STRUCTURE AND STRATIGRAPHY OF THE AJDABIYA TROUGH AREA, EAST SIRT BASIN - LIBYA

GHANUSH, HUSSIN,B

STRUCTURE AND STRATIGRAPHY OF THE AJDABIYA TROUGH AREA, EAST SIRT BASIN - LIBYA

Hussin Basheir Ghanush

A thesis submitted for the degree of
Doctor of Philosophy (PhD)

Department of Earth Sciences
Durham University

2015

ABSTRACT

The structural style within the deepest parts of the Ajdabiya Trough is defined by a system of Early - Late Cretaceous syn-depositional fault blocks bound by normal faults and basement highs devoid of syn-rift sediments, which are buried under a thick succession of Cenozoic post-rift deposits. The range of fault orientations likely reflects the conflicting influences of the ~NE-SW regional extension direction and the dominant ~N-S trending basement fabric. Mainly NW-trending normal faults dissecting Cretaceous and older rocks have been inferred from 2D seismic reflection and potential field data. Other faults trend NE-SW and E-W, and mainly cut Miocene and older strata. Some of these faults have both sinistral and dextral strike slip components and are possibly linked to on-going seismicity in the Sirt Basin and the Cyrenaica Platform. Vertical displacements on these faults are several hundred meters and are defined by large throws on Cretaceous and underlying horizons. Structural mapping confirms the presence of relay ramps associated with overlapping faults developed in the hangingwalls adjacent to west downthrowing normal faults along the eastern margin of the Ajdabiya Trough. The seismic stratigraphic framework is organised into six mega-sequences that correlate to variations in relative sea-level and/or sediment supply during Late Mesozoic and Cenozoic times. The stratigraphic architecture of the trough is largely influenced by relative sea level changes and minimal tectonic effects during the Cenozoic; observed progradation of the Paleocene, Early and Middle Eocene sequences along the trough margin is attributed to relatively rapid sedimentation rates and relatively slow rates of increase in accommodation space. Depositional environments are interpreted using the resultant facies analysis and the characterisation of the seismic reflections indicated that the geological units were deposited in marginal marine, shallow shelf and moderately deep marine environments. Special consideration is given to the principle of seismic sequence stratigraphy analysis of carbonate depositional systems where the facies group took initially place on a homoclinal ramp which later developed into a rimmed platform. This analysis additionally reveals that similar depositional architectures can be divided into systems tracts. The earliest systems tract of the Lower Eocene sequence is interpreted as lowstand prograding wedge distinguished on the basis of the component facies that indicate the dominant depositional regime. Localized debris flow or mass transport complex formed during early highstand systems tract deposition began during the Middle Eocene. The tectono-stratigraphic analysis of the Ajdabiya Trough reveals that two major extensional pulses controlled the architecture of the trough during continental rifting with crustal stretching (β) factor ranging from 1.3 to 1.5 consistent with subsidence in the Ajdabiya Trough having been controlled by thermal cooling and isostatic adjustments of the crust beneath the trough. Growth strata within grabens and half-grabens denote persistent tectonic subsidence and demonstrate the progressive depocenter locus migration towards the north. In such a context, the current geometry of the Ajdabiya Trough is interpreted to have resulted mainly from rifting cycles and possible renewed continental extension. The investigations of the tectono-stratigraphic controls reveal that after a period of relative tectonic quiescence, post-rift tectonic reactivation affected the Ajdabiya Trough almost continuously since the latest Cretaceous to the Miocene. Burial history curves correlated with one-dimensional back-stripping assuming Airy isostasy shows that Cenozoic subsidence in the Ajdabiya Trough can be divided into three episodes of post-rift subsidence characterized by short and long-lived subsidence pulses and rapid sedimentation rates that may lead to development of overpressure by disequilibrium compaction.

TABLE OF CONTENTS

DECLARATION

No part of this thesis has previously been submitted for a degree at this or any other university. The work described in this thesis is entirely that of the author, except where reference is made to previously published or unpublished work.

Hussin Basheir Ghanush

Department of Earth Sciences

Durham University

August 2015

ACKNOWLEDGMENTS

I am pleased to have this opportunity to thank the many colleagues, friends, and the Department of Earth Sciences members who have helped me with this research project. I am particularly indebted to my supervisor Dr. Jonathan Imber, for sharing his expertise, wisdom, and for his invaluable advice, valuable support, and his great attitude. His careful editing contributed enormously to the production of this thesis. Jonny had a great patient to hear about new ideas and comments at many stages in the course of this research project. I am extremely grateful to my second supervisor Prof. Ken McKafrey for his support and for the insightful guidance and fruitful discussions that largely helped improving this research. To the Department of Earth Sciences staff for providing excellent administrational services, an enjoyable work place and supported facilities. Thanks to my annual review committee members, Prof Mark Allen and Prof Robert Holdsworth for their support.

I would also like to thank all the members of staff within the Department of Earth Sciences Gary Wilkinson, David Stevenson, Matthew Hepburn, and others for provide help and support during the course of the study.

I would like to thank Dr. Stuart Jones for his time, advice, and input into sequence stratigraphic work. This work was supported by the Libyan Petroleum Institute (LPI) and the National Oil Corporation (NOC). I am grateful to the Libyan Petroleum Institute and the Libyan Embassy for funding the study. I would like also to acknowledge Shell Libya and the NOC, for the use of their 2D seismic lines and numerous well data. I individually thank Mr. Basheir Megrab and Dr. Ide Molen from Shell Libya and Mr. Daw Zahmoul from the NOC. To my research colleagues in the Department of Earth Sciences (open plane), I specially thank Alexander Peace.

I would like to express my gratitude to my family in Libya for their immense support that lead this quest to completion, I am sincerely indebted to them all specially my mother Mrs. Fatima Nafati, and to the spirit of my father Mr. Basheir Ghanush.

This research would not have been possible without the encouragement and support of my wife Mrs. Loutfia Muamir and my children during our stay in the lovely city of Durham.

CHAPTER 1: INTRODUCTION

1.1 Overview

The Sirt basin in north central Libya (Figures 1.1 & 1.2) is a Palaeozoic - Mesozoic intraplate depression that contains, on average, a 2500 m thick sedimentary rock record. The sedimentary rocks are of mainly Cretaceous and Cenozoic age and host world-class petroleum systems (e.g. Gumati, 1985; Gumatti and Nairn, 1991; Baird et al., 1996; Hallett, 2002). The Mesozoic - Cenozoic rift system is manifest as a ca. 500,000 km² area dissected by intervening platforms and troughs (Figure 1.3). The basin deepens towards the east, reaching the largest depression in the Ajdabiya Trough area (the focus of this study), with total sediment thickness of about 7000 m (Figure 1.4) (Hallett, 2002; Abuhajar and Roohi 2003; Guiraud et al., 2005).

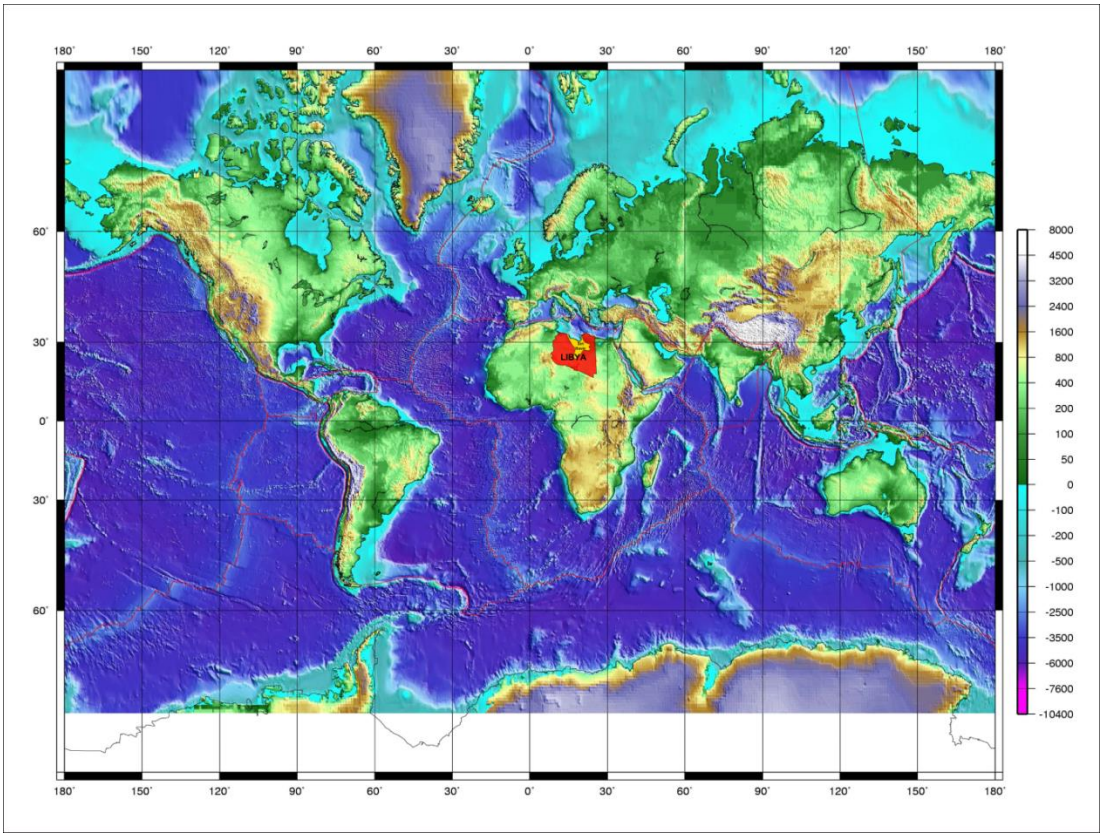

Figure 1.1: World topography and bathymetry map showing the location of Libya and Sirt Basin along the North African Margin close to the North Africa and South Europe active plate boundaries (Map available from the National Geophysical Data Centre, http://www.ngdc.noaa.gov/).

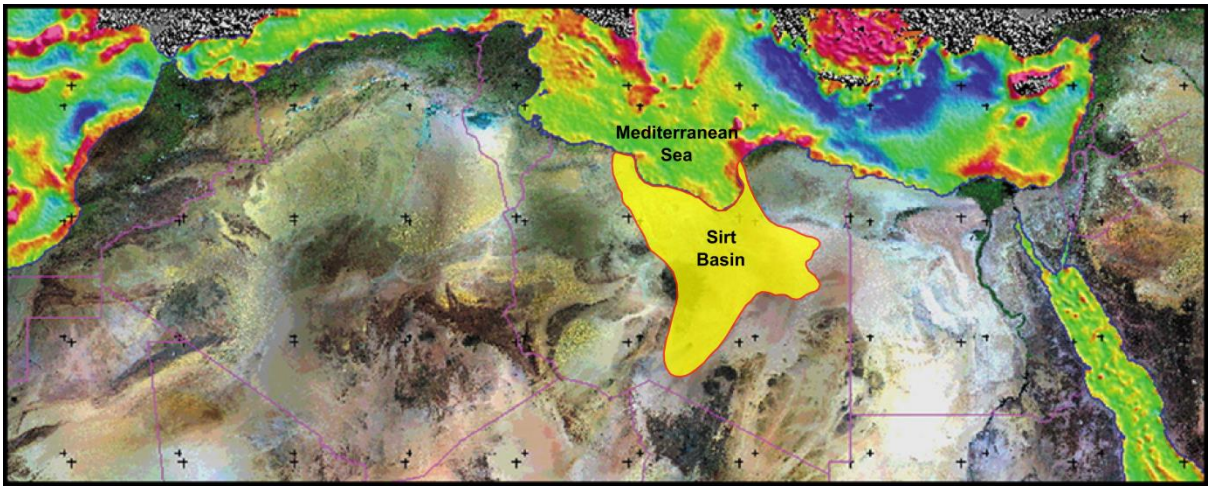

Figure 1.2: Satellite image of the North Africa and part from the Mediterranean Basin with location of the Sirt Basin in north central Libya. This map displays a contrasting view between the continental reliefs, in shades of grey-brown, and the Mediterranean seafloor morphology revealed by a red/green/blue colour grading scale. Map source (http://outreach.eurosites.info/outreach/DeepOceans/station.php?id=9)

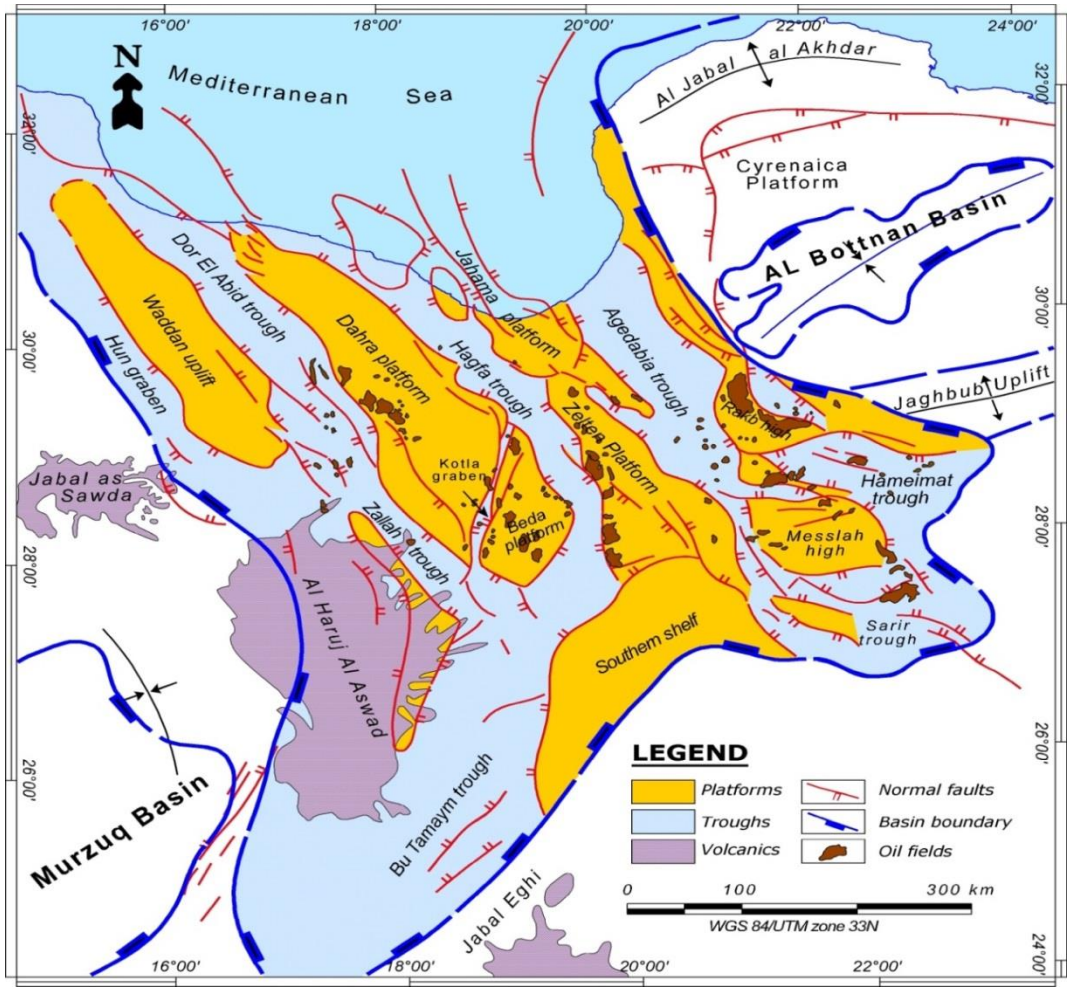

Figure 1.3: Structural map of the Sirt Basin highlighting key structural features. Map obtained from Mouzughi and Taleb, (1981).

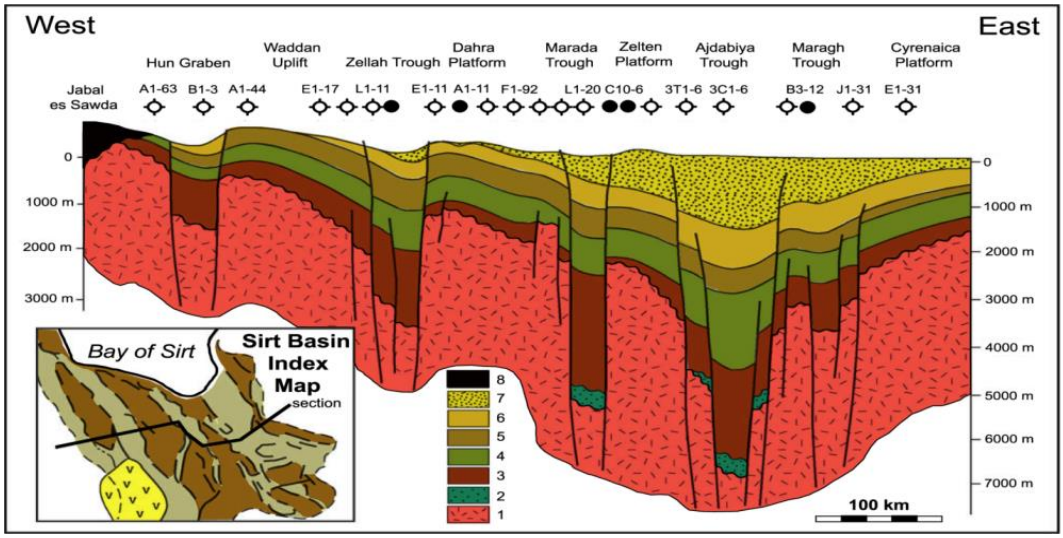

Figure 1.4: (a) Diagrammatic geological cross-section across the Sirt Basin, modified from Abuhajar and Roohi (2003), re-drawn from Guiraud et al., (2005), showing remarkable thickening in strata caused by dramatic subsidence and movement along major bounding faults in the Ajdabiya Trough. (1) Precambrian basement and Paleozoic quartzites; (2) Early Mesozoic(?) sandstones; (3) Late Cretaceous; (4) Paleocene; (5) Early Eocene; (6) Middle Eocene; (7) Late Eocene to Recent, (8) Cenozoic volcanics. Onset map shows the location of the cross-section, the brown and pale green colors are horst and graben features respectively and the yellow color indicates the Cenozoic volcanics.

The Sirt Basin is the youngest rifted intracratonic basin in Libya, formed by active subsidence and block-faulting that accompanied the collapse of the Sirt Arch in late Early Cretaceous times (Hallet, 2002) (Figure 1.5). The Sirt Arch formed during the Late Paleozoic time following inversion of early Paleozoic tectonic elements and was subjected to intense erosion that ultimately removed the entire Paleozoic succession (Hercynian unconformity) over the crest of the arch (Hallet, 2002).

Subsidence of the Sirt Basin reached a climax during the Paleocene and Eocene times (Gumati and Kanes, 1985; Abadi et al., 2008). The Precambrian basement and Early Paleozoic sediments of the basin were fragmented and subsided differentially to depths of more than 6000 m (Gumati and Schamel, 1988).

The Ajdabiya Trough with its thick Cenozoic section is located on the northern margin of the onshore Sirt Basin (Figure 1.3) close to the continent-ocean transition that connects stretched North Africa continental crust in the south with Central Mediterranean oceanic crust to the north (Casero and Roure 1994; Gaina et al., 2013). It is a complex graben mainly formed by Early Cretaceous rifting and Cenozoic post-rift subsidence (Baird et al., 1993; Ahlbrandt, 2001; El Arnauti et al., 2008), with basement-hosted extensional faults that presumably influenced syn-rift deposition but were not a primary control on the post-rift subsidence. This

post-rift subsidence contributed to the 7,000m thickness of Mesozoic - Cenozoic sediments accumulated in the depocentre (Rusk, 2001; Hallett, 2002).

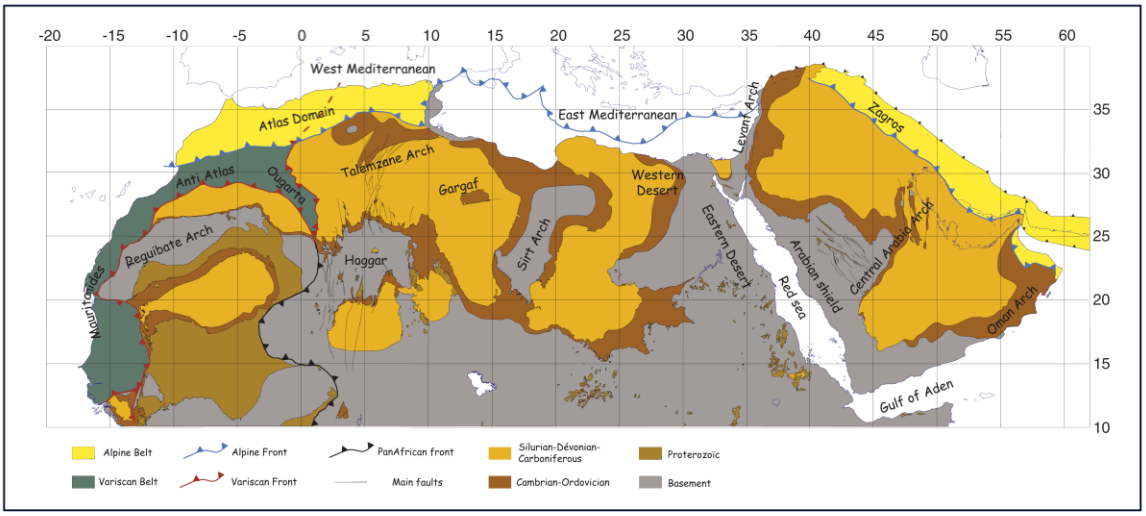

Figure 1.5: Simplified subcrop map of the Sahara and Arabia domains beneath the "Hercynian unconformity" showing the extent of the Sirt Arch and other features related to major arches with intervening Paleozoic basins in North Africa and Arabia. (Map obtained from Frizon et al., 2013)

1.1.1 Significance as a Petroleum Producing Province

The Sirt basin is a major oil producing region in Libya, and has been explored for over 50 years. Recoverable reserves are conservatively estimated at almost 24 billion barrels of oil in place. The majority of the Libyan hydrocarbon production comes from the Sirt Basin. Other discoveries have been made in the Ghadames and Murzuk Basins and, recently offshore discoveries have been made in the Pelagian Basin (Figure 1.6).

The prospective sectors of the basin encompass a total area of nearly 230,000 km^2, with a wildcat drilling density of one new field wildcat per 145 km^2 (Hallett and El Ghoul, 1996) . The average drilling rate is 3.3 wells per 100 km^2 (MacGregor and Moody, 1998) in areas, with an average field depth of 2,100 m. In comparison, the northern North Sea is three times more intensely explored compared to the Sirt Basin with average field depth of about 3,000 m (Montgomery, 1994; Ahlbrandt, 2001). Within the Sirt Basin, the petroleum discoveries were made on subtle traps such as hanging wall closure, relay ramps, and stratigraphic traps, many of which have not yet explored extensively. Recent drilling within deep troughs such as the Ajdabiya Trough suggests that clastic reservoirs beneath the carbonate reservoirs in the central Sirt Basin have potential (Hallett and El Ghoul, 1996).

Exploration activities in the Sirt Basin have led to the discovery of large quantities of oil and gas. The reservoirs range from depths of 500 m to more than 5000 m and produce hydrocarbons from rocks of Early Cambrian to Late Cenozoic age. Geochemical analysis suggests that shale sediments of Late Cretaceous and Early Cenozoic time are the source rocks for the Sirt Basin oil fields. The reservoir rocks are mainly sandstones and carbonates. Shales and evaporites form the seals in the basin. Normal faults and faulted anticlines are the major structural traps in the Sirt Basin, and Paleocene reefs form the major stratigraphic traps. The offshore area beyond 200 m depths is largely unexplored, but it has both significant hydrocarbon potential and significant exploration. The central portion of the Sirt Basin (Figures 1.6 & 1.7) is the main area of hydrocarbon occurrence. 21 major pools, with recoverable reserves in excess of 100 million barrels of oil have been discovered to date.

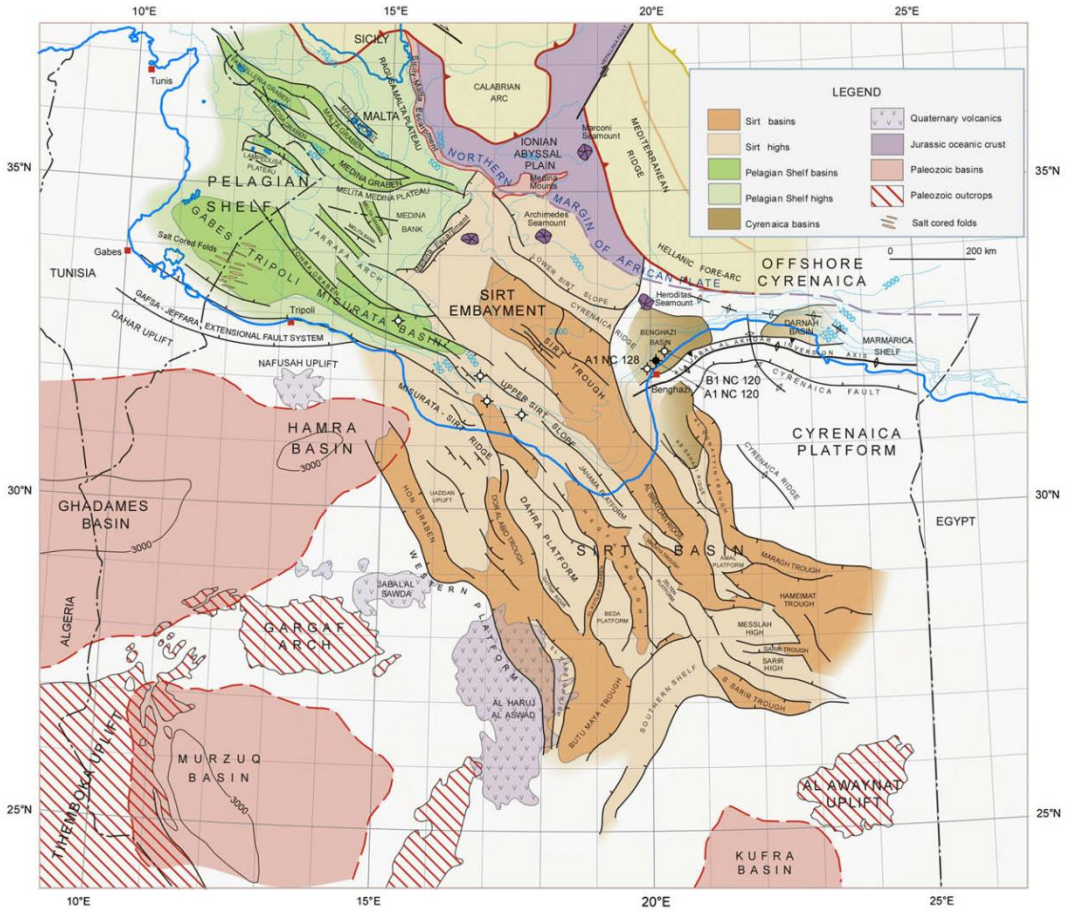

Figure 1.6: Tectonics and structural elements map for Libya and surrounding offshore areas. Structural highs and lows within the Pelagian Shelf, Sirt Basin, and Sirt Embayment are shown by lighter or darker shades respectively of the same color. Palaeozoic basins of Ghadames, Murzuq, and Kufra basins are shown in red color. Structures in sub-basins of the Cyrenaica region have not been so designated and are shaded brown. Map obtained from Fiduck (2009).

The majority of petroleum exploration activities in the Sirt Basin have been focused on structural highs with little attention to the deep troughs (Figure 1.7). Recent drilling within the Ajdabiya Trough has encountered oil shows in well A1-119 drilled on a structural high that bottomed in Upper Cretaceous strata (Hallett and El Ghoul, 1996). This suggests that significant potential could remain particularly in the grabens.

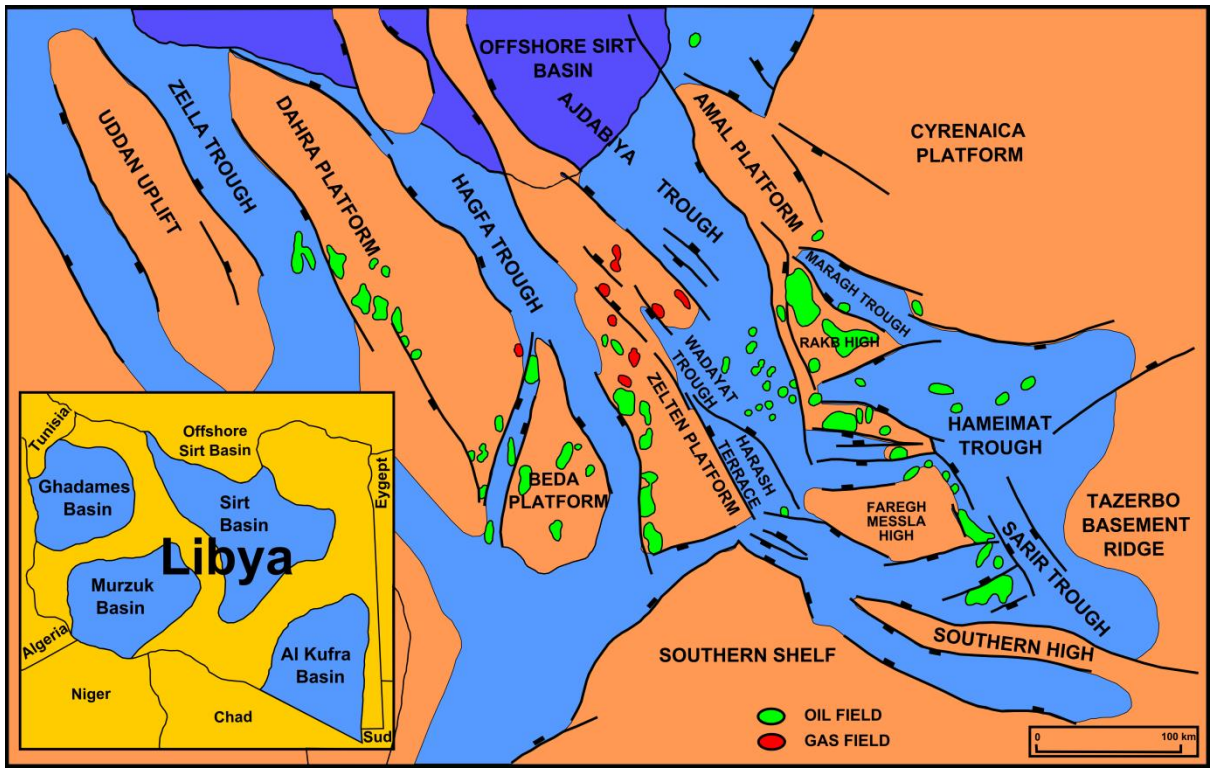

Figure 1.7: Map of eastern Sirt Basin area identifying major petroleum accumulations, main tectonic elements and depositional centres. Map redrawn from Burwood et al., (2003).

1.1.2 The Ajdabiya Trough: Background and Thesis Aims

During Triassic - Early Cretaceous time, as the Atlantic opened, the Sirt Basin went through a protracted phase of rifting (Figure 1.8). Although these events have been mentioned previously in several publications on the Sirt basin (e.g. Van Houten 1983; Rossi et al., 1991; Guiraud and Maurin, 1992; Maurin and Guiraud, 1993; Guiraud & Bosworth, 1997; Guiraud, 1998; McGregor and Moody 1998; Ziegler et al., 1999; El-Arnauti, et al., 2008), few details have been published, thus the structural geometry and the sequence stratigraphy of the rift are poorly known.

During the Late Cretaceous and throughout the Cenozoic, the deep troughs received large quantities of organic-rich shales, evaporites and clastic materials. At the same time, the

uplifted blocks were the sites of carbonate deposition, with reef development on the flanks and crests of the highs. The south-eastern part of the Sirt Basin is a siliciclastic, dominantly fluvial environment while the offshore penetrations show a marine carbonate-dominated depositional environment both in Cyrenaica and Tripolitania (Pelagian Basin).

The Ajdabiya Trough forms the connection between these two environments. To the south, the Sirt Basin is less disturbed and shallower; its continuation is marked by a thin succession of Early Cenozoic sediments (Conant and Goudarzi, 1976).

The Pre-Upper Cretaceous and Neogene history within the Ajdabiya Trough has not been investigated extensively in the literature, in part due to the almost total absence of outcrops and the previous lack of interest in the deep structures by the petroleum industry, the main sponsor for geologic studies in the area. The geologic history of the Ajdabiya Trough is dominated by the opening of the Tethyan seaway with the associated rifting and subsidence. This time of crustal thinning and subsidence is punctuated by brief periods of uplift and erosion. These are developed in response to shearing stresses, created non-uniform tectonic patterns (northwest-southeast horsts and grabens) over most of this part of the North African Margin during the Mesozoic and early Cenozoic (e.g. Schäfer, et al., 1980; Bosworth et al., 2008) (Figure 1.9). In comparison with contiguous areas in the Sirt Basin, and the Cyrenaica Platform to the east, the Ajdabiya Trough appears to have experienced a more complex geologic history. It is postulated that the crust beneath the NE part of Sirt Basin and Cyrenaica Platform has been affected by shear stresses that have recognized in the Western Desert of Egypt (Figure 1.10), but with much smaller magnitude and duration.

Topographically, there are no major structural features, exposed along the NE part of Sirt Basin including the Ajdabiya Trough area, except for the western part of the Sirt Basin and the Cyrenaica Platform to the east where excellent outcrop exists (Figure 1.11).

Previous studies around Ajdabiya Trough area were petroleum oriented and have concentrated on the southern part of the trough with more recent studies focussed on the offshore area (e.g, Gumati, 1985; Gumati and Nairn, 1991; Skuci, 1994; Hallett, and El Ghoul, 1996; Baird et al., 1996; Ahlbrandt, 2001; Hallett, 2002; Abadi et al., 2008; Witte, 2008; Fiduck 2009).

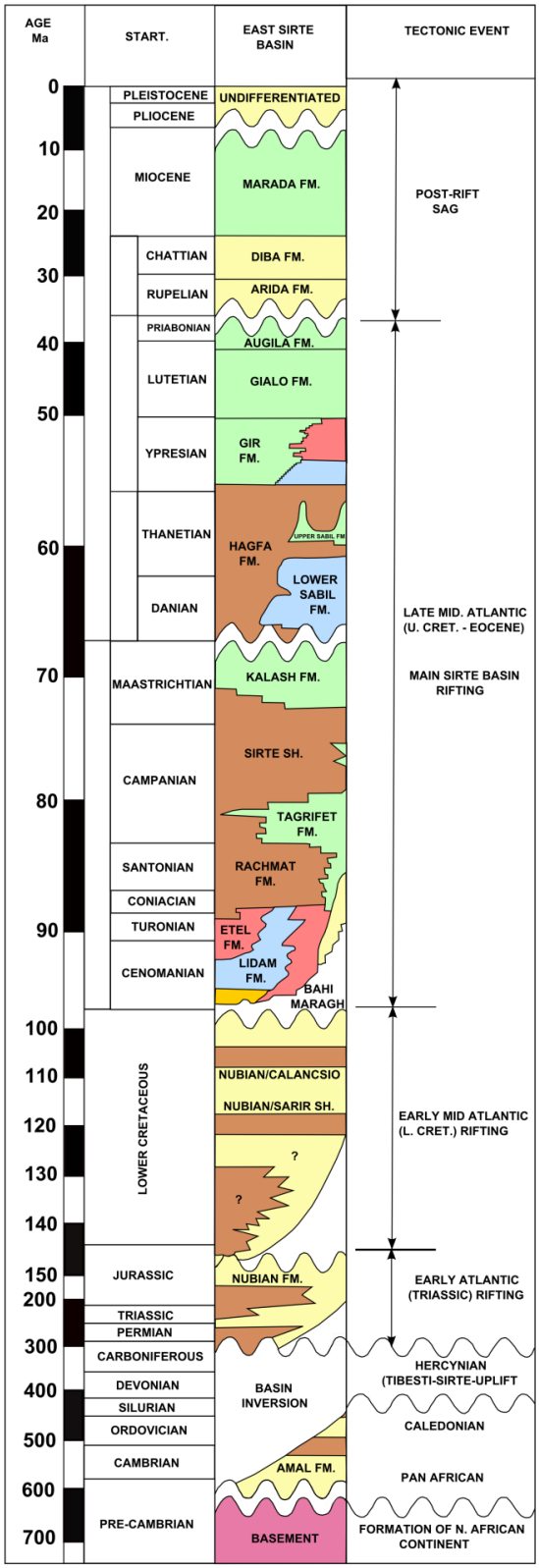

Figure 1.8: Generalized tectono – stratigraphic chart of the eastern Sirt Basin and Cyrenaica Platform modified from (Burwood et al., 2003).

Thus far petroleum exploration has focused on the mid-Cretaceous to Early Cenozoic rocks. Nevertheless, there is great potential for new hydrocarbon plays in the neglected syn-rift sequence and parts of the Cenozoic sequence. Understanding of the geometry and kinematics of the rift sequences (syn-rift and post-rift), as well as its infill cycles, will provide new insight into the tectonic evolution of the area and better understanding of the generation, migration, and trapping of the hydrocarbons in the basin.

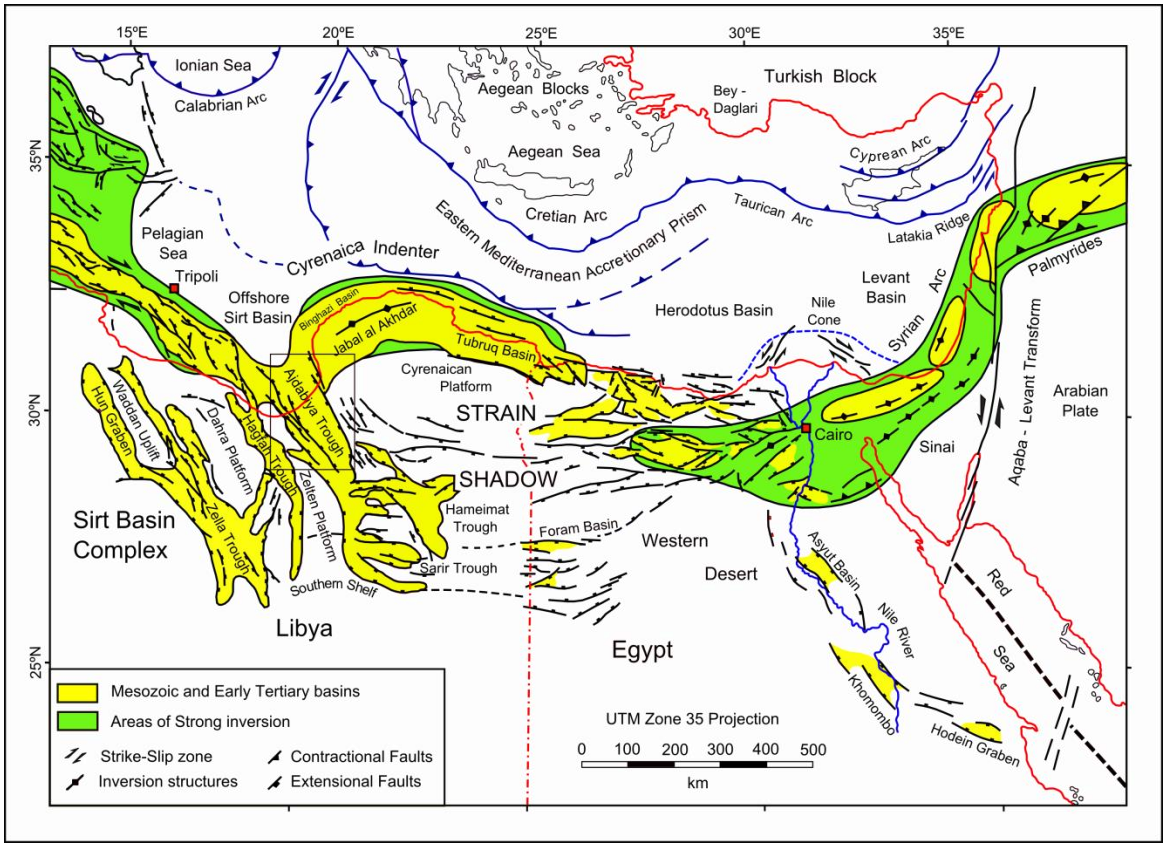

Figure 1.9: Tectonic setting of northeast Africa and the eastern Mediterranean collision zone, with location of Ajdabiya Trough (black rectangle) in the NE periphery of the Sirt Basin, from Bosworth et al., (2008).

There have been few studies of the subsurface geology of the NE Sirt Basin, and no detailed work on the structure and stratigraphy of the Ajdabiya Trough has been published to date.

The main aim of the study is to investigate the role of the previous tectonic events in the structural development of the Ajdabiya Trough area. It is also an attempt to correlate the kinematics of regional structures with the major events established within the Sirt Basin.

It is postulated that rifting was initiated in Sirt Basin during the Permo-Triassic - Cretaceous times (Gudarzi, 1981), reactivating pre-existing Paleozoic faults (Conant and Goudarzi, 1967;

Burke and Dewey, 1974). Rifting was possibly triggered by a lithospheric plume during the Cretaceous (Van Houten, 1983), with major subsidence occurring during the Late Cretaceous - Eocene (Gumati, 1985; Gumati and Nairn, 1991; van der Meer and Cloetingh, 1993; Abadi et al., 2008). The Ajdabiya Trough is considered to be part of the Sirt basin rift domain. Previous authors have identified a two phase basin history of syn-rift and post-rift subsidence (Gras, 1996).

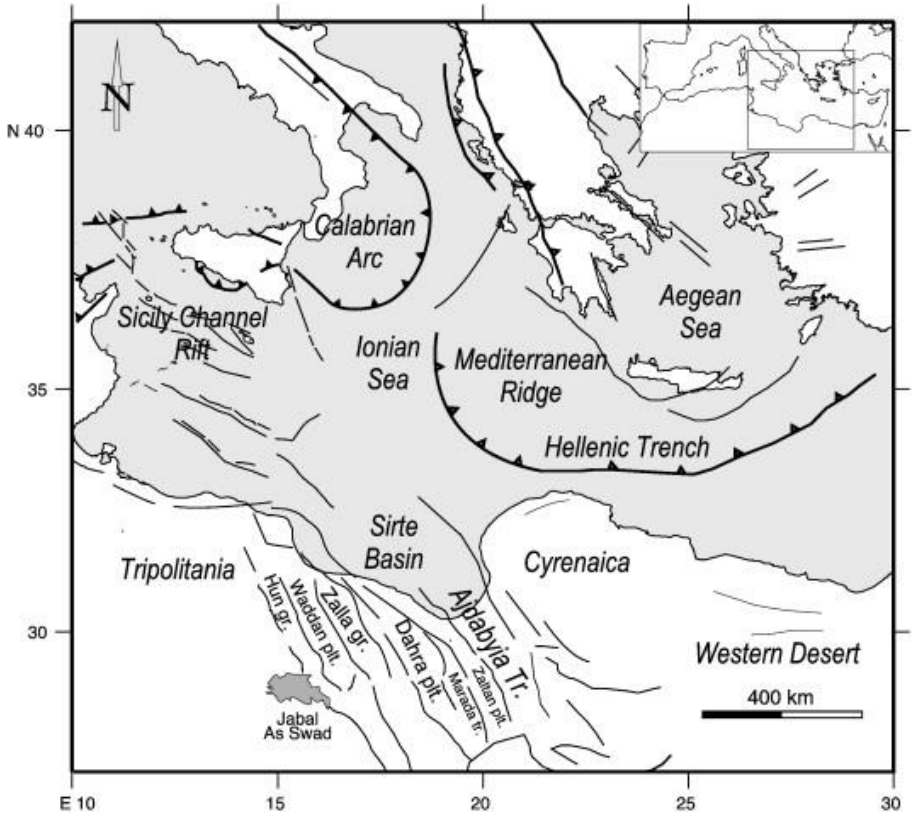

Figure 1.10: Tectonic sketch of the Central Mediterranean–North Africa area. Sirt basin is located in the northern African margin. Map from Capitanio et al., (2009).

The post-rift succession was developed during the end of the Mesozoic. The differential fault activity that formed subsiding grabens and uplifting platforms is believed to have been followed by a widespread Paleocene - Eocene regional subsidence phase (Gumati and Nairn, 1991; van der Meer and Cloetingh, 1993; Abadi et al., 2008). Subsidence and deepening of the entire Sirt Basin was accompanied by localized uplift in the western platforms (van der Meer and Cloetingh, 1993; Bosworth et al., 2008), possibly due to a strike slip component formed by variable alignments between tectonic structures and stress fields (Janssen et al., 1993; Anketerl, 1996; El Arnauti et al., 2008).

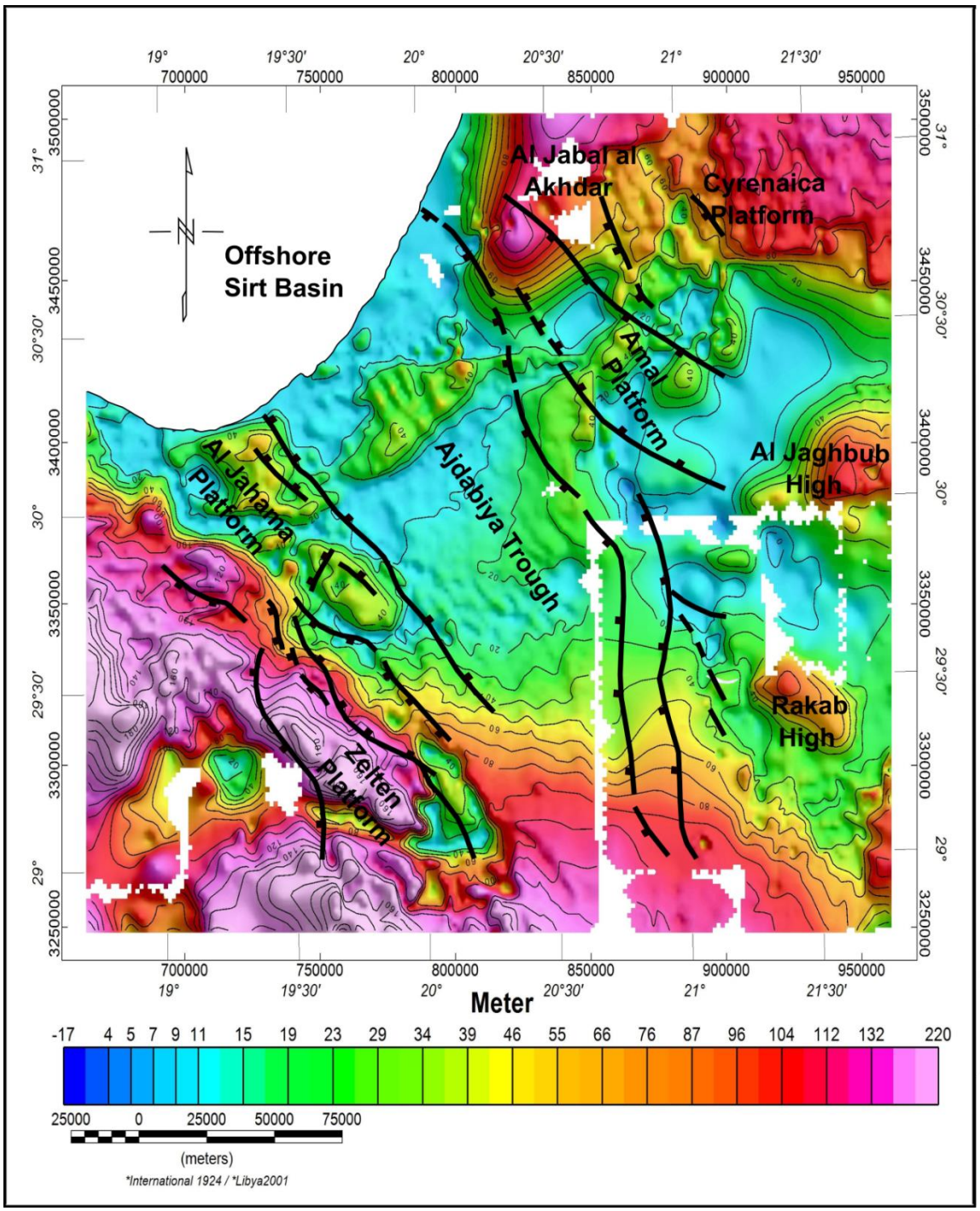

Figure 1.11: Topographic map of the eastern Sirt Basin including the Ajdabiya Trough and part of the Cyrenaica Platform. Surface outcrops are absent along the Ajdabiya Trough structural domain compared with the adjacent areas to the east and west.

As this major extensional event ended, the Sirt Basin underwent compression during Middle - Late Eocene times, tilting the basin northward and leading to abrupt subsidence in the north and uplift on the basin's southern shoulders followed by regional minor subsidence (van der

Meer and Cloetingh, 1993). Major tectonic subsidence within the Ajdabiya Trough therefore gave way to accommodation space produced by an interaction of regional and local tectonism and sea level changes leading to accumulation of a thick Mesozoic - Cenozoic sedimentary succession (Martin et al., 2008; Yanilmaz et al., 2008, Starkie et al., 2008).

The Ajdabiya Trough region has undergone extensional/compressional tectonics, however, the timing of the tectonic events and the details concerning the influence of tectonics upon the sedimentation are not well understood. These factors will be discussed in detail within the thesis.

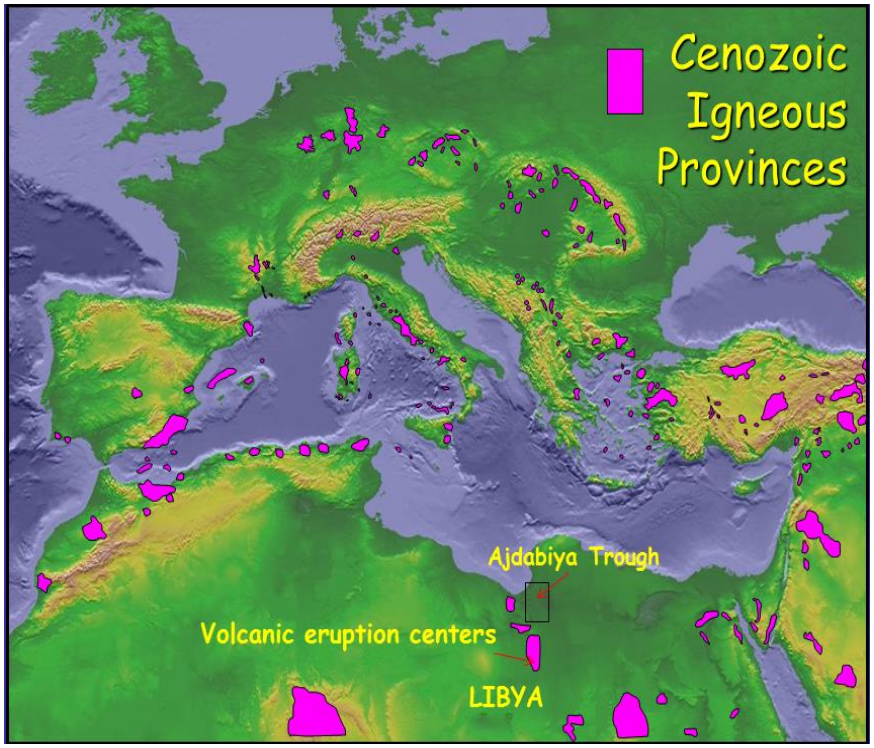

Figure 1.12: Digital topography of circum - Mediterranean area from NOAA showing the locations of Cenozoic igneous provinces (with both anorogenic and orogenic geochemical signatures) in purple. (http://www.ngdc.noaa.gov/mgg/image/2minrelief.html)

The overall aim is to outline a detailed tectono-stratigraphic framework within the Ajdabyia Trough area by analysing potential field and 2D seismic data correlated with well data from numerous wells. The trough recorded the largest continuous subsidence in the whole Sirt rift, thus offering the most significant estimates of its stretching history (Gumati and Nairn, 1991; Abadi et al., 2008).

The Ajdabiya Trough also lies close to areas of Cenozoic volcanic activity (Figure 1.12). Crustal structure and therefore subsidence may have further controlled Cenozoic tectono-

magmatic cycles through temporal variations in melt supply throughout the Sirt Basin (Figure 1.12).

1.1.3 Scope of Study

Within this context, I suggest that our tectonostratigraphic understanding of the Sirt Basin in general, and of the Ajdabiya Trough in particular, will benefit most by concentrating our study on the Cenozoic evolution of the trough, including an assessment of how the deeper, rift-related structures may have influenced the post-rift basin evolution. The main reason for this focus is that the seismic reflection images of the Cenozoic section are generally of good quality; but resolution decreases significantly at greater depths and there are few wells that penetrate the Cretaceous and older sections. The results of this study should shed much needed light on the recent structural evolution, on the hydrocarbon exploration history over the Sirt Basin. The general theme of this work is that the Ajdabiya Trough region is not an area with a single monolithic character through either time or space but comprises distinct domains each with individual tectonostratigraphic histories. One of my objectives is to identify and define the characteristics and histories of these individual domains. Tectonically the whole Sirt Basin evolved in the time dimension through a set of stages which are fundamentally different in the northern and the southern parts of the basin (Baird et al., 1996). As a consequence there are important differences in stratigraphy and structure between the different parts within the basin including the Ajdabiya Trough, which have substantial influence on regional interpretations of some unit distributions and on petroleum occurrence.

The remaining issues to be addressed in this work are threefold: 1) to investigate the upper crustal structure and Cenozoic stratigraphy of the Ajdabiya Trough. 2) To determine the geometry of the extensional fault system and understand the role of fault reactivation in controlling the Cenozoic fault patterns. It has been suggested that dextral strike-slip tectonics may have played a role in controlling rifting, but is there any direct structural evidence for this? 3) To estimate tectonic subsidence during the Cretaceous - Miocene period with emphasis on rifting effects on the present - day subsurface geometry of the Ajdabiya Trough.

The research is based on approximately 4000 kilometers of 2D seismic lines, and numerous wells mainly bottomed in the Upper Cretaceous section with potential field gravity and magnetic data. The seismic data were provided by Shell Libya Gmbh. The well data were

provided by the National Oil Company of Libya (NOC) and the potential field data were made available by the Libyan Petroleum Institute (LPI). In and around the Ajdabiya Trough region, many of the wells are drilled by commercial companies, and tend to be located over structural highs, anticlines, and other types of oil traps, this sampling bias result in a lack of details on the deep structure within the Ajdabiya Trough. Well logs, either on or close to the seismic lines, and surface data were used to calibrate markers that represent sequence boundaries. As a result of these interpretations structural and isopach maps for particular horizons were prepared. The gravity and seismic data were also used to identify faults associated with the rift structure. This thesis also addresses the stratigraphy of the syn-rift and post-rift (thermal-subsidence phase) sequences.

I interpret the study area as a major graben, striking NW-SE and tilted toward the northeast. This hypothesis is based on the presence of extensional structures aligned in NE-SW, NW-SE, and E-W directions and the north eastward thickening of the sedimentary section. The 2D seismic reflection data enables us to determine the geometries of the extensional faults but has not allowed imaging of the deep crustal structures. Despite the amount of data, the extensional fault system of the Ajdabiya Trough region is poorly understood because it is obscured due to the considerable depth of the Cretaceous sedimentary section and because of the presence, at shallow and mid crustal levels, of possible volcanic sequences and igneous intrusions as evidenced from the gravity and magnetic interpretations (chapter 4), and the study of Witte, (2008).

1.2 Study Aims and Objectives

In view of the factores mentioned above, the specific aims and objectives of this research are as follows.

1. Conduct gravity/magnetic and 2D seismic interpretation (i.e., maps, models, horizons, faults, sequence boundaries).
2. Construct geo-seismic cross-sections showing stratigraphic correlations, major sequences and fault structures.
3. Prepare gravity/magnetic maps showing regional structural trends with other map suites from 2D seismic and well data showing structure and sediment thickness distribution.

4. To construct a tectonic framework for the Ajdabiya Trough region and an assessment of the sedimentary cover overlying the Upper Cretaceous section.
5. To identify the main seismic-stratigraphic units and correlate them with, borehole data; recognizing systems tracts within depositional sequences by means of logs and seismic reflection patterns.
6. To identify and map faults in the Ajdabiya Trough and to enable comparison and correlation between fault geometries within different sectors (evaluation of displacement variations, timimng, growth and linkage of faults**)**.
7. Evaluate the subsidence based on interpretation of available well data, in order to establish the tectonic evolution, sedimentary distribution and thermal history.
8. To characterise the structural architecture of the Cenozoic post-rift strata and explain the controls of tectonic inversion throughout the thinned continental crust; to construct a seismo-stratigraphic framework that can explain the distribution, geometry and significance of correlative growth strata;
9. To develop one of the first tectono-stratigraphic models for the syn- and post-rift sequences in the Ajdabiya Trough, Sirt Basin.

1.3 Thesis Outline

The thesis is arranged in eight chapters, dealing with specific aspects within the study framework.

Chapter 1: Introduction

This chapter provides an introduction to the research study and presents the main aims and objectives of the thesis, as well as the outline of the thesis.

Chapter 2: Geological Framework and Regional Geodynamic Setting of the Ajdabiya Trough

In this chapter the general geological background of North Africa and the Sirt Basin, will be introduced, concentrating on their evolution and dynamics, with implications for the understanding of Cenozoic tectonics and their relationship to the earlier rifting episodes. The

Geological framework and regional geodynamic setting of the Ajdabiya Trough will also be outlined and the rationale and the hypotheses to be tested in this study defined.

Chapter 3: Dataset and Methodology

In this chapter a short explanation of the physical basis of the geophysical and geological datasets, the datasets used and the software packages that were required will be given.

In the second part, concepts of seismic interpretation, in particular focusing on the applications of 2D methods, a short review of data processing and modern interpretation tools is provided. In the third part, a general view of the fundamentals and applications of seismic and sequence stratigraphy in studying basin stratigraphy and sedimentary processes at continental margins ends with the general interpretation approach to this study.

Chapter 4: Gravity and Magnetic Data Interpretation

This chapter utilizes different techniques for better interpretation and understanding of gravity and magnetic data in terms of geology in Ajdabiya Trough. Using existing geological and geophysical data as a foundation this part of the study ultimately seeks to construct an updated tectonic setting of the Ajdabiya Trough region employing gravity and magnetic imaging and modeling.

Chapter 5: A Seismic Stratigraphic Approach to the Depositional History analysis of the Cenozoic strata

In this chapter models for the stratigraphic and sedimentological evolution of rift basins are reviewed at the basin scale and at the graben and/or half-graben scale. Different models have been presented for the geotectonic evolution of rifts (pure shear, simple shear, heterogeneous stretching and volcanic- or plume-related rifts) and these are reviewed. The chapter will introduce the idea behind the interpretation of the depositional sequences and their relationship to the rift structures and the regional extension in the Sirt Basin. It will also provide details about the main control on sedimentation and their relationship to basement structures that have played a significant role in developing the rift structures. The different stratigraphic signatures of the geotectonic models are discussed in terms of the nature and the

occurrence of pre-rift strata, syn-rift unconformity, syn-rift strata, post-rift unconformity and post-rift strata. A seismic stratigraphic framework in the Ajdabiya Trough area focusing on recognition of depositional megasequences or individual sequences that evolved during the period from the Cretaceous to the Miocene and on a more local scale is presented. This highlights distinct geological relationships such as variations in facies, thickness, and characteristics as they relate to the boundaries of individual structural blocks within the trough.

Chapter 6: Quantifying Subsidence History during Mesozoic to Cenozoic

In this chapter, the results of the subsidence analysis during the Mesozoic to Cenozoic are presented. The results of subsidence analysis and the results from backstripping wells in the Ajdabiya Trough during the post-rift subsidence period are given. This then provides an overview of the structural framework and overall architecture of the Ajdabiya Trough on a regional scale, making use of reflection seismic sections, geological sections, isopach maps and observed subsidence profiles (burial history curves or plots).

Chapter 7: Cenozoic Structural Evolution of the Ajdabiya Trough

The focus in this chapter is on the structural setting and generalized Cenozoic evolution of the Ajdabiya Trough. A case study analysis in which the results of seismic mapping undertaken to interpret the post-rift strata, the fault geometry and their links to the evolution of the variable rift megasequences in the study area is provided. Fault interpretations within the Ajdabiya Trough focusing on the duration of fault activity, fault geometry and patterns, timing of fault movement, growth characteristics and segmentation are described and discussed.

Chapter 8: Discussion and, Conclusions and Further Work

The final chapter presents a summary of the study and considers the main discussion items and conclusions that have been drawn. An integrated discussion of the main results deriving from core research themes revealed in the thesis is given followed by a synthesis of the conclusions from chapters 4, 5, 6 and 7 concerning the subsidence, stratigraphy and the fault analysis within the Ajdabiya Trough. Recommendations for future work are given at the end.

CHAPTER 2: GEOLOGICAL FRAMEWORK AND REGIONAL GEODYNAMIC SETTING OF THE AJDABIYA TROUGH

2.1 Introduction

This chapter summarize the geologic setting of the Sirt Basin and the Ajdabiya Trough and provide a brief overview on the mechanism and tectonostratigraphic implications of crustal extension; and summarise the geodynamic setting and regional geological framework of the Ajdabiya Trough by summarising and reviewing the published literature.

This chapter includes discussions of

- Rifting and crustal extension along continental margins.
- Tectonostratigraphic framework of the Sirt Basin and Ajdabiya Trough
- Geodynamic setting
- Crustal structure
- Subsidence and stratigraphical development of the Sirt Basin and Ajdabiya Trough
- Discussion

The Paleozoic tectonic framework in Sirt Basin has had a lasting effect on the overlying cover which is evident in the structural synthesis of the basin considered by group of researchers (e.g. Guiraud et al., 1987; Bayoumi and Lofty, 1989; Baird et al., 1996; Guiraud and Maurin, 1992; Janssen et al., 1995; van der Meer and Cloetingh, 1993; Pique and Laville, 1996; Wilson and Guiraud, 1998; Stampfli et al., 2001; Ziegler et al., 2001; Guiraud et al., 2001; Guiraud et al., 2005; Hallat, 2002; Craig et al., 2008; Abadi et al., 2008; Bosworth et al., 2008). The opening of the North Atlantic has had a large impact on the complex pattern of differential motion between Eurasia, Africa over the past 120Ma (Ziegler, 1988).

The location of the Ajdabiya Trough close to the Africa-Europe plate boundary zone means that the basin evolution is likely to have been characterized by active tectonic deformation, in addition to more typical sag-basin processes such as thermal subsidence and differential compaction (Skuci, 1994; Baird et al., 1996). A major NNW–SSE trending troughs and ridges

bound by master faults seen on geologic, seismic and potential field maps separates an ENE–WSW trending faults and shear zones (e.g. Anketell, 1996 and references therein). The Ajdabiya Trough area is characterised by NW–SE cross-cutting structures which reflect basement grain and/or location of major rift faults within the Mesozoic cover. These faults have remained active throughout the Mesozoic and part from the Cenozoic controlling structure and deposition (e.g. Capitanio et al., 2011). Although many studies on rifts worldwide have resulted in increased understanding of advanced stages of continental rifting, almost no research has focused on the processes that initiate and control the early stages of continental rifting. Because rifting gives rise to such a variety of geological processes, the chapter provides opportunities for relating deformation, igneous activity and sedimentation to their underlying driving mechanisms.

2.2 Rifting and Crustal Extension

2.2.1 Mechanism of Rifting and Crustal Extension

Active rifts is defined as rifting in response to thermal upwelling of the asthenosphere (Figure 2.1) and often develop large igneous provinces, whereas passive rifts are formed in response to a regional stress field and in large extent the result of plate boundary forces, with minor igneous activity (Corti et al., 2003; Ziegler and Cloetingh, 2004; Rosenbaum et al., 2008; Merle, 2011).

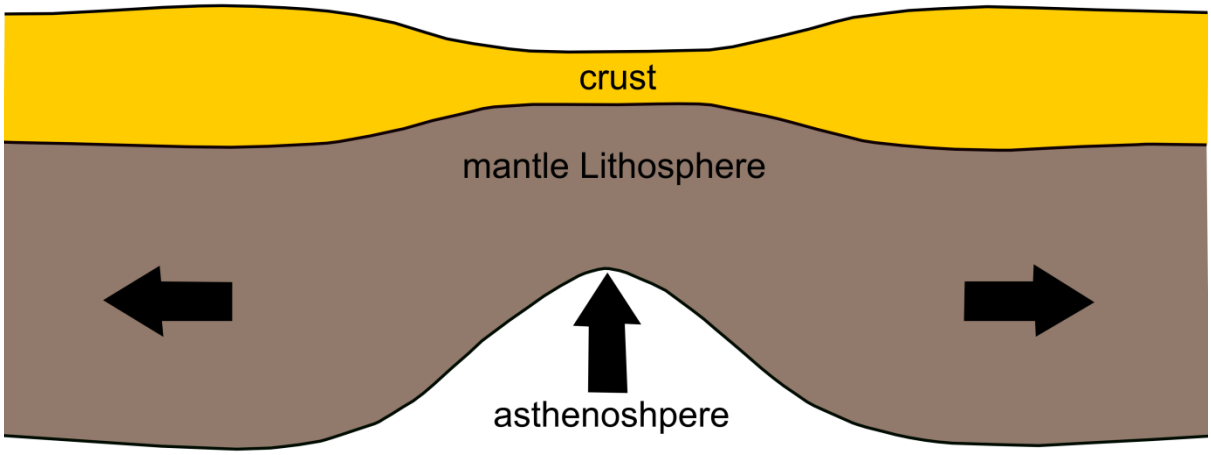

Figure 2.1: Schematic diagram of rift geometry showing the mantle flows acting underneath the rifted crust during extension, which might result in small-scale convection, (Redrawn from Steckler, 1985).

Rift systems are classified based on four models of geodynamic evolutions (Figure 2.2) that controlling the geometry and kinematics of continental rift basins (Merle, 2011), these are: 1) subduction-related rifts, 2) mountain-related rifts, 3) plume-related rifts, or 4) transform-related rifts.

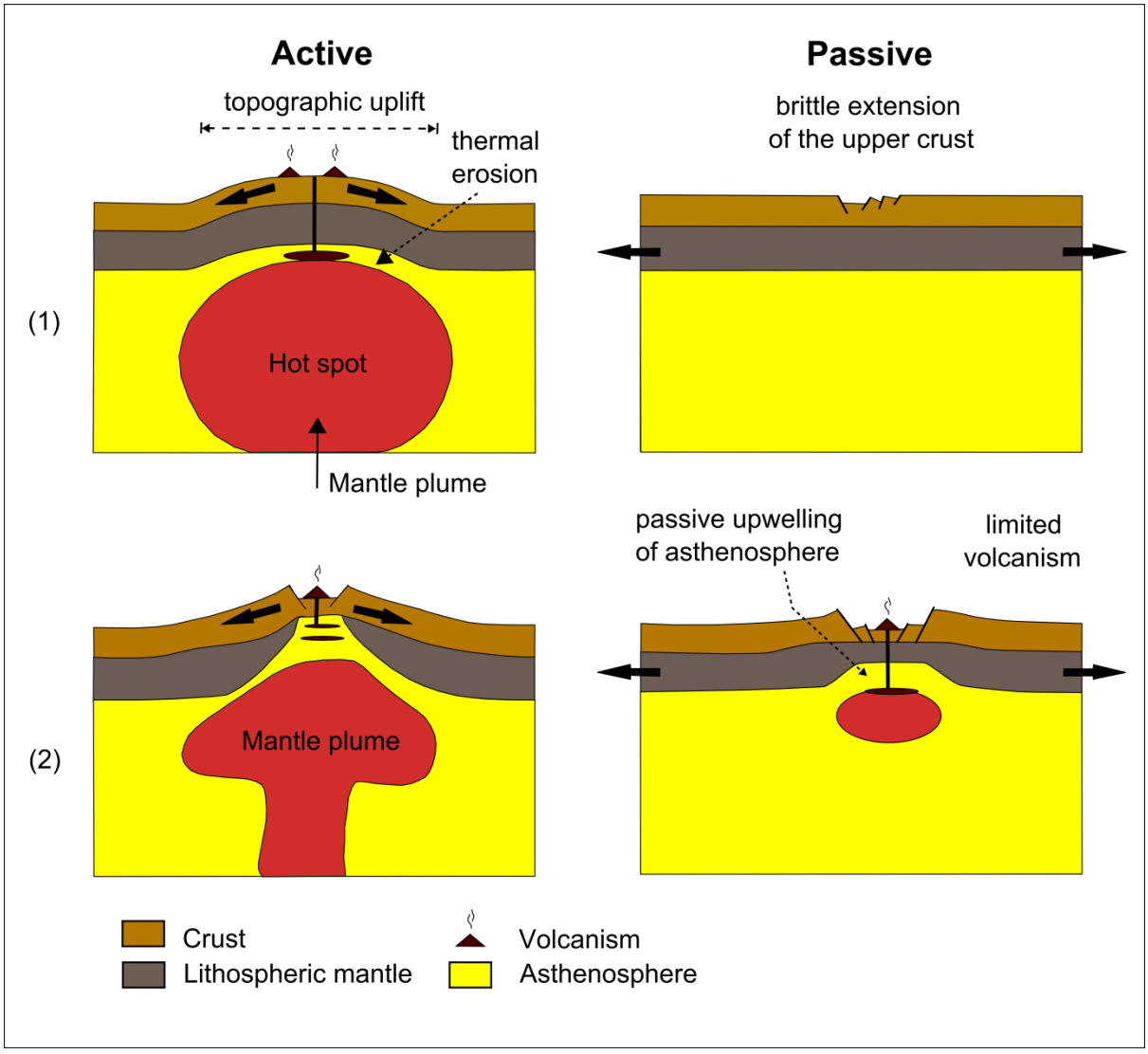

Figure 2.2: Schematic diagram illustrating different stages of continental rifting. Both (1) and (2) show Active rifting and Passive rifting models. Redrawn from Corti et al. (2003) and Merle (2011)

Continental rifting occurs as the response of rheologically complex continental lithosphere to extensional stress (Bott, 1992) and under the influence of a variety of plate tectonic regimes, which modify the rifts in moderate manner (Ziegler et al., 1995). These include convergence - related conditions, divergence related compression, collision related compression, shear, etc.

The structural style of rifts (Figure 2.3) is influenced by many factors; these include the thickness and thermal state of the crust and mantle-lithosphere at the onset of rifting in addition to the model and amount of crustal extension (Zigler, 1996). At syn-rift sedimentary level, the rifts are mainly influenced by the lithological composition of pre- and syn-rift sediments (Ziegler, 1996). Continental rifts are also characterized by volcanism, doming, and a tensional stress field which results in normal faulting in the upper crust.

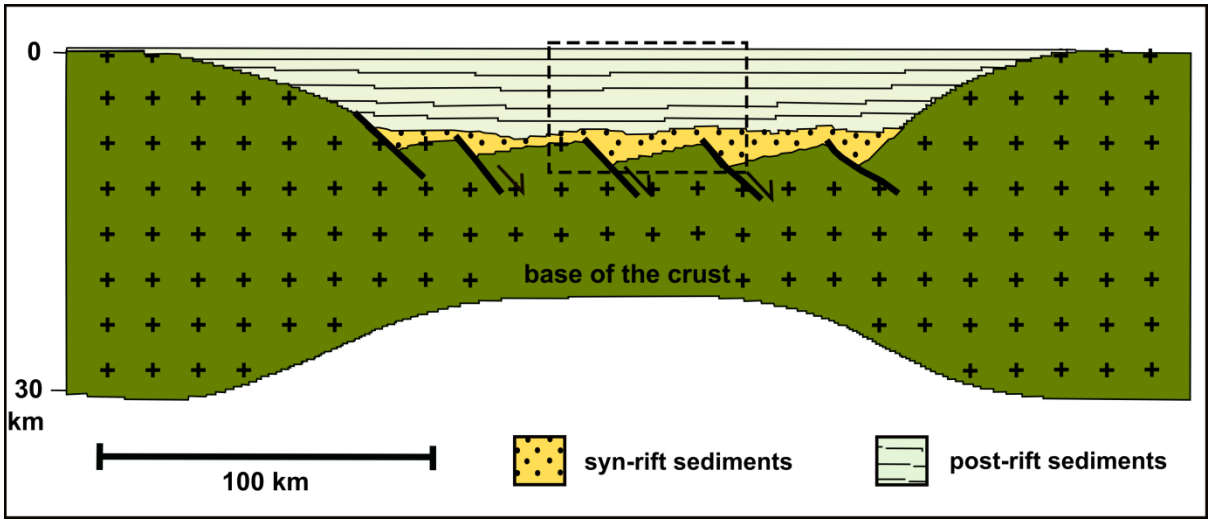

Figure 2.3: A sketch of a sedimentary basin that has formed by lithospheric stretching. The upper crust stretches by brittle faulting, while the hotter, lower crust and lithospheric mantle deform by plastic creep. Once stretching ceases, the region gradually subsides and fills with sediment (Redrawn from Lonergan and White 1999).

The geometry of continental rifts was assumed to be a typical graben structures with major planar normal faults on both sides of a subsiding grabens. On the other hand, listric faults produce asymmetric structures with downthrown block generating a half-graben structure (Bertotti et al., 2000). In McKenzie's pure shear model (Figure 2.4) (McKenzie, 1978) crustal stretching generated by an extensional force field occurs through a uniform continuous thinning of the ductile lower crustal thinning occurs below the surface rift, a process that is known as pure shear and lithospheric mantle and by normal faulting of the brittle upper crust. Lithospheric extension and thinning in Sirt Basin is intensified during the Early Cretaceous, due to movements between pieces or sub-plates within the African Plate (Van Houten, 1980; Fairhead et al., 2013). Crustal doming caused uplift and subsequent erosion, and intracratonic rifting.

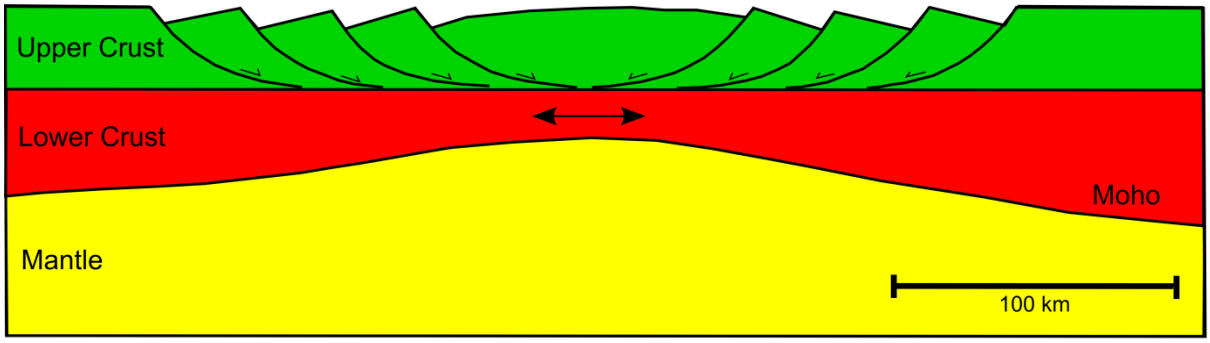

Figure 2.4: The uniform pure shear model of McKenzie.

It is hypothesised also that crustal thinning and riding above mantle magma plume are played significant role in the deformation of the Sirt Arch (Van Houten 1983). NW-SE oriented rift system and tectonism are developed during periods from Late Cretaceous – Cenozoic caused large scale basin subsidence and block faulting (Conant and Goudarzi, 1967: Baird et al., 1996; Hallett, 2002). The Sirt Basin represents the best-documented evidence for widespread extensional faulting within the African Plate during the Cretaceous (Browne et al**.,** 1985; Almond, 1986).

2.2.2 Kinematic Models of Rifting

A rift basin is defined as a large elongated tectonic depression bounded by normal faults that are formed as a zone of rupture in an extensional setting (Burke, 1977; Olsen, 1995). As a consequence, normal faulting occurs and the crust is displaced downward along the fault surfaces creating half-grabens or depressed areas inside the rift. According to studies on modern rift basins, such as the East African Rift system (Morley, 1988; Fairhead et al., 2013) the main rifts are markedly asymmetric with half-graben structures.

Several models have been proposed to explain the processes and geometries of the lithosphere during extension formed in rift basins (e.g. McKenzie, 1978; Wernicke, 1981; Lister et al., 1986; Rosenbaum et al., 2008; Merle, 2011). It is anticipated that deep crustal symmetry and asymmetry of rifted margins are invoked by differences of depth dependent controls of lithospheric extension (Lister et al., 1991). These differences are referred as the "simple shear" and the "pure-shear" models (Figure 2.5). The "pure-shear" model defined by McKenzie (1978) assumes homogeneous thinning of the lithosphere and used to predict

crustal thickness, subsidence history of symmetric passive margins, whereas asymmetric margins suggest a role for simple shear (Wernicke and Burchfiel, 1982). The simple-shear model predicts asymmetrical doming of a rift zone or even flexural uplift of an arch located to one side of the zone of upper crustal extension (Wernicke, 1981).

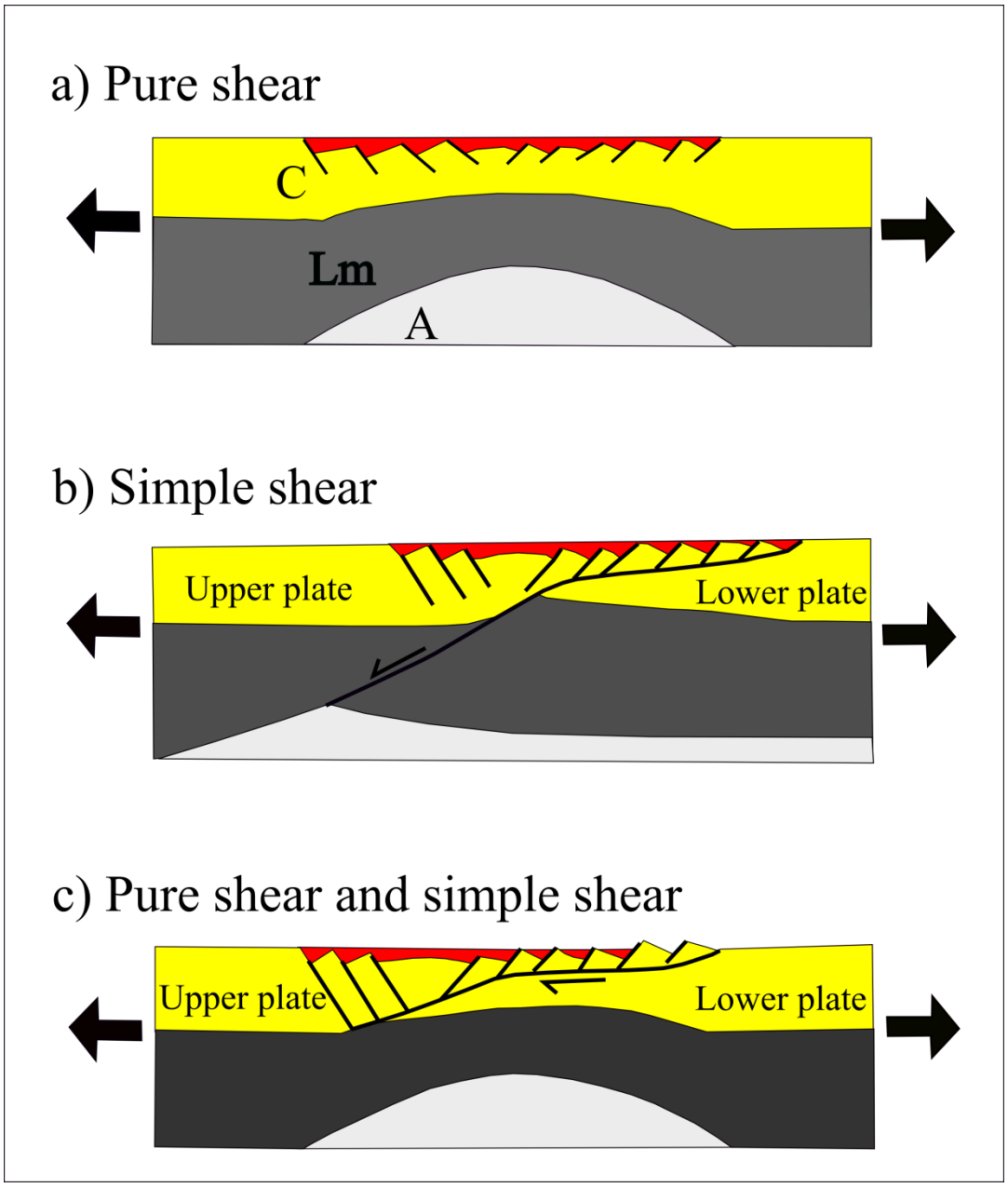

Figure 2.5: Different models of lithospheric extension proposed to explain the formation of rift basins and passive continental margins. a) Pure shear model is symmetric, with maximum heat underneath the middle of the rift. b) Simple shear model is dominated by a generally low angle shear zone that produces an asymmetry on the rift. c) Combination of lithospheric scale pure shear and simple shear stretching within the crust, Re-drawn from Keen et al. (1989).

Rift basins are characterized by, a significant extension and highly structured basement resulting from rotations and tilting of fault blocks bounded by high-angle normal faults (Lister et al., 1986 and Etheridge et al., 1989). The main factor controlling extension events in rift basins is a heat loss during rifting which leads to an increase in syn-rift subsidence and the subsequent development of post-rift (e.g. Reston, 2009). The "pure-shear" model of McKenzie (1978) assumes instantaneous and uniform extension of the lithosphere (homogenous thinning) and the crust with passive upwelling of hot asthenosphere to maintain isostatic equilibrium.

The lithospheric stretching model proposed by McKenzie (1978) is a kinematic model that allows for the thermal structure and subsidence history of a basin to be determined from the amount of crustal and mantle stretching. The total amount of thinning during extension usually is described by the stretching factor (β), (Figure 2.6) which is the ratio of the initial and final thickness of the crust as outlined by McKenzie, (1978) whose suggest that stretching is responsible for heating of the lithosphere and the basin subsidence, which mainly controlled by a molten asthenosphere and by variations in densities between the crust, lithosphere and the asthenosphere that governed by geothermal gradients and lateral heat flow. Subsequently, Wernicke (1981) and later Coward (1986) postulated that the upper crust has thinned and normal faults occur above a basal detachment (thin skinned tectonics).

Both McKenzie and Wernicke pointed that rift basins can be asymmetric and that extension is mainly controlled by deep detachment faults formed under simple-shear.

As an example, the models have been very often used in passive rifting settings to account for a large variety of observations like rates of subsidence and/or uplift of the basement, differential stretching, and lithospheric detachments (e.g. Cloetingh et al., 1995).

Continental rift zones are generally associated with a series of discrete, but kinematically linked basins along the length of the rift system (e.g., Bosworth, 1985; Rosendahl, 1987). Fault-bounded sedimentary basins are formed by crustal extension and marked by repeated episodes of normal faulting and large differential uplifts, over long period of time; forming asymmetric rift basins bounded by border faults whose offset decrease from a maximum near the segment centre to zero at segment tips. At large scale, hangingwalls is the block positioned over the border fault where possible drag folds form as a result of fault propagation into monocline structures developed by differential compaction at the fault tip.

2.2.3 Patterns of Subsidence during Rifting

Subsidence is probably the most important process that influences the infill of any basin. In the case of rift basins, subsidence progressively takes place as an isostatic response to crustal thinning. According to Dickinson (1974), subsidence can form according to the following processes:

1. Thinning of crust due to stretching, erosion, and magmatic withdrawal.
2. Thickening of mantle lithosphere during cooling.
3. Sedimentary and volcanic loading of both crust and lithosphere.
4. Tectonic loading of both crust and lithosphere.
5. Dynamics effects of asthenospheric flow.
6. Crustal strengthening.

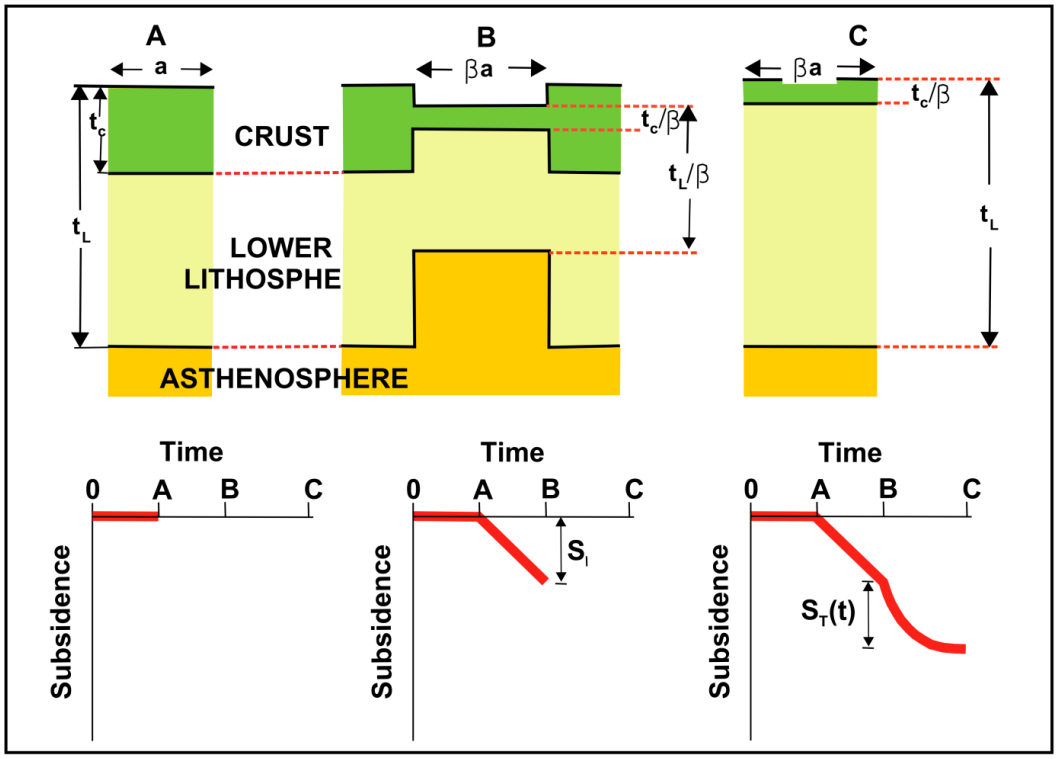

Figure 2.6: Principal features of the McKenzie's (1978) subsidence model. A: Initial conditions. A thermally equilibrated continental lithosphere of total thickness t_L consisting of a crust of thickness tc and a lithospheric mantle of thickness tm= (tc – t_L) overlies a partially molten asthenosphere. B: Uniform instantaneous stretching (β). At the time t = 0, uniform instantaneous mechanical extension of the lithosphere by a factor β occurs causing vertical thinning of both the crust (thickness = tc/β) and the mantle-lithosphere (thickness = tm/ β = (tc – t_L)/β). Since the temperature of the material remains unchanged during the extension, isostatic compensation causes upwelling of hot asthenosphere. The resulting gradual decaying of the thermal perturbation produces an initial instantaneous subsidence, S_I. C: Post-rift evolution. The cooling of the lithosphere following rifting causes a second phase of relative slower thermal subsidence, S_T (t). (Redrawn from Cacace et al., 2008).

For some authors (e.g. McKenzie, 1978) the main mechanism of subsidence in rift zones is stretching, although the mechanisms through which this type of deformation is produced are still not clear enough. Other scientists however, think that extension is not the only factor that controls subsidence in a rift during the syn-rift stage but that the sediment load also plays an important role in this process (Ziegler, 1995), and that the mechanical stretching of the lithosphere and the thickness and thermal state of the crust are factors than also can influence the structural style of the basin.

The magnitude of subsidence in rift basin depends on the geometry of crustal thinning and density of the rift infill. The subsidence is accommodated primarily by extensional faulting.

Maximum subsidence may occur in the hangingwall of the fault near the fault segment centre, while maximum footwall uplift is also observed at the centre of the fault (e.g. Morley, 1988; Gawthorpe et al., 1997).

Subsidence pattern during a rift phase is characterised by an initial period of slow subsidence and limited movement on bounding faults (rift initiation) associated with an initial isostatic subsidence (S_I) (Figure 2.6) in response to crustal thinning, subsequently followed by more rapid subsidence (rift climax) as a result of increase in accommodation space and finally culminated by period of final stage and dimensioned subsidence (Gupta et al., 1998).

It is dominantly accepted that during extension of the continental crust, tectonic subsidence in many rift basins is the main driver for the creation of new accommodation space.

Tectonic subsidence of continental crust can include periods of subsidence rates controlled by distinctive stages of faulting which plays a significant role in explaining the resulting sediment thickness and broad stratigraphic patterns in rift basins (e.g. McKenzie 1978; Watts et al. 1982; Gupta et al., 1998).

The final phase of tectonic subsidence is associated with the transition from pulses of rifting to thermally driven post-rift subsidence (S_T) (Figure 2.6) as heat is loss by conduction (e.g. Gupta et al., 1998). McKenzie (1978) proposed that as long as extension is instantaneous (i.e. less than 20 My) the initial subsidence will be complete before thermal subsidence begins. In rift basins, subsidence usually outpaces sedimentation, leading to an increase in accommodation space and minor eustatic variations lead to limited application of sequence stratigraphy applied to extensional settings.

2.2.4 Stratigraphy and Sedimentary Infill

During rifting rapid stages of tectonic subsidence followed by long period of tectonic quiescence is a criterion of many rift basins. During these stages sedimentation processes are characterized by gradual filling of the available accommodation space with overall progradational trend (Figure 2.7). Rapid subsidence will cause instant generation of the accommodation space which in turn will generate rift related sequence boundaries.

Sequence boundaries in this case are generated due to maximum flooding, which would initially develop a transgressive system tract, subsequently followed by highstand system tract formed during advanced rift phase as a result of decrease in accommodation space and due to lowering in the subsidence rates.

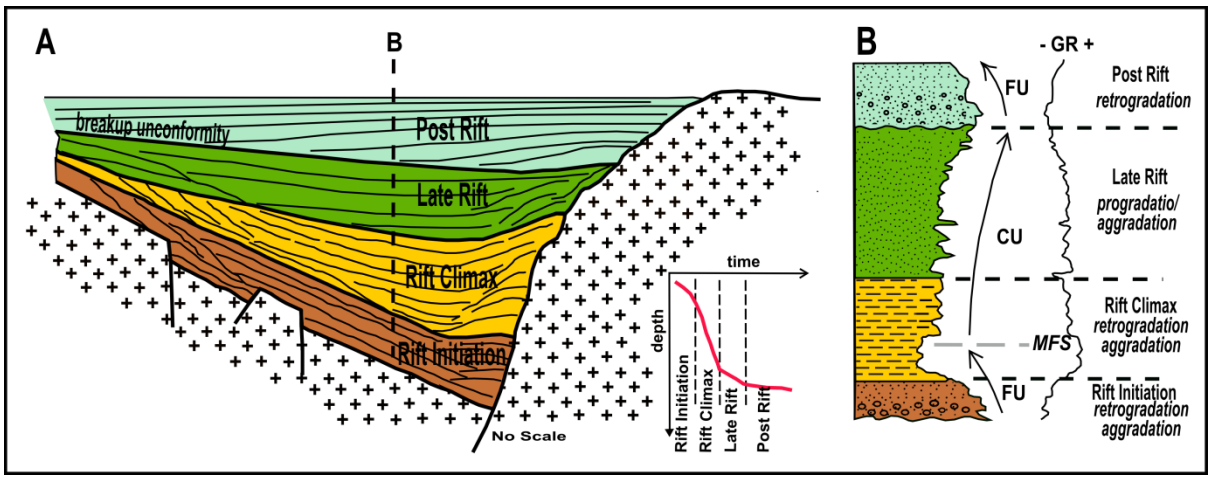

Figure 2.7 Schematic architecture and depositional sequences of tectonic systems tracts on a single phase rift event. A – Idealised seismic section across a sub-basin. B - In outcrop, borehole and wireline data. Redrawn from Pereira and Alves, (2012), based on simplified models obtained from Prosser (1993), Gawthorpe et al. (1994) and Ravnås and Steel (1998) and rift subsidence curve adapted from Gupta et al., (1998).

The final events of rifting are characterised by a decrease in the rate of tectonic subsidence and can be considered as thermal relaxation and are commonly associated with sedimentary infill of the accommodation space (e.g. Gawthorpe et al., 1994; Gupta et al., 1998).

Seismic reflection data show that late rift structures are characterized by gently diverging to sub-parallel reflectors that at its base, showing downlap reflector patterns at the centre of sub-basins, and strong apparent onlaps against fault and updip reflection terminations on the hangingwall (Prosser, 1993). The late rift stage on seismic data is also characterized by mainly high amplitude parallel and continuous seismic reflectors indicating cessation of

tectonic subsidence (Prosser, 1993) (Figure 2.7). Sediments associated with this stage are accumulated within progradational and/or aggradational sequences formed in response to relative changes in sea level and sediment loading.

2.2.5 Thermal Consequences of Rifting

As a consequence of extension, crustal thinning and geothermal gradient increases in response to lithospheric stretching (McKenzie, 1978). These physical changes affect lithospheric strength in different ways. The lithosphere tends to strengthen, as a result of crustal thinning or necking caused by replacement of weak crustal material by strong mantle lithospher during upward movement and mass conservation. This upward movement result in increased heat flow within rift zones. Weakening or strengthening of the lithosphere formed by a given amount of stretching also depends on the strength and rheology of the lithosphere and the total amount of extension. The thermal state of the lithosphere is affected by weakening of the crust and by subsequent filling of the available accommodation space (Sandiford et al., 2003).
Moho heat flow result from the thermal properties of rift basin and the distribution of heat sources in the crust allowing long-term lithospheric weakening. Accommodation space and filling of the rift basin could be modified as a consequence of isostatic compensation which in turn will increase the long term response to rift basin formation. The increase in the average crustal thermal gradient induces lateral heat flow that necessarily heats the Moho along basin margins, especially in narrow rift basins.
Subsidence in rift basin can be reversed if thermal uplift increases the isostatic subsidence that caused by lithospheric extension, this lead to uplift and erosion of the sedimentary fill within the basin (e.g. Ziegler, 1990).

2.2.6 Implications for Petroleum Systems

Rift basins may consist of deeply buried sub-basins and minor uplifts. The sub-basins (depressions), may occupied by source rock sediments (e.g. hot shales, lacustrine sediments rich in organic matter), and other sort of petroleum system elements. It is also important to highlight that igneous rocks accompanying rifting may also be beneficial to petroleum

systems. For example, the thermal effects of igneous intrusions may in some cases be sufficient to place immature source rocks within the oil window (Holford et al., 2013). Within rift basins, petroleum systems are correlated with syn-rift and post-rift stages of basin evolution, which characterized by the presence of source, reservoir, and seal lithofacies when combined with structural and/or stratigraphic trap style, determine the hydrocarbon habitat.

The growth and interaction of intra-basinal normal faults in particular can also lead to progressive confinement of petroleum systems in extensional basins. The recent history of petroleum exploration has depended greatly on the re-examination of known hydrocarbon provinces in light of new technology, and forms of analysis. Improvements in quality and scope of relevant geoscientific data have led to the identification of specific areas as important targets for further drilling (Sheriff & Geldart 1995). The maturity, migration and trapping must commonly be analyzed as relative to the state of the knowledge existing at any specific time. This can be achieved in the case of the Ajdabiya Trough area, where there is a large fault system distributed along a wide area. The distribution of faults within a hydrocarbon province is a key aspect in controlling fluid flow (Shepherd, 2009).

Fault seal estimates can be made, through the analysis of syn-rift and post-rift sequences and sedimentary facies developed in footwall and hangingwall structures (Yielding et al., 1997). Fault sealing capacities and reservoir characterizations could be achieved using a proper 3D seismic interpretation and modelling.

In order to achieve better results, detailed studies including fault growth developments, segmentation and fault displacement are necessary to build fault sealing models. For instance seismic interpretation alone does not usually provide enough data to evaluate the sealing potential of faults.

Fault zones may have the opposite effect on fluid flow in a direction normal to their plane (Yielding et al., 1997). It is, in fact, possible that the crushed and recrystallized material of the fault zone forms a permeability barrier or a seal to the movement of the fluids across the fault plane. The distribution and connection of the fault segments and the in-situ effective stress determine how effective the faults are in sealing or channelling the fluids. Fault sealing has been invoked to explain the existence of compartments with different fluid pressures in hydrocarbon reservoirs. The processes generally believed to generate a fault seal are geometric juxtaposition of permeable units against impermeable units.

Within the Ajdabiya Trough, hydrocarbon can be trapped by a proper sealing fault system that could exist along an interpreted fault blocks splays on the northeast edge of the study area. This proposed sealing fault system appears to have formed as a result of possible upward movement of an underlying magma during rifting episodes which has a great influence on hydrocarbon maturation and migration.

Seismic cross-sections and isochron maps of the syn-rift succession demonstrate that sedimentation was probably concentrated initially in the NW-SE trending grabens and halfgrabens. The fault system characterized with possible relay ramps and hanging-wall rollover structures of a large (throw 400ms) growth faults and are compartmentalized into a series of narrow blocks by smaller, predominantly antithetic and synthetic, growth faults. The growth histories of the master faults have been determined from detailed seismic structural mapping and analysis of fault displacement distributions. The growth of the identified faults is characterized by near instantaneous propagation followed by fault segment interaction and occasional fault linkage which may have a great influence on hydrocarbon potential in the area.

2.3 Tectonostratigraphic Framework of the Sirt Basin and Ajdabiya Trough

2.3.1 Tectonic and Stratigraphic Evolution

There are four main stages that shaped the tectonic evolution of the Sirt Basin, these are.

Basement Assembly (Neoproterozoic Cambrian 830 - 1520 Ma): The evolution of the Pan African basement terrains (700-600 Ma) during the assembly of Gondwana supercontinent (e.g. Craig et al., 2008) (Figure 2.8)

Passive Margin: Cambrian to carboniferous stable phase culminating ultimately in collision of Gondwana and Laurentia during the Devonian (Caledonian) and later during the Late Carboniferous (Hercynian Orogeny) (e.g. Jurdy et al., 1995; Bumby and Guiraud, 2005)

Break up: Progressive Permian - Mid Cretaceous rifting and breakup of Gondwana

Collision with Eurasia: Late Cretaceous - Tertiary and recent collision of Africa with Eurasia.

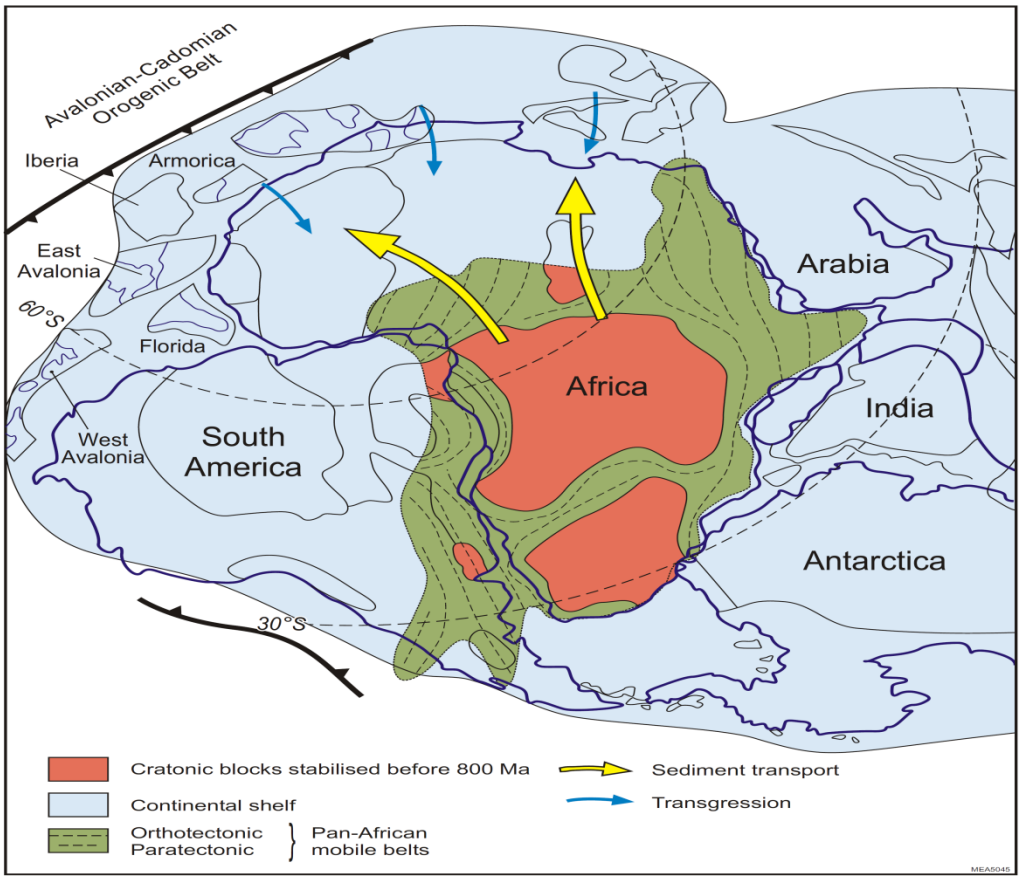

Figure 2.8: Generalised palaeogeography of Gondwana during the Early Palaeozoic from Craig et al., (2008).

In the Mid-Cretaceous the Tethys domain which extended from North Libya to Southern Aegan Sea (e.g. Guiraud & Bosworth, 1999; Stampfli & Borel, 2000) began to close due to change of motion of the African plate with respect to Europe**.** This movement presumably attributed to the operation of variable sub-plates within the African domain (Fairhead et al., 2013). It is postulated that a line of junction between two sub-plates extends from the Benue Trough in Nigeria to the Tibisti Massif in Libya (Hallett, 2002). Paleogeographic reconstructions of the Tethys domain show that the closure of the Tethyan oceanic space is interpreted as resulting from left-lateral transcurrent movements of the East Saharan domain in Barremian times (Dercourt et al., 1986; Janssen et al., 1995).

The rift system existed in the Sirt Basin is part of the East Tethyan rift system which propagated into the eastern Mediterranean and the Middle East (Coward and Ries, 2003).

The northward drift of Africa relative to Europe, emphasized by the opening of the South and Equatorial Atlantic Oceans (Craig et al., 2008), led to (1) the collision, and subsequent suture, of different cratonic blocks across the remnants of the Tethys ocean (Janssen et al., 1995).

Geophysical and field data indicate that the late Mesozoic rifting phase of the North Africa basement was accompanied by a series of aborted rifts south of the actual continental margin (Guiraud & Bosworth, 1999; Tawadros 2001; Craig et al., 2008). A late Cretaceous regional high subsidence rate, possibly associated with collapse in the Sirt Basin (Rusk 2001; Carr 2003), is effectively recognized in the Atlas mountains (Zouaghi et al., 2005) and in Libya's Kufrah, Murzuq, Ghadamis and Tripolitania basins (Figure 2.9). Changes in the intraplate stress field occurred during the Aptian time lead to changes in extension direction from N160–E to N–S, and NE–SW (Guiraud et al., 2005). Subsidence along NW-SE trending basement blocks occurred in Sirt Basin (Guiraud and Maurin, 1992; Hallett, 2002) with deposition of thick series of continental sandstone and shale (Bosworth, 1992).

During the Late Cretaceous rifting in the Sirt Basin was accompanied with deepening to the north of early formed Triassic basin associated with the opening of the eastern Mediterranean and with regional extension along NW-SE trending faults (Figures 2.10 & 2.11).

Along the North African Margin, several basins were active during Permo-Triassic, with localized renewed rifting in the Jurassic and/or Early Cretaceous.

Among these basins is the Palmyra Basin of Syria (Lovelock 1984), and the Western Desert Basin of Egypt, and the eastern part of the Sirt Basin (Thusu & Mansouri 1995). The larger structural elements exhibit a strong NNW-SSE to NW-SE structural grain, changing southward to ENE and WNW and form the tips of a major rift basin opened in the central Mediterranean.

The faults formed within the rift show both lateral and normal components and cross-cut Cretaceous fold axial structures within basin fill mainly dominated by basal clastics passing up into basinal shales and muds with transgressive shallow-water carbonates formed on structural highs. During early Cenozoic a period of rapid regional subsidence prevailed, where a north-facing carbonate platform developed over buried Cretaceous sequence. Initial Cretaceous subsidence in the Sirt Basin occurred at the same time as mild inversion in

Cyrenaica and western Egypt that may have been formed by block rotations associated with changes in extension directions from NW-SE to NE-SW (El Arnauti et al., 2008; Capitanio et al., 2009).

age	direction	geodynamic process	Plate tectonic relation
Late Carboniferous (Hercynian) (295-310 Ma)	ESE-WNW compression	uplift and postorogenic collapse	Separation of Laurasia from North Africa
Triassic - Early Jurassic (195-260 Ma)	SSE-NNW extension	central Atlantic rifting	Gondwana Breakup Seafloor Spreading in the Sentral Atlantic
M – L Jurassic (149 – 195 Ma)	SE-NW extension	Jurassic Rifting	Separation of North Africa and Europe - along major sinistral transcurrent shear zone
Early Cretaceous (140-149 Ma)	N-S extension	Cimmerian	Separation of Apulian Plate from North - - Africa, collapse of Sirt Arch
Early Cretaceous (115-140 Ma)	N-S extension	Early Cretaceous rifting	divergence
Early Cretaceous (97-115 Ma)	N-S extension	South Atlantic rifting	divergence
Late Cretaceous (63-97 Ma)	NW-SE to NE-SW extension	Gondwana Arc Collusion	Strong Rotation of African and Arabian - Plates in an anticlockwise direction.
Paleocene - Eocene (49-63 Ma)	SSE-NNW compression	Syrian Arc Inversion II	Slowing in the rate of convergence between Africa and Europe
M-L Eocene (49-34 Ma)	ESE-WNW compression	Alpine compression	Gondwana/Arc collision
Oligocene- M Miocene (49-34 Ma)	NE-SW extension	Gulf of Suez, rifting	Gondwana/Arc collision
Oligocene- M Miocene (23-15 Ma)	NE-SW extension	Red Sea, rifting	Collision of Africa with Eurasia along the northern margin of the Arabian Plate
M - L Miocene (15-6 Ma)	NE-SW compression	Red Sea, rifting	Collision with Eurasia along the - northern margin of the Arabian Plate
Miocene (6-0 Ma)	NE-SW compression	Red Sea, rifting	

Tabe 2.1: Deformation events in Sirt Basin correlated with plate tectonic events

Figure 2.12 summarizes the timing of tectonic events in the Sirt Basin in comparison with changes in relative motion vectors between the African and European plates documented by Dewey et al. (1973), Savostin et al. (1986), and Ziegler (1988). Paleo-stress data derived from Schafer et al. (1981) are also included. Burke and Dewey (1974) suggested that collapse of the Sirt Arch started during the Early Cretaceous related to dextral shear along the Gibraltar-Maghrebian shear zone forming a diffuse trans-tensional plate boundary between Africa and

the Italo-Dinaride block. Guiraud and Maurin (1991) suggest a Neocomian-Barremian onset of rifting resulting in the development of dominantly E-W-trending half-grabens associated with N140"E-trending faults for the Southern Sirt Basin. Bayoumi and Lofty (1989) found similar structures in the Abu Gharadig Basin located in the Western desert of Egypt (Figure 2.10). This Early Cretaceous rifting event is related to progressive northward propagation of crustal separation between Africa and South America and to changes in rates of seafloor spreading in the Central Atlantic (Figure 2.13) (Guiraud et al., 1992). A second stage of rifting, initiated at the end of the Early Aptian, in response to a NE-SW crustal extension (Guiraud et al., 1992).

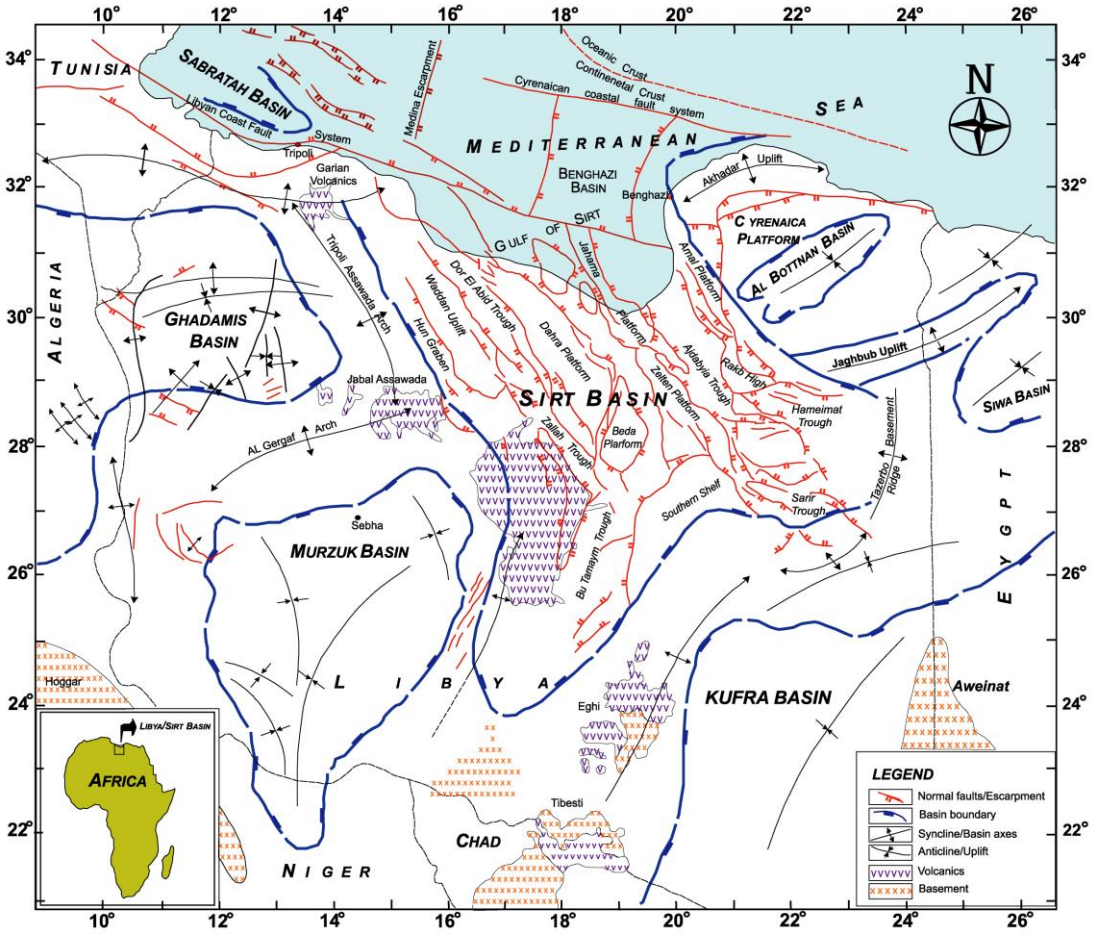

Figure 2.9: Tectonic map of Libya showing sedimentary basins and major tectonic elements, Ajdabiya Trough is almost located at the eastern periphery of the Sirt Basin near to Cyrenaica Platform. (Re-drawn from Taleb and Mesughi 1990).

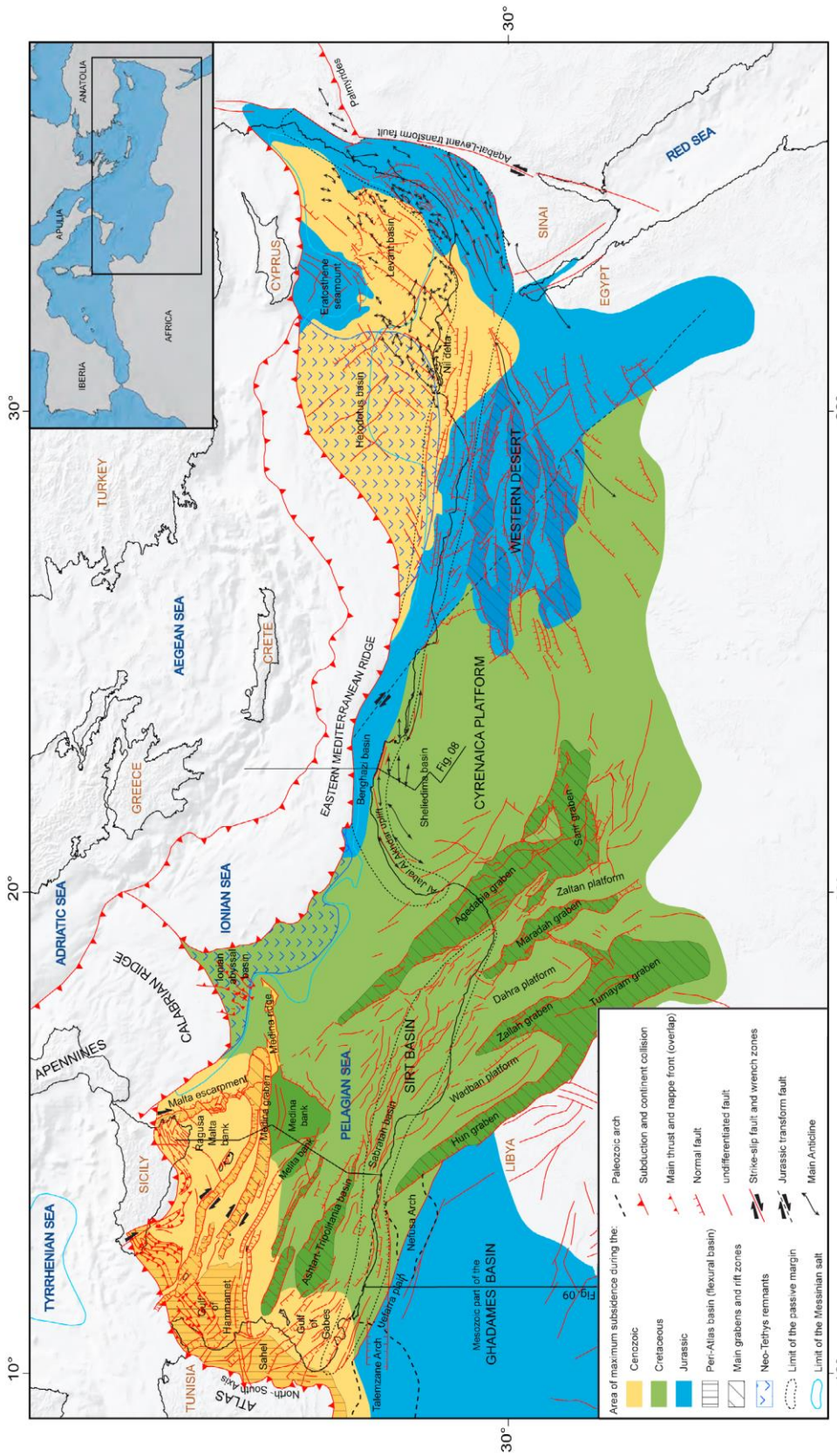

Figure 2.10: Structural map of the eastern and central Mediterranean, modified from Jongsma et al. (1985, 1987), Chamot- Rooke et al. (2005), Rusk (2001),Casero and Roure (1994), Finetti (1982), and Burollet (1991). Map obtained from Frizon de Lamotte et al., (2011).

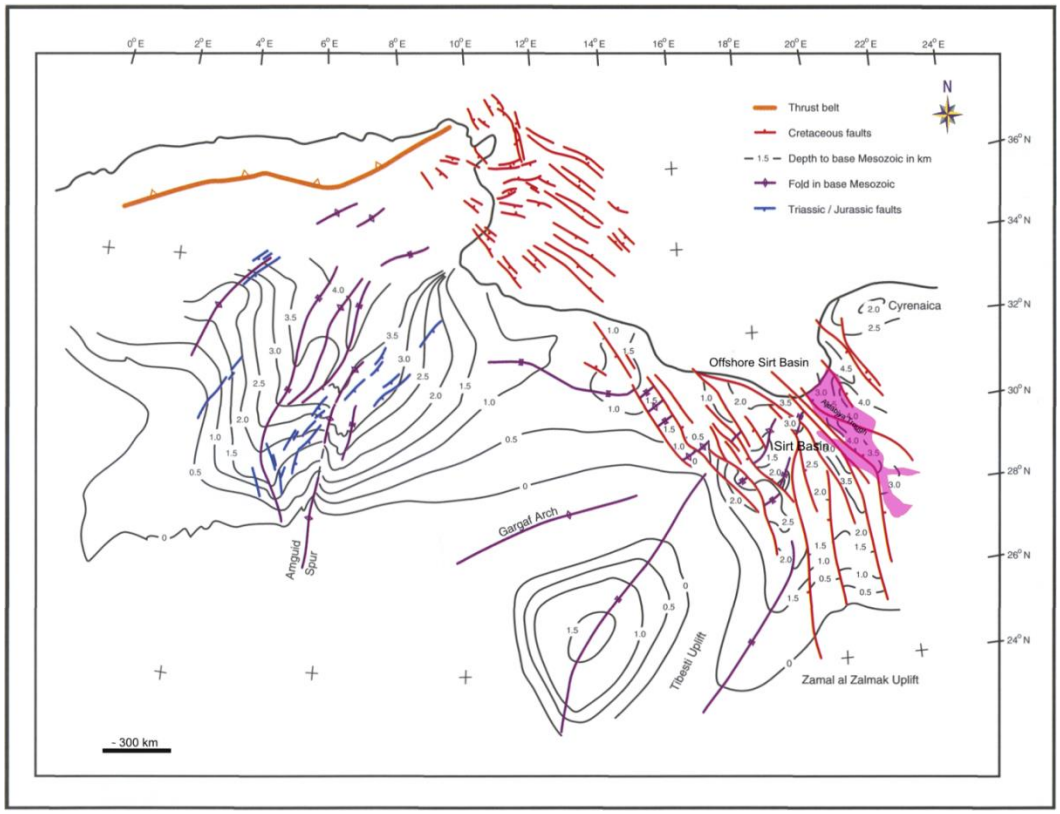

Figure 2.11: Map showing depth to the base Mesozoic in kelometers. Triassic faults in Algeria and Cretaceous Faults in Sirt and Pelagian basins (Tripolitania) – Libya. Map modefied from Coward and Ries, (2003).

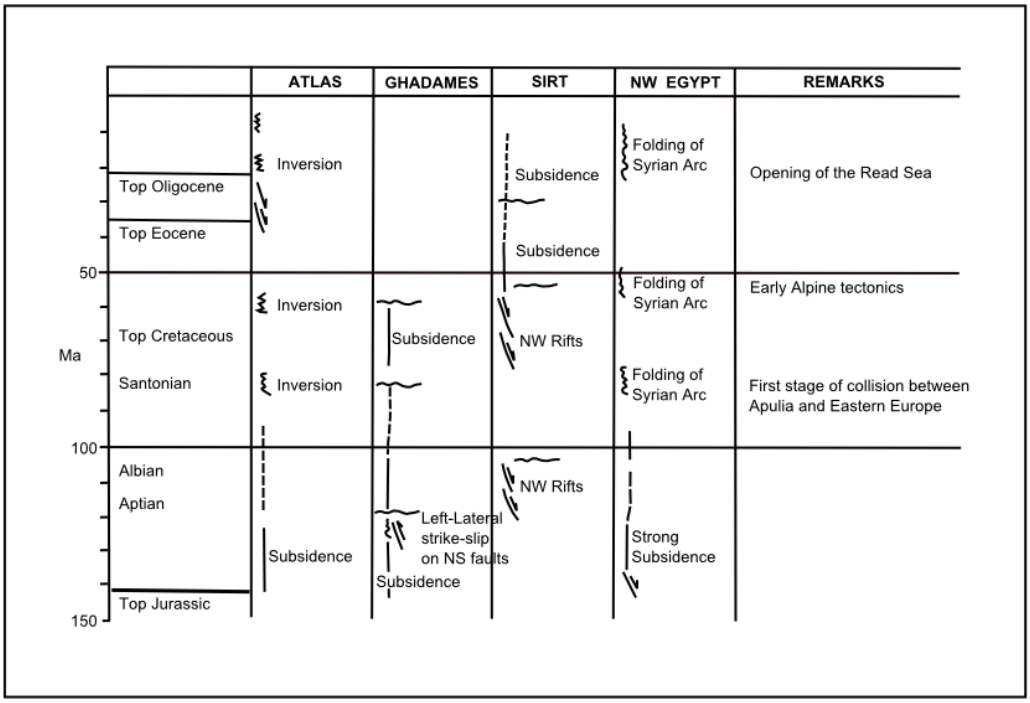

Figure 2.12: Chart showing the timing of uplift and subsidence across North Africa. Re-drawn from Coward and Ries, (2003).

Differential rates of sea-floor spreading in the Central and South Atlantic and contemporaneous rapid opening of the Equatorial Atlantic Ocean provide an explanation for the rejuvenation of crustal zones of weakness in Africa (Fairhead and Binks, 1991: Guiraud et al., 1992). According to the present analysis, active synrift subsidence in the northern part of the Sirt Basin started during the Late Campanian (73-74 Ma) and continued until the Late Palaeocene (Gumati and Nairn, 1991). Savostin et al., (1986) and Le Pichon et al., (1982) documented a change in the relative motion vector of the African and European plates from Ieft-lateral movement to convergence in the Campanian time (80 Ma) which coincides with the initiation of rifting (Figure 2.13) inferred from the subsidence analysis.

The Sirt Basin is considered to be an enigmatic feature in the complex Mesozoic-Cenozoic rearrangement of the Mediterranean tectonics, the rifting was significant in the eastern part of the basin (Ajdabiya Trough) and the area has been considered to be a part of the Mediterranean Tethys rifted margin (El-Arnauti et al., 2008).

During the Cretaceous-Tertiary boundary times, the Pre-Upper Cretaceous basement reached a maximum subsidence of 1200m in the southern part of the Ajdabiya Trough and about 200m in the Amal Platform (Gumati, 1985). The northern part of the Ajdabiya Trough showed much lower subsidence of less than 200m, which might suggest a present day thickness of the Maastrichtian, sequence to be around 100m. There are no wells that reach the Cretaceous in the extreme northern part of the Ajdabiya Trough but wells around it and to its south show the Cretaceous to be less than 100m in thickness.

During the Late Eocene, the Ajdabiya Trough reached a value of subsidence of 1800m and the present day structural configuration was almost reached during the close of the Eocene.

As suggested by several researchers and authors, it is a matter of debate the timing of rifting episodes in the area. Busrewil et al., 2008 suggested that rifting in the basin commenced in Triassic, intensified in the Jurassic – Lower Cretaceous and terminated in Upper Cretaceous. Overburden was largely deposited during the post-rift sedimentation stage (Oligocene and younger). Pre-rift and early syn-rift deposition was largely clastic whereas later syn-rift deposition was dominated by carbonate deposition, (Hallett and El Ghoul, 1996). Eighty percent of the drilling program in the basin has been on platform horst areas at depths less than 3,000 m. The Precambrian basement depth approaches 5000 m within the southern part

of the Ajdabiya Trough and is generally around 2000 m in the platform areas such as Amal Platform. The study area has experienced large scale normal faulting. These faults were considered to be mostly planar, basement – involved fault segments linked together by transfer zones. The nature of the displacement transfer varies with depth within these zones. The small scale structural details within the zones are obscure but some characteristics can be inferred by comparison with structural models from other settings, (Skuce, 1994).

2.3.2 Mesozoic Rifting in Sirt Basin

The time of Mesozoic rifting in Sirt Basin remains a matter of debate. Guiraud and Bosworth, (1999) suggested that rifting along the North African Margin which includes the Sirt Basin, has been created during Mesozoic time (Figure 2.14) and has led to crustal separation between southern Eurasia and Africa and east Mediterranean basins. Crustal extension associated with block faulting occurred in the Sirt Basin of Libya during the mid - and Late Cretaceous (Coward and Ries 2003). Dewey (1973) and Van Houten (1983) suggested that the Sirt rift took place at a time in the early Cretaceous when a significant shift in the absolute motion of the African Plate, from westwards to northwards motion, coincided with region passing over a fixed mantle hotspot. Burke and Dewey (1974) attributed this to widespread Early Cretaceous extension that they believed developed in a broad zone of strain between two African plates that were at rest relative to underlying mantle plumes (see also Burke and Wilson, 1972).

Basement structures in Libya is considered to be an inherited Pan-African and Palaeozoic structures trending NE-SW to ENE-WSW and have gentle to moderate dips to the southeast. However block faulting occurred along NNW-SSE to NW-SE zone of weakness cross-cutting earlier Palaeozoic structures at a high angle but possibly parallel to some of basement shear zones (Anketell, 1996; Coward and Ries, 2003).

The African plate has traditionally been considered as a rigid plate in plate reconstruction models and as such it was subject to possible intra-plate deformation (Fairhead et al., 2013).

The Early Cretaceous rifting episodes in West and Central Africa, located within Pan-African zones of lithospheric weakness (Daly et al., 1989), are related to the opening of the South and Equatorial Atlantic Ocean (Guiraud et al., 1992).

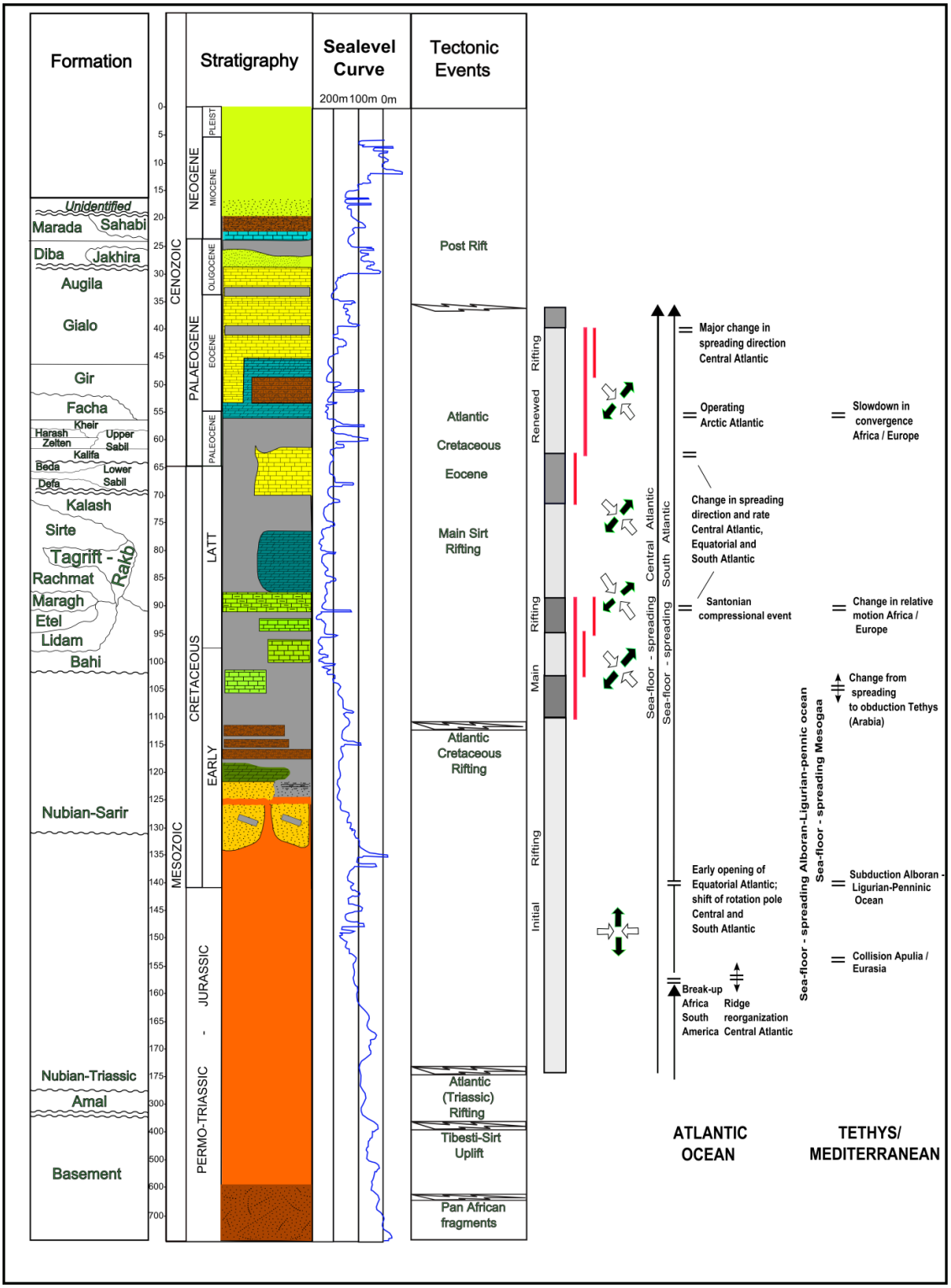

Figure 2.13: Tectonostratigraphic chart of the Ajdabiya correlated to major changes in the opening and closure histories of the Atlantic and the Tethys or Mediterranean areas. Paleostress directions are indicated by the orientation of maximum horizontal (compressive) stress (white) and minimum horizontal (extensional) stress (black) directions. The approximate stress directions are inferred from Guiraud et al., (2001), Cavazza et al., (2004), and Cloetingh et al., (2005).

The Cretaceous rift systems of West and Central Africa extend eastwards through southern Chad into South Sudan and Kenya (Fairhead et al., 2013; Binks & Fairhead, 1992) and it has been proposed that this rifting extended northwards to form the Cretaceous Sirt Basin of the eastern Mediterranean. It is hypothesised that rifting in the present day Sirt Basin is commenced during the Late Jurassic to Early Cretaceous time and became more active during Aptian – Albian time (Gumati & Nairn, 1991) and mainly characterised by E-W trending graben developments followed by a NW-SE trending extension system along the basin shoulders during the Cenomanian which then migrated towards the middle during the Maastrichtian. It is assumed also that the rifting in the Sirt Basin is probably linked to that of the Cretaceous West and Central African Rift System (WCARS) which formed the Benue Trough, Chad, Central African Shear Zone (CASZ) (e.g. Moulin et al., 2010). A latter trend was probably initiated during the Late Cretaceous and Early Paleocene with tectonic activity occurred in the Sirt Basin (van der Meer and and Cloetingh, 1996) accompanied by left-lateral strike-slip, as documented by onshore and offshore studies (Anketell, 1996).

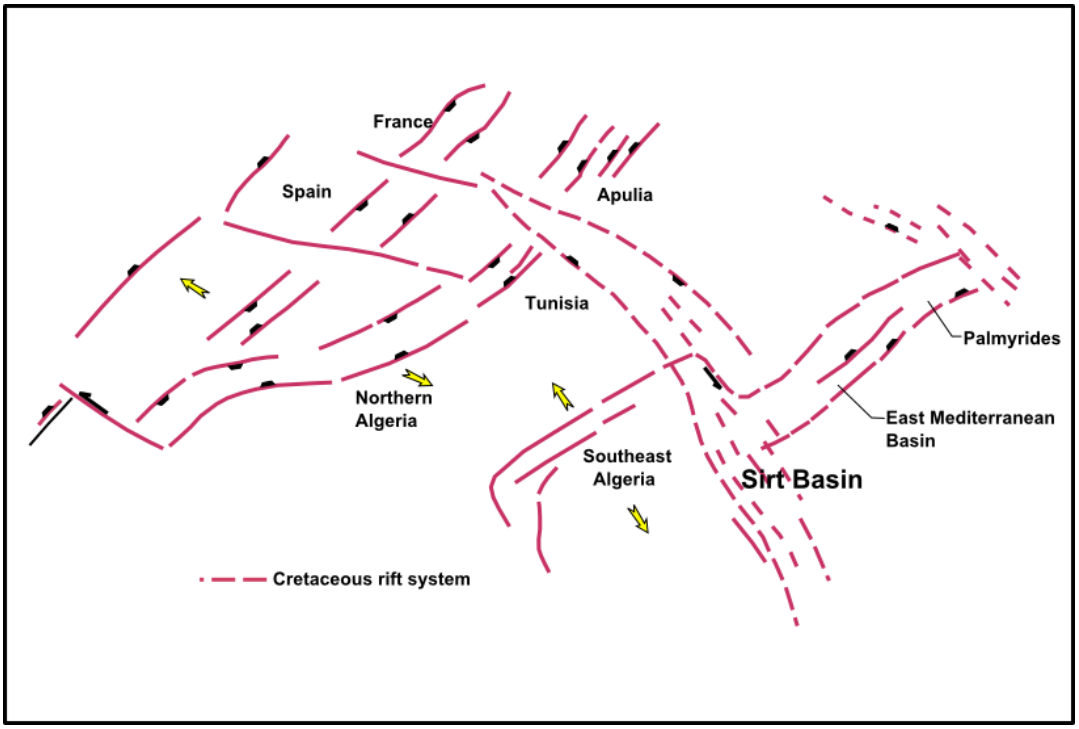

Figure 2.14: Sketch-map showing the pattern of Mesozoic rift basins in North Africa, the Mediterranean and the western part of the Middle East, re drawn from Coward and Ries, (2003).

During the first steps of the basin development, it formed an element of the NW-SE trending intercontinental basins which developed in the Nubian block (Figure 2.15). However, its main phase of subsidence began by the Late Cretaceous at the onset of Africa-Eurasia convergence. This has been generated by differential movements of the Africa Plate as a direct consequence of equatorial and southern Atlantic opening (Fairhead et al., 2013; Moulin et al., 2010; Guiraud and Maurin, 1992). Capitanio et al., (2009) propose an attractive hypothesis in which the pull exerted by the Neo-Tethys subducting slab below the Mediterranean Ridge (Figure 2.10), plays a major role in the rift development.

The rifting in the east-west trending troughs in the Sirt Basin such as the Sarir and Hameimat troughs is presumably related to the opening of the Central Atlantic and may also have been influenced by the left lateral opening of the Tethys Ocean (Abadi et al., 2008).

Convergence between Africa and Europe slowed down during interval between Cretaceous and Tertiary (Dewey et al., 1989). Collisional between Europe and Africa marked by a northwest – southeast to north – south oriented stress field at the early Eocene (Cloetingh et al., 2005). New phase of rifting resulted in a rapid subsidence particularly in the main troughs (Abadi et al., 2008). These have been formed as a result of Dextral Strike – Slip movement along plate margins (Anketell, 1996, Guiraud et al., 2001).

2.3.2.1 Syn-rift Phase Initiation and Rift Climax

The break-up of Pangaea involved the establishment of a spreading axis associated with igneous activity in northern Libya. These events correspond to the initial rifting phase in the Mediterranean region. Extensional fault system has been developed during Triassic time both offshore and onshore Libya, and several unconformities are present within the Triassic succession. Evidence from eastern Libya shows the presence of Triassic sediments which may represent the earliest deposits in incipient synrift grabens (Wilson and Guiraud, 1998).

In recent years major new information has been obtained from wells in the north eastern Sirt Basin which suggests that the rifting phase in the Sirt Basin began as early as the Triassic (Thusu, 1996). Samples from Amal Formation of pre-Upper Cretaceous age have been studied from well Al-96 (Jakharrah field), yielded a rich palynomorph assemblage of Middle Triassic age. Thusu 1996 suggested that the sequence was deposited in an incipient rift, marking the beginning of the synrift phase in the Sirt Basin.

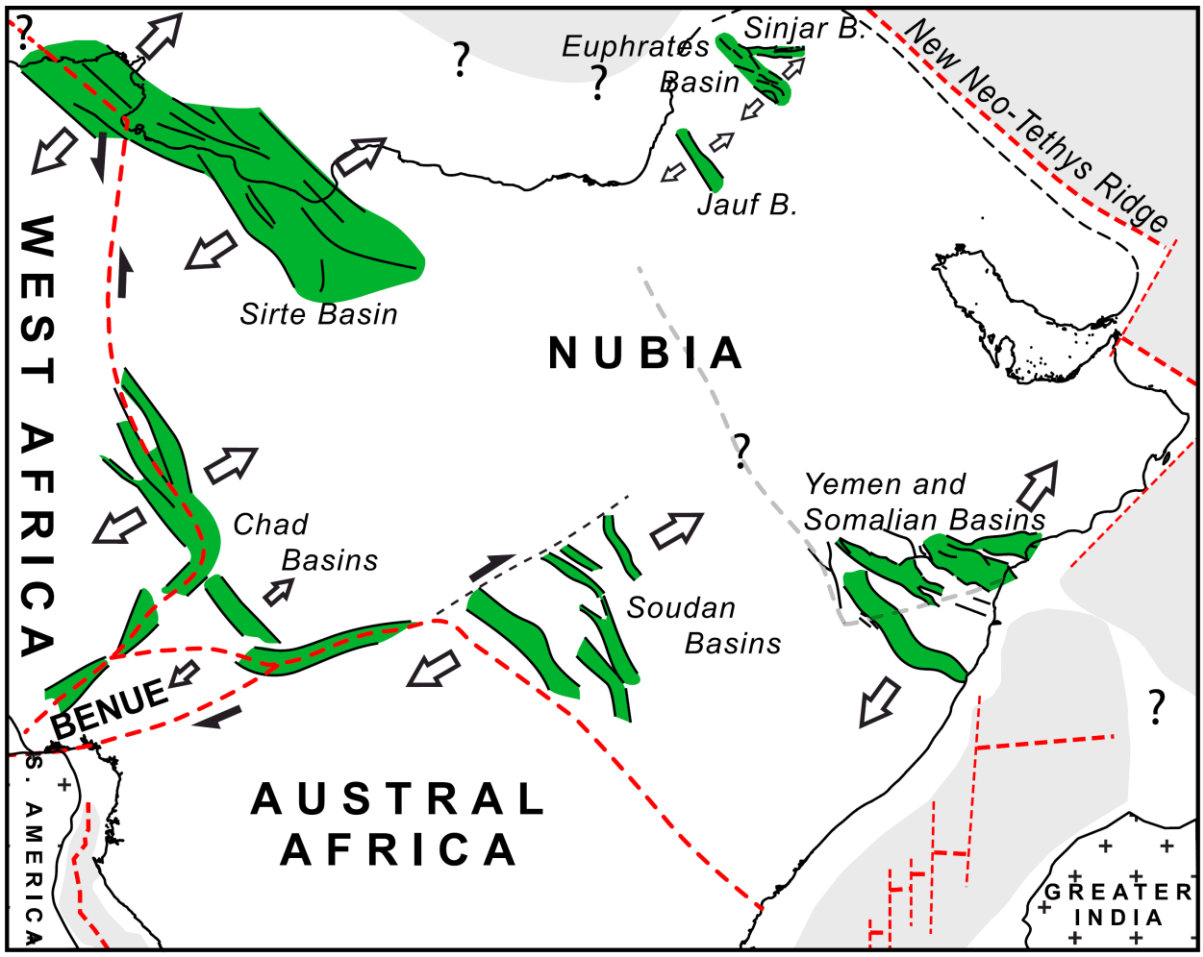

Figure 2.15: Schematic map of Nubia block showing the development of a wide rift system at the end of Early Cretaceous times. Map obtained from Frizon de Lamotte et al., (2011).

A prominent sedimentary and erosional break, locally marked by the Hercynian unconformity, supports the occurrence of important Late Paleozoic (Cambro-Ordovician) uplift and erosion (Figure 2.16). During the Triassic, sediments were initially deposited in topographic lows, and progressively on lapped the Hercynian Unconformity as sea level rose (Carr, 2003). The reactivation of previous Hercynian faults has been considered to be responsible for the location of the Triassic basin, under a NW -SE tensional field.

Evidence from the eastern Sirt Embayment shows the presence of Triassic and Jurassic rocks forming the oldest part of the syn-rift sequence, and the same situation may be present in other parts of the Ajdabiya Trough. The main syn-rift deposition occurred in the early

Cretaceous when the pre-Upper Cretaceous, Nubian (Sarir) Sandstone accumulated in rift troughs and topographic lows on the irregular pre-Cretaceous surface. The Nubian Sands are pass into a quartzitic facies in the northern Ajdabiya Trough.

2.3.2.2 Post-rift Phase Thermal Sag

Post-rift phase has established in the Sirt Basin with the closing of the Tethys Ocean during the Early to Middle Mesozoic time and accompanied by compressive tectonism (Şengör, 1979). By the Middle Albian the extensional deformation had decreased and declining heat flow lead to the beginning of a post-rift phase controlled by thermal subsidence.

The post-rift phase in the Sirt Basin is commenced during the Late Cretaceous time and characterized by graben fill system formed by marginal sagging and thermal subsidence (Gras and Thusu, 1998; Gumati and Nairn, 1991). It's underlying by Paleozoic pre-rift and Triassic to Early Cretaceous syn-rift phases.

After cessation of rifting by the Late Cretaceous time, the Ajdabiya Trough area has experienced a sever wide basin, post-rift subsidence during the Cenozoic time giving rise to accumulation of more than 4 km of sediments comprises Upper Cretaceous to Late Miocene rocks in its local depocentre. Thick evaporites were deposited during the Turonian time in the southern Ajdabiya Trough indicating period of tectonic quiescent. A thick succession of mudstones and subordinate limestones were deposited during the Cenozoic (e.g. Gir Formation) (Abugares, 1996; Baird et al., 1996), but the dominant deformation style was still normal faulting but less pervasive than during the synrift phase.

2.4 Geodynamic Setting

2.4.1 Tectonic Setting and Igneous Activity

The volcanism in the North African Margin and central Mediterranean area has been investigated by many authors (e.g. Zarudski, 1972; Di Paola, 1973; Finetti, 1982; Jongsma et al., 1985; Guiraud et al., 2005; Craig et al., 2008). Dercourt et al., 1986; Lustrino, 2000 attributed it to subduction related magmatism during the closing of the Tethys Ocean and the interaction between the Eurasian, African plates from 120 Ma to about 30 Ma.

In Sirt Basin, volcanic activity appears in frequent periods from Triassic to Quaternary (Guiraud et al., 2005; Craig et al., 2008; Busrewil et al., 2008).

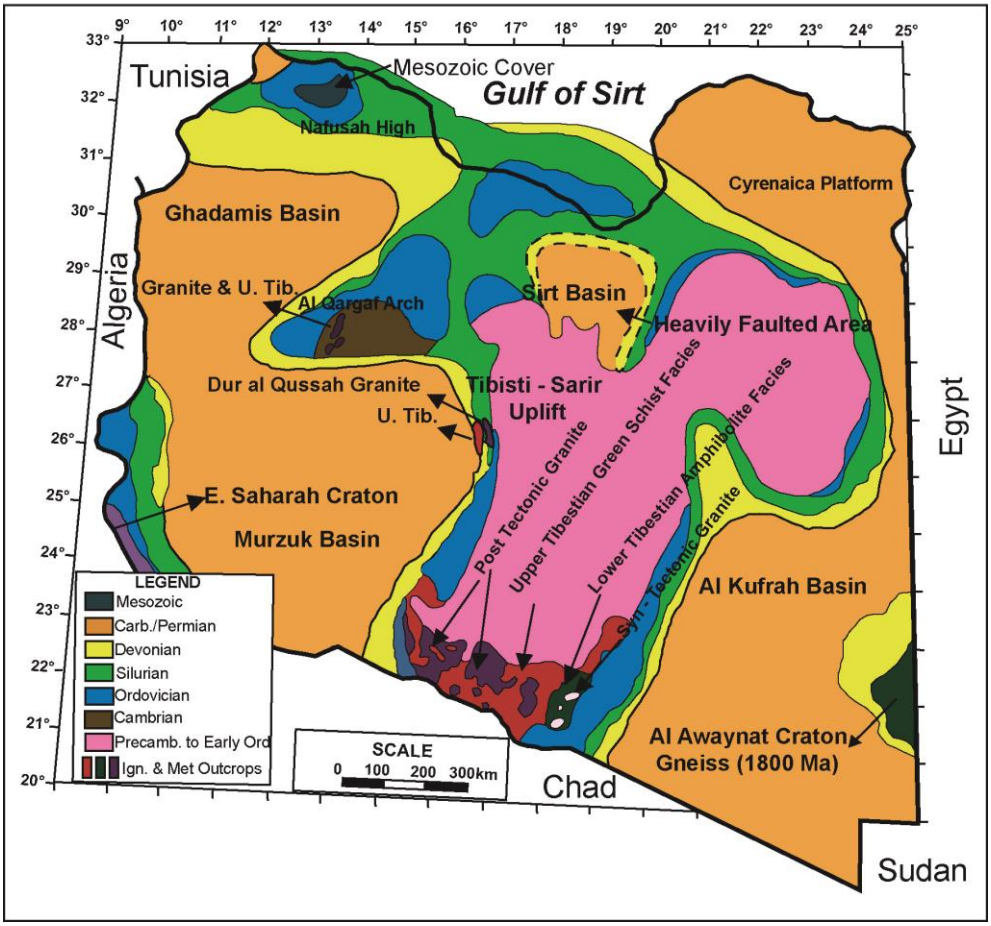

Figure 2.16: Regional subcrop map (Pre-Mesozoic), showing the regional uplift and erosion of the Sirt area during the Late Palaeozoic-Early Mesozoic. Most of the Palaeozoic sediments have been eroded and the Sirt area remained a high until the Late Mesozoic, at which time movement and deformation took place. (After Gumati and Nairn, 1991) The map also shows the age of the formations subcropping the Mesozoic unconformity. It represents a view of the deformed post-Hercynian surface, prior to the deposition of Mesozoic sediments. The deeply eroded Tibisti-Sirt Arch dominates the map, and other important uplifts are evident at A1 Awaynat, Nafusah, Al Qarqaf, and Tihemboka Highs. The data has mostly been obtained from oil wells. Small inliers on the Sirt Arch have not been shown. The extent of the Permian subcrops in Jabal Akhdar and in the Jifarah Trough is uncertain.

Major structures within the Ajdabiya Trough province is clearly elongated NW-SE and are probably associated with very active early volcanic activity, often associated with more or less symmetrical doming of the rift zone in the area (e.g. Klitzsch 1966, 1968; Woller & Fediuk, 1980; Busrewil & Wadsworth 1980a; Busrewil & Esson 1991; Busrewil & Oun 1991; Busrewil et al., 1996; Klitzsch & Ziegert 2000; Peregi et al., 2003). High volcanic activities are characteristics of Wrench-induced pull-apart basins and oblique-slip rift zones (e.g. Triassic grabens of North Africa: Hay et al., 1982). As a consequence of that, a major wrench

faults transect the entire lithosphere, and hence magma migrate to the surface (Wilson and Guiraud, 1992).

During the Late Jurassic rifting and subsidence occurred in the SE of Sirt Basin, while, during the Jurassic-Cretaceous transition, hiatuses and unconformities are observed within sedimentary sequences (Guiraud, 1998). At the Early Cretaceous (Neocomian-Earliest Aptian) a new phase of active rifting began along the northern African-Arabian margin within the intraplate domain, (Guiraud and Maurin, 1992). Active faulting also affected the Sirt Basin during this time (Wennekers et al., 1996; Hallett, 2002). Along the Libyan-Egyptian margin several E-W to ENE-WSW trending half grabens showed strong subsidence during Neocomian-Barremian time period, such as the Hameimat and Sarir troughs in the southeastern Sirt basin (Rossi et al., 1991 and Guiraud, 1998).The E-W trend pattern is probably controlled by the structural trend of the Pan-African and/or Late Proterozoic basement (Guiraud and Bosworth, 1999; Coward and Ries, 2003; Guiraud et al., 2005; Bumby and Guiraud, 2005). The most impressive African rift system which started in the early to late Cretaceous has its roots deep in the Pan African N-S and E-W trends (Maurin and Guirand, 1993; Selley 1997; Gras and Thusu 1998; Ziegler et al., 1999). The timing of the African rift system, with its NW-SE and E-W trending extension basins, is dated in Central Africa as late Early Cretaceous (Maurin and Guiraud, 1992), which is also supported by the distribution of the Aptian-Albian sediments of SE Sirt Basin.

Another rifting event started during the Early Campanian and continued to the Late Maastrichtian or the Palaeocene along the northern African-Arabian passive margin which was affected by tectonic instability, increasing from Middle Triassic times and highlighted by block tilting and local uplifts (Guiraud and Bosworth, 1997; Guiraud, 1998; Guiraud and Bosworth, 1999). Crustal thinning and spreading are probably initiated during this time (e.g. Robertson et al., 1996; Stampfli et al., 2001; Stampfli and Borel, 2002). Effusion of flow basalt accompanied rifting or faulting all along the Mediterranean margins, including the northeastern Sirt Basin (Wilson and Guiraud, 1998; Guiraud, 2001).

During Late Senonian rifting, the fault system trending NW-SE, was the result of the NE-SW extension of the African plate (Guiraud, 1998). This structural trend manifested by the Hun, Zellah, Marada, and Ajdabiya troughs of the Sirt Basin (Massa and Delort, 1984 and van der Meer and Cloetingh, 1993).

This structural system accompanied by the granite intrusions (152-127 Ma) and the extrusion of basic to inter-mediate volcanics (148-127 Ma) in trough and rift shoulders (Rossi et al., 1991; and Wilson and Guiraud, 1998). The occurrence of high level of magmatic activity in this basin is related to the opening of the East Mediterranean basin, (Guiraud, 1998). The close of the Oligocene was also the period when the NE moving African plate slowed down and whence the Sirt Basin area was on top of a mantle hotspot. The slowdown in movement of the plate allowed the subcrustal volcanics to pierce through to the surface. Highly alkaline basalt and phonolites were out to the W, SW and S of the Sirt Basin (Wilson and Guiraud, 1998).

2.4.2 The Tectonic Evolution of the Tethys Ocean

The term Tethys Ocean is formerly a marine realm lying along the Alpine-Himalayan-Indonesian Mountain ranges (Şengör, 1987). The reconstruction of the Permo-Triassic Pangea by Wilson (1963), found a triangular oceanic embayment gap opening eastward. This plate reconstruction model confirmed the existence and the singularity of the Tethys Ocean (Şengör, 1987). The Tethys defined, by Argand, 1924 as a narrow single mobile marine way bordered by two drifting continental masses of Laurasia and Gondwanaland (Şengör, 1987).

Şengör (1987) discussed the presence of wide and long orogenic belts between the Laurasian continental plates and microplates in the north and the Gondwanian continental plates and microplates in the south. African continental crust is displayed by the Pan-African Trans-Saharan belt, which crops out in the Hoggar Massif of southern Algeria (Figure 2.17). Boullier (1991) subdivided the belt into structural domains which included a 730 Ma pre-Pan-African suture zone in the east, and areas of Pan-African thrusting, crustal thickening and late Pan-African strike-slip ductile shear zones. These orogenic belts were the result of consumption and subduction of the oceanic plate of the Palaeo-Tethys (Şengör, 1987). Şengör (1984, and 1987) called these belts as the Tethyside Super Orogenic Complex (TSOC) El-Makhrouf (2004).

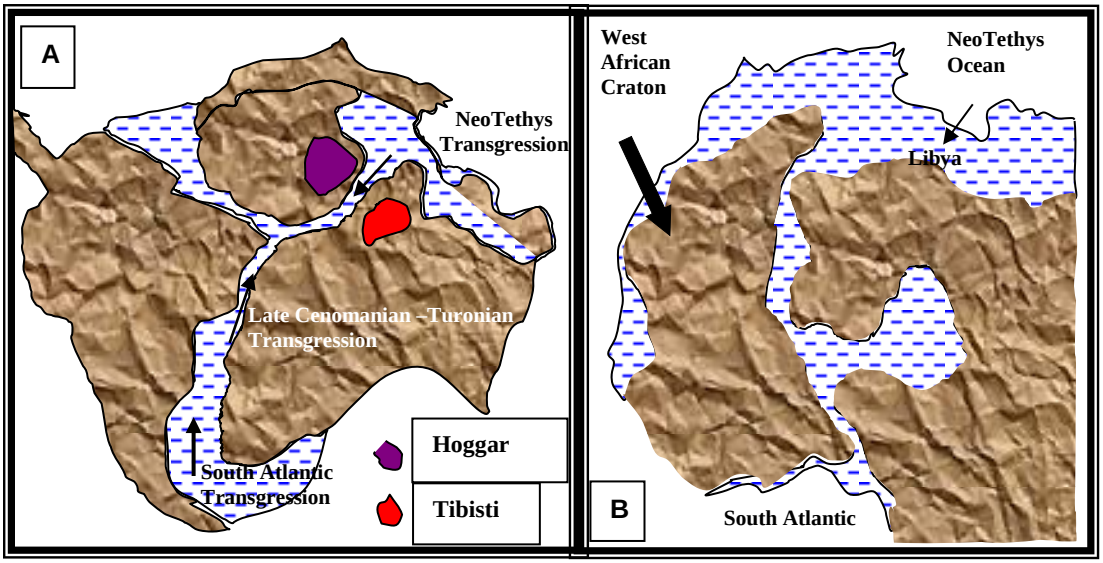

Figure 2.17: The Tethyside Super Orogenic Complex (TSOC) consists of two orogenic belts, which are independent and superimposed. The first and oldest orogenic belt was formed within the Late Carboniferous to Early Cretaceous time, as a result of the closure of the Palaeo-Tethys (Şengör, 1987). This orogenic belt called the Cimmerides, which discovered by Suess (1901). The youngest orogenic belt called the Alpides. It has been evolving since the Jurassic time.

2.4.3 Tectono-stratigraphic Evolution of the North African Platform

The timing of tectonic events affecting basins in North Africa corresponds closely with the major events in the fragmentation of Gondwanaland and Pangaea and the relative movements of the African, Laurentian and Eurasian plates (Jurdy et al., 1995; Anketell, 1996; Hallett, 2002; Bumby and Guiraud, 2005). The Mesozoic and Cenozoic evolution of the Tethys Oceans was also affected by the plate reorganizations caused by the breakup of Pangea. The opening of the Atlantic Ocean further complicated the geodynamic settings of the Laurasian and Gondwanan margins due to the changes in stress fields during different stages that characterized the breakup of Pangea. In particular, the movement and rotation of Africa, controlled by the opening of the central and southern Atlantic oceans, heavily controlled the relative motions among the numerous plates (which suffered alternatively both extensional and compressional tectonic regimes) in the Tethys. The present-day setting of south Mediterranean and Middle East regions is therefore the result of the global reorganization derived from the closure of the Tethys Ocean and the time-transgressive opening of the Atlantic Ocean.

The tectono-stratigraphic evolution of the North African Platform reflects an alternation of long periods of quiescence, subsidence, or rifting, separated by brief compressional events

(e.g. Guiraud et al., 2005). Prior to the opening of the NeoTethys Ocean, substantial crustal thinning took place in the Mediterranean sea area and E-W basins developed in the northernmost part of North Africa (Guiraud, 1998; Ziegler et al., 1999) suggested that Permo-Carboniferous arches were developed in NE-SW orientation that resulted in uplifting of the southern part of the Sirt basin while the Sirt basin itself underwent subsidence.

The African rift system is an example of classical rift developed within intracontinental terrains associated with normal thickness lithosphere characterized by magmatism, steeply dipping bounding faults, and long term extension (Leeder, 1995).

The Phanerozoic tectonic events of Libya are the product of the plate movements of Africa, influenced by inherited Late Precambrian Pan African trends (e.g. Guiraud, and Bosworth, 1999). Most of these tectonic events are associated with the more mobile Late Precambrian accretionary terranes. The Hercynian orogeny occurred during the Late Carboniferous to Early Permian (400-280Ma) producing a broad arching area within the Sirt Basin (e.g. Hallett & El Ghoul, 1996; Hallett, 2002) and caused variable metamorphic and reworking of older basement rocks. Late Hercynian (Late Palaeozoic) event also affected the Sirt Basin area during (Permo-Triassic) time and resulted in the exposure of the area of the Sirt basin for long periods of time (Figure 2.16). Mesozoic events affected the Sirt Basin can be related to the Syrian Arc system which resulted in the development of E-W arches in central Libya. These events were intensified during the Early Cretaceous, producing narrow active grabens and associated highs. They are related to the opening of the Mediterranean ocean during the Triassic and Jurassic and the development of the African Rift System associated with the opening of the South Atlantic during the Early Cretaceous. The most prominent event in Libya is the Sirt trans-extensional system associated with the African rift system and the associated sub-plate adjustments. This event resulted in the subsidence along three main directions, NNW, NNE and E, producing important depocentres.

During the Hercynian orogeny, the western part of Libya (Jabal Nafusa Highs) (Figure 2.16) also uplifted led to the erosion of the Paleozoic sequences and as deep as the Cambrian basement of the Gargaf Arch in the south east (Echikh, 1998) (Figures 2.9 & 2.16). The sedimentary infill of the Al Jefarah Basin of NW Libya (Figure 2.18), mostly of Carboniferous, Permian, and Triassic age (Swire and Gashgesh, 2004).

The integration of the paleogeographic time maps of Biju-Duval et al (1977) and the isopach maps of Wennekers et al. (1996) led to improved paleogeographic maps of the tectonic evolution of the Tethys Ocean (Figures 2.19, 2.20, 2.21, and 2.22) (El-Makhrouf, 2004).

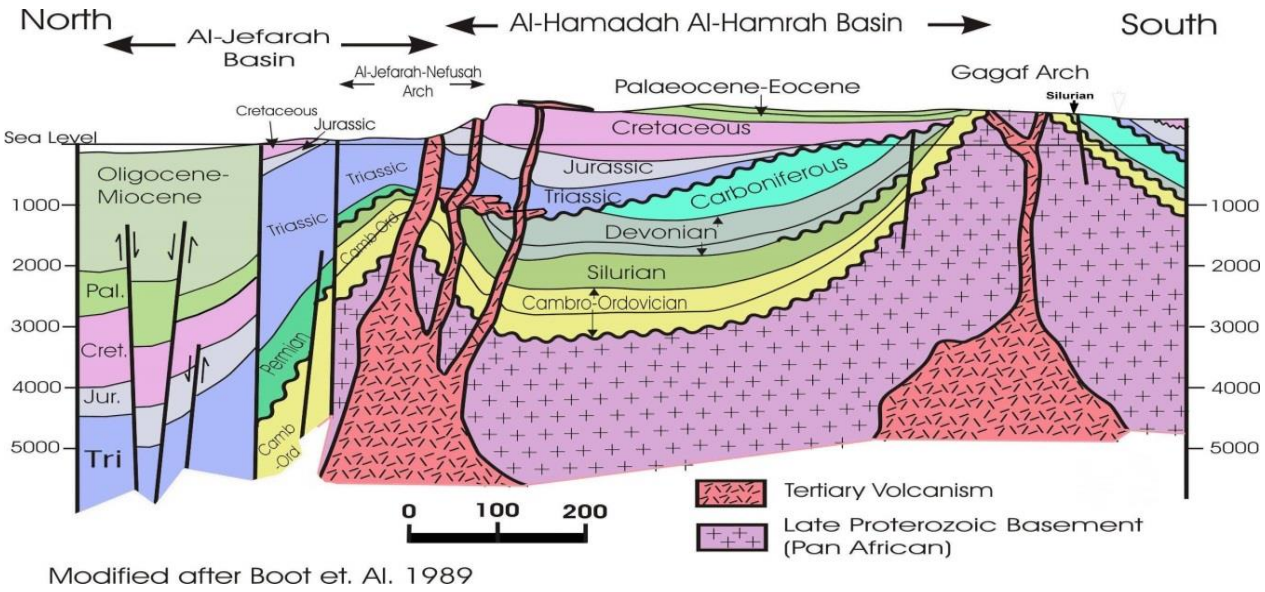

Figure 2.18: Generalized structural cross-section illustrate the tectonic evolution of the offshore Pelagian area, the Al Jefarah basin, Jabal Nafusa escarpment, and the Ghadamis (Al-Hamadah Al-Hamra) Basin obtained from El-Makhrouf 2004.

Plate I, (Figure 2.19) demonstrates that a broad and deep Tethys (Paleotethys) Ocean exists in the northeast of Europe. An evaporite facies belt extends from northwestern to the southwestern Europe and at the same time over North Africa, (El-Makhrouf, 2004). Carbonate platforms deposits were found all along the margins of the Tethys and along the areas of the future rifting (Biju-Duval et al., 1977). The Late Triassic is the period of extensional tectonics that took place. Because of this type of tectonics directly affected the sedimentation pattern and facies through subsidence during the Middle to Late Triassic (Swire and Gashgesh, 2004). **Plate II**, (Figure 2.20) show that the extensional tectonics is spread regionally during Liassic time (El-Makhrouf, 2004). During this time, Africa was moving left-laterally in relation to the opening of the central Atlantic with the deposition of evaporites and carbonate facies continued in the NW Libya and all over Tunisia (Biju-Duval et al., 1977) with deposition of continental sediments in the inner areas of Libya (Wennekers et al., 1996).

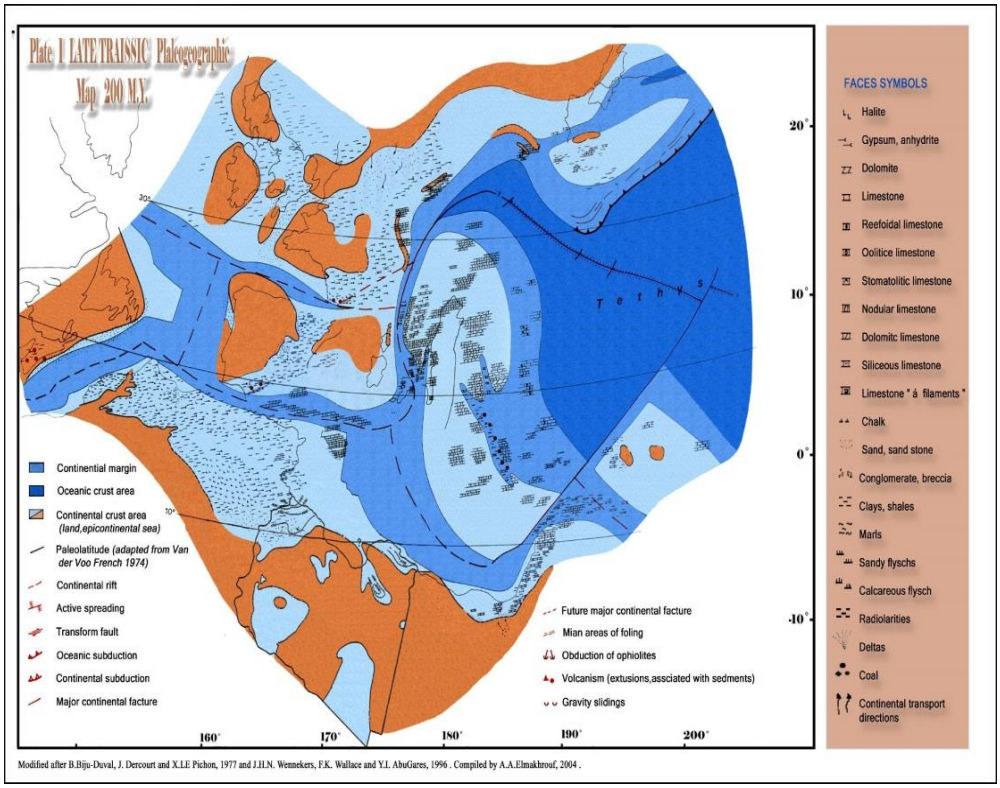

Figure 2.19: Late Triassic paleogeigraphic map 200 M.Y obtained from El-Makhrouf 2004.

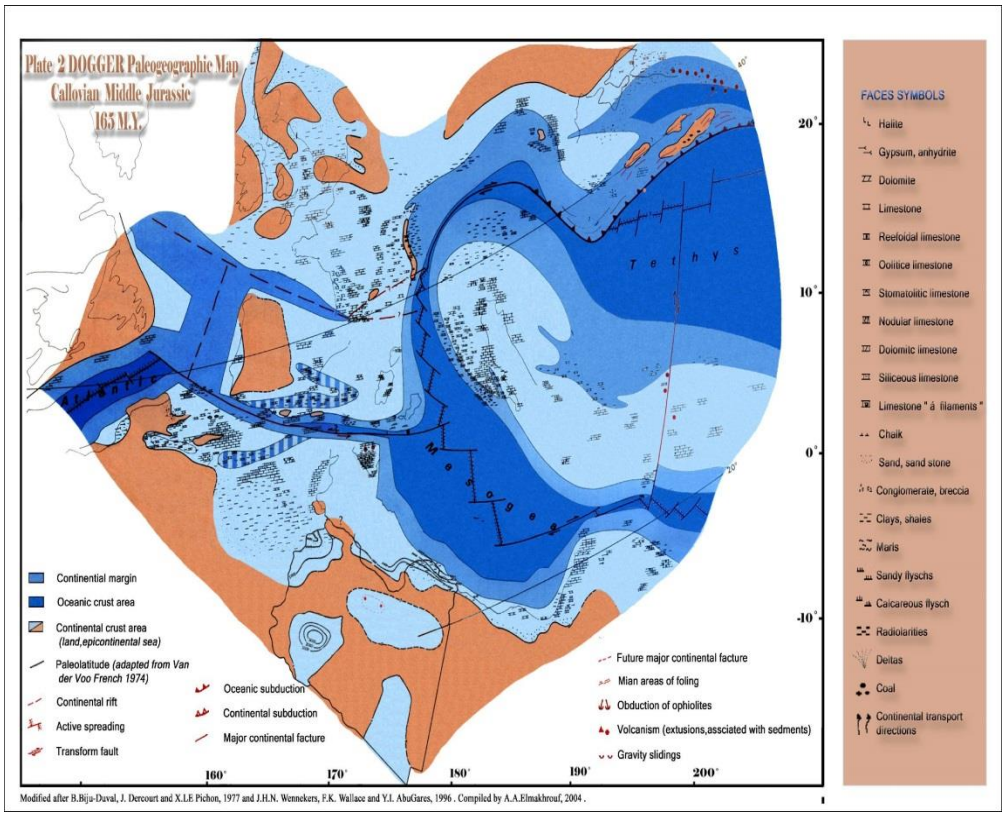

Figure 2.20: Paleogeographic map of Callovian Middle Jurassic 165 M.Y. obtained from El-Makhrouf 2004.

Plate III, (Figure 2.21) During Tithonian-Berriasian (Late Jurassic-Early Cretaceous), a major rifting event occurred with active subsidence, which led to the Neotethys transgression into the NW Libya, the Sirt Basin (eastern and western) with a high land in part of north western Libya (Al Jeffarah and Ghadamis (Hamada) basins).

Plate IV, (Figure 2.22) During Late Cretaceous (Campanian-Maestrichtian, 76-68 Ma), most of the northern half of Libya is covered by the Neotethys incursion (Figure 2.21) with active deposition of platform carbonates and deep facies in the centre of the Sirt Basin.

Three important phases have been reported by Biju-Duval et al. (1977) during modeling of the tectonic evolution of the North African Margins during opening of the Tethys Ocean. (1) During Mesozoic to Late Cretaceous, Africa was subjected to a left-lateral motion and high rate of movement (2-4 cm/yr), (2) After that during the Late Cretaceous and Ypresian (49 Ma), the motion is slowed because of the intercontinental collision, and right-lateral movement of Africa in relation to the spreading of Europe and North America, (3) Then, from the Ypresian on, as a result of intercontinental collision state, Africa moved rapidly to the east. Maurin and Guiraud 1993, suggested that Alpine deformation, inverting Early Cretaceous rift systems and reactivating older structures as far south as Central Africa. North south trending Pan-African faults were the most strongly reactivated lineaments during this phase.

In North African basins, the Palaeogeographic setting has been studied entirely during the main phase of the Alpine compression and in the Late Cretaceous time (Stampfli and Borel, 2002). As rifting waned, the North African Platform subsided and was blanketed by a succession of continental clastics, evaporites and carbonates during the subsequent Mesozoic (Boote et al., 1998). The stratigraphic nomenclature for Libya is complex, mainly due to the large number of oil companies operating in many small concession areas. This is most pronounced in the Sirt basin. For this reason, the discussion of the stratigraphy is mainly based on megasequences of Cretaceous – Miocene age.

The divisions are generally controlled both by global and local tectonic and eustatic sea level fluctuation events. In the Sirt basin and due to earlier influences of the Caledonian arch, older sequences may have been exposed at the core and this arch may have undergone further exposure during Permo - Carboniferous times. In the Nafusa region, an E-W uplift which started in Tunisia and extended into W Libya exposed Precambrian basement at its core.

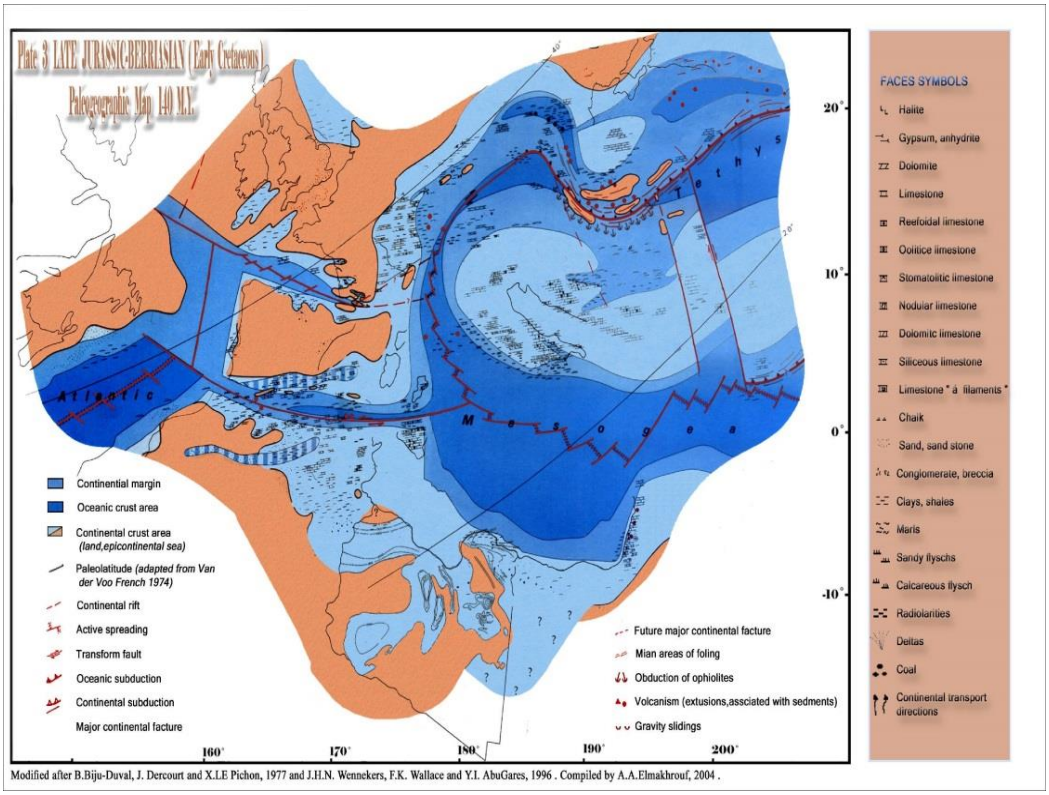

Figure 2.21: Paleogeographic map of Late Jurassic – Early Cretaceous 140 M.Y. obtained from El-Makhrouf (2004)

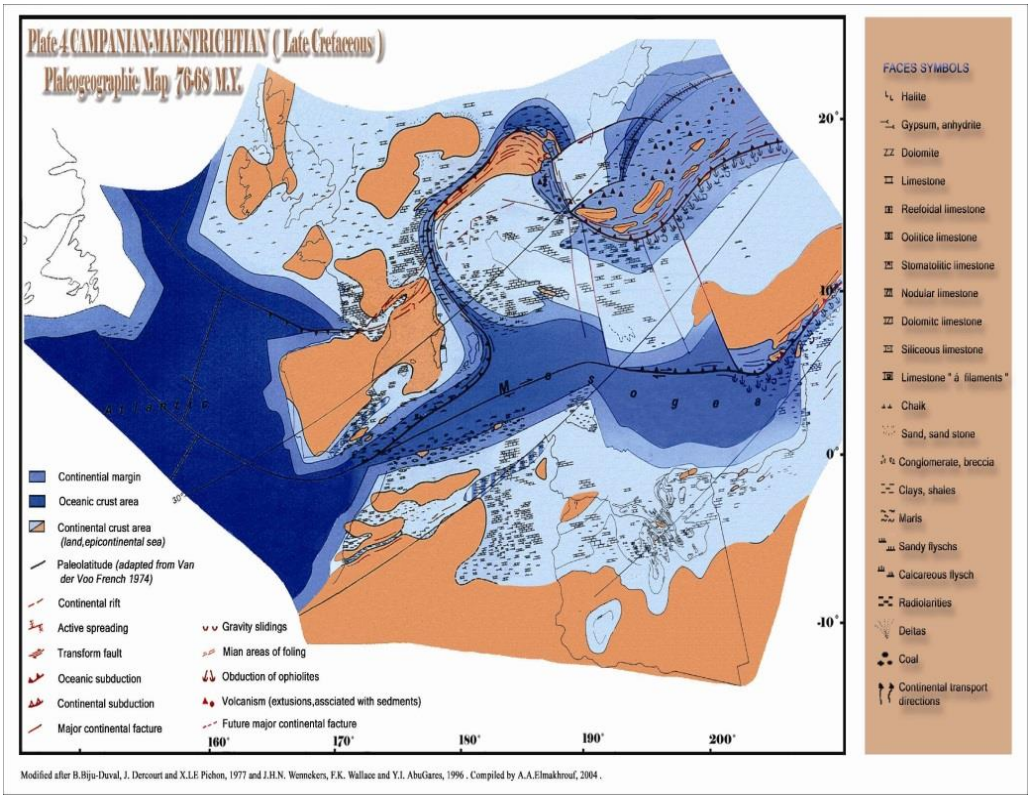

Figure 2.22: Paleogeographic map of Cambanian – Mastrechtian (Late Cretaceous) 76 – 68 M.Y. obtained from El-Makhrouf (2004).

Another NNE-SSW uplifted block occurred in eastern Kufra on top of the Awaynat High (Figures 2.9&2.16). The initial opening of the Neo-Tethys started during the late Permian in Northern Arabia at first, extending westwards slightly later during the earliest Triassic (Laubscher and Bernouli, 1977) (Figure 2.23).

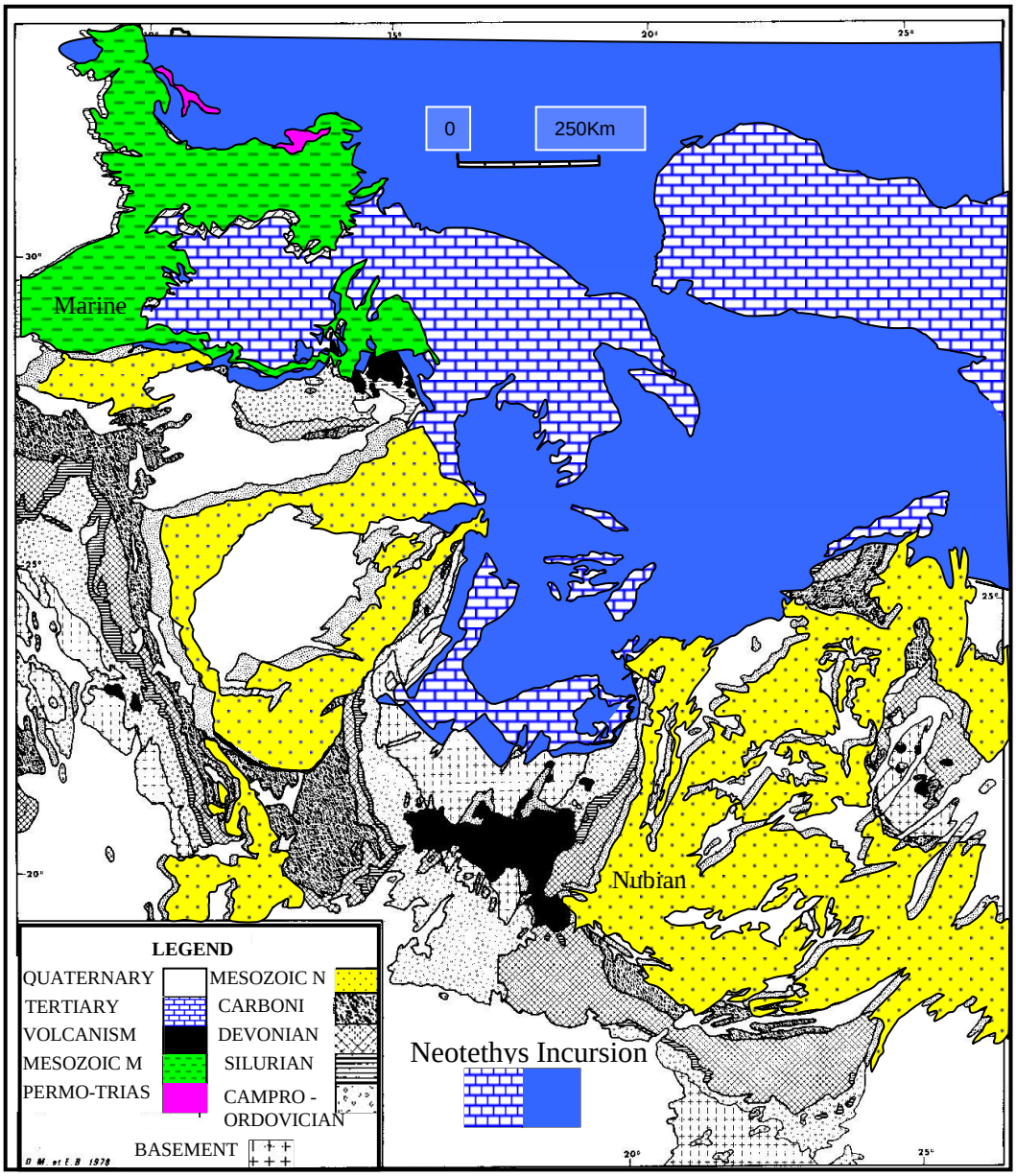

Figure 2.23: Sketch Geologic map of Libya, show the Permo – Triassic sediments at the NW (violet), the marine (dashed green) and Continental Mesozoic (dotted yellow) sediments, and the Tertiary carbonate and evaporite sediments (blue carbonate symbol) and the blue for the Neotethys marine incursion. (Map redrawn from Bellini and Massa, 1980).

An East-West marginal basin developed along the Cyrenaica-Nafusa line. This marginal basin had two branches to the south, one extending into the Ghadames basin and the other into the Cyrenaica Platform and Kufra basin. These arms were furnished by river systems running from Kufra in East Libya and the Gargaf in west Libya. The fluvial and fluvimarine sediments of W and E Libya pass northward into open marine carbonates north of Jabal Akhdar and the Pelagian basin (Figure 2.10). Such open marine sediments are referred by Ziegler et al. (1999).

In the central part the Upper Cretaceous-Paleogene megasequence is the product of the Sirt extensional tectonics, which started in the Aptian-Albian as E-W trending horsts and grabens and shifted to NNW-SSE trends from the Cenomanian onwards. These effects only influenced Libya north of the Gargaf-Dalma trend, although during the Paleocene, rifting also extended south of this line. The Tibesti high (Figures 2.6, 2.9, and 2.17) underwent extensional effects, which resulted in the development of a Paleogene basin in that area. Rossi et al., (1991) suggested that the extensional phase of the Sirt resulted from cratonic uplift, associated with triple junction extension. These blocks were not fixed in their movements. Analyses of the sedimentary sequences in the Sirt basin suggest that the present day platforms and troughs exchanged attitude few times during the Cretaceous and Paleogene. This is particularly pronounced during the Cenomanian to Campanian, where the sequence is variable and laterally interrupted. From the Maastrichtian onwards, the sequence is fully distributed throughout the Sirt basin. Carbonate reef build-up from the northern part of the Ajdabiya Trough was studied by Hladil et al., (1991) and showed that the reef-bearing carbonates range in age from Priabonian (U Eocene) to Serravillaian (Miocene).

The Paleocene was the time when the maximum area of the Sirt Basin and its surroundings were submerged. Previously, during the late Cretaceous, areas south of the Sirt Basin previously not submerged were eventually submerged. E-W trending blocks within the basin were activated and have influenced the pattern of sedimentation as such. Carbonates and shale were deposited at first, followed later by carbonates which accumulated on carbonate ramps, some forming foraminiferal - shoals. Some areas north of Cyrenaica may have been elevated during this time as well as the Jefarah Plain and the western offshore area (Figure 2.9). Deposition within the Sirt Basin extended southwest ward in the Tibesti region where the Paleocene Sea reached as far as the southern borders of Libya. The offshore blocks of Libya

were part of an offshore basin receiving basinal marl sand and shale (Guiraud & Bosworth, 1997; Guiraud, 1998). The Oligocene was the time of uplift for most of Libya, leaving behind a 400 km wide basin occupying the central part of the Sirt Basin, (Knyle et al., 1996; Guirand, 1998). This marine basin was filled in with carbonates, occasionally developed into a river system.

In some parts of the basin, especially at its connection to the Tethyan seaway, some carbonate reef builds were developed.

The close of the Oligocene was also the period when the NE moving African plate slowed down and whence the Sirt Basin area was on top of a mantle hotspot. The slowdown in movement of the plate allowed the subcrustal volcanics to pierce through to the surface. Highly alkaline basalt and phonolites were out to the W, SW and S of the Sirt Basin (Wilson and Guiraud, 1998). The Sirt Basin was almost closed during the Neogene, apart from its central part, which extended southeast wards into the Sarir low in SE Sirt.

2.5 Crustal Structure

Convergence between Africa and Europe slowed down during interval between Cretaceous and Tertiary (Dewey et al., 1989). Collisional between Europe and Africa marked by a northwest – southeast to north – south oriented stress field at the early Eocene (Cloetingh et al., 2005). New phase of rifting resulted in a rapid subsidence particularly in the main troughs (Guiraud et al., 2005). These have been formed as a result of dextral strike - slip movement along plate margins (Anketell, 1996; Guiraud et al., 2001).

The Sirt basin, is located on the northernmost part of the North African Margin (NAM) (Figure 2.24), and characterized with an African and Mediterranean (Tethyan) influence in its dynamic evolution and approximately 500 km wide Mesozoic - Cenozoic rift system comprising platforms and basins (Figure 2.25) that deepen towards the east, reaching the maximum depth in the Ajdabiya Trough area.

The tectonic history and stratigraphy of the Sirt Basin has been studied by several authors, among them Klitzsch, (1966), Conant and Goudarzi, (1967), Barr and Weegar, (1972), Goudarzi (1981), van Houten (1983), Harding (1984), van der Meer and Cloetingh (1993) and Wennekers et al. (1996), all argue that the tectonic history of the Sirt Basin is characterized by

a complex series of geologic episodes during supercontinent breakup that vary from compression and therefore to a broad and extreme extensional regime.

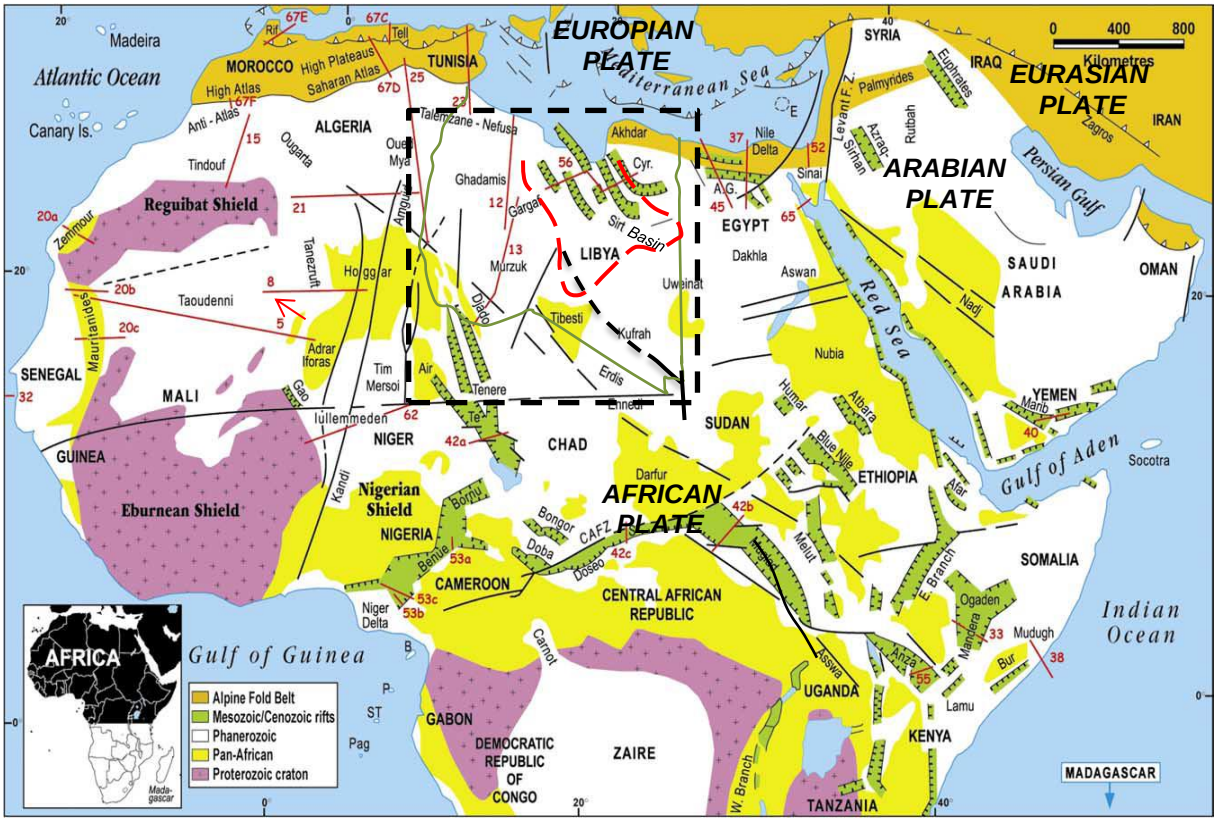

Figure 2.24: Schematic geological map of Northern Africa, Central Africa and Arabia, compiled from Wilson and Guiraud (1998), showing regional setting of Libya, almost surrounded by currently active plate boundaries. The major fault zones and Mesozoic-Cenozoic rifts are located. CAFZ, Central African Fault Zone; Cyr, Cyrenaica Platform. Rifting is moved northward from southern Atlantic during Late Jurassic-Early Cretaceous (e.g. El Arnauti et al., 2008), during this time the African plate moved to the ENE with respect to Europe and broke into sub-plates along major shear zones which were formed by the Central African Shear Zone (CASZ). Map from Guiraud et al., 2005.

Contemporary Sirt Basin extensions started ~180-160 Ma producing regional subsidence, block faulting and crustal thinning, accompanied by increasing heat flow and bimodal volcanism. Crustal rifting in the eastern part of the Sirt Basin such as the Sarir and Hameimat troughs (Figure 2.25) is presumably related to the opening of the Central Atlantic and may also have been influenced by the left lateral opening of the Tethys Ocean (e.g Piquep and Laville 1996; Wilson and Guiraud, R, 1998; Stampfli., et al 2001; Ziegler et al., 2001; Guiraud et al., 2005; Hallat, 2002; Craig et al., 2008; Bosworth et al., 2008).

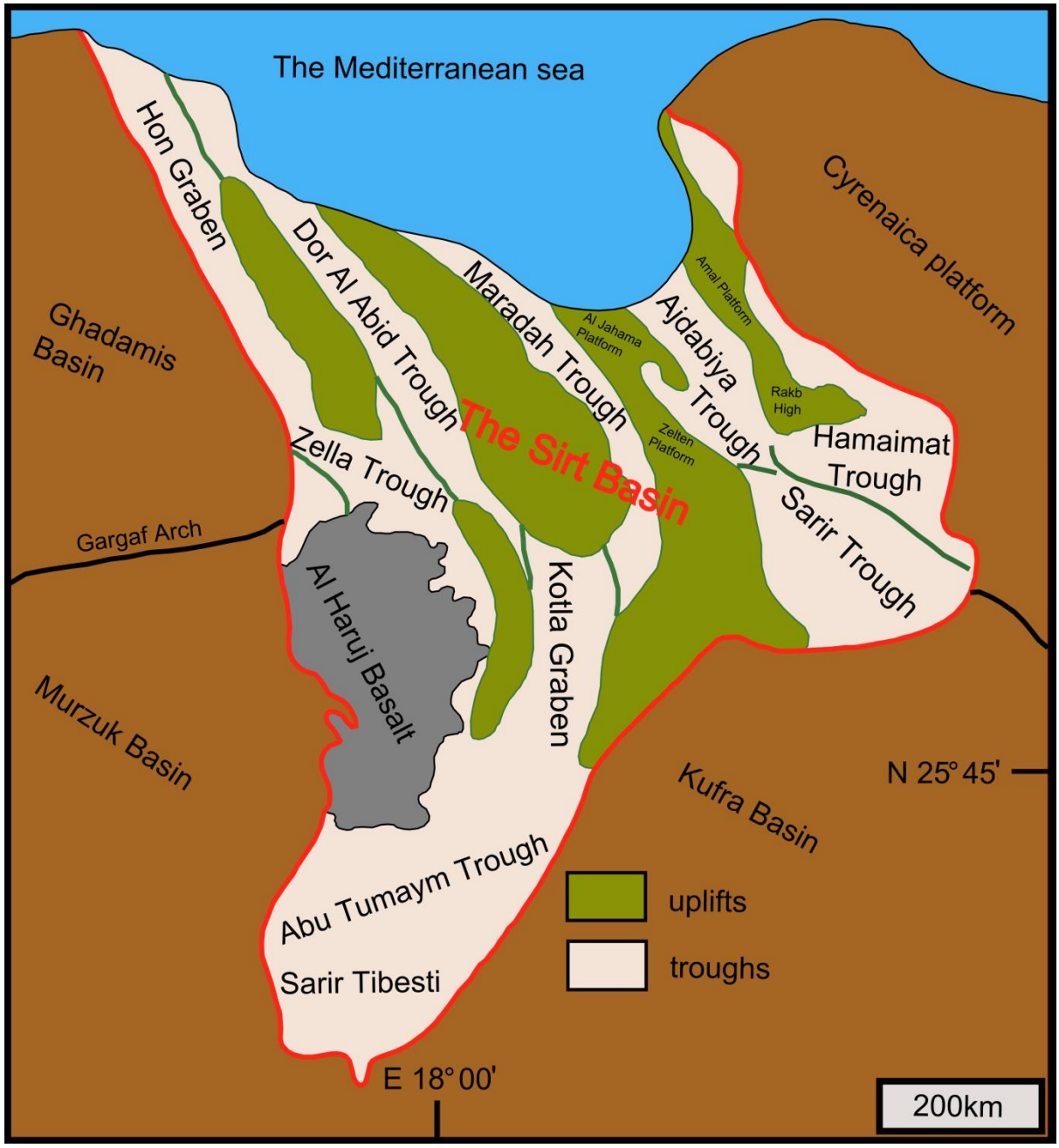

Figure 2.25: shown the location of Ajdabiya Trough relative to the major structural elements (uplifts and troughs) of the Sirt Basin.

2.5.1 Basement under the Sirt Basin

Basement under the Sirt Basin is Pan African in age (late Proterozoic –Early Paleozoic (Vail, 1991). It is mainly granitic in composition. The upper section appears to be quarzitic sandstone of Late Palaeozoic (Cambrian and Ordovician).

According to Vail (1991), four Precambrian basement zones can be mapped in Libya. The first and oldest is restricted to SE Libya. This covers the Tibesti to the south, the Al Awaynat to the south east and the whole of the Kufra basin (Figure 2.26). The second is restricted to SW Libya and is part of the East Saharan craton (Figure 2.16). This covers the Thamboka and Murzuk basin area. The third zone is the Pan African remobilised continental terrain, representing the W Tibesti area, and extends underneath the sedimentary cover towards the southern part of the Sirt basin with characteristic NE-SW trending structural elements.

The fourth zone is an accretionary belt that extends to the west into the Algeria, and characterized by NW-SE oriented structural trends. It is possible that the volcanics encountered in numerous wells reaching the basement in the Sirt basin might be representative of this unit.

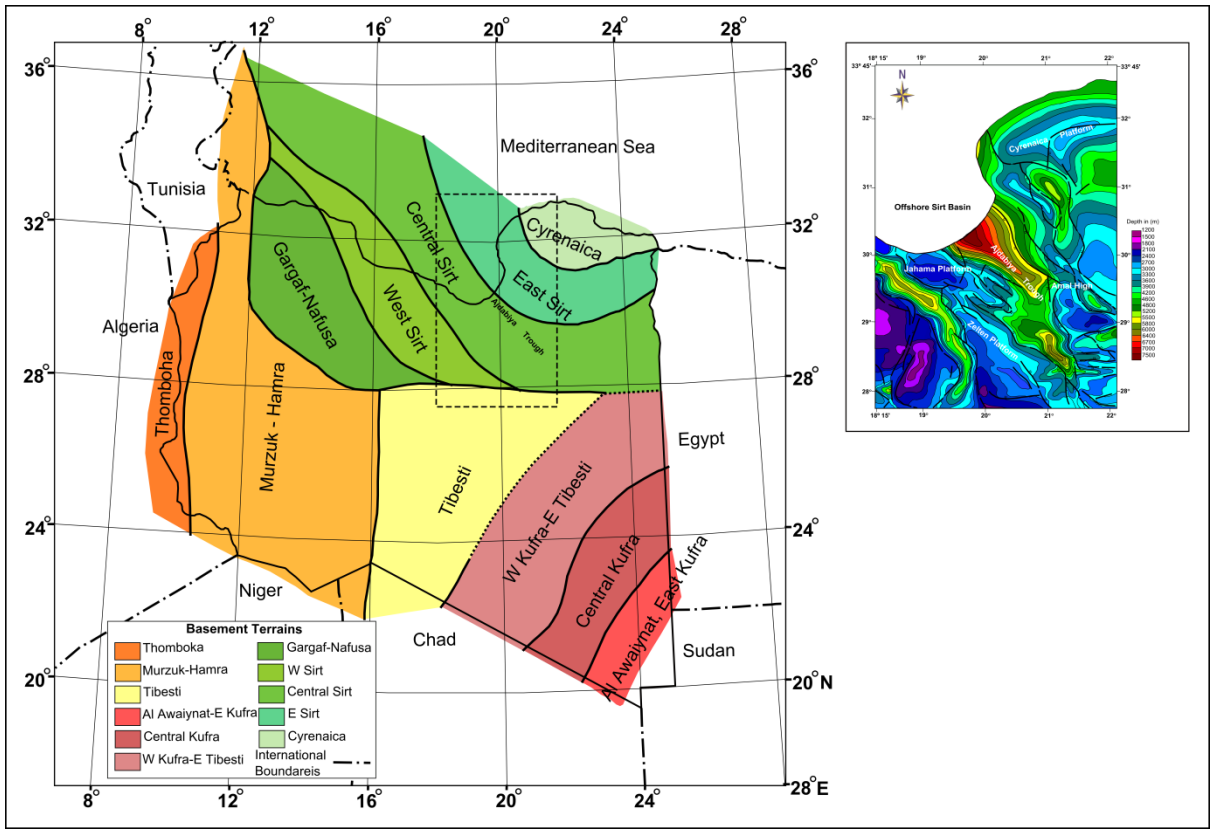

Figure 2.26: Distribution of basement terrains in Libya, with onset map showing basement depths within the Ajdabiya Trough and nearby areas.

Neoproterozoic mobile belts form basement terranes in the Sirt Basin. The structural grain and boundaries of these terranes fundamentally controlled the location and shape of the basin

and the locus of deformation and uplift. A NE-trending Proterozoic basement structural grain influenced the development of NE-trending Triassic-Jurassic growth faults in the Ajdabiya Trough and adjoining Cyrenaica Platform. These faults were the focus of SE-directed Late Cretaceous and younger inversion.

2.5.2 Central Atlantic Rifting (260-195 Ma)

The Late Permian Triassic and Jurassic marked the second phase of Gondwana breakup with the onset of the seafloor spreading in the central Atlantic, Triassic faulting is recorded particularly along the Tunisian Margin of the Pelagian Basin where N-S normal and E-W transfer faults developed (Ouali, 1985; Morgan et al., 1998). In the Sirt Basin extensional faulting is interpreted to be controlled by the NE- trending basement structural grain with reactivated NW trending Nabitah Orogeny - Oman. Movement was accommodated by inversion of shear zones. Movement on these zones was particularly focused on a crustal-scale system that extended from the south-eastern part of the Sirt to the Pelagian Basin incorporating the Ajdabiya Trough. This zone was the site of granitoid intrusion during this and younger Mesozoic - Cenozoic extensional events (Figures 2.26 & 2.27). Depth to Moho and Crustal thickness calculation (chapter 4) indicate significant crustal thinning beneath the offshore Sirt Basin, this thinning is interpreted to have commenced with the Syrian Arc at about 90 Ma (Gondwana/Arc Collision event).

2.5.3 Jurassic Rifting (195-149 Ma)

From about 195 Ma, opening of the mid Atlantic was accompanied by separation of North Africa and Europe along a major sinistral transcurent shear zone. South of this zone throughout Libya and North Africa, NE trending growth faults, some reactivated during the Late Permian Triassic, developed along a marginal zone of extended crust, portioned from unaffected areas to the south by major Pan African NE- trending crustal fracture zones (Najd Faults). The magnitude of extension was controlled by the fabric of the basement terranes being extended. Extension leads to the onset of sea floor –spreading in the eastern Mediterranean.

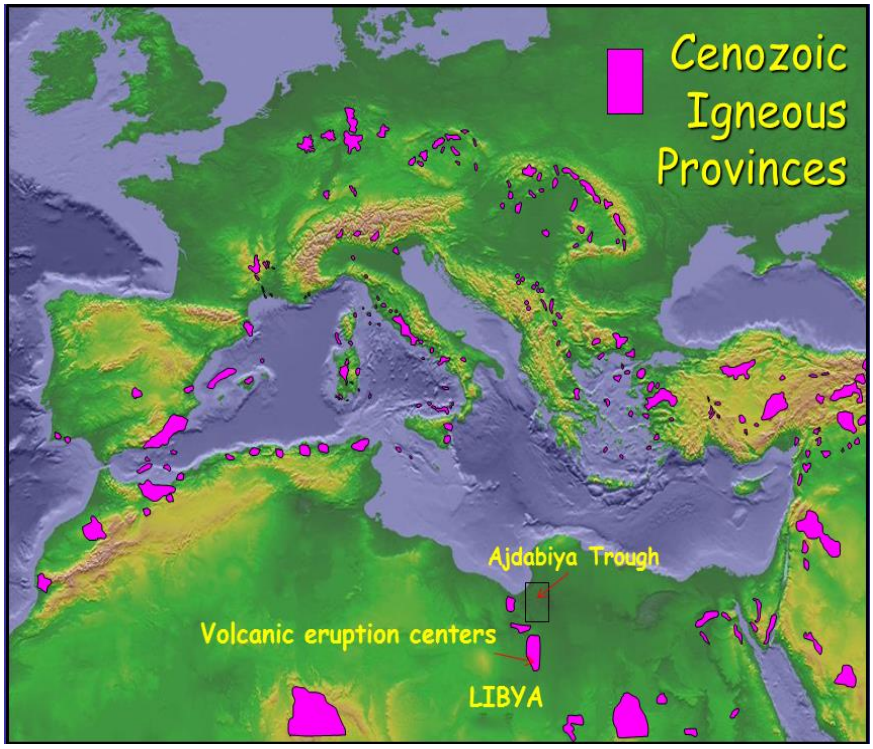

Figure 2.26: Digital topography of circum - Mediterranean area from NOAA showing the locations of Cenozoic igneous provinces (with both anorogenic and orogenic geochemical signatures) in purple. (http://www.ngdc.noaa.gov/mgg/image/2minrelief.html). NOAA National Oceanic and Atmospheric Administration.

Within the Sirt Basin, predicted NE-trending extensional faults form a series of en echelon half-graben and graben features. NW-trending transfer zones link major extensional components with major NE-tending bounding faults. The Hameimat and Ajdabiya Troughs were likely to have been significant depocentres.

2.5.4 Cimmerian (149-140 Ma)

Early Cretaceous rifting (140-115 Ma): and south Atlantic rifting (115-97Ma). At 150 Ma onset of sea floor spreading in the North Atlantic caused the south European micro plate be decupled from Atlantic spreading system, This resulted in regional plate movement between North Africa and Europe from NW to NE resulted in regional uplift and inversion in the latest Jurassic Early Cretaceous, accompanied by a worldwide valanginian drop in sea level and opening of the Neotethys.

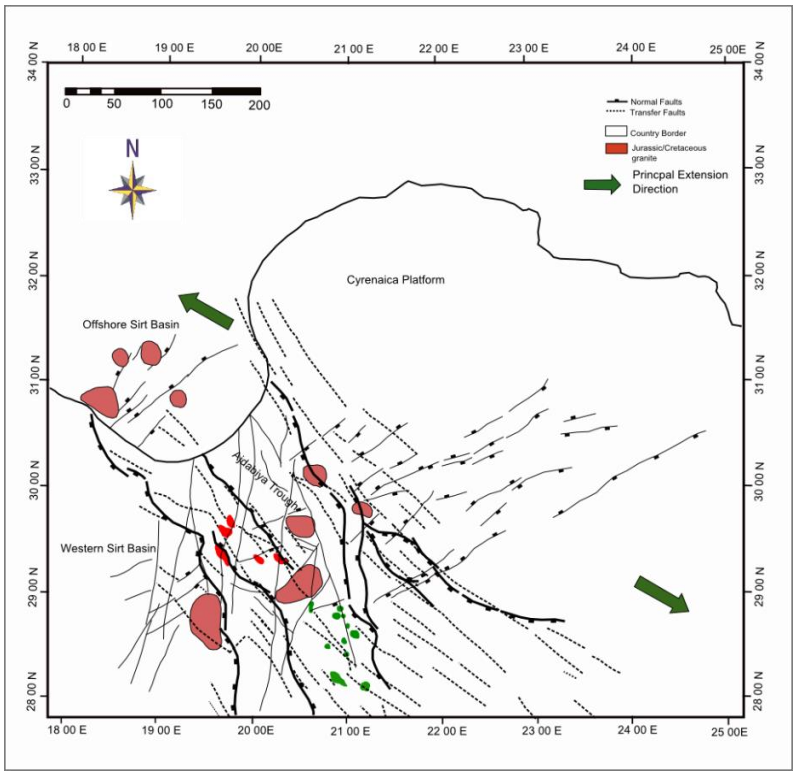

Figure 2.27: Generlized map of Jurassic rifting (195 – 149 Ma) and extension direction inferred during opening events of mid Atlantic. From about 195 Ma, opening of the mid Atlantic was accompanied by separation of North Africa and Europe along a major sinistral transcurent shear zone. South of this zone throughout Libya and North Africa, NE- tending growth faults, some reactivated during the Late Permian – Triassic, developed along a marginal zone of extended crust, partitioned from unaffected areas to the south by major Pan African NW-trending crustal fracture zones. The magnitude of extension was controlled by the fabric of the basement terranes being extended. Extension led to the onset of sea floor spreading in the eastern Mediterranean. The Jurassic rifting event caused major subsidence in the Sirt Baasin and Cyrenaica Platform (El Arnauti and Shelmani, 1985). Subsidence was controlled by reactivated NE-trending normal faults.

North south extension between the southern European micro plates and North Africa caused reactivation of faults in the Sirt Basin, Jurassic NE trending faults and Proterozoic N trending faults underwent oblique normal reactivation. There was also development of E-W trending growth faults. These three fault trends controlled subsidence of the main Cretaceous depocentres in the Sirt Basin with most growth on E-W structures (eg. Hameimat and Ajdabiya Trough), (Ahlbrandt, 2001).

2.5.5 Gondwana Arc Collision 97-63 Ma)

Plate constriction indicates that the Neoteyhys had began to close by the end of the Early Cretaceous. A NW-SE compressive regional stress regime was established by Middle

Cretaceous. Collision of Europe with Africa and Arabia commenced during the Santonian at about 87 Ma (Ziegler et al., 2001). The Santonian event is characterized by a major Unconformity within the marine to shallow marine strata with local folding, inversion, thrust faulting and uplift focused on NE trending Jurassic growth faults. Subsidence accelerated within the Sirt Basin along reactivated NW trending faults. Some of the Cambrian Ordovician sequences on structural highs were not completely transgressed untile the Mastrichtian.

The effect of the tectonic evolution i.e. graben subsidence plus concurrent progressive incipient macrobasinl subsidence on depositional environment are shown by the progression from subareial, peripheral marine and shallow marine in the earlier stages to a comparatively deeper marine palaeobathmetry during the Santonian-Coniacian and Campanian stages (Baird et al., 1996). Dextral transpression is interpreted along the North Cyrenaica Fault system and Western Desert of Egypt (El Arnauti et al., 2008). Within the Sirt Basin, this period is characterized by a continued pull-apart and transtensional subsidence. The deformation was accompanied by localised uplift along Pan African fracture zones sub parallel to the coast, concentrated in the northern part of the area. During the initial stages of the event new NE trending extensional faults developed to form domino style array between inverted Proterozoic and Jurassic structures.

2.6 Subsidence and Stratigraphical Development of the Sirt Basin and Ajdabiya Trough

The history of the Sirt Basin is characterized by a complex post- Hercynian lithospheric deformation, which is intimately linked to the opening and closure of the Tethys and the Atlantic oceans (e.g. Ambrose, 2000; Ahlbrandt, 2001).

The basin originated in Late Cretaceous times, when localized basins developed under influence of intense wrenching of the crust due to the dextral shear movement between Laurasia and Gondwana (Hallett, 2002). Subsequently, localized Cretaceous sub-basins were joined together in the Tertiary when a main phase of stretching took place with deep basement faults accommodating the extension (Baird et al., 1996; El Arnauti et al., 2008; Bosworth et al, 2008).

2.6.1 Subsidence Development

Tectonic subsidence in Sirt Basin is considered by several authors (e.g. Van Wees et al., 1996; Abadi et al., 2008) based on assumption of uniform lithospheric stretching model (McKenzie, 1978; Royden and Keen, 1980) with the assumption that the response of the lithosphere under the basin to the internal and external load is locally isostatic. Subsidence studies within the Ajdabiya Trough (Abadi et al., 2008) indicates that this is a marked phase of increased subsidence rates characterized with lithospheric extension ranging from 1.03 - 1.3 (e.g. Gumati, 1981; Gumati and Kanes, 1985; van der Meer and Cloetingh; 1992; Ceriani et al., 2002; Abadi et al., 2008).

Subsidence occurred in pulses, based on temporal variations during the period of the Cretaceous (Cenomanian – Maastrichtian, 98.9 – 65 Ma) (Abadi et al., 2008). This indicates strong variations in subsidence mechanism mainly concentrated in the eastern part of Sirt Basin, which has a direct link and interaction with the basin fault framework. In contrast to the subsidence in the western part of the basin represented by a NW-SE aligned troughs, a rapid and continues subsidence shifted to the eastern part of the basin and forms the Ajdabiya and Hameimat Troughs (Baird et al., 1996; Pawellek, 2007).

Significant changes from the thermal subsidence curves were observed from previous studies (Gumati 1985; Abadi et al., 2008 and references therein). Subsidence curves, show that subsidence was continuous throughout Late Cretaceous and Tertiary times, reaching a maximum during the Paleocene and Eocene (Gumati and Nairn, 1991; van der Meer and Cloetingh, 1993; Abadi et al., 2008). During Eocene time, the Sirt Basin undergoing dawn-warping conditions, marine transgression gave way to advent circulation and extensive evaporite sedimentation due to inversion tectonics to the north (Knyle et al., 1996; Fiduk. 2009). Although the subsidence analysis provided fundamental information concerning the quantification of tectonic subsidence over different parts from the basin, the spatial and temporal distributions were poorly constrained.

2.6.2 Stratigraphic Development

It is postulated that the structural and stratigraphic architecture of the basin has been developed during four main supra-regional tectonic phases, which can be observed all over

North Africa, and which correspond to the complex evolution of the Atlantic and Tethys Oceans (e.g. Burke & Dewey 1974; van Houten 1983; Guiraud & Maurin 1992; Cavazza et al. 2004). These are:

1. Late Carboniferous to Early Jurassic rifting.
2. Middle Jurassic to Early Cretaceous left lateral wrenching.
3. Late Cretaceous to Middle Eocene right lateral wrenching.
4. Late Eocene to the present right lateral wrenching and north-south compression.

Magmatic activities of Permian age are centreed on the offshore areas and the northern part of the Sirt basin (Wilson and Guiraud, 1998). The offshore activity is basaltic while Triassic - Permian granites (256 Ma) and granodiorite (230 Ma) were encountered in some wells in western Sirt Basin. Basalts (213-218 Ma) and microsyenite sills (245 Ma) are also encountered in wells from the Amal horst (Cahen et al., 1984; Massa and Delort, 1984). These activities are anorogenic and might have been triggered by the opening of the Neo-Tethys. Transpressive-dextral tectonic activities continued at different rates and strengths well into the Palaeogene and the Neogene in the North African basins (Guiraud, 1990; Guiraud et al., 2005). In Sirt basin area inversion evidenced from compressional structures are rare, but diastrophic events (uplift, subsidence, tilting, faulting and intrusions) are prevalent (Goudarzi 1980, Gumati and Nairn, 1991; van der Meer and Cloetingh, 1993; Abadi et al., 2008).

The magnetic interpretation show that the south-eastern part of Ajdabiya Trough is characterised with high amplitude magnetic anomaly signature (~500 nT) possibly attributed to the existence of igneous intrusions or signatures of major fault zone where basement rocks are possibly juxtaposed against Mesozoic carbonate units.

Gravity and magnetic modeling integrated with seismic profiles show thickening of strata to the east possibly attributed to the tilting of the trough. At the north eastern part of Ajadabya Trough, the Tertiary especially the Oligocene - Miocene section is more thickly developed and the Upper Cretaceous probably more thinly developed.

In addition to the gravity and magnetic modeling, the structural alignment and extent of these features can be detected by regional and residual mapping of the gravity and magnetic anomalies.

2.6.2.1 The Paleozoic sequence (Stratigraphic architecture of the Palaeozoic succession around syn-tectonic highs)

The Palaeozoic sequence in Sirt Basin is highly influenced by successive epirogenic events that have removed over 4000m of Palaeozoic rocks (Hallett, 2002). In contrast, about 5000m of Paleozoic sequence is estimated to be present within the offshore Sirt Basin. The top of the Palaeozoic is generally marked by an unconformity surface which represents latest Permian or earliest Triassic transgressive surface. The stratigraphic units of the Palaeozoic within the Sirt Basin are presented in the following.

2.6.2.1.1 Infracambrian-Silurian sequence

The Infracambrian-Silurian sequence is patchily distributed due to removal of sediments largely during the early and late Palaeozoic arching, and partly due to Mesozoic arching. The sequence is almost totally removed within the present day Sirt basin due to NNE-SSW "Caledonian" uplifts, N-S "Hercynian" uplifting and E-W Jurassic-Early Cretaceous uplifts.
The Infracambrian-Silurian sequence is divided into two sequences on the basis of unconformities within the sequence. These are:

- **Late Precambrian-Infracambrian**

The Cambro-Ordovician of Libya generally rests on granitic or metamorphic rocks.
In the Sirt basin, numerous wells reached volcanic rocks that lie below the Gargaf Group. In some wells volcanics were fully penetrated, with underlying metamorphic basement. As far as we can gather, no age determination is available in literature for these occurrences.
Dacite, rhyodacite and ignimbrites are also described from the Northern Sahara region of Ouguarta ridge and sandstone and carbonates from the Tassile region of SE Algeria are also described in positions below the Cambrian sequence, and above granitic and metamorphic basements (Fekirine and Abdalla, 1998). Whether these volcanics represent Infracambrian rifts or the arc system products associated with the final reconstitution of the Late Proterozoic of Afro Arabia (Vail, 1991) is not clear.

- **Cambrian-Lower Ordovician**

This sequence constitutes the major part of the Gargaf Group. This group is only subdivided into its various formations in the Murzuk and Kufra basins. In the Ghadames, Sirt and Cyrenaica areas, no subdivisions were offered by the well logs of the operating oil companies. The reconstructed thickness suggests a sudsiding depocentre on the Tibesti High extending northwards into the Sirt basin.

2.6.2.2 The Mesozoic sequence, UpperJurassic – Campanian-Maastrichtian: Terrestrialrift (Synthesis: tectono-stratigraphic evolution).

2.6.2.2.1 Triassic-Lower Cretaceous

The Triassic-Lower Cretaceous sequence, represented by an E-W extensional phase during the opening of the Neo-Tethys, has two characteristic sedimentological domains. Triassic and Jurassic are generally absent in the Sirt basin while Lower Cretaceous clastics are encountered in SE Sirt and in some grabens in central Sirt. In the Cyrenaica platform some Jurassic and Lower Cretaceous sequences are encountered in the E-W Jaghbub trough, with the Lower Cretaceous units reaching up to 1250m. Arching during the Early Triassic and the Early Cretaceous resulted in an almost complete removal of the Paleozoic from the Sirt basin. During the Late Jurassic and Early Cretaceous, the Sirt basin was still elevated apart from some narrow N-S grabens which still retained the Pre-Upper Cretaceous Mesozoic sequence, often referred to as Pre-Cretaceous in well logs. Upper Jurassic and Lower Cretaceous clastics were laid down on both flanks of the Sirt basin (i.e. the Ghadames and the Cyrenaica) and were strongly affected by E-W horst and graben development.

2.6.2.2.2 Early Synrift Deposits

Rifting in Sirt Basin began approximately during the latest Jurassic and resulted in extensive deformation of the basement with earliest syn-rift deposits encountered in shelf wells comprising the Nubian Sandston facies, which subdivided to sandstone and shale beds reaches a maximum thickness of 1200 m in the Hameimat Trough (Figure 2.25).

The Upper Cretaceous unconformity (Cenomanian age) marks the transition into late- to post-rift sediments, which consist principally of marine carbonates and shales.

Evidence from the eastern Sirt Embayment shows the presence of Triassic and Jurassic rocks forming the oldest part of the synrift sequence, and the same situation may be present in other parts of the Ajdabiya Trough. The main syn-rift deposition occurred in the early Cretaceous when the Nubian (Sarir) sandstone accumulated in rift troughs and topographic lows on the irregular pre-Cretaceous surface and pass into a quartzitic facies in the northern Ajdabiya Trough. The Nubian may pass into a marine facies in the northern part of the trough.

2.6.2.2.3 Late Synrift Deposits

According to Hallette (2002), both siliciclastic, dominantly fluvial environment and carbonate dominated deposition can be a consequence of the early stages of submergs controlled by eustatic sea level changes, within the Ajdabiya Trough. A pervasive sequence of Jurassic – Lower Cretaceous synrift sandstones and shales blankets the SE Sirt Basin (e.g. Ambrose, 2000) and may be similar syn-rift sequence formed within the Ajdabiya Trough during this period. The sequence onlaps major bald basement highs and thickens into a number of grabens and half grabens. The Ajdabiya Trough underwent extensional deformation during the Cretaceous time and possibly extended to the Paleogene (e.g. Abadi et al., 2008), by which late synrift sequences could be developed as a consequence of variable cycles and trends of marine inundation. For instance the deposition of Late Cretaceous Sirt Formation (Figure 2.8) as a black laminated organic rich shale is due to high organic productivity and restricted marine circulation deposited during Maastrichtian to lowermost Campanian time. Thus, deep marine rift basins are enriched in organic muds, which makes them excellent petroleum source rocks in the area (e.g. Roohi, 1996 a, b).

The latest synrift stage is a character of the Late Cretaceous time and characterized by high rates of extensional faulting (Gras and Thusu, 1998) therefore there may be sufficient sediment yield potential to exceed the accommodation space generating deep depositional enviroments, in addition to that deepest post-rift depcentres coincide with syn-rift sediment accumulations (Gras, 1996).

2.6.2.3 The Cenozoic Sequence

The Cenozoic tectonic history of the Sirt Basin is marked by rather subtle changes in stress regimes due to tectonic settings and events in a broader regional context. The Sirt Basin was always quite remote from any plate boundaries and thrust fronts. The nearest major tectonic feature is the frontal thrust of the Aegean arc, which is more than 450 km away from the onshore Sirt Basin.

The regional tectonic setting has been summarised adequately by Hallett (2002). For the basin fill, this means that there are no major inversions of troughs and drowning of individual platforms. All major structures remained as they were at the end of the Early Cretaceous, with adjustments due to regional, not local, stress regimes. An exception must be made for Oligocene and Neogene volcanism which was widespread along the TripoliTibisti axis, to the west and south of the Sirt Basin. It is not entirely clear what this volcanism is related to, perhaps the passing of the Cameroon hotspot (c. 14 Ma), followed by the Hoggar hotspot. These also caused relative "uplift," in western area here Cretaceous and Tertiary Sirt Basin sediments are now in outcrop, whereas sedimentation largely continued well into the Neogene and the Quaternary further east.

2.6.3 Tectono-Stratigraphy of Post-rift Strata

Post-rift strata in Sirt Basin has been considered for several decades that attributed to differential thermal subsidence, based on the general acceptance that the only significant post-rift tectonic process experienced by passive margins is lithospheric cooling, expressed by a simple uninterrupted thermal sag pattern of subsidence (Sleep, 1971; McKenzie, 1978).

The seismic character of the post-rift sequence in the Ajdabiya Trough consists of continuous reflections and gradual changes in thickness.

Tertiary successions in the Ajdabiya Trough were deposited during thermal and drift phases of the Sirt Basin and separated from the Upper Cretaceous strata by a major unconformity. NW-SE trending faults are dominant during the Cretaceous time interrupted by E-W faults may offer additional accommodation space for the post-rift sediments during possible reactivation cycles. The Paleocene rifting phase is separated by a period of tectonic quiescence from the Late Cretaceous subsidence during Maastrichtian time. During the Palaeocene, the basin deepened with markedly thick deep marine sections developed in the

central part of the Ajdabiya Trough. Carbonate build ups were deposited in the marginal areas. The Paleocene strata are characterized also by variations in lithology in marine continental interface (Bezan, 1996). In the north east part of the trough carbonate and clay succession indicates marine shelf conditions. During Eocene time, the Sirt Basin undergoing dawn-warping conditions, marine transgression gave way to advent circulation and extensive evaporite sedimentation due to inversion tectonics to the north (Knyle et al., 1996, Fiduk. 2009). Within the Ajdabiay Trough, carbonate progradation is formed during Eocene transgression event followed by period of sea level fail. These followed by subsidence and transgression events. Subsidence during the Eocene occurred in the Ajdabiya Trough formed a single larger elongated depression tilted to the north east toward the Mediterranean Sea, with no fault activity observed which indicates that sediment loading and thermal relaxation play an important role in the subsidence process. The absence of faulting during post-rift stage may also suggest a component of lithospheric folding (Cloetingh et al., 1999), which may be related to the mantle upwelling as evidenced from large areas in Europe (Cloetingh and Van Wees, 2005). Narrow to basin wide deposition caused by the post-rift thermal subsidence, mainly attributed to fluctuating of intraplate stress field and/or migration of rift activity caused by the strain bordering of the previously stretched lithosphere (Abadi et al., 2008; Cloetingh et al. 2005). Must of what has been addressed at present about the post-rift stratigraphy and structure in the study area, was inferred from disconnected seismic surveys and a fraction of the exploration drilling within the basin. The Oligocene – Early Miocene time was marked by a reduction of tectonic subsidence rates within the basin, and local folding of the earlier sediments. Open marine conditions existed during the middle Oligocene – Late Miocene.

2.6.4 Heat Flow in the Ajdabiya Trough

Heat flow measurements from drill core and cuttings were carried out in Sirt Basin (Suleiman, 1985: Nyblad et al., 1996) show that the heat flow obtained from platforms are higher than from the troughs. These could be related to the large thickness of sediments within the trough compared to the platforms or could possibly arise from heat refraction associated with fault block structures. It is probably caused by present or recent igneous activity during the late

Permian and Triassic (Hallett, 2002). To evaluate the contribution of upper crustal heat production to surface heat flow, heat production of basement rock at different localities was measured by Nyblad et al., (1996). Geologic cross-sections constructed by Gumati and Kanes (1985) as well as modelling of Bouguer gravity anomalies associated with the platforms (Suleiman et al., 1991), suggest offsets of a few kilometres along bounding faults separating the platforms and troughs. In the south-western part of the Ajdabiya Trough, heat flow appears to be higher in the central rift zone than in the surrounding area (Galushkin et al., 2015).

2.7 Discussion

The aim of this chapter was to introduce the geological framework within the Ajdabiya Trough area, NE onshore Sirt Basin. This was accomplished by demonstrating the principles behind the development of rift basins and crustal mechanism with details outlining the geodynamic and geologic evolution along the North African Margin and the Sirt Basin. Along with previous works in the Sirt Basin, this study provides new insights into the geological evolution of the Sirt Basin and Ajdabiya Trough as well as contributing to the wider geological debate regarding Early Cretaceous rifting in the Sirt Basin. Different kinematic models of rifting have been outlined. This provides an integrated analysis of the evolution of the rift basins and important clues regarding the development of subsidence patterns and stratigraphy. The Ajdabiya Trough experienced a number of rift stages suggesting a complex post-Hercynian history. As a consequence of a complex Mesozoic -Cenozoic tectonic history, the characteristics of the crust in the Ajdabiya Trough significantly differ from the other localities in the basin. Rifting in Sirt Basin occurred in different stages each being characterized by specific crustal thinning factors which provides information on the geometry of rifting and suggesting that crustal thinning either accommodated by pure or simple shear geometry (McKenzie, 1978; Wernicke, 1981).

The development of tectonics in Libya during the Paleozoic and Early Mesozoic was controlled by the evolution of the Gondwana supercontinent, whereas Tethys seas also had a significant influence on the tectonic development of Libya (Hallett, 2002). According to Miall (1985) most rifts have originated at divergent plate margins during the breakup of the Pangea supercontinent (Dewey and Bird, 1970; Bond and Kominz, 1984).

The tectonic history of the Sirt Basin is characterized by a complex series of geologic episodes during supercontinent breakup that vary from compression and therefore to a broad and extreme extensional regime. Specifically in the eastern part, these tectonic events have divided the basin into distinct geologic provinces. To the west, the basin is characterized by high heat flow, Eocene-Pliocene volcanism, thin crust and relatively high elevations (Hallett, 2002). Crustal extension associated with block faulting occurred in the Sirt Basin during the mid and Late Cretaceous. The block faults trend NNW-SSE to NW-SE, cross-cutting NE-SW trending earlier Paleozoic structures and possibly parallel to basement shear zones (Anketell, 1996; El Arnauti et al., 2008; Craig et al., 2008). Subsidence in Sirt Basin was continuous throughout Late Cretaceous and Tertiary times, reaching a maximum during the Paleocene and Eocene, when a major reactivation of faults occurred (e.g. Gumati and Nairn, 1991; van der Meer and Cloetingh, 1993; van Wees and Cloetingh 1996; Ahlbrandt, 2001; Abadi et al., 2008). Nature of faulting and later subsidence might have had an effect on charge pattern (fetch areas vs. charge volumes, as well as bypassed areas). Either Intra basin transversal structures related with block movement in addition to thermal effects of igneous intrusions on maturity of organic matter can be interesting for intra-trough structure development and hydrocarbon entrapment.

Significant changes from subsidence curves were observed from number of studies within the Sirt Basin (Gumati 1985; Van Der Meer and Cloetingh, 1993: Abadi et al., 2008). The subsidence curves and subsidence rate curves for the Sirt basin, constructed from the stratigraphic record, show that subsidence was continuous throughout Late Cretaceous and Tertiary times, reaching a maximum during the Paleocene and Eocene, when a major reactivation of faults occurred (Gumati andNairn,1991; van der Meer and Cloetingh, 1993; Abadi et al., 2008). During the Eocene time, the Sirt Basin undergoing dawn-warping conditions, marine transgression gave way to advent circulation and extensive evaporite sedimentation due to inversion tectonics to the north (Knyle et al., 1996; Fiduk. 2009).

Although the subsidence analysis provided fundamental information concerning the quantification of tectonic subsidence over different parts from the basin, the spatial and temporal distributions were poorly constrained. In this study, we intended to combine information provided by well information’s and thickness maps for the Late Cretaceous - Early Paleocene, Paleogene and Neogene periods, with the thickness of the sediments

observed in many wells at different periods (Late Cretaceous - Early Paleocene, Late Paleocene, Eocene, Early Oligocene, Late Oligocene and Miocene - Quaternary).

NW-SE structural grabens filled by thick successions of Late Jurassic – Late Cretaceous Nubian fluvial sandstone facies, which sometimes show a tripartite sandstone-shale-sandstone subdivision and occasionally had a marine (lagoonal) influence (Barr and Wegeer, 1972; El Hawat, 1992; Hallett, 2002). The structural grain of the Sirt Basin therefore relates to the Late Jurassic/Early Cretaceous rifting characterized by the development of syn-rift sequences. The syn-rift includes a sequence deposited during active rifting, typically showing rift-initiation development of normal fault blocks (Hallett, 2002). By the end of the Cretaceous rift cessation characterized by erosion in many places, suggesting tectonic adjustment due to the ending of the tensional regime and development of post-rift thermal subsidence stage.

CHAPTER 3: DATASET AND METHODOLOGY

3.1 Introduction

The aims of this chapter are to provide: (1) an overview of the techniques used to acquire and interpret the geophysical, geological and petrophysical datasets that underpin my study; and (2) to summarise key characteristics of normal and strike-slip faults in sedimentary basins. The latter aim will provide the necessary background to study and interpret the faults and faulted seismic stratigraphic sequences within the Ajdabiya Trough (see Chapters 5, 6, and 7). The present study was accomplished using a diverse dataset that includes 2D multichannel seismic reflection data, potential field data, wireline data and reports from hydrocarbon exploration wells, together with lithological information from a non-commercial well and other results. There are four stages to the workflow: data acquisition, data processing, data interpretation, and modelling, as summarised below. The seismic data have not been depth converted and so times in this study are presented with the vertical axis in two way travel time (TWTT). Numerous wells have been integrated with the seismic data to constrain the stratigraphic ages of the interpreted horizons down to the Early Cretaceous and to help in identifying the faults.

The economic potential of a sedimentary basin is normally assessed in a number of stages. Potential field methods are the primary tools of geophysical prospecting, and may reveal the presence of large sedimentary basins that can be subsequently investigated using advanced 2D and 3D seismic methods to identify particular target structures. Conventional seismic interpretation implies picking and tracking laterally consistent seismic reflectors for the purpose of mapping geologic structures, stratigraphy and reservoir architecture. In this thesis, 2D seismic reflection data, in combination with ground gravity and magnetic (airborne combined with draped satellite) datasets are used to understand the structure and stratigraphy of the Ajdabiya Trough.

3.2 Potential Field Data

Potential field data are generally acquired within offshore and onshore sedimentary basins, by means of ground, ship, aircraft or satellite surveys. Both airborne and shipborne surveying

produce much higher resolution datasets compared to satellite surveys, which usually focus on acquiring data on a regional and global scales.

Gravity and magnetic surveying measures the variation of the Earth's gravitational and magnetic fields due to differences in the density and magnetic susceptibility of the sub-surface geology, respectively. Gravity anomalies might be considered as an indication of a change of structural relief or lateral variation of composition within the basement or sedimentary sequence, such as might be caused by the presence of volcanic rocks, intrusive igneous rocks or other higher/lower density rock units. Magnetic anomalies might be considered to be related to the presence of magnetic crystalline basement or other magnetic materials (such as volcanic rocks) at shallow depths within a sedimentary basin. The composition of crystalline basement rocks is generally complex and lateral compositional changes can result in lateral susceptibility contrasts (Talwani et al., 1959; Blakely et al., 1999; de Castro et al., 2007) and hence magnetic anomalies. Both gravity and magnetic anomalies can therefore be attributed to geological variations in the Earth's crust.

Key uncertainties associated with the application and interpretation of gravity and magnetic methods include (Telford et al., 1990**)**:

1- The uncertainty in the determination of source parameters of both methods.
2- Basement heterogeneity leading to interference between anomaly sources.
3- Low amplitude anomaly signatures caused by the presence of homogeneous semi-infinite bodies.

Several processing and modeling approaches have been proposed to overcome these limitations, with different degrees of success. The potential field data can be combined with 2D&3D forward modelling, shallow core, deep borehole, and 2D & 3D seismic reflection data for better prediction of subsurface structures such as crustal structure, basement relief and faults.

3.2.1 Gravity Data

Gravity data provide a set of tools to interpret large-scale basin-wide studies using information about rock densities. Based on wide range of density distributions, geologists can make inferences about the distribution of strata and other structures. Collected gravity data is processed and assigned to a reference level, typically the mean sea level. The data acquired in

any survey area must go through a series of corrections before it can be interpreted, because the gravity field at a point is affected not only by subsurface material, but also contributions from other factors such as surface topography, tidal effects, latitude, and elevation, and errors/drift in gravity instruments deflections (Telford et al., 1990, and references therein).

In sedimentary basins, an elevation correction must be applied for the gravity data, either by the free air correction (which is generally used in marine surveying) or the Bouguer correction, in addition to corrections applied to variations in terrain (topography) and latitudes.

The free-air correction (*FAC*) allows for a reduction in the magnitude of gravity with increasing height above sea level. In other words, it corrects for the decrease in gravity with height in free air resulting from increased distance from the centre of the Earth, according to Newton's Law. To reduce to datum an observation taken at height *h* (Figure 3.1a), the free-air correction is represented as:

$FAC = 3.086hg$ (*h* in metres)

Where g is the gravity unit in $\mu ms^{-2} = 10^{-1}$ milligal (mgal).

The Bouguer correction (*BC*) accounts for the low density of sea water that is effectively replaced on land by an equivalent thickness of rock with a specified density (Figure 3.1 (b)). It is used to remove the effect of the rock mass by approximating the rock layer beneath the observation point to an infinite horizontal slab with a thickness equal to the elevation of the observation above datum. If ρ is the density of the rock, then:

$BC = 2\pi G\rho h = 0.4191\rho h$ g

($2\pi G\rho h$) *is the Bouguer slab correction (gravity anomaly), h in meters,* ρ in Mgm^{-3}.

The corrected gravity reading using the Bouguer correction is often referred to as the Bouguer anomaly which is generally expressed in mgals (1mgal = $10^{-5}\ ms^{-2}$) or gravity units (1GU = 0.1 mGal).

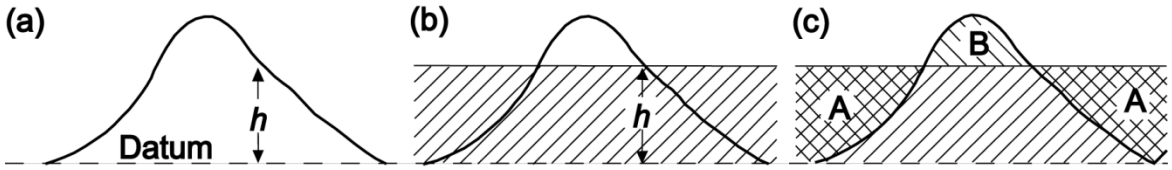

Figure 3.1: (a) The free-air correction for an observation at a height *h* above datum. (b) The Bouguer correction. The shaded region corresponds to a slab of rock of thickness *h* extending to infinity in both horizontal directions. (c) The terrain correction.

3.2.2 Magnetic Data

Magnetic anomalies are largely caused by the gradients produced by susceptibility boundaries. Magnetic susceptibilities of sedimentary and crystalline basement rocks are desirable for any magnetic data interpretation. Unfortunately, no magnetic susceptibility measurements are currently available for the rocks of the Ajdabiya Trough.

The juxtaposition of rocks with contrasting magnetic content may arise from a number of scenarios:

1. Lateral variation of magnetic content within a lithologic unit;
2. Fault movement, which may juxtapose rocks of differing susceptibility across the fault boundary;
3. Fluids preferentially moving along fault boundaries to either oxidize existing magnetic material, destroying the magnetic susceptibility, or the deposition/*in situ* chemical alteration of existing phases to magnetic minerals;
4. Structural juxtaposition bringing two different lithologic units adjacent to each other, i.e., isoclinal folds;
5. Migration of hydrocarbons to near surface areas forming magnetic minerals in the overlying sediments.

Magnetic anomalies could arise from the presence of magnetic crystalline basement or some other magnetic materials (e.g. volcanics) within the sedimentary sequence. The composition of the basement is generally complex and lateral composition changes can result in lateral susceptibility contrasts and hence magnetic anomalies. This and the bipolar nature of magnetic anomalies add to the complexity of interpreting magnetic data. In addition, the shape and intensity of the resultant magnetic anomaly, all other things being equal, depends on the location of the source within the Earth's magnetic field.

The interpretation of gravity and magnetic data can be aided by the application of several advanced processing, imaging and depth estimation techniques. These are discussed below. These techniques have been applied in this study with the principle aim of adding to the understanding of the regional tectonics and structures and calculating the depth to Precambrian – Late Palaeozoic basement beneath the Adjabiya Trough. The success of the

various techniques can vary often from area to area dependent on a number of factors such as data quality and coverage and the type of geological features giving rise to the anomaly.

Reduced to the pole magnetic anomaly: the reduction to the pole operation transforms a magnetic field to that which would arise from the same source placed at the north magnetic pole, i.e. it removes the bi-polar nature of the magnetic anomaly resulting in a single anomaly directly over the causative body.

Pseudo gravity: the pseudo gravity operation transforms a magnetic field to the gravity field which would arise from the same source geometry if the source magnetisations were replaced by geologically reasonable density contrasts.

Total horizontal derivative: this operation measures the rate of change of field in the X and Y directions and creates a resultant grid. This has the effect of highlighting high gradient areas such as might occur at faulted boundaries. Viewed on a regional scale it is useful for delineating structural trends.

Vertical derivative: this operation measures the rate of change of field in the Z direction. Again this has the effect of highlighting possible fault trends and has the effect of amplifying the near surface anomalies at the expense of the deeper anomalies. The horizontal and vertical derivatives of the gravity and magnetic data were used for detailed lineament analysis.

Analytic signal (total derivative): this operation is the Pythagorean sum of the X, Y and Z derivatives. This transform was particularly useful in delineating changes in the character of the magnetic field and hence in zoning the terrains of the Precambrian basement.

3D Euler deconvolution: Euler deconvolution was applied to the magnetic data to help determine the location and depth of causative bodies and help to further highlight trends. It can also be applied to the gravity data for the estimation of depth and location of bodies with density anomalies. Euler deconvolution is a method of solving Euler's Homogeneity equation for potential fields (Thompson, 1982). It can be expanded to work on gridded potential field data, a full discussion of which is given in Reid et al. (1990).

Spectral depth estimation: spectral depth estimation was used to determine the depth of specific causative bodies. It has been used in this study to estimate average depths of causative bodies, such as basement blocks, within the Ajdabiya Trough.

2D gravity and magnetic modelling: the gravity and magnetic responses of ten geological profiles have been forward modelled to attain a fit between calculated and observed gravity

and magnetic. The depth information in the models was constrained by well data and the sedimentary densities were estimated from well log analysis, magnetic susceptibility values were obtained from published studies. The results of the gravity and magnetic modelling are discussed in chapter 4 as appropriate.

3.3 Seismic Reflection Data

Seismic reflection surveying is the most commonly conducted geophysical technique and has been used since the 1930's. The technique has been applied to investigate hydrocarbon traps in upper crustal structures within sedimentary basins with depths of penetration in the order of several kilometres. There is a wide range in technical literature available upon seismic reflection surveying as a very large amount of research and development has been carried out within the hydrocarbon industry (Reynolds, 1997).

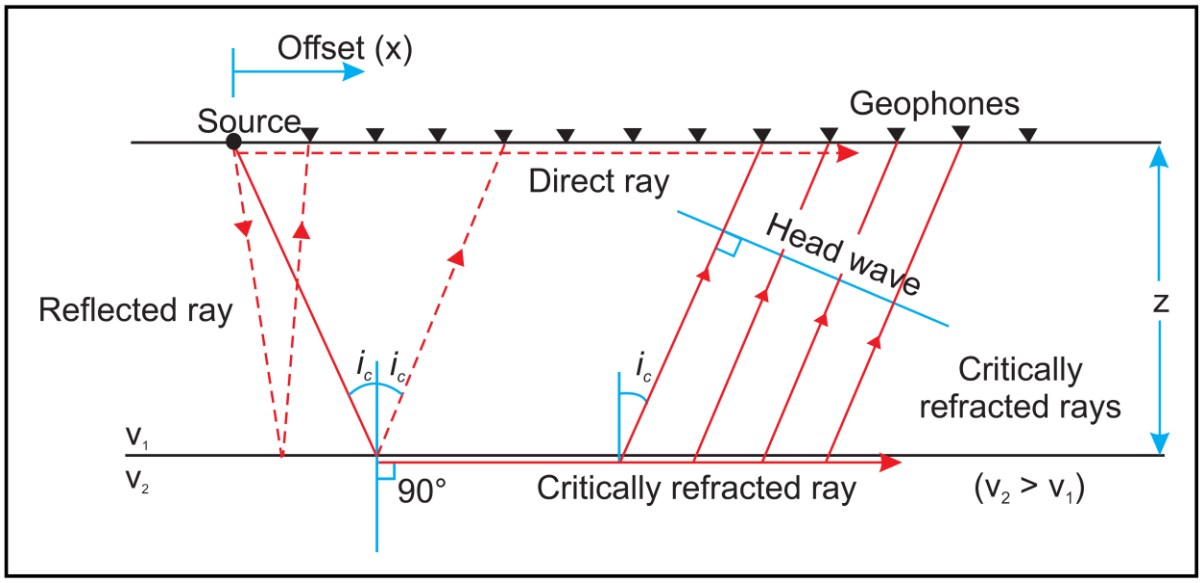

Figure 3.2: Raypath diagram showing a respective diagram for direct paths from source and reflected, rays up to geophones at the surface. The behaviour of a wavefront as it meets an interface of two media with contrasting acoustic impedances based on velocities V_1 and V_2. The angle of the incident wave (i_c) is the same to the reflected wave in an isotropic media. Obtained from Reynolds, (2011).

The basic concepts involve measurement of the time taken for seismic energy to travel from source (e.g. Vibroseis, air or water gun**)** at or near the surface, through the ground to an acoustical discontinuity between two lithologies of contrasting densities and velocities, and back up to a receiver or series of receivers (geophone or hydrophone) on the ground or sea

surface (Figure 3.2). The time required for seismic signal to travel from its source to a reflector and back is known as the two-way travel time (TWTT), and it is measured in milliseconds (ms) (equal to 1 x 10^{-3} seconds). An important step in seismic method is seismic processing which generally involves taking an acquired seismic data through a series of processing steps or processing sequence in order to produce finally processed seismic image.

The primary processing steps (Figure 3.3) are gain correction, trace editing, static correction, deconvolution, stacking, and migration and this is the order of their application in conventional processing. In areas of complex structure or where we are searching for more subtle traps, migration is done before stack.

A seismic trace consists of signal plus noise. The signal is that component of the seismic trace that contributes useful information to the interpretation of the seismic data. Seismic noise is both random and coherent. The procedures of seismic data processing are used to enhance the signal and to remove the noise from the seismic data. There are five main types of corrections and adjustments used in seismic processing: time, amplitude, frequency-phase content, data compressing (deconvolution), and data positioning (migration).

The objective of these processes is to properly align the data (statics and normal moveout), increase the signal-to-noise ratio (filtering, stacking), increase temporal (deconvolution) and spatial (migration) resolution, and to remove unwanted coherent noise (F-K, mute, tau-p transformation) (Yilmaz, 1987). The remaining signal can, depending upon the quality of the seismic data give a great deal of information about the sub-surface geology. Noisy data obscures this information. The geologic information desired from seismic data is the shape and relative position of the geologic formations of interest. In areas of good data quality it is possible to produce estimates of the lithology based upon velocity information." (Savit and Dobrin, 1988).

3.3.1 Convolutional Model of Seismic Data

The convolutional model of seismic data is used to provide a theoretical basis for seismic data processing. In this model the earth is modeled as a series of discrete layers. At the boundary of each layer we derive an impedance response based upon the physical properties of the earth. This sequence of impedance responses is combined to produce the earth's impulse response (Yilmaz, 1987).

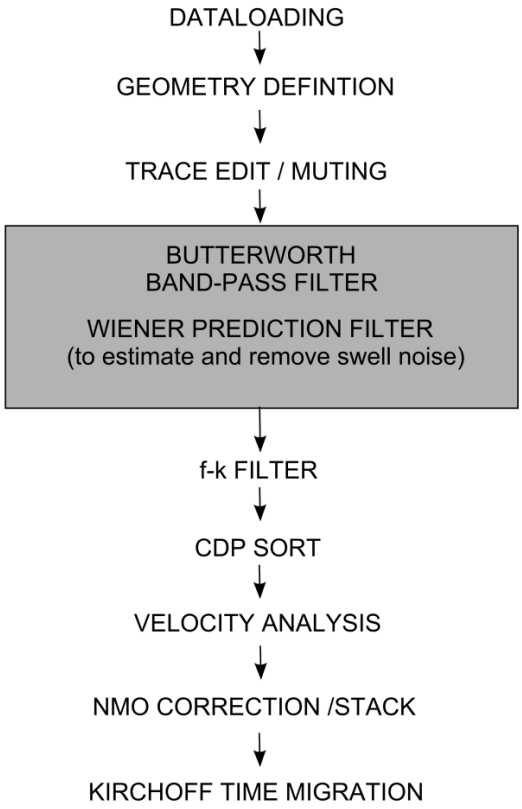

Figure 3.3: Processing steps applied to conventional seismic using Butterworth and Wiener filter processing flows (Yilmaz, 1987).

The input energy can be modeled as a wavelet. The convolution of the wavelet with the impulse response plus the addition of random noise is the basis of the convolutional model and can be described by

$x(t) = w(t) * e(t) + n(t)$

where

x(t) is recorded seismic trace

w(t) is seismic wavelet

e(t) is the earth impulse response

n(t) is the random noise

To this simple model we can add coherent noise, spherical divergence, attenuation, multiples, diffractions, refractions, and anisotropic effects to create a very complex model.

This more complex model can be represented by

$x(t) = w(t) * e(t) * a(t) + n(t)$

Where

a(t) is the coherent noise

From this model we can see that the goal of processing is to remove the effects of the source and noise from the recorded seismic data, leaving the impulse response of the earth. This represents the geology of the earth.

3.3.2 Preprocessing

This part of the processing sequence includes a description of the acquisition geometry of the line and initial gain corrections to compensate for propagation and spreading of seismic waves in a spherical manner (spherical divergence) and attenuation. Sometimes the data are filtered prior to deconvolution to remove noise using either a bandpass filter or linear filters like F-K filtering.

Gain correction – increases the amplitudes that are reduced due to absorption and geometrical spreading of the energy from the point source as a function of time.

Trace Editing – Removes incorrect data such as bad traces in order to improve the signal-to-noise ratio.

Statics corrections – removes the near surface effects by removing the travel time differences from trace to trace to improve signal to noise ratio due to elevation and weathering layer changes, the data must be corrected to a reference datum.

Signature deconvolution – removes the source wavelet effect to increase the resolution of the seismic dataset such as the removal of bubble pulses from airgun sources in marine surveys.

3.3.3 Deconvolution

Deconvolution improves the temporal resolution of the seismic data. Deconvolution uses the autocorrelation of the seismic trace to derive an inverse operator to compress the seismic data.

3.3.4 Stacking

Seismic data is acquired with many traces that reflect from a common midpoint (CMP) (Figure 3.4), each trace having a different shot/receiver pair. The data from a CMP is added together, after appropriate corrections, to increase the signal-to-noise ratio of the seismic data. The main processes prior to stack are velocity and statics.

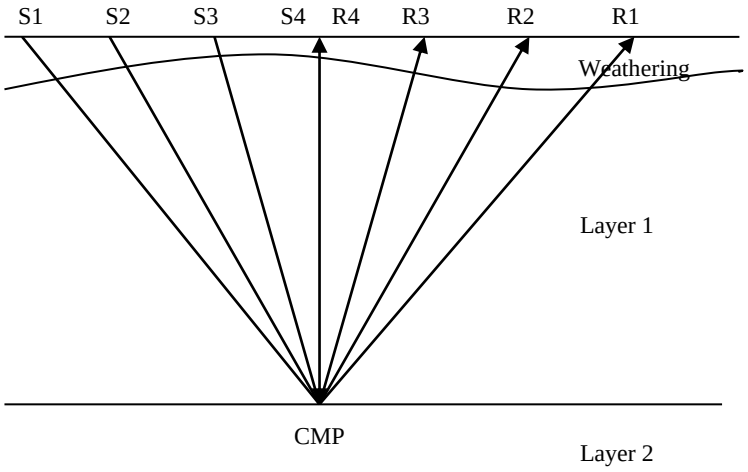

Figure 3.4: CMP (from Yilmaz, 1987)

Prior to stacking we must compensate for the portion of the travel path that is through the weathering layer and for the different distances that the energy travels through the earth due to shot/receiver offset. The CMP gather (Figure 3.5) at the right is a simple seismic experiment. There are three horizons that produce the events seen at 500 ms, 1000 ms, and 1500 ms. There is some background noise that mostly obscures the event at 1500 ms. In addition there are unresolved statics on this gather. This can be seen as the small shifts on the events. The offset range for this gather starts at 25 m and extends out to 2375 m. Figure 3.6 shows the statics applied to the CMP gather. After this application the seismic events show a smooth curvature. Statics are usually not a concern in marine processing. The sea bottom is generally very uniform and the geologic layers very slowly in thickness and velocity. Land surveys, such as carried out in the Ajdabiya Trough, often have very large statics and this is a very important step in the processing of these data.

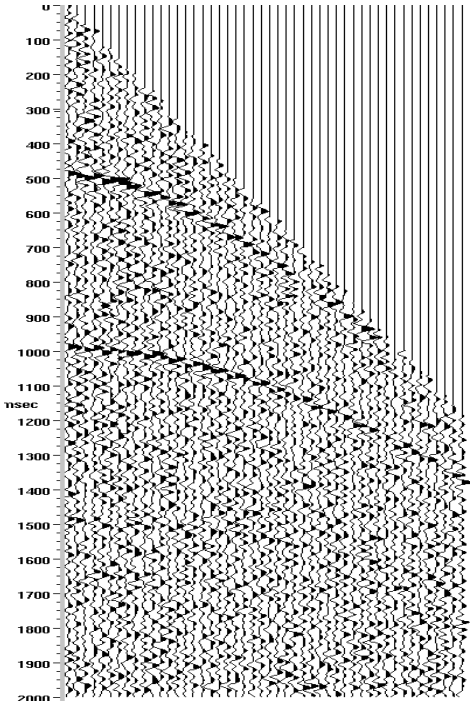

Figure 3.5: Synthetic data (Yilmaz, 1987)

The moveout that can be seen on (Figure 3.7) is described by the following equation.

$$T_x = \sqrt{T_o^2 + \frac{X^2}{V_{RMS}^2}}$$

Where

T_x = Time at offset X

T_o = Time at offset Zero

X= Offset

V_{RMS} = Root Mean Square Velocity

RMS velocity is related to the interval velocity and can be used to get an estimate of the geologic velocities for depth conversion.

Figure 3.5 shows the application of normal moveout. The seismic events are now lined up at 500 ms, 1000 ms, and 1500 ms. The events are now positioned properly to allow us to stack the data.

In practice, the velocity used in processing is called a stacking velocity which is related to the RMS velocity by the cosine of the geologic dip on the horizons.

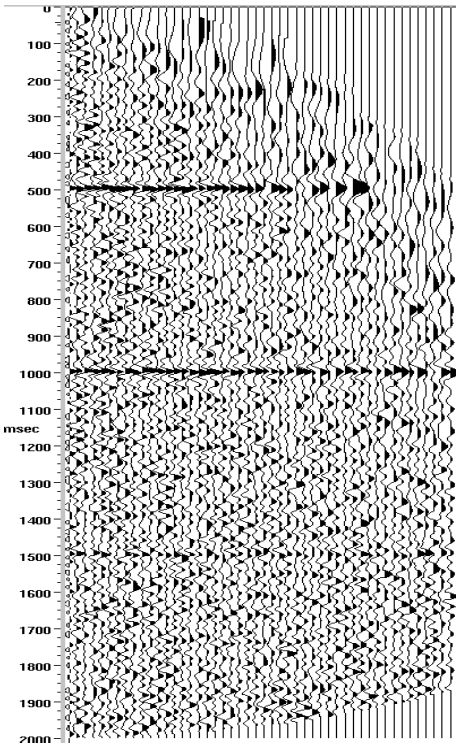

Figure 3.6: Statics applied (Yilmaz, 1987)

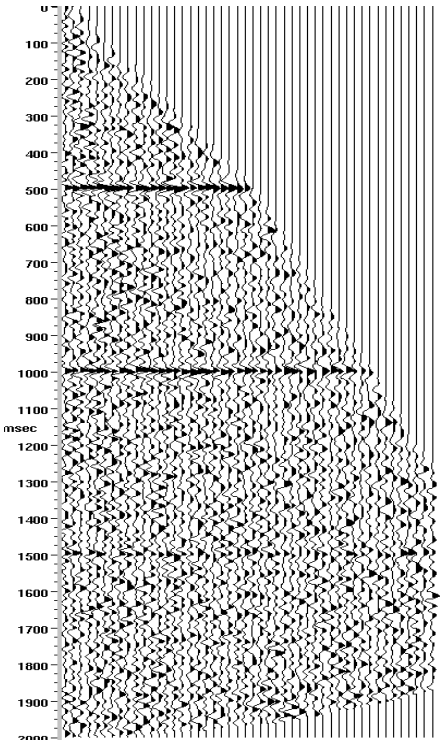

Figure 3.7: Normal move out applied (Yilmaz, 1987)

Prior to stack we removed the distorted data that appears at far offsets and shallow times on (Figure 3.6). The stacked section is supposed to represent a zero-offset section and this data has been seriously distorted and must be removed prior to stack as shown on (Figure 3.7). It can also be useful to apply an inner trace tail mute to remove near-zero offset multiple energy which is not well-suppressed by the F-K demultiple or stack. The stacked section (Figure 3.8) at the right clearly shows three events. The weak event at 1500 ms has been enhanced enough that it can be easily interpreted.

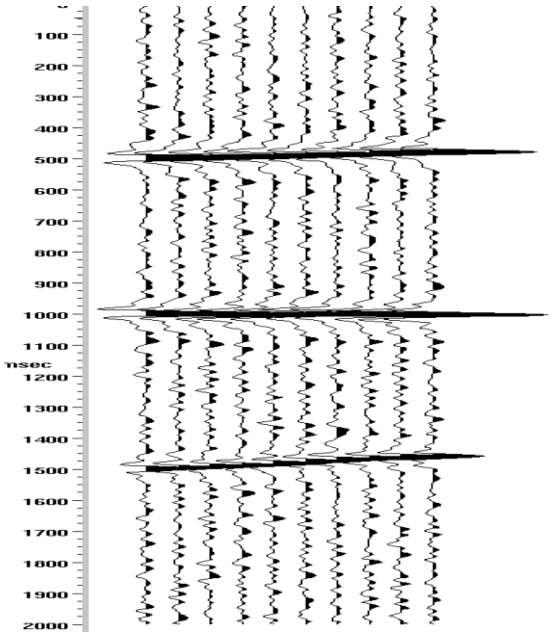

Figure 3.8: Stack section (Yilmaz, 1987)

3.3.5 Filtering

During seismic wave propagation, some frequencies do not carry seismic information and in this case will clutter the section with extraneous noise. Much of this unwanted information can be eliminated by using a frequency filter to pass the frequencies containing the seismic information. Many types of noise have the same frequency range as the seismic data so that this type of filter will not eliminate the noise without damaging the signal.

Some types of noise can be separated from the seismic data via a two dimensional filter. Examples of these types of filters are F-K filters and radon transforms work in this way. Stacking is also a two dimensional filter and is the most powerful filter available to the processor (Yilmaz, 1987).

3.3.6 Migration

Figure 3.9: Model of migration problem

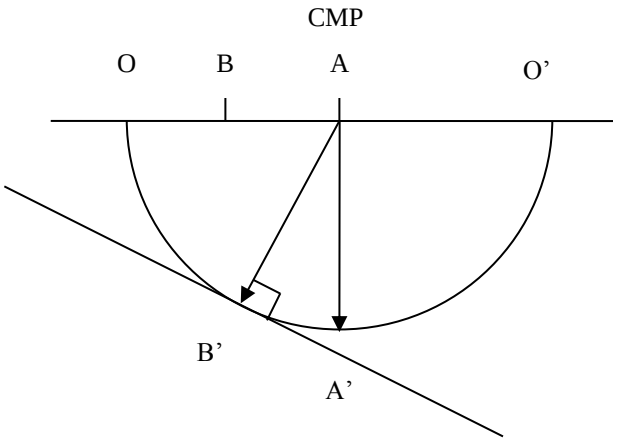

Migration is the process that determines the true spatial position of reflecting interfaces on the seismic section. In the presence of dip, the true reflection point is not the common mid-point but is updip from this location. The data is assumed to be located at the CMP position (Figure 3.9) and it must be moved to the correct location underneath station B. If we have a source and receiver located at station A on the surface the true reflection point will be located at B' for the boundary shown on this figure. This is the point at which the interface between the two layers is tangent to the half circle O – O'. The arc defines the position of all possible locations of the signal recorded at station A.

On reflection time profiles the attitudes of inferred fault traces and other non-registered geological elements are usually in conflict with the above definition of migrated time. This is due to the fact that the interpreter's concept with regard to the true shape of these features in the depth domain is commonly copied in the migrated time domain with disregard of the effects of the scale conversion (Kleyn, 1983). Figure 3.10 is a synthetic example showing the incongruity of migrated depth and migrated time configurations.

Seismic techniques use the coherency image to mask any original migration in order to get a coherency enhanced focused migration for different levels within the section. This image will provide an accurate depth profile for any interesting features such as basement involved normal fault systems (Hatton et al., 1986, Savit and Dobrin, 1988).

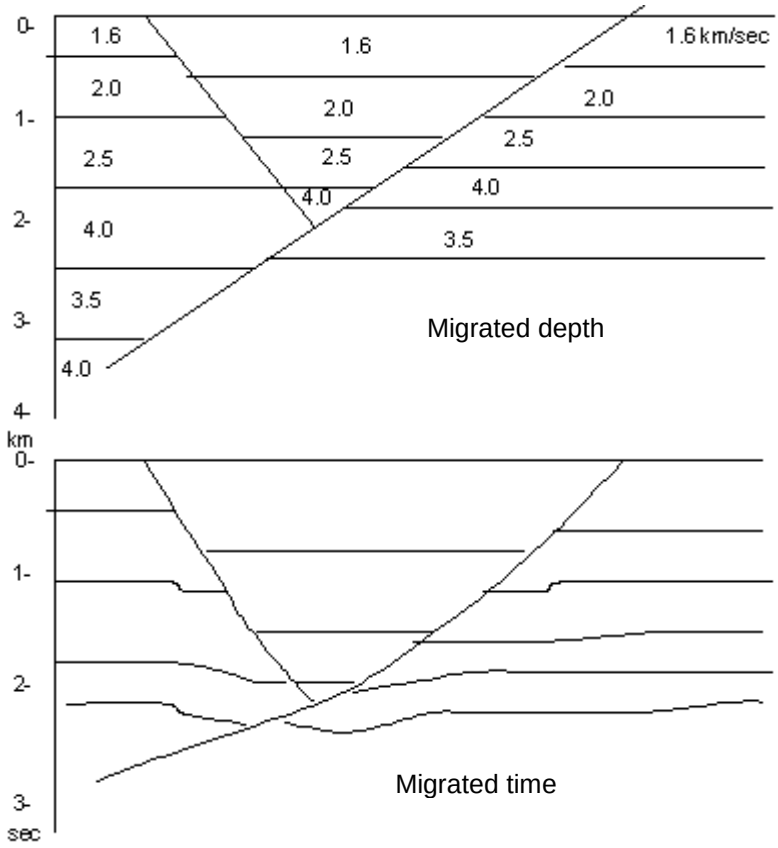

Figure 3.10: Migrated time from migrated depth (adapted from Kleyn, 1983).

3.3.7 Improving the Display of the Processed Seismic Dataset

A band pass filter is applied to remove both low and high frequency noise that was created by the earlier steps in order to compromise between seismic resolution and the noise effects. After validation applied to the data, it then scaled to a suitable level for display. The most common application of seismic reflection technique is the determination of subsurface geology and estimating the depth to bedrock at a much higher resolution to what potential field data is capable. This is due to the large contrast in seismic velocity between intact bedrock and unconsolidated superficial deposits. The most important problem in seismic reflection surveying is the conversion of two way travel times (time domain) to depths (space domain). The link between time and depth is seismic velocity, a parameter which is not simple to define.

3.4 Well Data

Well logging or borehole logging is the practice of making a detailed record of the subsurface geology penetrated by a borehole but is expensive compared to the aforementioned geophysical methods. A variety of datasets are obtained from wellbores, e.g. cutting-logging, core-logging, petrophysical logging and geophysical logging etc. It is a key technology in the petroleum industry and widely used for exploration activities.

Rock cuttings brought to the surface by a circulating drilling mud while drilling and can be used to understand information about the lithology at each stage of drilling process, and fluid content of the borehole while drilling with an interpretation made as to which stratigraphic interval each sample belongs. Core samples obtained from wells can lead to improved interpretations of sedimentological systems, depositional environments and give a better understanding of small-scale fault and fracture orientations which are not visible on seismic reflection data. Other data obtained from wells are based on geophysical wireline well logs that employ continuous recording of a geophysical parameter along a borehole. For example, the resistivity log measures the resistance to an introduced current flow between two electrodes and show continues plot of formation resistivity from bottom to top of the well. Gamma ray logs also record the amount of natural gamma radiation emitted by the rocks surrounding the borehole.

Common geophysical logs include calliper, gamma ray, single-point resistance, spontaneous potential, normal resistivity, sonic, density, electromagnetic induction, fluid resistivity, temperature, neutron, etc. Geological interpretations are mainly deduced from variations obtained from these measurements such interpretations may include identifying stratigraphic sequences (Rider, 1991). One of the first pieces of work involving the application of wireline logs to sequence stratigraphy was that of Van Wagoner et al., (1990).

The wireline logs are often displayed in the form of composite Log which is defined as a set of curves, usually depth-matched and spliced (joined) so that measurements are available over the greatest possible depth interval within a given wellbore. When combined with final well report, the composite log can give important information which can help in prediction of geological models of the area.

Seismic data are recorded and commonly interpreted in vertical two-way time; well logs, measured in depth, must be tied to seismic using a time-depth curve in order to provide a

known data point from which subsurface interpretations can be made. Sonic log measurements and density logs are combined to produce an impedance model which can be ray-traced and convolved with a basic seismic pulse to create a synthetic seismogram that can be compared directly with the observed seismic data.

3.5 Datasets Used in This Study

The data used in this study were primarily gravity and magnetic data and around 10,000 km of 2-D seismic reflection profiles and information from over 20 wells (Figure 3.11) and (Table 3.1). These data were provided by the Shell Exploration and Production Libya GmbH as part of collaborative work with the National Oil Company of Libya (NOC). Seismic data were mainly migrated 6.0 seconds TWT SEGY digital records, collected using Vibroseis sources during the 2005 and designed for deep target structures but suited to image shallow structures also. The seismic acquisition layout is designed to include symmetrical 480 channel split spread, 25 receiver-group spacing, 6km maximum offset, and a vibroseis shot interval of 25m. Additional data (red lines on figure 3.11) is provided by Petro-Canada Libya.

In order to investigate the tectono-stratigraphic evolution of the Ajdabiya Trough, selected exploration wells were analysed, in order to correlate both regional and local stratigraphy with the seismic data (Figure 3.11).

Data from the exploration wells (Table 3.1) includes.

1- Well reports from previous companies working in the Sirt Basin
2- Wireline data includes the typical industry dataset

- Gamma Ray (GR)
- Spontaneous Potential (SP)
- Density (RHOB)
- Sonic (DT)
- Lithology and rock type

Formation top data were available for all wells, with wire-line logs available for around a quarter of the holes.

The gravity and magnetic data set has kindly been made available by the Libyan Petroleum Institute (LPI). The gravity data consists of Bouguer anomalies onshore (Figure 3.12) compiled with a reduction density of 2.67 g/cm^3, and using the 1980 formal ellipsoid formula.

The process of preparing a gravity compilation of Libya was started in 1992 with data gathering and preprocessing carried out mainly in Libya under the project named "Libyan Gravity Compilation". The final project in this compilation was formally agreed in a contract signed 20 July 2000. The project comprised addition of new data, correction, compilation and integration of data, map production for the whole country and subareas, interpretation, and report preparation for whole Libya and subareas.

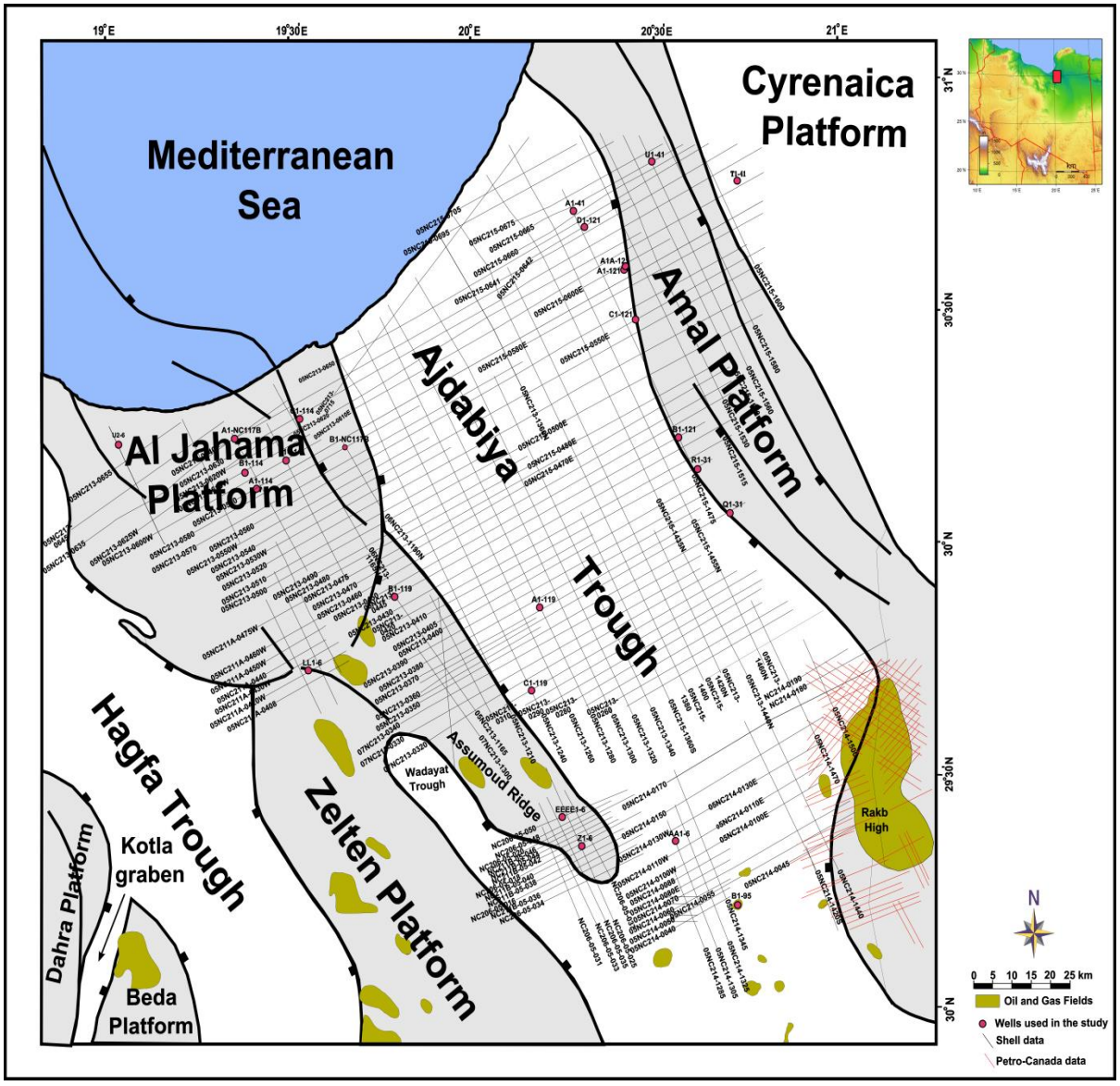

Figure 3.11: 2D seismic and well database map showing locations of selected data sources used in this study. Wells used in this study are marked in red.

Well Name	UTM		TD (m)	Formation	Logs Available
	X	Y			
A1-12	514674	3222908	3033	Nubian.	Lithology and rock type
A1-41	430897	3397537	4180	U.C.	Lithology and rock type
A1-114	421818	3302612	2900	Gargaf. Fm.	GR,SP,DT, time/depth
A1-119	444286	3384636	4145	U.C. Tagrift.	GR,DT
A1-121	482630	3274649	2590	L. Eocene.	GR,DT
A1A-121	444369	3384436	3500	Gargaf. Fm.	Lithology and rock type, time/depth
A1-126	479725	3343332	3420	Basement.	Lithology and rock type
A1-NC103	436175	3279249	3400	Paleocene.	Lithology and rock type
A1-NC117B	352511	3343132	2823	Gargaf. Fm.	Lithology and rock type
A1-NC154	458485	3284611	4348	Maragh. Fm.	GR
A3-126	479725	3274653	3225	Nubian. Fm.	Lithology and rock type
A3-LP3C	488007	3343707	3450	Paleocene.	Lithology and rock type
B1-6	419982	3305770	2674	Nubian. Fm.	Lithology and rock type
B1-121	447341	3253034	3408	Gargaf. Fm.	GR,SP,DT
B1-119	384355	3283384	3308	Gargaf. Fm.	GR,DT, time/depth
B1-LP2E	488090	3252833	3000	Paleocene.	Lithology and rock type
C1-119	420065	3283183	3670	Paleocene.	SP
C1-121	447424	3371861	3780	Gargaf. Fm.	GR,DT
CCC1-6	453570	3227252	4600	U.C.	Lithology and rock type
D1-6	435968	3281419	3749	Paleocene.	SP
D2-12	518405	3304182	3004	U.C. Rakb C.	GR, DT
D1-114	328524	3334008	2740	Gargaf. Fm.	Lithology and rock type, time/depth
EEE1-6	318668	3307619	2639	U.C.	Lithology and rock type
F1-41	482720	3451543	2000	Paleocene.	Lithology and rock type
HHH1-6	405236	3232969	3383	Nubian.	Lithology and rock type
HHH1-59	361730	3302072	3000	Pre. U.C.	Lithology and rock type
I1-6	375604	3352587	4604	Paleocene.	SP, RE
K1-31	430747	3288262	4115	U.C.	Lithology and rock type
KK1-6	446375	3242397	4300	U.C.	Lithology and rock type
LL1-6	378678	3232771	3383	U.C.	Lithology and rock type
N1-31	514287	3356381	3116	Gargaf. Fm.	Lithology and rock type
NN1-6	471861	3232569	4048	U.C.	Lithology and rock type
Q1-31	451440	3325503	4648	Silurian.	GR, DT, DTL
QQ1-6	438047	3263523	3400	Paleocene.	Lithology and rock type
R1-31	463355	3336139	3994	Maragh. Fm.	GR, DT, DTL
U2-6	312056	3341639	2926	Gargaf. Fm.	GR,DT
U1-41	451523	3409243	5421	U.C.	GR,DT, time/depth

Table 3.1 – Summary of the onshore wells used in this study. Coordinate transformation from European Libyan Datum 1979 (ELD79) to WGS84, using the Geodetic Ellipsoid International 1924.

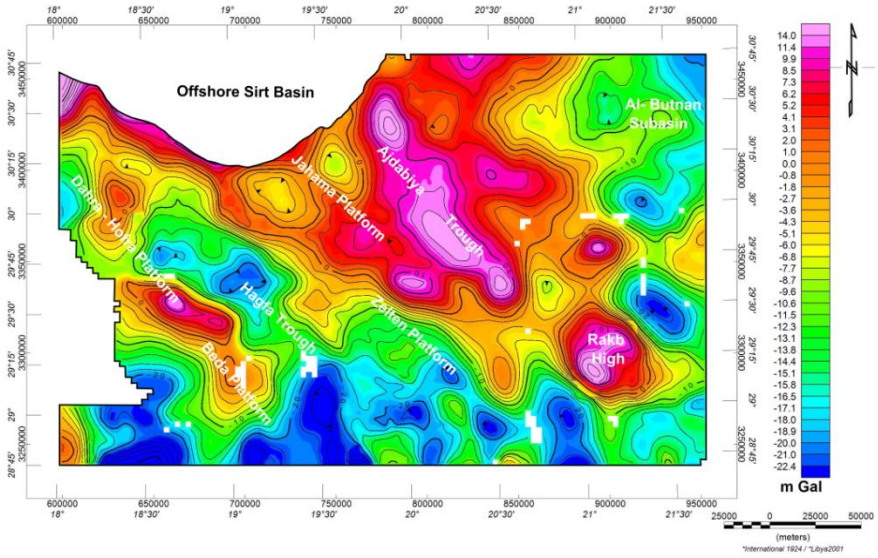

Figure 3.12: Bouguer gravity map of Sirt Basin with location of the Ajdabiya Trough

The magnetic data of the Ajdabiya Trough (Figure 3.13) is based on a compilation of aeromagnetic survey data merged with draped satellite data. The data provided by the Libyan Petroleum Institute were already in residual form, after subtraction of the appropriate reference field. Further processing was carried out for closer comparison with the gravity. Merging of the different datasets was done by the Geophysical Exploration Technology Limited (GETECH - Leeds), throughout the African Magnetic Mapping Project (AMMP). The compiled magnetic dataset has an average resolution of 1 x 1 km over most of Libya.

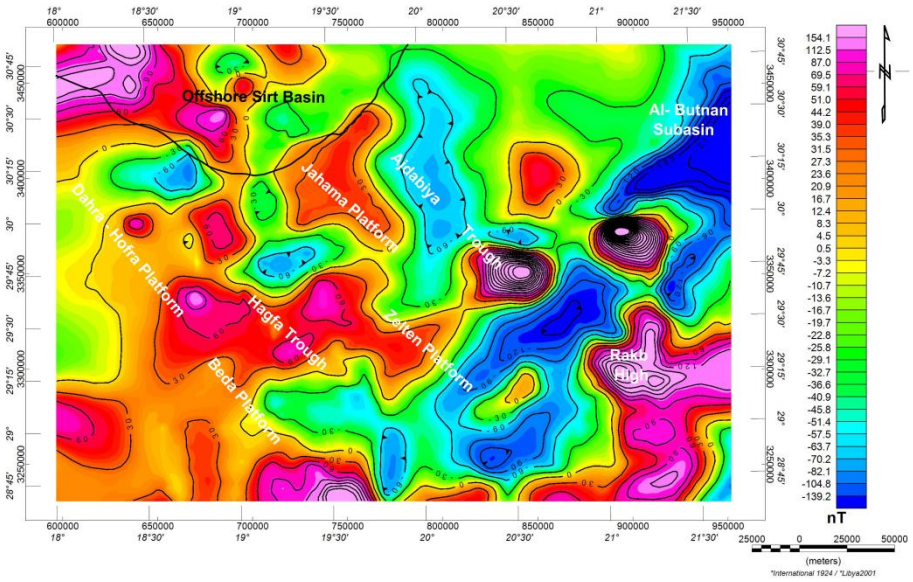

Figure 3.13: Magnetic map of Sirt Basin with location of the Ajdabiya Trough

The borehole data used in this study are based on hydrocarbon exploration well data (Table 3.1) obtained from the Libyan National Oil Company (NOC). Most of the boreholes are located over platform areas and structural highs around the Ajdabiya Trough and mainly bottomed within Upper Cretaceous strata. For the study purposes, the selected wells are chosen in the vicinity of the seismic profiles where possible in order to accomplish better seismic interpretation and gravity and magnetic modelling.

For the modelling purposes, no direct measurements of magnetic susceptibility has been done, in this case magnetic susceptibility data used in the magnetic modelling has been obtained from published articles and reports as introduced in chapter 4. In the same context the density of the sediments has been obtained from different sources, (The Libyan Gravity Compilation Project, 2001, Makris, and Yegorova, 2006, Casten and Snopek, 2006). Published values are

mainly based on analysis of well logs (density and sonic) and core sample analysis from the Sirt, Ghadames, Murzuk, Jefara and Cyrenaica areas (Essed, 1978). The density contrast was constructed by assuming a constant basement density of 2.67 g/cc and subtracting mean sedimentary densities as used in the 2D gravity and magnetic modelling.

3.6 Methodology and Software

The subsurface structure and stratigraphy of the Ajdabiya Trough were analysed using the data mentioned and described above. Interpretation of the seismic reflection datasets were carried out using commercial software (Landmark, Trap Tester, and 2DMove). For the gravity and magnetic interpretation, I used the Geosoft (Oasis Montaj) version 6.2.1.

3.6.1 2D Seismic Derived Surfaces

Six horizons were mapped on 2D seismic reflection profiles throughout the study area to produce time structure and time thickness (isochron) maps. The six horizons mapped are: (1) '*Late Cretaceous*' – base of the Cenozoic deposits; (2) Harash - Kheir Formation or its equivalent Upper Sabil Formation as the '*Top Paleocene*' (the post-Late Cretaceous deposits); (3) '*Lower Eocene*' (Gir Formation); (4) '*Middle Eocene*' Gialo Formation which considered to be the '*Top Eocene*', as it was difficult to resolve the Top Eocene Augila Formation using the available seismic data; (5) '*Top Oligocene*'; and (6) '*Top Miocene*'.

The preliminary age assignments of the sedimentary succession are based on calculation of time – depth relations and comparison with recent studies in areas close to the Ajdabyia Trough (e.g. El-Shari, 2008). The conversion from two-way travel time to depth used a number of velocity-depth functions through the sediment column. These were constrained from borehole data, and show a considerable spatial variation along and across the strike of the Ajdabiya Trough. An example is the A1-114 well which has been used in the calculations. The well is cut by the seismic line 05NC213-0590 and used as a start point for the horizons picking. The data used is shown in (Table 3.2) below.

The drafts of the time structure maps were compiled at scale of 1:1000 000. The final maps were produced digitally with the Oasis Montaj mapping system using a 500 m gridding interval. The maps are defined throughout the study area where possible with appropriate isochron maps equivalent to the thickness of the stratigraphic units.

The isochron maps are used to illustrate vertical time thickness variations between the mapped horizons throughout the Cenozoic and provide information on the distribution of the subsidence and sediment fill that shaped the Ajdabyia Trough area at different times during the Cenozoic and possibly related to thermal and/or tectonic affects (Gumati and Nairn, 1991; Janssen et al., 1995; Ahlbrandt, 2001; Hallett, 2002). It will also help in sequence stratigraphy and fault interpretations.

Depth subsea (m)	Formations/ reflectors	TWT subsea (ms)	Interval Velocity (m/s)
205	Top Carbonates	240	1715.655
258	Top Miocene	297	1832.174
800	Mid Miocene	706	2652.088
1352	Base Miocene	1176	2346.193
1637	Top Eocene	1380	2793.291
1995	Near Base Eocene	1578	3620.148
2499	Top Palaeozoic	1797	4607.417
2847	TD	1929	5268.195

Table3.2 Cenozoic reflectors, ages and interval velocities utilized in the depth-conversion of the Ajdabyia Trough based on data obtained from well A1-114 located at the northeastern part of the trough.

3.6.2 Interpretation of 2D Seismic Data

The aim of the 2D seismic interpretation was to develop a general overview of the structure and stratigraphy of the Ajdabiya Trough by viewing selected strike and dip sections across the study area. This provided a regional understanding of the subsurface structures and the location of major fault blocks in the area. Other orientations (dominant dip direction) were used to ascertain more detailed structural patterns. The basic interpretation of seismic horizons and faults has been carried out using the Landmark work station which was supported with a full suite of interpretation tools including autotracking, fault and horizon picking, etc. The second stage began with mapping selected seismic reflectors across the study area which mainly related to top of significant strata, unconformities, and main sequence boundaries. Interpretation of the subsurface is performed on suites of vertical seismic sections with structures being correlated from line to line to build up a map view of particular horizons. Picking horizons on every line was a labour-intensive task due to low data resolution in some places. Under ideal conditions, such as a continuous reflection that has

significantly higher amplitude than surrounding events, it might be possible to autotrack a horizon in a simple manner; otherwise a point picking option is used. Conversely, in areas of high noise or geologic complexity, it was difficult to autotrack the horizon in this case. The results of the autotracking were checked and manually edited where necessary.

Presumed syn-rift and pre-rift reflectors in fault related hanging-wall structures are the deepest reflectors mapped for limited areas related to particular rift related graben features. The top pre-rift reflector marked a seismic onlap surface separating well-defined, gently dipping reflectors of the pre-rift from the seismically transparent syn-rift strata. Within the syn-rift package of each fault block a top syn-rift reflectors were mapped. These reflectors are assigned to a likely Pre - Upper Cretaceous age. The interpreted reflectors defined the top and the bottom of the syn-rift sequences and have been used to describe the structure and the evolution of the graben and half-graben structures revealed by the syn-rift stratigraphy. Fault sticks have been picked along the 2D seismic lines. Fault surfaces were constructed by correlating fault sticks using interpretation processes in Landmark and the Traptester software following procedures described by Freeman et al., 1990 and summarized below in section 3.7.7. Usually more reliable descriptions of a faulted surface can be obtained if the three-dimensional properties of a fault network are observed directly (Willemse et al., 1996), but this has not been possible owing to the lack of 3D seismic reflection data. Fault traces picked on vertical sections can be used to model the fault surfaces, which are then viewed in perspective to give an immediate assessment of the plausibility of the interpreted fault geometry (Coffeen, 1984). The faults in the area were interpreted on each strike and dip lines. Dip lines strike approximately perpendicular to the northwest-southeast trend of fault strikes, allowing determinations of fault throws.

Displacement-distance profiles of the interpreted faults were constructed from the throws (in ms TWT) of the mapped reflectors. In addition, fault attributes and dip lines were used to constrain fault locations in two dimensions and to assess the occurrence of fault segmentation and linkage locations.

3.7 Faulting in Rift Basins

3.7.1 Basin Development and Geometry

Deposition within rift basins is largely controlled by normal faults that bound tilted blocks and half grabens (Roberts & Yielding, 1991). Asymmetric basins develop as a result of oblique extension (Withjack et al., 2002). Examples of such type of geometries have been extensively described from recent rifts (e.g. the East African Rift), based on variable data type and analogue models (e.g. Leeder and Gawthorpe, 1987; Lambiase and Bosworth, 1995; McClay et al., 2001).

Many workers have presented geometric and physical models of hangingwall collapse along vertical or steeply dipping shear surfaces (e.g. Withjack et al., 1995 and references therein), including pronounced shear along active fold hinges called axial surfaces which, are held at depth to fault bends and extend upward through syn-rift strata which commonly onlap pre-rift rocks (Xiao and Suppe, 1992; Shaw et al., 1999). Faults within an extensional domain often changing their polarity in response to changes in stress regime (Gawthorpe and Leeder, 2000; McClay et al., 2001). Thickening and fanning of syn-rift strata toward a boundary fault are important components of syn-depositional faulting (Schlische and Withjack, 1999). In a cross section oriented parallel to the boundary fault, the basin commonly has a synclinal geometry with occasionally rollover structures such as broad anticlines (Schlische & Anders 1996, Withjack et al., 1998).

As fault displacement and basin subsidence increases during continued extension, isolated fault segments interact and link to form through-going faults that control overall basin geometry and deposition (Gawthorpe et al., 1994; Gupta et al., 1998). The period of maximum subsidence and fault displacement rates along such through-going structures is referred to as the "rift climax" phase.

3.7.2 Fault and Graben Geometry

Most rifts consist of a system of half-graben shaped basins bound by system of normal faults, the polarity of which often changes along trend across accommodation zones (Rosendahl et al., 1992). The latter are characterized by complex fault geometries involving local positive and negative flower-structures and folding (Morley et al., 1990). Lambiase and Bosworth,

(1995) identified four distinct structural stages that control the rifts each with individual tectono-sedimentary responses, which include: 1) initial faulting; 2) development of half-graben morphology; 3) filling of half-graben; and 4) regional subsidence (Figure 3.14).

Rifts mainly developed with an approximate order of width of a few hundreds of kilometres where intense normal faulting generates horst-graben geometry. Such examples are the narrow rifts of the Rhine Graben, the Gulf of Suez, and the East African Rift (Buck, 1991; Davison, 1997).

Normal faults within rift basins are active during the deposition of sedimentary sequences they cut. Growth strata can be deposited in asymmetric depressions (the hanging-walls), while the footwalls are often uplifted and subjected to erosion and mainly controlled by several factors including, basin subsidence, location of the fault and any changes in eustatic sea level. Relative movement between hangingwall and footwall controls the sediment thickness across any fault with the thickest sediment thickness accumulated within the hanging wall indicating fault growth stage.

During fault movement, the oldest strata are generally subjected to long time period of fault movement compared with the younger one. In this case the amount of fault offset on any particular horizon is the accumulation of all fault movements following its deposition. The process will result in increasing the offset with depth with variations in offset from maximum at the centre to minimum or zero at the fault tips (Barnett et al., 1987; Walsh and Watterson, 1991). This produces the syncline-shaped basin in longitudinal section. In traverse section, the displacement of an initially horizontal surface that intersects the fault is greatest at the fault itself and decreases with distance away from the fault (Figure 3.14). This produces foot-wall uplift and hanging-wall subsidence, the latter of which creates the sedimentary basin. However, this basic geometry can be modified by fault propagation and forced folding (Gawthorpe et al., 1997; Withjack et al., 1998).

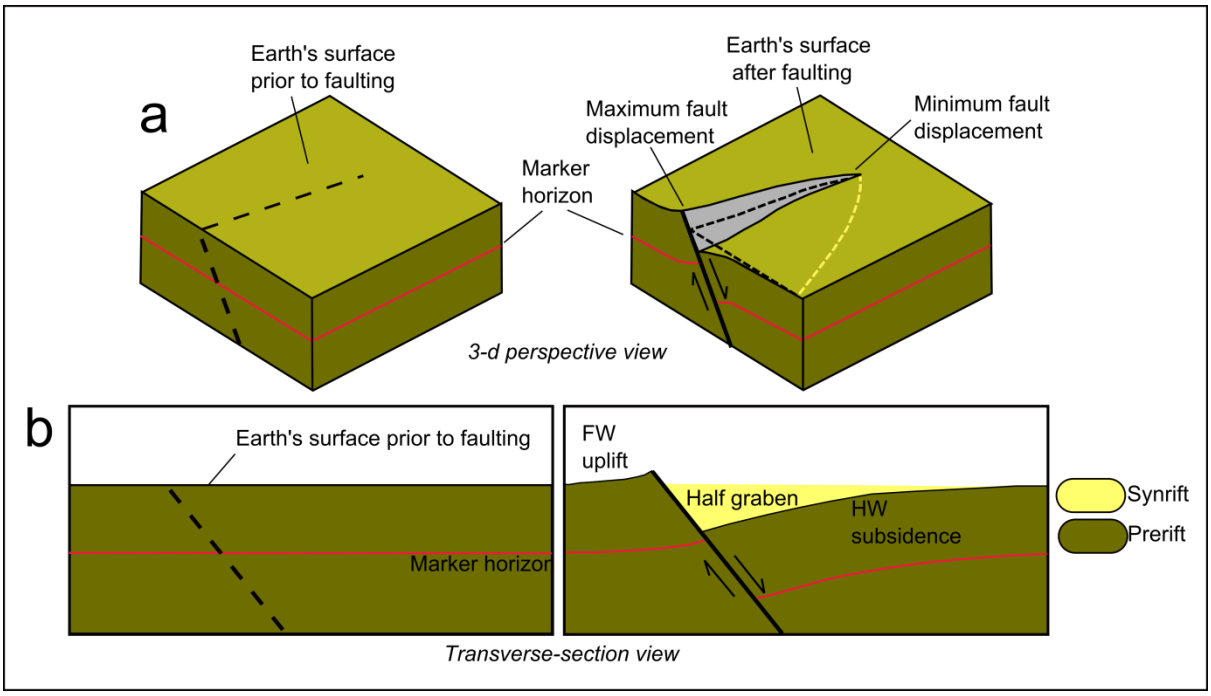

Figure 3.14: Fault-displacement geometry. (a) Perspective diagram before (left) and after faulting showing how normal faulting uplifts the foot-wall block and produces subsidence in the hanging-wall block. The yellow dashed line shows the outer limit of hanging-wall subsidence and marks the edge of the basin. Displacement is a maximum at the centre of the fault and decreases toward the fault tip. (b) Traverse section before faulting (left) and after faulting and sedimentation showing foot-wall uplift and hanging-wall subsidence, (redrawn from Withjack et al., 1998).

Some normal faults flatten with depth, causing collapse of the attached half-grabens and the formation of an inclined rollover panels (Figure 3.15), with growth strata thickening abruptly toward the fault above the rollover panels (Shaw et al., 1997). Geometric models of fault slip and hanging-wall collapse have been studied by Withjack et al., 1995, including pronounced vertical and steep shear along active fold hinges called axial surfaces are extend upward through pre-rift and syn-rift strata (Xiao and Suppe, 1992), and then subsequently deformed into kink bands or inclined rollover panels (Figure 3.15). Fault bend folds have long been recognized as forming due to slip along subjacent faults with flat-ramp-flat geometry in areas of thin-skinned deformation (Wilkerson et al., 2002; Kerr and White, 1994).

Progressive strain gives rise to a rotational subsidence of individual fault blocks. This accounts for the accumulation of wedge-shaped sedimentary units which expand towards the foot-wall fault and thin towards the leading edge of the hanging-wall blocks. As long as the lithosphere retains a certain amount of strength during rifting, the subsidence and uplift pattern of such fault blocks conforms closely to the flexural cantilever model (Kusznir &

Ziegler, 1992). An extreme form of listric faulting, controlling the development of core complexes, can occur during extension of originally thickened crust at high strain rates and stretching factors, involving ductile flow of the middle and lower crust (Bertotti et al., 2000).

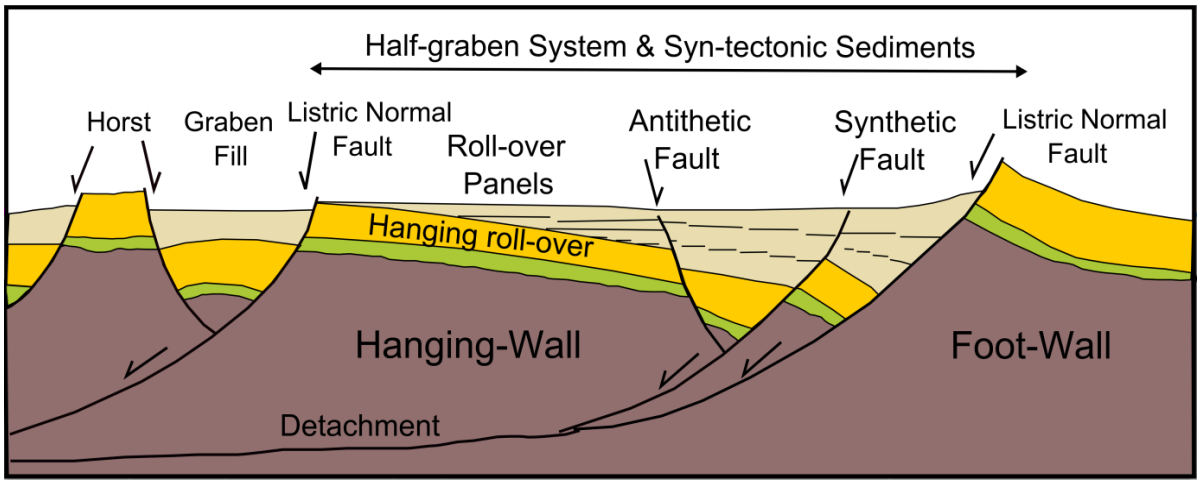

Figure 3.15: Schematic of cross section of normal faults in an extensional regime, (adapted from Burbank & Anderson 2001).

3.7.3 Fault Growth

Normal fault systems at all scales are commonly segmented (Jackson and White, 1989). Fault-segment boundaries are recognized by bends in the fault trace, overlaps, offsets, apparent deficits in hanging-wall subsidence, and differences in the age of faulting on either side of the segment boundary (Schlische and Anders, 1996; Gawthorpe et al., 1997). Faults in extensional basins may grow by the processes of radial propagation and/or segments linkage, (Figure 3.16) (e.g. Cartwright et al., 1995).

The characteristics of fault growth will determine the rate at which space is created in which sediment can be deposited, and also influence the resultant geometry of the infilling sedimentary bodies. Studies into the growth of individual faults suggest that displacement rates may increase through time due to the relationship between slip increment and fault length. This implies that if the rate of sediment supply remains constant through time, the potential for subsidence to outpace sedimentation will increase with the duration of fault movement (Waterson, 1986).

A fault growth model has been proposed by Watterson (1986) for a variety of faults by plotting maximum displacement against width:

$$D = W2/P \qquad (3.1)$$

Where D is maximum displacement, W is the maximum dimension of the fault surface normal to the slip direction and P is a variable relating to rock properties.

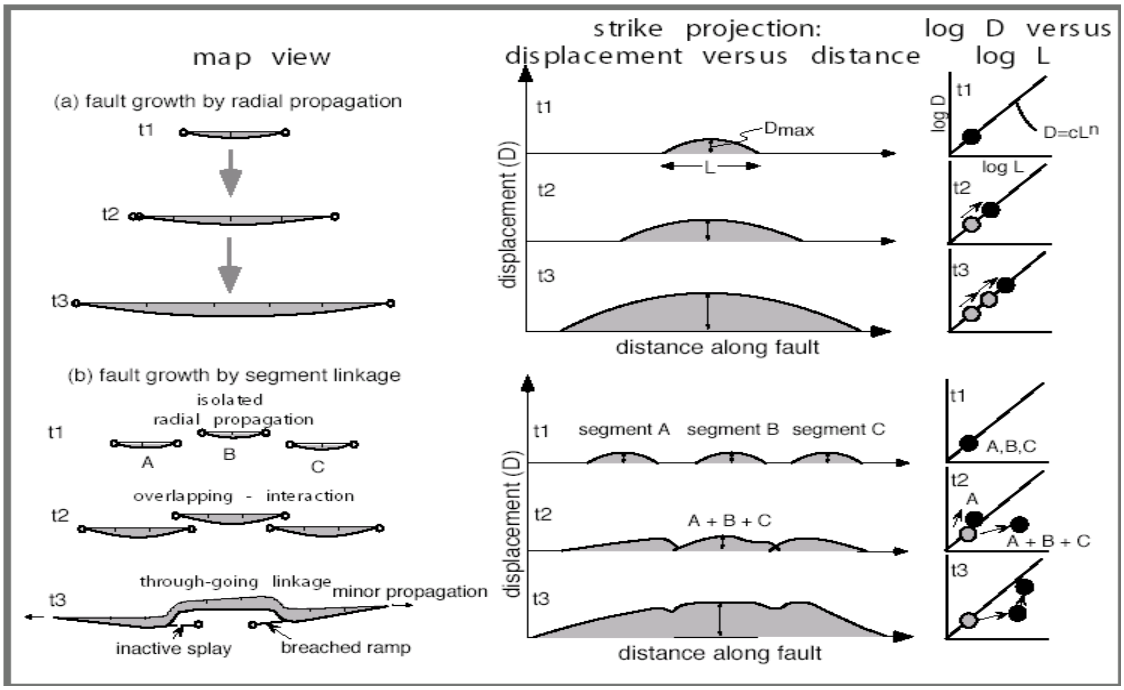

Figure 3.16: Schematic block diagram illustrating the alternative model of fault growth (a) Fault growth by radial propagation. (b) Fault growth by segment linkage. During fault growth by radial propagation, an individual fault simply lengthens and accumulates more displacement through time. Plots of displacement versus fault length (right column) show a steady increase in displacement as the fault grows. Map view on the left shows a different scheme for fault growth, whereby small individual faults gradually link up to create one large, and through-going fault. Whereas the accumulation of displacement follows a predictable path for the individual segments, when they link up, displacement becomes considerably less than that predicted for a fault of this length (see right-hand column). Through time, the slip deficiencies near the points of segment linkage are reduced. From Burbank & Anderson (2001).

Walsh et al., 2002 proposed an alternative model based on observations from syn-sedimentary growth faults. They hypothesised two fault growth stages, the fault growth during the first stage being largely controlled by the abrupt lateral propagation of the fault tips until full fault length obtained (Figures 3.16 and 3.17) while in the second stage the fault grows mainly by the accumulation of displacement where the fault length is established in its early history (Wilson et al., 2009). Patterns of fault growth and linkage are likely to be complicated where pre-existing basement fabrics and structures exert an influence on syn-rift structural development (Wilson et al., 2009). Interaction and linkage of faults with adjacent faults is

established during the early stage of fault growth. Synthetic faults which have the same polarity of dip of the main faults can overlap and act as a single coherent fault.

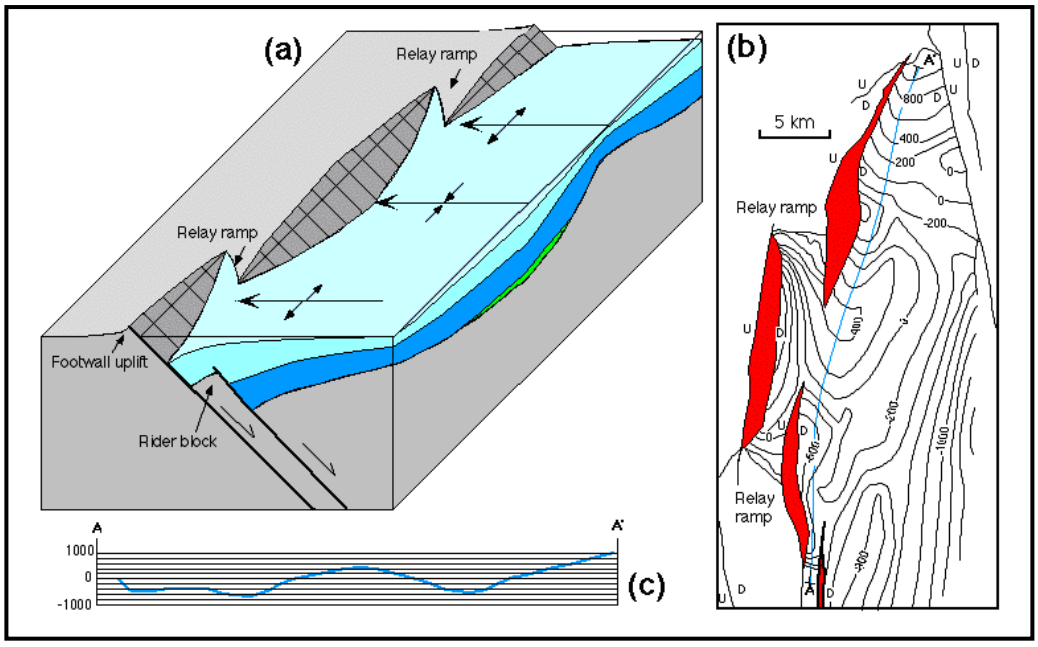

Figure 3.17: (a) Geometric relationship among a segmented normal fault system, relay ramps, transverse folds, and rider blocks, simplified from Schlische (1993). (b) Structure-contour map showing relay ramps between offset fault segments. (c) Longitudinal profile.

Fault segments within a larger array are commonly kinematically linked (Larsen, 1988; Morley et al., 1990; Peacock and Sanderson, 1991; Walsh and Watterson, 1991; Dawers and Anders, 1994; Trudgill and Cartwright, 1994). Discontinuous fault segments which are linked by ductile deformation of the fault volume, e.g. the transfer of displacement between adjacent fault segments of a segmented fault array is mostly accommodated by ductile strain in the form of a relay ramp, which develops in the overlap zone (Peacock and Sanderson, 1991) (Figures 3.17, 3.18 and 3.19). In perhaps the most common linkage involving overlapping faults, the displacement on one fault decreases with complimentary increase in displacement on the other; a relay ramp forms within the zone of overlap (Childs et al., 1995). Individual faults within the array display along-strike variations in fault displacement. However, displacement gradients are higher in the vicinity of overlapping fault segments (Trudgill and Cartwright, 1994). Fault segments have variable lengths and variable amounts of overlap and spacing in relay zones. The amount of mechanical interaction between adjacent fault segments

is affected by these parameters and is evidenced in the slip distributions and displacement fields (Willemse et al., 1996). Summed and contoured displacement profiles of two overlapping faults will give a more accurate picture of displacement patterns in regions of displacement deficit and resemble a model of an ideal isolated fault (Peacock and Sanderson, 1991; Walsh and Watterson, 1991; Childs et al., 1995), (Figure 3.18e,f).

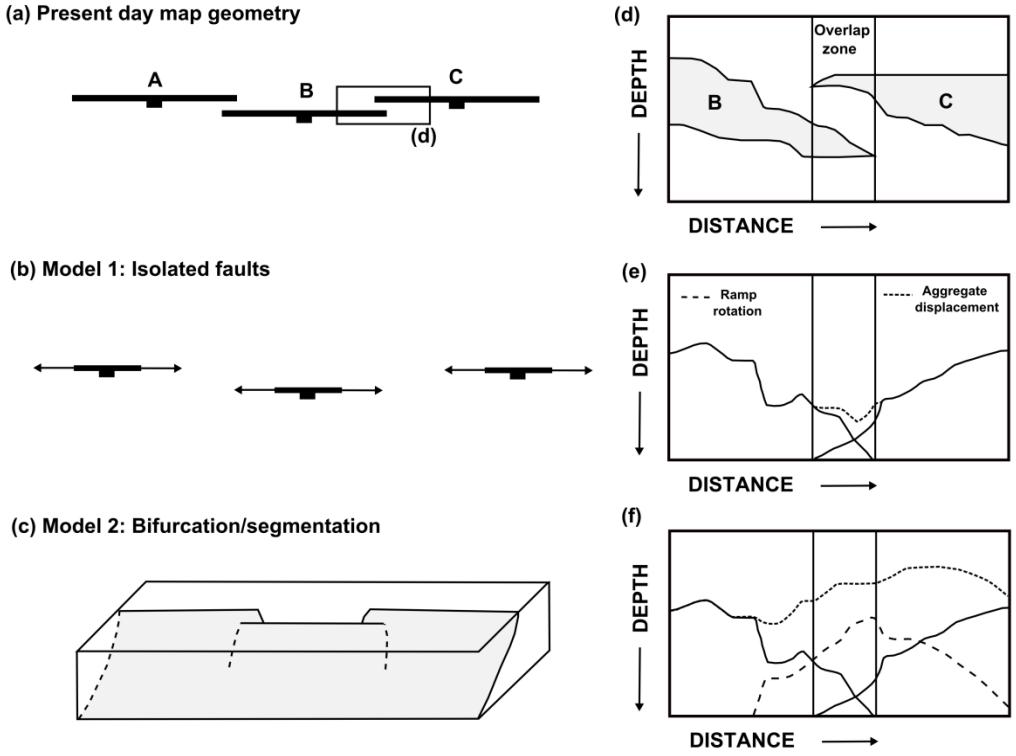

Figure 3.18: Show present day fault geometry and relay zones with model of fault growth formed by propagation of isolated fault segments with alternative model of fault growth due to bifurcation of a kinematically coherent array of unconnected segments. Throw profiles (Right) demonstrating displacement minima within aggregate profiles related to overlap zones and ramp rotation kinematics. (Re-draw from Marsh, 2008).

3.7.4 Reactivation

Many studies have suggested that reactivation of pre-existing faults and fabrics play an important role in controlling the evolution and architecture of rift basins. Faults and shear zones are often long-lived zones of weakness which probably has impact on fault geometry and may undergo reactivation in preference to the formation of new faults during regional deformation (e.g. Holdsworth et al., 1997).

Pre-existing fabrics can be discrete or pervasive (Morley, 1999). Discrete fabrics include faults and pre-existing shear zones which represent a mechanical weakness at upper and lower crustal levels (e.g. Daly et al., 1989)., Pervasive fabrics (e.g. cleavage and metamorphic foliation in pre-rift basement) are present throughout a large volume of rock and impose a strong strength anisotropy that is able to influence the development and architecture of rift systems (Morley, 1999). These appear to control the orientation of new rift faults and influence the formation of basin bounding faults. Discrete fabrics tend to influence more isolated structures in terms of their geometry and orientation.

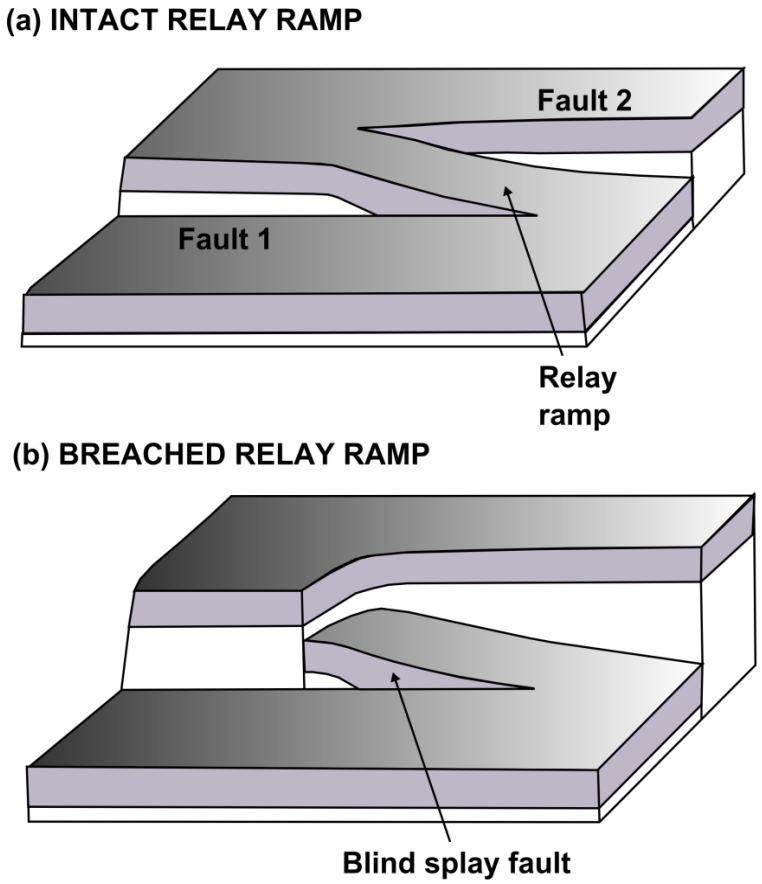

Figure 3.19: The geometry of relay ramp, a) block diagram of an intact relay ramp. b) With increasing displacement and fault growth the relay ramp is breached by one or both faults.

The change of fault orientation during extension is an effect of both local and far-field stresses and controls fault kinematics. Faults change orientation due to a deflection of the local stress field (Brun, 1999) with localised re-orientation of structures due to the influence of pre-

existing fabrics within the rift. Faults are either parallel to basement fabric or perpendicular to the extension direction or combine of both. In Sirt Basin, the faults have orientations parallel to the basement fabric that are inherited from Pan-African structure grain and both the Neo-Tethyan extensional event and the Late Cretaceous-early Eocene Syrian Arc compressional event (e.g. El Arnauti et al., 2008).

3.7.5 Post-sedimentary Normal Faults

Post-rift sedimentary normal faults formed in rift and sag basins basically exhibits elliptical fault surfaces (e.g. Barnett et al., 1987: Walsh and Watterson, 1988).

Fault displacement in this style is increasing towards the centre and decreases in all directions (Figure 3.20) until it reaches zero at the fault tips (Barnett et al., 1987) where the displacement is accommodated by systematic elastic strains in the rocks adjacent to the fault maintaining balance between rocks on either side of the fault.

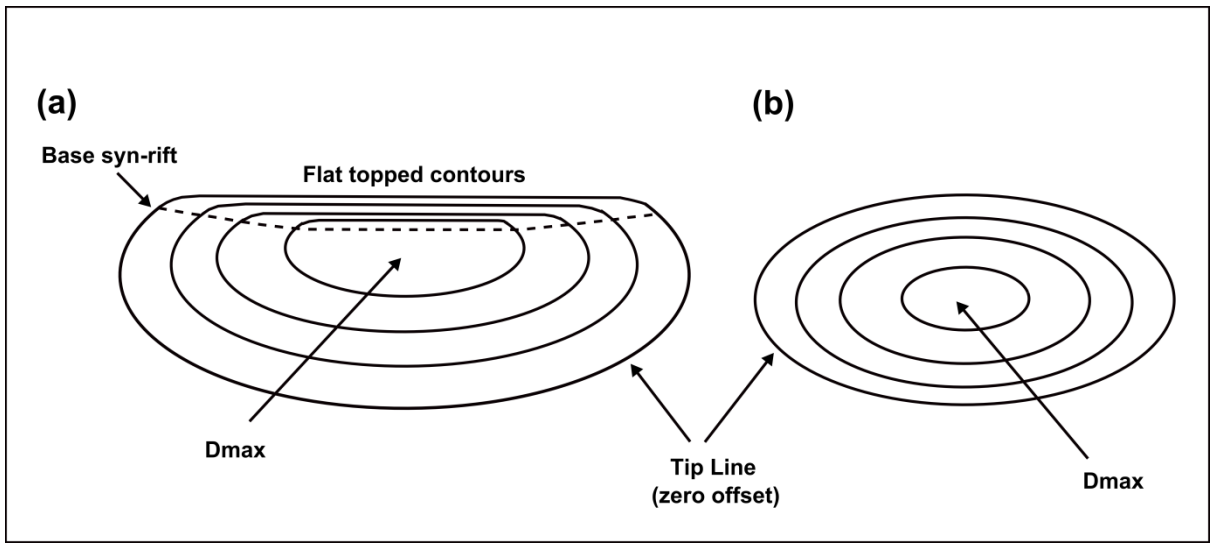

Figure 3.20: Schematic diagram of contoured displacements (a) on a simple syn-sedimentary fault surface with maximum displacement (**Dmax**) above the centre of the fault and with tip line loop corresponding to zero displacement contours. The dashed line marks the base of the syn-sedimentary part of the faulted sequence, and below the line the contours resemble a post sedimentary fault as shown on (b) where the contours are concentric ellipses. Re-draw from Marsh, 2008.

Variations in displacement across the fault surface can be measured in vertical and horizontal directions and represented by the term displacement gradient which is strongly influenced by the properties of the host rocks adjacent to the fault. In ideal case of fault style where the

length of the fault is about twice that of it is vertical axis; the horizontal displacement gradient is also twice the vertical displacement gradient (Walsh & Watterson, 1991). The main causes for post-rift normal faults include later tectonic events, diapirs (either mud or salt), and gravitational collapse. Post-rift faults are observed within the Ajdabiya Trough.

3.7.6 Fault Correlation Using 2D Seismic Reflection Data

Correlation of fault sticks picked on multiple 2D seismic reflection profiles is based on procedures described by Freeman et al., 1990 as shown schematically in Figure 3.21.

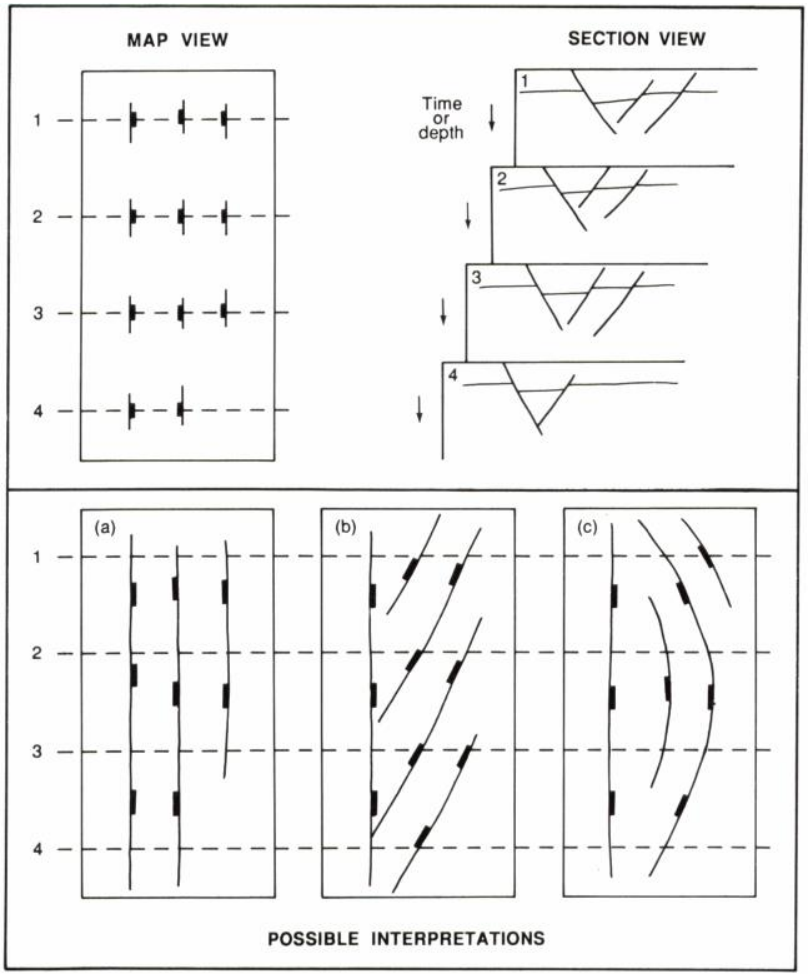

Figure 3.21: Cartoon illustrating that the correlation of faults seen on seismic sections is not necessarily simple or straightforward. (from Freeman et al., 1990).

It is based on building a set of interpretation models for similar fault picks. The upper part of the figure defines the positions of horizons and faults. The picked faults are correlated in

order to establish the fault patterns. Fault planes are interpreted as linear trends taking the largest fault from seismic line to line. Large and small faults mapped in the same structural domain are likely to have similar orientations (Freeman et al., 1990). The fault correlation can be aided by correlating the throw contour patterns across fault network that can correspond to areas of missing interpretations.

Throw contouring is a powerful method used to identify mis-picks. Smooth variations in fault throw over its surface are typical of a good correlation (Freeman et al., 1990). Inconsistent throw patterns should prompt the interpreter to re-examine the fault picks. In the lower panel (Figure 3.21) faults correlation has been made based on their sense of systematic throw variations and large movement. The regularly changing value of the throw, with only one maximum, indicates a correct correlation of fault planes (Freeman et al., 1990).

3.7.7 Interpreting the Timing of Fault Activity

The timing of fault activity can be achieved based on an analysis of the amount of offset on each mapped horizon cut by the fault (e.g. Childs et al., 2003). The timing of fault movements was determined based on the knowing (or estimating) the ages of the affected sedimentary sequences. The tectonic movement will normally give rise to changes in the physical characteristics of sedimentary sequence, such as changes in thickness and the degree of deformation.

Timing of fault movement can be recognized throughout the growth of strata against the mapped faults indicating that these faults were active during time of deposition. The criteria are based on the recognition of deference in thicknesses between the footwall and hanging wall thicknesses across the fault. Thickening and fanning of strata in the hangingwall of the fault during fault growth stages can be correlated with the idea that sedimentation keeps pace with basin subsidence (e.g. Childs et al., 2003).

During fault movement time, old strata will be subjected to a long history of movement compared with the younger sediments. In this case initial faulting and older syn faulting horizons (Figure 3.22) will record large offsets than younger syn-faulting horizons by which timing of fault activity to be established (Childs et al., 2003).

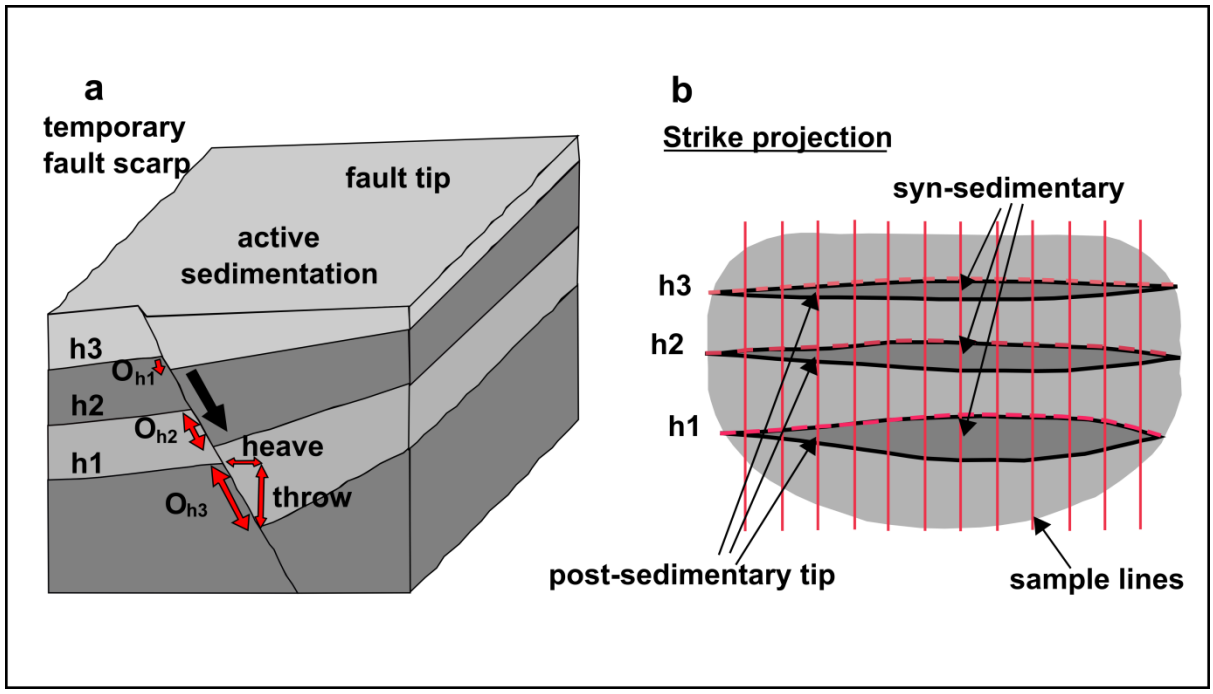

Figure 3.22: a) 3D model showing stages in the development of a syn-sedimentary tectonic fault intersecting three horizons h1 – h3. Decrease in offset along younger horizons may indicate syn-sedimentary fault movement. b) A strike projection of the same fault surface, the variations in offset are sampled along orthogonal sample grid lines. The fault centre shows a decreasing upwards offset consistent with syn-sedimentary fault movement from horizon h1 onwards; in contrast the fault tip shows equal offset on all three horizons indicating that movement occurred after the deposition of h3. The fault has grown with lateral propagation indicating that the fault tips are younger than the fault centre.

Within rift basins, fanning of seismic reflectors can be observed within hangingwall of normal faults indicating syn-tectonic faulting. The degree of fanning in the pattern of synrift deposits is controlled by the magnitude of rotation of the normal faults (Cartwright et al., 1995). The associated growth strata show fanning and growth wedge model with decrease of dip on overlying young strata. During basin subsidence, fanning pattern of seismic reflectors would develop also if sedimentation kept pace with the subsidence. Onlapping of successive strata against previous horizons would be observed also with bedding attitude decreases upward.

3.7.8 Recognizing Strike-slip Faulting from 2D Seismic Reflection Data

Very high reverse fault dips are typically produced by normal fault reactivation or in strike-slip settings (e.g., Harding, 1990). The interpretation of strike slip faulting using 2D seismic data is particularly ambiguous especially for the recognition of slip vectors and sense of offset (e.g., Harding, 1990). The criteria for recognizing strike slip faulting on 2D seismic sections

using the methodology of Harding (1990), is based on recognizing the following characteristics on multiple profiles: (1) faults often consist of variable traces; (2) faults tend to change dip and dip direction along strike, (3) complex fault interactions are apparent in seismic reflection cross sections (so-called positive or negative flower structures); (4) basement involvement in faulting; (5) en echelon fault patterns and development of through-going master fault along strike. Wide spacing and limited lateral extent seismic lines also increases uncertainty during strike slip faulting picking, which may omit some of the deformation on faults that lie outside the realms of the seismic survey.

Strike slip interpretations made from poor quality 2D seismic data are often improved using well data, 3D seismic dataset, additional 2D regional seismic lines and plate reconstructions. .

It is postulated that the aftermath of Cretaceous rifting in Sirt Basin was interrupted by contractional (inversion) and strike slip events (Anketell, 1996; Guiraud et al., 2001; Bosworth et al., 2008; Capitanio et al., 2009). It has been suggested that the Ajdabiya Trough might be a zone of strike-slip faulting (e.g. El Arnauti et al., 2008) but it is now generally agreed to be the site of extensional faulting. Evidence for Late Cretaceous dextral transtensional and transpressional strike-slip faulting is observed and discussed in Chapter 7.

Strike-slip faults in Ajdabiya Trough can be identified on seismic sections and appear to be formed from a series of steeply-dipping, basement-rooted faults with distinctive positive flower structures in Miocene strata.

3.8 Seismic and Sequence Stratigraphic Analysis

3.8.1 Fundamental Concepts and Historical Development

Seismic stratigraphy is a method to interpret stratigraphy from seismic data (Mitchum, et al., 1977). It is a combination of seismic sequence analysis and seismic facies analysis (Mitchum et al., 1977). The seismic facies analysis is the recognition and mapping of facies units within seismic sequences using fundamental parameters such as reflection configuration, continuity, amplitude, frequency, and internal velocity. The fundamental principle of seismic stratigraphy is that within the resolution of seismic method, seismic reflections follow gross bedding surfaces and they approximate time lines (Emery & Myers, 1996).

During seismic stratigraphy analysis, seismic sections are subdivided into sequences of reflections related to genetically sedimentary sequences (Kearey et al., 2002).

Both 2D & 3D seismic data provide evidence of stratal terminations (lapouts), stratal stacking patterns, stratigraphic surfaces and depositional elements in the subsurface (Posamentier et al., 1999).

The concept of sequence stratigraphy has been developed since the 1970s, based on the idea of understanding the distribution of the sediment bodies within a sedimentary record (Figures 3.23 & 3.24).

The approach is mainly based on prediction of what so called stratal stacking patterns which mainly analysed within a temporal framework.

Within any sedimentary sequence the startal stacking patterns evolve in response to the interplay of accommodation space and sedimentation influx. The nature of these patterns reflect a combination of depositional trends (Figures 3.25, 3.26, 3.27, 3.28, and 3.29) that include progradation, retrogradation, and aggradation patterns (e.g., Posamentier et al., 1988; Galloway, 1989; Hunt and Tucker, 1992; Posamentier and Allen, 1999; Catuneanu et al., 2009).

Unlike other stratigraphic techniques which may include correlation using lithology, fossils and others, the sequence stratigraphy is a genetic, process-based approach to stratigraphy (Emery and Myers 1996). It recognizes packages of strata each of which was deposited during a particular phase in a cycle of relative sea-level change.

The sequence stratigraphic approach yields depositional patterns through the analysis of the order in which strata were laid down, and explains the geometric relationships of sedimentary strata and the elements formed by the strata within a deferent sedimentary environment.

The packages of strata in a sequence record are bounded by stratal surfaces and it is correlative surfaces. These surfaces are formed within chronostratigraphical cycles including unconformities and their correlative conformities formed during cycles of sea level fluctuations (Coe et al., 2002).

The sequence strartigraphy is aimed to provide a chronostratigraphic framework based on correlation and mapping of stratigraphic sequences and sedimentary facies (Emery and Myers, 1996) in order to predict lines of evidence when analysing the fill of a sedimentary basin (Coe et al., 2002).

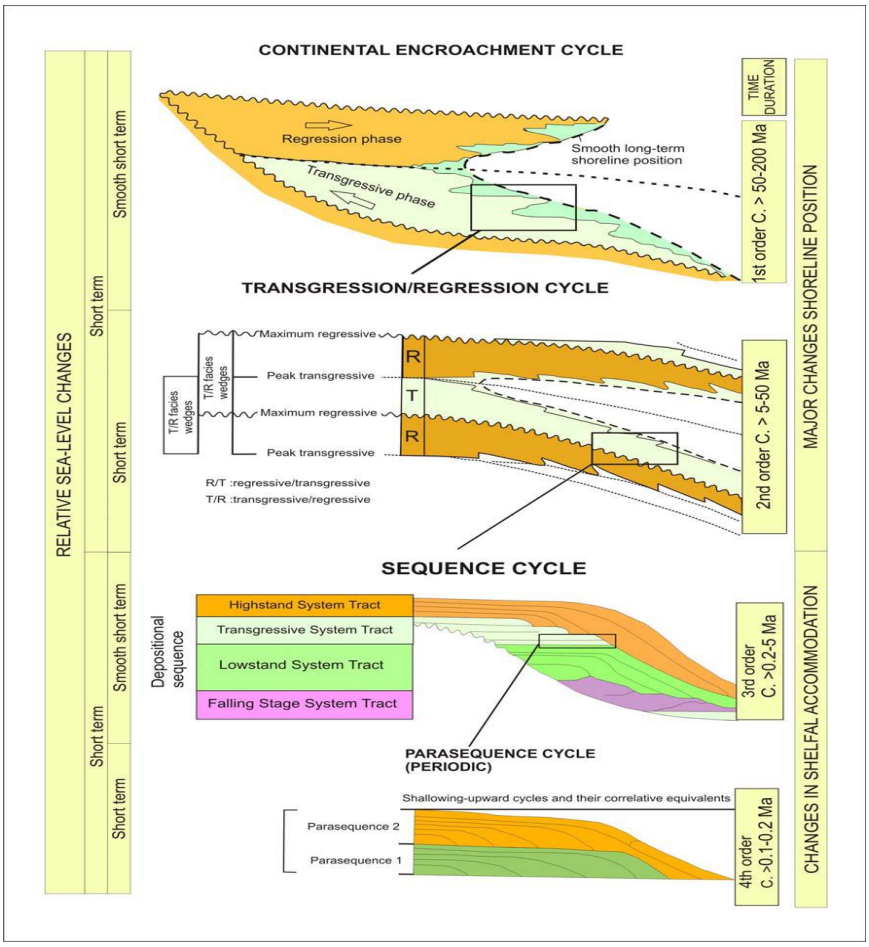

Figure 3.23: Hierarchy of stratigraphic cycles (After Duval and Vail, 1992).

In order to understand the origin of the depositional elements within any depositional setting, the sequence stratigraphic framework can be established through the analysis of a different packages of datasets , including conventional and high-resolution seismic data, wireline logs, cores, outcrops and palaeontologie and geochemical data (Posamentier and Allen, 1999).

A "eustatic cycle" refers to a period of time during which sea-level falls from a highstand position through a lowstand, and returns to a highstand (Van Wagoner et al., 1990). Depositional sequences of geologic history are induced by different order eustatic cycles and distinct orders of sea level variations (Vail, 1987). The largest changes occurring every 200-300 million years (first order).

Intermediate changes occurring every 10 – 80 million years (second order), and the smaller change occurring every 1-10 million years (third order). Vail et al., 1991 modified the

sequence classification approach in which six orders of boundaries were defined solely on boundary frequency.

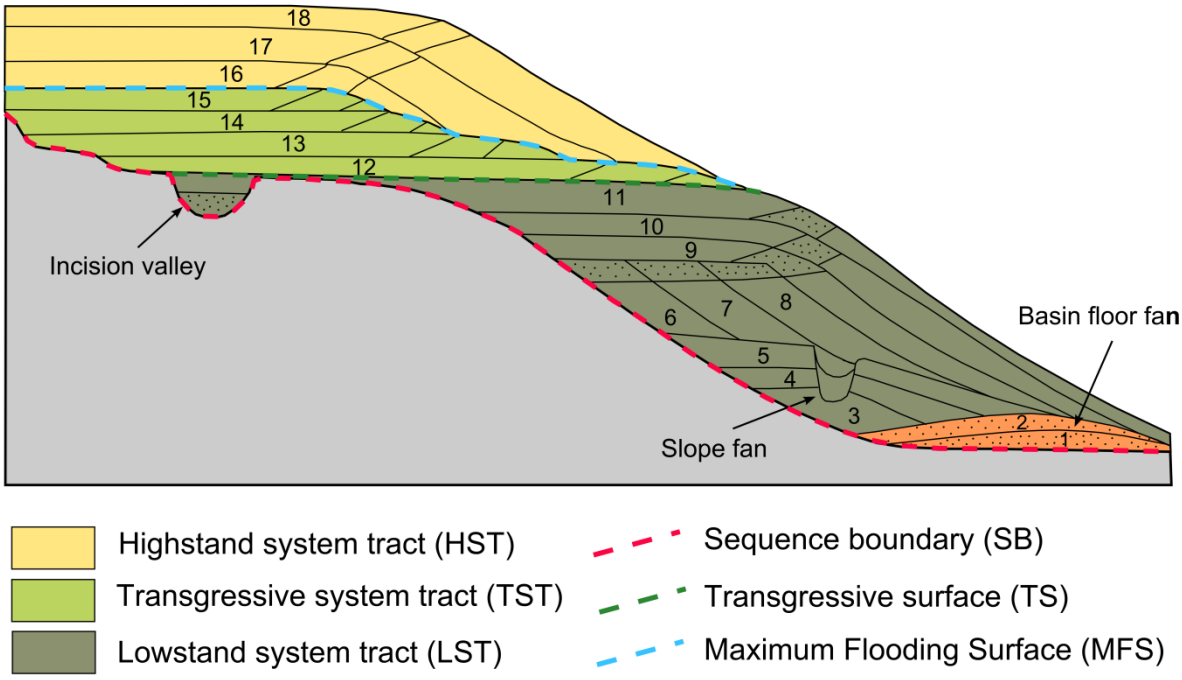

Figure 3.24: Depositional model of sequence stratigraphy, numbers indicate sequence of deposition. The sequence has a lithological scheme with sequence system tracts; and key surfaces. SB = sequence boundary: TS = transgressive surface MFS = maximum flooding surface: LST, TST, HST, = Lowstand, Transgressive, Highstand Systems Tract. (Redrawn from Emery and Myers, 1996).

The six orders and their characteristic boundary frequencies in this hierarchical scheme are:

1th order - 50 Ma

2nd order - 3-50 MA

3rd order - 0.2 - 5 MA

4th order - .08 - 0.5 MA

5th order - .03 - 08 MA

6th order - .01- .03 MA

First-order eustatic cycles (continental break-up cycles), have time duration of *c*.50 to *c*.200+ Ma (Figure 3.23). They show onlapping against cratons and represented by major tectonically controlled unconformities (Duval and Vail, 1992).

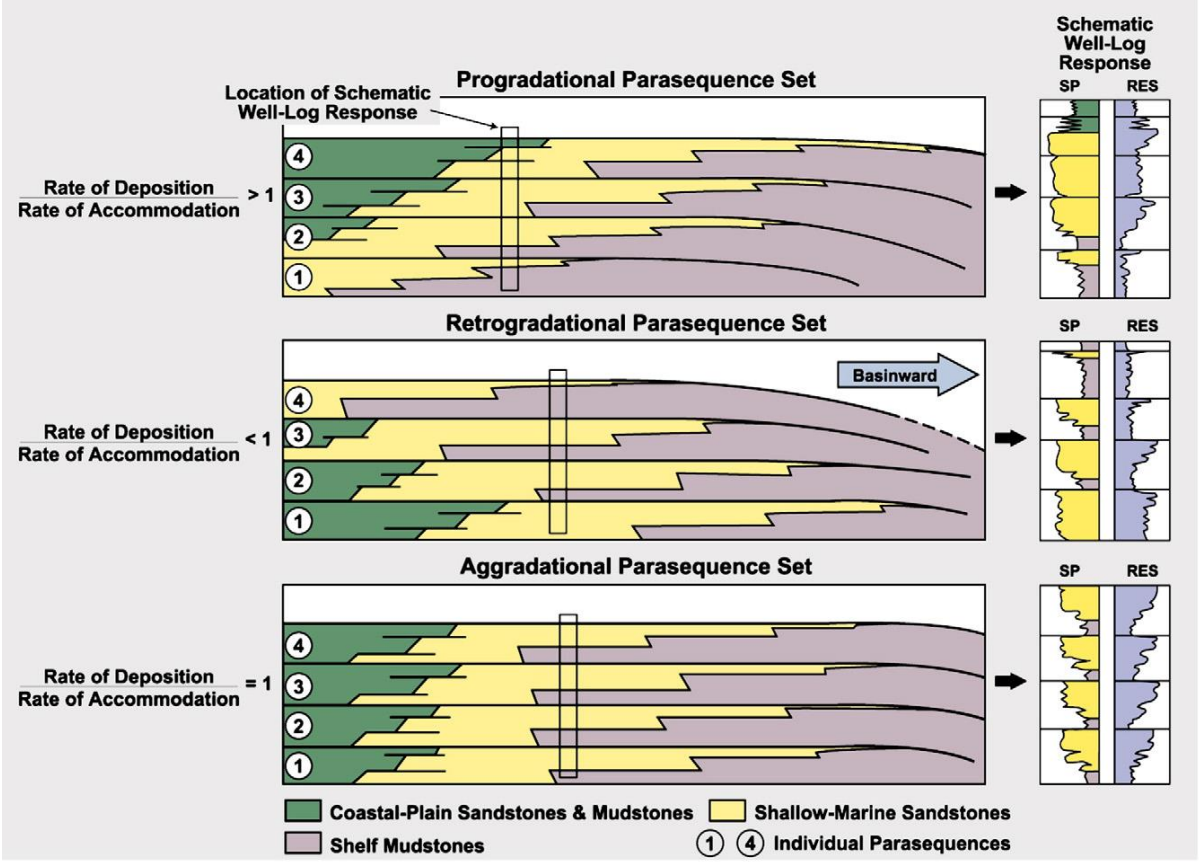

Figure 3.25: The three stacking patterns: Progradational, Retrogradational and Aggradational (from VanWagoner et al. 1988)

Second-order eustatic cycles have time duration in the range of 9 to 10 million years. It is defined as a composite stratigraphic sequence by Van Wagoner et al. (1990).

The second order cycle is caused by changes in the rate of tectonic subsidence and long-term displacement of the shoreline (Vail et al., 1991: Duval and Vail, 1992).

The majority of sequences are third order cycles which have time duration in the range of 0.2 to 5 million years. They are caused by glacial eustasy (Haq et al., 1987) stress release at plate margins (Cloetingh, 1992) and tectonically driven variations in sediment supply (Galloway, 1989).

Fourth and fifth order cycles are assigned to parasequences (Figures 3.23 & 3.25) within main depositional sequences which are of one order higher than the parasequences (Church & Coe, 2003).

Higher-order eustatic cycles (fourth and fifth-order cycles), pronounced as parasequence cycles which are made up of beds and bed sets and have time duration in the ranges of 0,1 to

0,2 and 0,01 and 0,02 million years respectively. Parasequences caused in response to the interaction among the rates of eustasy, subsidence and sediment supply (Van Wagoner et al., 1988).

Sequence stratigraphic analysis develops a chronostratigraphic framework of cyclic, generally related strata. A depositional sequence is bounded by a surface of stratal discontinuity or their marine correlative conformities created by erosion or non-deposition (e.g. Posamentier et al., 1988; Van Wagoner et al., 1988, 1990; Hunt and Tucker, 1992); genetic stratigraphic sequences, bounded by marine maximum flooding surfaces (MFS) (Figure 3.24) which represent the maximum landward extent of deep-water deposition (Galloway, 1989); and transgressive-regressive (T-R) sequences, bounded by maximum regressive surfaces (MRS) (Johnson and Murphy, 1984; Johnson et al., 1985).

These sequence boundaries were defined by prominent reflectors at the base between deposits revealing high acoustic impedance contrast combined with the concept of three main types of sequence boundaries:

1- The Exxon model or concept of subareal erosion (unconformity) and their correlative conformities in depositional sequence developed by Mitchum (1977).

2- Using the maximum flooding surfaces (MFS) in *genetic stratigraphic sequences* that of Galloway (1989).

3- The term transgressive surfaces (TS) in *trangressive-regressive (T-R) sequences.* (e.g. Embry and Johannessen, 1992; Catuneanu et al., 2011; Enge, 2008). The T-R sequence was subsequently redefined by Embry and Johannessen (1992) as a unit bounded by only one type of surface, a maximum flooding surface (MFS), which generally consists of both unconformable and conformable portions. It includes the subaerial unconformity and the marine portion of the maximum regressive surface and thus this sequence type is seemingly compatible with the Mitchum et al., (1977) definition of sequence.

Sequence boundaries as represented by one or several of the MFS, MRS, and TR boundary types were determined by the type of reflection terminations (lapout) against the seismic boundaries (downlap, toplap and onlap) (Figure 3.30) (Mitchum et al., 1977).

Aggradational stacking pattern occurs when the sediment supply and the rate of creation of topset accommodation volume are roughly balanced. In that case the facies at the top of each

parasequence is similar (Emery and Myers, 1996). In a retrogradational stacking pattern the facies become upward more distal (Emery and Myers, 1996).

After having defined seismic sequences, seismic facies analysis is the next step in the work flow. With this method, environment and lithofacies within the sequences are interpreted from seismic and geological data. Reflection configuration reveals informations about depositional processes, erosion and paleotopography (Mitchum et al., 1977).

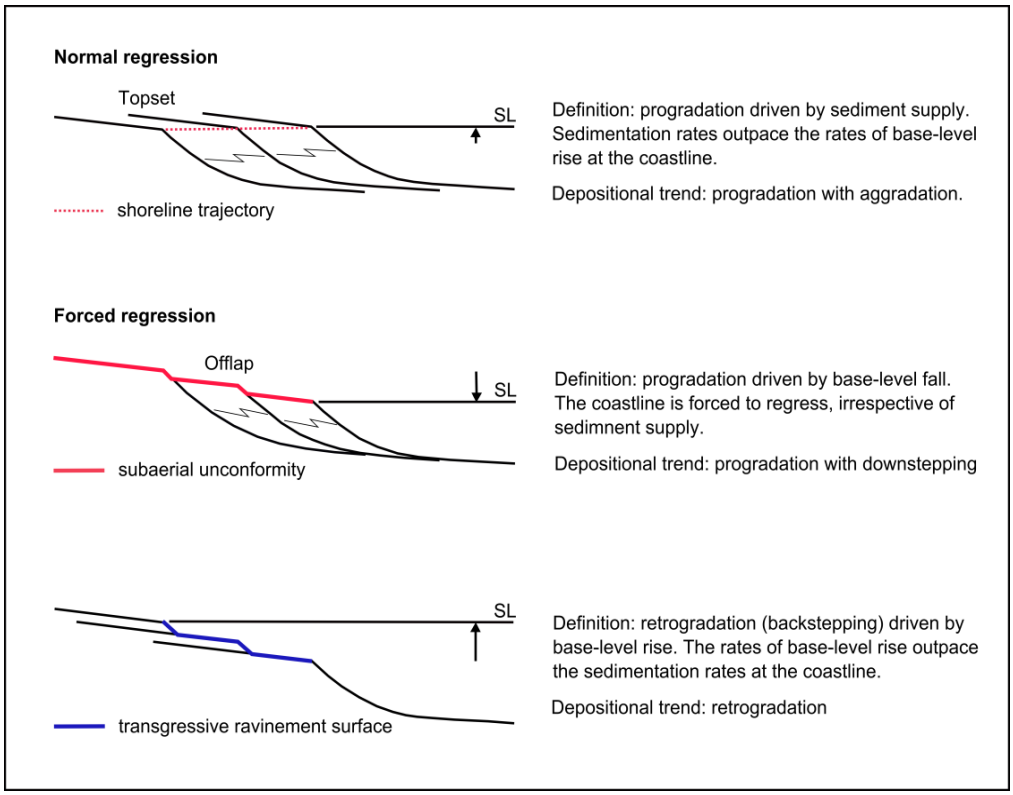

Figure 3.26: Stratal stacking patterns that define the genetic types of deposit which are the fundamental building blocks of the sequence stratigraphic framework: normal regressive, forced regressive and transgressive. Zigzag lines indicate lateral changes of facies within individual sedimentary bodies. (Re-draw from Catuneanu et al., 2009).

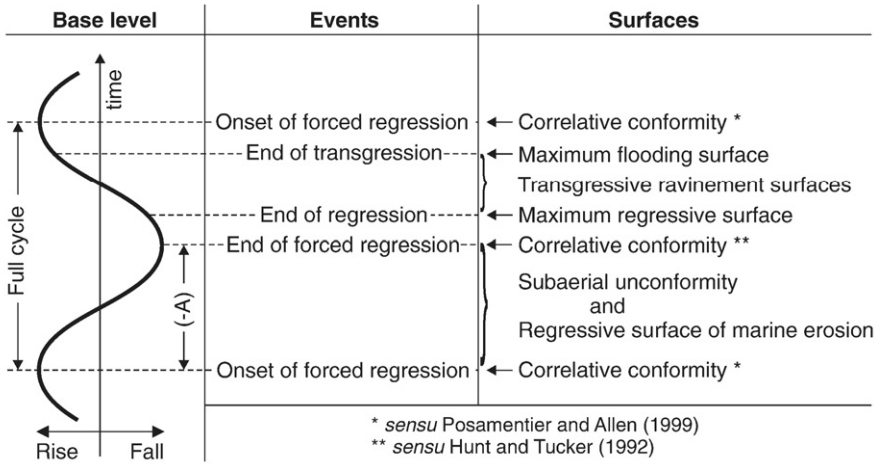

Figure 3.27: Timing of the seven surfaces of sequence stratigraphy relative to the four events of the base-level cycle (Obtained from Catuneanu et al., 2009).

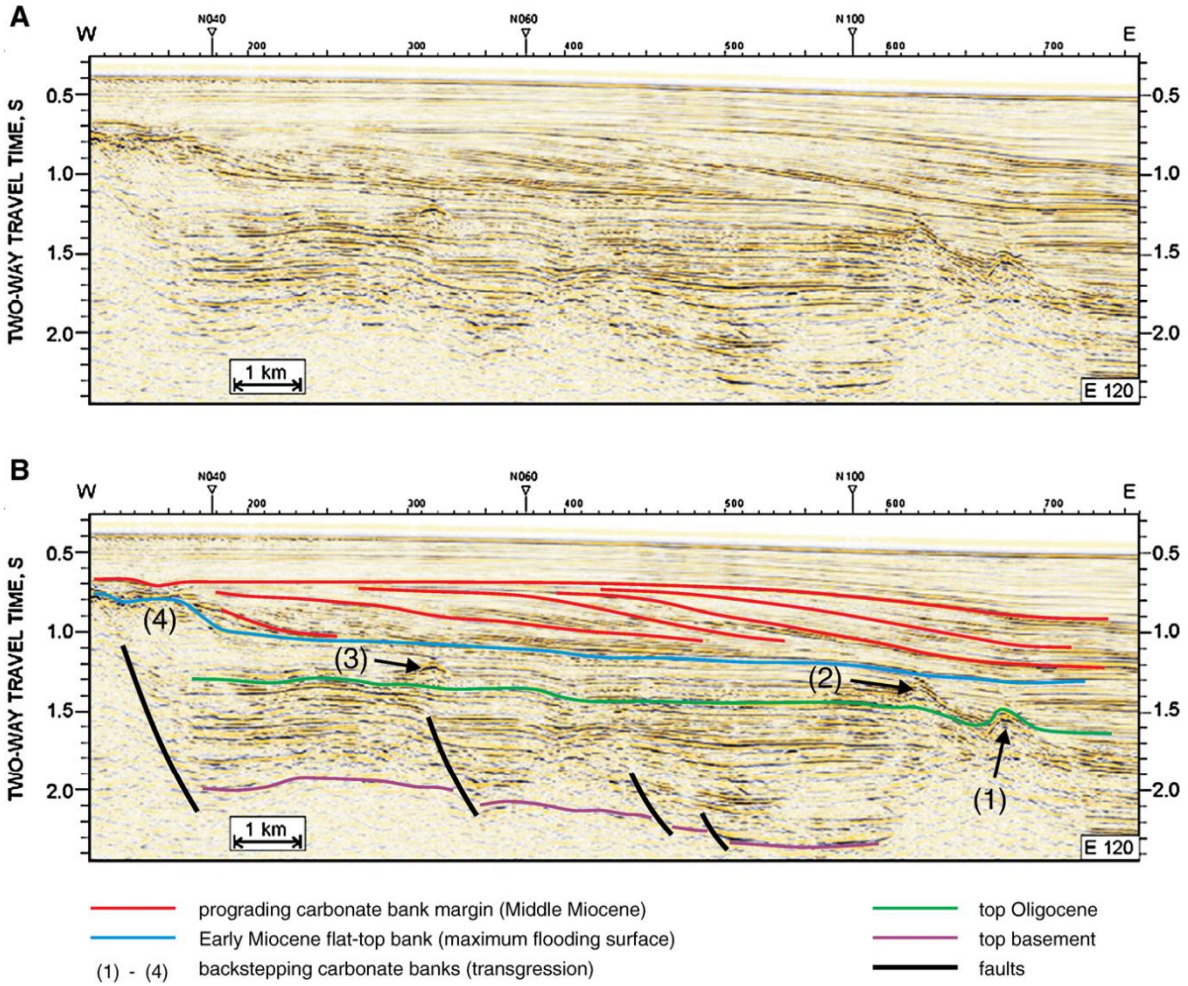

Figure 3.28: Uninterpreted (A) and interpreted (B) seismic line showing depositional trends change from retrogradation to progradation. The boundary between the transgressive and highstand systems tracts is represented by the maximum flooding surface (downlap surface). Obtained from Catuneanu et al., 2009.

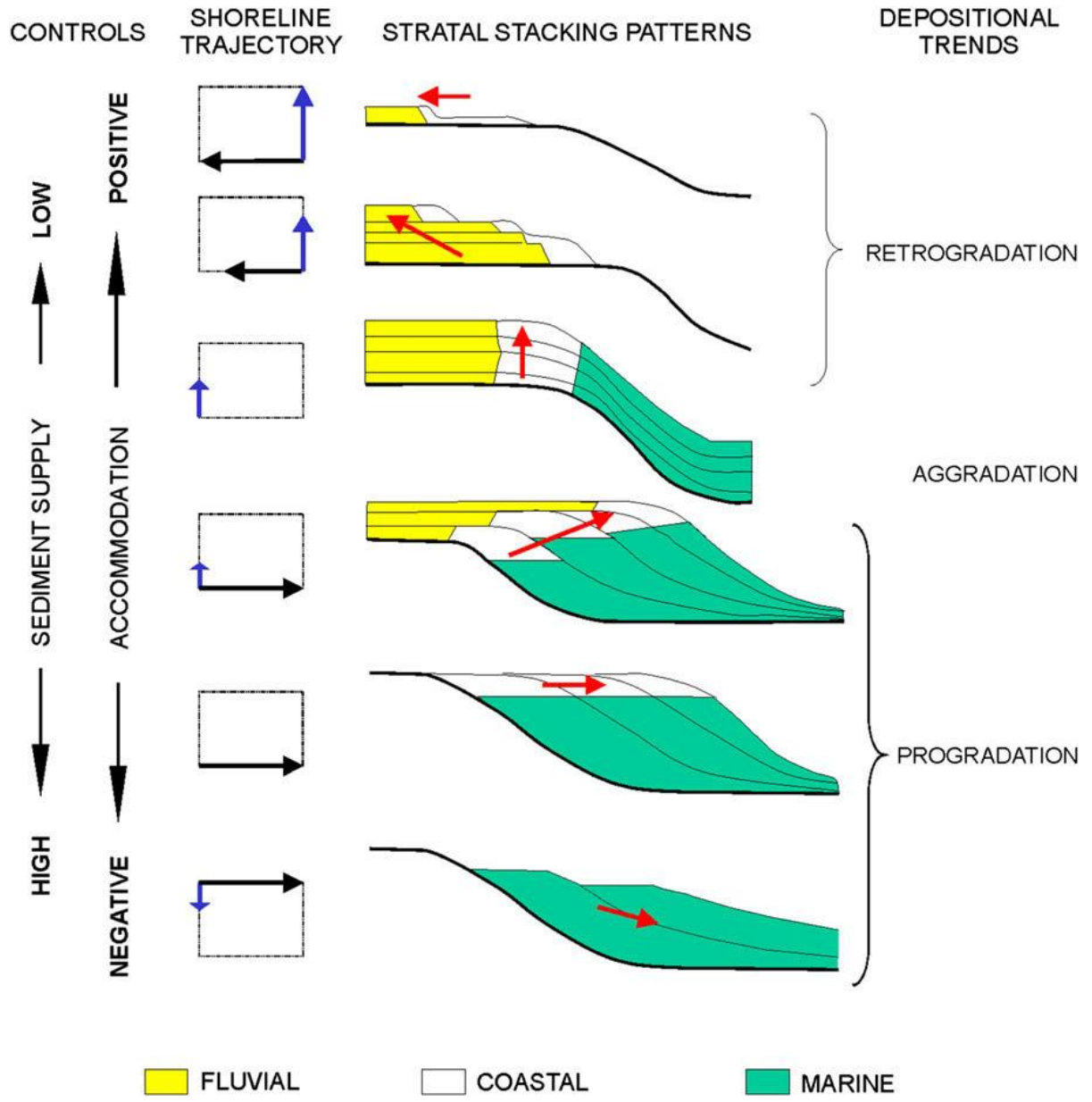

Figure 3.29: Depositional trends (progradation, retrogradation, aggradation) as a response of the interplay of accommodation and sediment supply. Black arrows represent the horizontal (progradational or retrogradational) component, blue arrows the aggradational component, and the red arrows the resultant shoreline trajectory. (from VanWagoner et al., 1990).

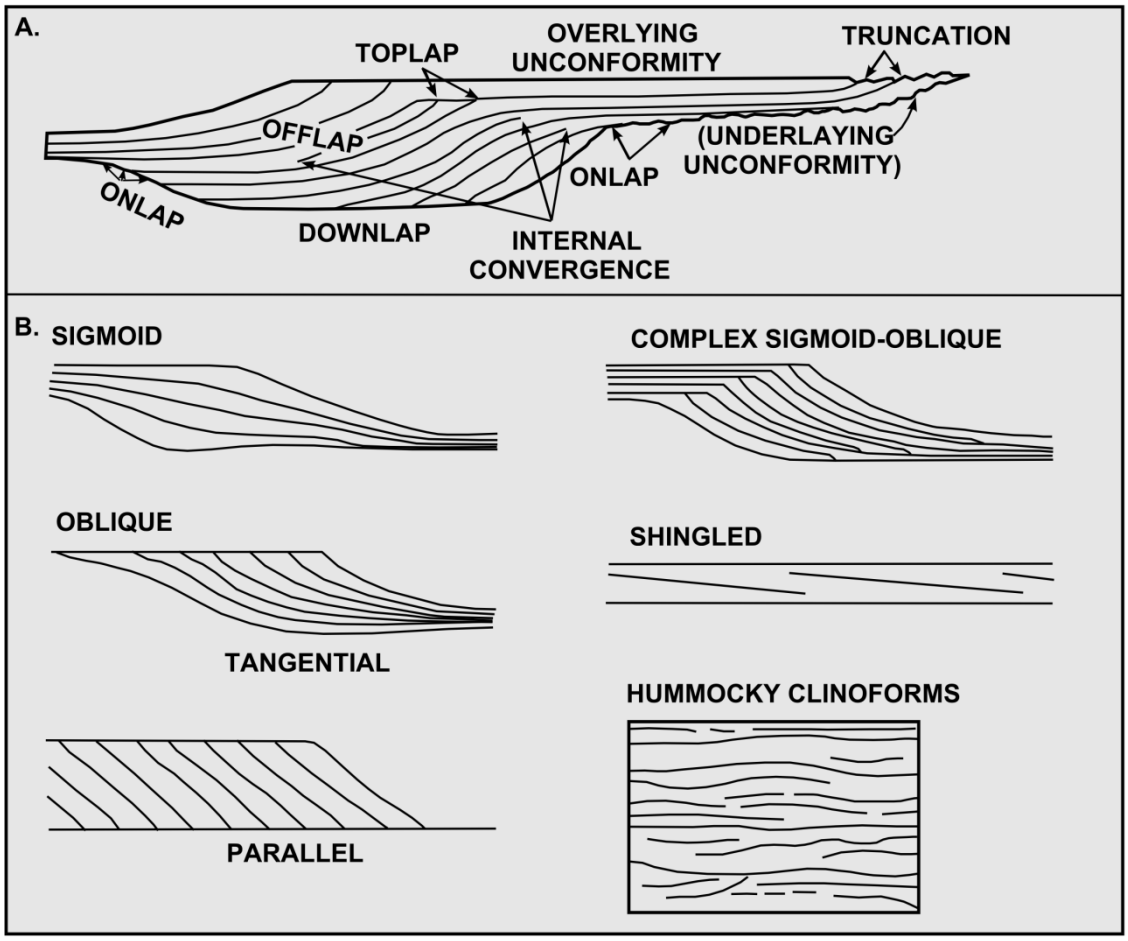

Figure 3.30: (A) Seismic stratigraphic reflection terminations within idealized seismic sequence (B) Seismic reflection patterns interpreted as prograding clinoforms (Redrawn from Mitchum et al. 1977).

3.8.2 Building Blocks of the Sequence Stratigraphic Framework

The depositional sequence, which is the basic stratigraphic unit in sequence stratigraphy, is considered to be a succession of genetically related strata bounded by unconformities and their correlative conformities (Mitchum et al., 1977).

A stratigraphic sequence composed of three different types of sequence stratigraphic units, including sequences, system tracts (Figures 3.31 & 3.32), and parasequences (Figures 3.23 & 3.25). Within sequence stratigraphic framework, these units are mainly defined by bounding surfaces, stratal stacking patterns, and detailed facies relationships (Figures 3.26 & 3.30). Within the stratigraphic domain, these units are defined with a temporal and spatial scales related to the mechanism of their formation. A sequence can be divided into separate parts, termed systems tracts that define the parts of the sequence in terms of rising or falling relative

sea-level. Systems tracts are demarcated by key surfaces. The system tracts are independent of spatial and temporal scales and considered as the linkage of synchronous depositional systems, forming the subdivision of a sequence within stratigraphic framework (Brown and Fisher, 1977).

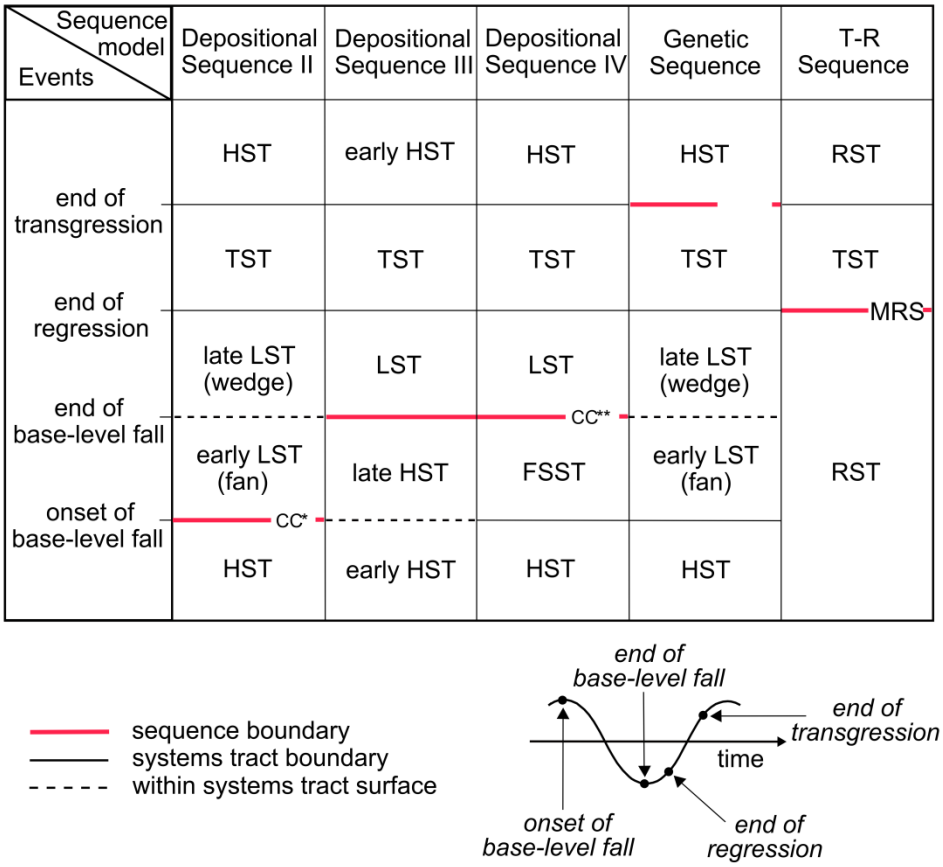

Figure 3.31: Nomenclature of systems tracts, and timing of sequence boundaries for the various sequence stratigraphic approaches. LST – lowstand systems tract; TST – transgressive systems tract; HST – highstand systems tract; FSST – falling-stage systems tract; RST – regressive systems tract; T-R – transgressive-regressive; CC* – correlative conformity in the sense of Posamentier and Allen (1999); CC** – correlative conformity in the sense of Hunt and Tucker (1992); MFS – maximum flooding surface; MRS – maximum regressive surface. (Redraw from Catuneanu et al., 2009).

The lowermost systems tract in the stratigraphic sequences is named the Lowstand Systems Tract (LST) which includes deposits that accumulate during the onset of relative sea-level rise on top of a Forced Regressive Systems Tract (FSST), and subaerial unconformity formed during sea level fall (Catuneanu et al., 2011). This systems tract has also been termed the Late Lowstand Systems Tract (Posamentier et al. 1988; Posamentier and Allen, 1999) or the Lowstand Prograding Wedge Systems Tract (Hunt and Tucker, 1992).

The "transgressive surface" (TS) represents the first significant flooding of the basin margin during rising relative sea level.

The Transgressive Systems Tracts TST comprises the deposits accumulated between the "transgressive surface" (TS) and the maximum rate of relative sea level rise (MFS). The maximum flooding surface (MFS) documents the change from the TST to the Highstand Systems Tract (HST). Sediments deposited during the late stage of relative sea level rise represent the onset of the Highstand Systems Tract (HST) (Brown and Fisher, 1977). The HST lies directly on the MFS and includes the aggradational and progradational deposits that form when sediment accumulation rates exceed the rate of increase in accommodation space.

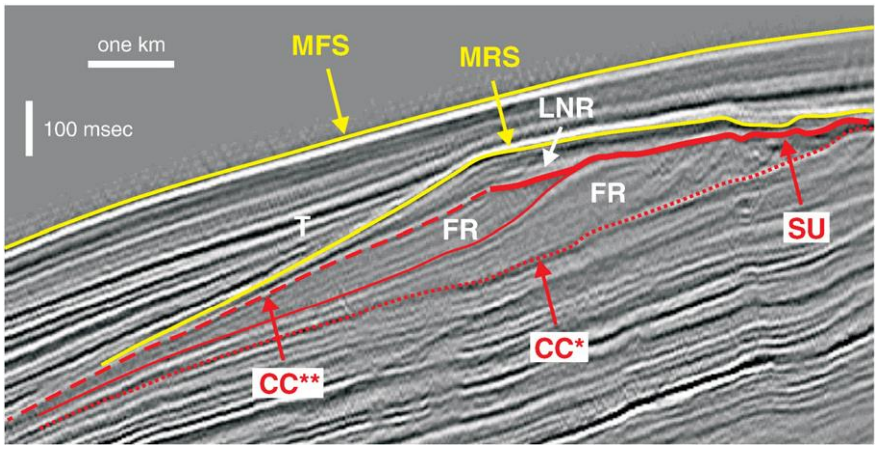

Figure 3.32: Seismic line in the Gulf of Mexico showing different genetic types of deposits. FR= forced regressive; LNR = lowstand normal regressive; T = transgressive; SU = subaerial unconformity; CC* = correlative conformity sensu Posamentier and Allen, 1999 (=basal surface of forced regression); CC** correlative conformity; MRS = maximum regressive surface; MFS = maximum flooding surface. Obtained from Catuneanu et al., 2009.

The stratigraphic architecture of rift basins is sensitive to a variety of factors, including basin geometry, and other factors. The stratigraphic architecture of sedimentary succession in rift basins is strongly controlled by interplay of tectonics through fault movements, uplift and subsidence. In rift basins, climate eustatic fluctuations may operate at low and high frequency levels as a control on stratigraphy and sediment supply which mainly expressed by bed thickness variations related to tectonic activity. Accommodation space in these basins is generated mainly by tectonic subsidence in response to pulses of extension and fault reactivation, followed by period of tectonic quiescence. During this stage no new

accommodation is generated and the basin becomes fully filled with sediment as the sediment supply gradually consumes the available accommodation space.

In rift basins, and during extensional subsidence cycles, the stratigraphic record is mainly dominated by progradational depositional trends; with coarsening upward successions fill any available accommodation space (Figure 3.33).

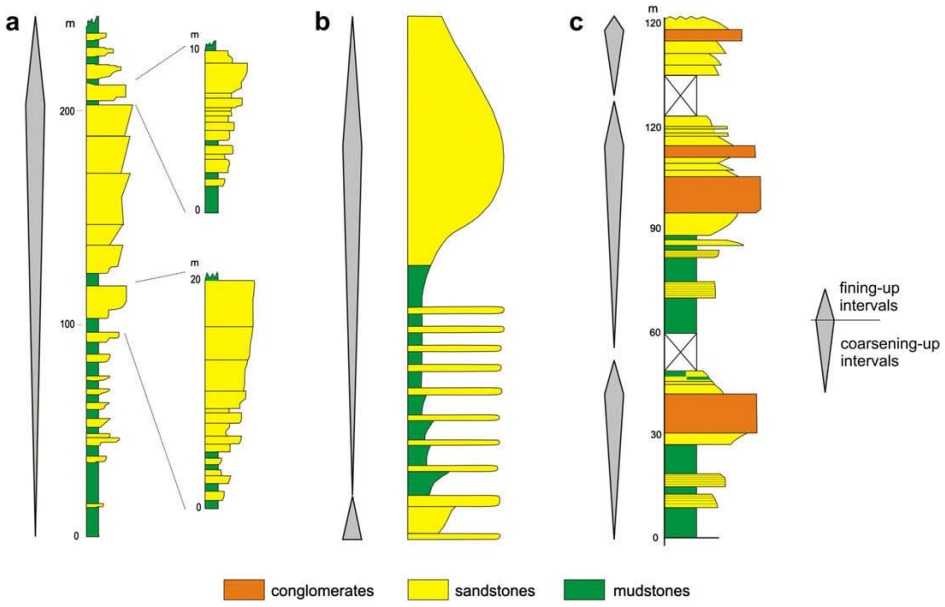

Figure 3.33: Stratigraphic columns showing the coarsening-upward vertical stacking pattern that is typical of sequences accumulated in rift basins. The fining-upward trends that are observed at the top of sequences may correspond to spans of time toward the end of each tectonic cycle when denudation of source areas, as well as the decrease in the differential relief between the source areas and the basin, combine to decrease the efficiency of sediment supply to the basin. (from Martins and Catuneanu, 2009).

A full cycle tends to include a short retrogradational portion (transgressive systems tract TST) will have accommodation space greater than sedimentation rate resulting in landward-steeping units which corresponds to the tectonic pulse of extensional subsidence. This followed by progradation geometry during tectonic quiescence (highstand system tract HST) where the accommodation space less than sedimentation rate, so basin-ward steeping units (Martins and Catuneanu, 2009) and facies with prograding geometry downlaps on the MFS. The succession is dominated by thinning upward patterns of depositional parasequences often dominated by peritidal facies with well-developed exposure surfaces.

CHAPTER 4: GRAVITY AND MAGNETIC DATA INTERPRETATION

4.1 Introduction

Potential field methods involve measuring the Earth's gravitational and magnetic fields using highly sensitive instruments. The measurements can be made on the Earth's surface, both on land and the sea bottom, from ships or from aircraft. The data are then processed in a number of ways to emphasize gravity and magnetic anomalies. These gravity and magnetic anomalies can be attributed to variations in density and magnetic susceptibility in the Earth's crust and are a major advantage in mineral and hydrocarbon exploration. Traditionally, gravity and magnetic imaging have been extensively used to reveal internal basin geometry, based on the contrasts of density and magnetic susceptibility between the sedimentary rocks and their crystalline basement (Talwani et al., 1959; Blakely et al., 1999). Restrictions are imposed on the application of these methods by 1) the basic ambiguity in the determination of source parameters from gravity and magnetic data, 2) the interference of sources from the heterogeneous basement and 3) weak potential field signatures associated with semi-infinite horizontally extended bodies. Several processing and modelling approaches have been proposed to overcome these limitations, with different degrees of success. The imagery can be combined with modelling, shallow core, deep borehole, and both 2D & 3D seismic data for better prediction of subsurface structures such as crustal structure, basement relief and faults.

Within the Sirt Basin area, gravity, magnetic and seismic data have been gathered, and as a result the basin is far better known than any other area in Libya, although it can fairly be claimed that the deep troughs such as Ajdabiya Trough are still under-explored. There is a consensus that regional and local tectonic influenced sedimentation in the NE Sirt Basin has played a significant role in the development of the Ajdabiya Trough structural styles (e.g. Baird et al., 1996; El Arnauti et al., 2008).

This chapter utilizes different techniques for better interpretation and understanding of gravity and magnetic data in terms of basement and other structures in the Ajdabiya Trough region, located approximately between latitudes 28º N to 31º N and longitudes 19º E to 21º E and extended along north–south length of about 250 km (Figures 4.1).

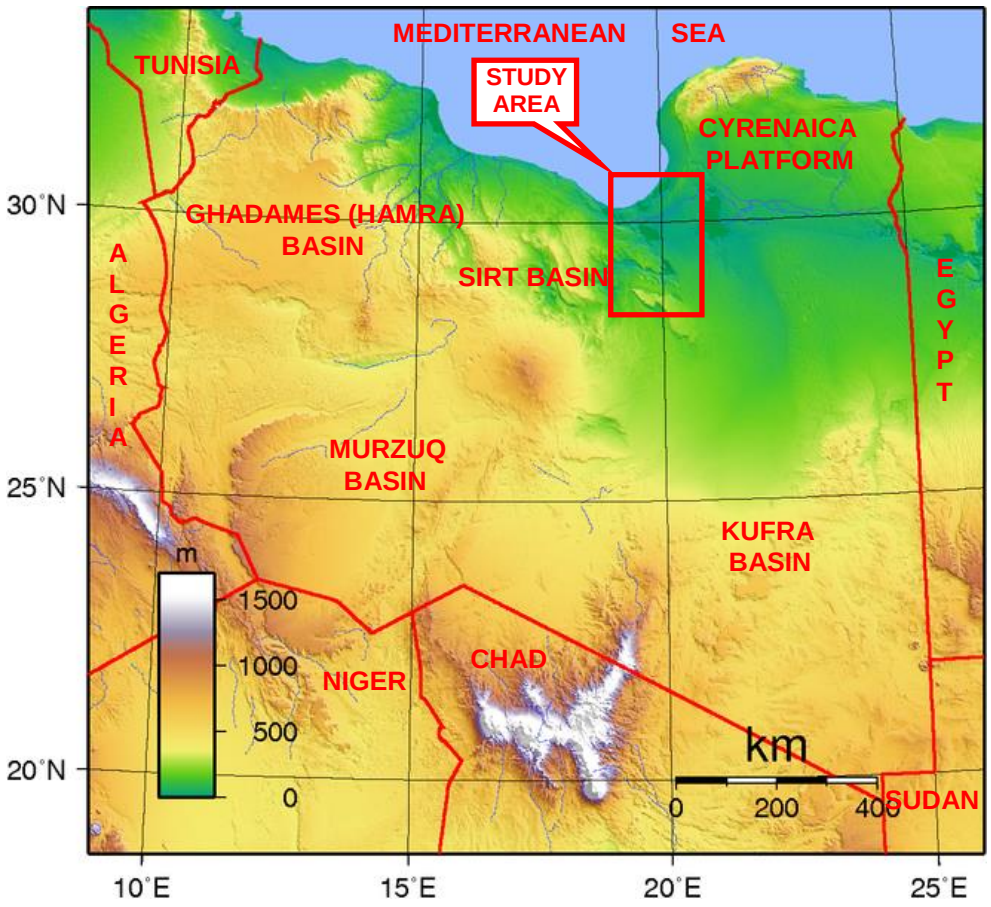

Figure 4.1: Topographic map of Libya and location of the Ajdabiya Trough in the northeastern part of Sirt - Basin. (https://vec.wikipedia.org/wiki/Giografia_de_la_Libia)

4.1.1 The Aims of the Study

The aim of the present work is to contribute to the understanding of the tectono-structural architecture of the Ajdabiya Trough and its deformed basement. I integrate gravity and magnetic data in order to map shallow features and deep crustal structures that controlled the structural framework of the trough and are possibly related to reactivated rift faults and shear zones of Pan-African and post Hercynian ages (e.g. Conant and Goudarzi, 1967 ; Burke and Dewey, 1974) .

The interpretation of gravity and magnetic data can be aided by the application of several advanced processing, imaging techniques. These techniques have been applied in this study with the principle aim of adding to the understanding of the regional tectonics and structures and calculating the depth to crystalline basement. The success of the various techniques can

vary often from area to area dependent on a number of factors such as data quality and coverage and the type of geological features being imaged.

Observed magnetic and Bouguer gravity anomalies were both forward modelled with the aim of analysing intra-crustal features such as igneous intrusions, basement features, sedimentary basin extent and depth to the Moho. Models considered the geometry of the upper crustal structures and explored different scenarios for crustal thickness variations causes short wavelength gravity anomalies. The subsurface relief, and heterogeneous composition (e.g. mafic/felsic basement underplating), of basement rocks give rise to medium to long wavelength gravity and magnetic anomalies. Some of these anomalies can be correlated to near surface features such as the Cenozoic volcanic belt of the western Sirt Basin and the offshore area (Figure 2.26) (e.g. Capitanio et al., 2011), others may be correlated with faults. Some may be related to deep features associated with sub-surface structures such as the main trough bounding faults. Others have no obvious association with the surface geology.

Magnetic anomalies have a complicated relationship to their source bodies. This is partly because of the oblique dip direction of the total field and the magnetization which produces asymmetry. Furthermore, the magnetization is dipolar. The dipole nature of the magnetic source results in a more complicated field than a monopole source as in gravity. These factors prevent direct correlation of the causative body to the magnetic anomaly. Shallow magnetic sources produce prominent short wavelength anomalies and these add to the complexity and may make the identification and interpretation of the medium and long wavelengths anomalies difficult. For these reasons, it has been found useful to use the simpler pseudo gravity anomalies to assist interpretation of the longer wavelength anomalies. An overview of the workflow adopted in this study to interpret and model the gravity and magnetic data is provided in Figure 4.4.

In summary, the gravity and magnetic responses have been forward modelled along selected profiles, and compared with observed the potential field data. The forward models were constrained in accordance with seismic reflection interpretations (Chapters 5 and 7), changing the deep crustal structure to obtain the best fit with the gravity and magnetic observations. The key products of the study provided as digital grids and maps are:

1. Tectonic element maps estimated from different depth levels, dependent on tectonic style and history during Mesozoic to Cenozoic.

2. Approximate depth to Precambrian acoustic basement map from gravity and well data.
3. 2D gravity & magnetic models.

4.1.2 Structural Framework of the Ajdabiya Trough

The structure of the Ajdabiya Trough (Figure 4.2), especially in the deeper part is not clear. It has been described by Parsons et al., (1980) that it is a half graben characterized by different structural patterns and styles along it is margins, the difference in the nature of faulting on opposite sides of the trough may be responsible for the structural asymmetry (Baird et al., 1996). The northern margin of the trough is defined by a horst structure known A1 Brayqah High (Hallett and El Ghoul, 1996), which is covered with Palaeocene carbonate rocks and Oligocene - Miocene shale (Wennekers et al., 1996).

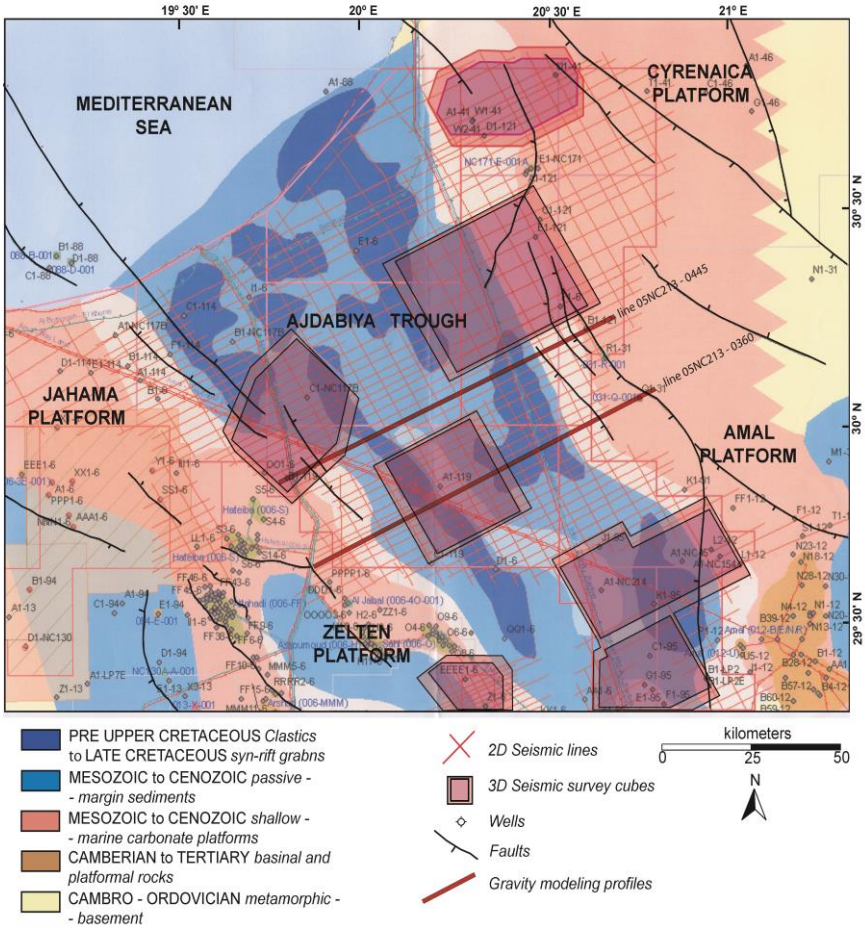

Figure 4.2: Map showing seismic coverage in the Ajdabiya Trough along with geology and locations of selected seismic lines used for the gravity modelling.

The southern margin (Figure 4.3) is characterised with a gentle slope (ramp margin) with small faults down to the basin. The western side of the trough close to the Jahama Platform (Figure 4.2) is very little known, but it is believed to be a sharp faulted margin (Hallett, 2002). The eastern flank of the trough is more complex. The northeastern margin abuts against the Cyrenaica and the Amal Platforms, with a series of terraces which may represent relay-ramp faulting (Hallett, 2002).

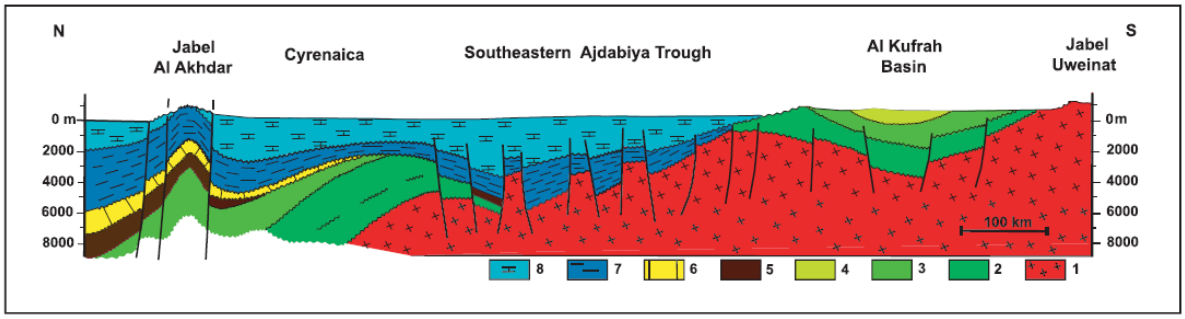

Figure 4.3: Geological cross section extended from Al Kufra Basin to Cyrenaica Platform passing through south-eastern Ajdabiya Trough, where carbonate ramp structure controlled by extensional faults. (Redrawn from Hallett and El Ghoul, 1996).

4.1.3 Summary of Previous Work

Results of previous gravity studies in Sirt Basin were presented by view authors, (Essed, 1978, El-Butroukh and Zentani, 1980, Suleiman, et al, 1991, The Libyan Gravity Project, 2002). They all argue that the gravity field in the area has been significantly influenced by lower crustal structures formed during the Early Cretaceous - Tertiary in response to crustal extension causing active subsidence resulting in the collapse of the Sirt Arch and movements along active basement faults (F.D van der Meer, 1993; Hallett, 2002). The major tectonic trends of the Sirt Arch are also believed to have controlled the post- Hercynian structures of the Sirt Basin (Goudarzi 1980; F.D van der Meer 1993).

From this study, a low amplitude positive gravity anomaly of about 15 mgal is observed in the centre of the Ajdabyia Trough. This relatively low amplitude signature is a characteristic of weak rifted margins and implies that this part from the Sirt Basin is locally compensated and not supported regionally by the strength of the lithosphere (e.g. Watts & Marr 1995). This observation supports the possible primary assumption of the subsidence mechanism in the study area (i.e. local isostatic equilibrium).

The gravity and magnetic maps show that fault trends in the study area are dominantly NW-SE and NE-SW or NNE-SSW, of which the latter have the appearance of strike-slip faults. During the Cenozoic, regional right-lateral strike-slip has been inferred along major fault zones in the Cyrenaica region (Anketell, 1996; El Arnauti et al, 2008), possibly resulting from compression in this region (El-Arnauti et al., 2008). It is suggested also that dextral strike slip reactivation of the North African Megashear System from Paleocene to Middle Eocene times promoted sinistral transtensional reactivation of north-west-striking, collision-parallel faults in the Sirt Basin (Janssen et al. 1995; Anketell, 1996).

From a gravity and magnetic point of view, it would appear that the gravity and magnetic sources that are bounded by these faults are due to reactivation and possible intrusive igneous activity as result of alternating positive and negative source susceptibility and density values. The transtensional opening of the Neo-Tethys during the Early Mesozoic was associated with sinistral strike slip movements which were reversed during Late Cretaceous to Paleocene time into dextral transpressional shear movements contemporaneous with the opening of the North Atlantic (Smith, 1971) and recently outlined by El Arnauti et al., 2008. The large distinct changes in the gravity anomalies are interpreted to be produced from possible transitional crust, at the middle of the trough and/or stretched crust possibly represent the differential crustal extension during the Mesozoic. The slight increase in Bouguer gravity compared to the transitional crust possibly indicates a higher amount of stretching for this crustal segment. This could be associated with changes in Tethyan oceanic crust and inversion of previously subsiding rift basins on the southern Tethyan margin (El Hawat and Abdulsamad, 2004). These were associated also with increased magmatism that peaked during the Turonian event (90 m.y), in Egypt, Sirt Basin and the Pelagian shelf (North West offshore Libya) (El Hawat, 1997; El Hawat and Argnani, 2000).

4.2 Gravity Analysis

4.2.1 Data Set and Methods

The study area is comprised of approximately 25,000 square km and covers approximately 100 km in an east-west direction and 250 km in north-south direction (Figures. 4.1 and 4.2).

The Bouguer gravity map of the study area is produced using data obtained from the Libyan Petroleum Institute (LPI).

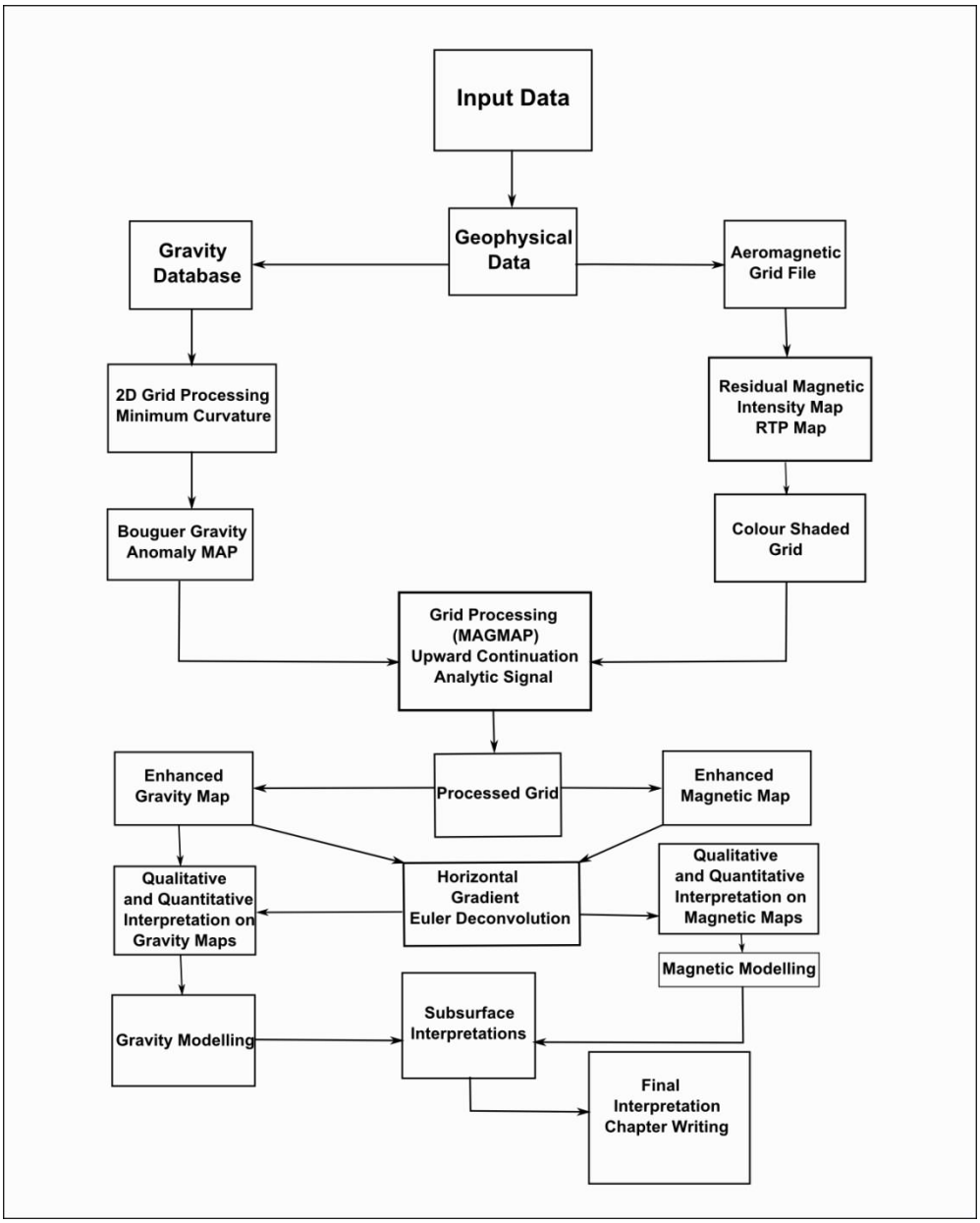

Figure 4.4: Flow chart of the methodology

A gravity data set covering the Ajdabiya Trough and the adjacent areas has been constructed from the LPI data using data window process. Gravity data collected from different sources were merged and reduced to the mean sea level and processed to produce Bouguer gravity

anomalies using the 1980 international gravity formula (Morelli, 1976), and estimated local bed rock density of 2.67 g/cm³. About 32144 gravity observations (Figure. 4.5) represent the data set used in this study. There are a number of gaps around the Ajdabiya Trough area due to the lack of gravity surveys in these regions. Most noticeable are the gaps located to the southeast near Amal Platform and Rakab high, and to the northeast near Cyrenaica Platform. To overcome any voids in the data coverage, different interpolation techniques were employed during the image processing stage. After trying different grid intervals, the merged data were then gridded at an interval of 3.0 km and contoured using the minimum curvature technique (Briggs, 1974), in order to produce the Bouguer gravity anomaly map for the study area. The minimum-curvature method interpolates the data to be gridded with a surface having continuous second derivatives and minimal total squared curvature.

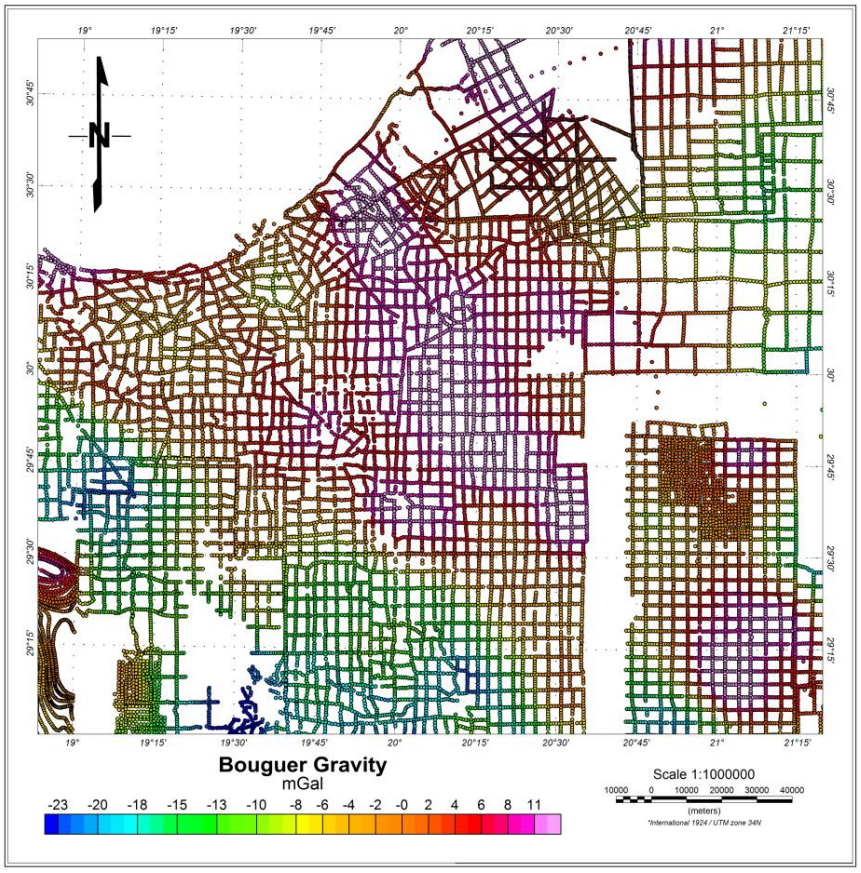

Figure 4.5: Map showing the distribution of the gravity data used in this study. The variable colored circles represent the station locations with different Bouguer gravity values according to the map color-code. The data were compiled from different surveys and mainly converted from maps to digital numbers. Other data obtained from contour maps (samples from this data showing at the SW corner of the map) .Data obtained from the Libyan Petroleum Institute (LPI) as part from the Libyan Gravity Compilation project (2002).

4.2.2 Bouguer Gravity Map and Data Filtering

The resulting Bouguer gravity map of the Ajdabiya Trough is shown in Figure 4.6. The map shows that mainly long wavelength anomalies related to large-scale deep seated structures are predominant. A gravity anomaly over the centre of the trough ranges from lows exceeding 0 mGals (1 milligal = 10^{-5} m/s^2; yellow) to +15 mGal (warm orange). The Ajdabiya Trough basin is expressed as a broad, nearly elongated region in which gravity values are 5-15 mGal lower than regional values.

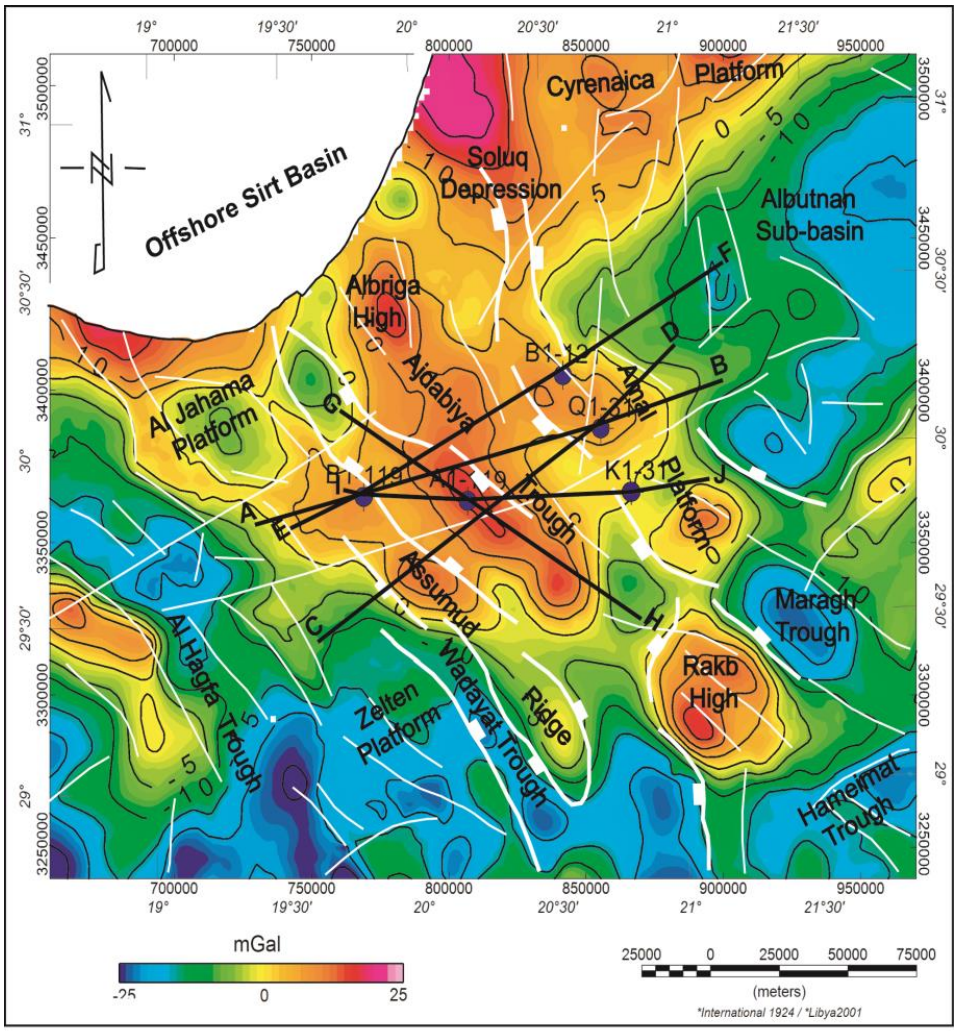

Figure 4.6: Bouguer gravity map of the Ajdabiya Trough and the nearby areas in simple and shaded relief display showing variable distribution of the gravity values related to major structural elements identified on the Bouguer map. Blue and black circles on the maps are wells used in the gravity modelling. White and black lines are gravity lineaments indicating extensional faults and shear zones, (A-B, C-D, E-F, G-H, and I-J are locations of modelled gravity and magnetic profiles) on both maps.

Four regions dominate the gravity field from east to west: (1) the gravity high (up to 23 mGal) in the Cyrenaica Platform and Solouq Depression to the northeast; (2) an arc shaped gravity low (relative, from 0 mGal to -20 mGal), which represents the eastern most sub-basins and troughs (Albutnan sub-basin, Maragh Trough etc); (3) a series of gravity highs (from 0 mGal to +15 mGal) in the centre of the Ajdabiya Trough, and Al Jahama and Zelten Platforms to the west; (4) The low gravity up to -22 mGal southwest of Ajdabiya Trough, the area coincides with Al Hagfa Trough and part from the Southern Shelf.

The positive gravity anomaly of about 15 mGal at the middle of the trough can possibly be attributed to influences of deep sources (e.g. crustal thinning, and igneous intrusions) and/or shallow sources mainly caused by low density contrast between adjacent sedimentary sequences possibly composed of surficial or reworked clastic sediments and/or a lateral transition and switch from carbonate to clastic sediments. The majority of the low amplitude positive gravity anomaly is associated with the Ajdabiya Trough central part. It is also interpreted to mark the position of a possible ridge identified by Hallett and El Ghoul (1996). Gravity modelling highlights the possibility of an asthenospheric uplift within the upper mantle. This asthenospheric uplift may result in uplift of the crustal basement; therefore creating positive anomalies of low amplitude that are superimposed on negative anomalies raising from thick low density sediments mainly clastics as lithological variations observed between carbonate rich platform areas and more muddy rocks of the basin centre. The positive gravity anomalies could also indicate dense rocks such as the igneous material or deep crustal rocks.

4.2.2 .1 Anomaly Separation

A common practice in potential field (gravity and magnetic) interpretation is to separate anomalies based on their wavelengths, or anomaly widths. This practice is based on a rule of thumb that the short wavelengths (detailed features) are produced by shallow sources, whereas the long wavelengths (broad features) are produced by deep sources.

During the first stage of the gravity interpretation, it is difficult in some cases to recognize smaller or shallower features from the simple Bouguer gravity map. In such cases, one can see

the importance of anomaly separation routines which consist of removing regional anomalies resulting from the deep seated structures so as to emphasize residual gravity anomalies (Figure.4.7) associated with subsurface source of primary interest.

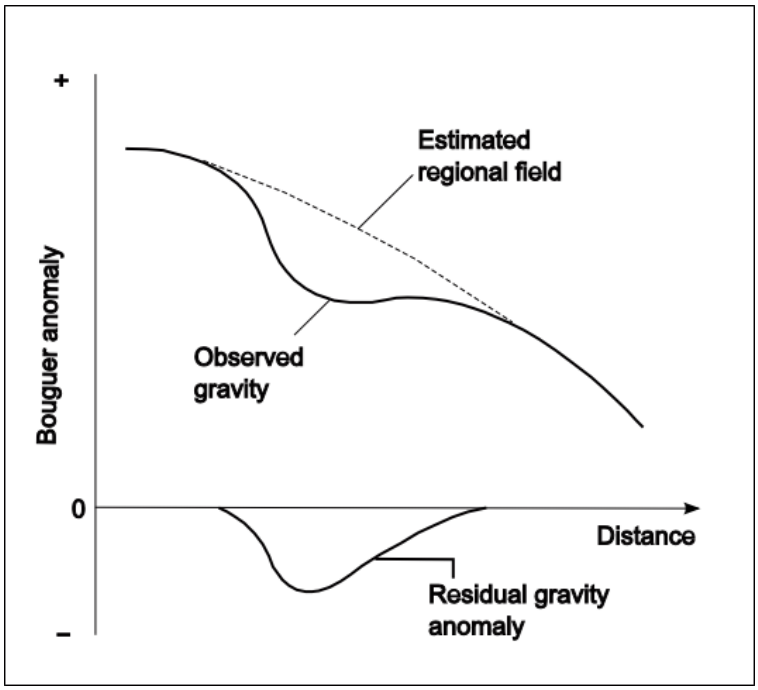

Figure 4.7: The separation of regional and residual gravity anomalies from the observed Bouguer anomaly.

4.2.2.2 Upward Continuation

The regional - residual field separation of the Bouguer anomaly has been studied using the "upward continuation filtering technique". In this technique filtering separation using differential upward continuation (Paul et al, 1966; Jacobsen, 1987; Blakely, 1996) can be used to determine the gravity response arising from different depth intervals below surface (Figure 4.8). Complete separation of responses is not possible; however, the approach is useful for discerning shallow from deep sources, and highlighting pertinent features and structures dominant within the depth interval of interest.

Using this approach, the data are upward continued to various heights above the datum level (usually the sea level) and one grid is subtracted from another to approximate the response from as specific depth interval. High wave number anomaly components are effectively removed by transformation of gravity data measured on one datum to some higher levels.

Therefore, on higher levels the regional patterns of variations tend to be more clearly displayed.

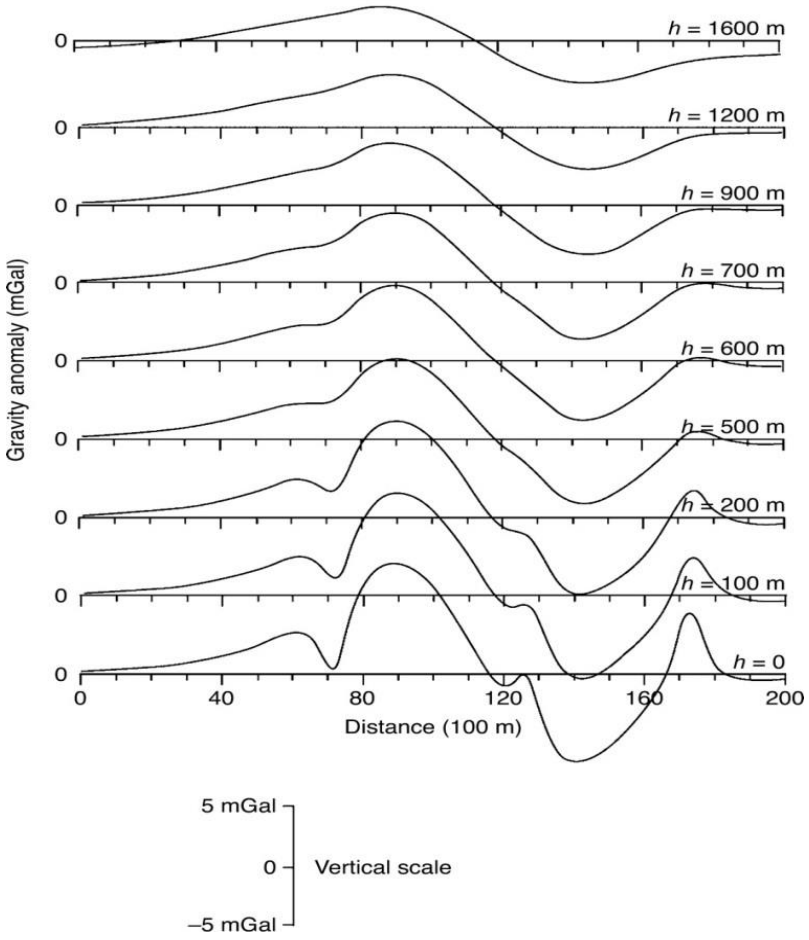

Figure 4.8: Diagram showing upward continuation of the gravity data to different heights.

In this study the Bouguer gravity field is continued upward to variable levels using the Geosoft - Oasis Montaj software (version 6.1). Upward continuation of the Bouguer anomaly field to variable levels yields variable anomaly slices for different depth intervals and calculates the response from sources deeper than depths of approximately half the upward continuation level (Jacobsen, 1987). The depth intervals obtained starting from 0.5 km up to 10 km (Figures 4.17 and 4.18). Comparative study of these intervals indicates that relatively long and short wavelength anomalies related to different structures do exist at different depths.

4.2.2.3 Horizontal Gradient

Horizontal gradient filtering of the gravity anomalies adopted in this study provided much better definition of the geological contacts within the study area. The horizontal gradient method has been used extensively to locate contacts of density contrast from gravity data (Cordell, 1979) or pseudogravity data (Cordell and Grauch, 1985). It use the two first-order horizontal derivatives of the gravity (or magnetic) fields (Phillips, 1998), which reveal the anomaly texture and highlight anomaly-pattern discontinuities. The amplitude of the horizontal gradient (Cordell and Grauch, 1985) is expressed as:

$$HG = \sqrt{\left(\frac{\partial \mathrm{g}}{\partial x}\right)^2 + \left(\frac{\delta \mathrm{g}}{\delta y}\right)^2} \qquad (1)$$

Where $\left(\frac{\partial g}{\partial x}\right)$and $\left(\frac{\delta g}{\delta y}\right)$ are the horizontal derivatives of the gravity field in the x and y directions.

The high component of the horizontal gradient anomaly tends to overlie the edges of any causative bodies (geological structures) if the edges are vertical and well separated from each other. It is maximum over the boundaries of geological structures mainly related to horst or graben features, masses extending horizontally and vertically, fault blocks, and volcanic intrusive bodies, (Blakely, 1995). The method is also robust to delineate either shallow or deep in comparison with the vertical gradient, which is useful only for the shallower structures. In this case, major fault zones and fold structures associated with lateral fault movements can be mapped and traced by computing the horizontal gradient of the gravity anomalies within Ajdabiya Trough area.

4.2.2.4 Euler Deconvolution

Euler deconvolution has come into wide use as an aid to interpreting profile or gridded gravity and magnetic survey data. The technique is used to help determine the location and depth of causative bodies and help to further highlight trends in density and magnetic susceptibility anomalies. Euler deconvolution is a method of solving Euler's homogeneity equation for potential fields (Thompson, 1982). It can be expanded to work on gridded potential field data,

a full discussion of which is given in Reid et al, (1990). 3D form of Euler's equation can be defined as:

$$x\frac{\partial g}{\partial x}+y\frac{\delta g}{\delta y}+z\frac{\delta g}{\delta z}+\eta g=x_o\frac{\partial g}{\partial x}+\ +y_o\frac{\delta g}{\delta y}+z_o\frac{\delta g}{\delta z}+\eta b \qquad (2)$$

Where $\frac{\partial g}{\partial x}$, $\frac{\delta g}{\delta y}$, and $\frac{\delta g}{\delta z}$ are the derivatives of the field in the *x*, *y*, and *z* directions, η is the structural index value that needs to be chosen according to a prior knowledge of the source geometry. ηg, ηb (b and g are the total field components or potential function). By considering four or more neighbouring observations at a time (an operated window), source location (x_o, y_o, and z_o) and *b (the potential function)* can be computed by solving a linear system of equations generated from equation (2). Then by moving the operated window from one location to the next over the anomaly, multiple solutions for the same source are obtained.

4.2.3 An Overview of the Gravity Anomalies

The range of the Mesozoic - Cenozoic sediment densities in sedimentary basins is generally lower than that of most enclosing Palaeozoic sedimentary and crystalline rocks. Thus, medium to high negative gravity anomalies would be expected where the preserved strata in the basins are thick. Unlikely this is not the case in the Ajdabiya Trough area where low amplitude positive gravity anomaly is dominated and centred above the centre of the trough. However, the geometry of sedimentary basins is commonly not readily apparent from Bouguer anomaly maps because of the dominance of large-amplitude regional gravitational fields. During interpretation of the gravity data and after regional gradients of the gravity anomalies are removed using regional residual anomaly separation technique, the internal structures of the basins are usually discriminated, especially where there are major faults and thick sedimentary sections. Interpretation of basin geometry using gravity maps is further complicated by the presence in some areas of large volumes of intrusive bodies, dikes, and basalt flows (mafic / felsic basement); however, the large density contrast between these structures (density ~ 3.0 gm/cm^3) and the Mesozoic - Cenozoic sedimentary rocks (density ~ 2.5 to 2.7 gm/cm^3) facilitates meaningful analysis of intra-sedimentary volcanics (e.g. Busrewil et al., 2008; Witte, 2008).

Recognizing potential field lineaments require a conceptual interpretation scenario, based on an understanding of the geology and structure of a given area. This knowledge is commonly inferred from magnetic and gravity maps. Interpretations of lineaments and structures can be very important for structurally controlled deposits, intrusion-related deposits. Interpretation can be visual or semi-automated using some filtering techniques (e.g., horizontal gradient). Within Ajdabiya Trough, localised NW-SE and N-S trending gravity lineaments are associated with positive gravity anomalies. The amplitude of these anomalies ranging from 5-15 mGals and are developed at the intersection of a NW-trending gravity high and an ENE-trending gravity high possibly attributed to major shear zone inherited from Pan-African orogeny and linked to the South Cyrenaica Fault Zone (e.g. Anketell, 1996). The gravity anomalies reveal about 200 km long, elongated, NW-trending gravity highs with peak values of 0 mGals and amplitudes of 5-15 mGals. These variations were ultimately related to structures formed during successive tectonic events, which indicate, that the present-day structural configuration of the Sirt Basin results from the interplay of Palaeozoic, Mesozoic and Cenozoic tectonism. Interpretation of the 2D seismic data (chapter 7) confirms that the Ajdabiya Trough area is affected by fault systems whose orientations are different owing to changes in tectonic regimes.

The compiled Bouguer anomaly map of the study area (Figure 4.6) was generated from the coverage shown in figure 4.5. The map shows a clear regional gradient from relatively low gravity values of less than –25 Gal in the NE (Cyrenaica region) and to the SW (Al Hagfa Trough) to positive gravity values ranging from 15 - 20 mGal in the Ajdabiya Trough depocentre and over the Rakb High to the SE. The regional trend may also be influenced by a variation in sedimentary densities as a study of well logs from the Libyan basins (Essad, 1978) shows that in general the density of the sedimentary rocks increases from the SW (Murzuk region) to the NE (Cyrenaica).

The Bouguer garavity map points out mainly three distinctive areas: a predominant positive gravity trending NW–SE to N–S in the centre of Ajdabiya Trough bounded by NW-SE to NE-SW regional low gravity trends on the west and the east sides of the trough. The positive anomalies are mainly located within areas occupied by the Ajdabiya Trough complex as well as by the Rakb High to the south east and part from the Cyrenaica Platform at the north east. The positive anomaly over Cyrenaica Platform to the northeast (Figure 4.6) occurs over

outcrops of Oligocene to Miocene carbonates (El-Hawat and Shelmani 1993).To the west of Ajdabiya Trough a negative gravity zone is surrounded by regions of positive gravity anomalies parallel to the Al Hagfa Trough structural trend. The regional positive anomaly trending NW–SE, seems to represent the signature of dense rocks in the centre of Ajdabiya Trough area. The regional structure is characterized by a broad positive gravity in the centre bounded by gradients increasing towards the east and the west. It may be inferred from these observations that the basement is deepening towards the north of the region. Indeed, using gravity modelling and spectral analysis of gravity data, Spector and Grant, (1970); Regan and Hinze, (1976) obtained the crustal thickness beneath the Ajdabiya Trough to vary from 26 km in the centre to 35 km in the east and west boundaries. An inferred Moho depth map show that the crust is thinning towards the central part of the region.

The gravity mapping also shows that the study area is most likely characterized by large scale fault systems along with subordinate faults of variable trends and strikes. Seismic data confirm that these faults are mainly rift faults with different dips and strikes most likely basement reactivated faults and present within Early Cretaceous syn-rift sequences (e.g. Roohi, 1996b; Hallett, 2002).

To the north of the study area, the faults are trending NW-SE and NE-SW, while to the south the faults are predominantly trending NW-SE and E-W. The E-W trending faults may have initiated during the Early Cretaceous rifting (140-115Ma), probably in response to NS extensions along the edge of the Neo-Tethys, (Dercourt et al., 1993; Robertson et al., 1996; Guiraud, 1998; Guiraud et al., 2001; Bosworth et al., 2008), resulting in the development of E-W to ENE-WSW trending grabens and/or half-grabens (Figure 4.9) that showed strong subsidence during the Early Cretaceous rifting (Neocomian-Barremian times), notably the Hameimat and Sarir in the south-eastern Sirt Basin (Rossi et al., 1991; Gras and Thusu, 1998).

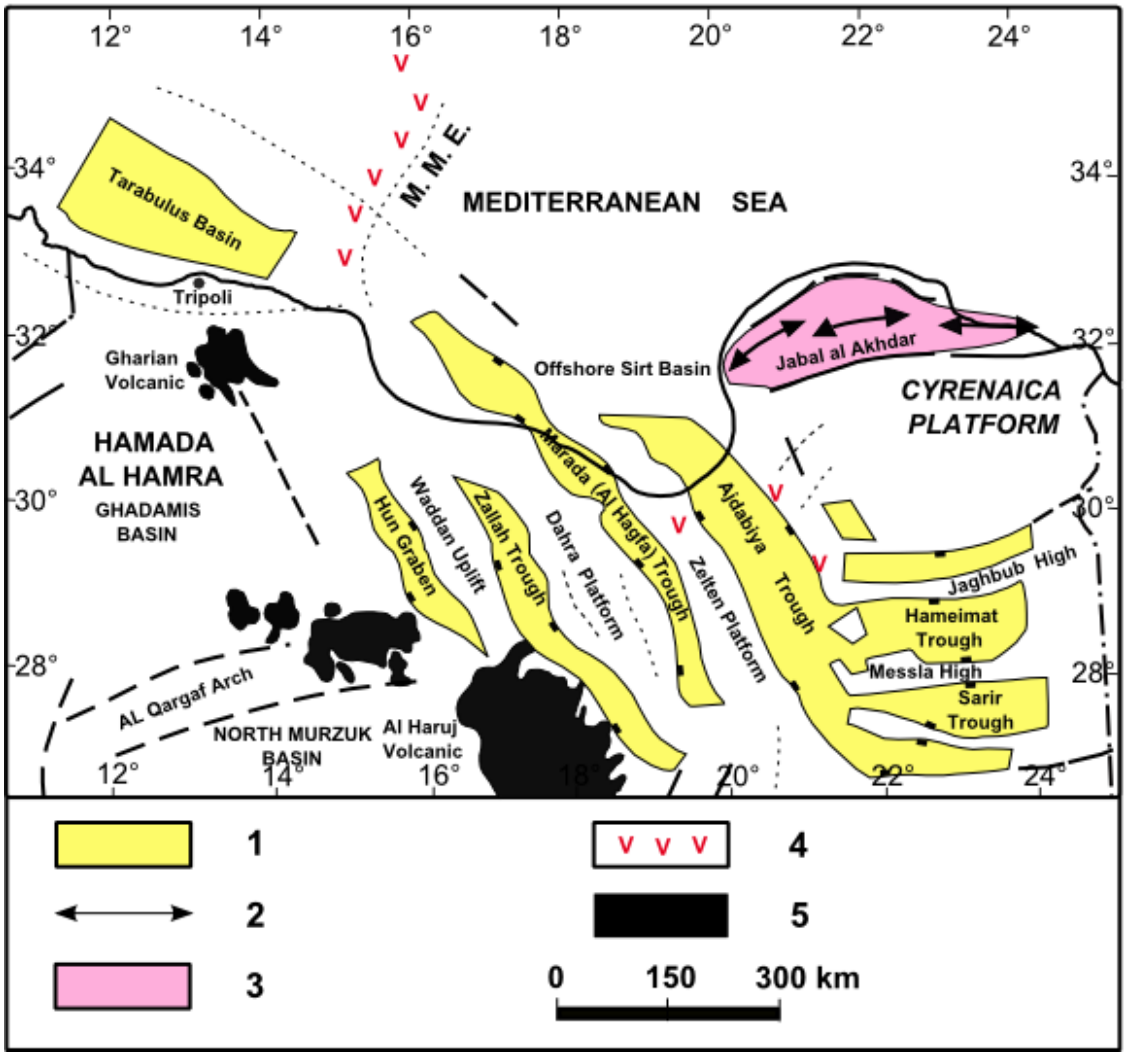

Figure 4.9: Present-day schematic pattern of Cretaceous tectonic units along the Libyan Tethyan margin, modified from Guiraud & Bosworth (1997). l, Cretaceous rift or subsiding basin; 2, anticline axis; 3, Late Cretaceous (Senonian 88.5–65 Ma) inverted area; 4, Cretaceous magmatic occurrence; 5, Miocene to recent volcanism. M.M.E., Misratah-Malta escarpment. Map re-drawn from Guiraud (1998).

4.2.3.1 Gravity Response Arising from Cenozoic Section

The observed gradient in Bouguer gravity anomalies (Figure 4.10) ranges from an average of about 0.02 mGal/km to about 0.04 mGal/km. High gradient areas on the map are likely to represent faulted boundaries. The map shows that the study area is characterised with a tectonic zone comprised of variable tectonic trends, affecting the Cenozoic section. An E-W trend is characteristic of the south-eastern part of the zone, the NW-SE trend covers the major part of the zone and the NE-SW trend characterise the northeast part of the zone. A possible geological interpretation is that the earliest structures developed along the E-W trend during

the early Cretaceous, possibly in response to extension along the edge of the Neo-Tethys, resulting in the development of E-W troughs and highs across the northern part of Libya (Bosworth et al., 2008).

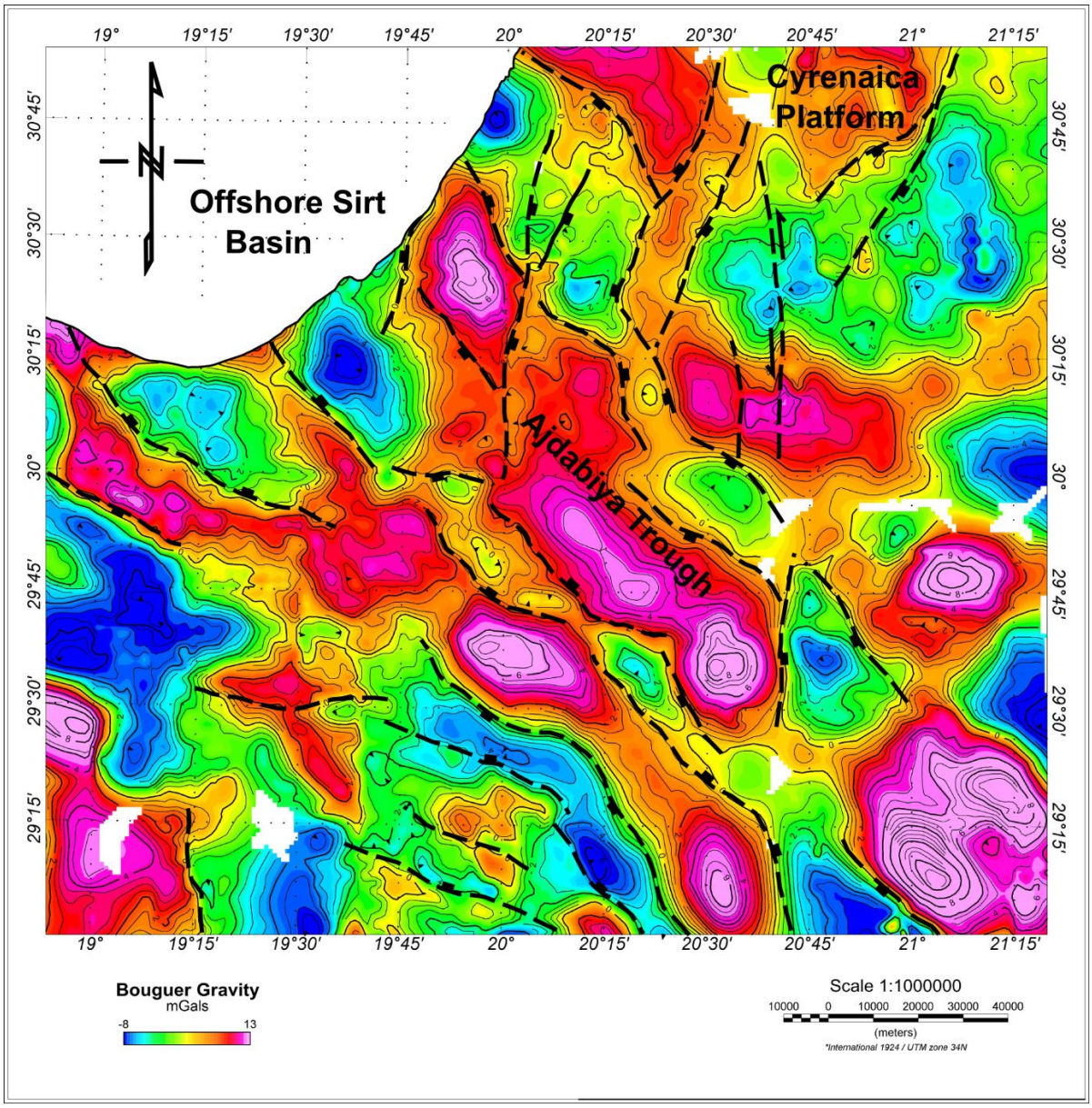

Figure 4.10: Bouguer gravity map produced from upward continuation to 4 km level, showing main faults that cut the Cenozoic succession, along with an inferred strike slip fault at the NE part.

At the north east side of the map, an abrupt change in gravity contours along N-S trending region characterized by an intermittent gravity low may be the imprint of strike-slip fault that links with similar structures observed in the Cyrenaica region from north to south (El Arnauti

et al., 2008). This possible strike slip fault seems to cut the Cenozoic sediments and extend downward into the Mesozoic section. It is possibly linked to very deep source as deformation in the lower crust and upper mantle was distributed over a broad region of the eastern Ajdabiya Trough and over Cyrenaica Platform (El Aranauti et al., 2008).

4.2.3.2 Gravity Response Arising from Mesozoic Section

The Bouguer gravity map (Figure 4.11) varies from -5 mGals in the southwest and northeast boundaries of the Ajdabiya Trough to about 4 mGals in the centre of the trough, thus a gravity relief of about 9 mGals is observed giving average gravity gradient of 0.04 mGal/km over about 100km. The general trend of gravity contours is NW-SE following the major Cretaceous trend in the Sirt Basin. The low amplitude positive gravity anomaly over the centre of the trough (~4 mGal) may be attributed to the presence of high density sediments (e.g carbonates or/and evaporites) or due to influence arising from high density body beneath the sedimentary cover close to the Moho. The positive gravity anomaly could be also related to volcanic structures or deep ridge as proposed by Hallett and El Ghoul (1996).

4.2.3.3 Gravity Response Arising from Paleozoic – Mesozoic Section (7km level)

Bouguer gravity anomalies arising from Palaeozoic and deeper sources over the Ajdabiya Trough are shown in Figure 4.12. The Bouguer gravity is dominated by a regional field at the central area, the source of which is possibly deeper in the crust and may be related to changes in basement density and variations in crustal thickness. Trends in the Bouguer gravity anomalies are comparable with the basement trend within the study area. Paleozoic deformation within the Ajdabiya Trough is controlled by Precambrian structural patterns such as faults which existed prior to the deposition of the Mesozoic sediments (Baird et al., 1996).
Another hypothesis is that this could be related to very low contrast in densities between the sediments, or could be related to thinning of a preserved Palaeozoic section at the centre of the trough. The low amplitude gravity anomaly is also possibly due to volcanics or due to lithological variations and changes in depositional environments (e.g. carbonate to shale transition).

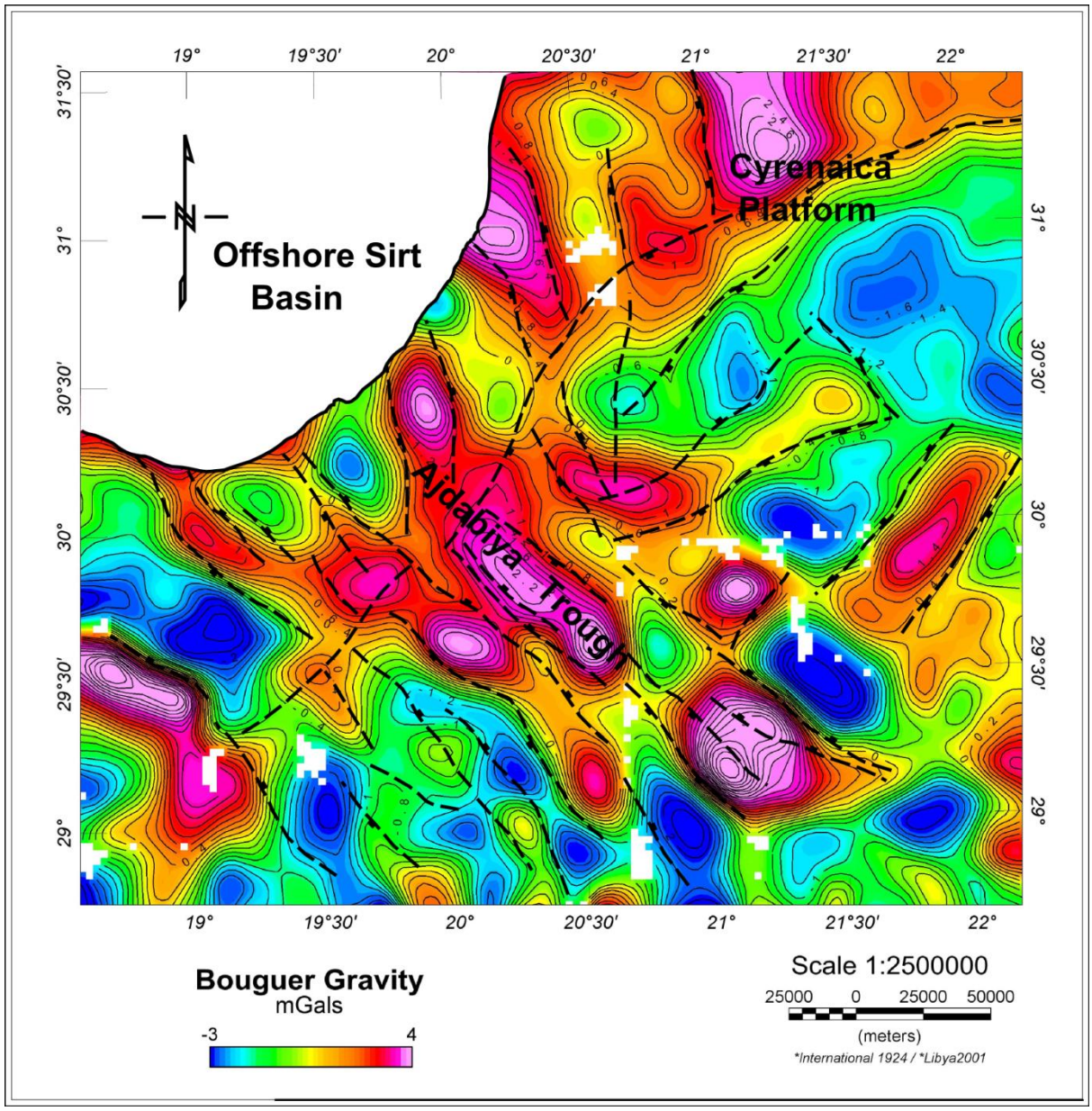

Figure 4.11: Bouguer gravity map produced from upward continuation to 6 km level, showing main faults, cut the Mesozoic succession with extended strike slip fault at the NE part.

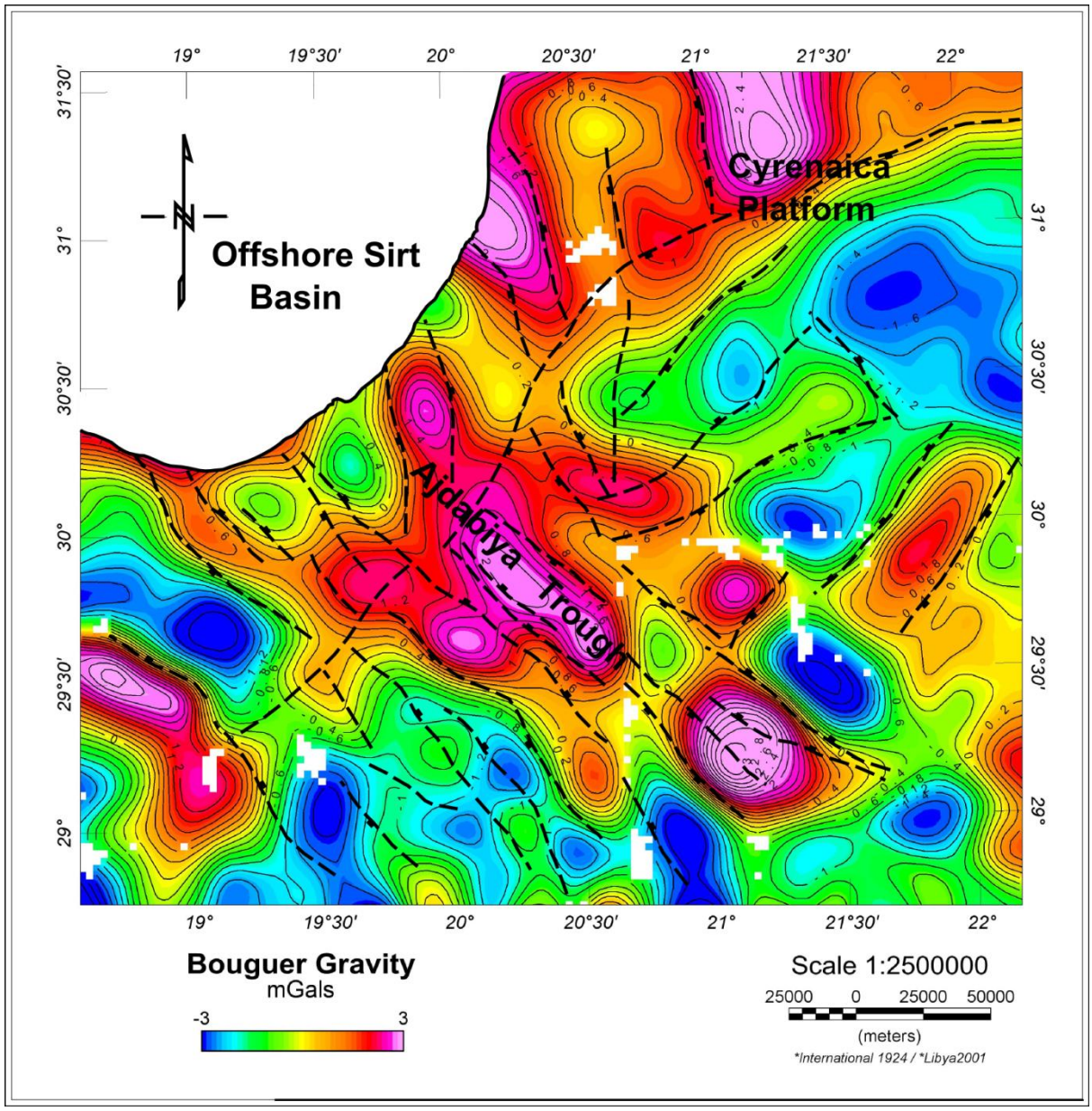

Figure 4.12: Bouguer gravity map produced from upward continuation to 7 km level, showing main faults, cut the Palaeozoic - Mesozoic succession with extended strike slip fault at the NE part.

4.2.3.4 Detailed Results from Upward Continuation and Horizontal Gradient

1-Slice (0.5 – 1km)

With the help of upward continuation technique, the gravity anomalies are separated into a series of spatial components assumed to be associated with different "depth slices". This way, upward continuation may be regarded as a pseudo depth slicing technique, whereby structures may be traced through the crust (Jacobsen, 1987). Several additional lineaments and deep

structures (faults) are apparent on enhanced depth slices of the gravity data. Overlaying the depth slices (Figures 4.13 - 4.18) shows clear indications and continuation of fault zones at a basement to upper-crustal level into the shallow depths across the Ajdabiya Trough area. The upward continuation maps at large depths confirm that the regional-scale faults characterized the deeper structure setting of the Ajdabiya Trough, and affected the shallow structural scheme.

It is postulated the main trough bounding faults were subject to movement during Mesozoic time (e.g. Baird et al., 1996) and may facilitate that possible variation in the structural style of the main basement blocks within the trough. The maps show that these faults have been significantly offset by either sinistral or dextral movement (e.g. El Arnauti et al., 2008) along zone of weakness defined by long offset gravity lineaments (Figures 4.13 - 4.17). Alternatively, these apparent offsets may be the result of rift segmentation. In addition, there are possibly zones of mafic and felsic intrusives (Busrewil et al., 2008; Witte, 2008), or uplifts marked on the maps (Figures 4.13 - 4.17).

An upward continuation to a height of ca. 1000 m suggest, that the gravity anomalies arise principally from variations in basement topography. A major uplift of Albregha High (Hallett and El Ghoul, 1996) is placed at the north-western part of the study area. The most noticeable features on the upward continuation map of the gravity anomalies are the ENE–WSW trending basement shear zones crossed by NW-SW lineaments bounding uplifting horst and subsiding graben features. These include the Rakab High and Amal Platform to the east and Al Jaham Platform, Zelten Platform and Assoumoud Ridge to the west (Figure 4.13).

The major structural characters of the Ajdabiya Trough area are the NW–SE and NE-SW trending structures which are mainly widespread in the area as a result of phases of rifting and fault reactivations.

It is observed that identified faults from the horizontal gradient map are superimposed on depths to basement undulation zones (areas of steep gradients). It is interesting that good correlations have been obtained between the basement undulation from gravity data and known faults in the study area (Chapter 7). Other undulation features traced from the equivalent horizontal gradient map are the expressions of folding during the Cenozoic (e.g. El Arnauti et al., 1996). The mapped gravity highs in Ajdabiya Trough area and northern

Cyrenaica may be also associated with fundamentals of WNW-ESE strike-slip faulting in response to transpressional tectonics (e.g. Anketell, 1996; El Arnauti et al., 2008).

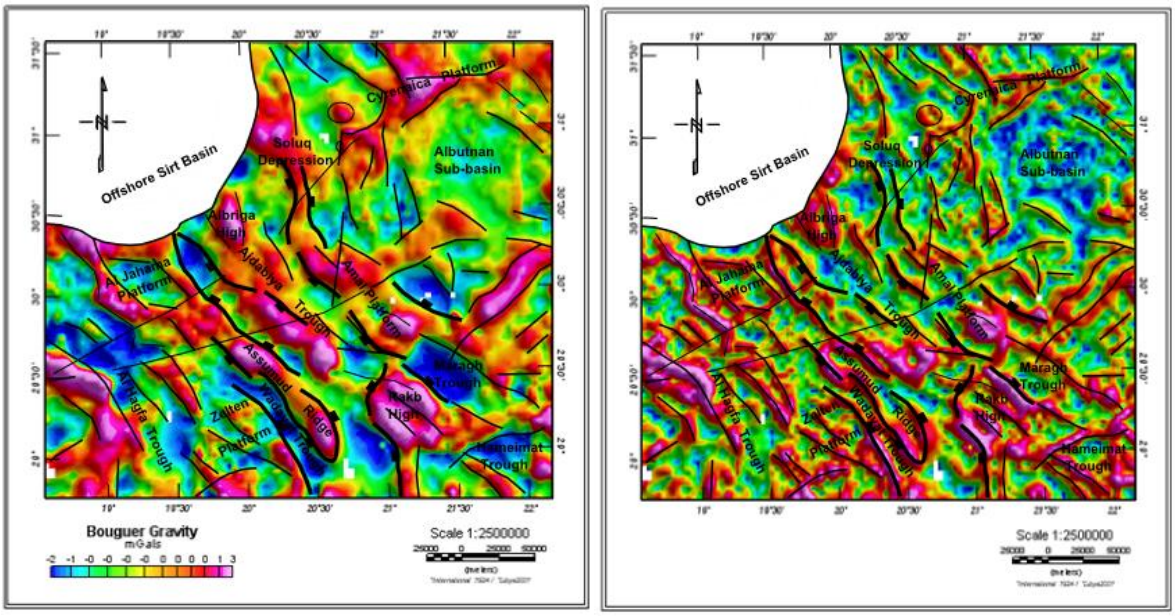

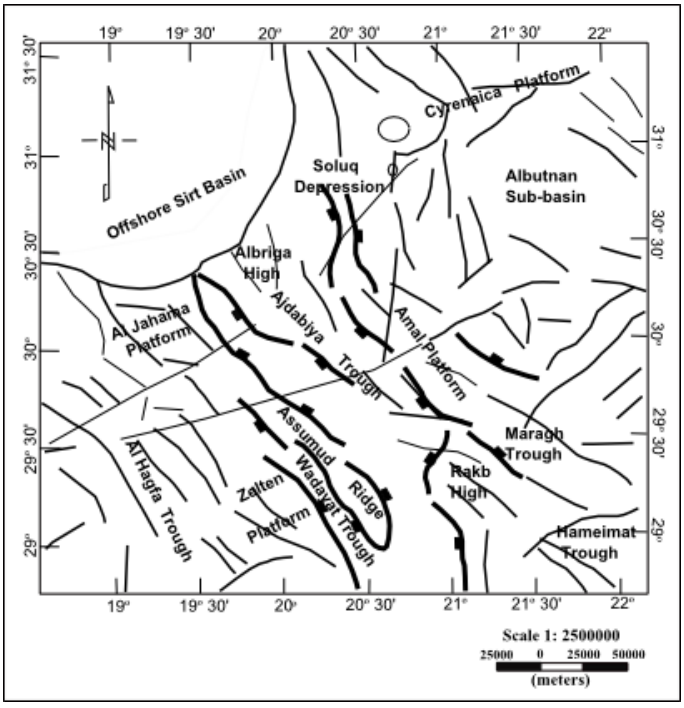

Figure 4.13: Upward continued Bouguer gravity to 1000 meter (Slice 0.5 – 1km) (a) and it is equivalent total horizontal gradient (b) with lineament interpretations below. (a) Most prominent gravity lineaments interpreted from the Bouguer gravity anomaly, and its gradient enhancements superposed on Bouguer anomalies. Lineaments from shallow depths show good expressions of major faults bounding main horst and graben features with other details outlining other fault structures and possible shear zones.

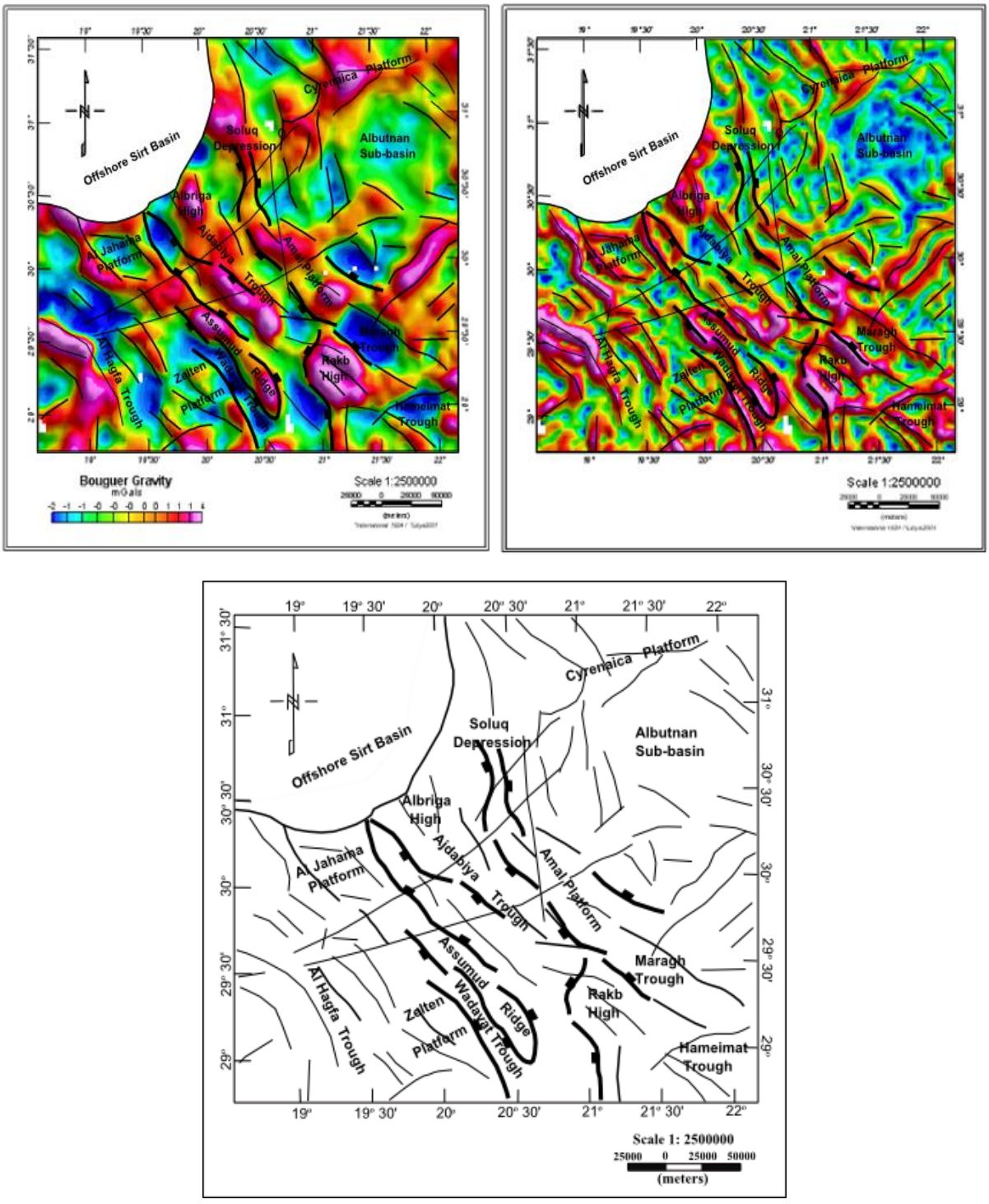

Figure 4.14: Outlining the upward continuations of the Bouguer gravity anomaly with equivalent total horizontal gradient slice of 1 – 2km ("pseudo-depth slices", Jacobsen, 1987). Upward continuation image portray anomalies from source depths (indicated on depth slices) greater than half the level of upward continuation (Jacobsen, 1987).

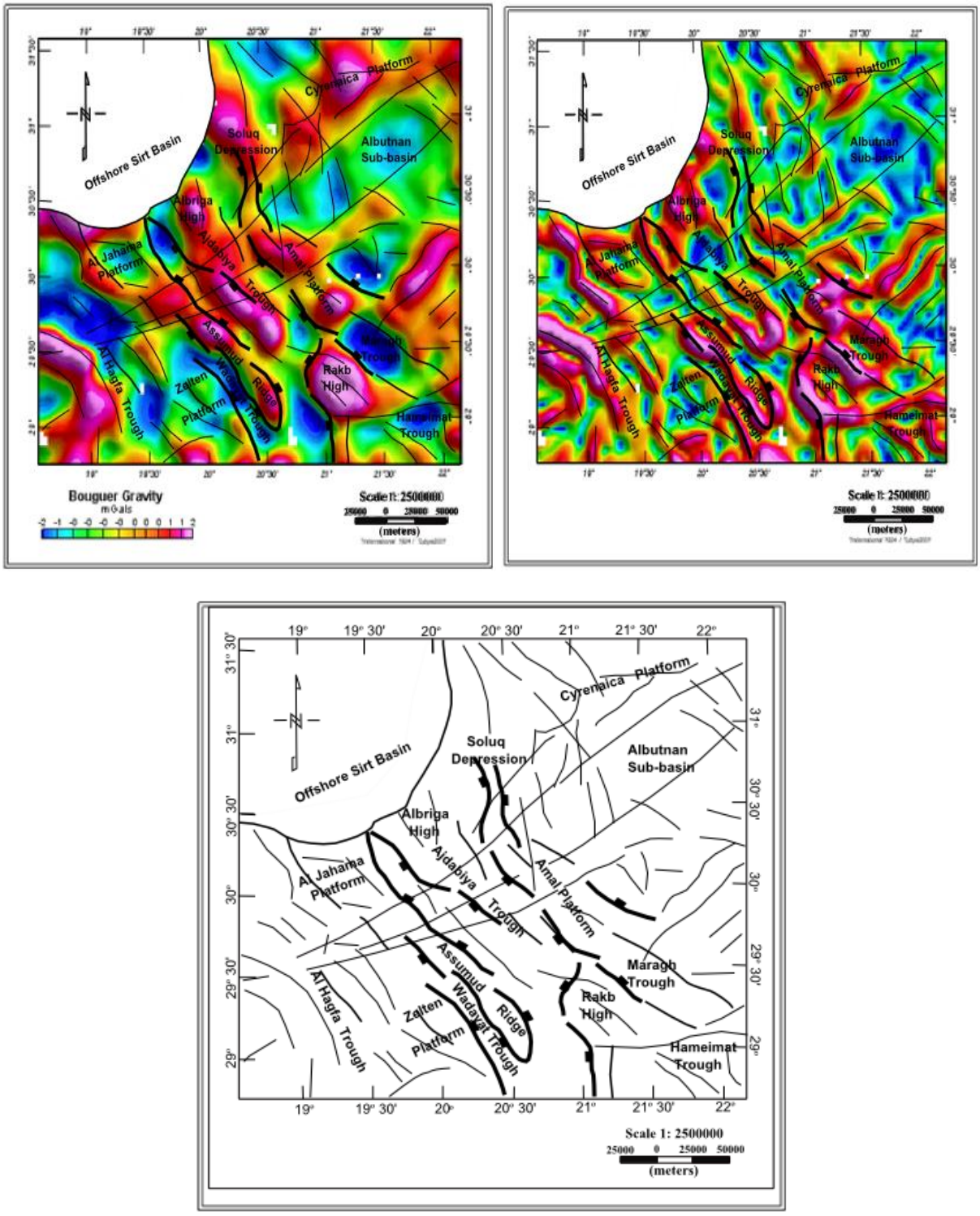

Figure 4.15: Outlining the upward continuations of the Bouguer gravity anomaly with equivalent total horizontal gradient slice of 3 – 4km ("pseudo-depth slices", Jacobsen, 1987). Upward continuation image portray anomalies from source depths (indicated on depth slices) greater than half the level of upward continuation (Jacobsen, 1987).

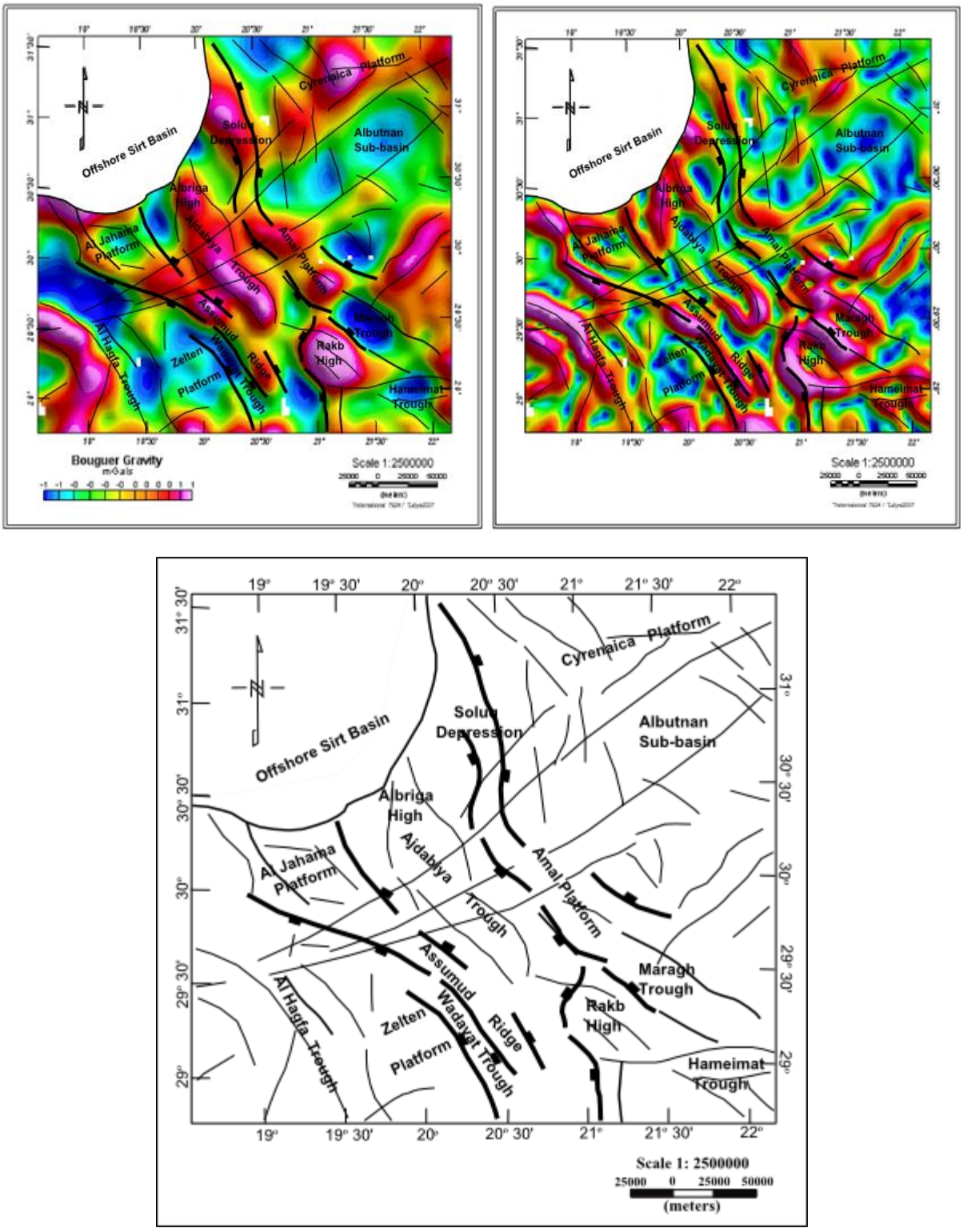

Figure 4.16: Outlining the upward continuations of the Bouguer gravity anomaly with equivalent total horizontal gradient slice of 5 – 6km ("pseudo-depth slices", Jacobsen, 1987). Upward continuation image portray anomalies from source depths (indicated on depth slices) greater than half the level of upward continuation (Jacobsen, 1987).

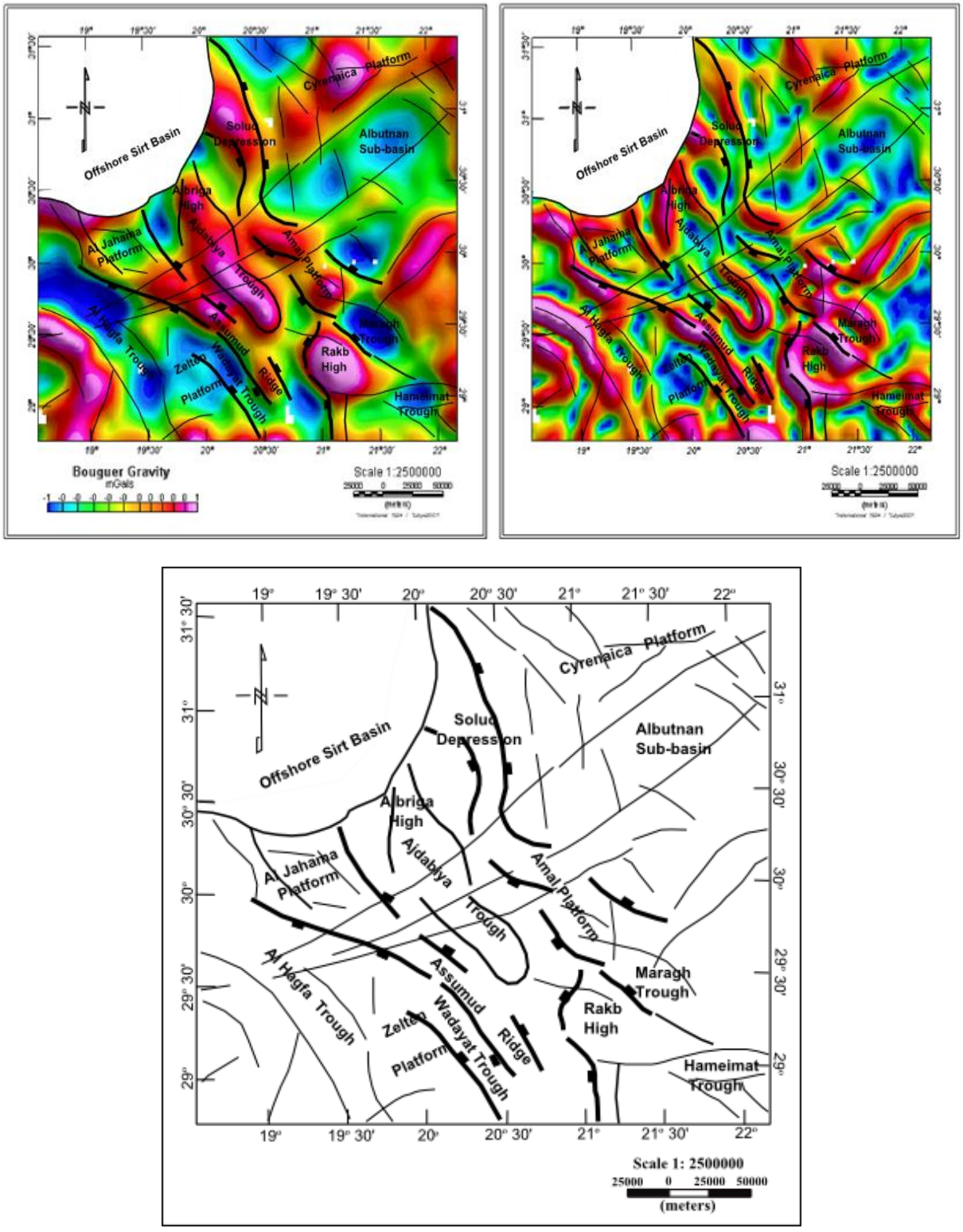

Figure 4.17: Outlining the upward continuations of the Bouguer gravity anomaly with equivalent total horizontal gradient slice of 6 – 7km ("pseudo-depth slices", Jacobsen, 1987). Upward continuation image portray anomalies from source depths (indicated on depth slices) greater than half the level of upward continuation (Jacobsen, 1987).

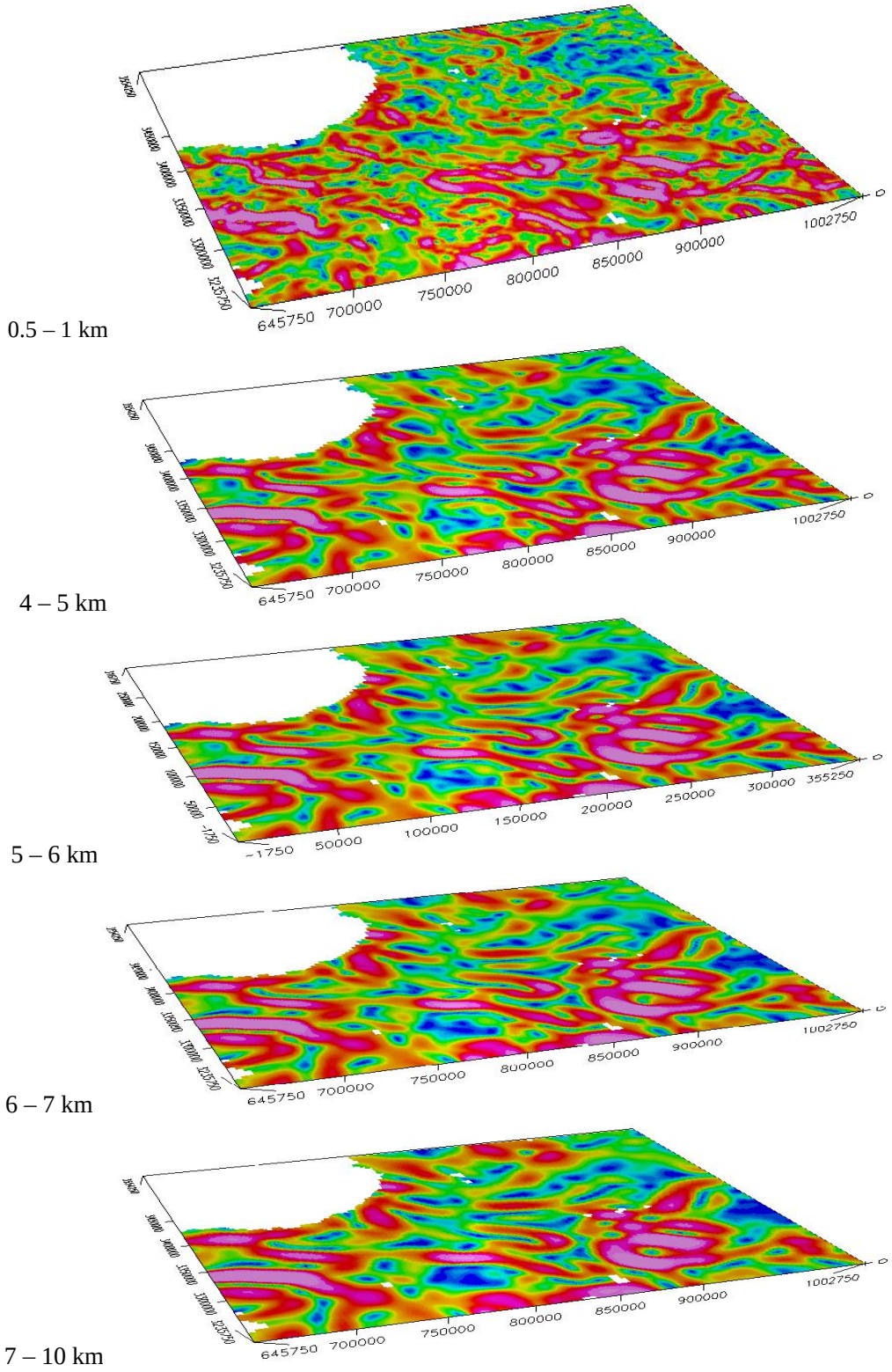

Figure 4.18: Upward continuation slices of the Bouguer gravity field ("pseudo-depth slices", Jacobsen, 1987). The Upward continuation images portray anomalies from deep source depths of about 10 km up to shallow depth of 0.25 km.

To summarise, it is observed on all maps that the gravity low in the Cyrenaica region is traversed by NW-SE or N-S cross lineaments, which are probably faults, and cut to the southwest by the dominant NW-SE Sirt faulting which slightly bend towards the N-S in southern Ajdabiya Trough. The upward continuation of the gravity data is adequate for picking out local anomalies; however in northern Cyrenaica region the maps show residual high gravity which would be associated with thick carbonate sequence or uplifted basement of the late Cretaceous inversion (Al Jabal Al-Akhdar anticline) (e.g. El Arnauti et al., 2008). This high area possibly continues offshore and could therefore be part of a large feature involving uplift and northward, development of oceanic crust. Within the Ajdabiya Trough isolated gravity lows represent individual grabens with possible significant sections of Cretaceous and Tertiary sediments fill, but these are represented by only moderate - low values on the gravity maps. This suggests possible local basement changes as well as local crustal thinning.

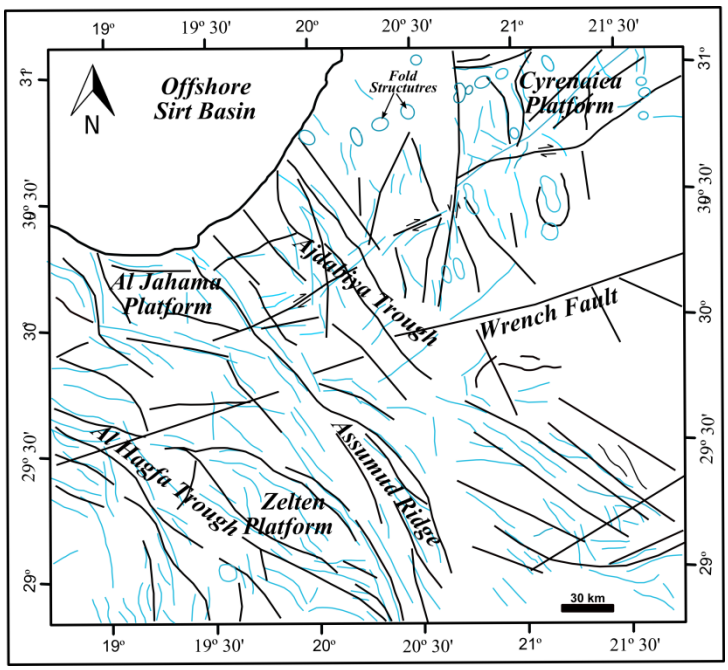

Figure 4.19: Summary of main lineaments deduced from the upward continuation maps. The lineaments are striking in NE – SW, NW–SE, and NNW–NNE directions with fold structures in northeast Ajdabiya Trough and Cyrenaica Platform. Black features are obtained from deep sources mainly Paleozoic - Mesozoic source while blue features are Cenozoic source.

These aspects are discussed further in the gravity modelling section, below. All the upward continuation maps (Figures 4.13 - 4.17) permit mapping of many fault segments, and fold structures (Figure 4.19) particularly in NW-SE, NE-SW trends persist north-westwards from

eastern Ajdabiya Trough until termination at a probable cross fault further west, NW-SE features are broken into segments by N-S and NE-SW probable strike-slip faults.

4.2.4 Results of Euler Deconvolution Method

The Euler method has been applied to the residual data using moving windows of 7km x 7km and 20km x 20km. I have assigned various structural index values and found that structural index (SI) of (0) gives good clustering solutions for faults and (SI) of (1) gives good clustering for other structures. However, many other cases have been studied using various combinations of structural indices and window sizes which are not described below.

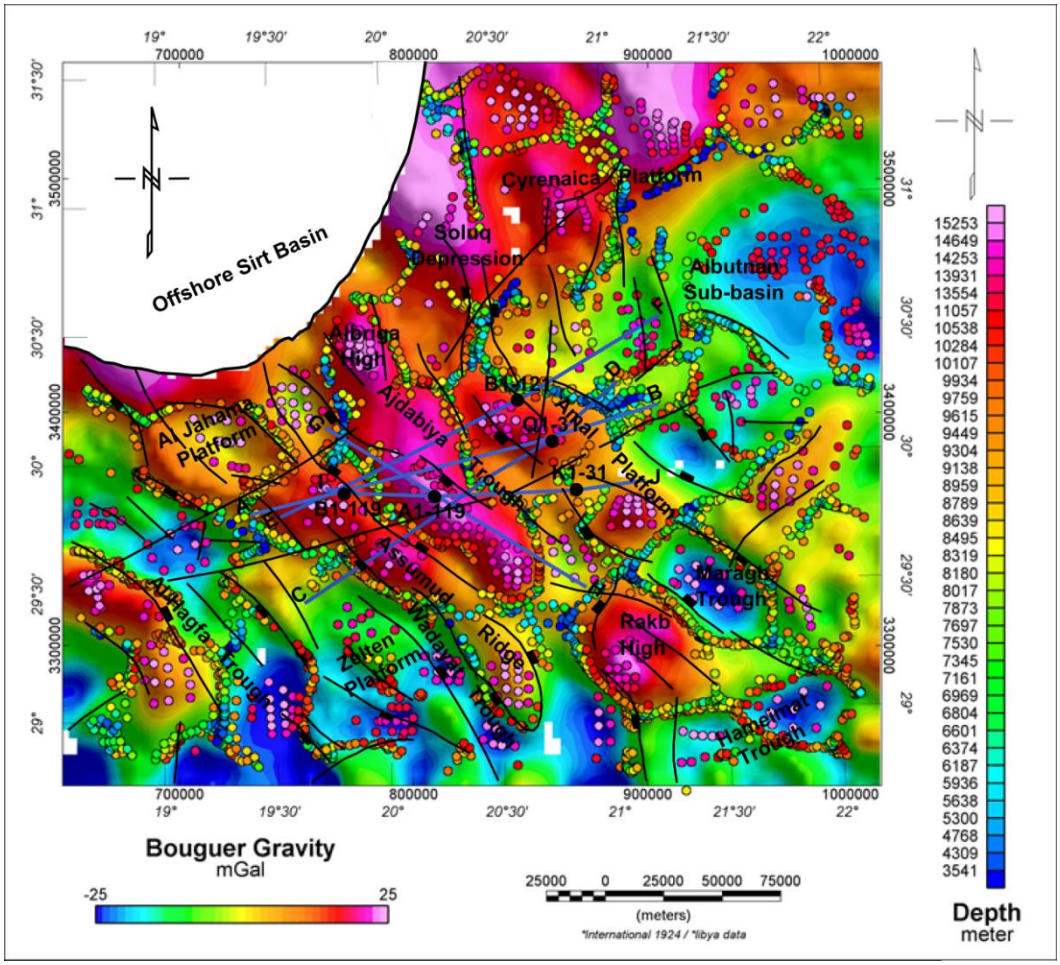

Figure 4.20: Euler Deconvolution applied to gravity dataset of Ajdabiya Trough and the nearby areas. Grid spacing: 3.0 km. Structural Index SI = 0.0. Window Size: 7x7. The depth solutions obtained using the Euler deconvolution technique, show regular depths (coloured circles), representing clear NW-SE trend of rift signature, Euler solution clusters support a basement source at around 4 - 10 km depth as might be expected in this area. NW-SE trend following the Sirt Rift (variable colour circles) can be traced. Wrenching in the area mapped along major NE-SW trend (orange - reddish coloured circles) (eg. El-Badrawy and Soliman, 2000).

It is seen that the Euler depth solution and the derived results from the upward continuation analysis are well correlated. After studying the Euler deconvolution, it seems that there are many trends identified through Euler deconvolution study indicated by the locus of source points as the faults and structural lineaments. The results suggest that the structural trends are predominantly elongated in the NW-SE and ENE -WSW directions.

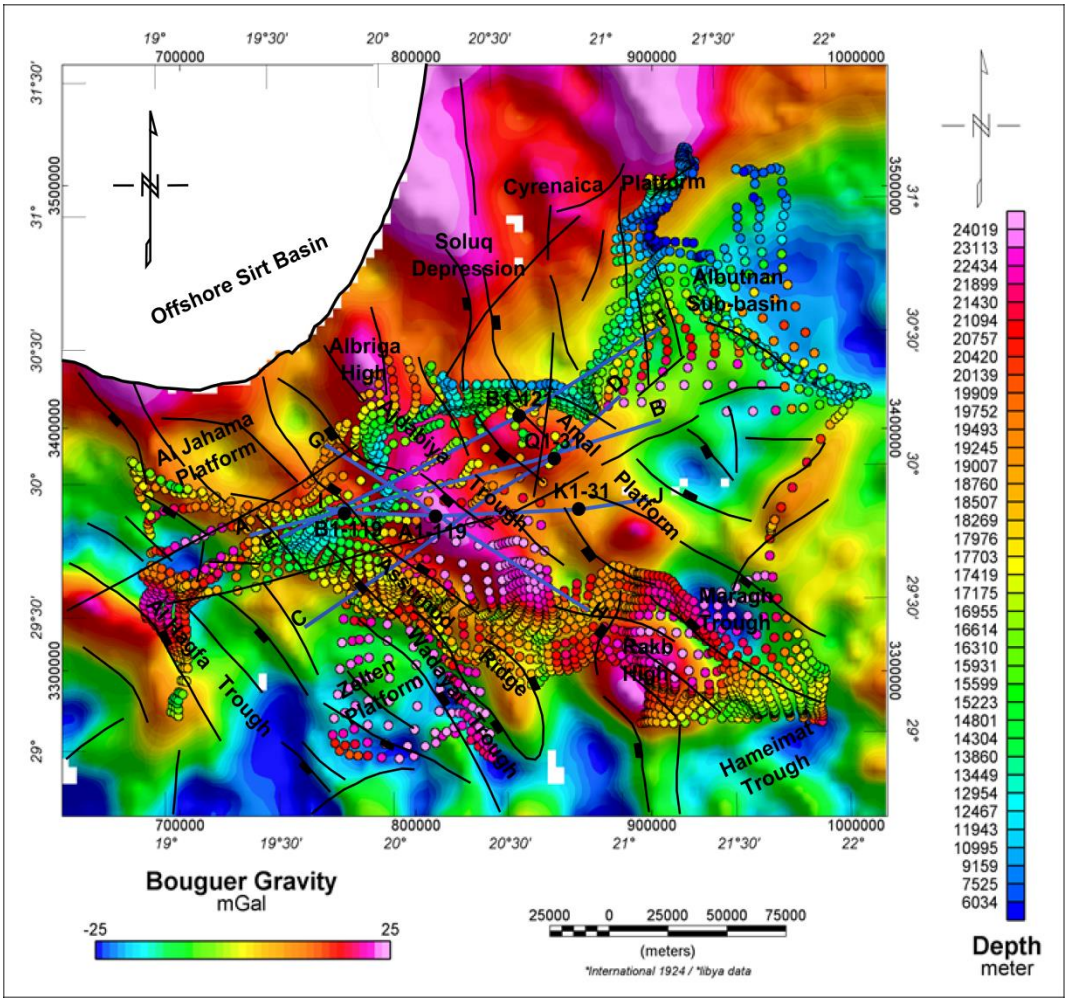

Figure 4.21: Euler Deconvolution applied to gravity dataset of Ajdabiya Trough. Structural Index SI = 1.0, Window Size: 20x20, limiting distance from centre of window Max D: 30km, Grid spacing: 3.0km. Depth uncertainty of dz ≤ 15% and a horizontal uncertainty of dxy ≤ 20% are retained, which results in an obvious reduction of solutions, although the clustering of solutions at the centre of the Ajdabiya Trough remains apparent. The significant arrangements of solutions in the range of 15 to 28 km above the Ajdabiya Trough broad anomaly are significant enough to serve for discussion.

The basement depths estimated through Euler deconvolution technique are varying from about 4 km to 10 km. Within the central part of the Ajdabiya Trough, the basement depth

calculated is more than 10 km. Depth solutions obtained from the gravity data (Figures 4.20&4.21) show significant variations from south to north ranging from approximately 2 to over 20 km below sea level clearly highlight the overall structural framework of the area, including likely influences from basement faults. A number of deeper Euler solution clusters (red warm colours) were observed in the central zone indicating the probability of intra-basement intrusive bodies.

The basement faults trends are again NW-SE and ENE-WSW. There exists a good correlation between these faults derived independently from seismic reflection data (chapter 7) and enhanced gravity data.

4.3 2D Gravity Modelling and Densities of the Main Rock Types

In order to facilitate gravity interpretation, the gravity responses of three geological profiles have been modeled to attain a fit between calculated and observed gravity using 2D modelling technique. The 2D modeling was performed with the GMSYS modeling software extension of the Geosoft Oasis montaj software package. GM-SYS Profile is a program for calculating the gravity and magnetic response of a geologic cross-section model. The software allows the user to digitize a profile from maps in Geosoft. In general, the extent (x-coordinate) and depth (z-coordinate) of the profile to be modeled and the Earth's gravity and magnetic field parameters (Strength, Inclination, and Declination) are defined. With the given coordinates a topography, gravity and magnetic profile can be extracted from geo referenced grids or maps. The presented models are pure 2D models.

The method of gravity modelling enables us to test the conformity between the calculated gravity response of modelled bodies in a vertical geological cross-section and the gravity effect measured in the field. In addition to the gravity anomalies assessed from the field measurements, densities of rocks, shapes and the depth extent of geological bodies have been considered. To minimize the risk of non-realistic model solutions, the following sources were respected and integrated into the models: The data from boreholes, especially of those situated near the lines of the modelled cross-sections; any previous gravity models such as those from the Sirt Basin and Cyrenaica Platform (Libyan Gravity Compilation Project, 2002; Witte, 2008),; rock densities obtained from previous studies such as those from (Essad, 1978;

Libyan Gravity Compilation Project, 2001; Makris, and Yegorova, 2006; Casten and Snopek, 2006) and results of 2D seismic interpretations and fault analysis (Chapter 7).

Within the Ajdabiya Trough area, I used the forward models to test the hypothesis that igneous intrusions are assumed to be the main source of the positive gravity anomalies observed in the central Adjabiya Troughin the modelled cross sections, along which was the gravity modelling performed.

Within the Ajdabiya Trough, the positive gravity anomalies presumably caused by multiple mantle intrusions which may have been initiated as a result of weakening of the crust under extensional forces associated with the Sirt Basin rifting events. AI assumed a density of 2.98 g/cc shown in the models intended to represent a homogenous unit of intruded material that is now anomalously denser than the adjacent crust; instead, it should be taken to represent the average properties of a region rock volume containing of high density igneous Iintrusions. The shape of the hypothetical hypothesised high-density intrusions is open to considerable modification because of ambiguities in modelling gravity data. However gravity minima are mainly related to the marginal clastic-rock-filled basin depocentres. Thus, it follows that the minima at least partly reflect the broad gravity anomaly caused by an increased depth to Moho along the axis of the rift shoulder which may partly have existed during the rift initiation due to possible lower crustal intrusion or underplating.

The models created by GM-SYS extend to a crustal depth of about 40 km, and therefore the whole Ajdabiya Trough crustal structure can be modelled. This is advantageous as the observed gravity field is contributed to by the entire geologic section. To accurately model the upper crustal, residual components requires accurate definition of the regional, lower crustal density variations, such as Moho relief. Positive gravity anomalies are normally assumed to be caused by mass excess located at depth. In some cases, the positive regional gravity response from extended crust, giving rise to an elevated Moho, can be relatively well constrained from the gravity profile itself. However, gravity models are not unique and it is not possible to unequivocally determine the cause of a gravity anomaly in full extent.

The modeled profiles in this study were chosen so as to traverse the major structural features in the area such as fault boundaries, structural highs and lows.

The depth information in the models was constrained by depths obtained from formation tops in selected wells (Q1-31 and B1-121) from Amal Platform to the east, (B1-119) from Al Jahama Platform to the west, and (A1-119) near the centre of the trough.

Once basin structure was determined, densities were altered in order to fit the observed gravity anomaly. I found that the geometry of the lower crust-mantle boundary (Moho) – which is not well-constrained by either borehole data or seismic reflection profiles – also had to be varied to fit the observed gravity response. The sediment densities used in the modelling are outlined summarized in Table 1. These density values for sedimentary rocks are mainly based on analysis of well logs (density and sonic) and core sample analysis from the Sirt, Ghadames, and Murzuk basins, Jefara Plain and Cyrenaica Platform (e.g, Essed, 1978). The density contrast was constructed by assuming a constant basement density of 2.67 and subtracting mean sedimentary densities as used in the 2D gravity modeling. In the same context, assemblages of Ordovician, Silurian, and Devonian strata have been recovered and studied from Palaeozoic successions in wells from east Sirt Basin for the purposes of extracting real densities (Woollam and Pearce 2006). Within the Ajdabiya Trough, the wells used in the gravity modelling (B1-119, B1-121, and Q1-31) are bottomed at Cambro–Ordovician quartz-rich sandstone.

Table. 1 Density values of the main rock complexes (used for the gravimetric modelling of the cross-sections along the profiles 1, 2 and 3)

Rock Complex	**Density [g.cm^3]**
Main data sources: The sediment densities were estimated based on published values and previous models, published values are mainly based on analysis of well logs (density and sonic) and core sample analysis from the Sirt, Ghadames, Murzuk, Jefara and Cyrenaica areas (Essad, 1978), (Libyan Gravity Compilation Project, 2001, Makris, and Yegorova, 2006, Casten and Snopek, 2006).	
Mid Eocene and Younger	2.35
Lower Eocene	2.40
Paleocene	2.40
Upper Cretaceous	2.50
Lower Cretaceous	2.50
Nubian	2.54
Carboniferous	2.55
Devonian	2.55
Silurian	2.60
Gergaf (Quartzitic sandstone)	2.74
Igneous	2.91
Upper Crust	2.74
Lower Crust	2.84
Mantle	3.20

4.3.1 Modeling Process

Profiles AB, CD, and EF were constructed, along the NE-SW direction across the main strike extent of the Ajdabiya Trough area (Figure 4.6). Profile AB contains proven Paleozoic strata beneath possible Pre-Upper Cretaceous unconformity (Figure 4.22).

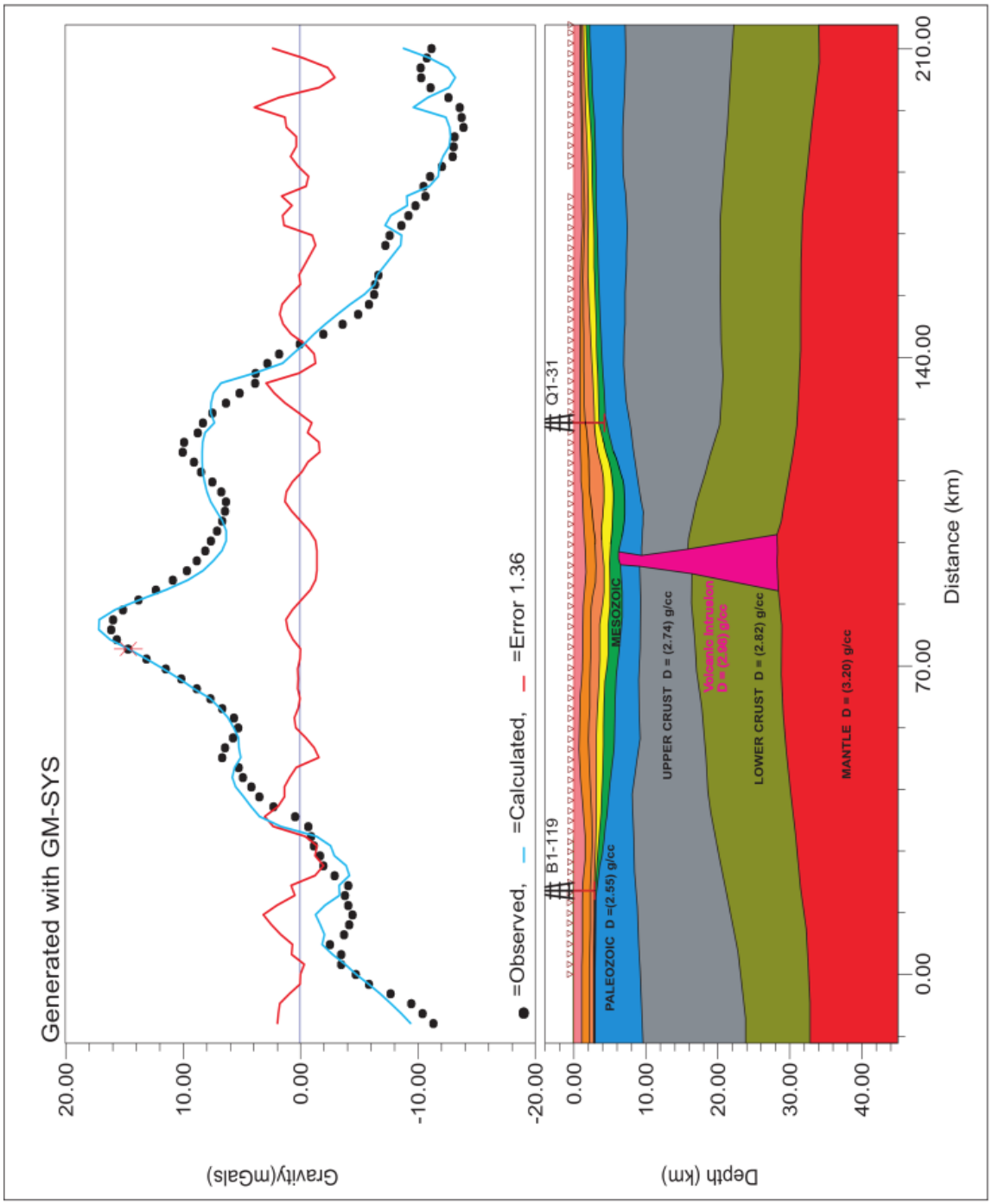

Figure 4.22: The AB gravity model showing extensional geometry and sequences of Mesozoic to Cenozoic strata developed over underlying Paleozoic section include basement fault blocks proven by seismic. The model suggests a local crustal thickening on both sides of the trough. Igneous intrusion is placed to compensate for the modelling density and the positive gravity response. The calculated gravity profile (blue solid line) is the predicted gravity from this model and the black circles represents the observed gravity. Densities are in g/cc. Line location shown on figure 4.6.

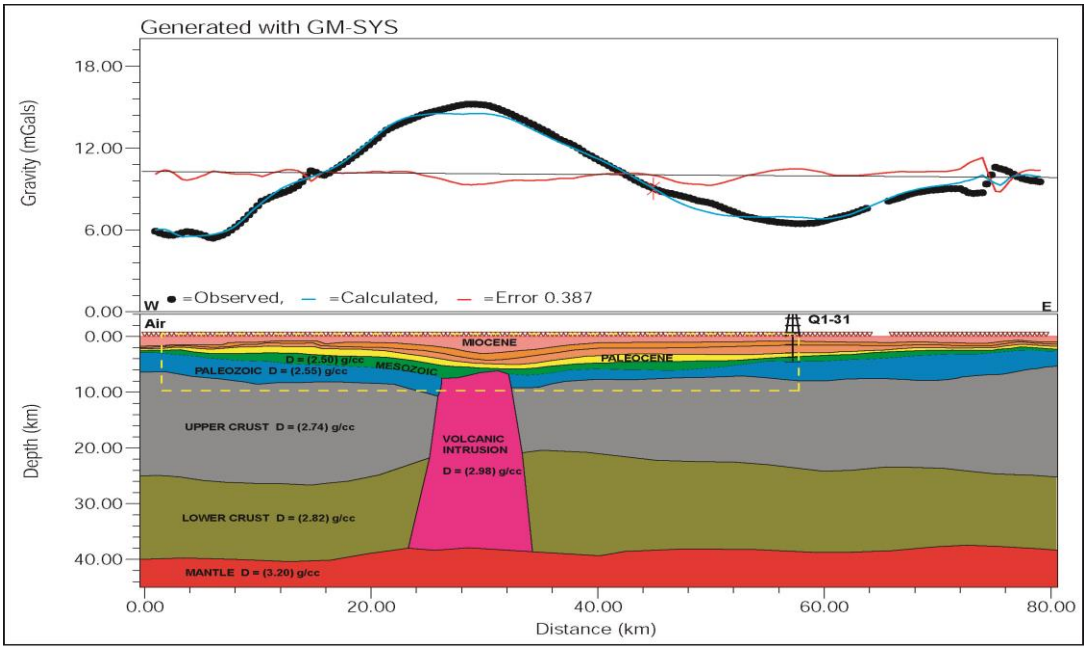

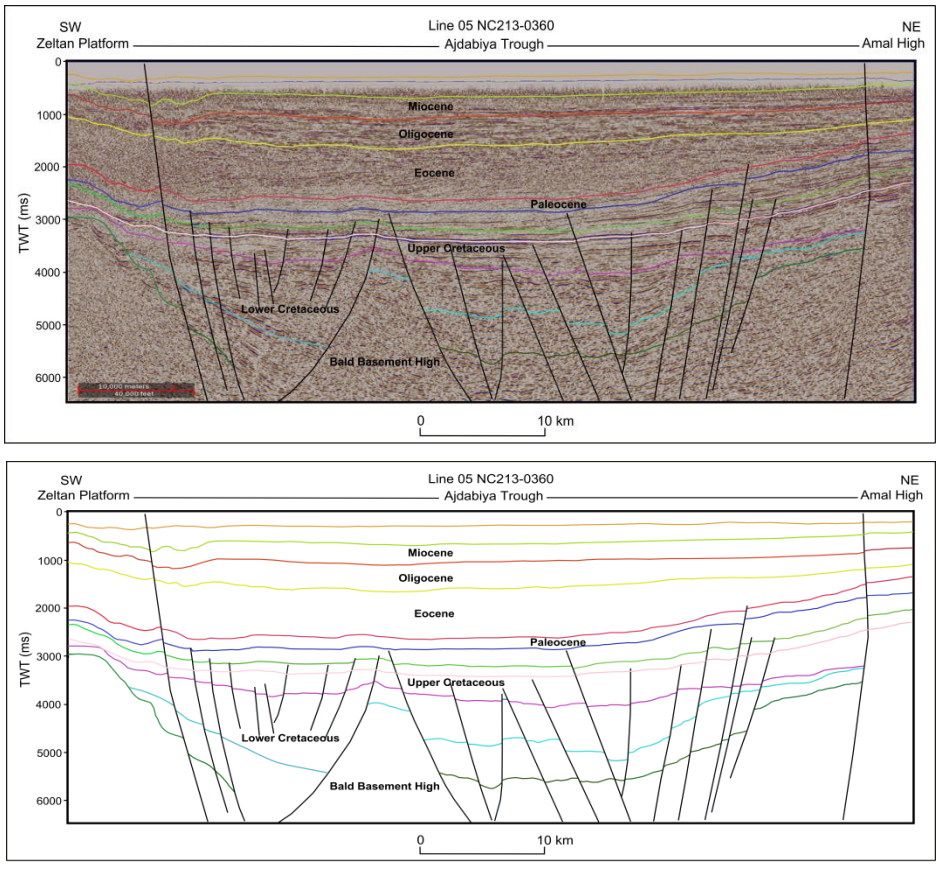

Figure 4.23: CD gravity model along the seismic line **05NC213-0360** which highlithed with yello dashed rectangle on the geological model**.** The model shows variations in sediments thickness which matches the seismic profile at shallow depths and indicating graben asymmetry. There may be some uncertainties at the deeper part where high density anomaly or intrusive bodies and/or significant crustal root were indicated by the gravity modelling.

Further south on profile CD (Figure 4.23), which constructed along the seismic line 05NC213-0360 (Figure 4.23), a presumed Paleozoic section of a few hundred meters is present, thickening considerably away from the main basin area to the east. In the central area, a thinner Mesozoic sequence is interpreted. This can be observed also on the interpreted seismic line 05NC213-0360 (Fig. 4.23 & Chapters 5 and 7).

The models show that our best fit model to the observed gravity anomaly in the Ajdabiya Trough is achieved simply by thinning the crust. However it is necessary to assume a greater density at depth in the centre of the trough to account for the positive anomaly. However, these vertical densities were increased with depth and lateral density variations were assigned (Figure 4.24).

In general the gravity anomalies appear to reflect the horst-graben systems of the area. However two areas on the AB and CD profiles show inconsistency between the gravity and the geological models which are worthy of discussion. The area between 50 and 120 km in profile AB is coincident with the Ajdabiya Tough, and is strangely represented by positive gravity anomaly. A profile presented by Hallett and El Ghoul, (1996) and derived from several wells shows a thick Neogene and Paleogene sequence (> 4 km) in the centre of the trough, although the precise location of the profile is not clear. However it is in the central area of the trough where Hallett and El Ghoul's profile is controlled by the well (A1-119), about 30km south of profile AB. The area coincident with the Ajdabiya Trough on profile CD also shows a relative gravity high (Figure 4.24). The trough is mapped north from Hallett and El Ghoul's profile but using the same sediment thickness does not fit the observed gravity.

There might be two explanations for this incompatibility. There may be a change in composition of the basement to a higher density material (possibly intrusives or metamorphics) in this area. Such a change could be related to a deep ridge identified by Hallett and El Ghoul, (1996) in the central trough area. This is presented as the case in the models. In contrast to the Hallett and El Ghoul, (1996) model which required high density sediments to have been emplaced deposited and preserved, the higher density in our models are achieved via high density an intrusive igneous body.

The area between 115 and 130 km on profile AB coincides with a gravity and structural low (Figure 4.22).

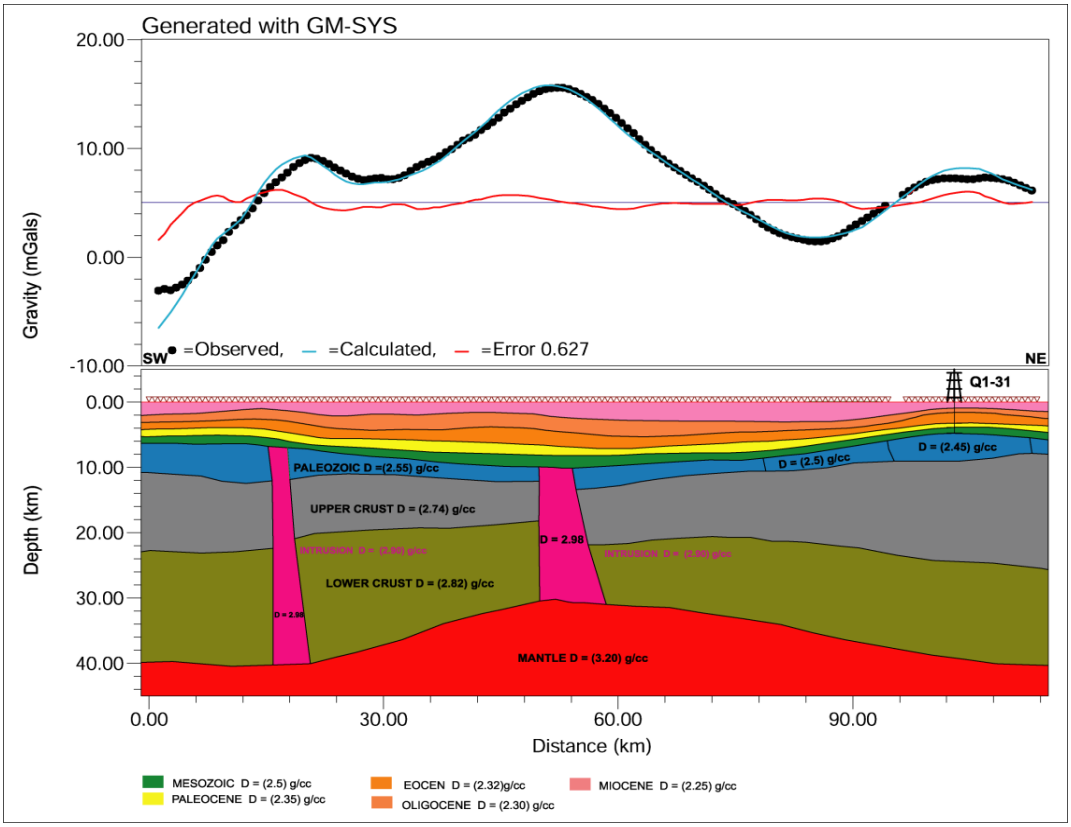
Generated with GM-SYS
Gravity (mGals)
20.00
10.00
0.00
-10.00
=Observed, =Calculated, =Error 0.627
SW
NE
Q1-31
Depth (km)
0.00
10.00
20.00
30.00
40.00
PALEOZOIC D =(2.55) g/cc
D = (2.5) g/cc
D = (2.45) g/cc
UPPER CRUST D = (2.74) g/cc
D = 2.98
LOWER CRUST D = (2.82) g/cc
MANTLE D = (3.20) g/cc
0.00
30.00
60.00
90.00
Distance (km)
MESOZOIC D = (2.5) g/cc
PALEOCENE D = (2.35) g/cc
EOCEN D = (2.32)g/cc
OLIGOCENE D = (2.30) g/cc
MIOCENE D = (2.25) g/cc

(a)

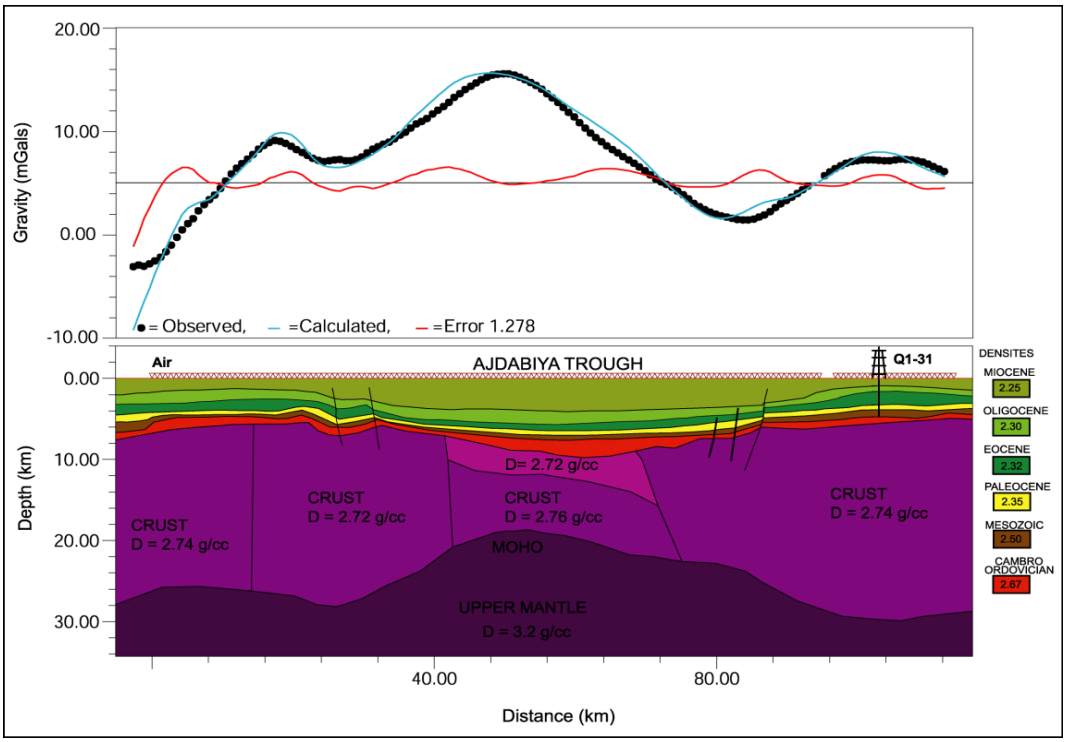
Gravity (mGals)
20.00
10.00
0.00
-10.00
= Observed, =Calculated, =Error 1.278
Air
AJDABIYA TROUGH
Q1-31
Depth (km)
0.00
10.00
20.00
30.00
D= 2.72 g/cc
CRUST
D = 2.74 g/cc
CRUST
D = 2.72 g/cc
CRUST
D = 2.76 g/cc
CRUST
D = 2.74 g/cc
MOHO
UPPER MANTLE
D = 3.2 g/cc
40.00
80.00
Distance (km)
DENSITES
MIOCENE
2.25
OLIGOCENE
2.30
EOCENE
2.32
PALEOCENE
2.35
MESOZOIC
2.50
CAMBRO ORDOVICIAN
2.67

(b)

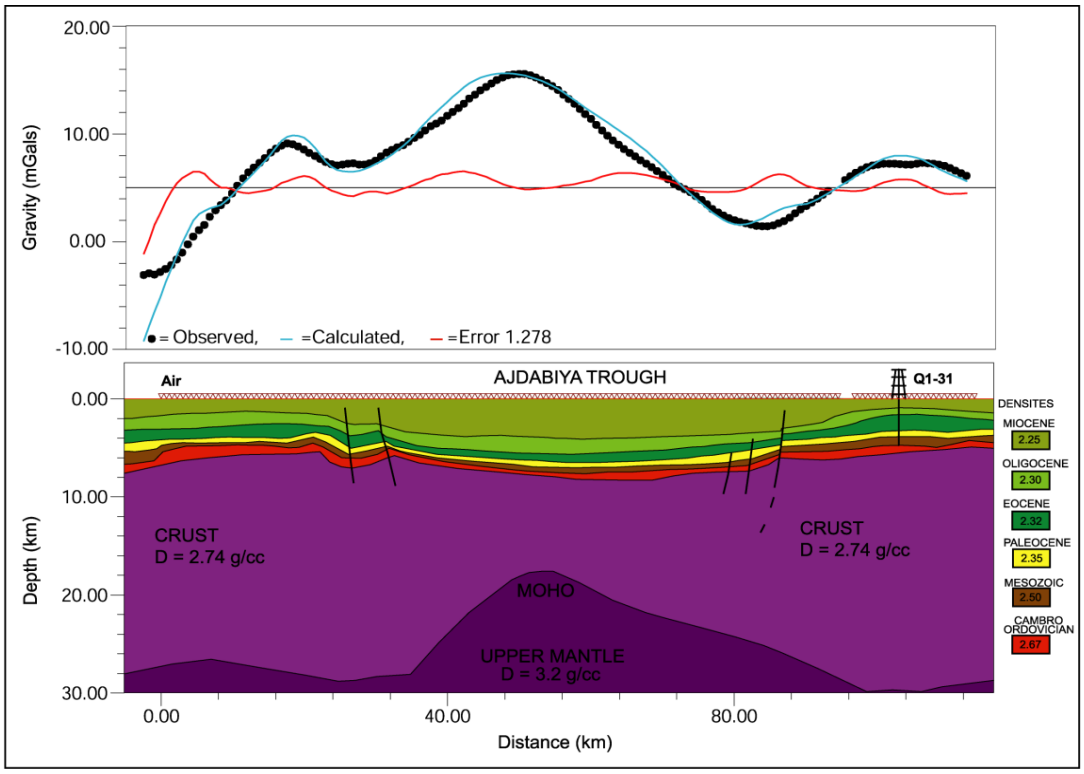

(c)

Figure 4.24: Three different scenarios for a cconceptual geological crustal model across the Ajdabiya Trough along the CD gravity profile outlining different hypothesis for the crustal morphology and the nature of the extensional geometry beneath the Ajdabiay Trough. (a) Positive anomalies are modelled by positive density contrast bodies associated with the carbonates that constitute the Ajdabiya Trough to the SE. (b) Profile was inverted under the assumption that the anomaly is due to a variable density interface. This interface is the contact of the lower crust and of the cover of Paleozoic sediments. (c) High density lower crust is interpreted to be mafic underplated material superimposed over a shallow Mantle which contributes to the low amplitude positive gravity anomaly.

However, the well Q1-31 located at the eastern edge of the gravity low and bottomed at Paleozoic section. Therefore a dramatic thickening of the Paleozoic strata beneath this well would be required to fit the gravity anomaly. This may be possible but alternative models were presented in profiles AB and CD where a basement compositional change is introduced to help compensate for the gravity low. This density (2.67 g/cc) could be related to a lower density granitic rock type. In addition the gravity modelling is evident at the centre of the trough with the presence of high density section (possibly Paleozoic remnants) beneath the Mesozoic sediments (Pre-Upper Cretaceous). These and further aspects need to be tested in future, in conjunction with the seismic evidence.

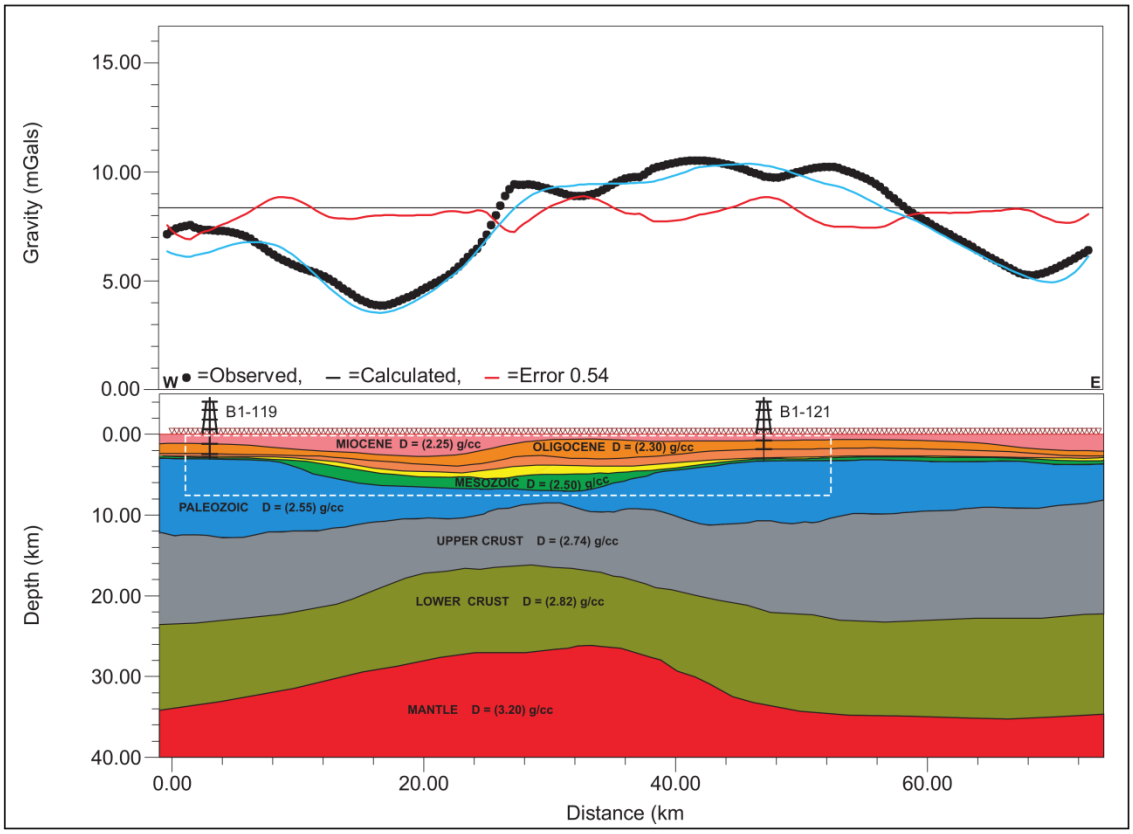

(a)

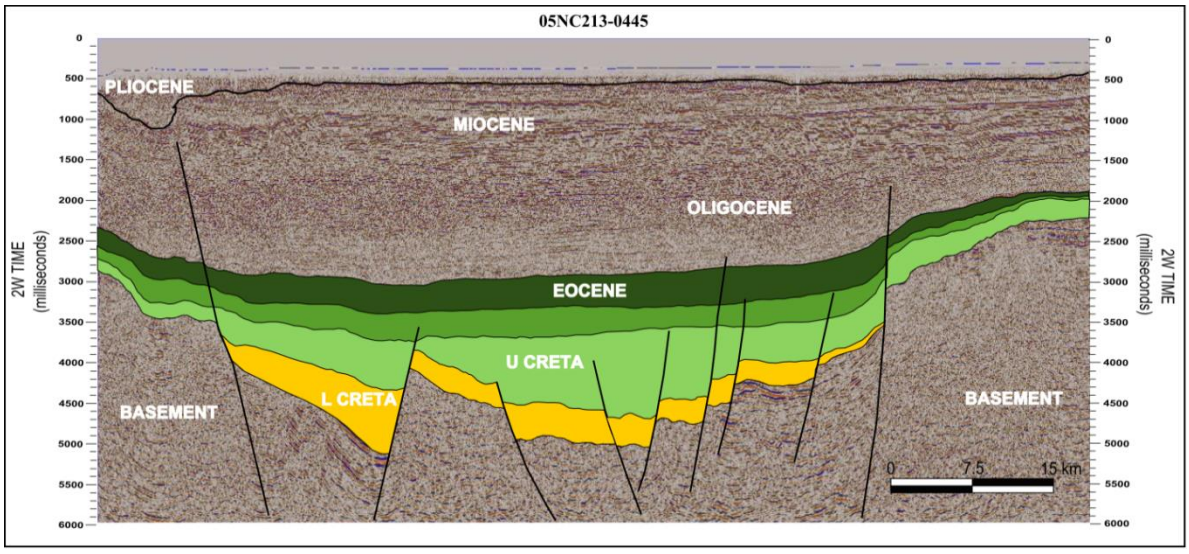

(b)

Figure 4.25 (a) Profile EF runs northeast-southwest along seismic line 05NC213-0445 (b) across the Ajdabiya Trough. Area equivalent to the seismic line on the EF gravity model is outlined by the Ajdabyia Trough borders limit. Crustal thickness as predicted by the gravity model exceed 30 km. Boreholes uniformly cover the marginal areas of the Ajdabyia trough from north to south over a total distance of ~200 km, and detail the whole sedimentary sequence around the Ajdabyia, about 4 km thick. The broad thinning of the crust at the central part of the model calls for more intensive stretching that formed during extensional events.

In the 2D gravity model EF (Figure 4.25a, b, c), along the seismic line 05NC213-0445, additional interpretation of the broad gravity high over the Ajdabyia Trough was attempted by hypothesising a crustal body that plunges into the lower crust to a depth exceeding 17 km, as long wavelength broad structures related to the Sirt Basin rift evolution at this level were constrained by the Euler Deconvolution analysis (above).

However, the comparison of gravity data with the seismic observation suggests a shallower source depth, within the upper crust. At shallow section it is interpreted that the preserved thicknesses of the sediments indicate a seaward shift of the main depocentre of the trough caused by thermal subsidence (Gumati and Nairn, 1991; van der Meer and Cloetingh, 1993; Abadi et al., 2008), and thickening towards the basin margins. Since Tertiary, the sedimentary successions have been affected by margin instability, sea level change which leads to growth of stratigraphic sequences and basin subsidence.

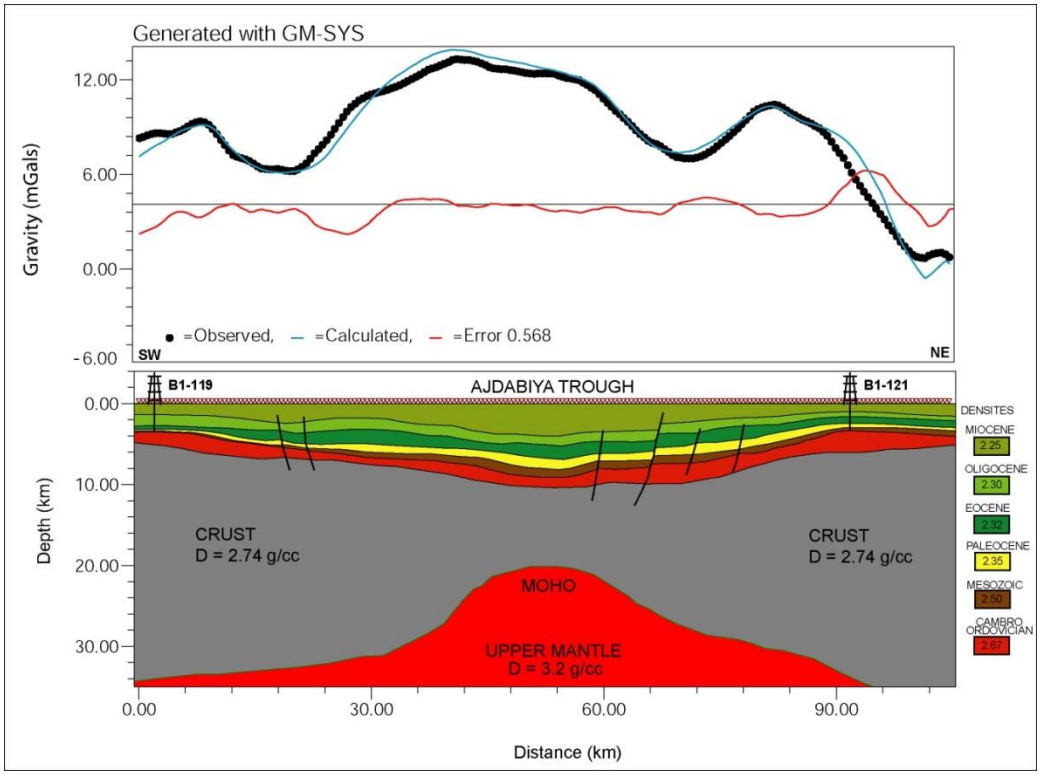

(c)

Continue to Figure 4.25: (c) Second scenarioe for the EF model show strong regional trend at the centre of the trough. This is interpreted as due to a dramatic crustal thinning and rise of the Moho from around 35 km depth at the profiles ends to about 23 km depth at centre of the trough. The two model hypothesis show a general thickening of the Palaeozoic sequence to the northeast. Consistent with this thickening Palaeozoic a significantly deeper basement is interpreted to the north.

4.4 Magnetic Analysis

The key component of the magnetic analysis in this study involved image enhancement of existing ground magnetic and aeromagnetic data sets acquired by different survey air companies (contractors) for the oil companies (clients) during the period from 1968 - 1977. The same data were integrated with draped satellite magnetic data to form the complete magnetic data set for the purpose of the African Magnetic Project (AMMP) compiled by the GETECH Company. This data enabled the interpretation to be extended over large areas of Libya where there was little well information. The AMMP was a compilation of all available airborne, ground and marine magnetic data for the whole of Africa. The data, which cover a variety of resolutions, vintages and types, were merged into a unified 1km grid at a constant 1km elevation above terrain. The magnetic data coverage for Libya is shown in figure 4.26.

After correction of the measurements for the temporal variations of the magnetic field, the total magnetic intensity (TMI) anomaly was deduced by subtracting the theoretical geomagnetic field or IGRF (International Geomagnetic Reference Field) at each station.

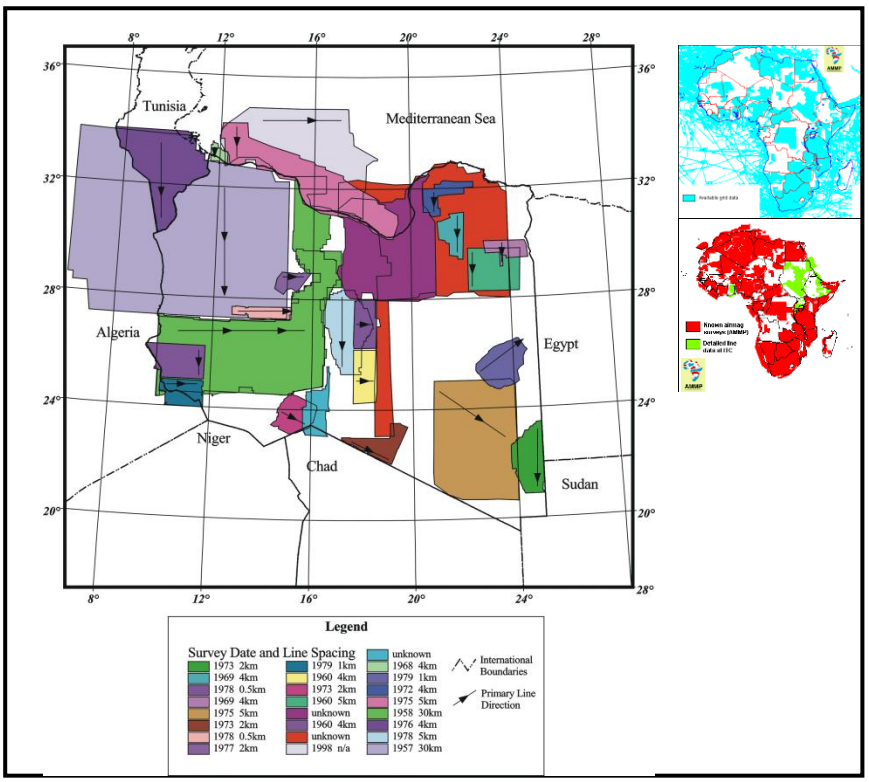

Figure 4.26: Map showing magnetic surveys over Libya (inset is the data available for the AMMP)

The TMI anomaly data were then upward continued to a height of a mean clearance of 1 km before they were merged into a unified digital grid, which has a cell size of 0.01 degree (i.e. 1. km). This grid enabled us to establish a residual magnetic anomaly map for the Ajdabiya Trough (Figure 4.27). The data provided by GETECH were already in residual form, after subtraction of the appropriate reference field.

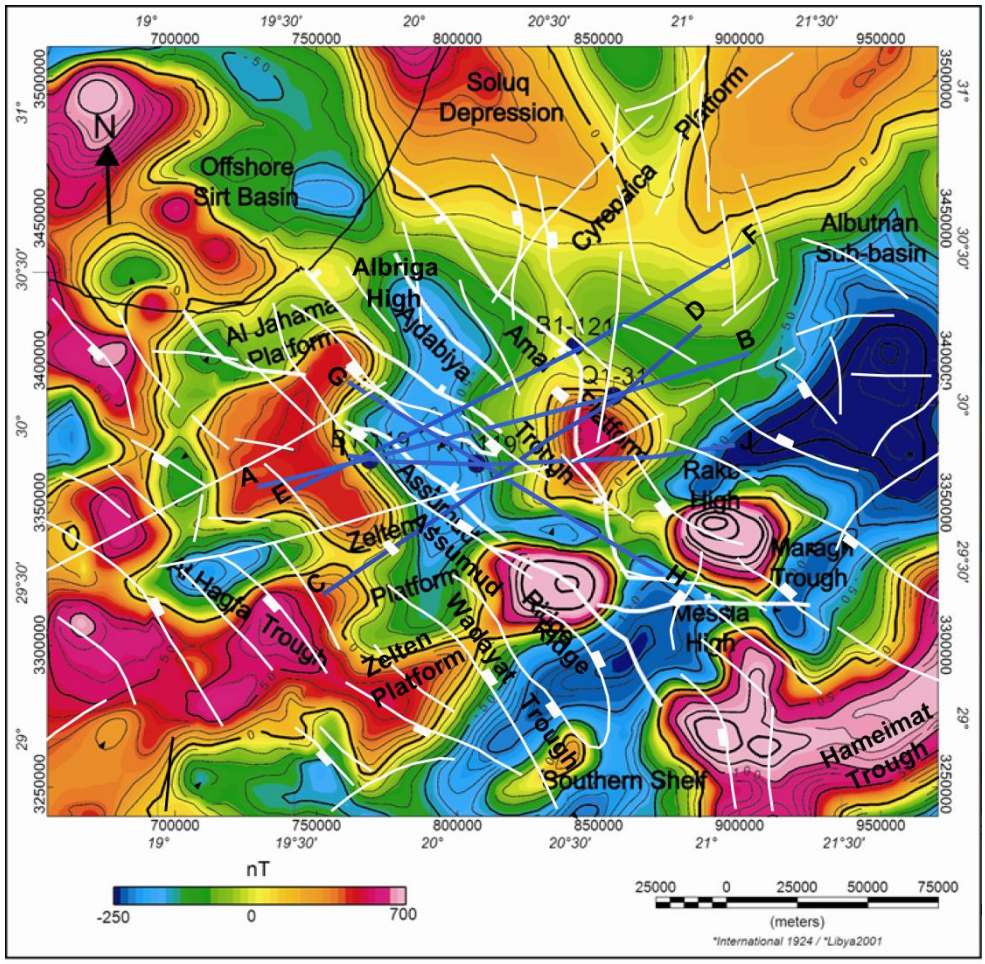

Figure 4.27: Residual magnetic anomaly map of Ajdabiya Trough and adjacent regions. Data are a subset from the compilation of AMMP aeromagnetic data by GETECH (1990). Warm colours (reds) are magnetic highs; cooler colours (blues), are magnetic lows. White lines are faults deduced from the gravity interpretation.

4.4.1. Reduction-to-Pole (RTP)

Inspection of the residual magnetic anomaly map (Figure 4.27) shows long wavelength anomalies dominant in the centre and the eastern part of the Ajdabiya Trough. Other high magnetic anomalies can be traced from the map along the western part of the map and over

the offshore area. These anomalies contain both positive and negative portions of the magnetic response (polarity). One of the main problems with acquiring magnetic data over a small area is that a large (wavelength), deep sources will create a magnetic anomaly whose total signature may not be covered by the aforementioned survey. At the latitude of this survey, the positive parts of most anomalies lie to the south of the centres of their causative sources, which is the reason why I needed to apply the reduction to pole (RTP) process.

A reduction-to-pole (RTP) transformation is standardly applied to magnetic data to minimize polarity effects (Blakely, 1995). These effects are manifested as a shift of the main anomaly from the centre of the magnetic source and are due to the vector nature of the measured magnetic field. The RTP transformation usually involves an assumption that the total magnetizations of most rocks align parallel or anti-parallel to the Earth's main field. This assumption probably works well for the Paleozoic and Mesozoic units in the study area, which are the focus of the interpretation. The magnetic data for this study were recalculated in an operation so that the magnetic maps would appear as if the inducing field was vertical (i.e., the area was at a magnetic pole). At vertical inclination, magnetic anomalies are located over their causative bodies for all strikes if the bodies are approximately vertically sided.

At the general geographic position of the survey areas, the expected ambient magnetic field at Ajdabiya Trough area should have the following characteristics, as calculated from IGRF formula (2008), the dip angle (inclination) = 42° and the declination angle = 2.5°.

In this study the RTP magnetic data, computed from the grid of residual-field magnetic data, is shown in figure 4.28. Geosoft FFT package contains a utility to selectively suppress the amplitudes of the higher frequency anomalies during the RTP operation (Pearson 1998). The absolute amplitudes of the shorter wavelength anomalies may be slightly suppressed but their spatial locations should be correct for interpretative purposes.

The study area is characterized by a number of major long wavelength anomalies and narrow short wavelength anomalies. The negative anomalies of up to -400 nT at the centre of the Ajdabiya Trough and on the north eastern edge of the map (Al Butnan Sub-basin) are mainly due to the presence of low susceptibility rocks. The presence of linear, negative and positive anomalies next to each other is due to the general geometry of magnetic anomalies (Telford et al., 1990). The anomalies with the highest amplitude of 900 nT is situated at the centre of the Ajdabiya Trough. I hypothesise that these high amplitude anomalies are caused by igneous -

-intrusions; this hypothesis is consistent with previous investigations in the area that showed a high thermal maturity (Burwood et al., 2003).

To the east of the trough the anomalies are mainly caused by the Rakb High massif. To the south west of the trough observed abnormally high degrees of thermal maturity have been observed in well AA1-6, which has previously been attributed to local volcanic activity (Gumati and Schamel, 1988).

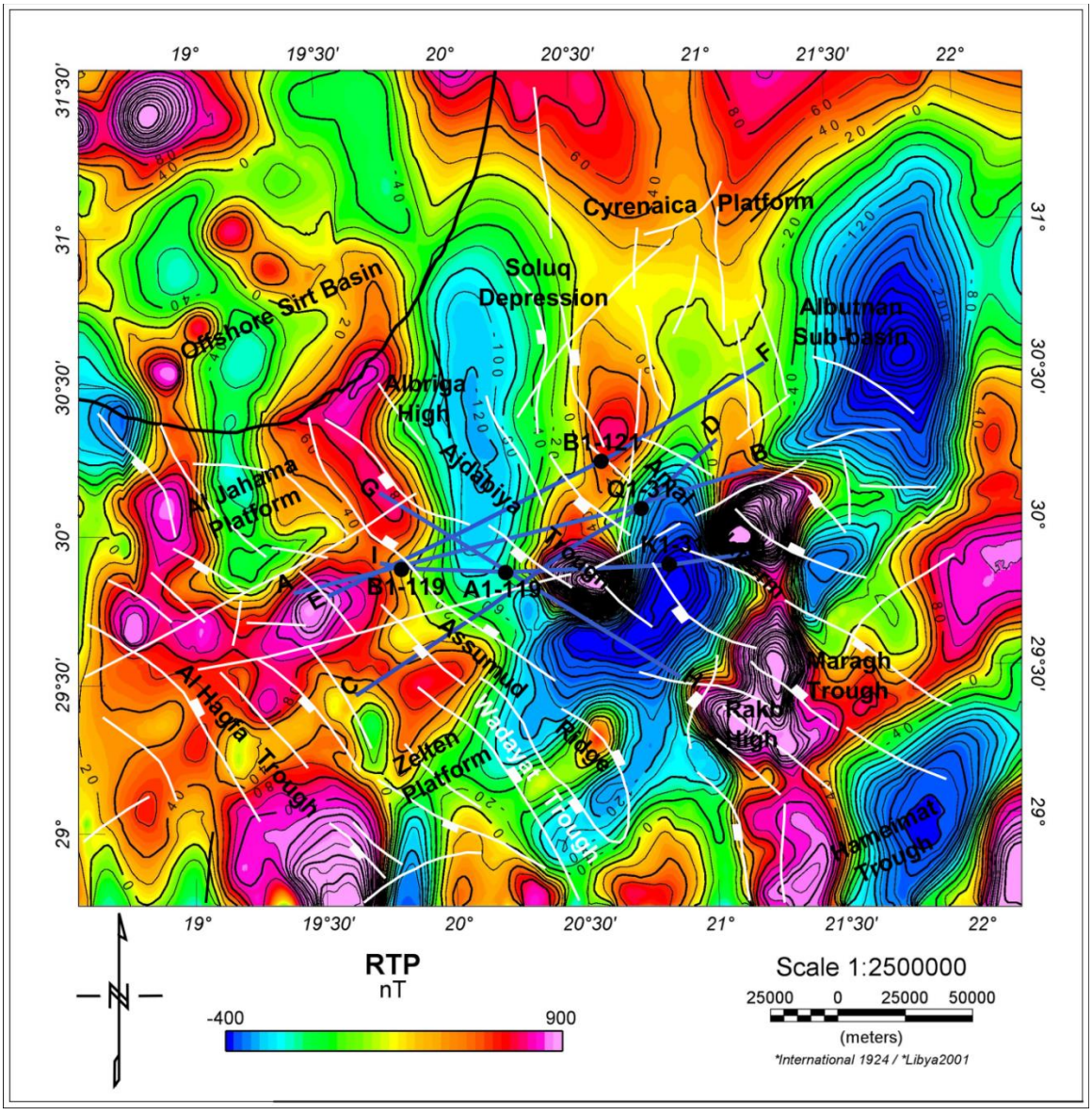

Figure 4.28: Reduction to the pole (RTP) magnetic map of the Ajdabyia Trough and the nearby regions showing the major structural elements superimposed over structural highs and lows of variable magnetic content. Contour interval is 10 nT.

The positive anomaly in the north-east is a branch of a positive magnetic anomaly north of Cyrenaica Platform with high amplitude of up to 100 nT. This positive anomaly is caused by the rocks of the Al Jabal Al Akhdar Mountain for which an inversion scenario are discussed (El Arnauti et al., 2008).

Again the northeast-southwest trending (roundish) positive anomaly in the central part of Ajdabiya Trough has not been matter of thorough investigation yet compared with the western part where igneous intrusions and sills where the main cause of the magnetic anomalies. North-West of the Ajdabiya Trough and on the offshore area, roundish anomalies with amplitudes ranging from 60 - 200 nT are probably also the result of igneous intrusions.

4.4.2. Spectral Analysis

Spectral analysis is a technique used to analyse characteristics of potential field data (magnetic and gravity) in the frequency domain by using Fourier Transformation (FFT). The expressions for the potential field in the frequency domain have simple and direct forms with separated factors including physical properties, horizontal dimensional geometry, top depth, bottom depth, earth field vector, etc. The parameters of a body can be estimated by analysing the energy spectrum of the anomaly. The spectral analysis method is used to investigate the frequency content of potential field and make statistical estimation of depths to the top of the causative bodies (Spector and Grant, 1970; Regan and Hinze, 1976). These authors considered an ensemble of bodies with varied depth, width, thickness, density and/or magnetisation as a statistical model and made the assumption that the observed gravity and magnetic anomalies were caused by several ensemble blocks. The technique is based on the principle that the potential fields measured at the surface are the resultant effect of the sources at various depths. These depths can be determined from the radially averaged power spectrum of the potential fields at the surface (Blakely, 1995).

The radial power spectrum of the magnetic data indicates the presence of three magnetic depths assembles. The shallow ensemble extends over a wide spectral band (wavenumber 1.5 – 1.0) and is attributed to intra-sedimentary anomalies. The deep ensemble (wavenumber < 0.125) is steep and of higher intensity than the shallow ensemble and is attributed to deep seated basement rocks. The third ensemble is between the deep and the shallow ensembles

(wave number 1.0 – 0.2) are probably related to the transition zone between both the upper most basement and the intra-sedimentary rocks.

The logarithm of the power spectrum plotted against radians/km is shown in (Figure 4.29). The plot shows a discrete series of linear segments with slopes proportional to the average depths of the density interfaces. The deepest interface with a maximum depth of 10 - 15.0 km corresponds to the basement depth. The other layers at depths of about 4.0 and 2.0 km correspond to Mesozoic and Cenozoic sediment depths respectively.

Based on the average wavelengths derived from the radial spectra, a set of Low-pass, High-pass & Band-pass filters are produced for the purpose of achieving a set of rough anomaly separation images. These are used to isolate certain features and assist in a comprehensive geological interpretation of the complete dataset.

In this study, I used a band pass filtering to separate the RTP field into shallow and deep structure components. The magnetic interpretation has been built using all of the aforementioned filter and residual maps. It comprises information gleaned from all of these maps as well as depth information calculated using 3D Euler technique (Reid et al., 1990). Riding on top of the larger wavelength anomalies are smaller, subtle gradient changes and high frequency features.

These features may be important to understanding magnetic basement components related to structural inversion, and the reactivation of basement faults and movements on the overlying fault systems. The shallower magnetic sources (Figure 4.30) within Mesozoic – Cenozoic sediments produce the highest frequency anomalies and have also been enhanced by this technique.

Spectral separation (High pass filter) was chosen as the best representation of the regional field. A spectral separation equal to approximately 30 kilometres (full wavelength) was subtracted from the RTP (Figure 4.28).

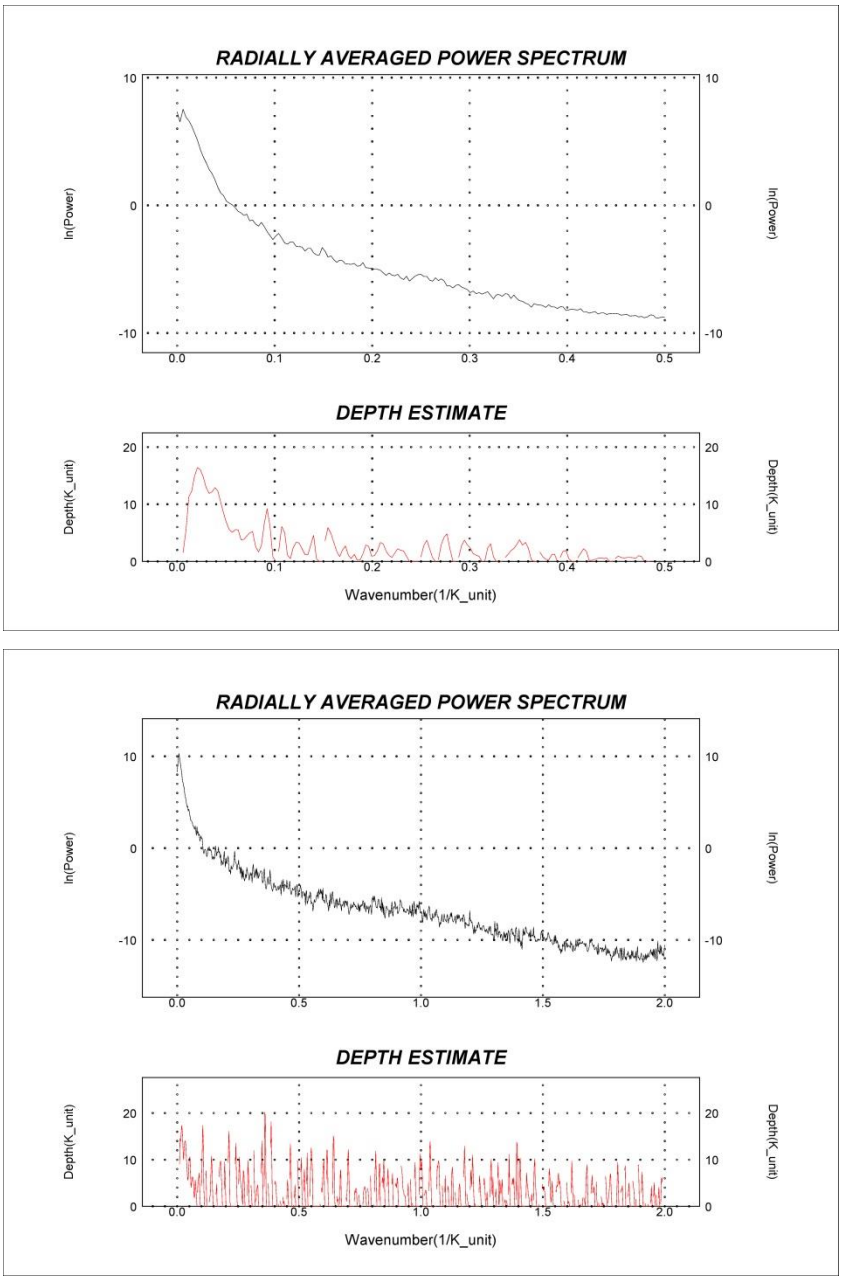

Figure 4.29 The power spectrum of the Bouguer anomaly and the magnetic intensity of the central part of the Ajdabiya Trough respectively. The average height of the red spikes defines depths to the various density interfaces.

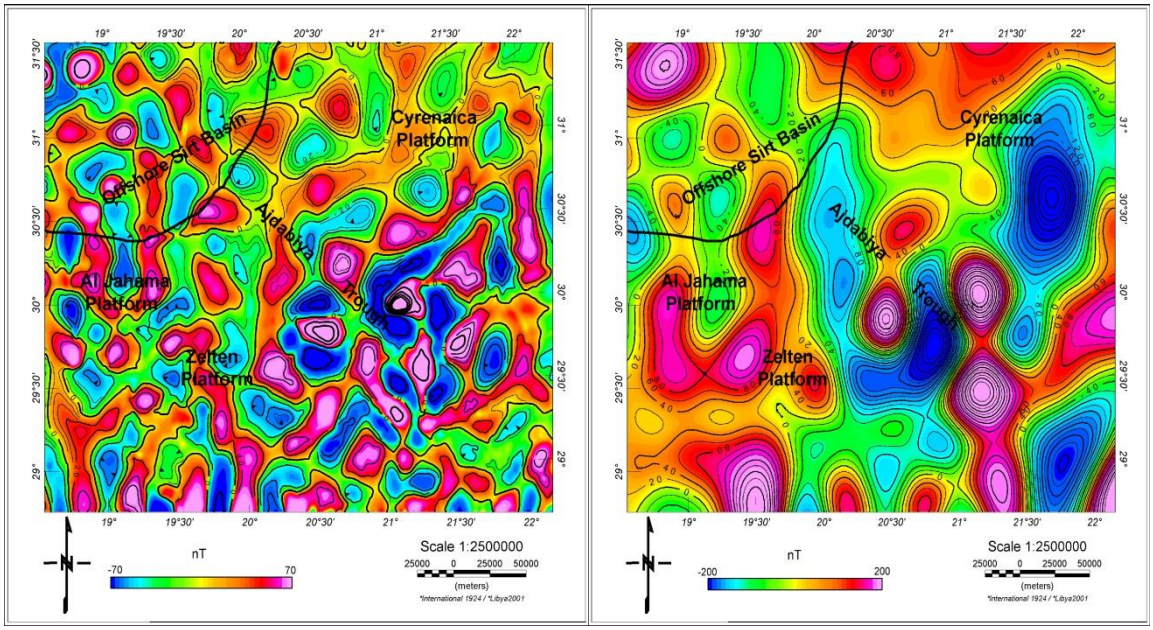

Figure 4.30: (a) Shallow sources magnetic anomaly map and (b) deep sources magnetic anomaly map obtained from band pass filters of the wave numbers of the RTP anomaly component using spectral analysis.

4.4.3. Horizontal Gradient Method

The reduced to pole magnetic anomaly over a vertically sided susceptible body reaches its maximum over the centre of the body and has the steepest gradient (horizontal derivative) over the edge of the body. The anomaly curve has its inflection point at the edge of the body where the anomaly changes from convex to concave. This point is where the horizontal derivative of the gradient (i.e., the second horizontal derivative) is zero. Therefore, if the points where the second horizontal derivative goes to zero are located, then the positions of the faults can be inferred.

Both the residual-field and RTP of the TMI magnetic data reveal subtle, northeast-trending linear anomalies superposed on the larger magnetic anomalies (Figures 4.27 and 4.28). The band pass filter maps (Figure 30 a&b) are enhanced more the shape of the identified anomalies. These anomalies are largely corresponding well to mapped faults that bound major basement blocks and offset basin-fill sediments (Smith et al., 2002). To enhance the signature of these faults, the horizontal gradient method was applied to the magnetic data. The horizontal-gradient method as outlined above (Cordell and Grauch, 1985; Blakely and Simpson, 1986) is based on a principle from gravity methods that steep gradients occur over near-vertical contacts between units with differing physical properties. Lithological

boundaries related to lateral changes in density and fault locations can be determined by computing the horizontal derivatives of the gravity anomalies (Blakely and Simpson, 1986; Blakely, 1995). Horizontal gradients related to shallow structures exhibit high values and form relatively short lineaments.

For magnetic data, the same principle can be applied after transforming the data into a form that is mathematically similar to gravity data, called pseudo-gravity (Blakely, 1995). The pseudo-gravity transform has some special characteristics that reduce the dominance of the shallow magnetic sources and enhances the amplitude of magnetic anomalies from deeper magnetic source rocks. The pseudo-gravity transform was applied to the RTP grid from the Ajdabiya Trough (Figure 4.28) using the FFT filter package available in Oasis montaj.

The broad, north south trend in the RTP image becomes the most dominating feature in the pseudo-gravity image (Figure 4.31) and it is difficult to recognize the small-scale features. The dynamic range of the short wavelength features that is evident in the RTP image is much lower in the pseudo-gravity image. Local peaks in the magnitude of the horizontal gradient of the pseudo-gravity (Figure 4.32), give the locations of steepest gradients between magnetic anomalies. Linear anomalies, probably related to N-S trending faults are clearly evident after application of the horizontal gradient method. The enhancement provides a more comprehensive view of fault patterns than previously available by any other method.

Further analysis was required to give estimates of the depths of interpreted faults. The first step of this analysis was to separate the anomalies of the map based on anomaly width. A horizontal gradient map was calculated for the deep and shallow sources (Figure 4.33 a&b). The maps shows besides the obvious long-wavelength anomalies on the deep sources map, linear, short-wavelength anomalies are present whose visibility is enhanced by the shaded relief image. A system of variable trending anomalies of short wavelengths is clearly visible on the map.

The major central and eastern anomalies lie exactly in the areas of a NW-SE striking fault system that passes eastward into the NE-SW and N-S fault systems. Though the majority of linear magnetic anomalies show good spatial correlation with fault structures previously inferred from gravity and seismic (Chapter 7) data, not all anomalies can be explained by faults.

There are a number of NE-SW to NNE-SSW structural trends dominates the study area. I hypothesise this trend may represent compressional and shear fractures related to Pan-African and/or Hercynian deformation zones associated with final closure of the ocean separated Laurussia and North Africa during the Late Carboniferous – Early Permian (~315 – 295Ma) (Badalini et al., 2002), and to movement accommodated by inversion of shear zones (Ziegler, 1989; Guiraud et al., 2005).

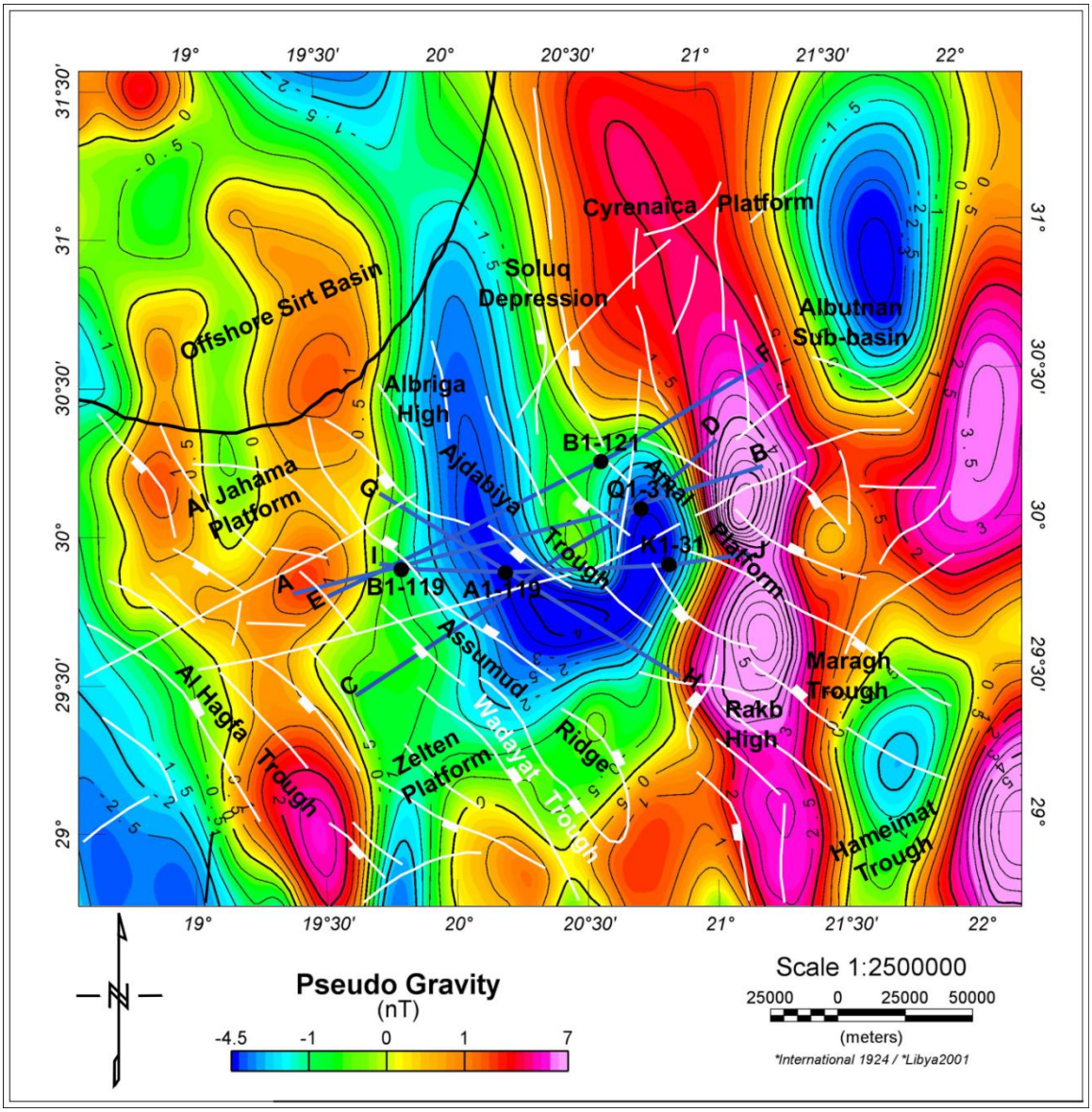

Figure 4.31: Pseudo-gravity map of the RTP magnetic field

Coward and Ries, (2003) suggest that NE-SW Pan-African structural trends are cut by inversion structures and reworked Paleozoic normal faults with oblique compression from NW-SE to NNW-SSE. Anketell (1996) interpreted these NE-SW faults as resulting from a paleo-stress field associated with the interaction between Europe and Africa The NE-SW trend could also be attributed to Late Permian (Triassic – Jurassic) rift faults formed during the Central Atlantic Rifting (260 – 195Ma), the time which marked the second phase of Gondwana breakup with NW-SE stress field (Morgan et al., 1998).

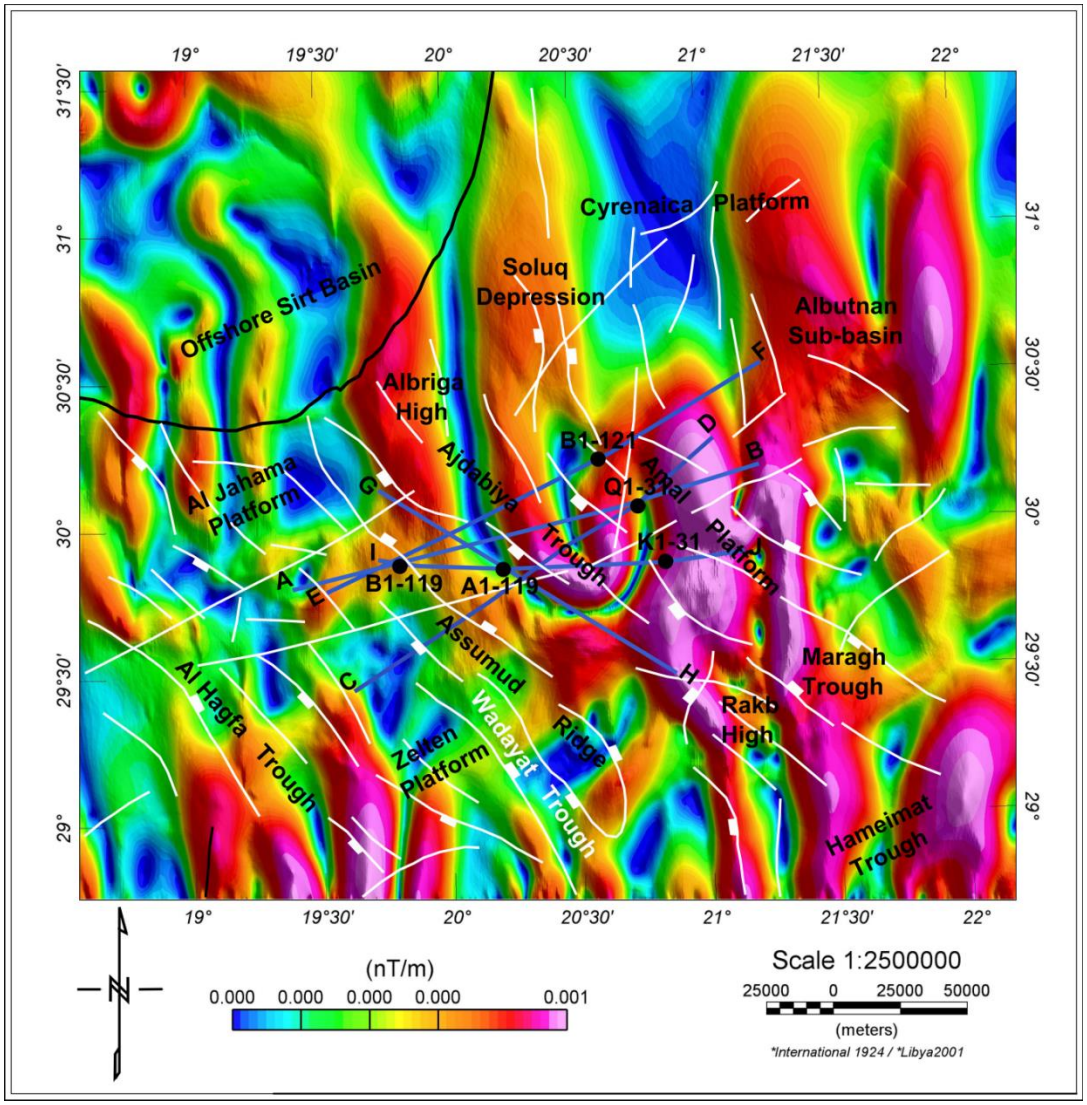

Figure 4.32: Total horizontal gradient of the pseudogravity field. Red warm colours indicate areas of maximum gradient readings mainly related to tectonic boundaries such as faults and other structures (Igneous intrusions…etc). Igneous intrusion in the offshore area is delimited by the high gradient round shape and it is in agreement with the results obtained from the previous maps.

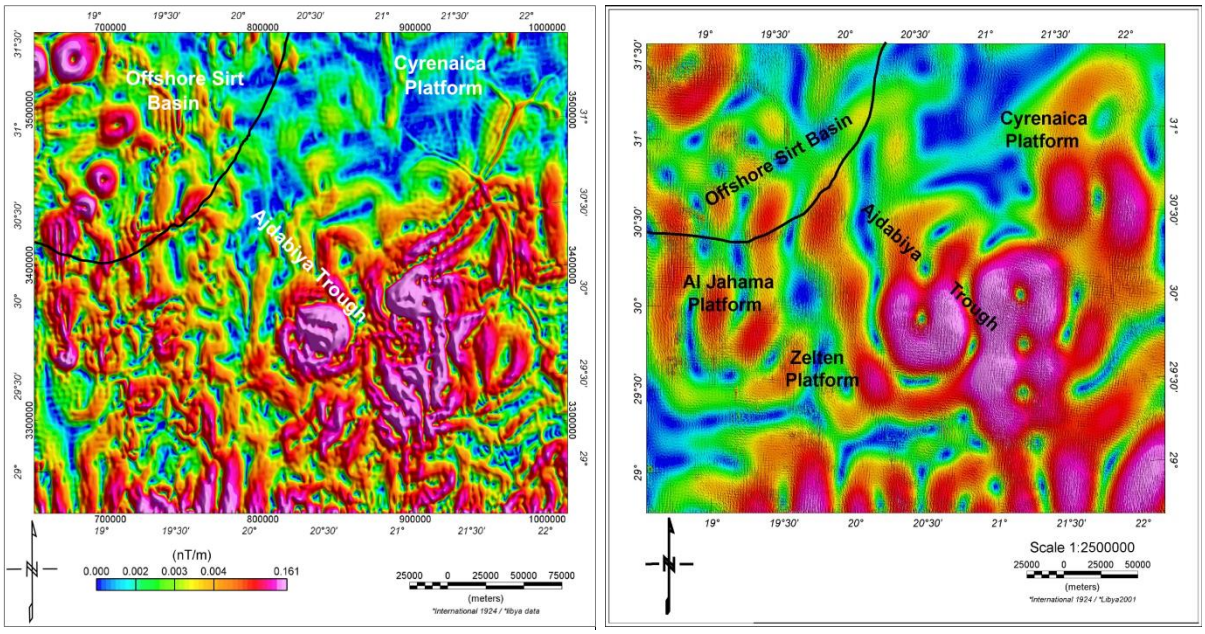

Figure 4.33: Total horizontal gradient maps of (a) Shallow source anomalies show evidence of variable fault trends cross cut each other's with signatures of igneous intrusions in both offshore and onshore areas. (b) Horizontal gradient of the deep source anomalies, clearly show edges of major structures (faults, basement blocks, anticline features…etc) superimposed over long wavelength and broad anomalies.

4.4.4. Analytic Signal

This transform was particularly useful in delineating changes in the character and edges of the magnetic field sources and hence to identify possible in compositional zoning within the Precambrian basement. The analytic signal method uses square of the partial derivatives in the x, y, and z directions. When applied, the analytic signal method generally produces good horizontal locations for contacts and sheet sources regardless of their geologic dip or the geomagnetic latitude. Analogous to the horizontal gradient, the analytic signal provides another look at the contacts and source locations.

The Analytic Signal is expressed as:

$$AS(x,y) = \sqrt{\left(\frac{dF}{dx}\right)^2 + \left(\frac{\partial F}{\partial y}\right)^2 + \left(\frac{dF}{dz}\right)^2} \qquad (3)$$

With F the measured field, are the spatial derivatives of the a particular Cartesian component of the field in *x*,*y*, and *z* directions. The analytic signal is used to locate the edges of magnetic source bodies, particularly where remanence and low magnetic latitude complicate

interpretation. Maps of the analytic signal for shallow and deep source anomalies over Ajdabiya Trough and near regions are shown in figure 4.34 (a, b).

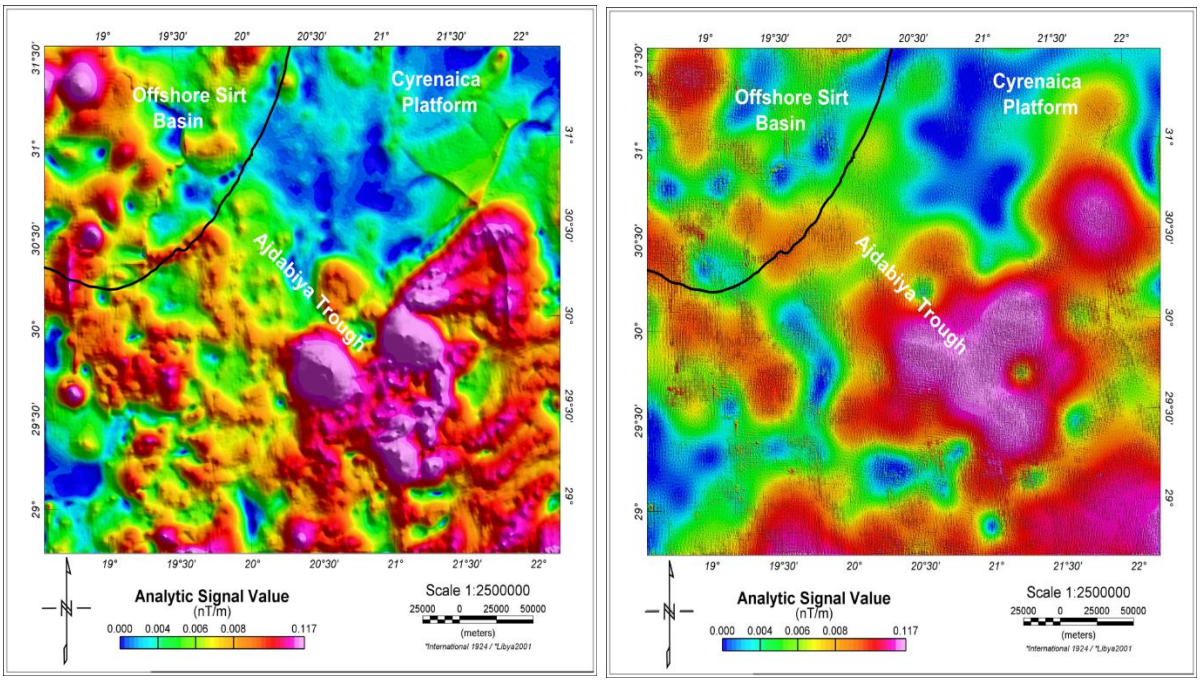

Figure 4.34: Analytic signal maps of RTP anomaly extracted for (a) shallow sources and (b) deep sources in Ajdabiya Trough and the adjacent areas.

Areas of high analytic signal seen in Figure 4.34(a) show a characteristic NE-SW trend and may be related to the site of the NE-SW Caledonian and Hercynian arching that shaped the Sirt Basin area (Goudarzi 1980). This structural trend is characteristic of Wadan Uplift to the west of Sirt Basin and Jaghbub High south of Cyrenica Platform (Figure 4.9). West of the Ajdabiya Trough, the maps show low - moderate analytic signal with isolated structures mainly related to a belt of igneous intrusions, the age of which is uncertain. This belt extends north-westwards into the offshore area of Sirt Basin as shown on the map (Figure 4.34a). In the central Ajdabiya Trough, the maps show high analytic signal with distinct causative bodies. Analysis of the magnetic data indicates that these bodies are within the basement. In the northern Ajdabiya Trough, the maps show moderate analytic signal with evidence of NW-SE structured trends in the central part and N-S in the outer part. In Cyrenaica region the maps show generally low analytic signal with mainly N-S trends.

4.5 3D Euler Deconvolution (3ED) Solutions from RTP

Analysis of the data for depth estimation purposes was approached in the following manner. Regional depth estimates were calculated from the computed power spectrum of the magnetic field (Spector and Grant, 1965). The spectral method uses a spectral plot of the grid which has the coordinate system of frequency number for the abscissa, and natural log for normalized power for the ordinate. The depths derived are only apparent average depths to source horizons. This spectral representation can be broken up into a series of straight line segments which are related to various groups of sources at varying depths. The depths calculated using this method for higher frequencies tend to be unreliable because they are often corrupted by short wavelength noise. Automated depth estimates were calculated using GEOSOFT 3-D Euler software. This technique allows a large amount of data, in gridded form, to be evaluated fairly quickly. Unfortunately, the technique is susceptible to filtering and noise considerations and therefore, the results must be carefully viewed and calibrated. A significant advantage of the Euler equation is that it is insensitive to magnetic inclination, and declination.

The Euler deconvolution was applied in this study to the reduction to pole field (RTP). The analysis is based on estimation of Eulers homogeneity – an equation that relates the field (magnetic or gravity) and its gradient components to the location of the source, with the degree of homogeneity N, which may be interpreted as a structural index (Thompson, 1982). The structural index as mentioned in the gravity section is a measure of the rate of change with distance of a field. For example, in a magnetic field a narrow 2D dyke has a structural index N=1, while a vertical pipe gives N=2. In a gravity field, a pipe has a structural index of 1, while a sphere has a structural index of 2. Reid et al., (1990) have shown in their study that a magnetic contact which includes faults will yield an index of 0.0 - 0.5. These ranges of indexes were used for the Euler depth solutions shown on the magnetic interpretation maps in this study. During magnetic interpretations, the 3D Euler Deconvolution method requires no prior information about the source magnetization direction, and its results are not affected by the presence of remnant magnetization. The method traces the edges and depths of source bodies as a function of its gradient (Thompson, 1982: Reid et al., 1990). Source location from 3D Euler Deconvolution solutions can be used for delineation of structural and lithological trends (Reid et al., 1990).

A location where these solutions tend to cluster is considered to be the most likely location of the source.

Euler deconvolution is carried out on the RTP grid (Figure 4.28) and gives an estimation of source depths of magnetic anomalies and hence an estimation of depth to crystalline basement features and basement trends and/or intra-sedimentary volcanics. To delineate contacts, structural indexes of 0.0 – 0.5 are tested with the best results obtained using the 0.0 structural index. The distribution and clustering of solutions along the boundaries of the anomalies is in a good illustration (Figure 4.35). Only few scattered solutions are not significant on the map. The obtained results show that a number of NE-SW to NNE-SSW structural trends dominates the study area, which have a gentle to moderate dips towards the centre of the Ajdabiya Trough (Figure 4.35).

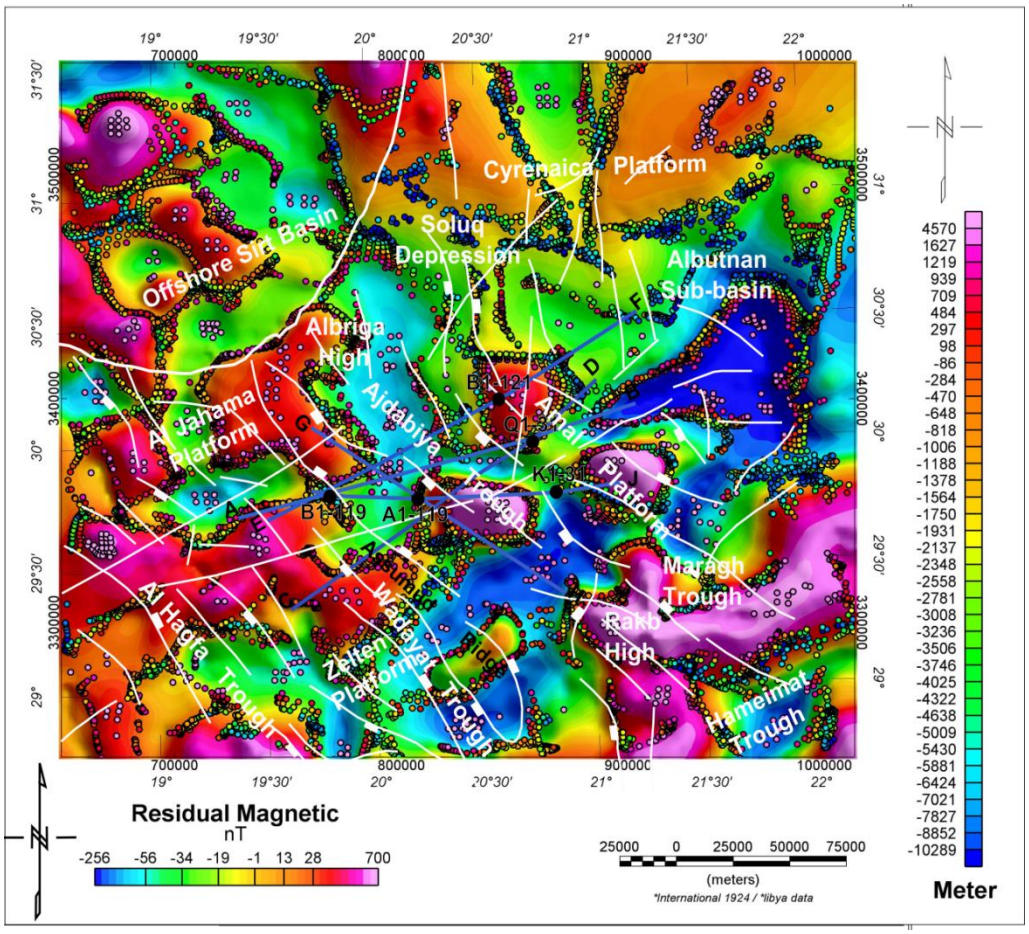

Figure 4.35: Depth Estimations by Euler Deconvolution applied to the RTP magnetic data of the Ajdabiya Trough. Grid spacing: 2 km. Structural Index SI = 0.0

In order to validate the solution clusters for the purpose of identifying other features, a different structural index has been set. Based on observations from the produced maps, a structural index of 1.0 is selected, which accounts for a magnetic anomalies possibly caused by igneous intrusions within the Ajdabiya Trough and the offshore area (Figure 4.35). The signatures of the positive anomaly in the north eastern edge of the map (Figure 4.36) are not showing significant solution clusters, but numerous significant source points scattered over the whole data set can be interpreted.

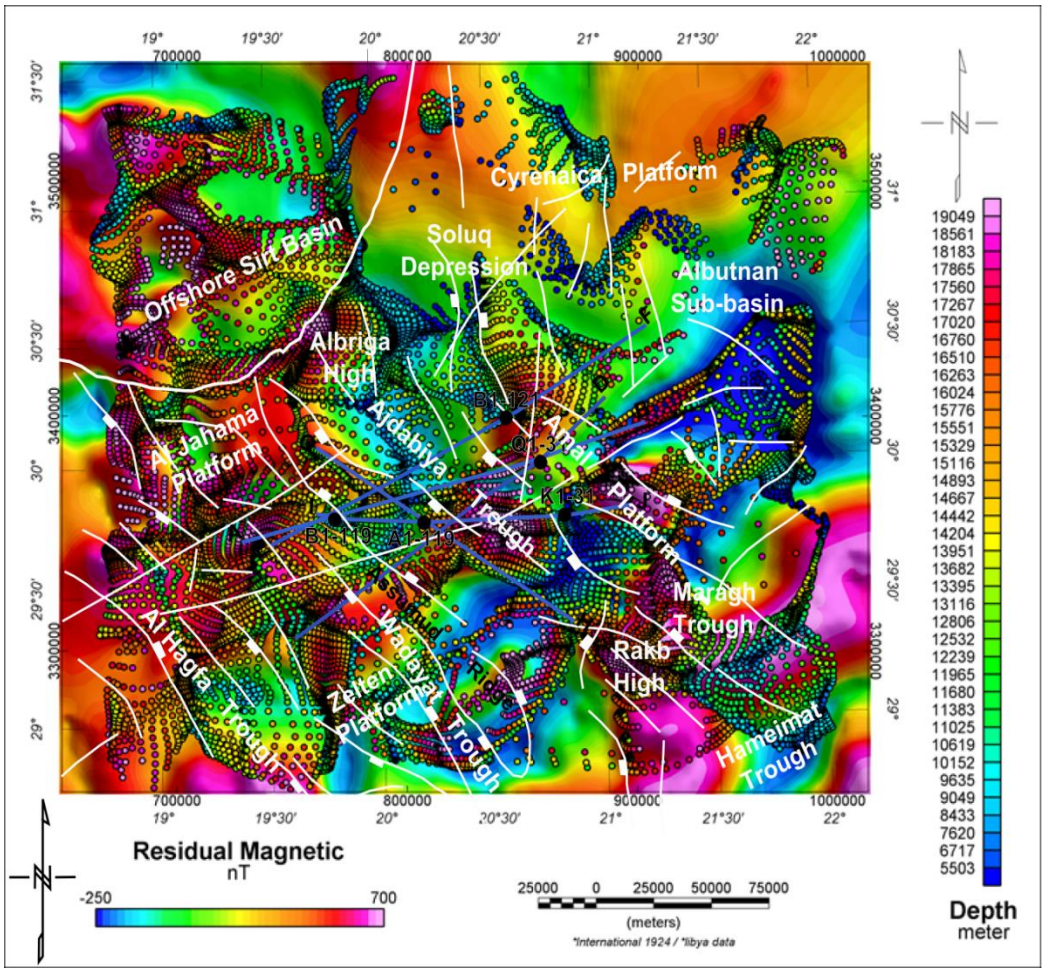

Figure 4.36: Presents the depth estimation solutions calculated for a structural index of 1.0. The application of the Euler deconvolution yields a cluster of source points in the Ajdabiya Trough area and above other large scale anomalies, which are fully present in the dataset.

Apart from the Ajdabiya Trough anomaly and the Rakb High (Figure 4.36), two anomalies east and south of the Ajdabiya anomaly show good clustering of solutions. The corresponding depth estimations are in the range of 3000 to 6000 m and 4000 to 7000 m respectively. The

dense clustering of solutions above the centre of the Ajdabiya anomaly suggests a depth to the top of the source between 6000 - 7000m which comparable with results obtained from the gravity modelling. The reduction of solutions by an adaptation of selection criteria involved the elimination of solutions with high uncertainties, which were scattered over the whole survey area.

4.6 Magnetic Modeling

The identification of high susceptibility horizons in the Ajdabiya Trough area by the Euler Deconvolution and the linear anomaly correlation encouraged the test of the results by building 2D models across the identified structures and proposed igneous intrusions.

The basement and Palaeozoic sedimentary cover succession in the Ajdabiya Trough have undergone significant deformation (folding, extensive erosion and faulting) during the Pan African ~530 to ~500 Ma and during the Late Palaeozoic (Hercynian Orogeny) ~ 310 – 295 Ma (Hallett 2002) and were subsequently reworked by rifting and extensional structures during the Mesozoic time (Baird et al., 1993; Ahlbrandt, 2001; El Arnauti et al., 2008). This has generated a set of clear magnetic and gravity responses from basement and the sedimentary sections observed in the maps generated. The NW-trending, high magnetic anomalies at the middle of the trough may be attributed to the presence of basaltic intrusions. Well A1-119 located at the central part of the Ajdabiya Trough (Figures 4.2, 4.6, 4.28, and 4.30) cut Cretaceous granitic basement at 4.3 km depth in a zone with gravity and magnetic high (Hallett and El Goule 1999). This magnetic and gravity high is possibly affected by local uplifting during the Cenozoic time (Hallett, 2002). Hallett and El Goule 1999 suggested the presence of ridge structure in this part. The magnetic maps show a northwest-striking magnetic high that extends across the Amal Platform to the east (Figures 4.27 & 4.28). It seems that the northeast edge of this anomaly, caused by ultramafic rocks, coincides with a major fault zone in the area as discussed by Anketell, (1996). The coincidence of the identified fault zone and significant gravity gradients could also suggest that the much younger fault zone has reactivated older basement features. However, it is also possible that a younger fault could give rise to significant structural expression within the basement.

The 2D models (GH & IJ) (Figures 4.37 & 4.38) have been broken up into 8 layers representing (from the top down)

1. Late Oligocene – Miocene Unit
2. Eocene – Early Oligocene Unite
3. Paleocene Unite
4. Mesozoic Unite
5. Unites between basement and base of the Mesozoic – (Camberian / Ordovician)
6. Upper Crust
7. Lower Crust
8. Mantle

The forwared models were calculated using variable susceptibilities (0.0001 – 0.002 SI units) for the Paleozoic basement. These susceptibilities were chosen as a first guess to fit the major anomaly trending NW/SE associated with the significant fault system in the area. The magnetic content inferred with the susceptibilities would be consistent with a fairly metamorphic and igneous lithology.

The basement fill model represents an attempt to fit the observed anomaly by changing the susceptibilities within the basement and the deeper section (Upper and lower crust unites) (Figure 4.37). This was done with a manual fitting to try and maintain the basic structural picture. For the most part faults were kept in the same locations and minimal change was applied to the layers to obtain this fit. The major changes to top of basement occurred on the northwestern end of the GH profile. The higher frequency content of the data, at the northwestern end of the model, precludes a good fit using susceptibility changes only within the Upper and Lower Crust.

The model utilizes a very low susceptibility (0.0 – 0.0008 SI unites) much lower in the column to fit the shorter wavelength anomalies on the southeastern side of the section. This susceptibility is consistent with those measured in metamorphic rocks (e.g. Clark and Emerson, (1991). As such, it may be showing different lateral variations in the chemical composition (lithology) or subtle structural variations and thicknesses within the basement unit. The changes made to the model occur approximately around the Paleozoic – Mesozoic boundary. These predominant variations may be observed at this location in a number of the filter maps supplied, specifically the Horizontal Gradient, and Residual RTP maps.

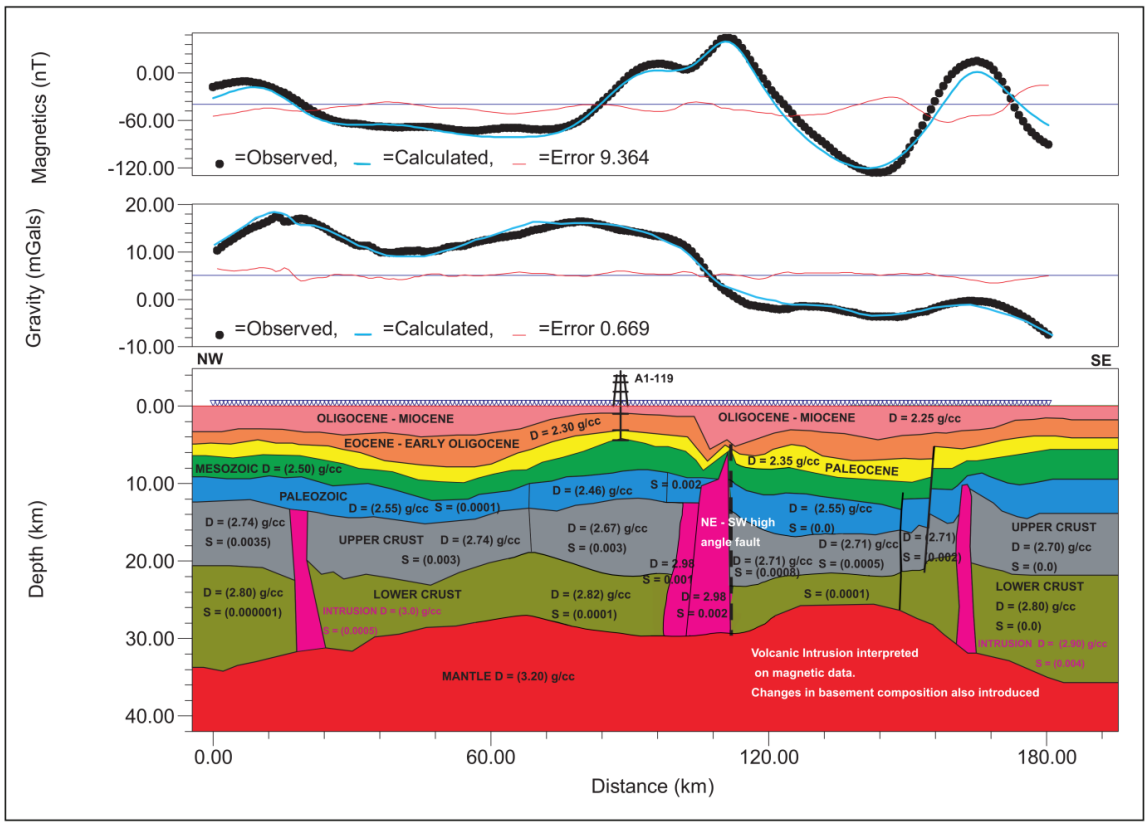

Figure 4.37: NW – SE gravity and magnetic (GH) model from central Ajdabiya Trough. The modelled gravity and magnetic anomalies are shown with unconstrained intrusive bodies. In general the volcanic activities in Libya are believed to have been concurrent with movements along deep-seated fractures perhaps in connection with the .great orogenic pulse of the Alpine cycle (Goudarzi, 1959). Crustal thickness varies under Ajdabiya Trough indicating stretching and undulations formed due to sediment loading and subsidence. Densities in g/cm3 are adopted from different sources (Libyan Gravity Compilation Project, 2001, Makris, and Yegorova, 2006, Casten and Snopek, 2006'). Published values are mainly based on analysis of well logs (density and sonic) and core sample analysis from the Sirt, Ghadames, Murzuk, Jefara and Cyrenaica areas (Essed, 1978), magnetic susceptibilities are given parenthetically with some constrains from local and regional studies.

Additionally, the Euler depth estimates are shallow in this area. The computed depths are actually matching those shown on the 2D models (Figures 4.37 & 4.38), so that the configuration of the igneous body in the model (IJ) should be considered a maximum depth solution for these high frequency intrusion and volcanic layer signatures.

The string of NE-SW anomalies correlates with a high angle normal faults shown in the basement (Figure 4.37). From a magnetic point of view, it would appear that the magnetic sources that are bounded by this fault are due to reactivation and possible intrusive activity. This conclusion arises from the alternating positive and negative source susceptibility values needed to accommodate the observed anomalies. The sharp rise in the magnetic field to the north is undoubtedly owing to the large magnetic anomaly south of the study area. Even

though we are seeing the effect in the magnetic field, the major bulk of the magnetic source lies at the centre of the study area.

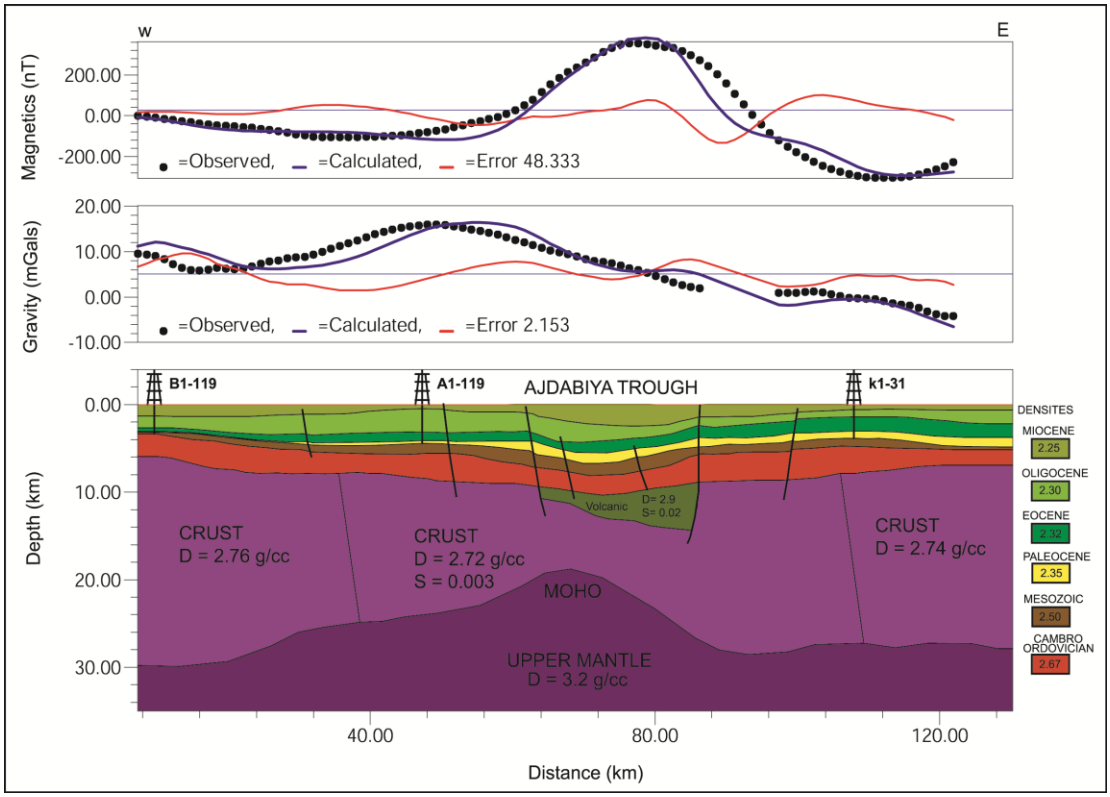

Figure 4.38: Geologic crustal model across the central part of Ajdabiya Trough in EW direction, based on gravity and magnetic data and well control along profile (IJ) (see location in Figure 12). Main trough bounding faults are indicated. High density lower crust is interpreted to be mafic material.

4.7 Crustal Thickness (Moho depth)

Crustal thickness (Moho depth) is an important control on subsidence. Gravity interpretation shows that low-amplitude, positive Bouguer gravity anomaly exists over the Ajdabiya Trough, possibly attributed to an elevated Moho beneath attenuated crust. Gravity and magnetic modelling has therefore been used to estimate crustal thickness variations. Varieties of approaches have been used to estimate the Moho depth map under the Ajdabiya Trough area. This incorporated 2D forward modelling along profiles set in different directions within the trough, in addition to other information from studies in Sirt Basin (e.g. Doser et al., 1995; Marone et al., 2003). The 2D modelling of the gravity data for particular anomalous regions clarified some uncertainties about the depth and origin of the anomaly in question.

Moho depths along variable gravity and magnetic profiles are extracted at regular spacing of about 2.0 km interval. For modelling purposes, the lithospheric column was divided into different layers, comprising mantle, lower crust and upper crust with variable densities and magnetic susceptibilities. The latter includes Palaeozoic, Mesozoic and Cenozoic sediments. A Moho depth of ca. 26 km is estimated beneath the Ajdabiya Trough (Figure 4.39). The Moho is 26 to 33 km deep in the centre of the trough and sharply deepens towards the northeast and southeast respectively, where it remains around 35 - 40km. Other work suggests a Moho depth of ca. 23 - 30 km, below the Sirt Basin (Doser et al., 1995; Marone et al., 2003). To the north of the Ajdabiya Trough, within the offshore Sirt embayment, the Moho is present at 30 km depth (Marone et al., 2003).

This suggests that the region could be an extension of the northern African margin beneath the Mediterranean Sea, an idea supported by its shallow bathymetry. Our estimates of Moho depth show that the mantle is obvious and elevated beneath the Ajdabiya Trough and distinct from adjacent regions. This elevated Moho is consistent with rifting and crustal thinning beneath the Ajdabiya Trough.

The Moho is deeper (35+ km) in SW Libya and more shallow (possibly around 26 km) in NE Libya. The regional trend may also be influenced by a variation in sediments densities as a study of well logs from the Murzuk and Cyrenaica areas (Essed 1987) shows that the density of the sedimentary rocks increases from the SW (Murzuk region) towards the NE (Cyrenaica Platform). A high density area in the lower crust, suggested by modelling gravity data, has been deemed too local to cause subsidence across the basin (Holt et al., 2012).

The model in figure 4.40 (b) show a strong regional trend as the Sirt Basin area is approached. This is interpreted as due to a dramatic crustal thinning and rises of the Moho from around 35 km depth or more in the south to about 26 km depth at the end point of the profile.

The profile shows a general thickening of the Paleozoic sequence to the north, although on several wells, this has been recorded as undifferentiated strata. Consistent with this thickening Paleozoic a significantly deeper basement is interpreted to the north indicating remarkable subsidence. Instead Bijwaard et al., 1998 and Widiyantoro et al., 2004 as outlined in Capitanio et al., (2009), have suggested that a deeper high velocity zone in the Western Mediterranean region including Sirt Basin area and extending down to lower mantle depth

visible in seismic tomographic image is evidence of a thick cratonic lithosphere, which may causes the subsidence under the Ajdabiya Trough.

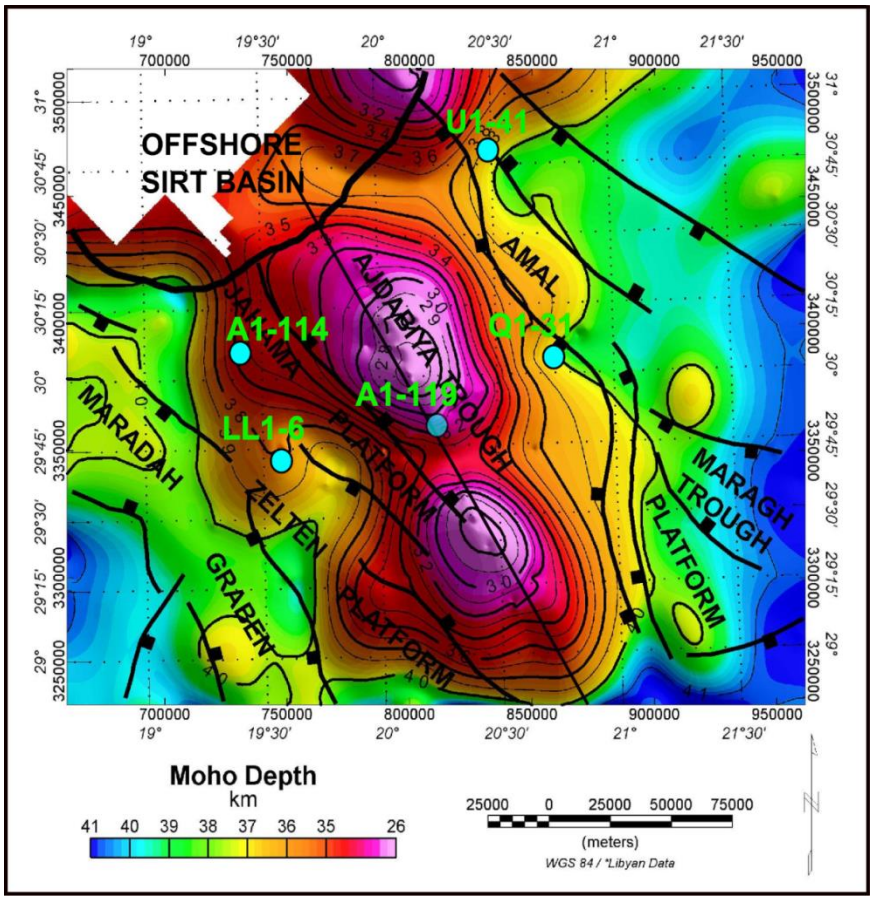

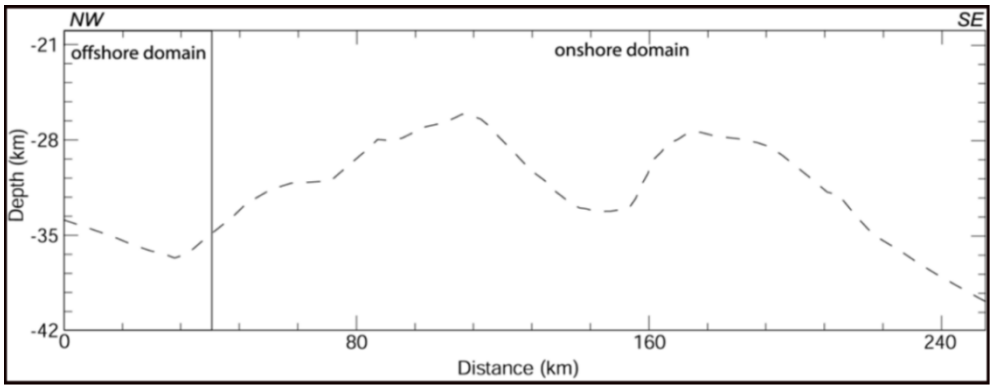

Figure 4.39: (a) Moho depth map shows that the Ajdabiya Trough having crustal thicknesses on the order of 35 km, thinning to 26 km toward the centre, similar to thicknesses presented in the gravity and magnetic model (Figure 4.35). (b) Moho depth profile underneath Ajdabiya Trough. Though the finer details of the crustal structure are impossible to resolve at such a regional level, the shape of the Moho presented here resembles that presented by (Doser et al., 1995, figure 4.38 a,b). The folding of the Moho at the centre of the trough is an indication of mantle upwelling or raising of the thermal anomaly which control the ongoing post-rift subsidence.

Thickening of lithosphere is presented to account for the cause of subsidence in North Africa Palaeozoic basins including Ghadames and Al Kufra basins in Libya (Holt et al., 2012). This could be compared with the post-rift thermal subsidence mechanism in the Ajdabiya Trough despite the broad gap in the time span and the basins forming history.

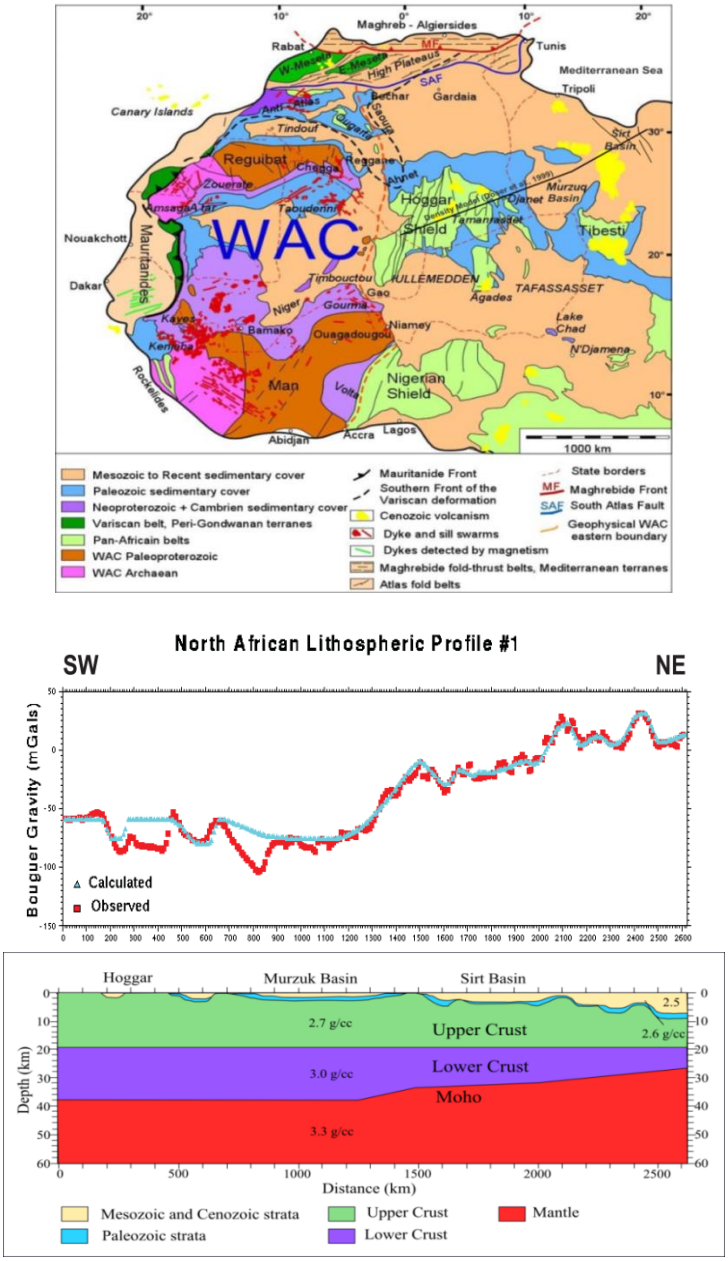

Figure 4.40: (a) General geology of the West African craton showing the location of the density model studied by Doser et al., 1999. Modified last version obtained from Ennih, N & Liégeois, J.P. (2008). (b) Simplified model of the Earth's crust across Murzuk and Sirt Basins from near vertical reflection seismic data with regional gravity profile. The model is re-drawn from Doser et al., 1999.

4.8 Summary and Conclusions

The chapter presented an integrated potential field dataset including Bouguer gravity, and combined draped satellite and aeromagnetic data that shed new light on the nature of the Mesozoic - Cenozoic tectonic and the crustal structure within the Ajdabiya Trough area. A combination of digital enhanced gravity and magnetic maps, coupled with depth to basement map and joint 2D magnetic and gravity models, used to map the subsurface geology and deeper crustal structure of the region. Specifically, I interpreted the data to compile an enhanced structure maps portraying the subsurface extent of Palaeozoic basement, Mesozoic and Cenozoic sedimentary infill and faults. The structural interpretation, based on the analysis of gravity and magnetic patterns and lineation's, reveals faults and possible igneous intrusions. ENE-WSW Left-lateral shear zones identified from the gravity and magnetic interpretation maps may have facilitated the emplacement of Pre-Cambrian intrusions (e.g. Busrewil et al., 1996) and accommodated NW-SE extension of the Sirt Basin and reactivated pre-existing fabric during the Early Mesozoic.

The 2D gravity and magnetic modelling provide better constrained mapping to the tectonic and crustal structures of the Ajdabiya Trough region. The result of the modelling provided a good fit to the observed and calculated gravity and magnetic anomalies. The uncertainty errors in the modelling fits were approximately 0.5 - 2 % for the gravity data and 10 - 48% for the magnetic data. Regarding the magnetic data, the high error in the fitting was due to the strict constraints imposed on the magnetic model which include the reduced number and geometries of magnetic sources in addition to their physical properties (magnetic susceptibilities of the sediments and the bed rocks). However, these limitations were necessary to relate each causative body with prior information from independent geological and geophysical studies. Further studies concerning the magnetic heterogeneity of the basement rocks are necessary to geologically constrain the joint modelling and to minimize the large misfit in magnetic properties.

Since the late Palaeozoic to Early Mesozoic and during the late Cenozoic periods, the Ajdabiya Trough region was intensely deformed due to rifting episodes and extension periods that caused thickening of the upper crust and thinning of the lower crust. Crustal structures of the Ajdabiya Trough region are closely correlated with tectonic activities of the eastern Sirt Basin and Cyrenaica Platform to the east (e.g. El Arnauti et al., 2008). The system of the

Ajdabiya Trough has been deformed by medium to high-angle extensional faults which cut down to the middle crust (Baird et al., 1996).

Basement depth map deduced from the gravity data (Figure 4.41) has shown information's about the basement depths within the trough, and provided a good indication of the regional tectonic setting.

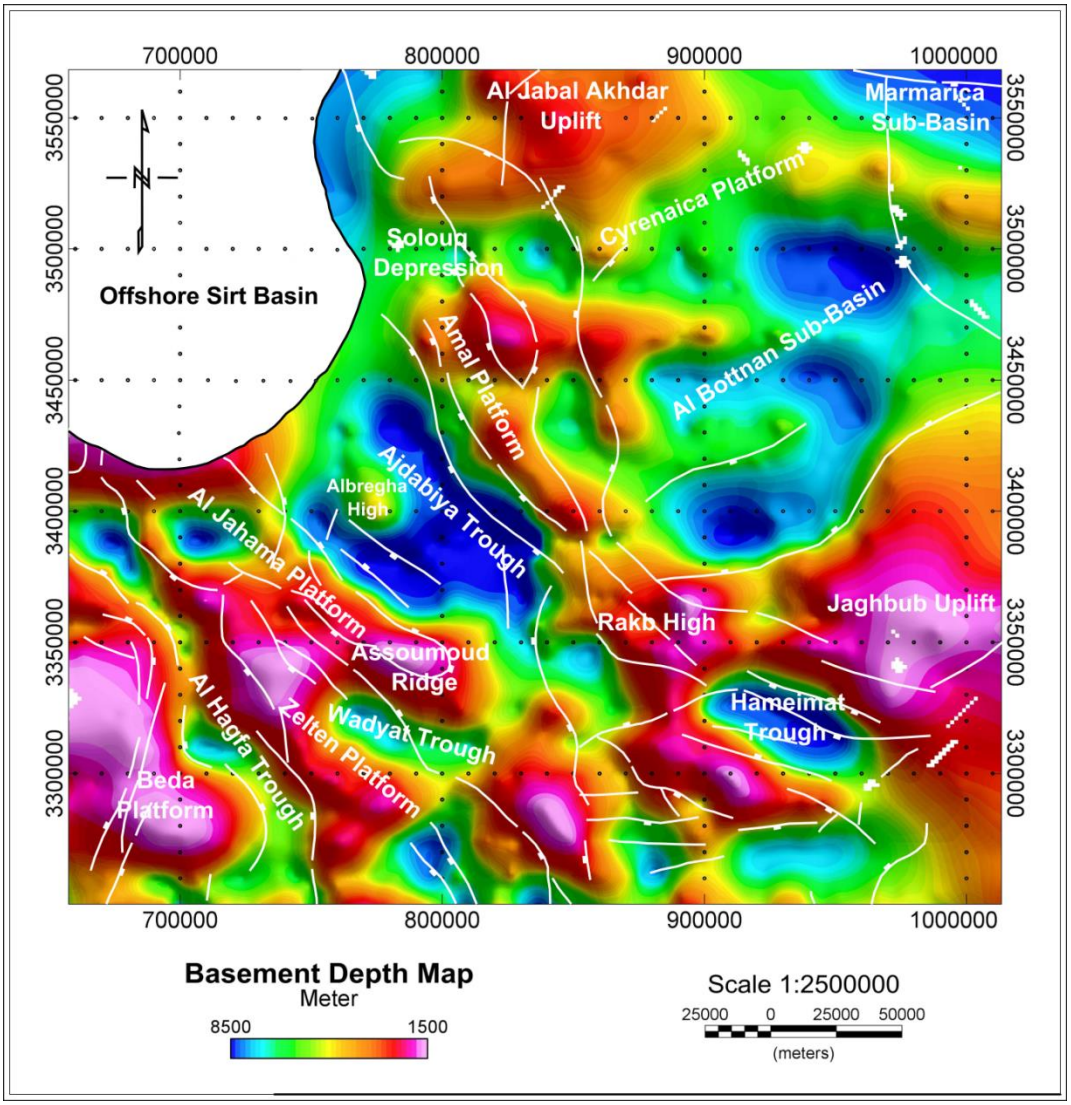

Figure 4.41: Basement depth map deduced from the 2D gravity modelling, 3D Euler deconvolution, and well data, showing the Ajdabiya Trough structural framework clearly surrounded by major structural elements includes major troughs and platforms. The basement morphology is in agreement with that basement depth map obtained by Witte, 2008 Figure. 4.43.

2D gravity modeling of the gravity data was used to define the internal architecture of the Ajdabiya Trough using series of gravity profiles (Figure 4.42) following the same

methodology used to predict the Moho depth map in figure 4.39. Additional 3D Euler deconvolution of the gravity and magnetic data guided the determination of the intra-sedimentary and intra-basement potential field source geometries.

The results of the combined gravity and magnetic modelling reveal an extended graben structure that comprises two main elongated depocentres that are separated by intra-rift horsts probably bald basement highs. This was correlated well with basement map produced by Witte, 2008 in the Ajdabiya Trough area (Figure 4.43).

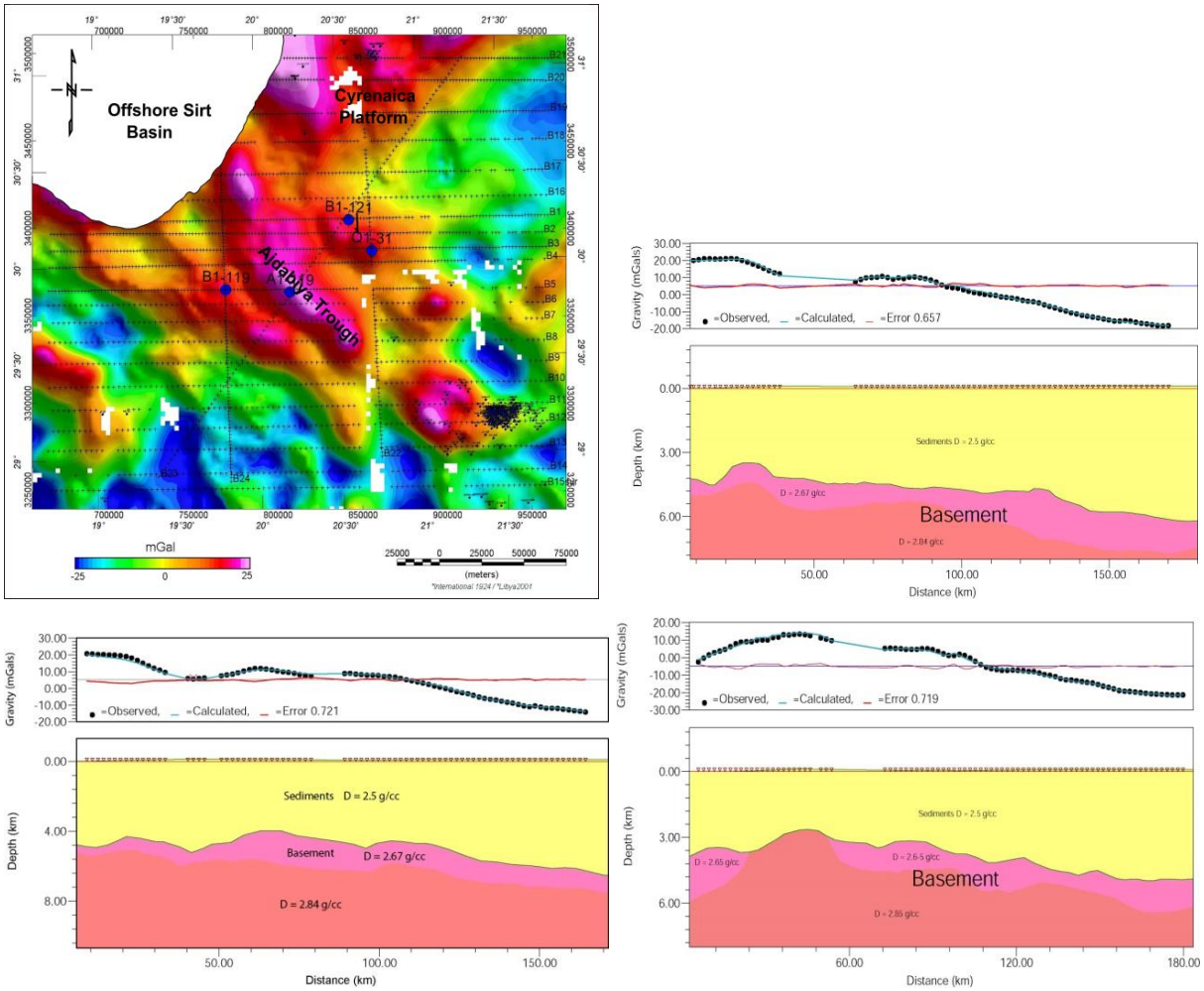

Figure 4.42 Bouguer gravity map of the study area with locations of modelling profiles used to predict the basement depth map and samples from the interpreted profiles.

A complex NW-SE and NE-SW-trending system of faults controls the rift architecture in the area. The gravity and magnetic modeling show that the internal geometry of the trough is characterized by a system of asymmetric graben vary greatly in the orthogonal direction to the

main basin axis, possibly due to the presence of intra-basement heterogeneities (Figure 4.41). Positive gravity and magnetic anomalies possibly related to intra-basement sources beneath and around the rift axis. These gravity and magnetic signatures, suggest that Mesozoic - Cenozoic mafic intrusive possibly constitute the basement blocks and possibly play a significant roles during subsequent stages of extension and fault reactivations.

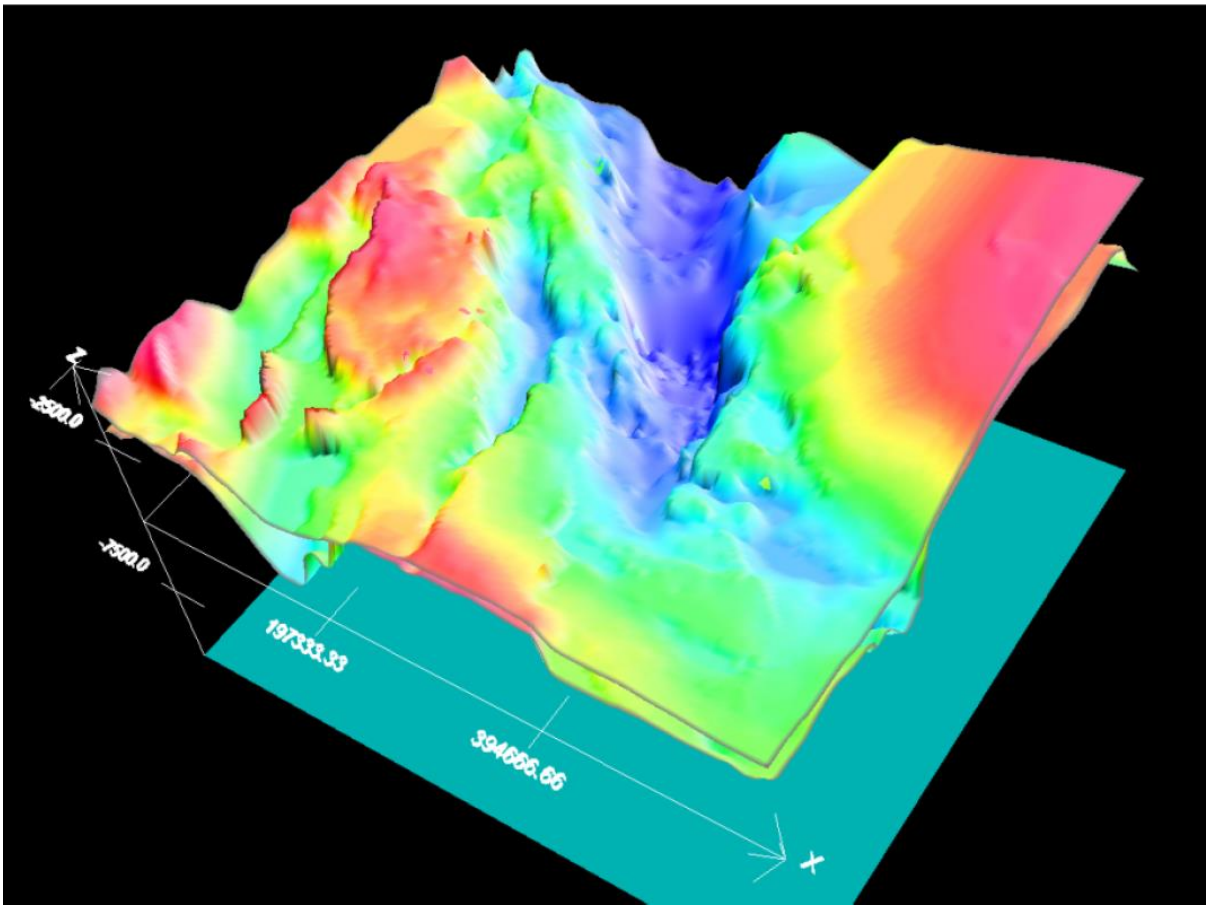

Figure 4.43: 3D modelling of near Basement interface in Ajdabiya Trough using gravity and magnetic data. (Obtained from Witte, 2008).

NE-SW trends indicate wrenching or shear zones that cut the Sirt Basin area and extended to the Cyrenaica Platform (Anketell, 1996: El Arnauti et al., 2008). Associated fold structures were recognized near the Cyrenaica region on horizontal gradient maps. This could be related to inversion tectonics occurred during the Santonian time (e.g. Anketell et al., 1996; El Arnauti et al., 2008). NW-SE trending structures are predominant, along with subordinate of E-W trending features, parallel to structures formed during rifting stages (e.g. Baird et al.,

1996; Ahlbrandt, 2001; El Arnauti et al., 2008), in addition to N-S, and NE-SW trends possibly inherited from Pan-African orogeny and Late Palaeozoic deformations.

It has been suggested that an impressive African Rift system which started in the early to late Cretaceous has its roots deep in the Pan African N-S and E-W trends (Ziegler et al., 1999; Maurin and Guirand, 1993). At shallow levels (ca. <0.5 km), short wave length and high frequency anomalies are interpreted to be a fault and fold structures and mainly die out into the deeper strata.

The African plate was subducted underneath the Eurasian plate during the tectonic interactions between the two plates (e.g. Capitanio et al., 2009). This affected major part from Sirt Basin including the northern part of the Ajdabiya Trough (Figure 4.44), which was subsequently affected by NE-SW crustal extension due to the bending of the continental crust of the African Plate formed NW-SE trending structures in the northern part of the Ajdabyia Trough and give way to a high dense material form the mantle to be in shallow depths as recognized from the gravity and the magnetic models. This subsequently followed by thinning of the continental crust beneath the northern part of the Ajdabyia Trough with possible subsequent emplacement of oceanic crust (e.g. Ahlbrandt, 2001). The region is also characterized by high heat flow, and mildly deformed (stretched) continental crust (e.g. Nyblad et al., 1996; Burwood et al., 2003; El Arnauti et al., 2008). The NE-SW tectonic extension within the northern part of the Ajdabiya Trough is more recent than southern parts, which is possibly related to the late stage of formation of the Sirt Basin, during the collision between the African and Eurasian plates (McKenzie, 1970; Jackson and McKenzie, 1984a, b, 1988).

The idea is supported by independent evidence of magmatism in the Sirt Basin (Capitanio et al., 2009), it could explain the stretching during the Paleogene, although this process could possibly account for the Neogene evolution of the Sirt domains, when tilting, regional subsidence and magmatic activity took place (Ade-Hall et al., 1974; Schäfer et al., 1981; van der Meer and Cloetingh, 1993).

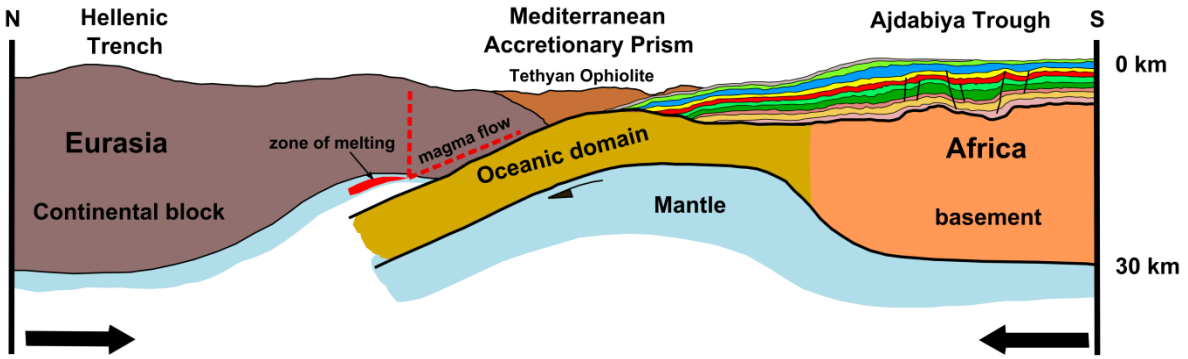

Figure 4.44: Hypothesized geological model showing subduction of African Plate beneath the Eurasian plate. The African plate is moving to the north. In this case, the lighter Eurasian plate made of lighter continental crust and underlying mantle, rides over the denser African plate.

High angle NE-SW basement fault recognized from the magnetic and gravity maps and the models separated the northern part of the trough from the southern part. It seems to be that the southern part of the trough is dominated by NE-SW trending fault system of the same generation and possibly inherited Hercynian reactivated faults. The analysis shows that a modern, high-resolution aeromagnetic survey is needed to confirm these interpretations.

The produced maps present preliminary results as magnetic anomaly maps. These magnetic observations are provided as a supplement to this study. Future work will generate further interpretive maps and models of these anomalies and will involve joint analysis of these data and the other data, with the main goal of understanding the geological structures development of Ajdabyia Trough.

CHAPTER 5: A SEISMIC STRATIGRAPHIC APPROACH TO THE DEPOSITIONAL HISTORY ANALYSIS OF THE CENOZOIC STRATA

5.1 Introduction

Rifting and extensional basin formation are key factors in the geological evolution of the continental lithosphere (Cloetingh et al., 2013). Substantial progress has been made during the last decades towards the understanding of thermo-mechanical processes controlling the evolution of rifts and extensional sedimentary basins (Watts, 2001). An important tool in sedimentary basin analysis is sequence stratigraphy, in which various sedimentary sequences are related to pervasive changes in sea level and sediment supply (Figure 5.1).

During rifting rapid stages of tectonic subsidence followed by long period of tectonic quiescence is a criterion of many rift basins. During these stages sedimentation processes are characterized with gradual filling of the available accommodation space (Figure 5.1) with overall progradational trend. Rapid subsidence will cause instant generation of the accommodation space which in turn will generate rift related sequence boundaries.

Sequence boundaries in this case are generated due to maximum flooding, which would initially develop a transgressive system tract, subsequently followed by highstand system tract formed during advanced rift phase as a result of decrease in accommodation space and due to lowering in the subsidence rates. During initial rift stage a narrow disconnected basins with restricted faults mainly formed. These mainly show sufficient size and depth to record facies like structures (e.g. Gawthorpe and Leeder 2000; Morley et al., 2007). Sequence boundaries are also generated due to fall in sea level and defined by unconformity (subaerial erosion) surfaces and their correlative surfaces.

Sequence stratigraphy is a useful for understanding the organization of the stratigraphic framework of sedimentary basins. It is adopted to understand the organization of the stratigraphic framework and has been developed within the context of tectonically stable sedimentary basins where accommodation formed upon long term thermal subsidence in response to global sea level variations (Vail et al., 1987; Posamentier et al., 1988).

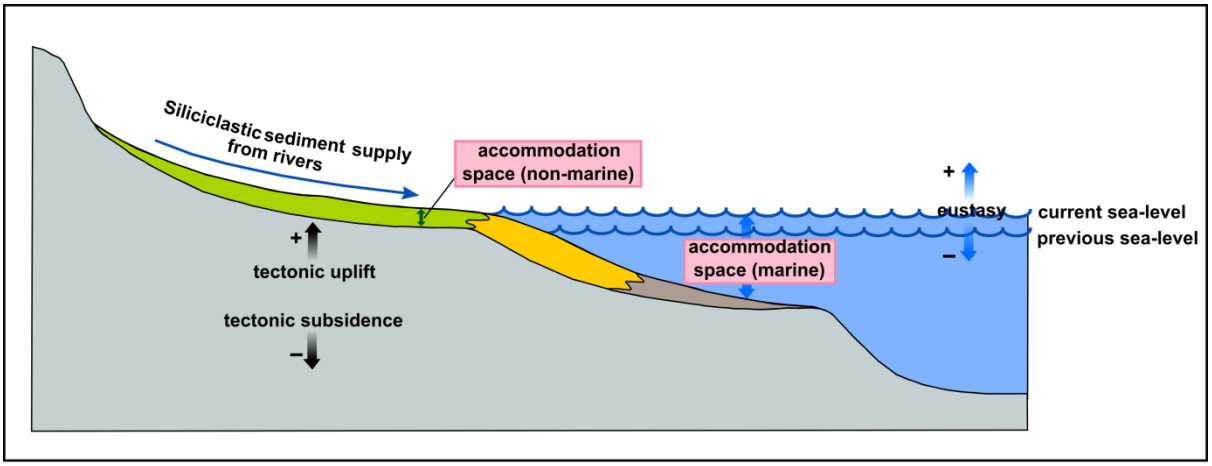

Figure 5.1: Sediment accommodation space and its relationship to eustatic sealevel, tectonic uplift and subsidence. Marine accommodation space created during a rise in relative sea-level has been partially filled with sediment (yellow and dark-grey), whereas the nonmarine accommodation space created during the rise in relative sea-level has been totally filled with sediment (yellowish-green). (Redrawn from Coe et al., 2002).

Quantitative sequence stratigraphic models can be related to crustal behaviour during basin subsidence, and to the effects of regional (tectonically driven) and global (eustatic) sea-level changes (Van Wagoner et al., 1990). In Sirt Basin for instance, the evaluation of the subsidence histories addressed by group of researches among them, Gumati & Nairn 1991, van der Meer and Clotheing, 1996, Abadi et al., 2008, and others suggested the presence of repeated cycles of thermal activation (e.g. Galushkin et al., 2014) and the extension of the lithosphere of the basin, were accompanied by unconformities in the sedimentary sequences and periods of fast accumulation of sediments (Yanilmaz et al., 2008).

The Cenozoic tectonic history of the Sirt Basin is marked by rather subtle changes in stress regimes due to tectonic settings and events in a broader regional context (Hallett, 2002). Cenozoic sedimentary sequences in Sirt Basin (e.g. Paleocene and Eocene carbonates), contain large accumulations of hydrocarbon which have the target for numerous exploration wells drilled in the region since the early discovery in 1957 (Hallett, 2002; Abouessa et al., 2012). The Cenozoic rocks contain major oil and gas accumulations in the subsurface in a variety of different facies, including reefs, bioherms and nearshore sands. Cenozoic outcrops are widespread in Libya, and show predominantly shallow-water marine lithologies (Baird et al., 1996; Hallett, 2002). Therefore understanding the Cenozoic stratigraphy in much detail would certainly lead to a better understanding of the basin structural and stratigraphic evolution.

The aim of this chapter is to evaluate the Cenozoic stratigraphy and tectonic development of the Ajdabiya Trough region using 2D seismic reflection profiles and borehole data including gamma rays, sonic, and resistivity logs.

Well-log sequence correlation and tectono- stratigraphic sequence mapping have been applied to the subsurface data set. The stratigraphic framework is based on wireline log signatures, well cross section, seismic facies mapping, stratal geometry and termination patterns on seismic sections, and isopach maps, and attempt to interpret them in the context of previous studies within the Sirt Basin (e.g. Abugares, 1996; Bezan, 1996; Bezan and Malek, 1996; Spring and Hansan, 1998; El Hawat, 2008; Martin et al., 2008; Yanilmaz et al., 2008, Starke et al., 2008).

The Cenozoic strata in Ajdabiya Trough area are composed of lithological cycles, suggesting cyclic sedimentation grading from platform and shelfal carbonates to siliciclastic and mudstone sediments towards the depocentre (Yanilmaz et al., 2008). This sedimentary package may reflect fundamental controls, such as accommodation space and sediment supply. Then the stratigraphic framework in this chapter provides an account of sequences and depositional facies in the study area and the controls on their deposition and distribution with constrains on the spatial and temporal tectonic development of the Ajdabiya Trough region, throughout the Cenozoic.

5.2 Sirt Basin Stratigraphy

The Cenozoic tectonic history of the Sirt Basin is marked by rather subtle changes in stress regimes due to tectonic settings and events in a broader regional context. A gradual restriction of sediments to the basinal area could be formed by a gradual long-term fall of eustasy, causing a regression or a relative fall and exposure.

For instance, Eocene carbonate depositional system within the Sirt basin can be considered as a non-rimed carbonate ramp system (e.g. Spring and Hansen, 1998; Baaske et al., 2014). The ramp model is considered most appropriate for the eastern flank of Ajdabiya Trough also. Wide depositional facies systems appointed on the basis of available well data confirmed the absence of margin stabilization systems and support the carbonate ramp model. Recently acquired 2D & 3D seismic data also support the ramp model and steepness due to influence of underlying structures.

Within the Sirt Basin significant facies variations occurred (Figure 5.2) during the Upper Cretaceous - Tertiary, and characterized by the development of stratigraphic sequences of predominantly deep and shallow marine carbonates, shales, sandstones and evaporites (Bellini and Massa, 1980; Van Houten, 1980; Anketell, 1996; Hallett, 2002). Sedimentation was controlled by tectonic and eustatic influences, locally inducing high sedimentation rates, the distribution of the various lithologies being governed by ridge-and-trough paleotopography.

Analyses of the sedimentary sequences in the Sirt basin suggest that the present day platforms and troughs (Figure 5.3) exchanged attitude few times during the Cretaceous and Paleogene. This is particularly pronounced during the Cenomanian to Campanian, where the sequence is variable and laterally interrupted. From the Maastrichtian onwards, depositional sequences are fully distributed throughout the Sirt basin and can be divided into seven sequences, these are.

5.4.1 Upper Cretaceous Sequence

5.4.2 Paleocene Sequence

5.4.3 Lower Eocene Sequence

5.4.4 Middle Upper Eocene Sequence

5.4.5 Oligocene Sequence

5.4.6 Miocene Sequence

The mapping in this section is based on stratigraphic analysis of over 50 wells, and covers all of the major study area. Analysis of the well database, and literature references were used to construct thickness and key horizon maps. The maps were created using the Oasis Montaj software used for the gravity and magnetic interpretation (chapter 4). The resulting data were gridded with standared minimum curvature gridding algorithms, using a gridding interval of 1000 m. The maps then contoured and exported into JPG files**.** One of the characteristic features of well logs in Libya, especially in the Sirt basin, is the variable stratigraphic nomenclature of the rock units, and therefore data from wells were referenced by age, rather than formational names. Thicknesses and tops files were created for time units rather than time-rock units. The values were automatically contoured within the areas of dense data coverage, and extended by interpolation into areas of limited data distribution. The resulting maps were used later for calculation of the thickness of the sedimentary cover within the stratigraphic framework in the Ajdabiya Trough.

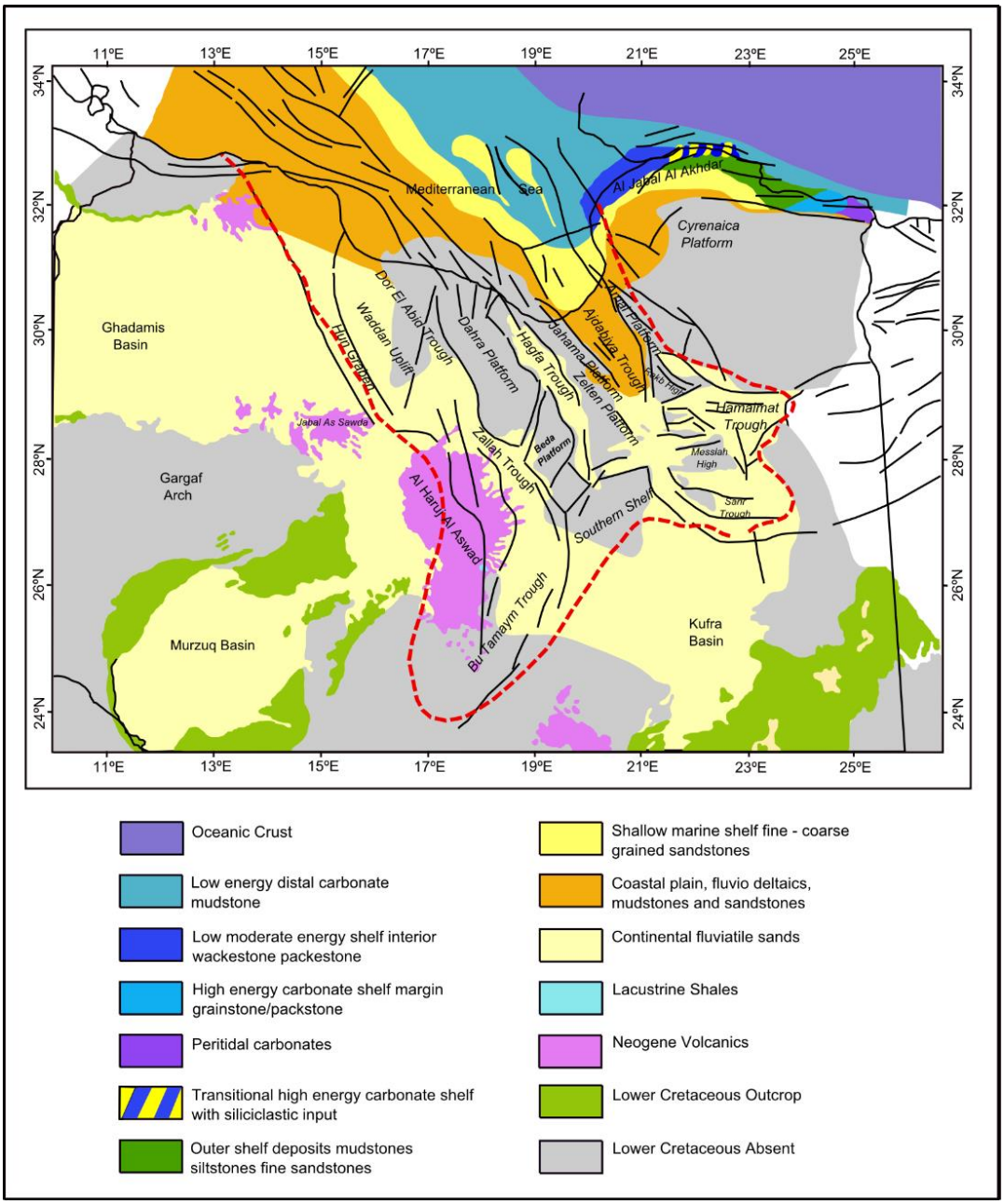

Figure 5.2: Structural elements and depositional environment (facies distribution) of various tectonic setting. The map is kindly provided by Shell Libya Gmbh.

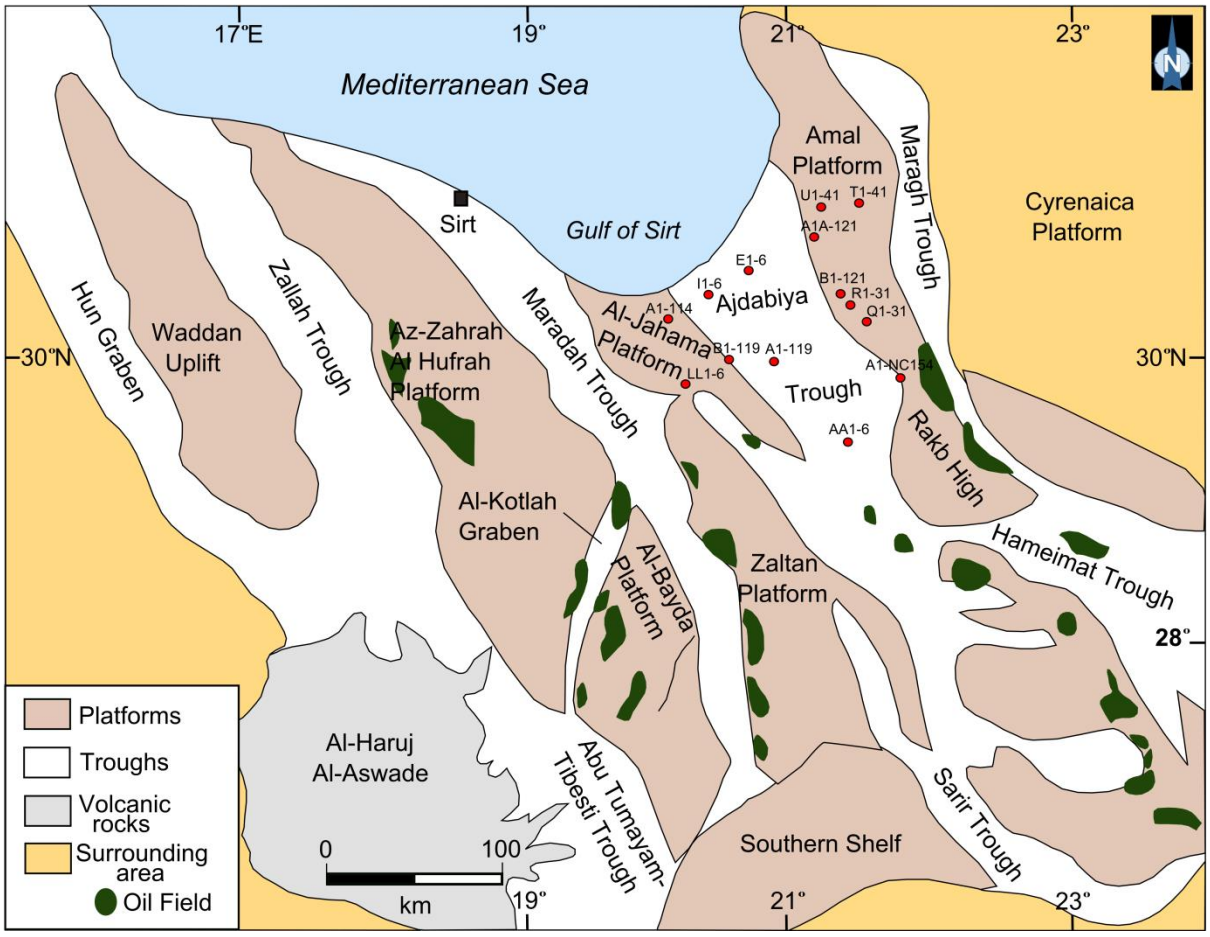

Figure 5.3: Structural elements of the Sirt Basin with location of the Ajdabiya Trough. Wells used in the stratigraphic correlation are highlighted in red circles. Map modified from Libyan structural map of Taleb and Mesughi 1990 and the modified map of Gibbs (2004) by Fiduck (2009). Oil and gas fields are drawn from Thomas, 1995 and Burwood et al., 2003.

5.2.1 Upper Cretaceous Sequence

In the Sirt basin, especially in S and SE the Bahi Sandstone (Cenomanian) (Figure 5.4) forms the basal part of the Upper Cretaceous marine sequence. Although Megerisi and Mamgain (1978) gave a large age range for the Maragh Clastics (Cenomanian-Maastrichtian) (Figure 5.4), and Barr and Weegar (1972) restricted it to the Coniacian-Santonian, the formation still forms the basal part of the Upper Cretaceous sequence (Figure 5.5) whatever its age. The distribution of the Maragh Clastics and the Bahi Sandstone are in some cases intermingled and it might be argued that both formations are equivalent to each other in both facies and age. The other alternative is that the Maragh Clastics sandstones represent the basal clastics of any unit found above it.

This configuration suggests that before the advent of the deposition of the dominantly marine units of the Sirt basin, it was preceded by fluvio-marine, probably deltaic sedimentation. These entire basal clastic occurrences, including the Maragh and Bahi, might therefore range in age from Cenomanian to Maastrichtian, or even Paleocene. During the Turonian-Campanian number of formations was lumped within so called the Rakb Group (Barr and Weegar, 1972,) although the name Rakb has been used in many concession areas to formation level only.

The Sirt Shale (Campanian - locally Maastrichtian) represents the upper part of the Rakb Group (Figure 5.4), and may occasionally be referred to as the Rakb Formation. It is composed of black to grey shale, and bioclastic limestone and sandstone with glauconite and fossil debris. The thickness of the Sirt Shale increases in troughs and diminishes over platforms, ranging from a few metres to over 600m. The Maastrichtian sequence is the most transgressive sequence of the Upper Cretaceous sequence (Wennekers et al., 1996). The names Waha Limestone and Kalash are the most common formation names used for the Maastrichtian sequence. The Kalash Formation (Maastrichtian-? locally Danian) is the most commonly used formation name. The Kalash Formation range from 27m to 247m in thickness (Eliagoubi and Powell, 1978). The Waha and Kalash formations composed of light grey to dark greyish green gypsiferous shale at the base, to brownish light green shale intercalated with yellowish grey fossliferous marl near the middle, and greyish-green shale at the top (Eliagoubi and Powell, 1978).

5.2.2 Paleocene Sequence

The Paleocene sequence (Figure 5.6) is distributed in NW-SE trending zones, coinciding with the Ajdabiya Trough structural trend. The Paleocene sequence is strongly influenced by ENE-WSW trending tectonic trends producing highs and lows in the thickness of the formations. However, this trend is interrupted by a NNW-SSE trend. The thickness in these occurrences ranges between 700 to 1300m. The Paleocene sequence is represented by the Hagfa Shale and locally Defa Limestone (Danian), Zelten (Landenian) and Harash (Landenian), Formations (Figure 5.4).

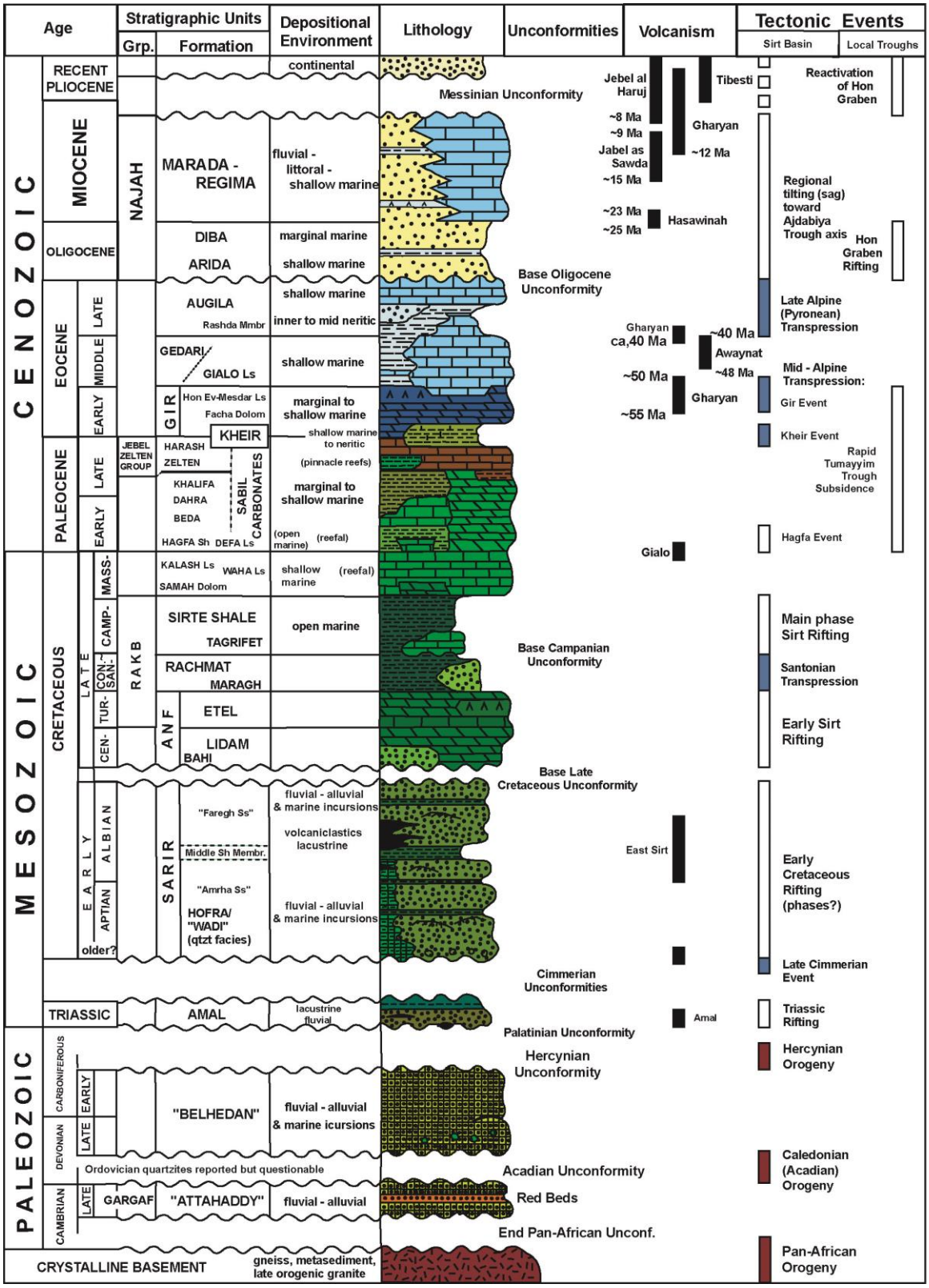

Figure 5.4: Tectono – **S**tratigraphy of the Sirt Basin, with major tectonic events and volcanism (vertical bars). (Redrawn from Guiraud et al., 2005).

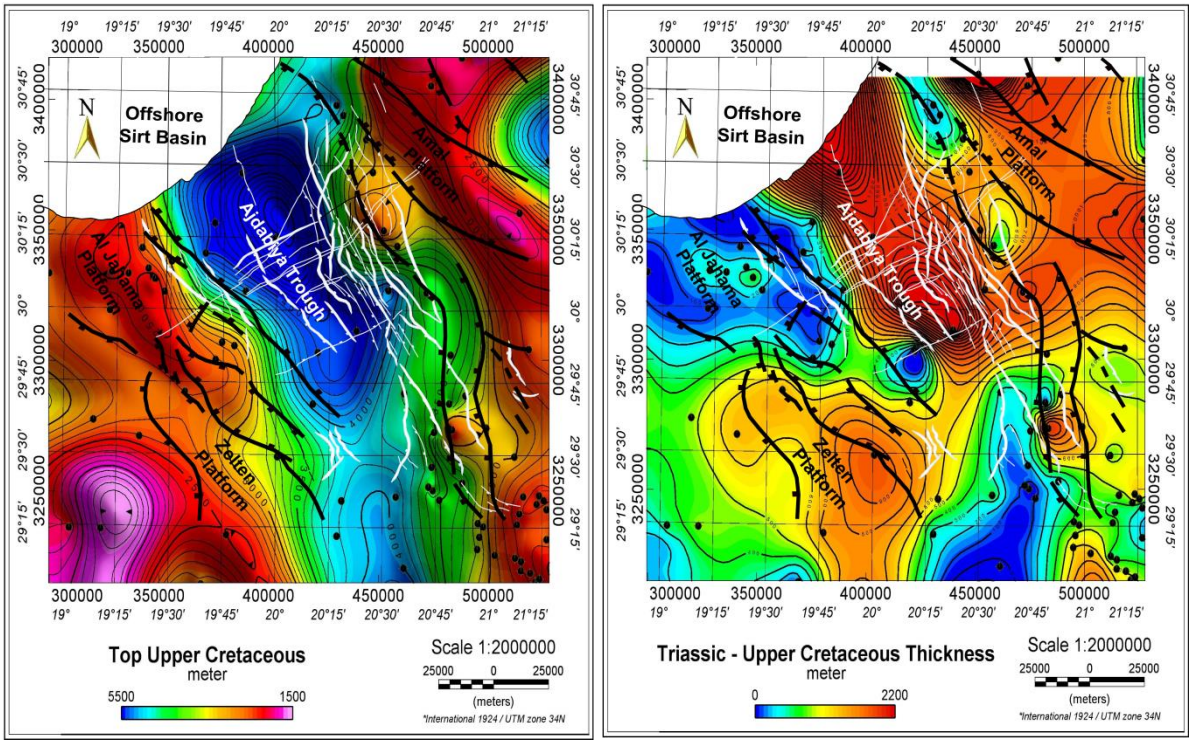

Figure 5.5: Depth and thickness maps of the Upper Cretaceous sequence in and around the Ajdabiya Trough obtained from well data. The maps show major NW-SW trend comparable with the major trend of the fault system in the area the thickness map show an evidence of remarkable deepening and thinning towards the north and north east respectively. White polygons are faults obtained from the 2D seismic interpretation, while the black lines are faults obtained from the gravity and magnetic interpretation.

In NE and SE Sirt basin, the Paleocene sequence is represented by the Lower Sabil (Danian-L Landenian), Upper Sabil (U Landenian) (Figure 5.7) (Barr and Weegar, 1972). The Paleocene sequence has been deposited in a middle shelf depositional environment, grading upward into an outer shelf environment in the upper part of the unit (Bezan, 1993; Yanilmaze et al., 2008). Strata of the Paleocene are the transgressive deposits of this depositional sequence. These strata were deposited above the transgressive surface overlying the Upper Cretaceous (Kalash Formation) and represent the sedimentological response to the onset of rapid relative sea level rise and increased accommodation within the Ajdabiya Trough during the Paleocene cycle (e.g. Bezn, 1996; Bezan and Malek, 1996; Baird et al., 1996; Hallett, 2002). Marine-shelf deposition was established throughout the study area. With the onset of transgression, carbonate deposition was initiated in the south-eastern part of the study area, an area that had existed as a persistent carbonate platform, as evidenced by the limestone's, dolomite and evaporites of the overlaying Gir Formation (Abugares, 1996) (Figure 5.4).

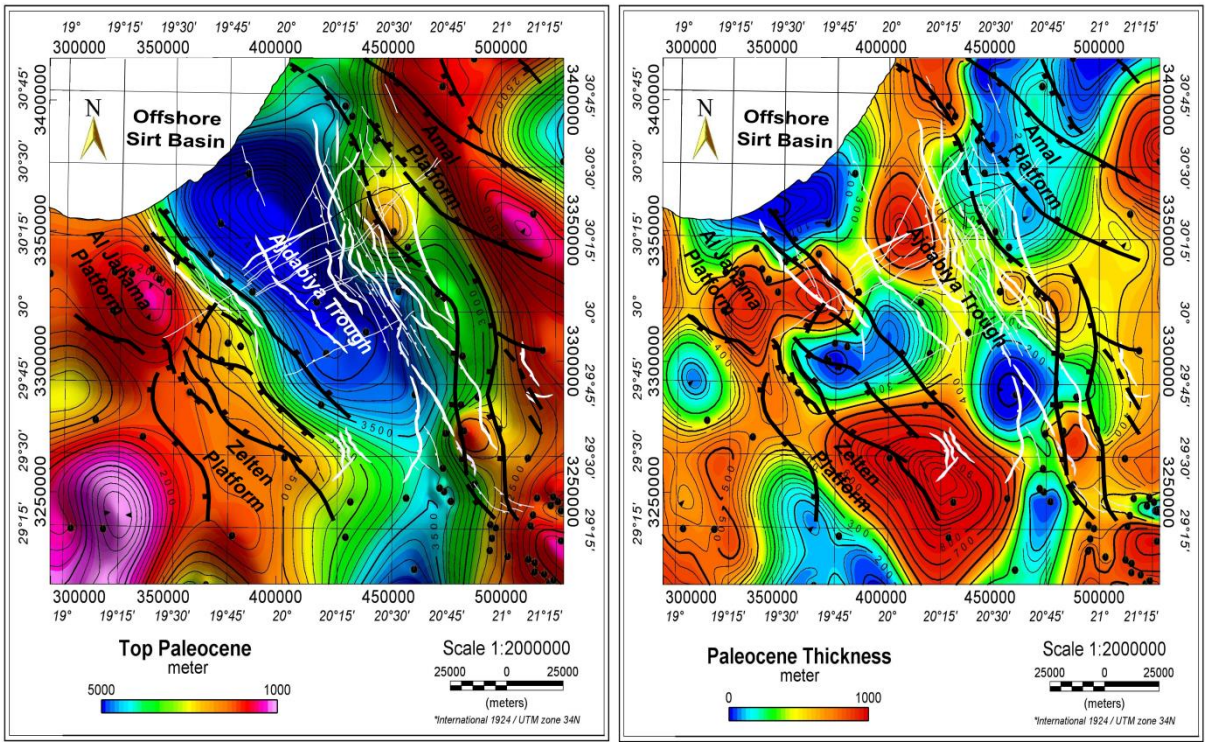

Figure 5.6: Depth and thickness maps of the Paleocene sequence in and around the Ajdabiya Trough obtained from well data. The maps show major NW-SW trend comparable with the major trend of the fault system in the area. The thickness map show an evidence of structural lows and highs developed during the Paleocene time with remarkable deepening and thinning towards the north and north east respectively. White polygons are faults obtained from the 2D seismic interpretation, while the black lines are faults obtained from the gravity and magnetic interpretation.

5.2.3 Lower Eocene Sequence

The Lower Eocene of the Sirt Basin is dominated by evaporites. The Gir Formation (Ypresian) or its lateral equivalents, the Domran, Gattar, Mesdar, Sitra, Bouran and Rouaga Formations, generally represent the lower Eocene sequence (Figure 5.8). The Gir Formation is distributed throughout the Sirt basin and its thickness, (including the Kheir Member) (Figure 5.7), is seemingly tectonically controlled. The Kheir Formation (Figures. 5.4 & 5.7) representing a maximum transgression section (Abougares, 1996; Yanilmaz et al., 2008) composed of shales followed by sabkha carbonate and shallow marine nummulitic banks of the Early-Middle Eocene. The carbonates and Anhydrites of this association are some of the widespread strata of the Sirt macrobasin and contain very little clay (Baird et al., 1996).

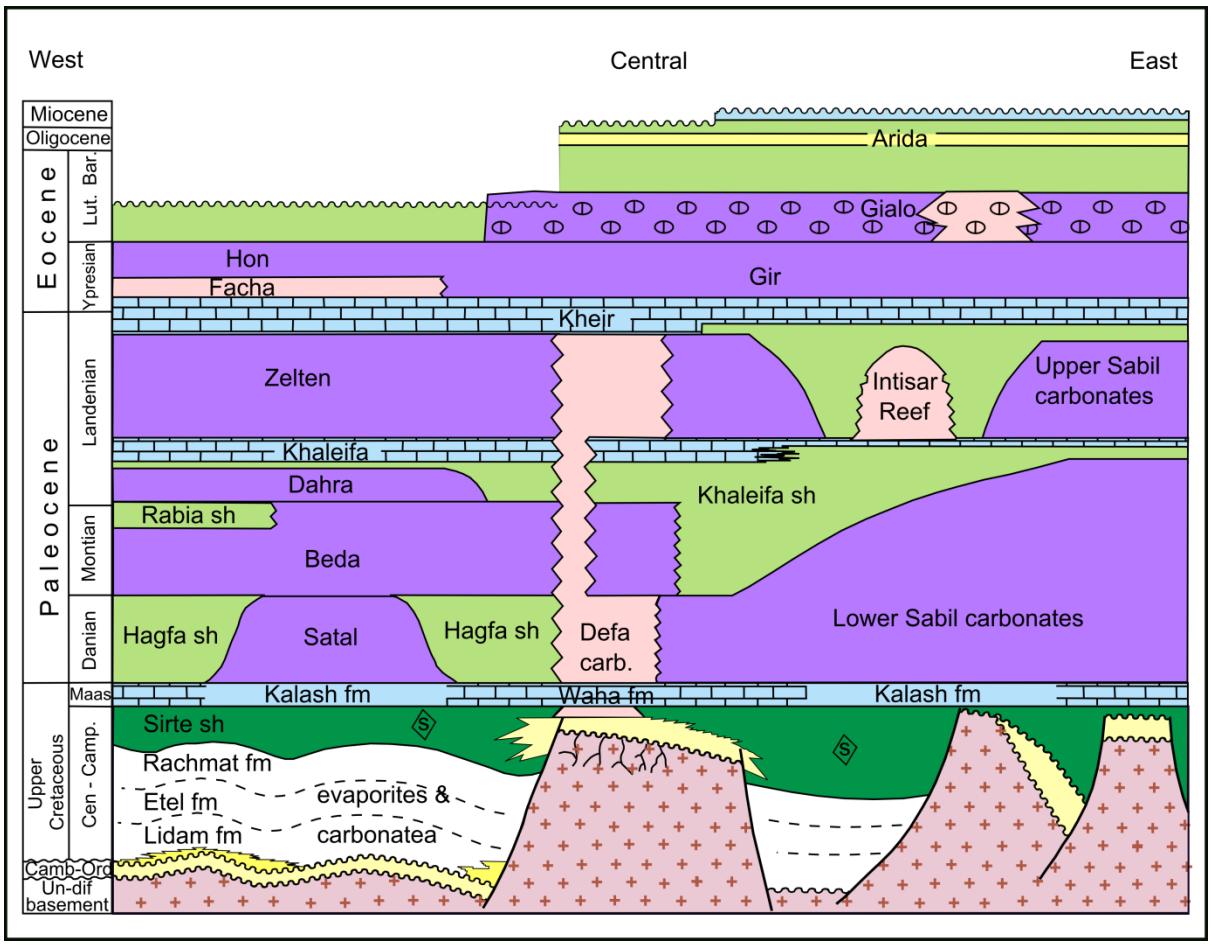

Figure 5.7: Sirt Basin lithostratigraphy show remarkable sequences developed during rifting and characterized by block faulting and both local and regional unconformities. During the Tertiary the sequences are mainly carbonate dominated along the shelf margins and switched to more muddy sequences towards the depocentres (Redraw from Thomas, 1995).

The Gir 'interval' represents one distinct sequence of the Lower Eocene regressive mega-sequence of the eastern Ajdabiya Trough characterized by basinward progradation of intertidal to supratidal system tracts. Eustatic sea level changes are marked in the Gir 'sequence' by Type 2 sequence boundaries (Vail and Todd, 1981), one significant transgressive system tracts, and numerous parasequences. This facies is interpreted to represent deposition in shallowest subtidal, intertidal, and supratidal settings (e.g. Yanilmaz et al., 2008; Starke et al., 2008; Martin et al., 2008). During the Early Eocene (54 – 49 Ma) the basin was affected by subsidence in most of the troughs and regression causing the presence of evaporites in the southern and western sides of the basin (Gir Formation). The Gir formation comprises shallow-marine carbonates and evaporites, with deeper-marine facies in the northern Ajdabiya Trough. A marked thinning of the Gir sequence of less than 90m occurs

towards the deep marine-outer neritic central and northern parts of the Ajdabiya Trough, indicating starved basin conditions (e.g. Abougares, 1996).

The biostratigraphy of the Gir Formation was examined by Abugares (1996). Based on both planktonic and nannofossil assemblages, he demonstrated that the Gir Formation in the Sirt Basin is of mid-Ypresian age, and that the contact with the overlying Gialo Formation is unconformable. The Gir formation can be divided into three members (Figures 5.4 & 5.7), the lower Kheir Limestone (sometimes also included into the Upper Paleocene Zelten Formation or defined as a separate formation) the Facha Dolomite and the Gir Evaporite. The Kheir Limestone (latest Paleocene earliest Eocene) is of shoal facies, usually predominated by large forams (*Nummulites*) (Barr and Berggren, 1980). It is composed of very fossiliferous white and cavernous limestone, occasionally chalky.

It's thickness reaches over 450m in two areas, an E-W zone in the offshore Sirt Basin and in SE part of the Sirt basin. The Facha Dolomite (Ypresian) which is a transition in facies between the shoal Kheir and the evaporitic Gir evaporites, is usually identified in the central part of the Sirt basin and might be either lumped with the overlying or underlying unit. It's thickness is usually around 100m, but values exceeding 350m may be found locally. These local thickness increases are probably due to mis-identification of the lower boundary of the overlying evaporitic unit. The Gir evaporite member (between 400m - 700m thick) is the most conspicuous part of the formation, and it is distributed along a NW-SE oriented zone, within Ajdabiya Trough. Within the Sirt basin, anhydrite forms 20 to 80% of the formation but no definite trend has been identified. It is obviously a product of the closure of the Sirt basin during the Ypresian, and the development of coastal sediments with tectonically active subsiding and uplifted blocks influencing the thickness of the sedimentary column.

5.2.4 Middle Eocene Sequence

The Middle Eocene sequence (Figure 5.9) extends in its distribution to the north Ajdabiya Trough. The maximum thickness of over 1000m is reached in the central trough occurrences (Figure.5.9b), decreasing northwest to less than 200m. The main representative of the Middle Eocene sequence is the Gialo Formation (Lutetian). It is composed of grey calcarenite and calcilutite, chalk and grey shale, fossiliferous and occasionally dolomitised (Barr and Weegar, 1972). The type and distribution of the Gialo depositional facies were influenced by basin-

floor architecture and environmental controls. Wennekers et al., (1996) described widespread shallow marine limestones which pass vertically and laterally into Upper Eocene Augila Formation.

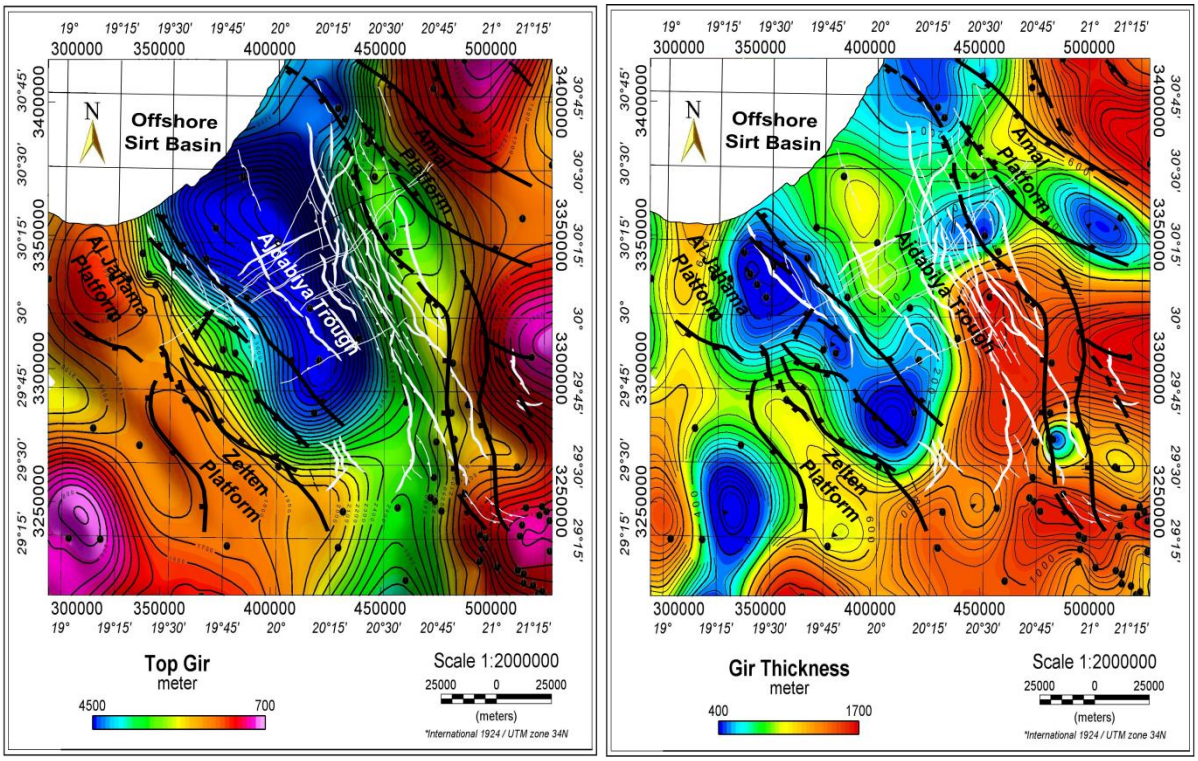

Figure 5.8: Structure and thickness map of the Lower Eocene (Gir sequence) obtained from well data, showing remarkably thick Lower Eocene sequence gradually thinning to the north and northwest implying the development of prograding sequences towards the north and northwest. White polygons are faults obtained from the 2D seismic interpretation, while the black lines are faults obtained from the gravity and magnetic interpretation.

These Middle Eocene sequence is deposited on a broad and shallow un-rimmed platform on the eastern flank of the Ajdabiya Trough with a gentle sloping surface (Spring & Hansan, 1998; Yanilmaz et al., 2008; Baaske et al., 2014). It's covered by facies exhibiting the characteristics of a peritidal environment in the east upon the present-day Cyrenaica Platform (Yanilmaz et al., 2008), followed by a subtidal platform lagoon where large foram-banks developed. In turn these shallow-water facies grade westwards into shoals, pelagic and open marine facies. The gradual change between shallow and deep marine facies is possibly related to transgressive-regressive cycles, which were dominated during the Cenozoic history of the new Tethys Ocean (Ziegler, 2001).

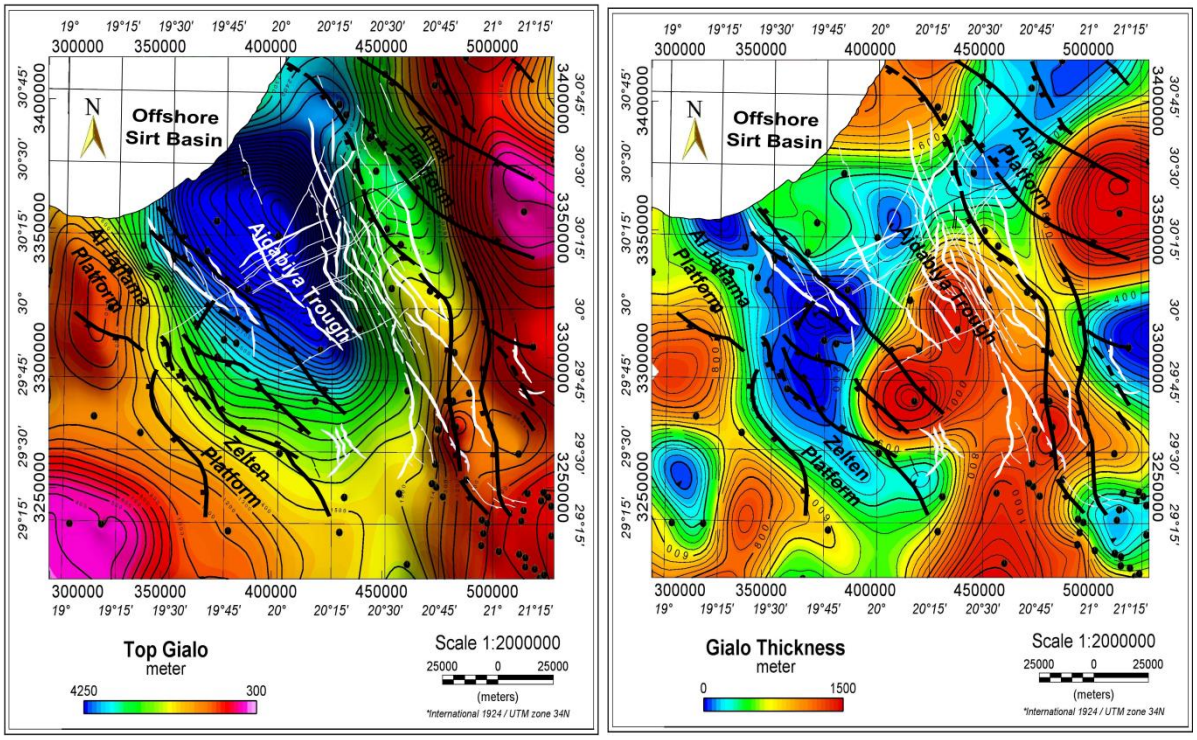

Figure 5.9: Structure and thickness map of the Middle Eocene (Gialo sequence) with equivalent thickness obtained from well data, showing remarkably thick Middle Eocene sequence gradually thinning to the north and northeast related to carbonate factory source at the south and northeast. White polygons are faults obtained from the 2D seismic interpretation, while the black lines are faults obtained from the gravity and magnetic interpretation.

5.2.5 Oligocene Sequence

Within Sirt Basin, the Oligocene sequence conformably overlies the Late Eocene (Augila Formation), and occasionally unconformably overlay the Middle Eocene (Gialo Formation) and underlies the Early to Middle Miocene Marada Formation (Figure 5.4). In the Sirt basin, the sequence is represented by the Najah Group, which is composed of Arida and the laterally equivalent Diba Formations (Figure 5.4).

In the north-eastern and south-eastern parts of the Sirt basin, the Najah Group extends into the Miocene and includes within it the Marada and Regima Formations. The Arida unit is composed of the alternation of thick bedded sandstone and claystone in the lower part with limestone intercalations, occasionally thick in the upper part. The thickness of the Oligocene sequences is increasing towards the Ajdabiya Trough depocentre (Figure 5.11) with gentle and occasionally prograding morphology owing to increasing in basin subsidence and sediment supply. To the east over the Rakb High south of Amal Platform (Figure 5.3), the thickness encountered in the range of 300 -500 m at about 400 - 500 m depth. West of the

Ajdabiya Trough the sequence thins to less than 300m and is composed mainly of open-shelf carbonates in an open shallow-shelf setting (Hallett, 2002). Within the Ajdabiya Trough the thickness of the Oligocene sequences reaches about 2000 m or more (Figure 5.11b).

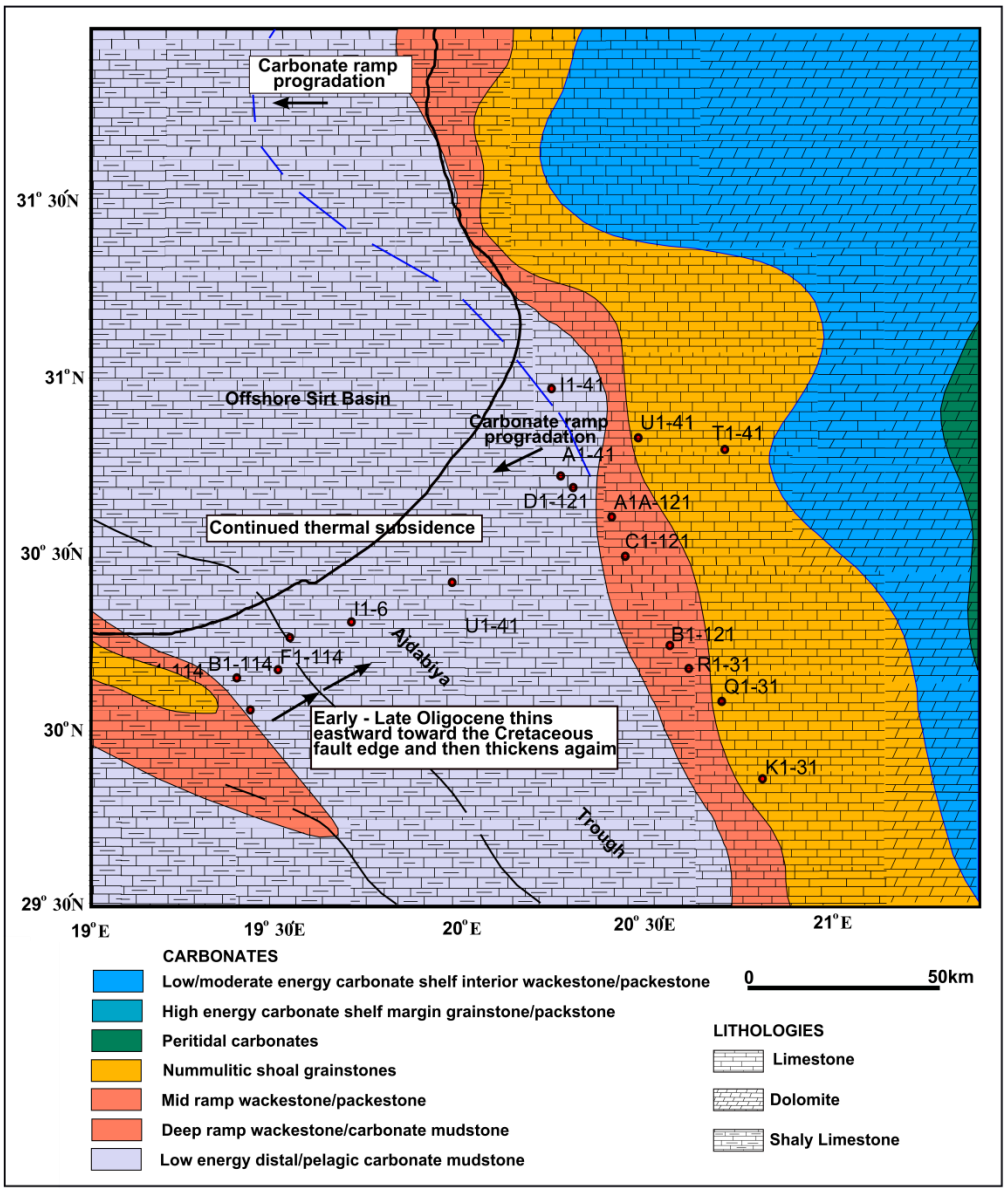

Figure 5.10: Middle Eocene (Gialo Sequence) palaeogeographic map (Redraw from Yanilmaz et al., 2008)

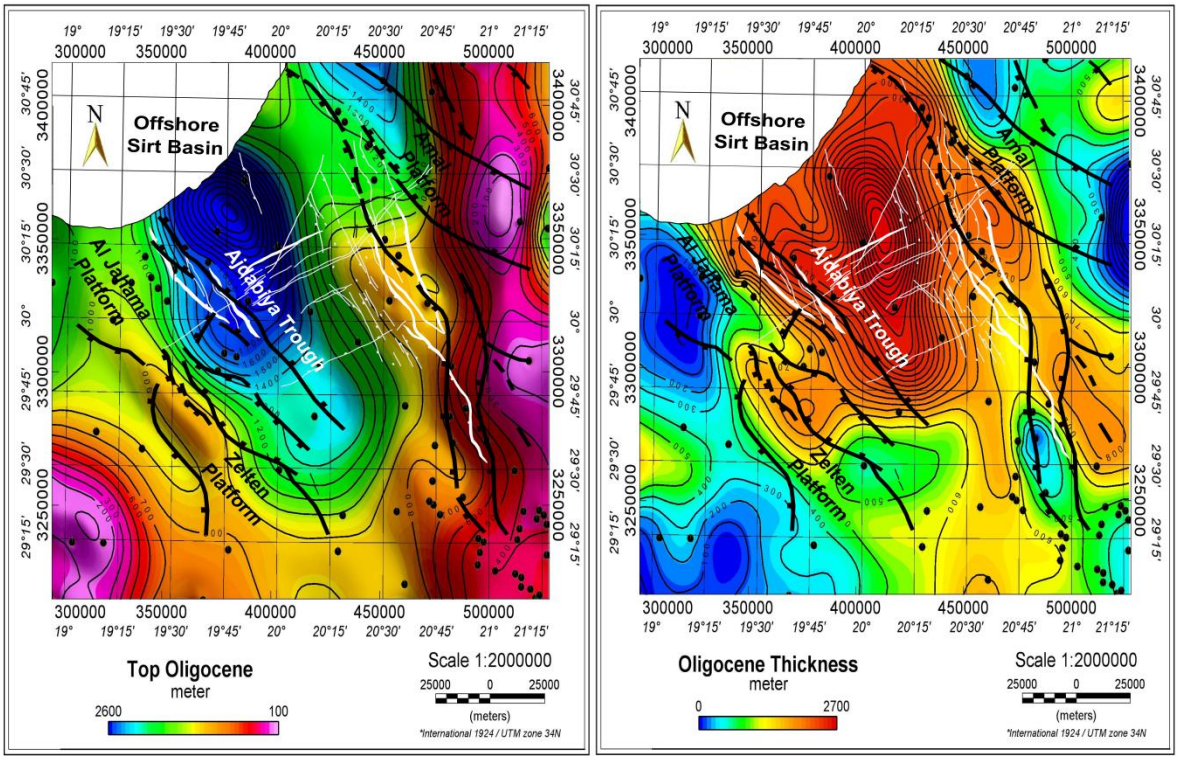

Figure 5.11: Structure and thickness map of the Oligocene sequence with equivalent thickness obtained from well data, showing remarkably thick Oligocene sequence gradually towards the offshore area and filling the accommodation space formed during periods of basin subsidence. White polygons are faults obtained from the 2D seismic interpretation, while the black lines are faults obtained from the gravity and magnetic interpretation.

Carbonate reef build-up from the northern part of the Ajdabiya Trough was studied by Hladil et al., (1991) and showed that the reef-bearing carbonates range in age from Priabonian (U Eocene) to Serravillaian (Miocene).The environment of deposition suggest that the L-M Oligocene sequence is the product of deposition in a narrow seaway (about 400km wide) extending NNW-SSE from the Sarir area in the SE (Figure 5.3) to the offshore area in the NW (e.g. Abouessa et al., 2012). The Ajdabiya Trough was influenced by much clastic material dumped into it both from the sides and the SE (e.g. Yanilmaz et al., 2008). However, some elevated blocks within the trough were possibly the site of carbonate reef build-up. Towards the depocentre the environment of deposition within the sequence becomes of open marine character.

5.2.6 Miocene Sequence

The distribution of the Miocene sequence (Figure 5.12) is largely in the central and northeastern parts (Ajdabiya Trough) of the Sirt basin where the thickness varies from 300m in its middle part and the platform areas to the west, to over 2000m in its northern part near the offshore area (Hallett, 2002). These occurrences are all of Miocene age, in places overlain by up to 200m of Quaternary sand. The Miocene sequence in Ajdabiya Trough is represented by the Marada Formation (Figure 5.4). This formation consists of a large number of lithofacies including shales, sandstones, sandy limestones and calcarenites (Barr and Weegar, 1972).

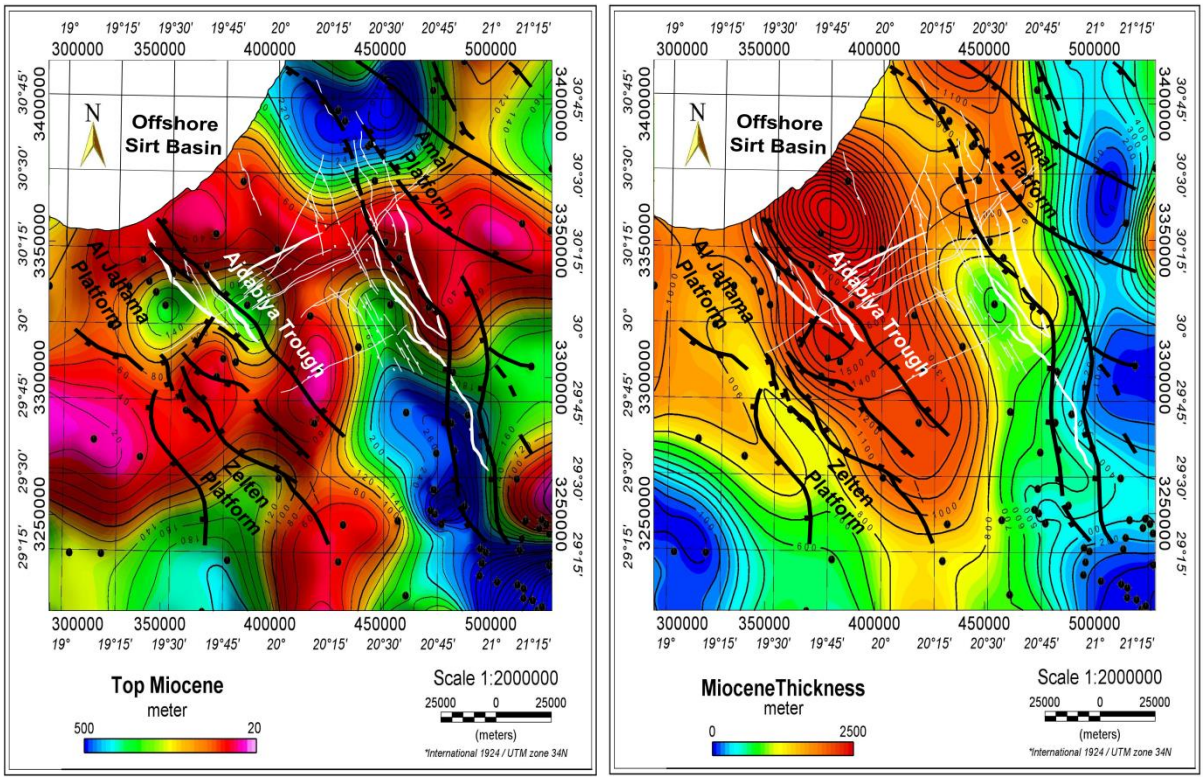

Figure 5.12: Structure and thickness map of the Miocene sequence with equivalent thickness obtained from well data, showing remarkably thick Miocene sequence gradually towards the offshore area and filling the accommodation space formed during periods of basin subsidence. White polygons are faults obtained from the 2D seismic interpretation, while the black lines are faults obtained from the gravity and magnetic interpretation.

The environment of the deposition is developed within a transition from peritidal to shoal facies (Hallett and El Ghoul, 1996: Yanilmaz et al., 2008). It is speculated between restricted lagoonal to the east of the trough towards the Cyrenaica Platform to low energy lagoonal and

grades to high energy shallow to mid ramp shoals (Yanilmaz et al., 2008) with possible development of patch reefs (Maneti, 1984). The Middle Miocene Marada Formation is a second-order stratigraphic sequence bound by well-defined unconformable boundaries (El Hawat, 2008). The unconformity separates the Middle and Upper Miocene strata. The Marada Formation conformably overlies shales and sands of the Oligocene Diba Formation (Wennekers et al., 1996). Overall the Miocene sequence forms a terminal phase in the post-rift megasequence infilling the Sirt Basin (e.g. Abadi et al., 2008; van der Meer and Cloetingh, 1993) and consists of vertically arranged lowstand (LST), transgressive (TST) and highstand (HST) systems tracts (Yanilmaze et al., 2008).

5.3 Stratigraphic Development of the Ajdabiya Trough

The Ajdabiya Trough is a unique rift feature on the African continent in that it occupies intra-continental position and has a thick Mesozoic to Cenozoic succession. The stratigraphic development of the early syn-rift and post-rift succession in the inner Ajdabiya Trough has been investigated using 2D seismic and well data (Figure 5.13). The major characteristic features of the trough are the normal faults, trending northwest-southeast, the rapid transition to deep central basin and basement relief. The basal section of the Ajdabiya Trough is comprised of a series of grabens and half-grabens formed during the Cretaceous rifting (Figures 5.7) these features have trapped up to 1500 m of Early to Upper Cretaceous sediments in the main depocentres, (Baird et al, 1996; Hallett, 2002). Despite the close proximity to active zone at Cyrenaica Platform (Figures 5.2) and the major plate boundary, preliminary observations show that the Ajdabiya Trough has been tectonically inactive since the late Eocene, however, a number of localized late Eocene to Oligocene and Miocene igneous activities are introduced (e.g. Oun et al., 2008).

Sedimentation rates within the trough are comparable to those of other deep marine rift basins (Baaske et al., 2014**)**. The lithological variations observed speculated between carbonate rich platform areas and more muddy rocks of the basin centre. The succession underlying the Upper Cretaceous sequence corresponds mainly to syn-rift sediments (Baird et al., 1996).

Syn-rift stratigraphy developed in response to active faulting, variable subsidence rates and variable topographic relief during deposition. Extensional fault geometry and pre-Cenozoic

topography characterized the rate and facies geometry of the oldest sediments in the Early to late Cretaceous time (Yanilmaz et al., 2008).

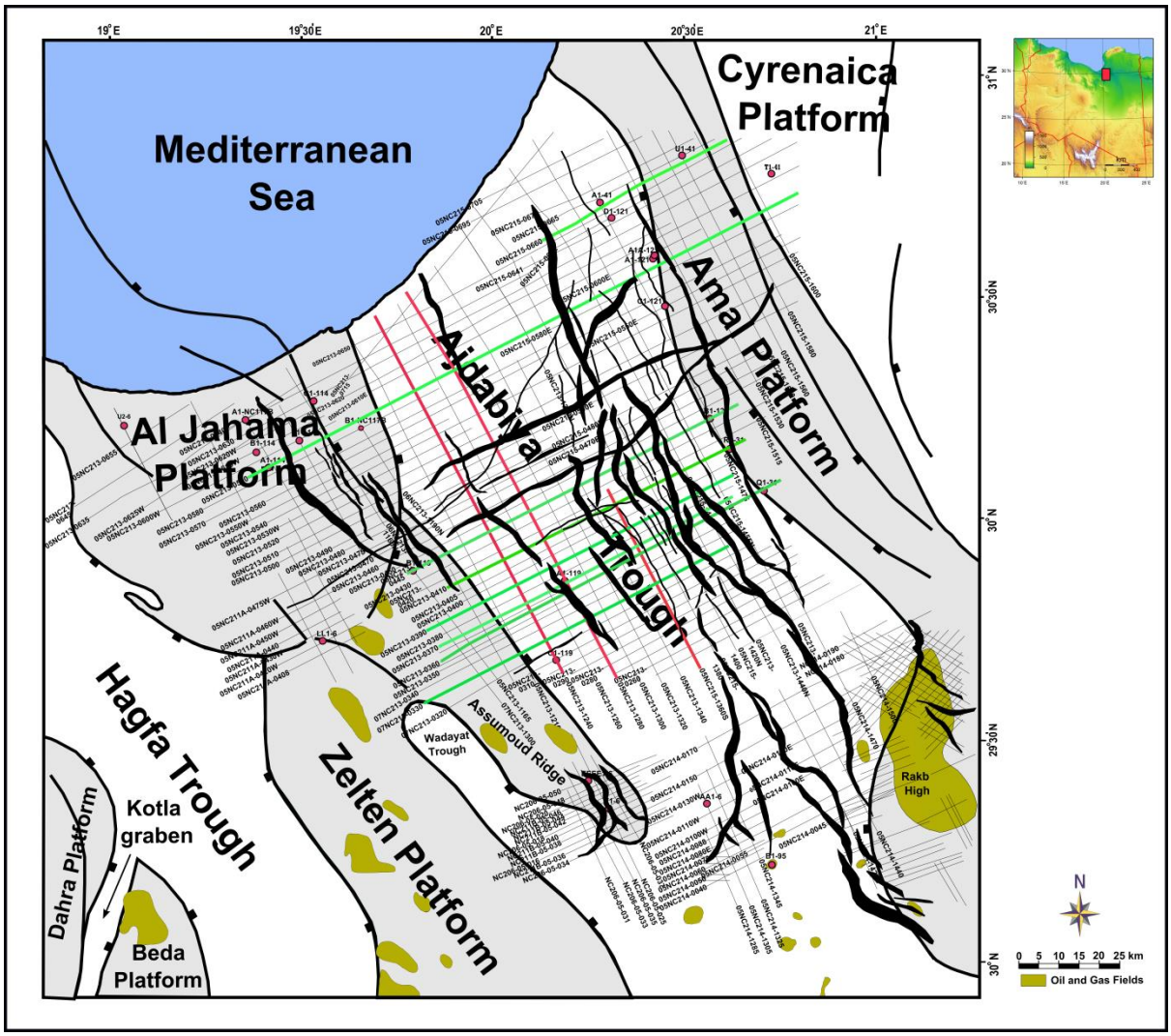

Figure 5.13: Location of Ajdabiya Trough in north-east Sirt Basin – Libya (red rectangle on onset) with 2D seismic coverage. Thick black lines indicate platform and trough boundaries bound by master faults. Green and red lines are 2D seismic lines used in the study. Red circles are wells used in tectonic subsidence calculations (chapter 6). Some of the wells are correlated with seismic profiles for predicting stratigraphic sequences.

This alternating foot-wall-hanging-wall geometry that characterized the Cretaceous fault system is an important factor determining the architecture and facies development of the various syn-rift fault blocks. Within the hanging-walls of the fault blocks, the strata can be subdivided into tectono-stratigraphic packages correlated with rifting stages. The rifting stages accompanied with fault initiation and re-activation phases are possibly Triassic – Early

Cretaceous age (Gras, 1996), and was characterized by rapid subsidence pulses (e.g. Gummati and Nairm, 1982; van der Meer and Cloetingh, 1993; Abadi et al., 2008) adjacent to major faults (Baird et al., 1996) such that the rift became structurally subdivided into sub-basins. Within the Ajdabiya Trough well penetration and seismic resolution in lower succession are generally poor, making observations of any possible Pre Cretaceous syn-rift geometries ambiguous.

This is a consequence of strong acoustic impedance of high density interface (high density strata or basement). 2D seismic sections show that reflectors are terminated against basement highs, suggesting deposition in grabens and half grabens controlled by SW-dipping normal faults. Average thickness of syn-rift sediments in the Ajdabiya Trough represents at least 1.0 s TWT (Figure 5.14). Well Q1-31 located on the Rakb High (Figure 5.3) traverses syn-rift sequence and contributes to define the remnant of the Cambro-Ordovician formations (Figures 5.15 & 5.16). Much of what is known at present about the Sirt Basin stratigraphy and structure was inferred from disconnected seismic surveys and a fraction of the exploration drilling within the basin. The Cambrian sediments are predominantly fluvial medium to coarse grained sandstones but recording common marine incursions (Barr and Weggar, 1972; Cepek, 1980). The Early Ordovician, fine-grained, and cross-bedded sandstones preserve predominantly shallow marine sediments (Turner, 1980). Cambro-Ordovician rocks subcrop the Late Paleozoic (Hercynian) unconformity over most of the trough with Precambrian basement subcropping in the south (Figure 5.16). Evidence from the eastern Sirt Embayment shows the presence of Triassic and Jurassic rocks forming the oldest part of the syn-rift sequence, (Dercourt et al., 1986; Anketell, 1996), and the same situation may be present in other parts of the Ajdabiya Trough. The main syn-rift deposition occurred in the early Cretaceous when the Nubian (Sarir) Sandstone (Figure 5.4) accumulated in rift troughs and topographic lows on the irregular pre-Cretaceous surface (Hallett, 2002). Within the Ajdabiya Trough the Nubian sand is pass into a quartzitic facies and it may pass into a marine facies in the northern part of the trough.

There was a period of erosion during the terminal Early Cretaceous. In some parts of southern Ajdabiya Trough this erosion removed the entire Pre Upper Cretaceous sediments (Nubian) section leaving basal Late Cretaceous sandstone resting on basement (Baird et al., 1996). The Late Cretaceous-early Tertiary transgression in Sirt Basin took place over a NNW trending

structural complex of horst-graben systems that influenced sedimentation during the early Tertiary period (Colley, 1964; Berggren, 1969; Bebout and Pendexter, 1975).

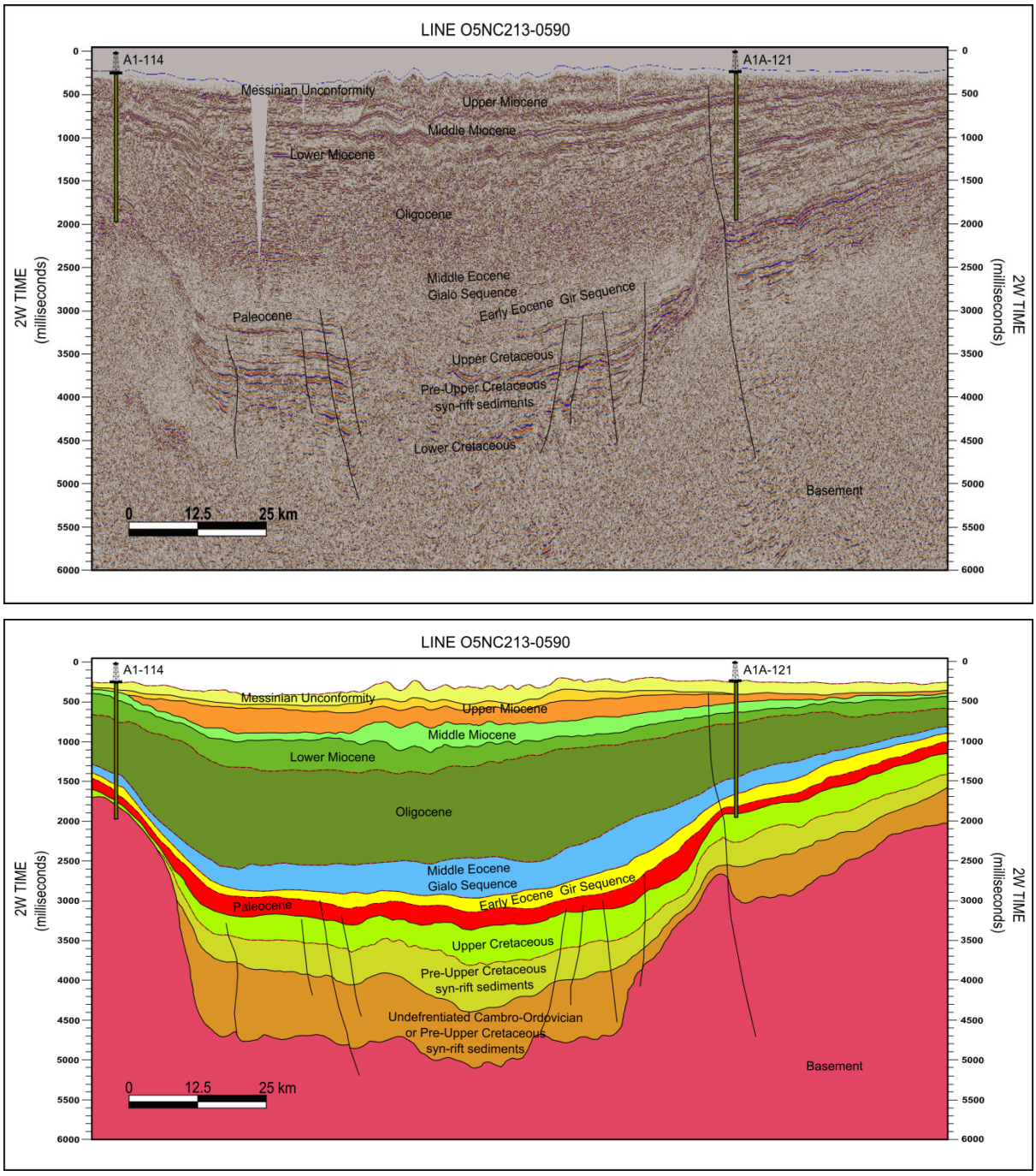

Figure 5.14: 2D seismic line 05NC213-0590 across the northern Ajdabiya Trough with interpretation below. Cretaceous – Paleocene rift faults appear to represent a propagation of reactivated eastward and westward dipping basement extensional normal faults interpreted as part of an underlying Pre- Cretaceous rift cycles.

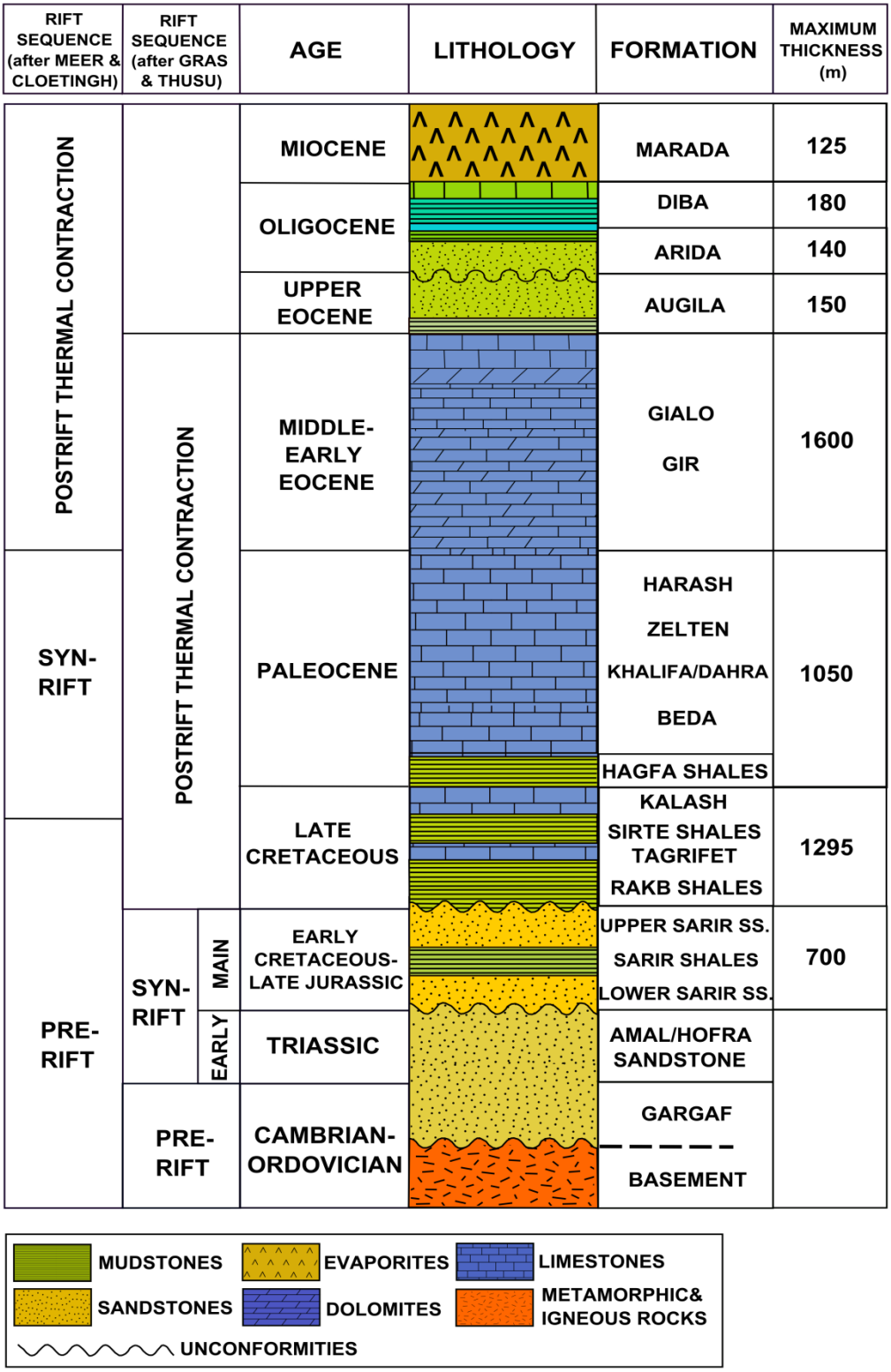

Figure 5.15: Generalized stratigraphic section of the eastern Sirt basin (redrawn from Ibrahim, 1991). Maximum thicknesses of different units are taken from Van der Meer and Cloetingh (1993). On the left, the related tectonic interpretations according to Van der Meer and Cloetingh (1993) and Gras and Thusu (1997).

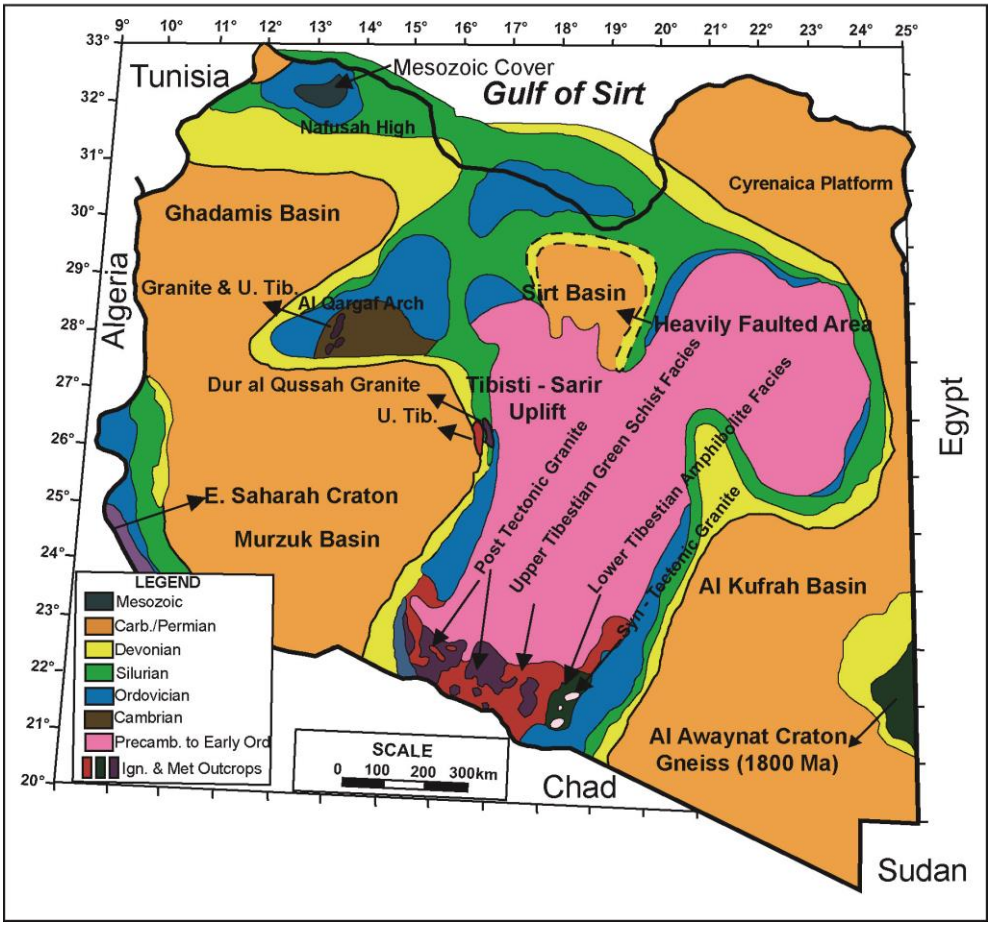

Figure 5.16: Regional subcrop map (Pre-Mesozoic), showing the regional uplift and erosion of the Sirt area during the Late Palaeozoic-Early Mesozoic. Most of the Palaeozoic sediments have been eroded and the Sirt area remained a high until the Late Mesozoic, at which time movement and deformation took place. (After Gumati and Nairn, 1991) The map shows the age of the formations subcropping the Mesozoic unconformity. It represents a view of the deformed post-Hercynian surface, prior to the deposition of Mesozoic sediments. The deeply eroded Tibisti-Sirt Arch dominates the map, and other important uplifts are evident at A1 Awaynat, Nafusah, Al Qarqaf, and Tihemboka. The data has mostly been obtained from oil wells. Small inliers on the Sirt Arch have not been shown. The extent of the Permian subcrops in Jabal Akhdar and in the Jifarah Trough is uncertain.

This forms the main post-rift Megasequence in the Ajdabiya Trough area. The post-rift Megasequence comprises Upper Cretaceous to Late Miocene rocks which reach a thickness of about 6000 - 7000m in the centre of the trough (e.g. Hallett, 2002). During the Maastrichtian, low-energy deep marine argillaceous limestone of the Upper Cretaceous (Kalash Formation) covered the Ajdabiya Trough and submerged the nearby horst regions such as the Rakb High, with relatively little change in facies. The Kalash Formation sediments were deposited during the Maastrichtian times (representing the maximum extent of Cretaceous marine transgression), (Wennekers et al., 1996); these sediments are consistent with those shown in

the Ajdabiya Trough at this time. During the early Paleocene sag phase commenced as fault related subsidence gradually ended, regional rift-basin subsidence ensued (e.g Abadi et al., 2008 and references therein). The Ajdabiya Trough deepened with markedly thick deep marine sections developed in the depocentre. Most of the post-Cretaceous rocks in the centre of the Ajdabiya Trough are argillaceous in character due to their deposition in a rapidly subsiding environment. Carbonate depositions extended from shelf margin towards the basinal areas during marine low-stand (Spring and Hansan, 1998; Yanilmaz et al., 2008), subsequently covered by wide spread of marine shales across former sites of carbonate deposition. Influx of coarse-grained extrabasinal clastics into rift virtually stopped. During the late sage phase, rates of regional subsidence continue with very rare fault activity (Gummati and Nairm, 1981; Abadi et al., 2008). Throughout the history of the rift sedimentation was controlled by the rate of subsidence relative to sediment influx rate. At the centre of the Sirt Basin the Paleocene section is shale dominated and well developed, but forms a complex relationship with the Lower Eocene due to high subsidence rates associated with rifting at the time. In places at the main central trough of the basin, pinnacle reefs are encased in Paleocene shales (Bezan, 1996; Yanilmaz et al., 2008) (Figure 5.17). Over structural highs on the other hand, the Paleocene section is carbonate dominated, and a disconformity is present at the Paleocene-Eocene boundary, whereas sedimentation appears to be continuous in the deep troughs. In the Paleocene, pinnacle reefs developed around the margin of the Ajdabiya Trough (Yanilmaz et al., 2008). Lower Sabil Formation, of carbonate build ups were deposited in the platform areas.

During the Early Eocene time, (54.8 - 49 Ma) (the beginning of the post-rift stag), the Sirt Basin underwent dawn-warping conditions; marine transgression gave way to advent circulation and extensive sedimentation due to inversion tectonics to the north (Knyle et al., 1996). During this interval the basin was affected by subsidence in most of the troughs and regression causing the presence of evaporites in the southern and the western sides of the basin (Gir Formation). The Late Eocene (37.0 - 33.7 Ma) was characterized by marine deposits due to a transgression event developed in the Early Oligocene. In this period subsidence was active along NW structure in the Ajdabiya Trough (Guiraud and Bosworth 1999).

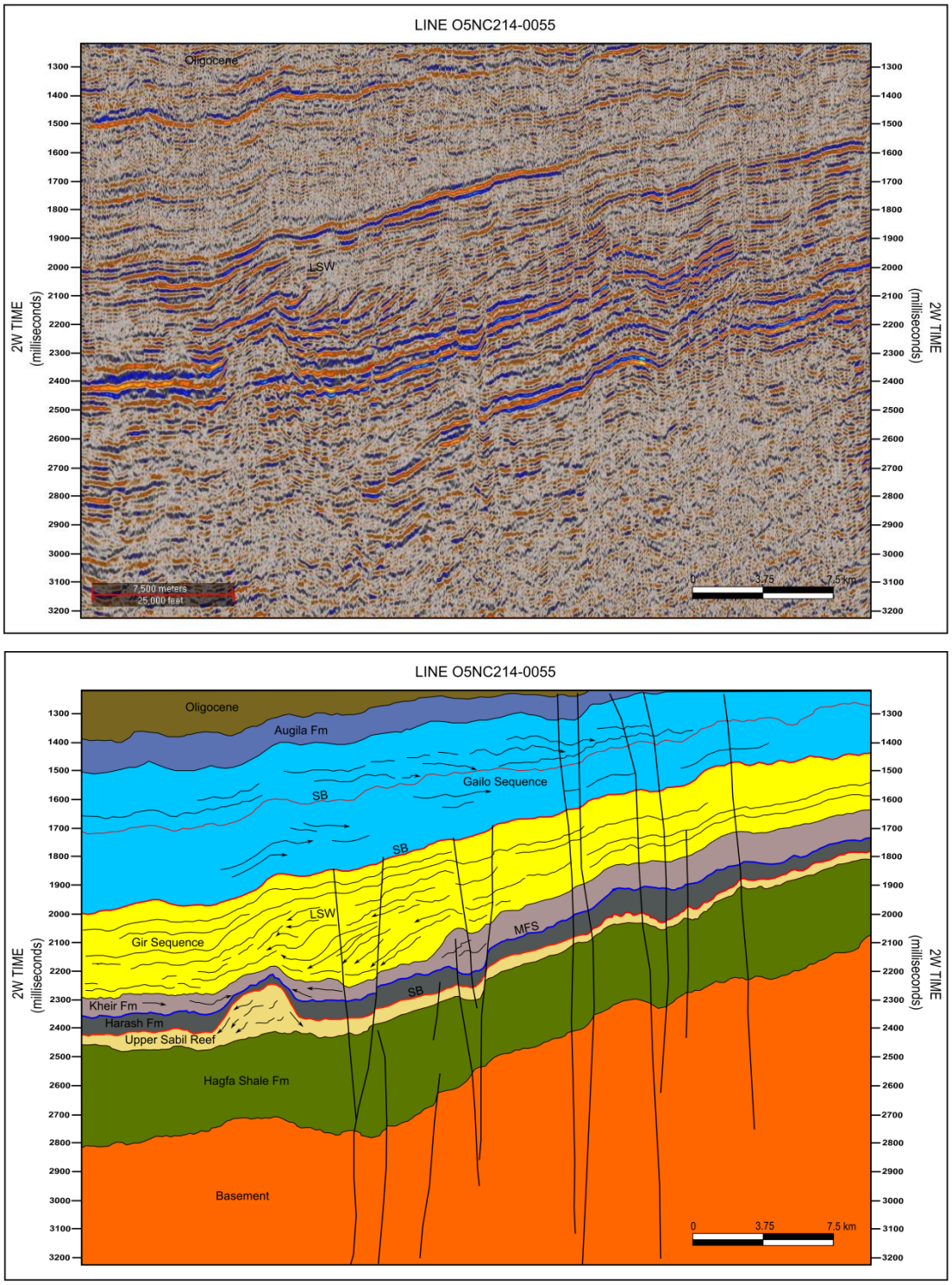

Figure 5.17: Seaward direction, mounded seismic geometry interpreted as reefal build-up of shallow marine carbonate unit of middle Paleocene (Upper Sabil Formation) which regionally thins to less than 20 ms, with the localized thickness increases representing pinnacle reefs towards the centre (e.g. Hallett, 2002). The section display typical reflection geometries and highlight the significant difference in seismic response of the Upper Sabil and overlaying formations. Steep shelf slope at top Upper Sabil level onlapped by high-amplitude parallel basinal reflectors of the Upper Paleocene Harash and Kheir Formations. For line location see figure 5.24.

The Eocene transgression is followed by a period of sea level fail and carbonate progradation into the trough areas. These followed by regional subsidence and transgression throughout the basin. The Oligocene – Early Miocene time was marked by a reduction of tectonic subsidence rates within the basin, and local folding of the earlier sediments. This phase was also associated with original uplift of the African Craton and marks the switch from carbonate to clastic dominated sedimentation within the rift system. Fine grained clastic sediments spilled into the offshore area to accumulate up to 3 km of section, suggesting continued subsidence and rifting in the area (Thomas, 1995).

The Sirt Basin underwent a regression during the Oligocene with a complex interplay between continental sandstones in the south and marine shales and carbonates in the north (Bezan and Malak, 1996). The main controls on the development and distribution of facies during Early to Late Oligocene were fluctuations in regional relative sea level and Palaeotopography.

To the west of Ajdabyia Trough (over the Al Jahamah Platform (Figures 5.2 & 5.3), the carbonate system received, increased amounts of clastic input through Late Oligocene to Early Miocene (Wennekers et al., 1996; Hallett, 2002). This is related to the development in the Sirt area of a major marine non marine shoreline complex which originated in the Oligocene in persisted through the early Miocene, with fluvial continental deposition in the southwest of the Sirt Basin and shallow marine sediments to the NE (Wennekers et al., 1996).

Open marine conditions existed during the middle Oligocene (Belazi, 1989). These characterized by variations in lithology in the marine continental interface (Bezan, 1996). In the north east part of the basin carbonate and clay succession indicates marine shelf conditions (Befiled and Wrigth, 1980).

5.4 Data Interpretation and Analysis

The analysis presented in this section is based on the seismic stratigraphic interpretation approach of a regional two dimensional (2-D) seismic reflection lines in conjunction of well data. Stratigraphic sequences were identified using 2D seismic data collected and processed by the Shell Libya Gmbh, in 2002 over an area of about 30,000 km². An additional 1380 km of low-quality regional 2D seismic lines, collected by Veba Oil Company in 1979 and reprocessed by Petro-Canda, were also used to fill gaps in the Shell dataset (Figure 5.13).

Depth (ft)	Formation	Lithology	Age
0 - 450		Calcareous sandstone and sandy lime packstones/wackstone	Miocene or younger
450 - 500		Sandy lime packstone – grainstone	Miocene or younger
500 -700		Dolomitic lime wackstone	Miocene or younger
700 -1000		Calcareous clay	Miocene or younger
1000 - 3674		Alternations of bioclastic lime packstone/ wackestone and calcareous shale or marl	Lower - Middle Miocene
3674 - 4227		Massive bioclastic lime packstone.	Lower - Miocene
4227- 4776		Calcareous claystones and marls with packstone intercalations from 4227 – 4362.	Oligocene – Lower Miocene
4776 – 5255	Upper Shale	Shale with marls from 5070 – 5165	Oligocene
5255 - 5875		Marl	UpperEocene -Lower Oligocene
5875 - 6140	Gialo Limestone	Foraminiferal Lime Wackstone	Middle – Upper Eocene
6140 - 6380		Argillaceous Lime wackestone with organic material	Middle Eocene
6380 - 7195		BioclasticLime packstones and wackstones with larger foraminifera. Shale intercalatios towards the base.	Lower Middle Eocene
7195 - 8180	Lower Shale	Shales with Lime mudstones and wackestones in the upper part (7196 – 7610). Becoming dolomitic and marly below 7930.	Lower Eocene
8180 - 9820		Mainly finely crystalline dolomite	No fauna Paleocene
9820 - 13,710		Lime mudstine and wackstones with dolomite streaks down to 10785.	Turonian - Maastrichtian
13,710 - 15,204	Rakb Shale	Calcareous shale becoming increasingly silty and sandy below 14400	Upper Cretaceous
15,204 - 17,102		Argillaceous Lime mudstone and wackestones	Upper Cretaceous
17,102 - 17,788	Basal Shale	Shales with interbeded Lime mudstones and occasional Sandstone beds becoming more frequent and quartazitic below 17600.	Partly Cenomanian

Table 5.1: Stratigraphic successions encountered in the well (U1-41) located along the northesatern part of the Ajdasbiya Ttrough (Figure 5.26) close to the Cyrenaican region. The data is summareized in terms of the main rock stratigraphic units and provide cluse to the depositional environment that spactulated along the eastern margin of the Ajdabiya Trough. Data obtained from the National Oil Company (NOC) internal reports.

Thickness and depth estimates from two-way traveltime are based on seismic stacking velocities obtained from check shot data.

The sequence stratigraphy of the Ajdabiya Trough reflects the interplay of several variables: A relative sea-level variations which influence the geometry of clinoform reflections, sequences, systems tracts, and the creation of disconformities, in addition to tectonic events, including the tectonic subsidence of the continental crust across the Sirt Basin which provides relevant accommodation space for sediments to accumulate with fault movement along the trough boundaries which presumably modifies the direction of sediment transport and accommodation space. The first step of the interpretation was identifying and mapping unconformities from 2D seismic reflection data (Figure 5.13), this considered being the main sequence boundaries within the study area. The 2D seismic mapping includes the calculation of aggregate thicknesses maps, e.g., the total thickness above the Cretaceous – Paleogene unconformity or the total thickness above the Paleocene – Early Eocene unconformity, etc. The second step was identifying potential sequence boundaries based on seismic reflection terminations: (lapouts) (Figures 5.14 & 5.17). I interpreted the Upper Cretaceous horizon based on the top-laps and/or erosional truncations that exist throughout the study area (Figure 5.25). The mapped unconformities based on correlation with check shot VSP data are the Upper Paleocene, the Early Eocene (Top Gir Formation|), the Middle Eocene (Top Gialo Formation), the Upper Eocene, the Top Oligocene, and the Early to Upper Miocene.

The well data provide information about the approximate age of the seismic horizons and their lithologies along the Ajdabiya Trough marginal domain. The correlation between well and seismic data yielded much better constraints on the age determinations for the mapped horizons and aid in the definition of the main sequence boundaries and depositional environments (Figures 5.18, 5.19, 5.20, & 5.21) and Table 5.1.

The last step was preparing contour and thickness maps. Thickness maps display the variation of sediment thickness in two way- travel time. They are important to understand the dominant locus of deposition, the changing thickness, the likely sediment-supply direction, and the nature of the prograding cycles that occurred.

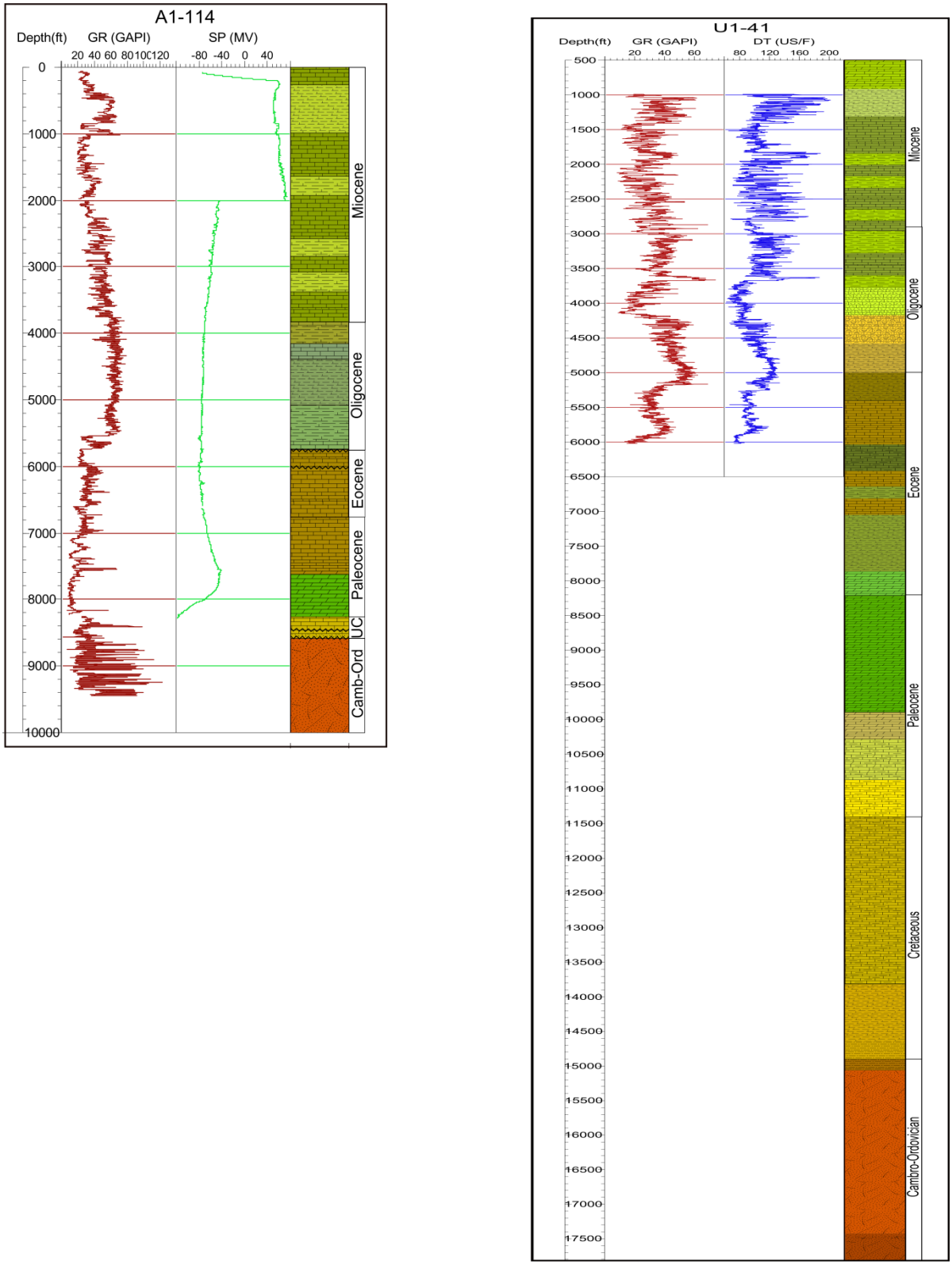

Figure 5.18: Samples of wells used in the correlation with the 2D seismic data

Sequence boundary and age	Reflection pattern	Seismic profile	Sequence boundary
Miocene (~ 23 - 5.0 Ma)	Strong - very strong amplitude, and good continuity	05NC213-0640	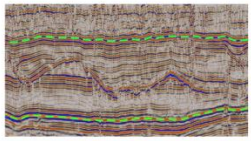
Upper Oligocene (~ 23 Ma)	Strong - very strong amplitude, and good continuity	05NC215-0665	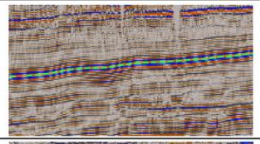
	Moderate - strong amplitude Moderate - good continuoty	05NC214-070	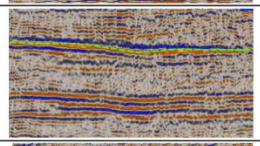
Middle Eocene (~ 41 Ma)	Moderate amplitude and Moderate continuoty with onlap below along internal sequence boundary	05NC214-1280	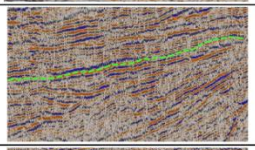
	Low amplitude and apparent continuity with complex terminolgy above indicating possible turbidites and channel levee system	05NC213-0330	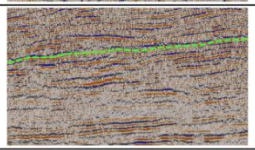
Lower Eocene (~ 47.8 Ma)	Moderate amplitude continuous with truncation below	05NC214-1280	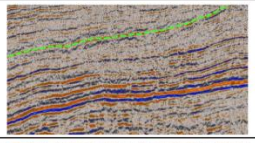
	Moderate - strong amplitude continuous onlap up with good continous progradation below	05NC213-1360	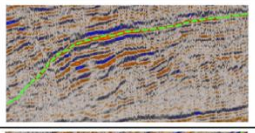
Upper Paleocene (~ 56 Ma)	Strong - strong amplitude continuous	05NC214-1280	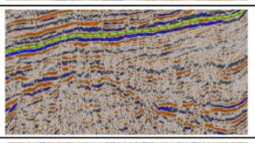
	Moderate amplitude patchy - continuous, truncation below	05NC214-0360	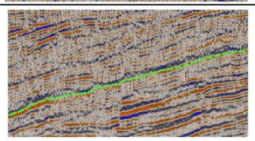
Upper Cretaceous (~ 65 Ma)	Moderate - strong amplitude Moderate - good continuous	05NC214-055	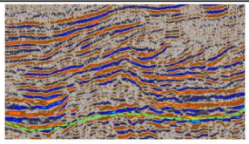
	Strong amplitude, continuous	05NC213-0330	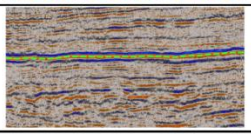

Figure 5.19: Reflection pattern with tentative ages of the main horizons acting as sequence boundary. Erosional truncations indicate potential sequence boundary. Some reflectors are associated with an undulating reflection or irregular surface.

5.4.1 Seismic and Sequence Stratigraphy

In this part, seismic and sequence stratigraphy analysis is undertaken and includes identification of sequence boundaries and interpretation of the internal reflection pattern of an individual sequences. The identification of sequence boundaries within the Ajdabiya Trough is based on analysis of selected 2-D seismic profiles crossing the trough into NE-SW and NW-SE directions and, complemented by wire line logs (e.g. Figures 5.20, 5.21, and 5.22).

The sequence boundaries are recognized based on the following. (1) On the criteria of the major unconformities and their correlative conformities which treated as a sequence boundaries (Haq et al., 1987), because they represent time-barrier surfaces which reflected on seismic profiles as truncations, surfaces of onlap, and downlap (Figure 5.22). (2) Possible incised valleys or channels and subaerial exposure surfaces can be used also to define sequence boundaries. (3) Abrupt changes in lithology and sedimentary facies can be represented as sequence boundaries which can be identified using the character of seismic reflections or the nature of the well logs.

The sedimentary succession in the Ajdabiya Trough is divisible into two groups of sequences separated by a basin-wide unconformity: (1) a Mesozoic sequence; composed of Late Jurassic - Cenomanian, siliciclastic dominated, syn-rift to early post-rift sediments (2) Cenozoic (Paleocene to Miocene), composed of carbonate – mudstone dominated sediments. The Eocene comprising sigmoidal clinoforms and carbonate dominated sequences named as Gir and Gialo sequences overlaying by Oligocene and Miocene sequences (e.g. Abugares, 1996; Beask et al., 2014). The Upper Miocene sequence is capped by a basin wide offshore Missinian unconformity recently addressed by Fiduk, 2009. The extensive erosional unconformity at the top of the syn-rift and early post-rift section forms an easily recognizable mapped surfaces; six unconformity-bounded seismic sequences overlie these surfaces (Figures 5.21 & 5.22) are recognized. The ages assigned to these successions are tentative and based (1) on presumed sequence age correlation (2) on limited data from wells (3) on the similarity in depositional style between the sequences and (4) on the division of the remainder of the sequences into a reasonable time-stratigraphic framework based on correlations with the Haq et al., (1987) sea level curve (Figure 5.20) and regional geology (Figure 5.2). The identified seismic units in the Ajdabiya Trough featuring particular reflection pattern, geological age and internal structure, and being separated by seven sequence boundaries.

These tectono-stratigraphic units correspond to distinct tectonic environments within the study area. Facies interpretations and lithology type within the identified sequences are outlined based on previous studies (Table.5.2).

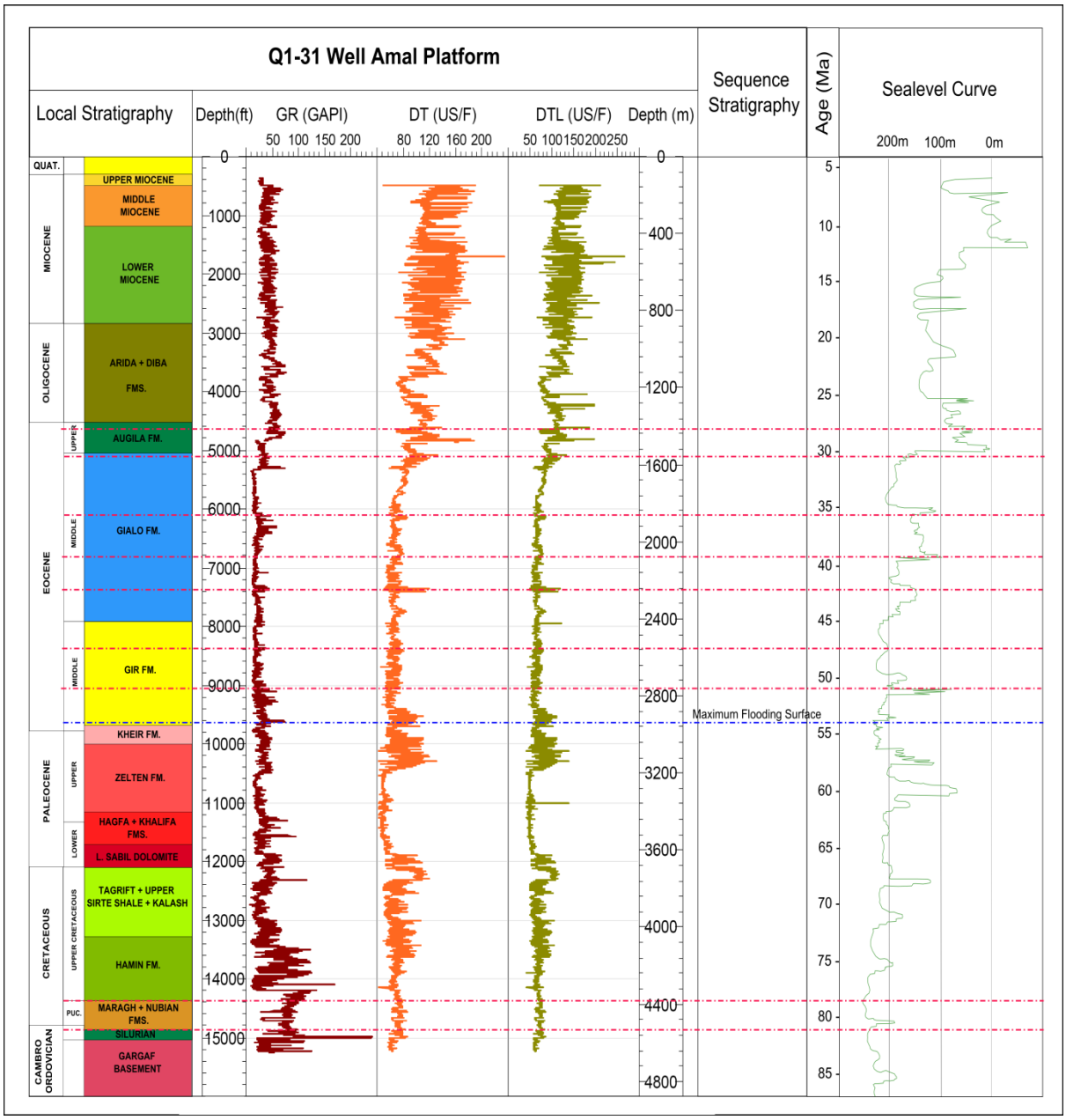

Figure 5.20: Distribution of sediments in sequences as a function of time and depth. Sea level curve in green is estimated based on Haq et al., (1987) and Kominz et al., (1998). Lithology details and wireline data are obtained from the well Q1-31 (see figure 5.14 for location). Red dashed lines representing main sequence boundaries and blue dashed line is maximum flooding surface (MFS).

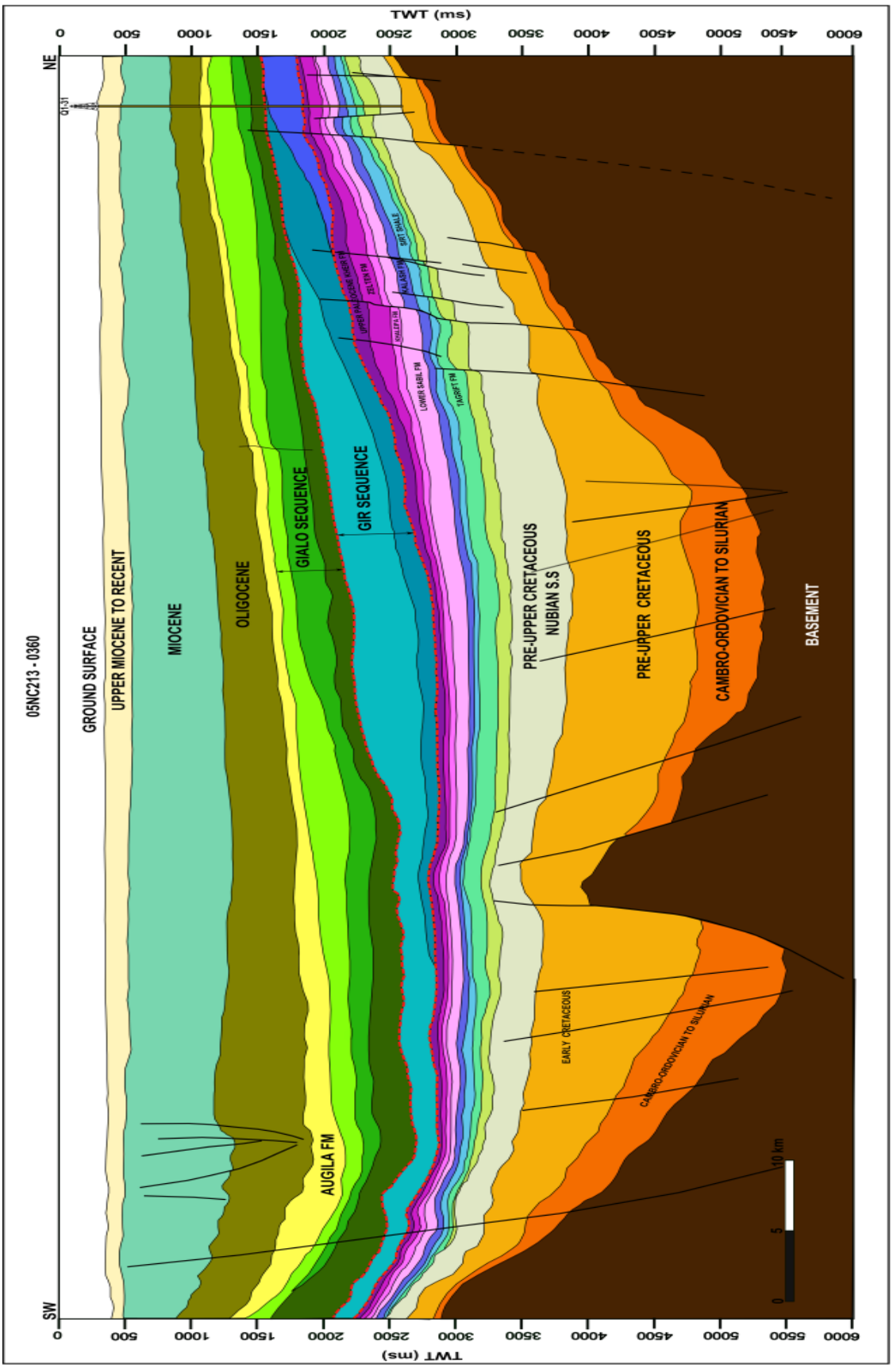

Figure 5.21: Interpretation of Seismic line O5NC2134-0360 across the Ajdabiya Trough (for location see Figure). Well-to-seismic tie and the lateral continuity of seismic horizons allowed identification of six mapable stratigraphic sequences. These are: (1) Upper Cretaceous sediments, (2) Paleocene sediments, (3) Early Eocene sediments, and (4) Middle Eocene sediments (5) Oligocene sediments, (6) Miocene sediments. All sequences are tied to various wells. The profile shows reactivation of Mesozoic faults during possible Paleocene-Eocene extension events. However, a subsequent postrift sequences are undeformed.

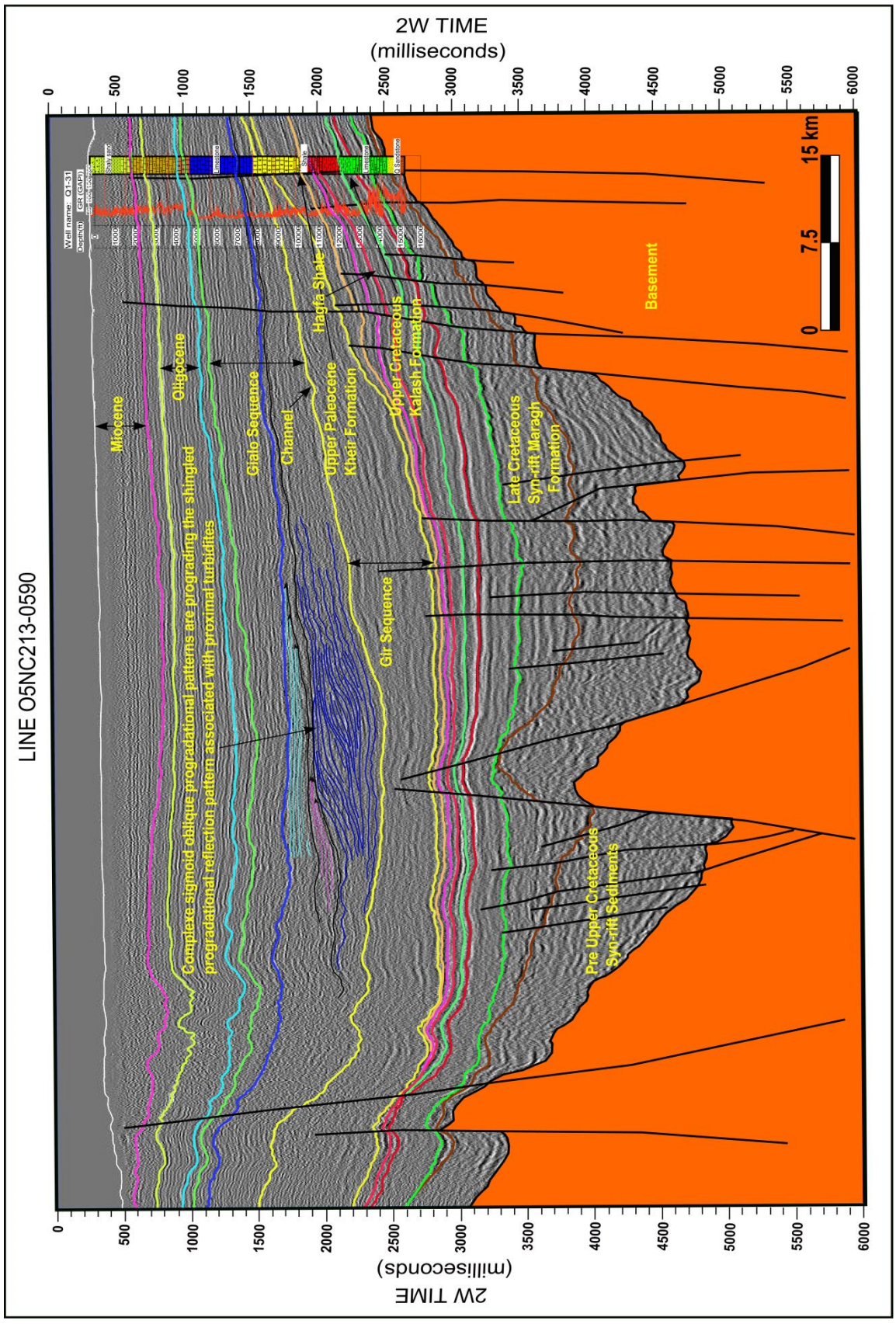

Figure 5.22: Interpreted 2D seismic section (Line NC213-0590) across the Ajdabiya Trough, evidencing the main sequences and tectonic systems tracts described in this chapter and thick syn-rift depocentres. The line showing a probable Paleocene to Early Eocene prograding rimmed carbonate platform. Deposition of the Late Paleocene – Early Eocene prograding wedge is controlled by a paleo-shelf break, subsequently eroded during the Paleocene-Eocene. Exploration well Q1-31 projected on the inner proximal margin.

5.4.1.1 The Upper Cretaceous Sequence (100 – 65 Ma)

The correlations between seismic profiles and individual depositional sequences with their bounding surfaces are made possible using time depth relationship obtained from check shout VSP data. Besides, strong amplitude contrasts and the characteristic reflection termination patterns on some seismic sections help to recognise the main depositional sequences.

In most of the studied seismic sections, no clear internal structure of the Upper Cretaceous sequence can be recognized possibly due to uniformity of lithology.

The Upper Cretaceous sequence shows a moderately continuous seismic facies, with parallel to subparallel configuration and occasionally displaying downlap patterns (Figures 5.20, 5.21, 5.22 and 5.23) which may reflect a characteristic of medium to high energy sedimentary environment. Variations in the depositional environments during the Upper Cretaceous are probably related to changes in global sea level, climatic changes, and rate of tectonic subsidence coeval with major sea level raise occurring during the Upper Cretaceous as outlined by Vail et al., (1977) and Haq et al., (1987). The Upper Cretaceous sequence in the Ajdabiya Trough as shown on the seismic sections exhibit basal aggradational geometry attributed to sea level rise that accompanied a widespread development of platform limestone and marine shale facies with considerable thicknesses. The Upper Cretaceous sequence includes deposits divided by an intra-Cretaceous unconformity at the base of the marine Upper Cretaceous sequence into two major depositional periods separated by well-defined sequence boundary (Figures 5.26). On the interpreted 2D seismic data, the sequence boundary truncates the underlying prograding sediment wedges and onlaped by the overlying strata in the southern part of the study area (Figures 5.22 & 5.23). On the well chart Figure 5.20, the Cretaceous sequence is divided into variable systems tracts by possible maximum flooding surface (MFS) observed through the long term and abrupt variations in the sea level curve. The Cretaceous strata are possibly developed within transgressive systems tract environment formed during an overall sea level rise followed by highstand system tract in which reflectors above the MFS downlap onto this surface (Figures 5.24 and 5.26). The sequence represents the first sedimentary sequence mapped within the Ajdabiya Trough based on correlation of seismic and well data in the study area. It is bounded by a Late Paleozoic (Hercynian unconformity) below and probably by Intra-Cretaceous (Aptian-Cenomanian) unconformity above (e.g. Thomas, 1995) and is characterized by reflections that are subparallel - chaotic,

closely spaced, relatively continuous, and fair to moderate amplitude (Figures 5.19, 5.21 and 5.22).

Sequence and age	Seismic line	Internal reflection pattern	Frequency	Intensity	Continuity	
Miocene Sequence	05NC213-0540	Parallel-subparallel, locally chaotic or wavy	Slightly variable to uniform	Low-moderate, locally transparent	Moderate to high	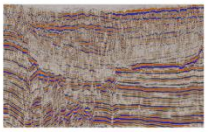
Oligocene Sequence	05NC213-0630	Parallel, locally wavy	Uniform	Moderate-high, locally transparent	Moderate to high	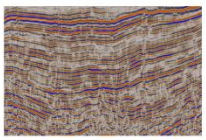
Middle Eocene Gialo Sequence	05NC213-1280	Subparallel locally wavy	Slightly variable	Low-moderate, locally transparent	Intermediate	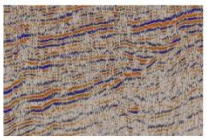
	05NC213-0330	Parallel-subparalle	Uniform, locally variable	Moderate, locally transparent	Intermediate -high	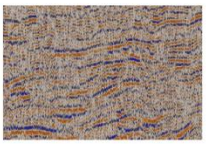
Early Eocene Gir Sequence	05NC213-1280	Subparallel, locally chaotic	Slightly variable	Moderate	Low -intermediate	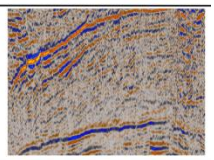
	05NC213-0360	Subparallel, locally chaotic	Uniform locally variable	Moderate-high	Intermediate -high	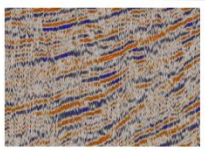
Paleocene	05NC213-320	Chaotic, locally subparallel	Varible	High-varible	Locally discontinuous	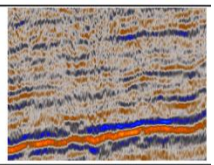
	05NC213-1360S	Parallel, locally suparallel	Uniform	Moderate-high	High	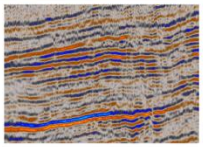
Upper Cretaceous	05NC213-1280	Parallel-subparallel	Slightly variable	Low-moderate	Occasionally high to Intermediate	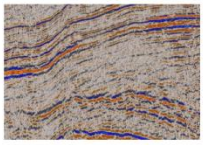

Figure 5.23: Seismic phases and sequences identified within the Ajdabiya Trough

Age	Lithology	Facies Interpretation	Reference
Middle - Upper Miocene	Calcareous sandstone and sandy lime Laminated packstone/wackestones, Dolometic lime wackestone, Calcareous clay.	Transition from peritidal to shoal facies grad to shallow and mid ramp facies.	Selley, (1971); Barr and Weegar,(1972); Maneti, (1984); Hallett and El Ghoul,(1996); Yanilmaz et al., (2008
Lower Miocene	Alternations and bioclastic Lime packstone/wackestone and calcareous shale or marl and massive bioclastic Lime packstone.	Transition from peritidal to shoal facies	Wennekers et al, (1996); Hallett, (2002); Yanilmaz et al., (2008)
Oligocene	Early Oligocene carbonate mudstones and late Oligocene shales. Calcareous claystones and marls with packstone intercalations and shale with marl. Deep water planktonic formaminiferal Limestone.	Restricted lagoonal to peritidal and high energy nummulitic shoals, pass basinward into deep ramp facies and pelagic carbonate mudstones periplatform bioclastic calcisilitites. NW prograding of Oligocene delta associated with deposition of turbidites sands.	Yanilmaz et al., (2008); Bezan, (1996)
Upper Eocene	Foraminiferal Lime Wackstone. Shale, and some streaks of limestone and Marl	Shales were probably deposited under inner to outer neritic open-marine conditions, whereas the sandstones and limestones were deposited in shallower, more restricted environments	Abadi et al, (2008)
Middle Eocene	Lime Mudstone and Argilaceous Mudstone, limestone, dolomite, and minor anhydrite	Shallow supertidal or intertidal to open marine facies. NW progradation of ramp facies. Shoreward shoals and lagoon.	Abadi et al, (2008); Barr and Weegar, (1972); Belazi, (1989); Abugares (1996).
Lower Eocene	Shale and dolomitic chacky Mudstone. Bioclastic Lime packstones and wackstones, shale interactions towards the base with lime mudstones and wackstones becoming dolomitic and marly below.	Shoal, mid and deep ramp carbonate facies. Progradation of shallow marine carbonates. Shallow-marine carbonates and evaporites, with deeper marine facies in the northern Agedabia trough	(Barr and Weegar, (1972); Bezan, (1996); Yanilmaz et al., (2008)
Paleocene	Arg. Mudstone and Shale. Packstones/wackstones depoited above wave base with Boundstone and crystalline dolomite. Deep shaly to shallow marine carbonate facies (e.g. AL Hagfa Formation).	Reefal build ups. Peritidal surounded by a low energy laggon, fringed by shoals, inner neritic facies of (Upper Sabil) shallow carbonates, which give way to pelagic distal carbonates.	Bezan, (1996); Spring and Hansen, (1998); Yanilmaz et al., (2008)
Upper Cretaceous Turonian - Maastrichtian	Lime Mudstone and wackstones with dolomite streacks.	The depositional environment is open marine, probably neritic high energy shelfal carbonate grading to low energy distal carbonate.	Abadi et al, (2008); Yanlmaz et al., (2008)
Upper Cretaceous Rakb Shale	Calcareous shale becoming increasingly silty and sandy.	Low energy subtidal shelf to low energy distal carbonate.	Yanilmaz et al., (2008)
Upper Cretaceous Cenomanian Basal Shale	Argillaceous lime mudstones and wackstones. Shales with interbedded lime mudstones and occasional sandstone beds becoming more frequent and Quartzitic below.	Quieter and possibly deeper water environment.	Barr and Weegar, (1972); Hallett, (2002)

Table 5.2: Lithology and facies interpretations in Ajdabiya Trough.

In general, the bottom and top of this sequence consist of higher amplitude, more closely spaced, and more continuous reflections than the middle.

The overall thickness of this unit varies from less than 300 ms (TWT) in the north to over 2000 ms (TWT) in the southern part of the study area (Figures 5.21 & 5.22). The sequence may extend with thick section to cover part from the Late Cretaceous (Cenomanian) period.

Reflections in this part are parallel to subparallel, low amplitude, relatively discontinuous, and widely spaced (Figure 5.22 & 5.24). Onlaping terminations are present, especially in the south-western part of the study area suggesting component of rifting and basin subsidence effecting this part during the Upper Cretaceous time. This sequence is composed of northwest–southeast oriented elongate syn-rift grabens separated by basement highs.

The thickness of these wedge-shape bodies increases southward to its thickest part (up to 500 ms TWT). The overlying strata of Upper Cretaceous age reflect sequential deposition of predominantly south-directed, high-frequency shelf-margin progradational wedges. A thin aggradational component at the top of the sequence represents a minor increase in accommodation space, probably resulting from sediment compaction and sag at the Cretaceous – Tertiary boundary (e.g. Skuze, 1994). Other sequence can be identified associated with Late Cretaceous (Turonian – Maastrichtian) sedimentary rocks based on the correlation of seismic data with the wells. It consists of reflections that are parallel to subparallel, relatively continuous, closely spaced, and moderate to high amplitude. The erosional limit of this sequence is in the northwest part of the study area. This sequence represents the end of the Cretaceous time and characterized by slow basin subsidence and decrease in accommodation space.

5.4.1.2 Paleocene Sequence (65 – 55 Ma)

The Upper Cretaceous sequence is overlain by parallel to shingled configuration interval defining the Paleocene sequence, which characterized by progradational-aggradational sedimentary patterns in most of the mapped seismic sections (Figures 5.22, 5.24, and 5.25). It is bounded by the underlying Cretaceous unconformity below and an early Eocene unconformity at the top. The sequence seems to be preserved in a wide area in the south but due to erosion occurred in the northern part of the study area, the sequence is fairly developed (e.g. Bezan, 1996). System tracks are not apparent in the Paleocene sequence in the north-western part because of the limitation of seismic data caused by significant erosion of the upper part of this sequence (Figures 5.22 & 5.25).

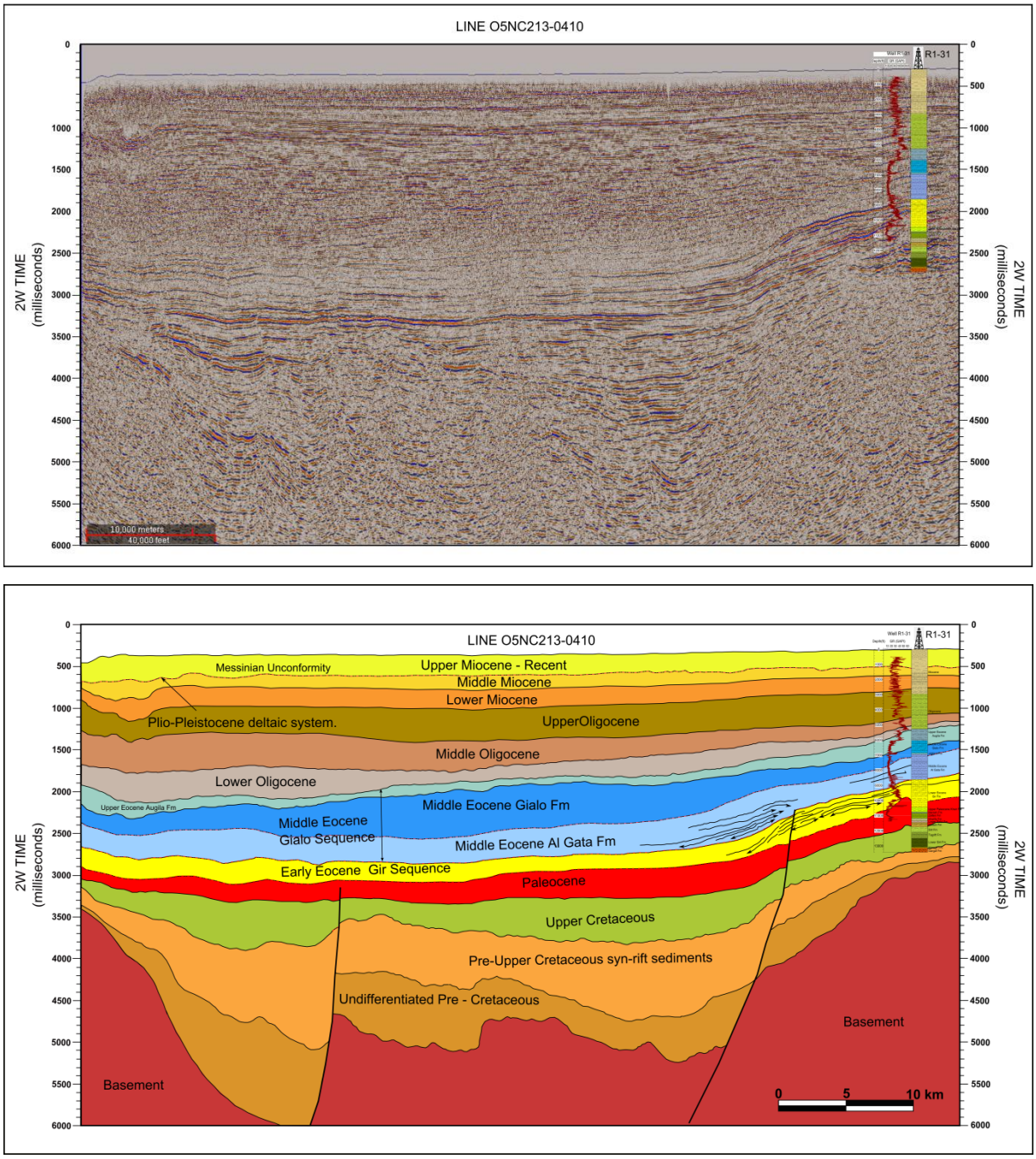

Figure 5.24: Seismic section above with interpreted copy below calibrated with borehole data showing remarkable sequences developed during rift period followed by Tertiary sequences. Sequence boundaries are marked by rift propagation unconformity and marine flooding surfaces. The Palaeocene–early Oligocene stratigraphic interval, consisting of alternating carbonates and siliciclastics of the Lower Sabil Formation to Augila Limestone, downlaps onto the base Tertiary surface. Carbonate clastics dominate the succession from the early Oligocene, with deposition of the Najah group. Primarily two dimensional progradation of the shelf edge above Early Paleocene occurs towards the northwest (shown on Paleocene thickness map).

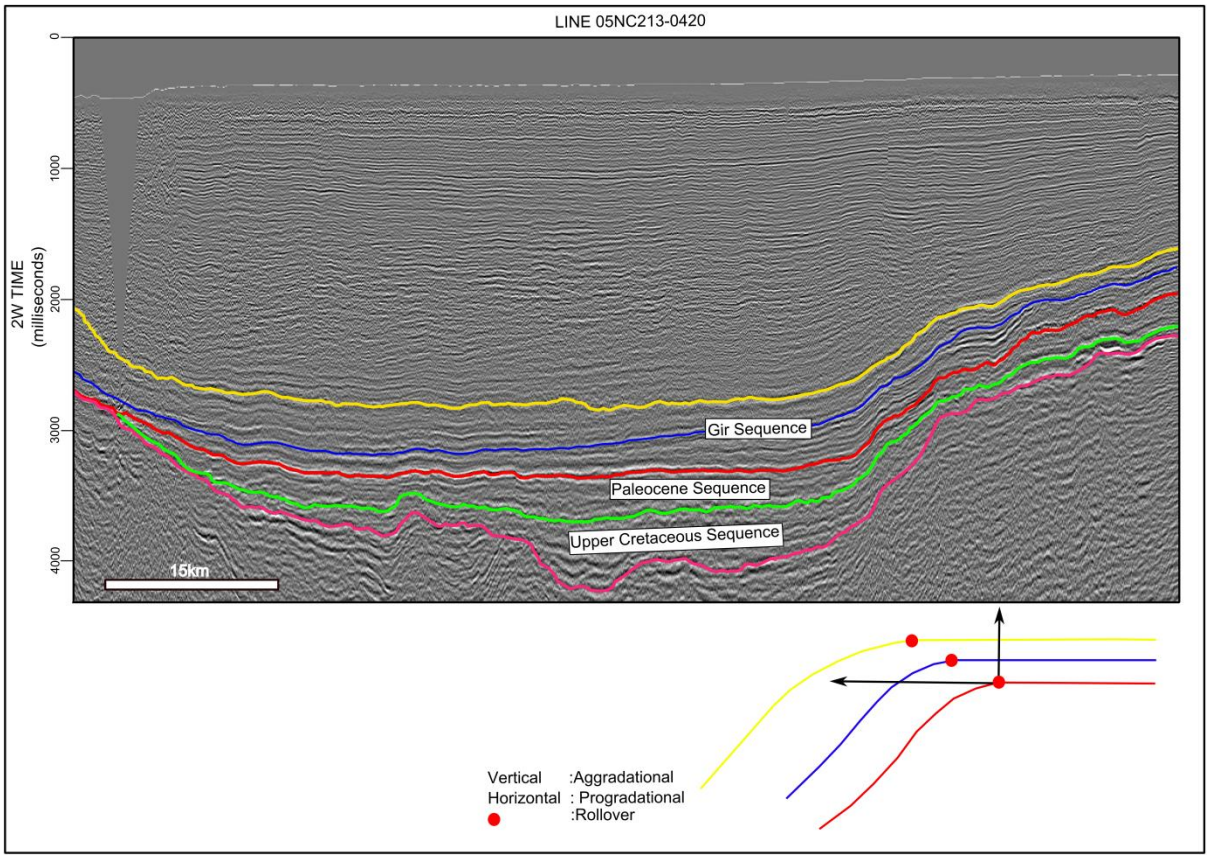

Figure 5.25: Seismic line O5NC213-0420 with interpreted system tract (top) and cartoon of clinoform rollover showing aggradational and progradational patterns.

Furthermore, the boundary correlates with the Upper Paleocene (Kheir Formation) (Figure 5.20) is characterized by a rough or irregular seismic signature caused by prograding or downlapping reflections (Figures 5.20, 5.21, and 5.22). A lowstand system tract and highstand system tract are present in the Paleocene sequence in the southeast portion of the study area, separated by a maximum flooding surface indicated by downlapping reflections (Figure 5.26). The different system tracts illustrate that relative sea-level fluctuated during the deposition of the Paleocene sequence. For example, the highstand system tract is the result of a decreasing rate of relative sea level rise and increasing rate of sediment supply that produced parasequence sets that began as aggradational and then became progradational (Figures 5.25, 5.26, and 5.27) (Van Wagoner et al., 1988). Moreover, based on the downlapping terminations in the low system tract, the sediment supply direction was from the southeast to northwest (e.g. Spring and Hansan, 1998; Yanilmaz et al., 2008).

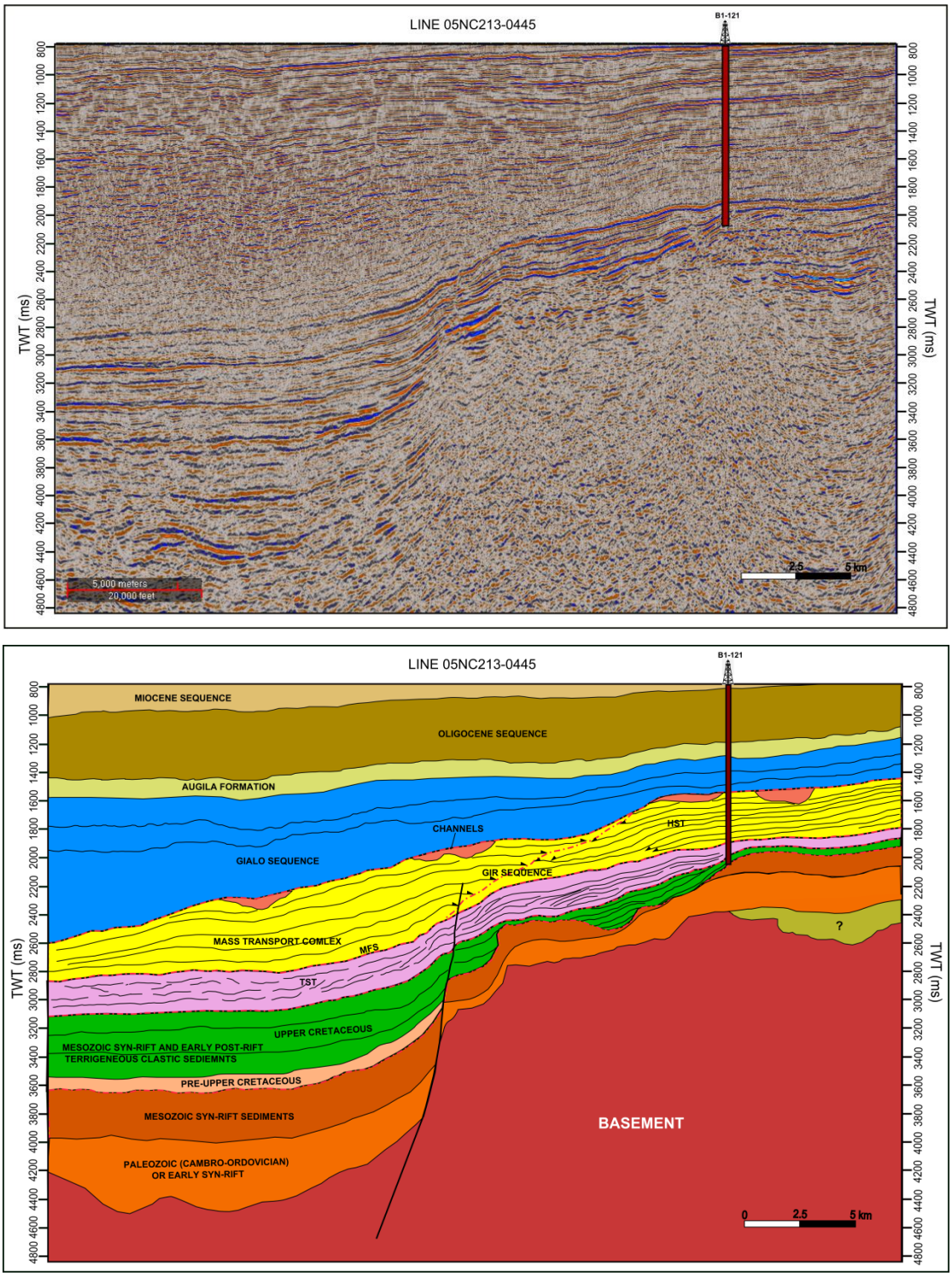

Figure 5.26: An interpreted portion from the seismic line 05NC213-0360 without colour annotation up and with colours down, show clearly the sequences developed along the eastern shelf of the Ajdabiya Trough. Palaeozoic-Upper Cretaceous sequences are considered to be formed within a rift domain controlled by faulting while Cenozoic sequences are mainly developed within ramp model platform with no or little fault control.
I postulate that, this indicates that the shelf edges are at all times submerged. However, partial exposure of the shelf, resulting in the formation of karst horizons or incesion inboard of the submerged shelf is observed.

Shale dominates the Paleocene sequence, e.g., the Hagfa Formation, suggesting that the depositional environment was inner neritic to outer neritic (e.g. Yanilmaz et al., 2008). This interpretation is supported by benthic and/or planktonic foraminifera analysis from the well data in the study area (Well Q1-31). For example, the sedimentary succession deposited during the period of relative sea-level fall and slow initial rise of relative sea level in the lowstand system tract has progradational patterns supported by the downlapping and onlapping terminations (Figures 5.26 – 5.28) (Posamentier and Allen, 1999). Clinoform geometries in the Paleocene sequence suggest that margin growth during the Early Paleocene to Late Paleocene had aggradational – progradational stratigraphic patterns (Figure 5.25).

This Paleocene sequence is variable in thickness within the study area and comprises the shallow to deep main sediments grading from carbonates at the shelf margins to shall towards the depocentre. The sequence is capped by the Early Eocene boundary unconformity which characterized on the seismic data, by high amplitude, high frequency reflector that can be traced across the study area.

This sequence boundary is clearly expressed on the well log. The GR logs show a large shift to higher values (Figure 5.20). The lithology contrast between the shale of the Kheir Formation and the evaporites of the Early Eocene (Gir Formation) across this sequence boundary is the major reason for these changes.

The Paleocene sequence is made of moderate high amplitude reflections which may be related to aggrading and rtrograding sedimentary facies under high energy conditions (Figure 5.27). This sequence was followed by stillstand or a slow regression (fall in sea-level), when the rate of sedimentation was greater than the accommodation space generation resulting in a basinward prograding facies. Toplap and downlap termination features mark a progress toward progradational deposition during the relative sea-level fall. The draw-down and possibly tectonic uplift caused local thinning of the Paleocene sequence (Figures 5.27 and 5.33). The upper part of the Paleocene sequence, whenever it is present, displays medium to high amplitude reflection features with variable to uniform signal frequency and irregular and parallel to locally sub parallel seismic reflection forming a hummocky patterns (Figures 5.27, 5.28, 5.30, and 5.33). These characteristics are interpreted as belonging to shallow to deep water environment, and transition from shoal sediments to more distal and pelagic carbonates (e.g. Yanilmaz et al., 2008).

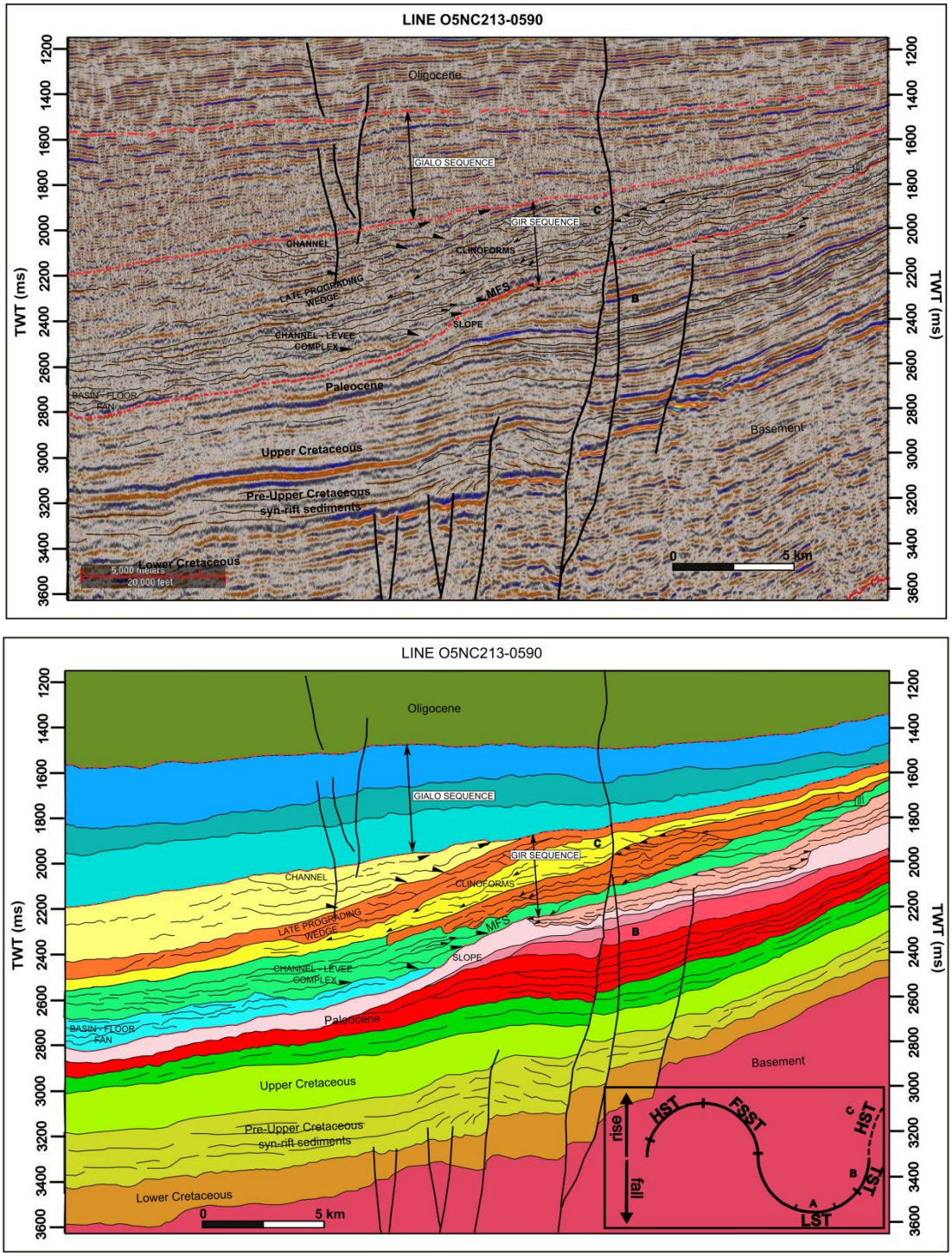

Figure 5.27: Facies analysis from dip-oriented seismic section in northeast Ajdabiya Trough (Line 05NC213-0590). See Figure 5.28 for location of seismic section. Shingled seismic configurations are most common in seismic intervals interpreted as shallow water to deep water prograding depositional sequences. The seismic section also shows the interpreted systems tract distribution in the Cretaceous to Eocene sequences. Parasequences show backstepping facies, retrogradational sets.

The sequence exists with thick Paleocene section in the south-eastern part of the study area (Figure 5.22), and is characterized by low to moderate amplitude, discontinuous to continuous, and moderately spaced seismic reflections. Prograding clinoforms display sigmoid geometries that are present in the upper part of the seismic data. The thickness of this sequence varies from less than 200 ms (TWT) to over 500 ms (TWT), becoming thinner toward the northwest. From the gamma ray and sonic log, a discontinuity peak at the base of the Upper Paleocene - Early Eocene (Kheir Formation) indicates a hiatus. This is associated with high gamma ray spike and static sea level curve with evidence of reworked sediments (e.g. Bezan, 1996; Bezan and Malek, 1996; Spring and Hansan, 1998; Yanilmaz et al., 2008), which indicate flooding (end of transgressive systems tracts or maximum flooding surface) above this unconformable surface. A significant response on the gamma ray, sonic logs and the sea level curve reflects an unconformity at the Cretaceous – Tertiary boundary. This corresponds to distinct evidence on the seismic for truncation of the underlying reflectors by a relatively high-amplitude reflector (Figure 5.19 & 5.23). A further response on the logs and the sea level curve related to the upper Paleocene Zelten Formation or its equivalent Upper Sabil Formation (Figure 5.20) reflects an unconformity formed during low stand system tracts as outlined by Spring and Hansen, 1998 whom suggested that the Paleocene (Upper Sabil Formation) was deposited as a shelf margin progradational delta.

Within the Paleocene sequence seismic reflections representing the high energy outer shelf facies. The facies onlapped parallel towards the topset beds with continuous low to medium amplitude reflections which reflect component of lagoonal environment (e.g. Yanilmaz et al., 2008, Starke et al., 2008, and Martin et al., 2008). It has been observed also a series of shallow marine high energy ramp related facies belts within possible low stand systems tracts with possible transition into shoal carbonate facies towards the depocentre of the trough. The shallow marine (lowstand) sediments as shown on the seismic section (Figures 5.21 & 5.28) is overlain by more distal (transgressive) marine sediments deposited as a result of continued sea level rise. The corresponding wireline log response shows gamma-ray and sonic logs show a blocky log response passing upward into an overall fining-upward trend. This relationship is perhaps best seen in well Q1-31 (Figure 5.20) as overmuch of the study area, the upper (more distal) part of the Paleozoic is eroded beneath the Mesozoic unconformity. The transition from shoal sediments to the more distal and pelagic carbonates during the Early

Paleocene to Early Eocene is generally abrupt and no well-developed ramp facies recognized (e.g. Spring and Hansen, 1998; Yanilmaz et al., 2008).

5.4.1.3 Early Eocene Gir Sequence (Progradational Carbonate Shelf) (54-49 Ma)

This Early Eocene (Gir Sequence) is the most extensive and geometrically most dramatic sequence within the Cenozoic succession. It is unconformably overlies the Paleocene sequence and exhibits sub-parallel, locally chaotic seismic reflections with a low to moderate amplitude response. It shows a variable to uniform frequency and oblique to sigmoid configuration patterns (Figure 5.19 & 5.23). Downlapping termination features express progradational deposition during this period (Figures 5.24, 5.25, 5.26, and 5.27). The depositional aggradation pattern at the lower part of the Gir sequence (Figures 5.20, 5.26, and 5.27) was accompanied by a maximum marine flooding in response to either maximum subsidence or sea-level rise during the Late Paleocene (Spring and Hansan, 1998).

Unconformity at the base of the Gir sequence could be the result of tectonic events and a sea-level fall. At the base of the Gir sequence, discontinuous seismic character often lie on erosional surfaces, particularly in uncompacted sediments which could be the result of a relative sea-level fall (Figure 5.20). The Gir sequence (Lower Eocene age) is expressed by moderate to high amplitude reflection features with a variable signal frequency content forming a complex sigmoidal configuration pattern (Figure 5.27). The upper part of the sequence is characterized by an alternation of horizontal sigmoid facies coastal toplap patterns. An onlap pattern at the topmost of the sequence reflects retrogradational and transgressive deposition, while onlap and diverging reflections at the base, indicate a subsidence and sea level rise also.

The sequence can be a really divided into three zones: (1) an inner shelf zone, (2) an escarpment zone, and (3) an outer shelf zone. The sequence overlies either relatively moderate to thin Paleocene succession within the inner shelf zone (Figures 5.22 & 5.28).

It is thicken at the inner shelf area (200 - 600 msTWT), and abruptly dips from close to the trough margin to more than 250 ms (TWT) into the basin across the shelf indicating possible rime ramp model (e.g. Spring and Hansan, 1998; Beask et al., 2014). The sequence in the outer shelf zone occasionally thicken owing to increase in accommodation space and sediment influx and extends basin ward towards the outer shelf from the base of the shelf

edge, where it wedges out by downlap onto the underlying unconformity (Figures 5.21, 5.22, 5.26, and 5.27).

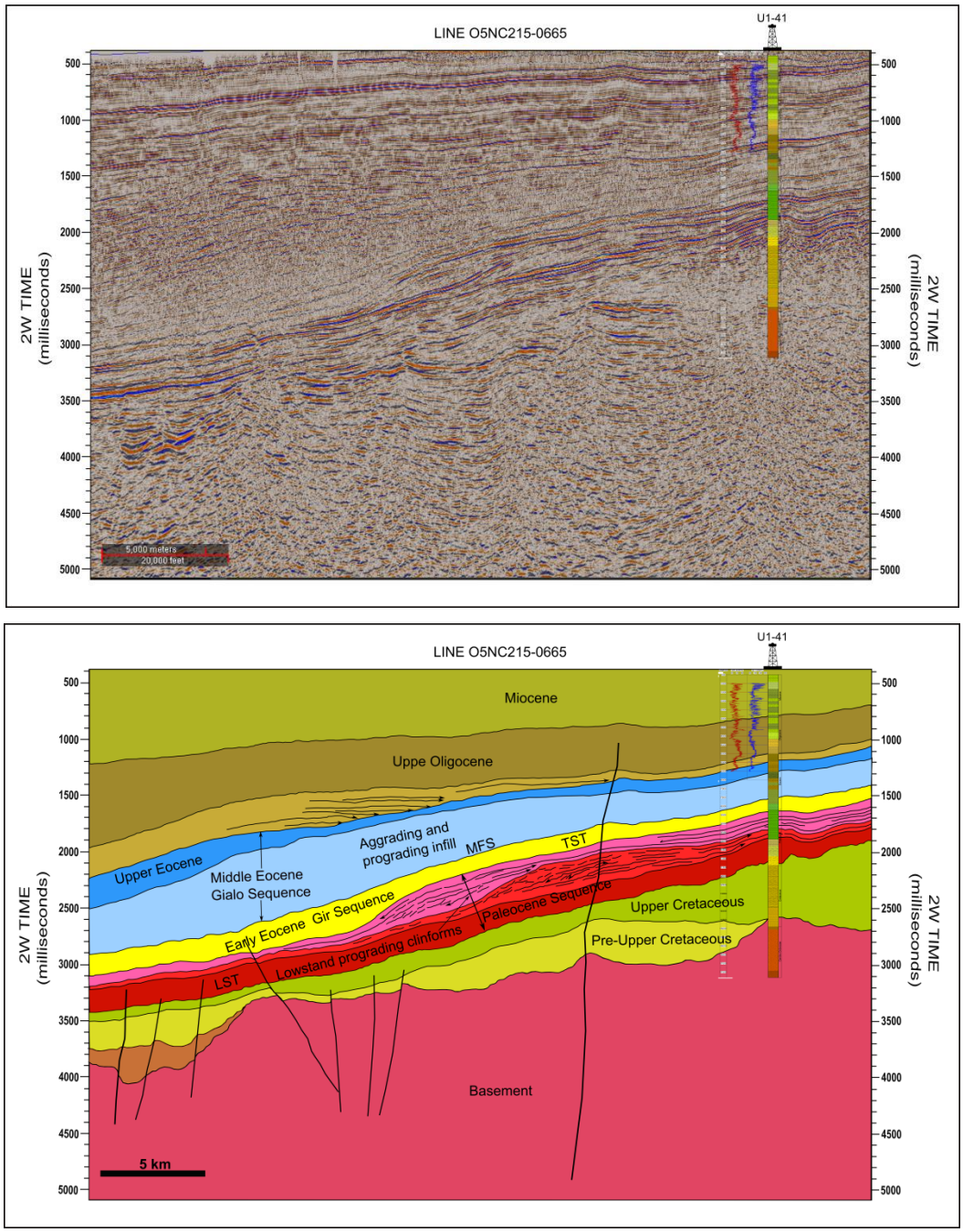

Figure 5.28: show a prograding clinoforms developed within the Paleocene sequence. The Paleocene sequence represents a change from slope deposition to non marine or shallow marine bypass or erosion, and the toplap surface is a local unconformity.

The basal sequence boundary unconformity is marked by reflections that downlap, in different parts of the basin, onto the Paleocene sequence boundary. The upper sequence boundary is a dramatic onlap surface onto which part from Gialo carbonate sequence terminated. This part is presumably related to transgression and sea leval rise during early stage of middle Eocene transgressive system tracts (e.g. Spring and Hansen, 1998 and references therein). Within the limits of seismic resolution, the Gir sequence forms the main body of the inner shelf zone and characterized by a broad clinoform structures with aggrading and prograding facies (Figures 5.27, 5.32, 5.33, and 5.35). Clinoforms range from gently dipping, almost planar ramps in the upper part of the sequence to more steeply dipping, oblique sigmoidal surfaces toward the basin centre. Reflections within the inner shelf zone are characteristically discontinuous and display considerable amplitude variation, contrasting with more continuous, moderate amplitude reflections in the outer shelf zone. A combination of seismic geometry, seismic facies, and the relatively simple structure beneath the inner shelf permits a confident correlation between stratigraphic successions.

5.4.1.4 Middle Eocene Gialo Sequence (Deep-Water Carbonate Sequence) (49-37 Ma)

The Middle Eocene (Gialo Sequence) is unconformably overlaying the Lower Eocene (Gir Sequence), this unconformity could be coincides with middle to late Eocene compressive event (Hallett, 2002). The patterns of this sequence show alternating periods of up-building and offlaping lopes (Figures 5.28, 5.30, and 5.33). The Gialo sequence also show a progradation along gently sloping depositional surfaces coincides with relative sea level fall during the middle to late Eocene (Figure 5.20). The Oligocene sequence is characterized by continuous and moderate to high amplitude reflecting horizons and locally transparent seismic facies and subparallel to divergent reflection patterns attributed to systematic deposition in broad platform settings (Vail et al., 1977).

An intra-Eocene unconformity at the top of Gialo Formation is characterized by raising sea level indicating an increase in paleobathymetry. This reflects an overall basinward shift in facies and cessation of carbonate deposition within the Middle Eocene Gialo Sequence (Figures 5.22, 5.27, 5.28, 5.30, and 5.33).

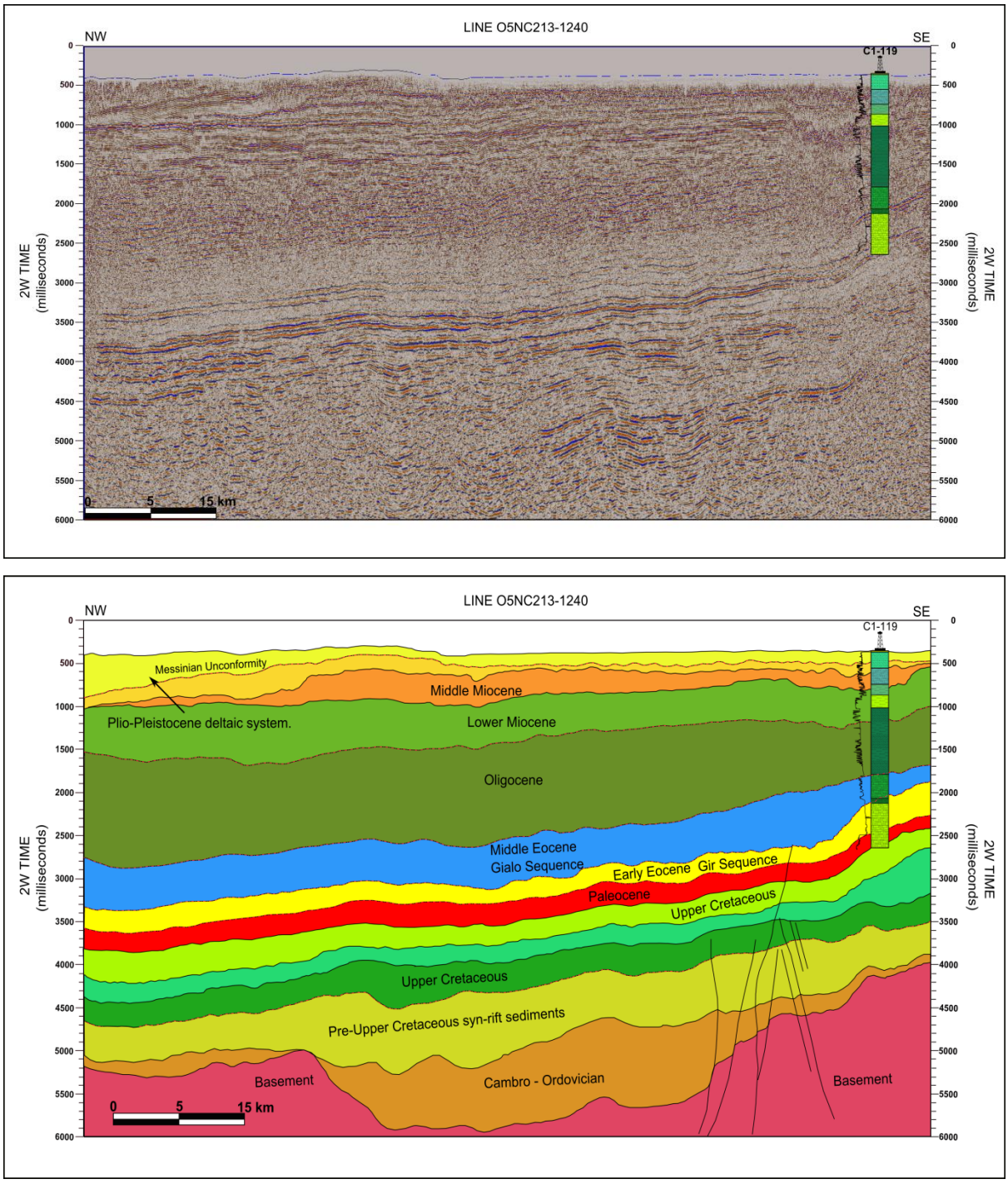

Figure 5.29: Seismic line 05NC213-1240 correlating with C1-119 well, uninterpreted (top) and interpreted (bottom). Horizons with strong-to-moderate-amplitude reflections are associated with top Late Cretaceous, top Early Eocene, and top Middle Eocene unconformities (based on the seismic character and the C1-119- well). See Figure 5.25 for location of seismic line.

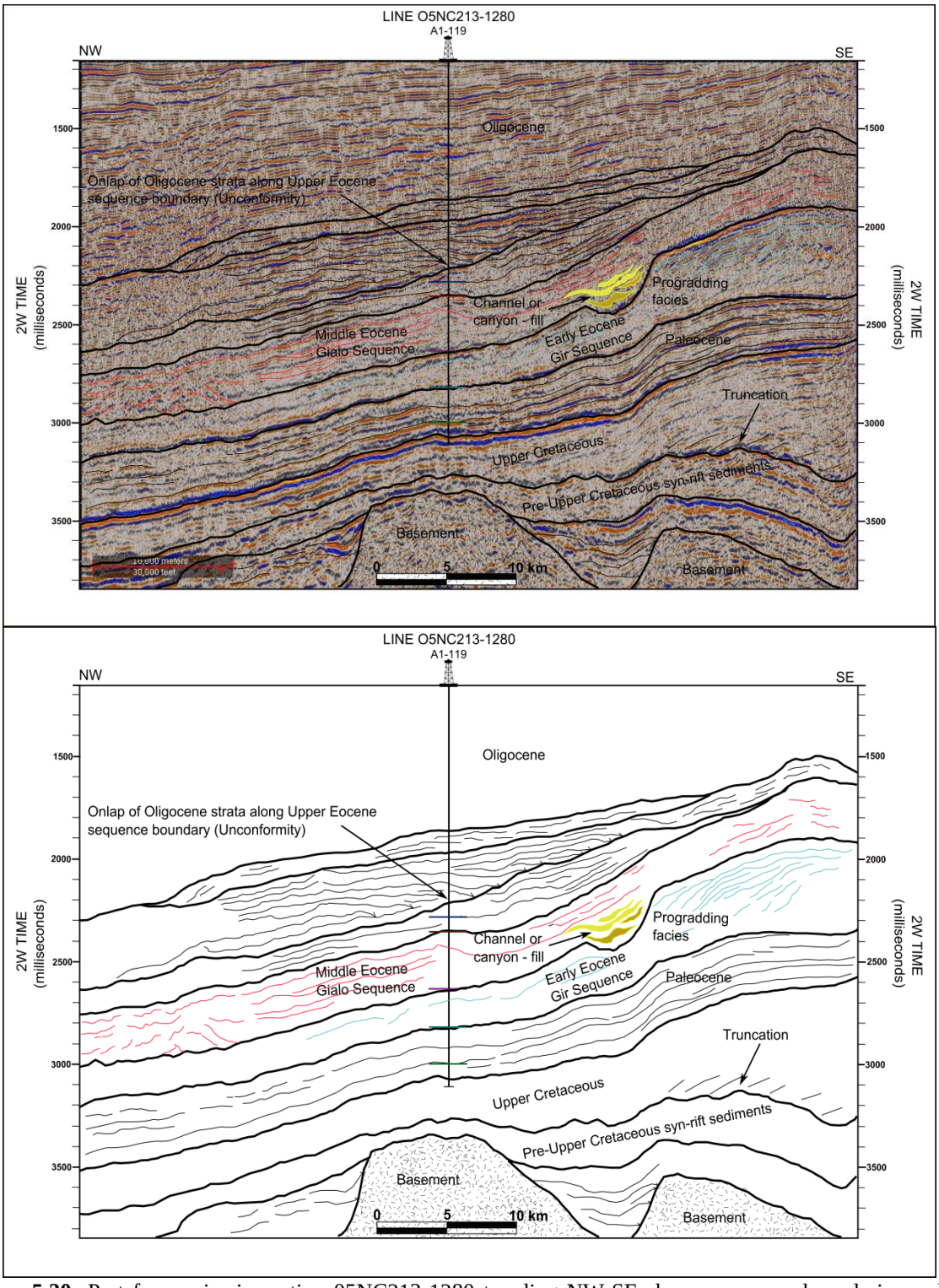

Figure 5.30: Part from seismic section 05NC213-1280 trending NW-SE shows sequence boundaries and lap outs. High amplitude area interpreted as erosional channel fills and surrounding low-amplitude area interpreted as lowstand bypass systems deposits in Gialo sequence.

This Gialo sequence is relatively thick sequence within the stratigraphic record. It occurs seaward and at a lower elevation than, the carbonate shelf (Gir sequence), but appears broadly

coeval with that sequence. The Gialo sequence is seemingly composed of three overlapping sediment parasequences (Figure 5.27) separated by unconformities. The lower sequence boundary onlaps landward against a possible siliciclastic wedge (e.g. Beask et al., 2014), and downlaps seaward onto the Lower - Middle Eocene unconformity.

The upper sequence boundary is a prominent reflection onto which younger sequences downlap. Internal unconformities indicate that parasequences downlapped and onlapped against each other's forming complex stacking patterns. With the exception of these sub-sequence boundaries, the Gialo sequence is characterized by a relatively coherent, continuous reflection character and variable, complexes structures (mass transport complex) at the centre of the Ajdabiya Trough (Figures 5.34, 5.35, and 5.36). The end of the Middle Eocene exhibit a facies changes (Figure 5.10) and the carbonates give way to shales (Augila Formation), possibly signifying the subsiding movements in the Ajdabiya Trough.

The depositional model of the Lower – Middle Eocene sequences represents a carbonate ramp developed during periods of lowstand and highstand system tracts (Figures 5.37 & 5.38). The model characterizes the facies distribution during periods of accommodation increasing (transgressive system tract), occurring by the end of Early Eocene.

The Middle Eocene facies distribution in the Ajdabiya Trough is probably influenced by the structuration and subsidence of the region. The general configuration is characterised by a ramp model progressively deepening toward the northwest. High energy facies can be deposited within these restricted areas, forming prograding shoals (Figures 5.30, 5.33, and 5.38). These shoals, prograding and evolve laterally into shelf lagoon to peritidal settings toward the east and southeast. The intertidal environment is characterized by the presence of ramp carbonates, dominated by limestone and evaporites (e.g. Yanilmaz et al., 2008). These facies laterally pass into large-scale prograding clinoforms of the Gialo Formation, dominated by mud-rich facies.

5.4.1.5 Oligocene Sequence (37-23 Ma)

Seismic profiles show that the Oligocene sequence consists of high amplitude and continuous seismic facies with parallel to subparallel configuration patterns (Figures 5.19, 5.22, and 5.23) and occasionally shows concordant reflection which suggests uniform rate of deposition in shallow water conditions (e.g. Wennekers et al., 1996; Martin et al., 2008; Starke et al., 2008;

Yanilmaz et al., 2008). Tied to wells B1-121 (Figure 5.31), C1-119, Q1-31, and U1-41, the facies of the Oligocene sequence is related to the shale of Arida and Diba Formations (Table 5.1) and (Figures 5.4 & 5.15). Locally the Oligocene sequence is unconformably overlying the Upper Eocene sequences.

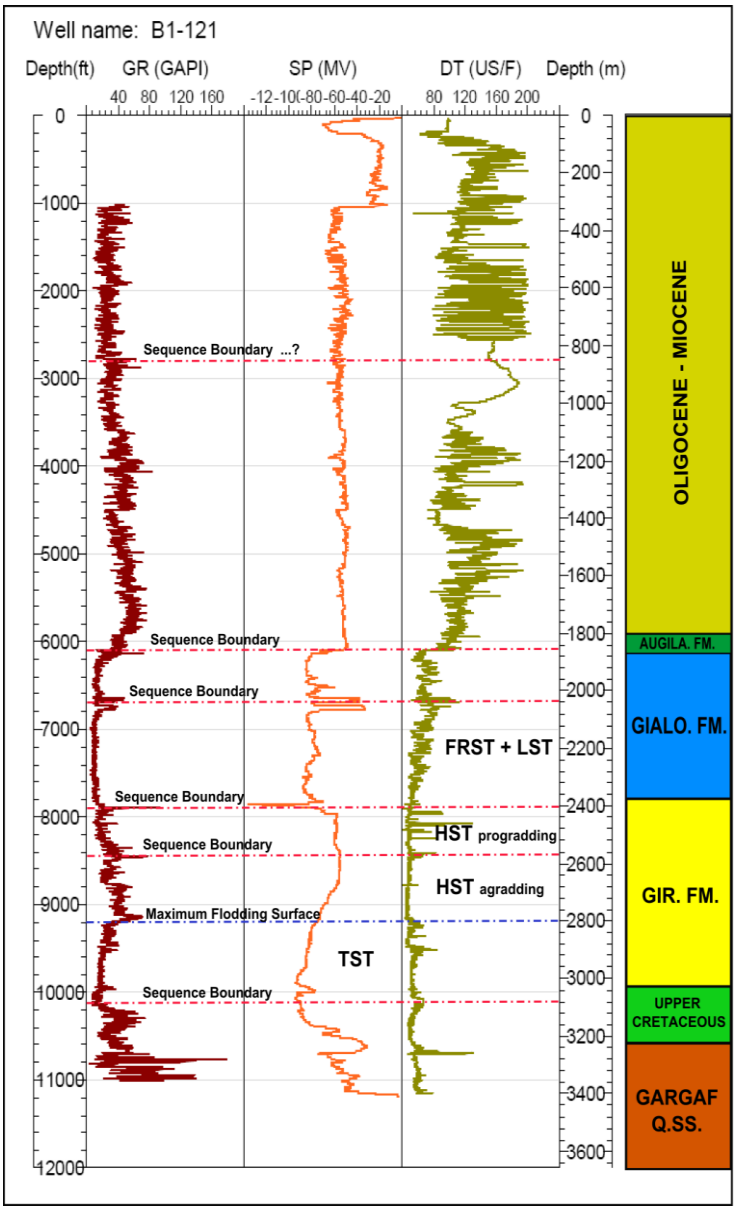

Figure 5.31: Interpreted stratigraphic surfaces in the logged section of well B1-121 located to the east of the Ajdabiya Trough (Amal Platform). Prominent stratigraphic breaks can be interpreted as sequence boundaries, marine-flooding surfaces (i.e., transgressive-surfaces of erosion) or system tracts.

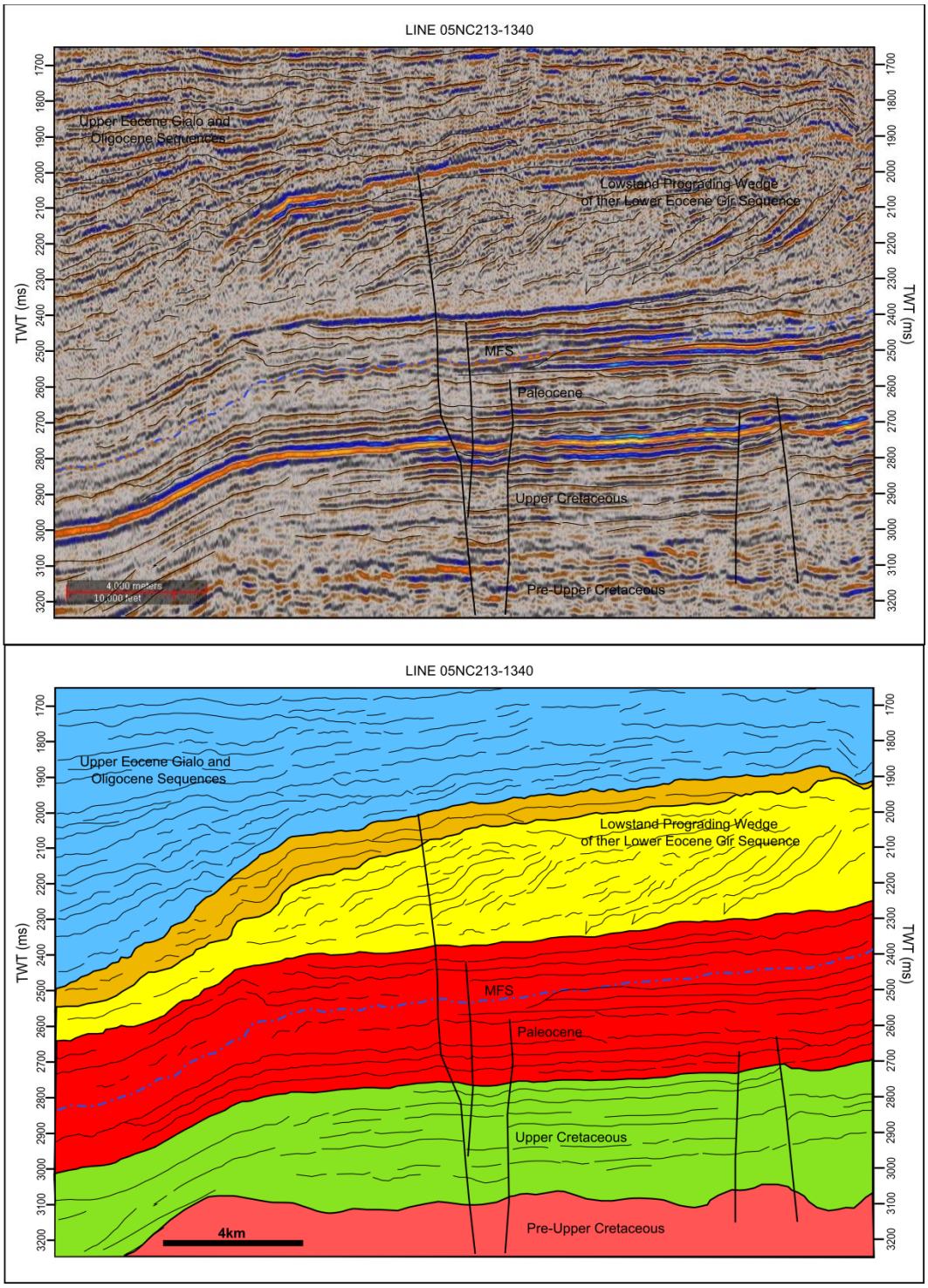

Figure 5.32: Seismic section 05NC213-1340 showing Early Eocene Lowstand Prograding Wedge. Possible Middle Eocene siliciclastic clinoform progradation across a carbonate ramp formed a depositional geometry featuring two breaks in slope. Progradational seismic facies on continental slope downlaps downdip on top of Paleocene Transgressive System Tract.

From south to north, the Oligocene sequence, shows a laterally continued through drawing concordant to sub-concordant stratal patterns (e.g. Line 05NC213-1240 (Figure 5.29).

This sequence latter is overlain by the clastic and carbonate sediments of the Miocene sequence (Marada Formation) (A1-114 well) (Figure 5.18). This seismic interval expresses a low energy lagoonal carbonates, fringed by high energy shoal carbonates (Yanilmaz et al., 2008). Ramp and pelagic environments developed basinward under sea level rise and a pronounced transgression.

The Oligocene sequence in Ajdabiya Trough (Figures 5.14 & 5.22) has an unconformable relationship with the underlying Upper Eocene (*Augila Formation*) and the overlaying Lower Miocene (*Marada Formation*), (Barr and Weggar, 1972; Benfield and Wright, 1980; Bezan and Malek, 1996). The reflection terminations for the Oligocene sequence show a clear separation of lowstand system tracts and highstand system tracts characterized by a progradation of ramp facies (e.g. Yanlmaz et al., 2008) (Tables 5.1 & 5.2). Sediments of this sequence deposited during period of relative sea-level fall and slow initial rise of relative sea level in the lowstand system tracts with progradational patterns supported by the downlapping and onlapping terminations (Posamentier and Allen, 1999). The downlapping terminations in the highstand system tracts show that the direction of sediment supply was from the southeast and northeast (Yalmnz et al., 2008). The thickness map of the Oligocene sequence shows that the major depocentre for this sequence is in the northeast portion of the Ajdabiya Trough indicated by the thickest preserved sedimentary rock (Figure 5.11). Wennekers et al., 1996 suggested that possible influx of clastic sediments from a deltaic system situated in the eastern part of the Sirt Basin may have augmented a NW progradation in the Ajdabiya Trough. The geometry of the Oligocene sequence as indicated on the thickness map (Figure 5.11) suggests that there may be possible of fluvial source flow that controlled the sediment transport of the Early Oligocene sequence associated with Middle to Late Eocene channel system were the Ajdabiya Trough margin growth during the Middle to Late Eocene was progradational accompanied by a localized debris flow or mass transport complex (MTC) toward the west (Beask et al., 2014).

During the Late Oligocene to Early Miocene, a carbonate platform model is not well developed and the sedimentation character show more gentle sloping. Shallow carbonate system may effectively prevent any progradation of mid ramp facies. To the west of the study area a restricted and open lagoons, tidal flates and possible eustrine channels could be developed due to retreat of the shore line within an E-W trend during most of the Oligocene.

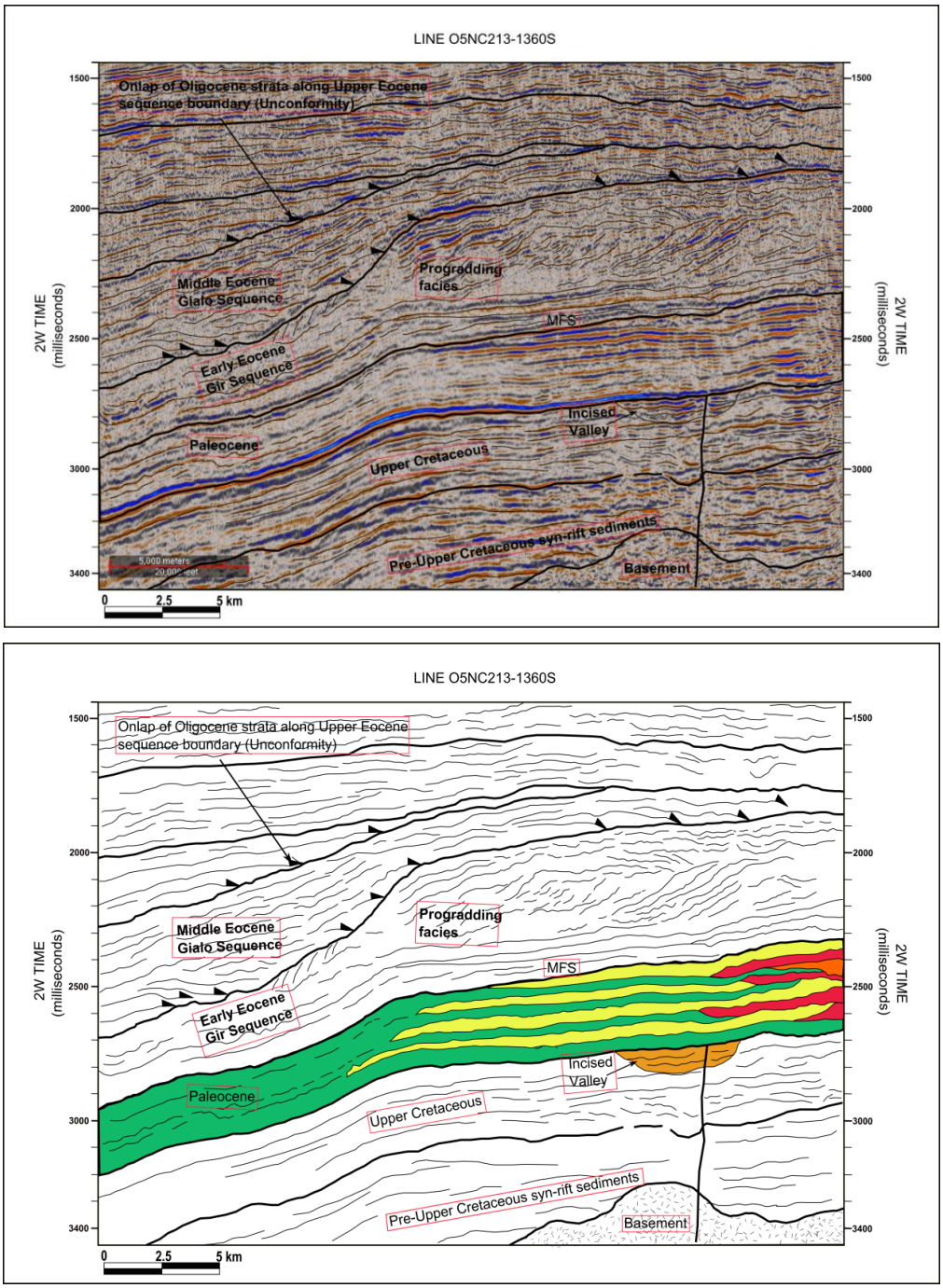

Figure 5.33: Seismic section 05NC213-1360S showing Early Eocene Lowstand Prograding Wedge. Possible Middle Eocene siliciclastic clinoform progradation across a carbonate ramp formed a depositional geometry featuring two breaks in slope. Progradational seismic faeies on continental slope downlaps downdip on top of Paleocene Transgressive System Tract.

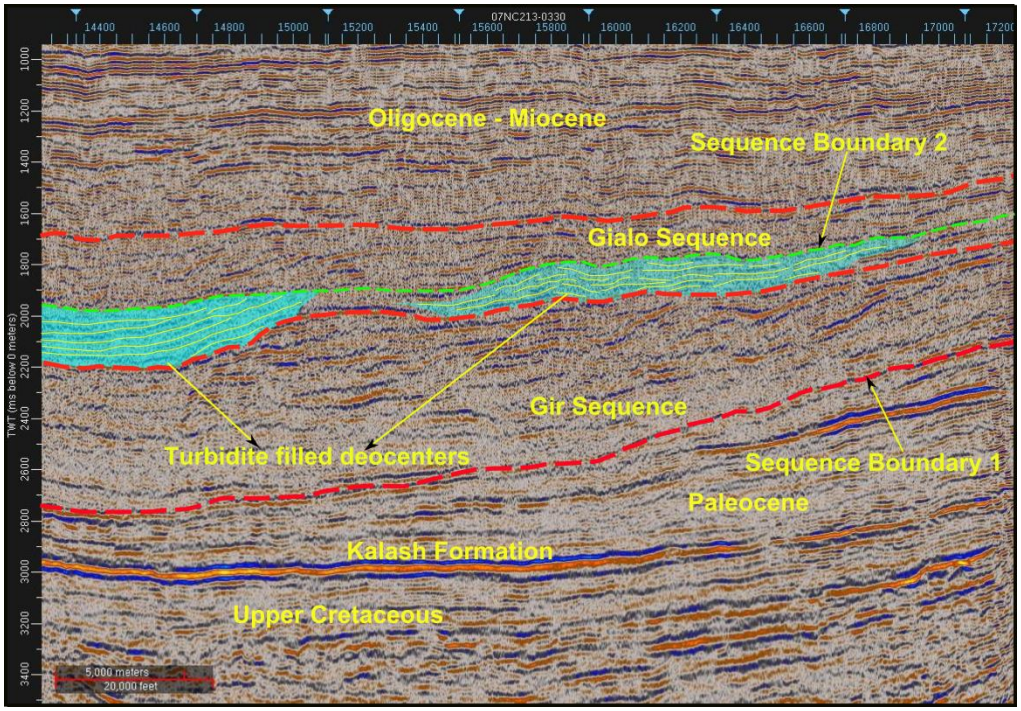

Figure 5.34: A part from strike oriented regional seismic line 05NC213-0330 crossing the study area in NW-SE direction. The blue colour seismic packages represent the confined nature of the "Gialo Sequence" turbidite system. This illustrates the shingled progradational reflection pattern associated with proximal turbidites lobes.

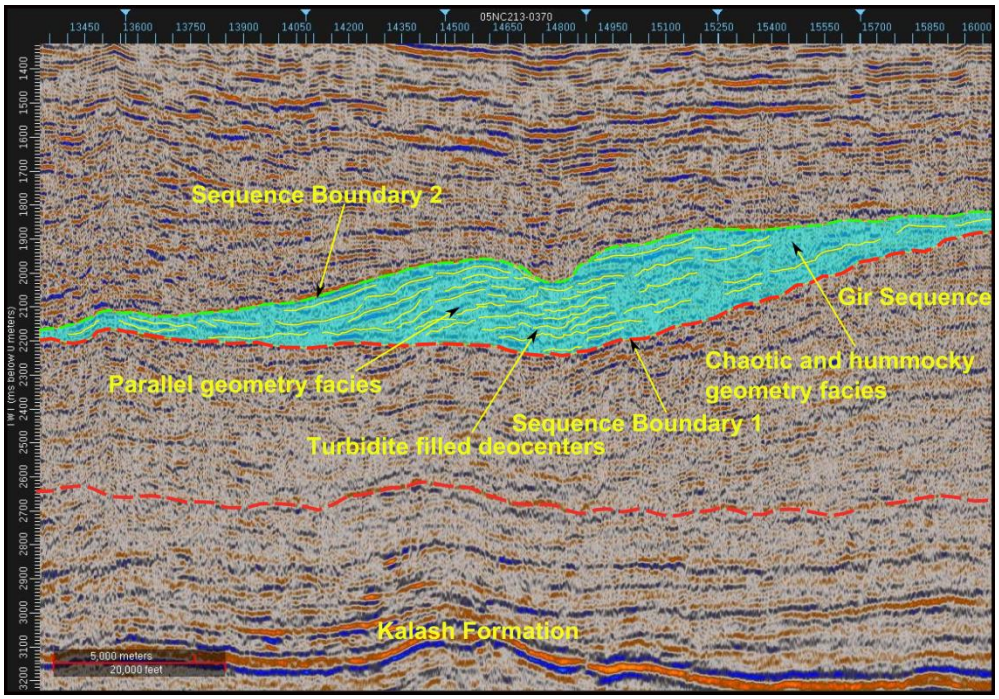

Figure 5.35: An oriented NE-SW seismic line crosses the southern depocentre perpendicular to the depositional dip direction. The blue color represents turbidite fill geometry and chaotic, hummocky, and parallel fill internal reflection configuration.

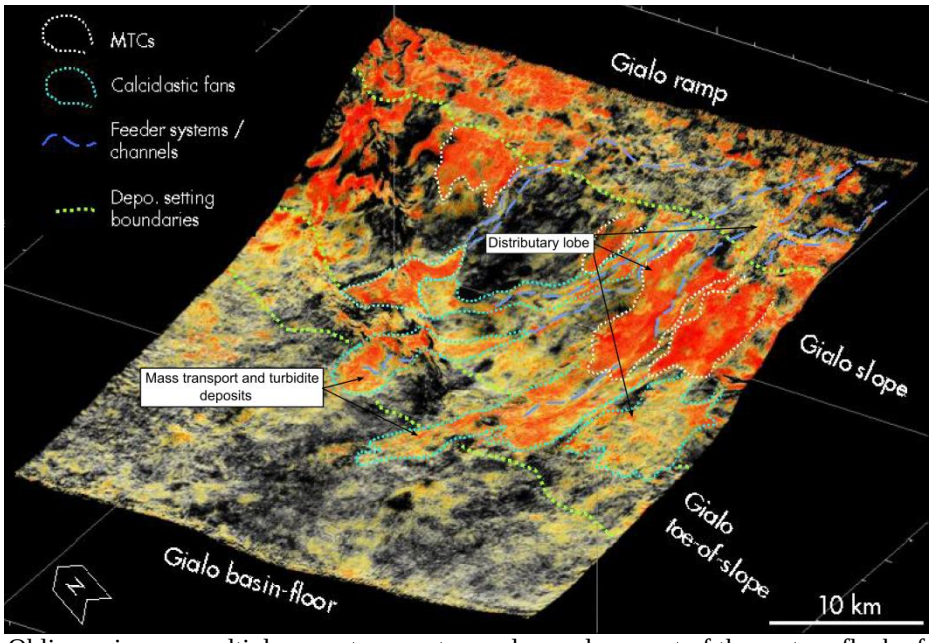

Figure 5.36: Oblique view on multiple mass transport complexes along part of the eastern flank of the Ajdabiya Trough. The seismic volume sculpting highlights the presence of depositional complex comprises multiple distributary channels and large-scale mass transport complexes on the upper part of the slope. The small-scale calciclastic fans on the toe-of-slope are turbidite systems and partly younger than the upper slope features. (Image obtained from 3D seismic interpretation by Baask et al., 2014)

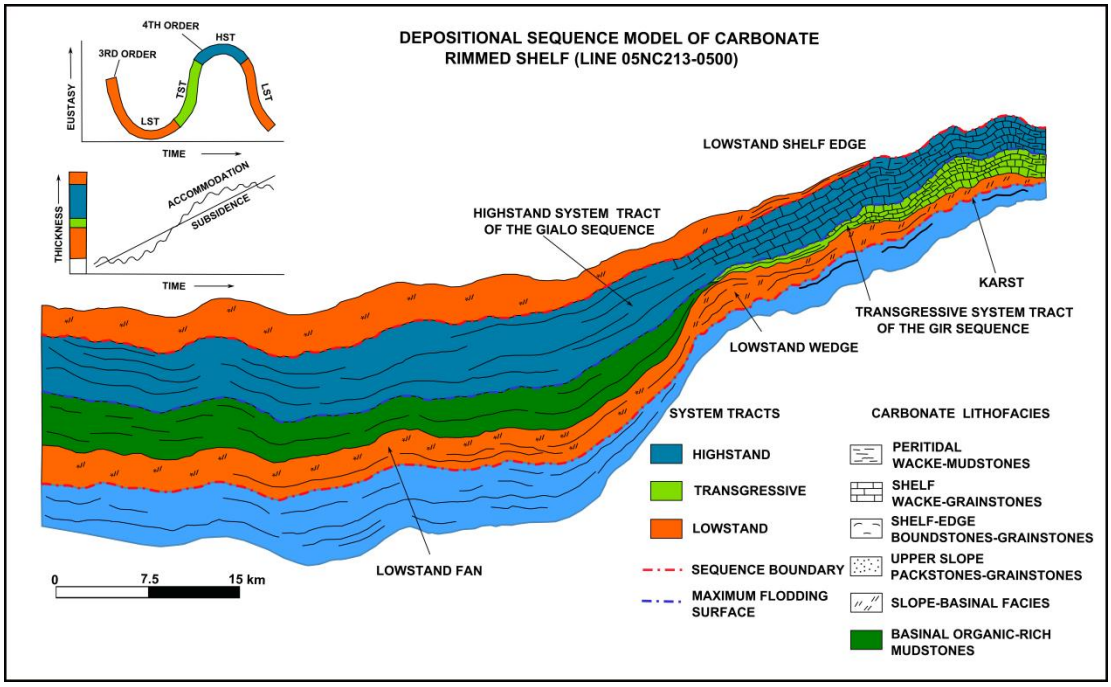

Figure 5.37: Depositional model for the Lower and Middle Eocene Gir and Gialo sequences based on idealized sequences and systems tracts model of Handford & Loucks, 1993.

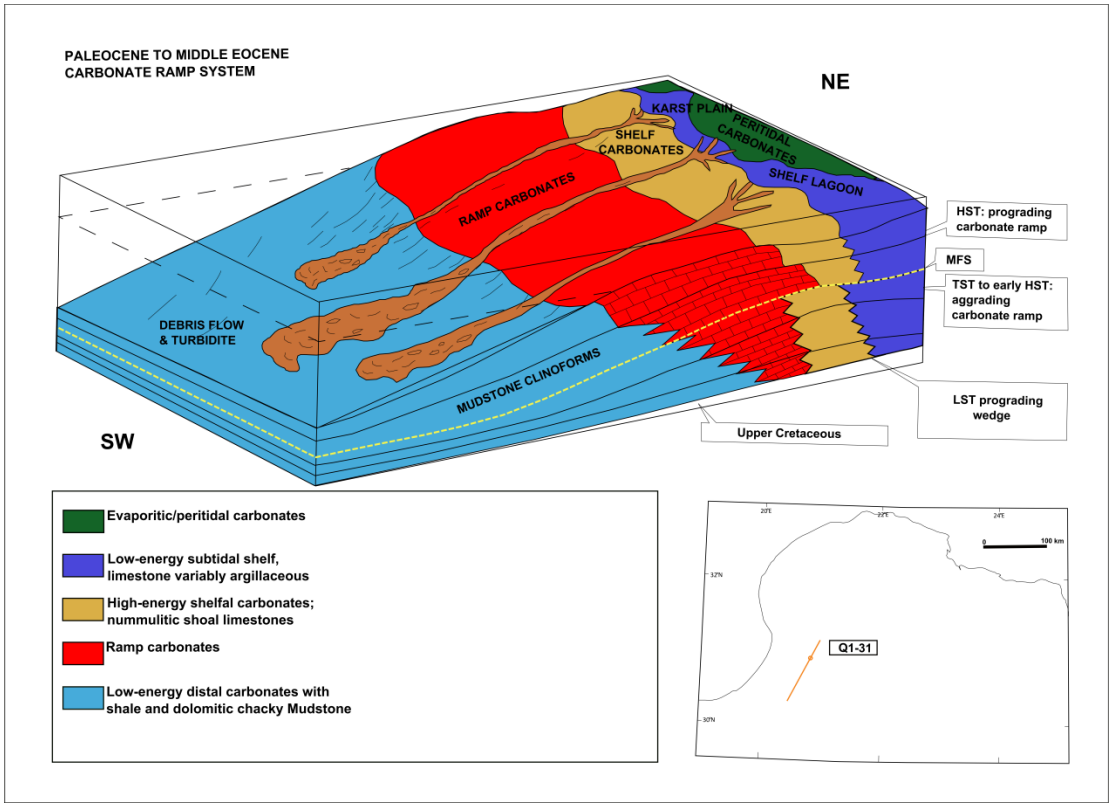

Figure 5.38: Depositional model of Paleocene – Middle Miocene system tracts. It is important to note the occurrence of HST debris flows and turbidites into the deeper portions of the basin. This clearly indicates an important sediment supply control on facies development and sediment by-passing and/or reworking from the shelf into deeper relatively sediment starved parts of the basin.

5.4.1.6 Miocene Sequence (23-0 Ma)

The Miocene exhibits continuous reflecting horizons with high amplitude response. The patterns within the sequence as observed from the majority of the seismic profiles show gentle deposition towards the basin centre interrupted by channel system at the top of the sequence. The ability of the carbonate system to prograde basinward is low with sedimentation keep pace with the basin thermal subsidence. Within high subsiding zones, within the Ajdabiya Tough, the Miocene sequence appears thicker and completes. The seismic facies of this sequence is very characteristic, marked by dominant low-amplitude and medium to low continuity reflections, indicating a transparent facies related to argillaceous and shallow marine depositional environment (Table 5.1). The internal reflections of this sequence show progradational clinoforms in sigmoid and shingled geometry, marking a shallow-to-deep water environment with low to high energy.

The Miocene sequence presents a parallel to sub-parallel seismic facies, clearly observed on the seismic profile and shows especially onlap and toplap structures, testifying to a uniform, vertical and aggrading sedimentation (Table 5.1).

In spite of many studies, the sequence stratigraphic analysis of surface and subsurface Miocene series and their correlation with various eustatic charts (Haq et al., 1987) still remain defective within the Ajdabiya Trough. Especially, no work has taken into account regional and local events (eustasy, tectonics, and climate) in order to clarify the role of each parameter in the control of sedimentation and the sequence organization in this environment. The works of Yanilmaz et al., 2008, Starke et al., 2008, and Martin et al., 2008 were focused only on the eastern part of the Ajdabiya Trough and Cyrenaica Platform using well data and geologic information's. Preliminary observations in this study show that within the Ajdabiya Tough, the Miocene sequence thickens towards the central area owning to continuing subsidence. The sequence varies in thickness from north to south and east to west several times along the main directions of the trough. The thickness ranging from about 200 ms (TWT) in platform areas mainly covered by lagoonal and peritidal to shallow marine environments to about 1200 ms (TWT) in outer shelf and pelagic environment. Entirely the facies of the Miocene sequence show more open marine conditions and different system tracts possibly developed.

The seismic facies of this sequence is very characteristic, marked by dominant low-amplitude and medium to low continuity reflections, indicating a variable amplitude seismic facies related to argillaceous and shallow marine depositional environment (Table 5.1). The internal reflections of this sequence show, a gradual deposition marking a shallow-to-deep water environment with low to high energy (e.g. Yanilmaz et al., 2008). The upper part seismic horizons of this sequence display very good continuity and high amplitude, corresponding to a platform carbonate and shale deposits towards the central area (bottom-set). In the northern part of the Ajdabiya Trough, where Upper Miocene (Messinian) deposits are preserved (Fiduck, 2009), this sequence is thick in the subsiding and bending part towards the offshore area and thicken also towards the tilted platform to the east. The deposit of the Miocene sequence probably synchronous to a major maximum flooding near 16 My, described by Vail et al. (1977), Loutit and Kennet (1981) in the Indian Ocean, and by Haq et al., (1987, 1988) in the Global Sea Level. This relative sea-level rise coincides with the opening of subsiding

grabens according to dextral and sinistral transtensional movements in the Cyrenaica Platform and along the Libyan costal areas (Anketell, 1996).

5.4.2 Post-rift Unite 1 (Early Cretaceous – Late Paleocene)

The internal reflections of post-rift unit-1 are parallel to each other, well continuous, showing low to moderate intensity, locally transparent, and the frequency varies slightly. The top of this unit is marked by seismic unconformity, which according to our interpretation is Late Paleocene – Early Eocene in age. This sequence is assumed to consist of a transitional facies between shallow - deep marine depositional environments correlating with the early - middle Paleocene, Hagfa Formation in the Amal High to the east (e.g. Thusu, 1996).

A lateral transition from inner ramp to outer ramp carbonates is recognized within Upper Paleocene cycles (Spring and Hansen, 1998). Wells on the southeast part of the Ajdabiya Trough shelf proved that the carbonates of the Sabil Formations are conformably overlain by the Hagfa Formation which consists of silty to calcareous shales, claystones and calcareous sandstones, deposited in deep-water marine condition (Bezan, 1996; Hallett, 2002) (Table 5.2). Carbonates locally continued up to unconformity, especially over structural highs around the Ajdabiya Trough. Locally, reef growth might have continued up to Upper Paleocene.

5.4.3 Post-rift Unite 2 (Late Paleocene - Miocene)

This unit is characterized by continuous subparallel to parallel reflections of low to moderate intensity, showing locally chaotic or wavy patterns (Figures 5.21, 5.24, 5.25, 5.29, and 5.45). Well A1-119 has penetrated the Upper Cretaceous to present post-rift strata and recovered a thick section of claystones, sandstones and carbonates with highly calcareous fossils (foraminifera) in slope bathyal or open marine environment (Yanilmaz et al., 2008). The lower sequence boundary in this unit shows moderate to strong amplitude unconformity surface and occasionally shows local truncation with the underlying sedimentary strata.

A Paleocene stratum thins toward the north and mainly eroded in certain localities within the Ajdabiya Trough. Paleocene to Early Eocene erosion present in the Cyrenaica Platform could have influenced the Paleocene section along the northern part of the Ajdabiya Trough. This is the case in well U1-41 (Figure 5.18) where the Paleocene section is thinner or almost absent.

The thick Cretaceous section observed in the well U1-41 shows that the basement configuration is more complex than other areas within or around the Ajdabiya Trough.

Small incised valleys cut into the Eocene recent sediments (Gialo Formation) and possibly extended few kilometres wide, indicating strong bottom turbidity currents or debris flow (Figures 5.26, 5.30, 5.37, and 5.38). These could be developed during a fall in base level. Tops of Gir and Gialo formations are other two unconformities in the post-rifting sequence. These unconformities separate the Lower and Middle Eocene formations with the age from about 54 - 37 Ma.

5.5. Lithostratigraphic Compilation Using Borehole Data

The study of sedimentary successions in the subsurface of the Ajdabiya Trough is based on borehole logs description compared to 2D seismic profiles. Well correlation cross-sections (Figure 5.39) show lateral variations in lithofacies and thicknesses occasionally displaying local gaps related to possible erosion or non-deposition.

The Upper Cretaceous sequence is at its lowest thickness of about 40m in the NW part of the Ajdabiya Trough (in well A1-114) (Figures 5.18, 5.39, 5.40, 5.41, & 5.42). Its thickness increases dramatically towards the NE (~1300m in well T1-41). It can, therefore, be assumed that the sequence is present throughout the study area, apart from small areas of erosion on top of the Al Jahama Platform to the NW where the sequence has been intensively eroded, along with many other Palaeozoic units. The erosion is probably the result of emergent of footwall structures and later to the east the erosion is attributed to localized 'pop-up' faulting (e.g. El Arnauti et al., 2008; Yanilmaz et al., 2008). NW-SE faulting in the Ajdabiya Trough also controlled the emergent of footwall structures of the main faults (e.g. Skuce, 1994; Baird et al., 1996). However, the sequence shows a local gap in A1-41 well near the western boundary of the Cyrenaica Platform (Yanilmaz et al., 2008). The Al Jahama Platform to the northwest, is subjected to continue transgression during the Upper Cretaceous (Campanian – Maastrichtian) evidenced by the presence of clastic sediments as a result of reworking of exposed Palaeozoic sediments of (Cambro-Ordovician age) (Yanilmaz et al., 2008).

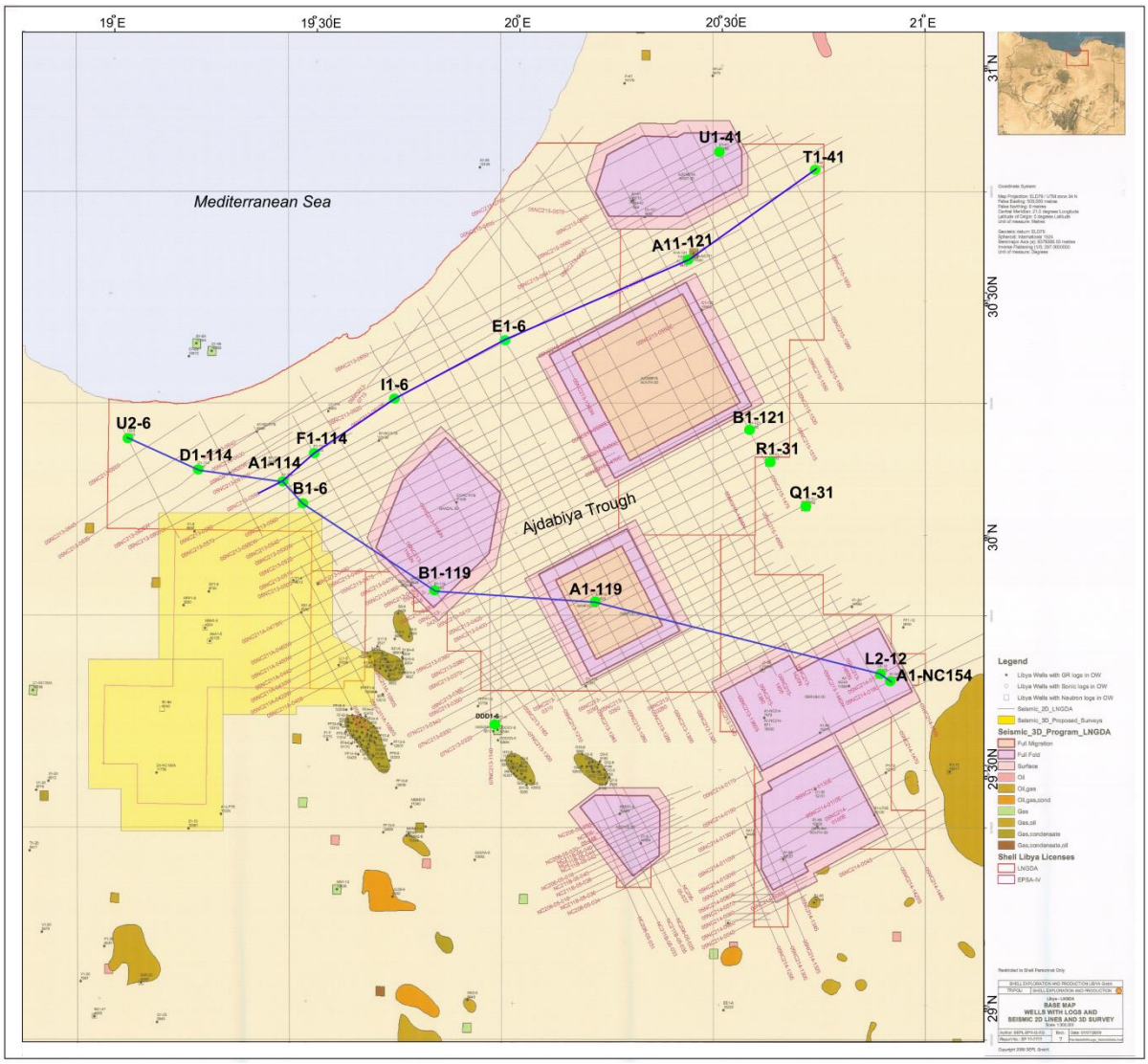

Figure 5.39: Location of constructed cross-sections based on correlation between wells superimposed on 2D&3D seismic coverage within the Ajdabiya Trough.

The facies of the Cretaceous sequence is considered to be deposited under a low energy shelf interior, fringed by a generally thin belt of high energy shoal facies which gave way to low energy distal pelagic carbonates. Repeated movements on the Ajdabiya Trough bounding faults created a series of stacked SW prograding carbonate and clastic cycles. For instance, Upper Cretaceous - Paleocene series conforms to thin pelagic marls and carbonates (Figure 5.19). In the Ajdabiya Trough area, Llewellyn et al., 1996 observed an intra - unconformity separating Early Maastrichtian Waha Formation and Late Maastrichtian Kalash formation (Figures 5.4, 5.7, and 5.15). The unconformity may correlate with Cretaceous – Tertiary boundary or Upper Cretaceous unconformity (Baird et al., 1996; Hallett, 2002). Regression is

responsible for the Upper Cretaceous unconformity was initiated during Maastrichtian times (Llewellyn et al., 1996; Wennekers et al., 1996), and was followed by progressive Late Maastrichtian through Early Danian transgressive sedimentation. Such an unconformity is thought to exist in the Al Jahama Platform area. For example, in the A1-114 well (Figure 5.18), the uppermost part of the Lower Paleocene organized in shales alternating with thin bedded limestone disconformably overly either remnants of Upper Cretaceous or Pre-Upper Cretaceous (Nubian Formation) sequences. In the Ajdabiya Trough, shales in the Upper Cretaceous decrease remarkably in thickness from south – north (A1-NC154: ~1200 m) and east – west (T1-41: 1300 m) towards the north (F1-114: ~ 50 m).

The Paleocene sequence is developed within ramp style platform geometry as observed from the cross sections (Figures 5.22, 5.27, 5.28, & 5.30). The facies geometries of the sequence are characterized by a low energy lagoon, fringed by shoals which give way to pelagic carbonates (e.g. Yanilmaz et al., 2008). Spring and Hansan (1998) suggested that a transition from shoal sediments to more distal sediments during the Paleocene was generally abrupt. Besides, these facies are eroded or none deposited in the north-west mainly in well F1-114 owing to localized uplift during the Late Paleocene in this part from Sirt Basin (e.g. Bezan, 1996), despite the preservation of thick Paleocene section that observed in wells A1-114 and D1-114, which may accumulated within a local depression as observed from the Paleocene thickness map (Figure 5.6). The Paleocene sequence which composed of shoal carbonates and pelagic shales is overlain by the Lower Eocene (Gir sequence). It consists of limestones interbedded with thin beds of marls and pelagic shales (Abugares, 1996). In the southeast and eastern sides of the study area, TI-41, A1-121, and U1-41 wells (Figure 5.18) displays the thickest limestone's of the Gir sequence 800 m and 700 m respectively, to the northwest, the Gir sequence decreases in thicknesses (A1-114, F1-114, and B1-6 wells). Further northwest over the Al Jahama Platform the Gir sequence show local gaps due to lateral pinch-outs (A1-114 well). In well U2-6, the Lower Eocene (Gir Sequence) lithofacies unconformably overlies Upper Cretaceous strata.

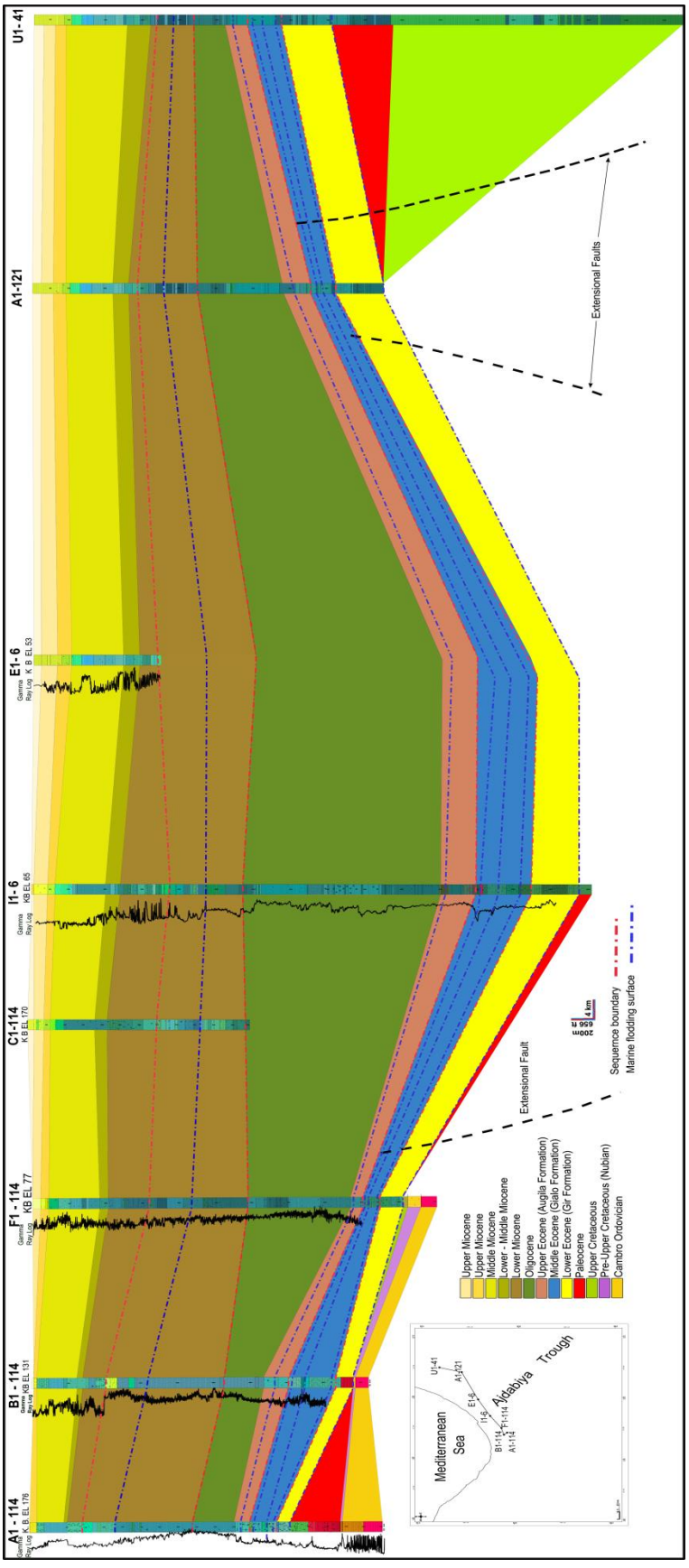

Figure 5.40: Lithostratigraphic correlation chart of the subsurface Ajdabiya Trough Late Mesozoic – Cenozoic successions across eight wells showing its lateral, vertical facies and thickness variations. Light green is the Cretaceous sequences; Orang, purple, and red are the Paleocene sequences. Yello is the Early Eocene Gir sequence, Blue is the Middle Eocene Gialo sequence, Green is the Oligocene sequence, Brown and above is the Miocene sequence. Red dashed lines are sequence boundaries (unconformities), and the blue dashed lines are correlated sea maximum sea level flooding surfaces. The vertical lines show the gamma-ray log. The inset map shows the location of the arbitrary cross-section correlated with the well data.

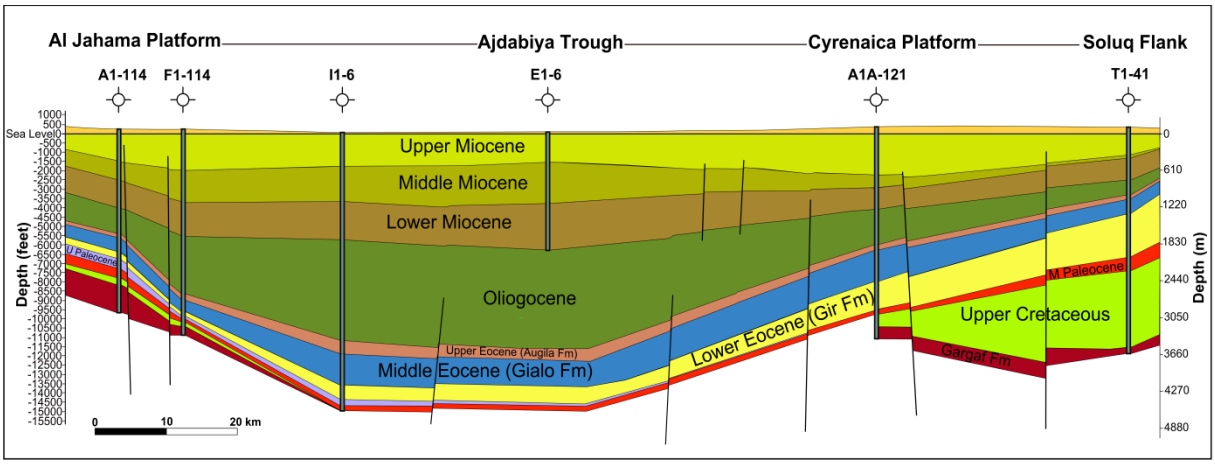

Figure 5.41: E-W cross-section based on well to well correlation depicting the identified sequences and show remarkable variations in thickness along the northern domain of the Ajdabiya Trough. (see Figure 5.39 for location)

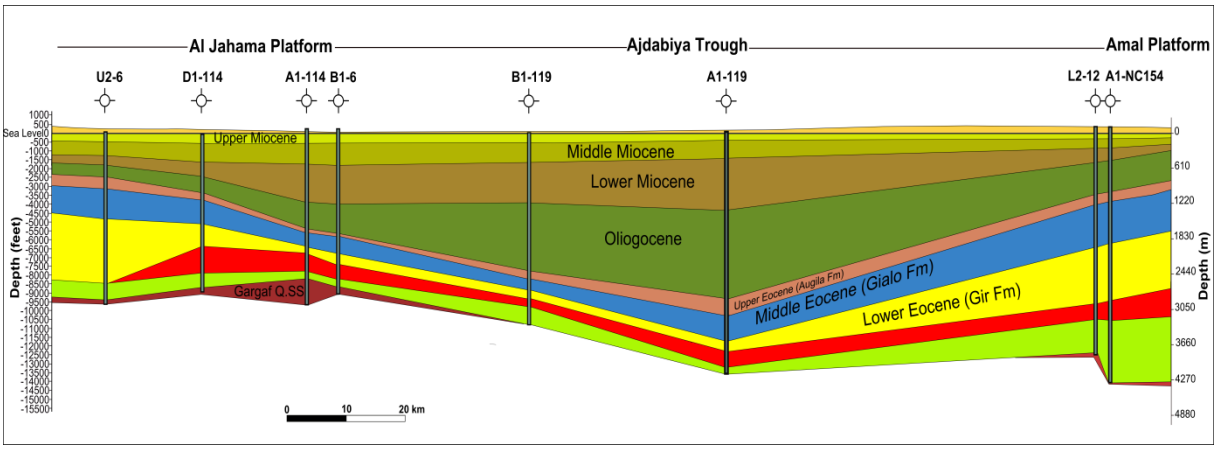

Figure 5.42: NW-SE cross-section based on well to well correlation depicting the identified sequences and show remarkable variations in thickness along the strike of the Ajdabiya Trough. (see Figure 5.39 for location)

The large thickness observed for the Gir sequence at the well U2-6 (Figure 5.42) may be related to basin subsidence, which dominated the northwest part of the Ajdabiya Trough during the Upper Cretaceous - Early Eocene times as observed from the subsidence analysis (chapter 6).

Middle Eocene (Gialo sequence) which contains limestone interceded with thin bedded of shales (Wennekers et al., 1996) is identified in all wells. The facies of the Gailo sequence which is represented by the Gialo Formation is changed laterally from limestone in wells (A1-114, B1-114, F1-114, C1-114, and I1-6) to shales in wells (A1-121, U1-41) with a distinct primary dip of the carbonate beds at the edge of a carbonate shelf to the east. To the west, the

Gialo Formation thins at F1-114 well. Therefore, the Eocene facies pinch out rapidly towards the north and northwest of the study area. At the centre of the trough towards the north at I1-6 well, the Gialo sequences consists of limestone's partly recrystallized and dolomitized, with benthic microfauna as observed from well reports. Over the Al Jahama Platform, Middle to Late Eocene thins eastward towards a faulted edge along the boundary of the Ajdabiya Trough and then thickens again toward the centre of the trough.

The sediments of the Oligocene sequence correspond to siliciclastic sands and detrital clays (Wennekers et al., 1996; Hallett, 2002). The Oligocene sequence measures the highest thickness in I1-6 well, which is located in the northwest (Figure 5.41). Facies of this sequence (Table 5.2) changes laterally from marls and shales as noticed in well I1-6 bearing planktonic foraminifera and trace fossils alternations to limestone beds (e.g. Yanilmaz et al., 2008, Starke et al., 2008, and Martin et al., 2008).

The Oligocene sequence is gently sloping towards the centre of the Ajdabiya Trough compared to the other Cenozoic sequences as a result of low gradient margins caused by the influx and the significantly infilling of the trough by the late Oligocene sediments.

The Miocene sequence thickens dramatically towards the north and the central area and unconformably overlies the Oligocene sequence. The sequence package consist of limestone and clayey limestone rich with fossils (e.g. benthic microfauna, e.g. El Hawat, 2008 and references therein). It is observed that subsidence during the Miocene continued to develop accommodation space subsequently the Miocene sediments thicken into the trough preserving more than 750 m in its axis. The well correlation show that the sedimentary successions started in Late Cretaceous are characterized by pelagic marl and limestone deposits with possible emersion and erosion. During the Paleogene times, the south-eastern part of the study area was the sites for the highest thicknesses of pelagic sedimentation. While the north-east and east-central parts were characterized by frequent gaps, thickness reductions and unconformities. The Paleogene – Lower Miocene sedimentation is characterized by frequent gaps, unconformities and considerably reduced thicknesses notably in the northern and north-eastern regions. It is likely that, tilting of blocks and subsidence due to tectonism, have, on a regional scale, exerted a control on lithofacies differentiation.

5.6 Development of Sedimentary Depocentres

The stratigraphic sequences described within the framework of the Ajdabiya Trough can be classified into variable tectono-sedimentary successions composed of early pre-rift, syn-rift and post-rift units. The pre-rift are mainly remnants of Paleozoic of Cambro-Ordovician age, the syn-rift composed of possible Triassic – Early Cretaceous units and the post-rift including Paleocene to Miocene strata.

Factors influenced the deposition and the thickness of the Cenozoic strata within the Ajdabiya Trough is controlled early by pre-existing basement highs that have caused the Upper Cretaceous and the Paleocene to be thin around those structures. Changes in Paleocene depositional styles are broadly influenced by underlying Cretaceous paleogeographic domains.

On 2D seismic sections, Upper Cretaceous horizons show broad regional similarities and show less structural complexity than the underlying structures including the basement, which suggest possible start of the post-rift stage or time of tectonic quiescent commenced by the end of the Upper Cretaceous as indicated also on some subsidence curves (chapter 6). Predicted Paleocene to Miocene thickness maps (Figures 5.43) show variations in structures and depositional trends during the Cenozoic time.

The drafts of the thickness maps were produced based on compiled time structure maps at scale of 1:1000 000. The maps were preliminary produced digitally with the Oasis Montaj mapping system using a 500 m gridding interval and then converted to adobe illustrator for further improvement. The maps are defined throughout the study area were possible with appropriate isopach maps (Figure. 5.43) equivalent to the thickness of the stratigraphic units.

The thickness maps show the variation in sediment thickness throughout the Cenozoic time. The extreme variations in sediment thickness indicating both an acceleration of graben subsidence in some areas and regional variability of the type which would accompany and suggest circulatory restrictions caused by rifting tectonics possibly in combination with regressive eustatics (Hallat, 2002).

The 2D seismic sections show moderate to thick sediments infill of Upper Cretaceous strata above rift depocentres and thin to no cover over bald basement highs in the rifted basement topography.

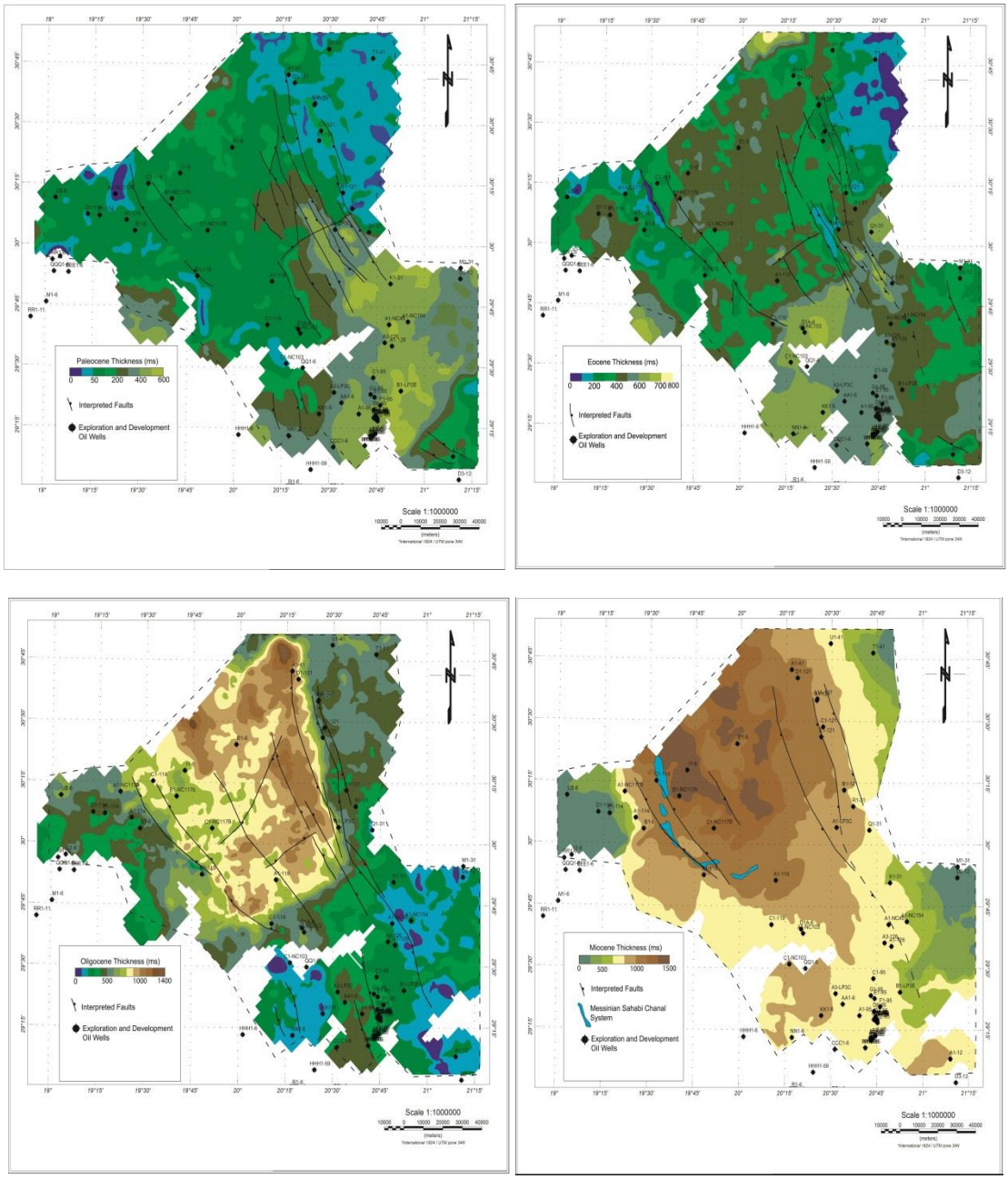

Figure 5.43: Thickness maps of Paleocene – Miocene sequences interpreted from 2D seismic data. Thickness variations in the Ajdabiya Trough are likely associated with the style of the underlying structures. The maps show the principal Cenozoic post-rift depocentres, largely controlled by inherited the syn-rift physiography. (a) Paleocene sequence shows that favored depocentres are located on the inner proximal and distal margin. (b) Eocene sequence shows favored deposition on the distal margin and a prograding wedge on the outer proximal margin. (c) Oligocene sequence shows the favoured depocentres are located to the northeast. (d) Miocene sequence shows favored deposition on the northwest.

The Paleocene thickness map shows that the Paleocene succession has a broad gradual form that thins gently from southeast to northwest indicating possible ramp model geometry (e.g. Spring and Hansen, 1998). A very subtle down-lapping pattern is visible within the Paleocene

interval shown on Figures (5.26, 5.27, and 5.32) developed within low stand system tracts (LST).

Marine conditions and carbonate dominated deposition within most of the Sirt Basin continued through the Paleocene until the end of the Eocene (Spring and Hansen, 1998). The Paleocene to Eocene interval shows a regional gradient of north to south thickening and a slight influence from deeper structure reflecting the transition from outer shelf-basinal to inner shelf facies (e.g. Spring and Hansen, 1998). Down-lapping and thinning to the north may suggest an easterly and southerly source for the overlaying Upper Eocene and Oligocene sequences.

The process of calculating thickness maps using both 2D seismic and well data can lead to misinformation about thickness changes for a given interval due to uncertainties associated with the used parameters. There are good correlations between the thickness maps obtained from the 2D seismic interpretation for the Paleocene – Miocene periods, with the thickness of the sediments observed in about 50 wells at different periods (Paleocene, Eocene, Oligocene, and Miocene). The two approaches allow us to characterize the distribution of the mapped stratigraphic sequences. Furthermore the maps obtained from the 2D seismic data are better constrained the vertical displacement (uplift and subsidence) in addition to information's about the fault activities within the Ajdabiya Trough. Both map products showed the thickness distribution of all six sequences and provided evidence of geographical location of depocentres north and south of the Ajdabiya Trough. Contrasting stratigraphies and thickness distribution from the maps are also used to detect the influence of tectonic setting on deposits formed during periods of sea level fall and rise.

5.7 Faulting and Subsidence Influences on Sedimentation

The seismic response within the Ajdabiya Trough in the south east exhibits a variety of horizontal to slightly inclined seismic reflections associated to chaotic and/or transparent facies. The stratigraphic cycles observed in early rift grabens are dominated by progradational depositional trends, formed during variable stages of extensional subsidence. The structural framework of the Ajdabiya Trough has been manifested by numerous tectonstratigraphic style and extensional fault system evolved during Mesozoic to Cenozoic time and resulting in the formation of grabens and/or half-grabens and rotated fault blocks. The rift infill in the deeper

part of the trough clearly exhibits restricted rift depositional systems of pre-Cretaceous to Paleocene period throughout the study area. Numerous tectono-stratigraphic units can be recognized from SE to NW cut by system of normal faults.

Importantly, the fault system within the trough was likely a reactivated normal fault system in the Palaeozoic basement (chapter 7). Some examples of compressional structures could also be found within the Cenozoic sediments as observed on some 2D seismic profiles (e.g. El Arnauti et al., 2008). As reverse displacement was initiated by east-northeast directed compression, upward propagation of each fault segment must have been strongly influenced by the mechanical stratigraphy of younger, well-bedded Mesozoic marine units. Some normal faults cut through the Cenozoic deposits, partly reaching the surface, indicating recent reactivation. The rift infill shows the typical wedge-shape structure bounded by major normal to possible listric fault components. Other faults are developed subsequently in the hanging walls of the master faults as subordinates. The rift fill graben features have been buried under slightly deformed thick post-rift sequences. The deeply subsided part of the Ajdabiya Trough is considered as a rigid continental block with few deformations during Cenozoic. Reef builds ups (Spring and Hansen, 1998) and channel complex systems developed also along the shelf margin of the trough (e.g. Beask et al., 2014) (Figure 5.44).

The deep-water areas in the Ajdabiya Trough would have been fault controlled. The faulting also significantly influenced and controlled the local facies development. The tectonic events during the Upper Cretaceous and Paleocene times are represented by normal faults deeping southwest and striking northwest - southeast (e.g. Baird et al., 1996; El Arnauti et al., 2008). It is postulated that early extensional faulting controlled subsidence in the Ajdabiya Trough while uplifting in the north-eastern part related to major geodynamic events was responsible for the generation of ramp and pelagic shelf geometries (Yanilmaz et al., 2008). These faults generally reactivated pre-existing extensional structures which are generated during an Early Cretaceous rifting. During the Early - Middle Eocene the sequences comprise essentially evaporites with limestone successions, locally dolomitized and dissected by extensional faults. They are deposited in a shallow marine environment, with clear unconformities emplaced at the base and top of the Gir and Gialo sequences. In the eastern part of the Ajdabiya Trough, a transpressive tectonics possibly related to compressional event in Cyrenaica during the Santonian (ca. 84 Ma) (e.g. El Arnauti et al., 2008), and later similar

pulses occurred through much of the Cenozoic (Bosworth et al., 2008) has generated fault propagation folds affecting the Upper Cretaceous to Miocene series in the northern part of the Ajdabiya Trough. In addition to tectonic inversion, this event has caused folded structures, subaerial exposure and erosion. Tectonic inversion of the same generation was reported by Guiraud et al., (2005) all-over the African-Thetyan margin due to convergence between African and European continental margins (Guiraud and Bellion, 1995; Guiraud et al., 2005).

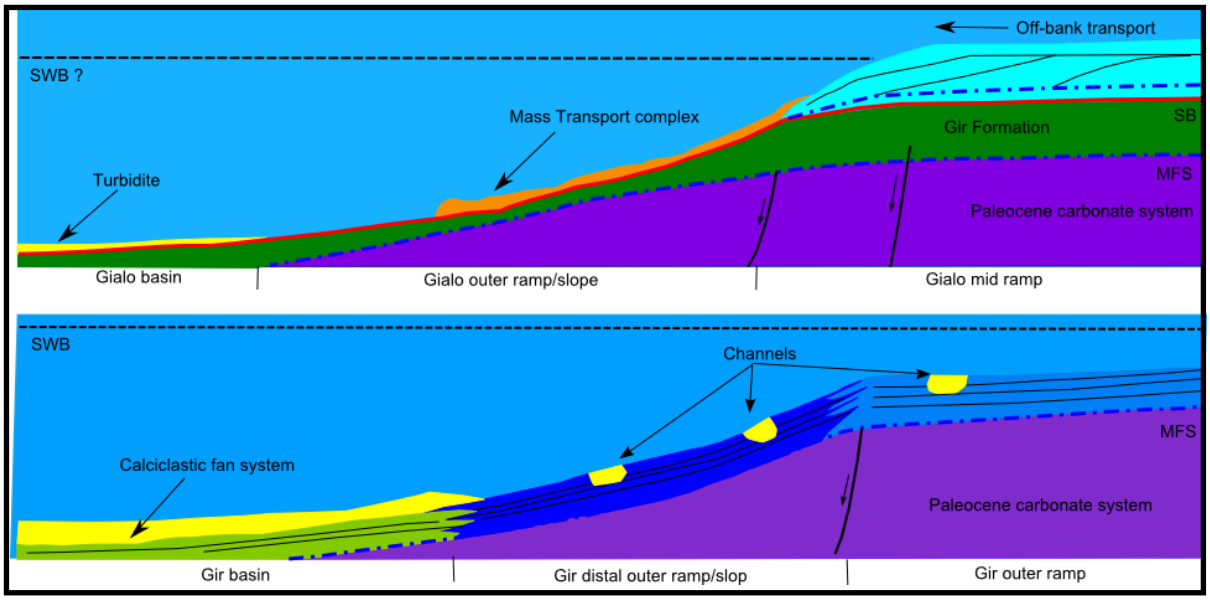

Figure 5.44: Depositional settings of the Early Eocene (Gir sequence) and Middle Eocene (Gialo sequence). Large areas of the Gir shelf are covered with fine grained carbonate sediments and clastic fan system. Continued lowering of the sea level during the Middle Eocene leads to progradation of carbonate system close to the shelf break. Mass transport complex associated with turbidites and small scale fan systems are also exist within the Gialo sequence. (Re-draw from Beask et al., 2014).

In contrast (Bosworth et al., 2008) attributed this to Far-field compressional stresses resulting from arc collisions with the northeast coast of Africa-Arabia propagated across the African plate. The platform margin faults were reactivated as sinistral wrench faults in the Eocene in response to the more rapid movement of the east African plate in relation to the West African Plate (El Arnauti and Shelmani, 1988). The Oligocene to Miocene strata in the Ajdabiya Trough unconformably overlies the Eocene rocks and can be divided into sequences separated by unconformities reflecting marine regressions and transgressions. During this period, the eastern part of the area was characterized by fluvial to shallow-water limestone's, dolomites and some evaporites which pass abruptly into deeper-water marls and mudstones in the Ajdabiya Trough (Hallett, 2002; El Hawat, 2008; Yanilmaz et al., 2008, Starke et al., 2008;

Martin et al., 2008). The western part of the trough is composed mainly of open-shelf carbonates in an open shallow-shelf setting.

5.8 Discussions

5.8.1 Rift-related Sequences

Lately major new data has been acquired from wells in the north eastern Sirt Basin which recommends that the rifting stage in the Sirt Basin started as early as the Triassic (Thomas, 1996). During Triassic - Early Cretaceous time, as the Atlantic opened, the Sirt Basin went through several phases of rifting. Although these events have been mentioned previously in several publications related to the evolution of the eastern Sirt Basin (Guiraud et al., 1987; Bayoumi and Lofty, 1989; Guiraud and Maurin, 1992; Janssen et al., 1995; van der Meer and Cloetingh, 1993; Pique and Laville, 1996; Wilson and Guiraud, 1998; Stampfli et al., 2001; Ziegler et al., 2001; Guiraud et al., 2001; Guiraud et al., 2005; Hallat, 2002; Craig et al., 2008; Bosworth et al., 2008), only few details are provided, thus the structural geometry and the sequence stratigraphy of the rift are poorly known and debated. Samples from Amal Formation of pre-Upper Cretaceous age have been studied from well Al-96 (Maragh Trough) south east of the Ajdabiya Trough, yielded a rich palynomorph assemblage of Middle Triassic age (Thusu and Vigran, 1985). Rifting is believed to have ended during the Late Cretaceous, with several thousand meters of sediments deposited during the Cenozoic, mainly post-rift phase. It is postulated that the aftermath of Cretaceous rifting in Sirt Basin was interrupted by contractional (inversion) and strike slip events (Anketell, 1996; Guiraud et al., 2001; Bosworth et al., 2008; Capitanio et al., 2009).

5.8.1.1 Pre-rift Unite (Palaeozoic – Early Mesozoic?)

This represents the acoustic basement and cannot be established as a united age. Parts may be made up of undifferentiated extrusive and intrusive rocks to Cambro-Ordovician quartzite sandstone as suggested by (e.g. Ambrose, 2000 and references therein). A pre-rift sedimentary unite is fragmentary and was mainly identified below Mesozoic grabens in the Ajdabiya Trough. We suggest that the Cambro-Ordovician represents the top of the Palaeozoic pre-rift sediments featured with reflector in moderate-strong, continuous amplitude, locally diffractive. Internally, the pre-rift sedimentary unit is characterized by parallel-subparallel,

intermediate-high continuous reflections with variable amplitudes. Figure 5.45, shows this unit in the upside part of a rotated block, with the uppermost part being extended along spur of basement high. A distinct Late Paleozoic (Hercynian) unconformity separates this unit from the sediments on top. The pre-rift strata seem to be deformed with series of fault related folds and may extend to Lower Triassic and include silisilclastics deposited in fluvial or shallow marine environment (e.g. Baird et al., 1996; Thusu 1996). Nonetheless, on the basis of the information accessible it is possible to characterize a general E-W drifting shoreline which denote the edge of a wide and low relief marine shelf, which thought to have prograded northwards through the Cambro-Ordovician.

5.8.1.2 Syn-rift Unite (Jurassic – Early Cretaceous)

In the Cenomanian, marine transgression in Libya was controlled by the sharp horst and graben relief, which was preserved after the collapse of the Sirt Arch (Finetti, 1982; Hallett and El-Ghoul, 1996 Hallet, 2002). Syn-rift and inter-rift strata show large variations in sedimentary architecture as a result of temporal and spatial variations in tectonic deformation and subsidence. The syn-rift unit is widespread in the Ajdabiya Trough and fills grabens and/or half-grabens. The unit is characterized by chaotic (locally subparallel) and discontinuous-moderate continuous reflectors with low frequency and various intensities (Figure 5.45), indicating variable cycles of rift-filling sediments.

The syn-rift infill is mixed of both marine and non-marine sediments and consists of basal continental to marine siliciclastics of Triassic, Late Jurassic (Pre Upper Cretaceous), and Cretaceous age, as well as marine carbonates and evaporites of Late Cretaceous and Tertiary age (Van der Meer and Cloetingh, 1996; Hallett, 2002; Boote, 2009). The main syn-rift deposition occurred in the early Cretaceous when the pre-Upper Cretaceous, Nubian (Sarir) Sandstone accumulated in rift troughs and topographic lows on the irregular pre-Cretaceous topographic surface and passing into a Late Paleozoic quartzitic facies in the northern Ajdabiyah Trough.

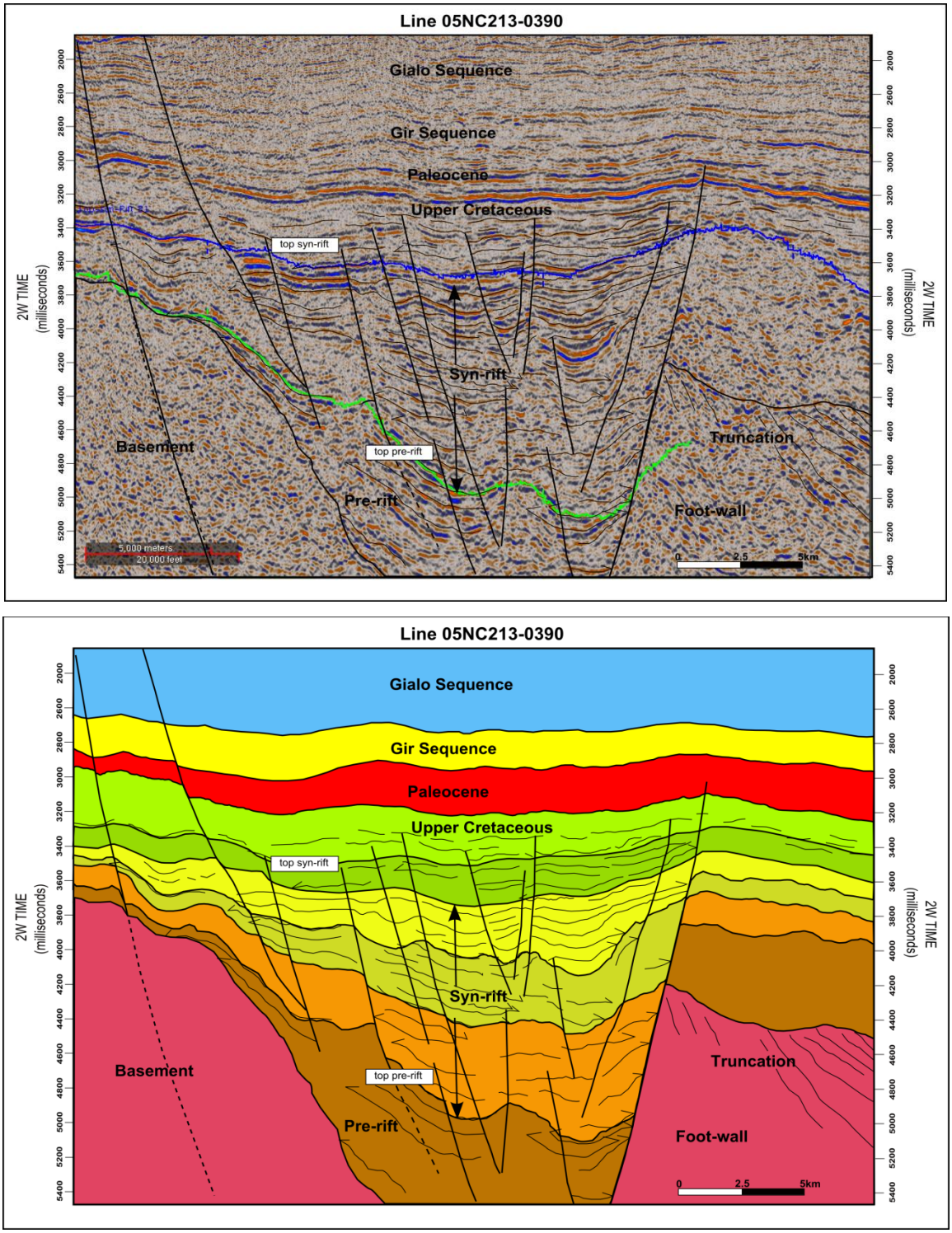

Figure 5.45: Seismic cross-section (05NC213-0390) above and interprteted copy below, illustrating syn-rift seismic stratigraphic architecture in the Ajdabiya Trough. The section show schematic multiphased syn-rift deposition on a tilted block at southwest. At the uplifted footwall a hiatus occurs, which is synchronous with deposition of the Rift Initiation (or Rift Climax) depositional sequences on the subsiding hanging wall. In the central part of the graben, strata above Late Paleozoic strata (Hyrcenian Unconformity) are sometimes parallel, defining a disconformity.

In the deep rift grabens, Cretaceous deeper water mudstones and shales may have been deposited under restricted conditions that are favourable for petroleum source rock generation (Sirt Shale). The syn-rift sequence shows moderate-strong amplitudes and patchy-continuous reflections, locally truncated underneath and onlaped against fault scarps or bald basement highs. The Upper part of the sequence is a regional (Upper Cretaceous) unconformity and represents the syn-rift to post-rift transition. Thusu, 1996 recommended that the sequence was deposited in an incipient rift, denoting the start of the syn-rift stage in the Sirt Basin. In the Ajdabiya Trough area, Cambro-Ordovician rocks subcrop the Late Paleozoic (Hercynian) unconformity over a large portion of the trough with Precambrian basement subcropping in the south. Evidence from the eastern Sirt Embayment (Hallett (2002), shows the presence of Triassic and Jurassic rocks forming the oldest part of the syn-rift sequence, and the same conditions may be present in the Ajdabiya Trough. Well Q1-31, located on the transition zone between the Ajdabiya Trough and the Amal Platform, penetrated some 600 m Lower Cretaceous marine sandstones and shales accumulated within graben and/or half-graben structures bounded by segmented faults (chapter 7). Continued rifting within the Ajdabiya Trough resulted in completely linked master faults and increased rotation of the associated half-grabens.

This led to a dramatic increase in subsidence of the trough depocentre and transgression of the slopes. The marine transgression may have caused reworking of previously deposited sands across structural highs as they subsided and became submerged. Biostratigraphical analyses indicate reworking of Lower Paleocene and Late Cretaceous material within the lower part of the Upper Paleocene (Harash Formation) (Spring and Hansen, 1998). Finally, the rift topography was filled with reworked coarse-grained, syn-rift successions and became capped by Upper Cretaceous marine mudstones. Post-rift thermal cooling continued in the latest Cretaceous and led to differential subsidence within the Ajdabiya Trough marked by shift in the early Cenozoic depocentres towards the rift axis.

5.8.2 Cenozoic Sequences

In this chapter stratigraphic sequences are identified by detailed seismic section analysis crossing the dip and the strike of the structures within the Ajdabiya Trough. A seismic stratigraphic scheme was developed within the trough by mapping and comparison of

reflection geometries and lapout facies observed on seismic sections and correlated with well data. The Ajdabiya Trough sequence stratigraphic framework consists of six sequences that correlate to sea-level changes during the Cenozoic period. Rift related sequences are also observed within Cretaceous and older strata, these could have an influence on the development of the identified sequences. Basement relief within the trough could also play a significant role in the development of the stratigraphic architecture of the trough.

Sea level cycles and sediment supply are the primary controls on the development of accommodation space and stratigraphic sequences within the Ajdabiya Trough. The recognized stratigraphic architecture of the trough is largely influenced by sea level changes and minimal tectonic effects during the Cenozoic, while observed progradation along the trough margin is attributed to increasing sedimentation rates presumably under control of main basin bounding faults (e.g. Baird et al., 1996). The sequence stratigraphic interpretation show significant development of prograding clinoform system along the shelf margin in the Paleocene, Early and Middle Eocene sequences, suggesting high sediment supply at the time of the deposition. Bending in the geometry of the margin (rimmed model) is likely the result of primary deposition rather than structural deformation.

System tracts are identified within the Paleocene to Eocene sequences. Progradational clinforms are interpreted as low stand systems tracts (LST) or low stand wedges during the Paleocene and Eocene. During the Early to Middle Eocene, the stratigraphic sequences are characterized with mass transport deposits in deep water and erosional unconformities in shallow water result during sea level low stands and characterized by channel incision. Channel flow generally bypassed the upper to middle slope region, resulting in debris flow turbidite deposits accumulating in lowstand wedges. While retrograding facies observed during late Paleocene and at the end of Early Eocene are considered to be part from transgressive system tracts (TST). The mass transport complexes are common along the slopes of the Eocene carbonate systems; they are especially frequent in the Middle Eocene Gialo Formation and interpreted as lowstand wedges (e.g. Baask et al., 2014). Early to Middle Eocene in the southern part of the Ajdabiya Trough was dominantly represented by mass transport successions towards the depocentre of the trough.

Type one sequence boundary corresponds to the boundary between Lower Eocene and Middle Eocene sediments and characterized with channel incision owing to possible sub areal

erosion. This boundary could be placed to the base of the mass transport deposits or the base of channel fill deposits based on the type of the setting.

Highstand system tracts (HST) are generally recognized on the outer shelf and slope as clinoform packages with reflection geometries indicating aggradation followed by slow then rapid basinward progradation determined from the relative thickness of individual clinoforms. Periods of transgression and sea level high stands are marked by shelf margin aggradaing and progradaing parasequences during the Middle Eocene (Gialo Sequence). Parasequences are indicated by short-lived sea level rises and falls developed within the Eocene sequences. This latter time period is marked by high sedimentation rates, minor incision, and lower slope infilling and rapid progradation of the shelf break. These deposits are the result of sea level lowering and incision in the outer shelf providing sediment conduits to the deep water regions. These deposits are likely bound by marine sediments forming possible stratigraphic traps during periods of transgression and highstand.

In the central Ajdabiya Trough, the overall retrogradational stacking pattern recognized within Paleocene and Eocene regressive parasequences provides evidence of a longer-term increase of accommodation space, probably reflecting the regional subsidence regime that shaped the study area. This is consistent with the general increase in thickness of depocentres from Paleocene to Eocene. However the Paleocene thickness has a reduced thickness at the depocentre compared to the Eocence sequence owing to minor thickness attained during deposition and/or high rates of erosion following the deposition. Possible causes would be a decreasing rate of regional subsidence, or drop in sea level. A static conditions of the sea level could be also influenced the deposition of the Paleocene sediments in different parts within the trough. The Gialo turbidite system within the Ajdabiya Trough is characterized with variable depocentres of different areal extent and lobe facies architecture (e.g. Baaske et al., 2014). Seismic data revealed that the sediment flow direction is estimated from northeast to southwest by channel-like features (e.g. submarine canyon and channel-levee geometry). The basin geography with the narrow shelf and steep slope gradient with high tectonic subsidence rate promoted the canyon formation. Relatively wider shelf and gentle slope gradient dominated a line type of source for the thick succession of mass flow and turbidity current deposits. The present-day shelf of the Ajdabiya Trough shows a system of canyons eroding down into the trough depocentre, and transporting sediments onto the slope where they are

deposited as turbidite fans. The Gialo turbidite system seems to be controlled by interaction of regional tectonics, and eustatic fluctuations in the Middle Eocene.

The tectonic control played significant role on sediment supply and local sea-level fluctuations (Bruhn and Walker, 1995). Along the north-eastern shelf the incised channel system developed during the Middle Eocene is presumably developed in response to tectonism formed by southeast to northwest trending basement-involved normal faults. The changes in thickness of the sediments are also controlled by the faulting and by a high basin subsidence rates. The facies diversity within the trough is linked to the basin tectonism and possible sediment input created during extensional periods. Carbonates developed along rimed platforms at the southernmost part of the Ajdabiya Trough, were influenced by the NW-SE structural framework (Spring and Hansen, 1998). On the contrary during the transition to possible compressional regime, the facies are mainly mud dominated due to changes in topographic gradient of the source areas.

Continues carbonate production during the Late – Middle Eocene caused a continuous progradation of the carbonate system towards the steep shelf.

The repeated cycles of limestone and marl dominated intervals in the shelf setting is indicating that the growth profile of the carbonate system along the eastern shelf of the trough is very sensitive to fluctuation in the sea level during the Middle Eocene which subsequently characterized by a stable conditions and decelerating in the tectonic subsidence due to low activity induced by the basement faults. The absence of high resolution biostratigraphic data did not allow calibrating the chronostratigraphic position of the cycles.

The definition of the carbonate platform margins in the Ajdabiya Trough much more subtle and gently sloping in the Late Oligocene to Early Miocene, compared to the earlier Tertiary sequences. This is the results of the Early to Late Oligocene sediments significantly infilling the trough thereby reducing the gradient of the margins. The large thickness of Late Oligocene in the Ajdabiya Trough represents a major phase of infilling of a basin that had (in the Cenozoic) become over steepened by preferential development of a carbonate system on its flanks. During the Late Miocene channel system associated with high sedimentation interpreted to result from periods of rising sea level and transgressive phases culminated in the formation of a maximum flooding surface.

CHAPTER 6: QUANTIFYING SUBSIDENCE HISTORY DURING MESOZOIC TO CENOZOIC

6.1 Introduction

Sedimentary basins form in response to subsidence of the earth's crust (Allen and Allen 2005). Basement subsidence is largely controlled by tectonic process amplified by sediment and water loads. Accommodation space in sedimentary basins produced by an interaction of global and regional tectonism and sea level fluctuations (Jervey, 1988). Eustacy is the change of the elevation of the sea level on a world wide basis relative to the stationary datum at the centre of the earth. During subsidence, accommodation space is controlled by eustatic sea level changes on local and regional scales (Bond and Kominz, 1984). Sediment accumulation formed by the increasing of the accommodation space will results in compaction of the earlier deposited sediments with significant downward movement of the base (Reynolds et al., 1991). Basin geometries formed within different tectonic settings are mainly controlled by different subsidence mechanisms including tectonic and thermal contributions (post-rift subsidence). Tectonic subsidence (TS) measures the tectonically controlled vertical movement of a basin which account for the difference between the elevation of a pre-rift continental crust and present day, sediment-unloaded, basement depth in a sedimentary basin (Sawyer, 1985).

With the advent of backstripping algorithms (Bond and Kominz, 1984; Steckler and Watts, 1978) in the late 1970s' and early 1980s', a phase of basin analysis commenced that aimed at backward modelling by reconstructing the tectonic basin subsidence from sedimentary sequences (Cloetingh et al., 2013). The technique of backstripping is commonly applied to extensional basins to determine the magnitude of lithospheric thinning from the observed post-rift subsidence (Sclater and Christie, 1980). Stratigraphic units within a sediment column are removed progressively from top downwards. The remaining sediments are decompacted and isostatically restored using Airy (1855) local loading model for isostatic compensation. Thus, the restoration accounts for new load conditions, paleo water depth, and the isostatic response to the change in loads.

Sediment backstripping can be performed in one of two ways. At a point location (1-D), commonly utilized to derive relatively complete tectonic subsidence curves at boreholes,

where there is detailed information on the stratigraphy and paleoenvironmental history of the area (Watts & Steckler, 1979). 1- D backstripping assumes that the sediment loads are locally compensated (Airy isostasy). Otherwise, sediment backstripping can be performed along 2D profile or using grids of 3D data. In these two cases, a regional model of flexural isostatic compensation is used. Compared to the 1D Airy backstripping, these methods provide more efficient analysis to the basin subsidence history on large scales (e.g. Watts & Torne, 1992; Stewart et al., 2000), with lack of details on basin stratigraphy compared with the 1D well backstripping.

Sedimentation and subsidence curves obtained from backstripping analysis can provide clues to nature of basin formation (Sleep, 1971). In order to estimate the subsidence history of any sedimentary basin, using this technique, present-day stratigraphic thicknesses must first be corrected to account for the loss of porosity due to loading from sediment and water above. Any study of subsidence at a sedimentary basin must consider the effects of each factor on the stratigraphy record. The analysis begins with data reduction to initial depositional conditions (decompacted thickness) as a main factor in the subsidence calculations.

Within extensional basins, subsidence is quantified using subsidence curves that typically show a clear distinction between syn-rift and post-rift periods (Cloetingh et al., 2013). Post-rift subsidence is mainly characterised with an exponential curve with decreasing subsidence rates and representing a combination of thermal equilibration and lithosphere flexure (Watts et al., 1982). 2D or 3D Modelling of flexure produced by sediment loading, tectonic loading and water loading is then carried out at chronostratigraphically significant intervals. Therefore, it is possible to assess temporal changes in the rheological response of the lithospher underlying sedimentary basin (Turcotte and Schubert, 1982).

The information used in this chapter is based on data published in the individual well completion reports and from revised stratigraphic reports (e.g. Barr and Weegar, 1972; Gumati and Schamel, 1988; Hallett, 2002). Paleontological data and correlation with outcrops were used for age and paleowater depth determination (e.g. Eliagoubi and Powell, 1980; Megerisi and Mamgain 1980; Ashour, 1996; Barbieri 1996; El Sogher 1996; Muftah 1996; Tmalla, 1996). The aim of this chapter is to review 1D Airy-isostatic backstripping technique and provide analysis of basin subsidence and extension factors (β values) in order to define appropriately the Cenozoic tectonic events in Ajdabiya Trough area with a particular

emphasis on the Late Cretaceous - Paleogene deformation pulses and placing them in the frame of the geodynamic evolution of the Sirt Basin. The analysis is based on set of petroleum wells obtained from areas close to the trough boundaries. Seismic and lithological techniques were also used. The wells in the analysis were drilled over four decades, so there is a possibility that dataset are inconsistent between wells. The wells are drilled by different operators each of them using different symbols and abbreviations assigned to different formation tops and ages which should be considered during the analysis. Some formations ages in the area are debated; for instance the Nubian formation is considered to be either pre-rift or syn-rift strata with different time scale within the Early Cretaceous series. All of these issues may give rise to uncertenites within the interpretations.

6.1.1 Airy Isostasy and Flexure

Isostasy is the term used to describe a condition to which the Earth's crust and upper mantle tend, in the absence of disturbing forces (Watts, 2001). Disturbances caused by tectonic extension, sedimentation processes and volcanism in any sedimentary basin, give rise to subsidence as the state of equilibrium between the earth's crust and the underlying mantle is achieved by the isostatic compensation of the subsurface structures. Geophysical data, such as seismic and potential field (gravity & magnetic), however, suggest that the Earth's outermost layers generally adjust to these disturbances (Watts, 2001).

Isostasy has implications in basin development where thickness or density of the crust is changed. This can happen in a number of ways, including stretching of the lithosphere, removal of the crust by erosion or tectonic processes, emplacement of denser material (e.g. dykes, thrust ophiolites), or filling a depression with denser material (e.g. replace water with sediment).

Airy model hypothesis (Figure 6.1) is based on assumptions that consider compensation to occur on a local scale as the compensation of the surface topography occurs directly below the subsurface. In any area, if the lithosphere rigidity is extended to a finite strength, then the compensation of topography will occur on a broad scale as it is supported by lateral strength of the plate and the vertical load.

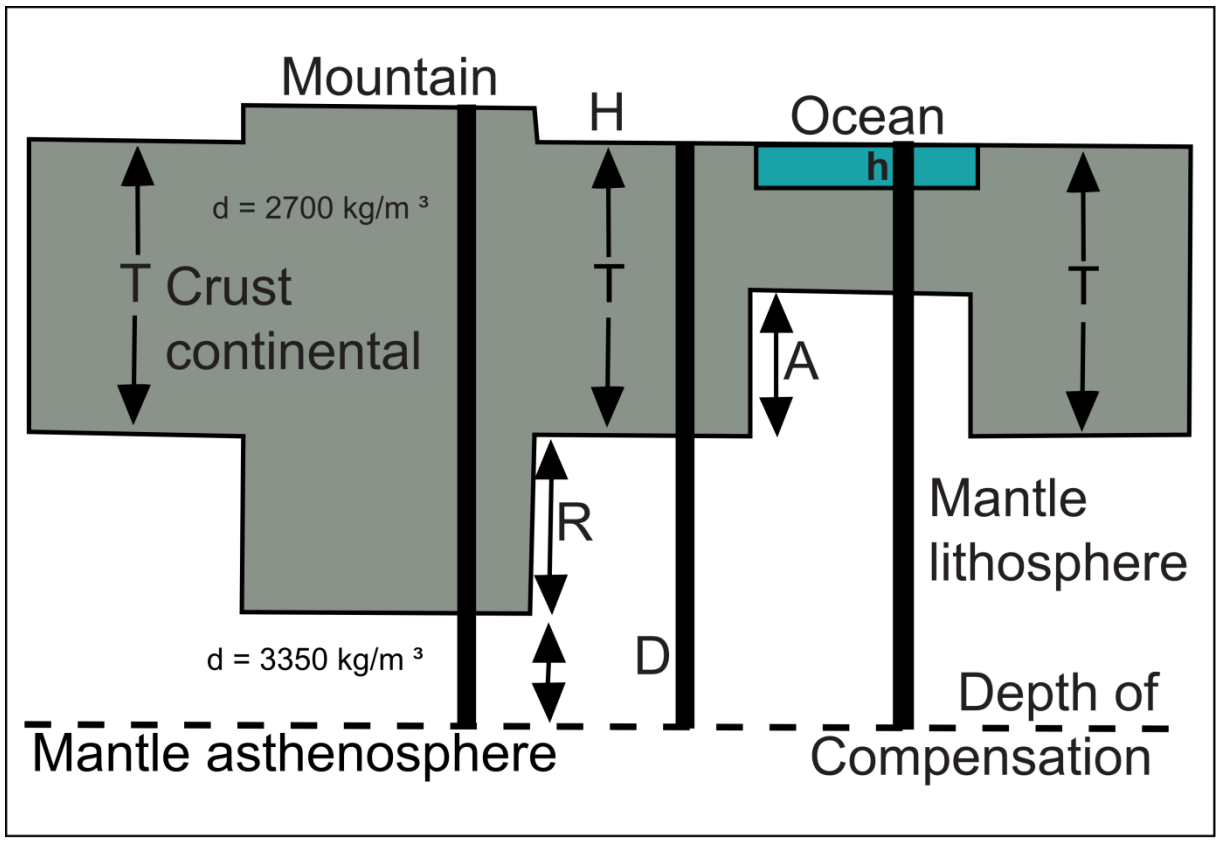

Figure 6.1: Airy mechanism of isostatic compensation. H, height of mountain above sea level; h, depth of water; T, normal thickness of crust; R, thickness of root; A, thickness of antiroot; D, depth of compensation below root.

The isostatic compensation under column 1= $p_c\mathrm{H} + p_cT + p_cR + p_mD$

The isostatic compensation under column 2= $p_cT + p_cR + p_mD$

The isostatic compensation under column 3= $p_wh + p_c(T - (h + A)) + p_m(R + D)$

The isostatic equilibrium 4= $p_c\mathrm{H} + p_cT + p_cR + p_mD = p_cT + p_cR + p_mD = p_wh + p_c(T - (h + A)) + p_m(R + D)$

Lithospheric flexure results in long wavelength topography with a distinct deflection profile caused by the application of an external force system (Allen and Allen, 2005). The downward deflection of the lithosphere is accompanied by a flanking upwarp or bulge (Figure 6.2). The degree to which elastic plate models reproduce lithospheric flexure is remarkable in view of the complex temperature, pressure and compositional dependence of strength and flow expected of the lithosphere and is an indication of the poor sensitivity of plate bending geometry to details of rheology, however, the lithosphere has a finite strength, therefore rigidity (Watts et. al, 1975).

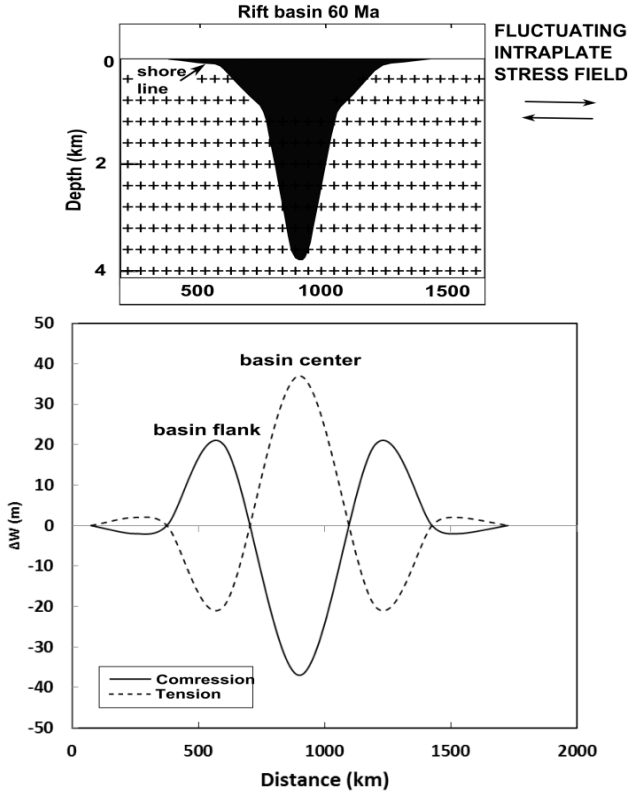

Figure 6.2: Flexural deflections at a sedimentary basin induced by changes in the intraplate stress field. Uplift is positive, subsidence is negative. In rift basin lasted for period of 60 Ma, sediments flexurally load an elastic plate. The flank and the basin centre are either uplift or subside due to change in deflections caused by changes in stress regime. The shape and magnitude of these stress-induced deflections evolve through time not only because of the increasing load, but also because of changes in the thermal structure of the lithosphere. (ΔW) in the lower panel is the vertical deflection produced by loading. re-draw from (Van Der Meer and Cloetingh, 1993).

6.2 Previous Work

A number of publications about the formation and the geological evolution of the Sirt Basin have been published. Subsidence history architecture in the Sirt Basin has been considered by a previous researchers and investigators (Gumati and Kanes, 1985; van der Meer and Cloetingh, 1993; Baird et al., 1996; Schroeter, 1996; Abadi et al., 2008, and others), using wells mainly drilled on structural highs. Based on that, it was difficult to establish and resolve the nature of the subsidence in details within the deepest areas in Sirt Basin such as the Ajdabiya Trough, because of lack of enough well data coverage and sufficient penetration; consequently it was difficult to correlate with examples from other areas.

In this chapter, I present a detailed quantification of subsidence in the Ajdabiya Trough area using wells and correlations from 2D seismic data. Subsidence analysis allows a quantitative reconstruction of basin evolution, sediment influx and deposition, and gives hints to the timing and types of tectonic driving forces within the area.

In the Sirt Basin (Figure 6.3) rifting was initiated during the Cretaceous (Goudarzi, 1981), reactivating pre-existing Paleozoic tectonic lineaments (Conant and Goudarzi, 1967; Burke and Dewey, 1974), and possibly triggered by lithosphere–plume interaction (Van Houten, 1983). Major subsidence is recorded during the Late Cretaceous - Eocene, over the entire basin (Gumati and Nairn, 1991). Pattern of tectonic subsidence observed in Sirt Bassin during the period from Cenomanian – Early Miocene can be characterized by a low subsidence rates from Cenomanian – Campanian reflecting the pre-rift period, the rapid subsidence period (Late Campanian – Paleocene) which reflects the actual rifting period during isostatic response of the lithosphere to crustal thinning (Van Der Meer and Cloetingh, 1993). The early Cretaceous stretching was followed by a Cenozoic thermal subsidence phase, which was especially severe in the Ajdabiya Trough. Tectonic subsidence is decelerating in Sirt Basin during the Cenozoic period predominantly characterized by post-rift phase driven by thermal re-equilibration modulated by plate interaction (Van Der Meer and Cloetingh, 1993). Within the basin a thick Cenozoic deposit loads the crust causing continues subsidence of the main basin depocentres.

It is observed that the general Cenozoic stratigraphic pattern in North African basins is that of a transition from lower Cenozoic carbonate strata to upper Cenozoic siliciclastic strata which coincides with a long-term eustatic fall in sea level since the middle Cretaceous and with a global climate transition from a Late Cretaceous – Early Eocene (Swezey, 2009).

Due to change in plate motions, compression and uplift occurred during the Early Eocene (Jansen et al., 1995), followed by an increase of subsidence rate during the Middle – Late Eocene and decelerating rates of tectonic subsidence during the Oligocene through Early Miocene (van der Meer and Cloetingh, 1996). The observed uplift in Early Eocene could have resulted from an increase of the level of horizontal intraplate compression; the subsequent Late Eocene subsidence can be explained by a sudden stress release or intraplate extension yielding isostatic rebound of the lithosphere. (van der Meer and Cloetingh, 1996). Differential fault activity on subsiding grabens and uplifting platforms was followed by a Paleocene –

Eocene widespread regional subsidence phase (Gumati and Nairn, 1991; van der Meer and Cloetingh, 1993; Abadi et al., 2008). Subsidence and deepening of the entire Sirt Basin was accompanied by localized uplift of the western platforms (van der Meer and Cloetingh, 1993; Bosworth et al., 2008), possibly attributed to a strike slip component (Anketell, 1996). Following extension, the Sirt Basin underwent compression during Middle – Late Eocene tilting the basin northward. This lead to abrupt subsidence in the north and uplift of the basin southern shoulders, followed by minor regional subsidence (van der Meer and Cloetingh, 1993).

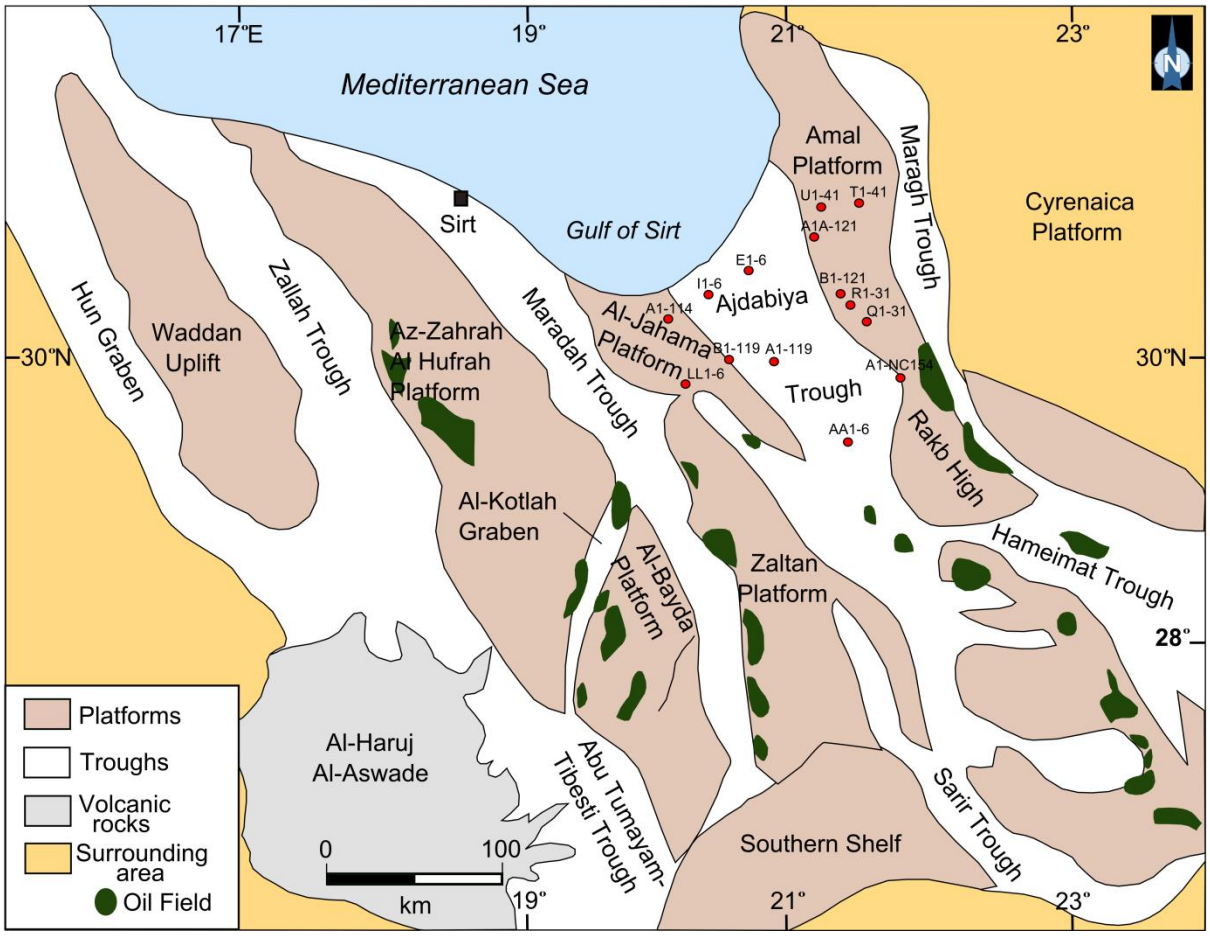

Figure 6.3: Structural elements of the Sirt Basin with location of the Ajdabiya Trough. Wells used in the subsidence calculations are highlighted in red circles. Map modified from Libyan structural map of Taleb and Mesughi 1990 and the modified map of Gibbs (2004) by Fiduck (2009). Oil and gas fields are drawn from Burwood et al., (2003).

In Ajdabiya Trough area a complex normal fault pattern evolved due to the extensional basin formation, during the Early Cretaceous and fault re-activation during Paleocene – Eocene

with possible sinistral and dextral strike-slip systems during Cenozoic (e.g. Baird et al., 1996; Anketell, 1996; El Arnauti et al., 2008) This could play important role in the tectonic segmentation of the basin fill and control the area tectonic subsidence. During the Eocene, subsidence in the Ajdabiya Trough was characterised by NE-ward tilting of a single elongated depression with no fault activity observed (Abadi et al., 2008). This observation indicates that sediment loading and thermal relaxation played an important role in the subsidence process. The absence of major faulting during post-rift stage may also suggest a component of lithospheric folding (Cloetingh et al., 1999), which may be related to the mantle upwelling as evidenced from large areas in Europe (Cloetingh and Van Wees, 2005).

The Ajdabiya Trough (Figure 6.4) records the largest continuous subsidence in the whole Sirt rift, thus offering important estimates of its stretching history (Gumati and Nairn, 1991; Abadi et al., 2008). However, the timing of tectonic events and the influence of tectonics upon sedimentation in the Ajdabiya Trough are not well understood.

Publications focusing on structural evolution of Ajdabyia Trough are limited, although several regional studies are available (El-Arnauti and Shelmani 1988; Gumati and Nairn, 1991; Skuce, 1994; Anketell, 1996; El-Arnauti et al., 2008).

Previous seismic studies have focused on the local near-surface features such as thickness of surficial sediments and structures mainly located on the rift flanks that are of importance in hydrocarbon exploration.

Gravity and magnetic data have been used to map the general basin structures and, basement morphology (Libyan Gravity Compilation Project LPI, 2001).

This chapter will present results of analysis of well data and industry seismic lines across the Ajdabiya Trough. After identifying the key features along the backstripped wells, the analysis will focus on the subsidence patterns, subsequently we discuss the role of faulting in the early post-rift subsidence history of the trough.

As a result of lack of seismic interpretations in the study of Abadi et al., 2008 their subsidence analysis did not provide details on intrabasin-scale features or on the roles of faulting in controlling the subsidence within the Sirt Basin. Their study area extended to covere the whole of the Sirt Basin, but few wells are used within the Ajdabiya Trough domain.

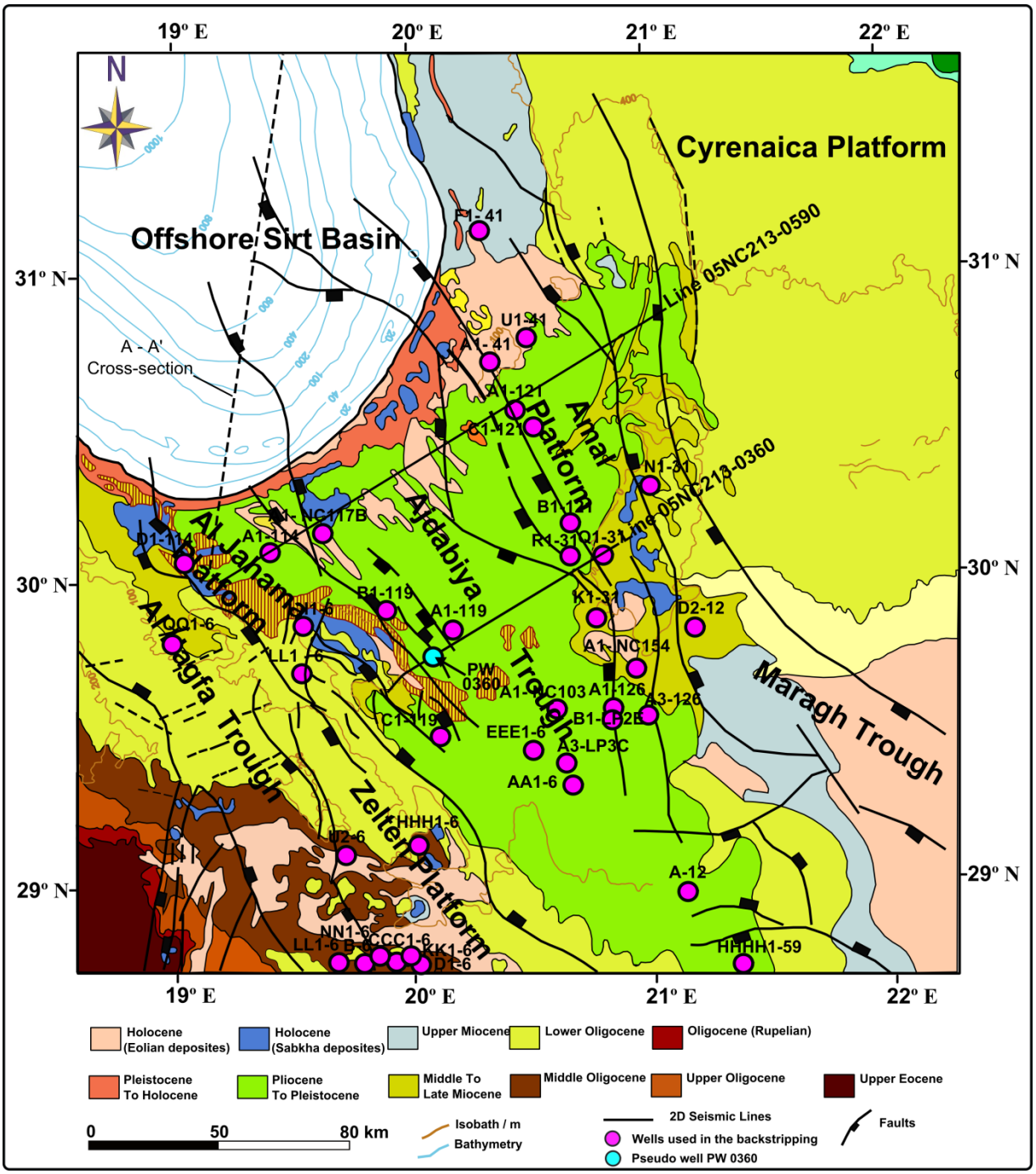

Figure 6.4: Map of Ajdabiya Trough showing surface geology and tectonic features. Red circles are the locations of wells used in this study; blue circle is location of pseudo well. Figure 6.4 show the location of Ajdabiya Trough along the northeast periphery of Sirt Basin. The trough is bounded on the north by the offshore area, to the east by the Amal Platform and Cyrenaica Platform, to the south by the southern shelf, and to the west by both Al Jahama and Zelten Platforms. The map is re-draw from the Geologic Map of Libya which compiled by the Industrial Research Centre of Libya (IRC) in 1985.

6.3 Influence of Deeper Structure on Late Mesozoic – Cenozoic Tectonics

It is postulated that the origin of Sirt Basin was related to the drift of mantle plume across the Cameroon Hotspot listed for about 150 Ma (Morgan 1983) (Figure 6.5). Crustal doming and thinning with fracturing of the thinned and weakened lithosphere occurred along the North African Margin associated with development of Cretaceous triple branching grabens system located along reactivated Pan-African structures (Dautria & Lesquer, 1989). Van Houten (1993) also interpreted fracturing in the Sirt Basin of Libya as a response to extension above a mantle plume during the Jurassic and Early Cretaceous. Conversely Anketell (1996) inferred that the Sirt Basin developed in response to strike-slip deformation along the North African Margin.

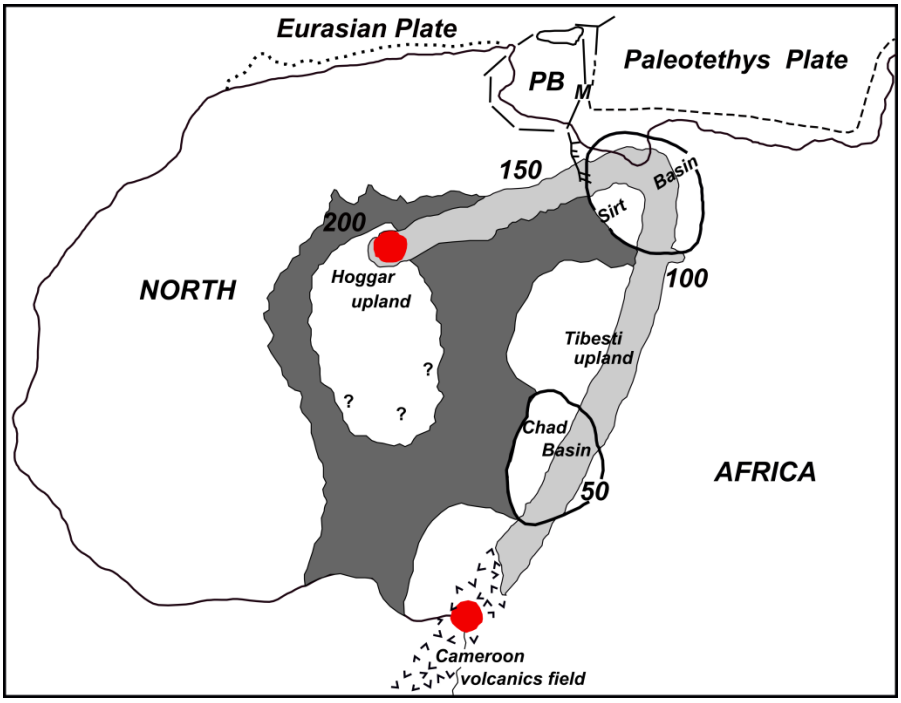

Figure 6.5: Hypothetical traverse of Cameroon fixed mantle hotspot based on reconstructed hotspot tracks involving Atlantic oceanic crust. Numbers = age in millions of years. Light grey path reflects drift of African plate westward until about 125 m.y. ago, then a shift to northerly drift. Dark grey outlines Late Cretaceous and early Cenozoic trans-Saharan seaways. PB = Pelagian cratonic block; M = Malta Escarpment lineament. Hoggar and Tibesti uplands provide geographic reference. At top, three lithospheric plates are assembled in their early Mesozoic position around a triple point, after Laubscher and Bernoulli (1977). Redrawn from Van Houten, 1983.

Large areas of the African lithospheric plate underwent crustal extension during the Jurassic to Early Tertiary (Beloussove, 1969; Burke and Whiteman, 1973), with a complex rift system extending from south-eastern Kenya to Libya during much of this time (Fairhead, 1988; Lambiase, 1989).

In Early Cretaceous time, the Sirt Basin was situated along major rift zone, trending NW-SE (Van Houten, 1993; Baird et al., 1996; Anketell, 1996; Hallett 2002).This major structural trend likely influenced the Mesozoic - Cenozoic tectonic development of the Ajdabiya Trough, as seen by Early Mesozoic extension (e.g. Baird et al., 1996; Anketell, 1996; Hallett 2002) that faulted the area into basins and highs along this inherited trend. This pattern was further emphasized by differential Cenozoic uplift and basin formation that contributed to the present structural style of the Ajdabiya Trough.

As mentioned above that the rifting in the Sirt Basin was characterized by a complex succession of major horsts and grabens, which have subsided at extremely variable times and rates (van der Meer and Cloetingh; 1996; Abadi et al., 2008). This mainly formed due to deep lithospheric attenuation and extension which is distributed in pulses in the corresponding upper crustal layers. Therefore, the amount of local subsidence measured at different areas within the basin shows considerable variability, as does the amount of crustal extension (β) factor derived from syn-rift and post-rift observed subsidence (Gumati and Kanes, 1985; van der Meer and Cloetingh, 1993; Abadi et al., 2008). The Ajdabiya Trough has a constant rate of post-rift tectonic subsidence unlike the exponentially decreasing rate observed for the other parts in Sirt Basin, which is more consistent with the subsidence predictions outlined by different investigators. This observation suggests that the basic mechanism for post-rift subsidence (i.e. thermal relaxation) cannot solely explain the pattern of subsidence of the deep part of the basin.

6.4 Subsidence analysis

6.4.1 Method and constraints

The definition of the Mesozoic - Cenozoic evolution within the Ajdabiya Trough has been aided by subsidence analysis, derived from the interpretation of 2D seismic lines and wells. To quantify vertical movements and associated sedimentation rates, seismic and wells have

been backstripped, illustrating key features of the post-rift tectonic evolution of the Ajdabiya Trough. The subsidence analysis is based on good coverage of 2D seismic and 37 wells (Table 6.1) are used to produce subsidence maps and 5 of them mainly located along structural highs where water depths are <100 m are used to produce subsidence curves.

It is postulated that, more than 3000 meters of sediments have been drilled in mainly post-rift sequence (Hallett 2002).

Well Name	TD (m)	Formation	Location
A1-12	3033	Nubian	Rakb High
A1-41	4180	U.C.	Soluqe Depression
A1-114	2900	Gargaf. Fm.	Al Jahama Platform
A1-119	4145	U.C. Tagrift	Central Ajdabiya Trough
A1-121	2590	L. Eocene	NE Ajdabiya Trough
A1A-121	3500	Gargaf. Fm.	NE Ajdabiya Trough
A1-126	3420	Basement	Zelten Platform
A1-NC103	3400	Paleocene	South Ajdabiya Trough
A1-NC117B	2823	Gargaf. Fm.	North Ajdabiya Trough
A1-NC154	4348	Maragh. Fm.	Rakb High
A3-126	3225	Nubian. Fm.	Zelten Platform
A3-LP3C	3450	Paleocene	East Ajdabiya Trough
B1-6	2674	Nubian. Fm.	Zelten Platform
B1-121	3408	Gargaf. Fm.	Near Amal Platform
B1-119	3308	Gargaf. Fm.	NW Ajdabiya Trough
B1-LP2E	3000	Paleocene	SE Ajdabiya Trough
C1-119	3670	Paleocene	West Ajdabiya Trough
C1-121	3780	Gargaf. Fm.	NE Ajdabiya Trough
CCC1-6	4600	U.C.	Zelten Platform
D1-6	3749	Paleocene	Zelten Platform
D2-12	3004	U.C. Rakb C	Rakb High
D1-114	2740	Gargaf. Fm.	Al Jahama Platform
EEE1-6	2639	U.C.	Assumoud Ridge
F1-41	2000	Paleocene	Cyrenaica Pltform
HHH1-6	3383	Nubian	Zelten Platform
HHH1-59	3000	Pre. U.C.	South Ajdabiya Trough
I1-6	4604	Paleocene	North Ajdabiya Trough
K1-31	4115	U.C.	Amal Platform
KK1-6	4300	U.C.	Zelten Platform
LL1-6	3383	U.C.	Zelten Platform
N1-31	3116	Gargaf. Fm.	Amal Platform
NN1-6	4048	U.C.	Zelten Platform
Q1-31	4648	Silurian	Amal Platform
QQ1-6	3400	Paleocene	Al Jahama Platform
R1-31	3994	Maragh. Fm.	Amal Platform
U2-6	2926	Gargaf. Fm.	Al Jahama Platform
U1-41	5421	U.C.	Soluqe Depression

Table 6.1: Wells used to construct the subsidence maps and curves in the Ajdabiya Trough.

The majority of the wells have not penetrated the proposed syn-rift sequences related to period of likely Jurassic - Early Cretaceous rifting within the Sirt Basin.

Subsidence is calculated by restoring the sedimentary column to its initial thickness and density, using observed thickness, ages of horizons, lithologies and associated porosities and inferred paleowater depths (Eliagoubi and Powell, 1980; Megerisi and Mamgain, 1980; Ashour, 1996; Barbieri, 1996; El Sogher, 1996; Muftah, 1996; Tmalla, 1996), and information obtained from the Libyan Petroleum Institute (LPI), for the wells B1-12, C1-12, and EE1-6, (Dr. Ammar Gamudi, personal communications). The density and the porosity were obtained from well logs and published works. Sample from this data is outlined in Table (6.2) obtained from subsidence analysis on Sirt Basin by van der Meer and Cloetingh (1996).

		Maximum porosity depth curves					Minimum porosity depth curves				
Parameters	ρ	ϕ_1	c_1	ϕ_0	c_0	z_Q	ϕ_1	c_1	ϕ_0	c_0	z_Q
Unit	g/cm³	_	km⁻¹	_	km⁻¹	km	_	km⁻¹	_	km⁻¹	km
lithology											
sand	2.65	0.29	0.216	0.40	0.51	1.0	0.20	0.480	0.20	0.480	0.0
silt	2.68	0.42	0.375	0.60	1.00	0.5	0.25	0.325	0.25	0.325	0.0
shale	2.72	0.50	0.475	0.70	1.10	0.5	0.37	0.470	0.53	1.050	0.5
carbonate	2.71	0.52	0.442	0.78	1.33	0.5	0.20	0.580	0.20	0.580	0.0
halite	2.03	0.00	0.100	0.00	0.10	0.0	0.00	0.100	0.00	0.100	0.0
anhydrite	2.95	0.00	0.100	0.00	0.10	0.0	0.00	0.100	0.00	0.100	0.0

Table 6.2: Density values and porosity parameters (after Bond and Kominz, 1984), used for the backstripping calculations, ϕ**1** and ϕ**0** are the surface porosities (given as a fraction), **c1** and **c0** are the characteristic depth constants (in km⁻¹) for the deep and shallow porosity-depth relation, respectively; z_Q is the depth (in km) at which the deeper porosity-depth relation takes over from the shallow one; ρ is the grain density in g/cm3, of the corresponding lithology (obtained from. van der Meer and Cloetingh, 1996).

The analysis in this chapter is based (1) on subsidence analysis inferred from deep wells situated in the trough and on its shoulders and (2) on inspection of maps (Late Cretaceous, Paleocene, Eocene, Oligocene, and Miocene time structure and isochrons maps) resulting from wells and 2D seismic interpretation. The combination of these two approaches allows the quantification of the tectonic subsidence and determination of possible fault activity during the different Cenozoic time periods.

The syn-rift succession has not been encountered or entirely drilled in most of the wells. For this purpose a pseudo well derived from 2D seismic interpretation has been modelled.

The location of the pseudo-well is projected above a presumed syn-rift depocentre in order to evaluate the subsidence of the deepest part of the Ajdabiya Trough, which is not constrained by drilling yet. The stratigraphic record for the syn-rift deposits is justified for the Early Cretaceous stratigraphic record, which is marked by relatively continuous sedimentation, lacking clear deep erosional unconformities excluding the Upper Paleozoic (Cambro-Ordovician) unconformity, while the post-rift possibly show sedimentary gaps due to possible erosions during Oligocene and Miocene. In the western Sirt Basin, about 1000m of Tertiary post-rift sediments of Late Miocene age has been eroded as reported by Gumati and Schamel, 1988. Therefore, the calculated post-rift subsidence mainly represents minimum values at some localities.

One-dimensional modelling of burial history was performed on 5 wells and pseudo well using modelling worksheet written on excel file (see Appendixe). The wells were chosen because they were drilled to a depth that penetrated a significant part of the geologic section of interest within the study area. The ages of stratigraphic units and unconformities were obtained from well reports. In this study no heat flow data has been used in the calculation.

6.4.2 1-D Well Backstripping

1-D well backstripping uses information on the lithologies, ages and depths of deposition of the main stratigraphic units to determine the tectonic subsidence (TS) at a point location, assuming that both sediment and water loads are locally (i.e. Airy) compensated. The first step in the 1-D well backstripping is to decompact the sediment column and reconstruct its original thickness and density, at the time of deposition (Figure 6.6a and b).

To quantify the subsidence history of sedimentary basins using Airy (1D) backstripping technique, stratigraphic data is obtained from a well or a point sample of a cross-section. When applied to the post-rift sequence of an extensional basin the Airy backstripping process consists of the following steps: (1) A sediment-loaded basement subsidence curve is constructed from the initial stratigraphic data by removing each layer in the sequence in turn (2) The remaining underlying sediment units are then decompacted (Figure. 6.6, b).

(3) As each layer is removed, the new sediment surface is set to a prescribed datum by assuming a depth of deposition for each stratigraphic interval, and, if desired, correcting sea-

level for long-term eustatic changes (Figure 6.7). (4) The sediment-loaded subsidence curve is corrected to an equivalent water-loaded subsidence curve.

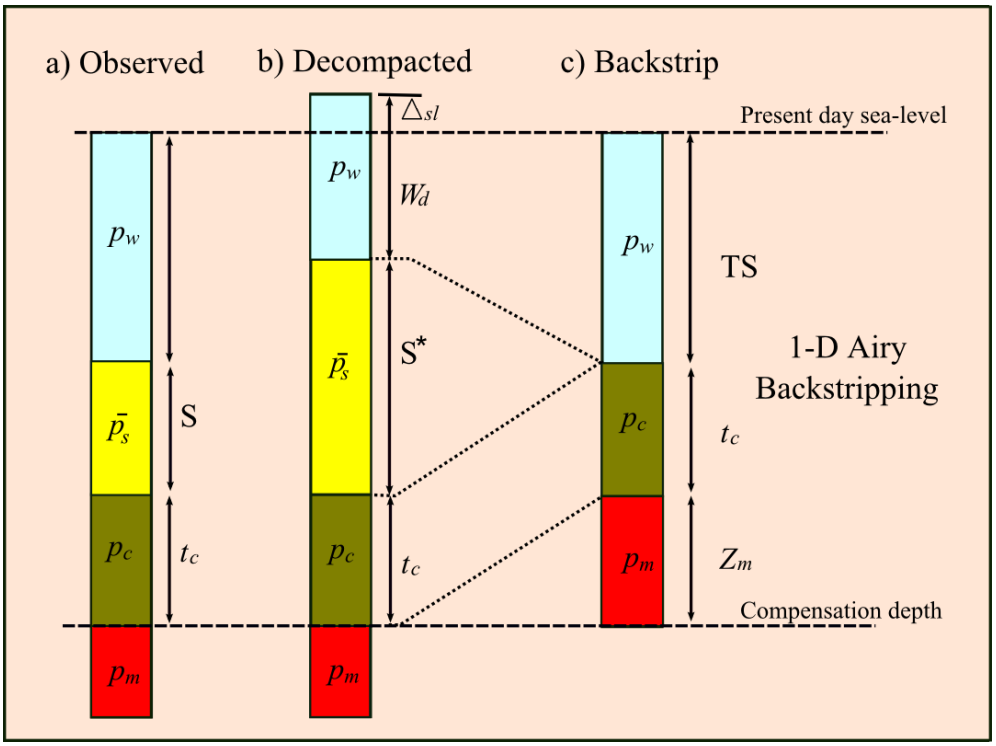

Figure 6.6: Rational of the 1-D backstripping technique: 1 layer example (modified from Watts (2001). Where (Δ_{sl}) is the mean sea-level height with respect to the present day. $\boldsymbol{p_m}$, $\boldsymbol{p_c}$, $\boldsymbol{p_w}$ are densities of mantle, crust and water respectively. $\dot{\rho}_s$ is the densities of the de-compacted sediment. ($\boldsymbol{S}^*$) and ($\boldsymbol{S}$) are decompacted and present day thicknesses. $\boldsymbol{t_c}$ is the thickness of the crust. $\boldsymbol{Z_m}$ is the compensation depth and ***Wd*** and ***TS*** are the water depth at the time of deposition and the recovered tectonic subsidence.

The loading correction from sediment to water is performed assuming 1D Airy (local) isostasy. This procedure produces the history of water-loaded basement driving subsidence. The water-loaded basement subsidence curve is usually compared with theoretical subsidence curves for specific values of a stretching factor, produced by the instantaneous stretching model of McKenzie (1978).

To correctly define subsidence rates, it is necessary to estimate how the sediment has changed thickness as a function of time and thus correct the present-day sediment thicknesses for effects of compaction. For this, exponential-type porosity-depth curves, such as those proposed by Bond & Kominz (1984), are commonly utilized. Alternatively, the porosity-depth relationships can be constrained from the porosity values measured in a particular well (e.g. Steckler & Watts, 1978), using different types of geophysical logs (e.g. sonic and density

logs). In this study, the principle of porosity calculation for each lithological unit corresponds to a mean value derived from maximum and minimum porosity depth curves (Skuce, 1994; van der Meer and Cloetingh, 1996) and based principally on the studies of Baldwin and Butler (1985) for shales; Sclater & Christie (1980) for sandstones; and Schmoker and Halley (1982) for carbonates. The tectonic subsidence is then calculated by removing the isostatic subsidence of the basement caused by the load of the sediments (Sclater & Christie, 1980; Bond & Kominz, 1984) using the assumption of the Airy isostasy.

In either case, from the porosity-depth curves the decompacted thickness (S^*) and average density ($\acute{\rho}_s$) of a particular sediment layer can be expressed in terms of the present-day layer thickness (S) and the porosities of the compacted ϕ_s and decompacted ϕ'_s layer, where p_w and p_g are the densities of the water and sediment grains, respectively.

$$S^* = S\ \frac{1-\phi_s}{1-\phi\prime_s} \qquad (6.1)$$

$$\acute{\rho}_s = p_w\phi'_s + p_g\ (1-\phi'_s) \qquad (6.2)$$

Recovering the basement depth in the absence of the sediment and water loads is now a simple exercise of balancing the pressures at the base of the decompacted and backstripped columns (Figure 6.6 b and c respectively). We have,

$$p_w g W_d + \acute{\rho}_s g S^* + t_c p_c g\ = TS\, p_w g\ + p_m g Z_m + t_c p_c g \qquad (6.3)$$

Where *Wd* and *TS* are the water depth at the time of deposition and the recovered tectonic subsidence, respectively, g is the average gravity and p_m is the density of the lithospheric mantle. t_c is the thickness of the crust. The portion of the mantle above the level of compensation depth (Z_m) is,

$$Z_m = W_d + S^* + t_c - (TS + \Delta_{sl} + t_c) \qquad (6.4)$$

Where (Δ_{sl}) is the difference between present day sea-level and the sea-level at some former time and was calculated using the long term euastatic component of sea level.

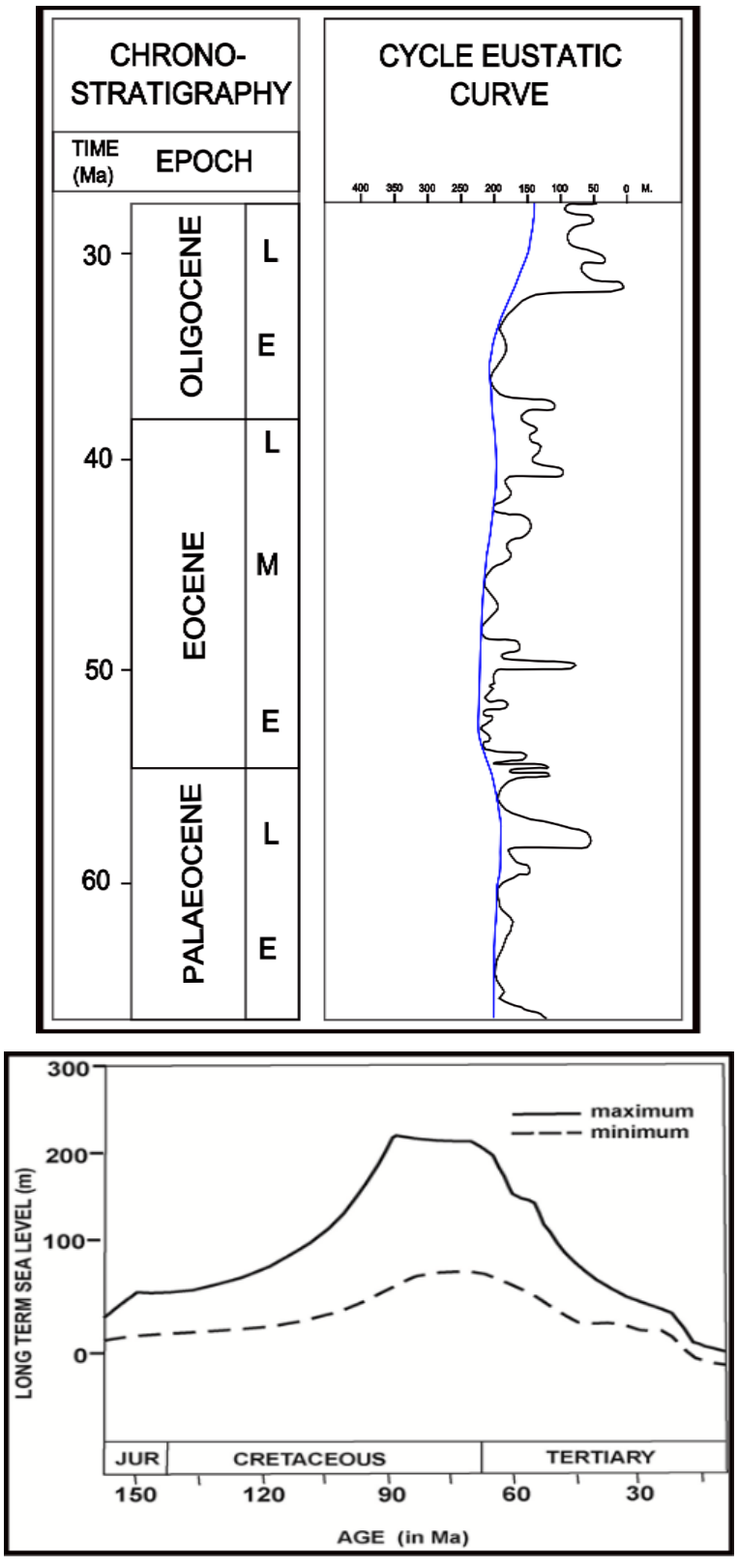

Figure 6.7: Long – term sea level changes used in the analysis of the tectonic subsidence. (a) Global sea-level curve for the Cenozoic (after Haq et al., 1987). (b) Sea level curves (after Kominz, 1984), solid and dashed lines indicate maximum and minimum sea level, respectively obtained from van der Meer and Cloetingh, 1993.

Upon substitution, and solving for the Equation 6.3, the tectonic subsidence is calculated using the formula (6.5) modified by Steckler and Watts (1978), which include corrections to sediment compaction, water loading and eustatic change.

$$TS = S^* \left(\frac{\rho_m - \acute{\rho}_s}{\rho_m - \rho_w}\right) + W_d - \Delta_{sl} \frac{\rho_m}{\rho_m - \rho_w} \qquad 6.5$$

Where *TS* is the tectonic subsidence, *Wd* and Δ*sl* are the water depth and sea-level height at a particular time, ρ_m the mantle density (Table. 6.3), the ρ_w and $\acute{\rho}_s$ are the densities of the water and de-compacted sediment respectively.

Parameter	Symbol	Value
Mantle density	ρ_m	3.33 gcm^{-3}
Water densrty	ρ_w	1.03 gcm^{-3}

Table 6.3: Parameters used as input for the synthetic modelling of the Sirte Basin adopting stretching models (McKenzie, (1978); Royden and keen, (1980).

Compaction was calculated using the equation (6.1), where S and ϕ_s are the thickness and porosity of the compacted layer and S^* and ϕ'_s are the thickness and porosity of the de-compacted layer respectively.

Equation 6.5 is known as the backstripping equation and includes three independent terms. From left to right these are, the sediment loading term, the water-depth term and the sea-level loading term.

The following paragraph provides a review about requirements and error sources of the subsidence calculation method adopted for this study. One main prerequisite of the method is that the stratigraphic record used for subsidence calculations has to be complete. In the case of using the well data, uncertainty comes from possible gaps in the record and that wells are not deep enough to penetrate all layers of interest. If stratigraphic information is derived from subsurface seismic data, uncertainties could occur during the conversion of seismic data from time to depth. Also uncertanites in correlating and extrapolating seismic reflections from well ties; lateral facies changes away from well ties. The lithology of the backstripped sections was identified from well logs, these included Lithology, Spontaneous Potential (SP), Gamma Ray,

and Sonic Logs. The time-depth conversion step used to predict accurate vertical thicknesses and correct for vertical exaggeration on stratigraphic thickness and dips on beds of the stratigraphic units.

Accuracy of chronostratigraphic age estimates of mapped horizons remains a major influencing factor, as rates are time averaged over stratigraphic intervals. For the purpose of the subsidence calculations, a depth-conversion of the time is performed using seismic velocities extracted from check shot data provided by the National Oil Company of Libya (NOC) (see Appendix). The utilized mean velocities for the Ajdabiya Trough is outlined in the previous sections, more explanations are given below.

Estimated velocities were assigned to the main stratigraphic units (Table 6.4) based on data extracted from the well A1-41 located at the northeastern part of Ajdabiya Trough. For the Upper Miocene 2.50 km/s, for the Oligocene 3.00 km/s, for the Eocene 3.30 km/s, and for the Paleocene 4.90 km/s.

Estimated uncertainties associated with velocities may produce in the final depth conversion a total error of 100 to 200 metres down to the base of the mapped stratigraphic intervals, such as the Paleocene interval, where well calibration was not possible.

The effects of velocity differentials upon the underlying sequences (i.e. the carbonates or the shales of the Cenozoic section) caused by the variation in thickness. Because the formation tops cannot be properly picked with enough accuracy, the calculations of the corresponding depths are sometimes obviously uncertain.

Lithological unit interval	**Interval Velocity (Vh), (m.s^{-1})**	**K value (s^{-1})**
Top Miocene to Middle Eocene (Gialo Formation)	2481	1.24
Middle to Lowe Eocene (Gialo – Gir)	3412	1.67
Top Eocene (Gialo Formation) to Top Paleocene (Hagfa Formation)	3950	1.75
Middle Eocene (Gir Formation) to Upper Cretaceous	5036	2.26
Top Eocene (Gialo Formation) to Top Paleozoic	4651	2.03

Table 6.4: Sample of velocity database used in the subsidence calculation, k is the rate of increase of velocity (compaction factor) per depth.

Due to different levels of sequence thicknesses prediction, some sedimentary sequences are far better constrained than the rest of the sections and this has affected the subsidence

calculations. As example the Cretaceous sequence is difficult to recognize from the 2D seismic data and not encountered in most of the wells.

6.4.2.1 Stratigraphy and Paleowater Depth

Backstripping analysis is fundamentally dependent upon the quality of paleowater depth information available (e.g. Roberts et al., 1998). In addition to the sediment loading, the water column provides an additional load contribution to the isostatic response of the system and, in turn, to the observed subsidence. Despite the importance of the water depth in the subsidence calculations, there is no direct and standard method to recover the water depth at any basin. For water depths, up to 200 m, as expected in Sirt Basin, estimating the water depth is easier and the errors associated are smaller. Even if the water depth used is wrong, a correction of a few 100 m will affect the shape of the subsidence curve much less than one of several 100 m (Holt, 2012). It is noticed also that the Ajdabiya Trough is remained under a small range of water column (50 – 200) meter during the post-rift period (Abadi et al., 2008), and then presumably in this case the paleowater depths corrections do not have a major influence on the subsidence calculations.

The paleowater depth data used in the subsidence analysis has been derived from published and unpublished studies within the Sirt Basin. Errors estimated for paleowater depth are interpreted as less than 50 m, using data from Barr and Weegar (1972), Eliagoubi and Powell (1980), Megerisi and Mamgain (1980), Ashour 1996), Barbieri (1996), El Sogher (1996), Muftah (1996), Tmalla (1996) and data obtained from wells (B1-12, C1-12, and EE1-6) based on unpublished joint study report between the Libyan Petroleum Institute and the Utah University entitled (Regional Chronostratigraphy of the Cretaceous Sections of the Sirt Basin Libya). Over the Cretaceous and Tertiary times, sediment facies change progressively with time throughout the Sirt basin, from terrestrial to marine (Barr and Weegar 1972). Abadi et al, (2008) among others suggested that, the Paleo-environments in Sirt Basin have been speculated between shallow marine to neritic which mainly formed within water depths not exceed the 200 meters. Palaeo-environment and palaeobathymetry have been determined on the basis of lithology and where possible, by analyzing benthic and planktonic foraminifera from within the Sirt Basin. Paleowater depth estimates (Figures 6.8 and 6.9) were inferred from lithology variations in each domain. The inner to outer shelf/slope transect can be

subdivided on the basis of the paleobathymetric distribution of different sizes of foraminifera assemblages (e.g. Muftah 1996; Tmalla 1996; Abouessa et al., 2012).

During most of the syn-rift periods, the entire Sirt Basin remained at shallow to moderate water depths (van der Meer and Cloetingh, 1993; Hallett, 2002). During the post-rift, while the platform areas remained under a very shallow water column (50 to 70 m), the entire basin experienced significant deepening related to thermal subsidence during the Tertiary time (van der Meer and Cloetingh, 1993; Abadi et al., 2008). Both lithostratigraphic and faunal parameters form the basis of the estimates of the paleowater depths in the Ajdabiya Trough (e.g. Muftah, 1996). Planktonic and benthonic forams are abundant in the Upper Cretaceous Kalash Formation (Tmalla, 1996). A mid-shelf environment is indicated by the large faunal diversity, which corroborates the suggestion by Barr and Weegar (1972) that the Kalash represents an open marine environment (Eliagoubi and Powell, 1996). During the Paleocene time the water depth is ranging from shallow at the basin margins to deep towards the basin centre. It is inferred that water depths never reached values greater than 200m (656 ft) (Bezan, 1996; Muftah, 1996) despite the argument made by Muftah, (1996) who suggested that water depths during the Upper Paleocene time could have reached depths greater than 200 m based on fauna assemblages and based on the study of Kaminski et al., (1988). At well A1-41 located at the north-eastern periphery of the Ajdabiya Trough planktonic foraminifera assemblage assigned for the basal Hagfa Formation of Upper Paleocene (Danian) age proved to belongs deep water environment, consequently an accompanying calcareous benthic foraminifera assemblage is interpreted as a deep water forms partly from shallow water source (probably slope derived faunas) formed as a result of synsedimentary slumping (Muftah, 1993). Based on the Libyan offshore analogues (Bernasconi et al., 1991) palaeowater depths for nummulitic shoals were probably on order of 25-35m. Barr and Weegar, 1972 divided the Upper Eocene (Augila Formation) into three units composed of shale at the bottom, quartz sandstone at the middle, and sandy limestone at the top. The environment is speculated between inner to middle neritic open conditions to shallow water.

The type and distribution of the Middle Eocene Gialo formation is influenced by basin-floor architecture and environmental controls. The basin floor was shaped through pre-Eocene structural development into a series of elevated platforms and deep troughs were dominated

by thick successions of lime mudstone containing rare fine skeletal fragments and nummulites, with deposition taking place in a deeper-marine environment.

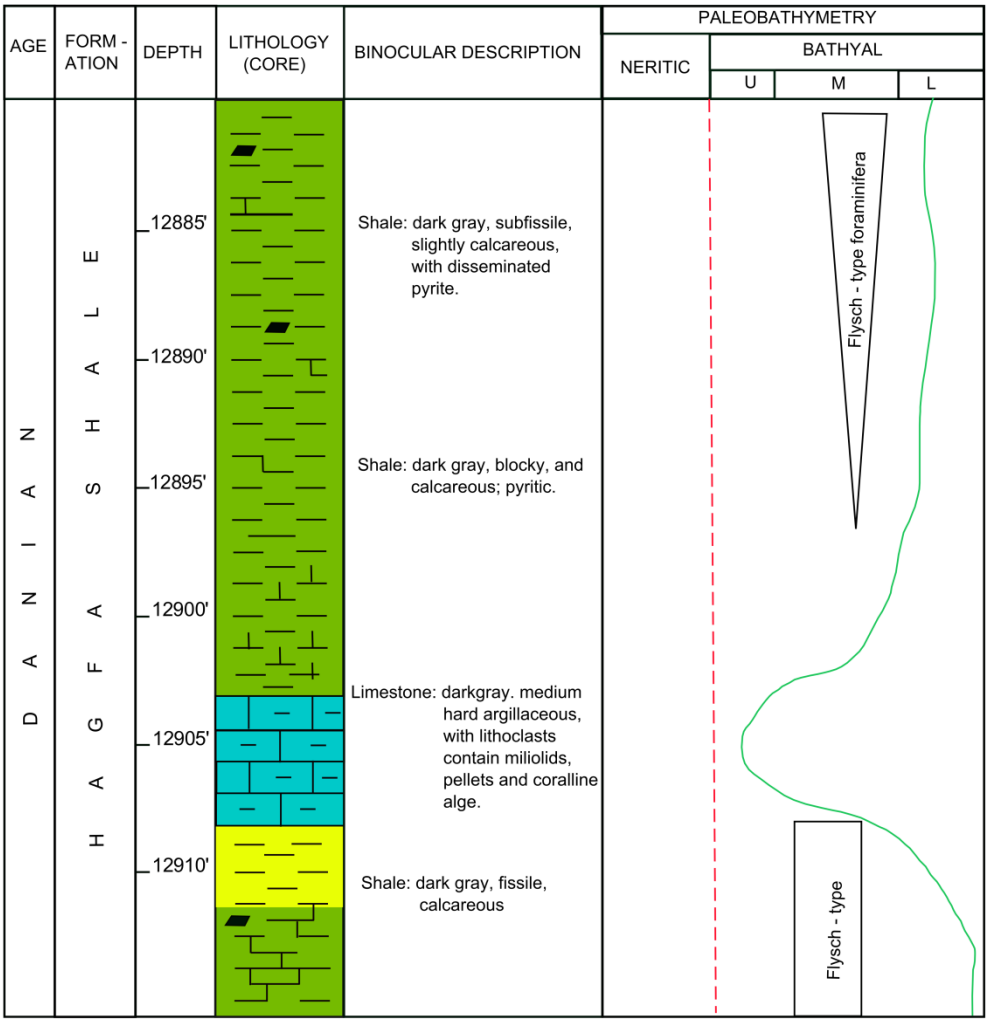

Figure 6.8: Lithology and interpreted paleobathymetry in the cored interval of the Hagfa Shale Formation (Danian) in well A1- 41, north-eastern Ajdabiya Trough. Re-drawn from Muftah, 1993.

The presence of planktonic foraminifera and the benthic assemblage are indicative of relatively deep-water outer ramp conditions. Also the presence of phosphatisation levels (e.g. Jarvis, 1992), which are typically more abundant in deeper-water environments between water depths of 50 and 150m, support this deeper water (>100m) interpretation.

The Lower Eocene Gir Formation overlain by the Gialo formation in most of the Sirt Basin and consists of a massive sequence of interbedded anhydrites and dolomites with subordinate amounts of limestone and shale formed in an open marine environment (Barr and Weegar,

1972). This formation is conformably overlain by the Gialo formation in most of the Sirt Basin. Foraminiferal banks developed in the Gir Formation sequence during phases of storm activity connected to eustatic sea-level rise and then foraminiferal production decreased when the rate of sea-level rise reached a minimum (e.g. Abougares, 1996).

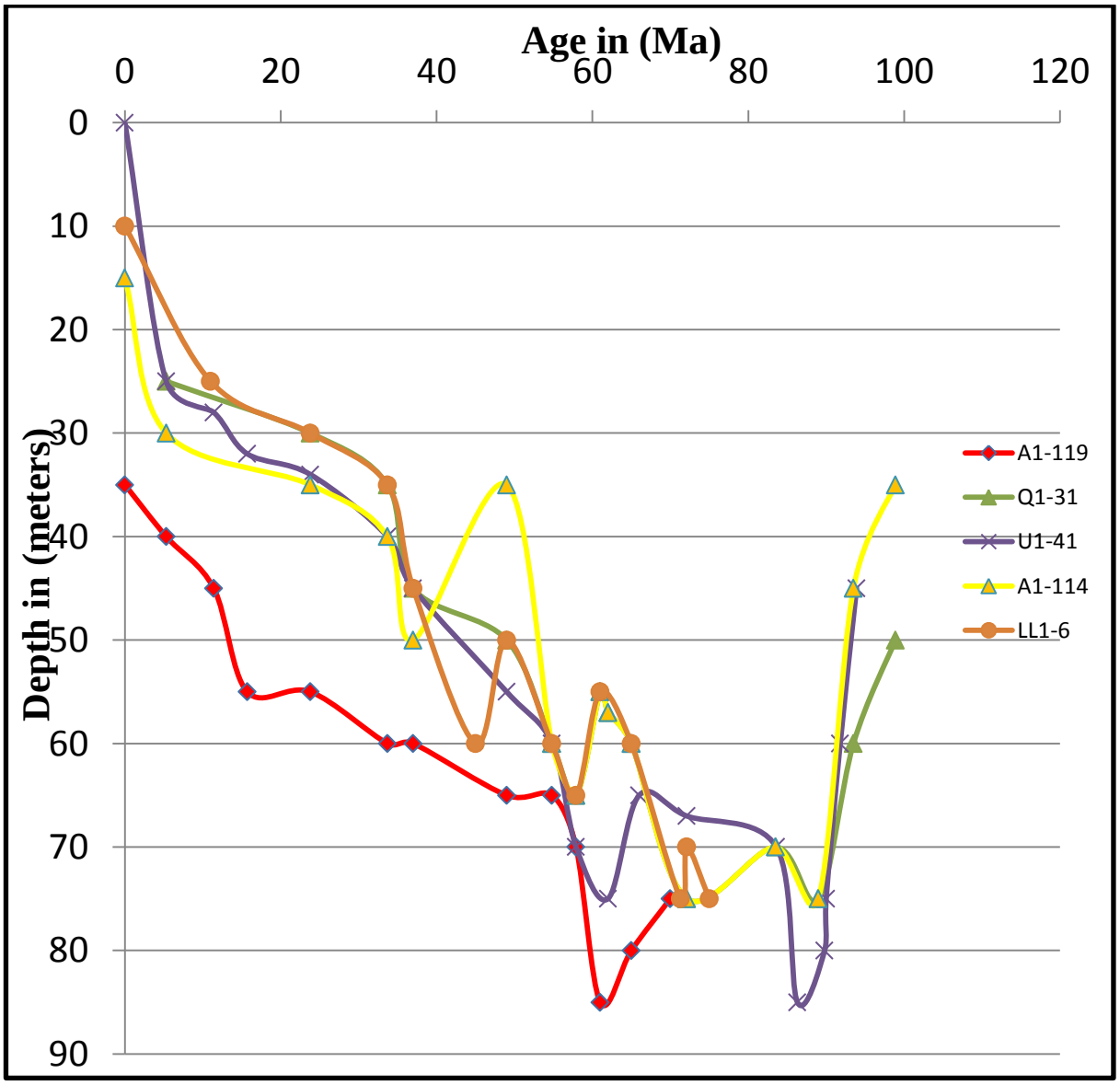

Figure 6.9: Estimated paleowater depth for the wells used in the backstripping analysis based on biostratigraphic studies in Sirt Basin and other published studies (e.g. Eliagoubi and Powell (1980), Megerisi and Mamgain (1980), Ashour 1996), Barbieri (1996), El Sogher (1996), Muftah (1996), Tmalla (1996)).

The Oligocene in Libya marks a period of regression in which the shoreline migrated northwards. There is evidence that minor oscillations occurred in the mid-Oligocene followed

by a minor transgression in the late Oligocene. An increase in the paleobathymetry reflects an overall basinward shift in facies and cessation of carbonate deposition.

The Upper Miocene Maradah Formation is characterized by a large number of lithofacies, including interbedded shales, sandstone, sandy limestone, calcarenite and gypsum (Barr and Weegar, 1972; Benfield and Wright, 1980). Gammudi (1996) considered the Maradah Formation Late Miocene in age, with infra-littoral (0-75 m) marine, including some brackish influence.

The Sirt basin was almost closed during the Neogene, apart from its central part, which extended south-eastwards into the south. Shallow water carbonates were laid down in these areas.

6.4.2.2 Decompaction

The purpose of the decompaction process is to estimate the total thickness of any sedimentary unit before it is buried and covered by sediment loading as the change of the stratigraphic thickness of any sedimentary unit is due solely to the loss in the volume of the total pore space. Tucker, (1991) suggested that there are two types of compaction formed during sediment burial. These are chemical and mechanical compaction. The mechanical process usually begins immediately after deposition and leads to closer partially of the sediment grains. As for the chemical process, the chemical compaction requires the existence of sedimentary cover composed of several hundred meters of burial resulting in increased solubility at grain contacts, and pressure dissolution seams (Tucker, 1991). Porosity decreases progressively with increasing burial, and the rates of porosity loss are generally lower in carbonate and higher in lime mud.

In order to estimate the amount of compaction (Figure 6.10), it is certainly assumed that the compaction of sediment is only caused by sediment loading and subsequent closure of the pore spaces (Sclater and Christie, 1980).

Although porosity directly describes compaction state, sonic velocity is widely used as an indicator of compaction because it is strongly dependent on porosity (e.g., Wyllie et al., 1956) and routinely logged in wells.

To remove the effect of the compaction the sedimentary units are moved up carefully using accurate porosity-depth curves.

The second assumption is necessary for decompaction that in normally pressured sediments porosity decreasing dramatically and exponentially according to equation given by Athy (1930).

$$\phi = \phi_0 e^{-cz} \qquad \text{Equation (6.6)}$$

Where ϕ is the porosity of the sedimentary unit at particular depth, and ϕ_0 is the original porosity at the time of deposition, c is the coefficient of the compaction, and z is the depth.

Commonly the predicted porosity values using equation (6.6) in addition to the values of the compaction coefficient and the original porosity are estimated from an integration and compilation of subsurface data "best suited" (Allen and Allen, 2005). Equation 6.6 can then be applied to any lithology, each with its own value for *c*.

The decompaction equation (6.7); is derived from the porosity-depth relationship. When the layer is moved up to a new depth and decompacted it expands. The volume of sediments does not change in mechanical compaction so the only thing that changes is the volume of the pore space. Therefore

$$z'_2 - z'_1 = z_2 - z_1 - \frac{\phi_0}{c}\left[e^{-cz_1} - e^{-cz_2}\right] + \frac{\phi_0}{c}\left[e^{-cz'_1} - e^{-cz'_2}\right] \qquad \text{Equation (6.7)}$$

Where $z'_2 \; and \; z'_1$ are the bottom and top depths of the decompacted layer and $z_2 \; and \; z_1$ are the present bottom and top depths of the layer.

Decompaction is performed using exponential porosity-depth relation characteristic to each lithology (Sclater and Christie, 1980). The predicted depth porosity curve (Figure. 6.13) obtained from well A1-114 located at the north-western part of Ajdabiya Trough (Figures 6.5) show an exponential reduction in porosity with increasing depth. The good agreement of the observed porosity and the model curve based on mechanical compaction also shows that mechanical compaction is the primary control on the reduction of porosity in the Ajdabiya Trough region, reflecting the fact that the Ajdabiya Trough Cenozoic sediments are predominantly mostly argillaceous rocks deposited above basement faults in which the porosity reduction is due mainly to mechanical compaction (e.g. Skuce, 1996).

Bore Hole Compensated Sonic log (BHCS) was run as the basic porosity tool in A1-114 well in addition to Epithermal Neutron (SNP) in order to determine which tool or combination of tools gave the most accurate porosity measurements.

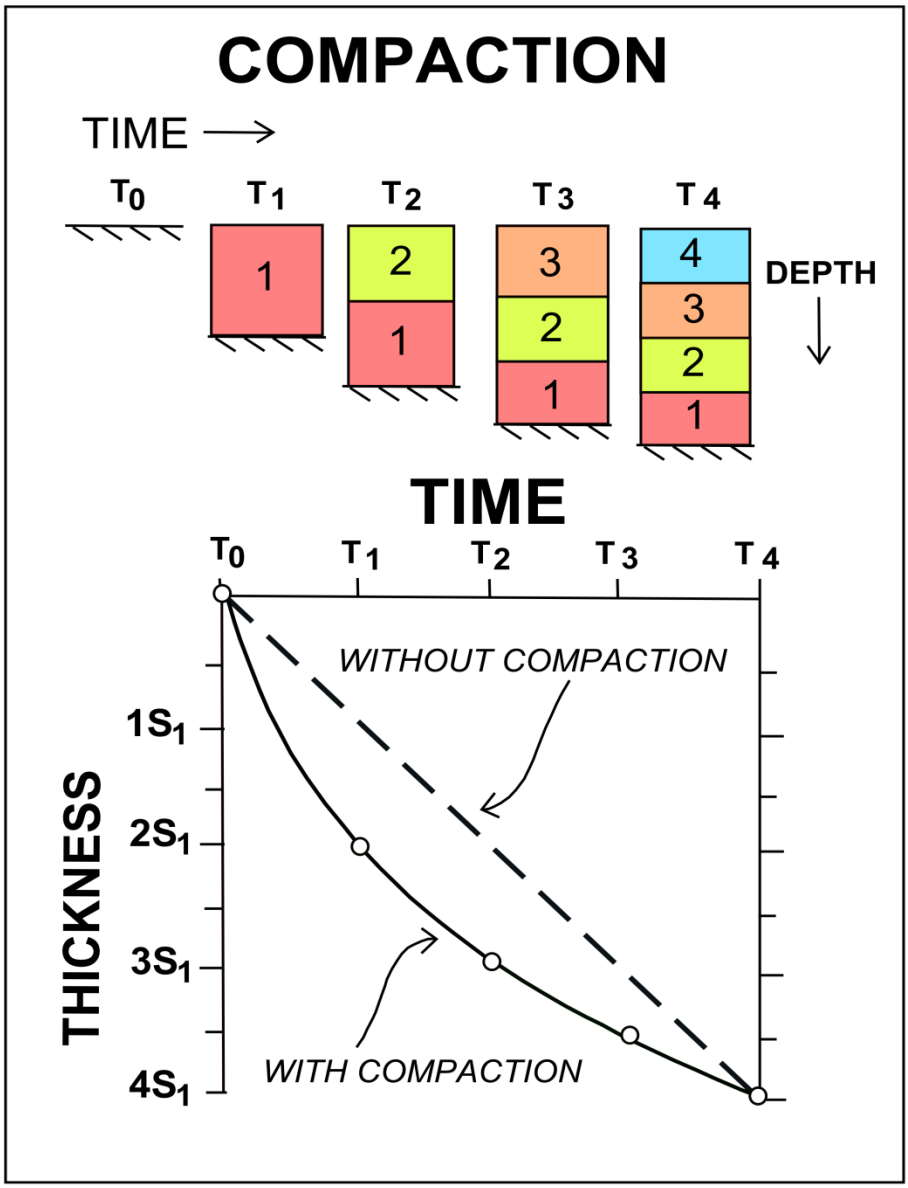

Figure 6.10: Removing the effects of compaction in geohistory analysis, by applying a 'compaction' correction. Horizontal axis is the time span in the geohistory record; the vertical axis is the variations in thickness of the compacted layer. (Re-drawn from Angevine, Heller and Paola, 1990)

Figure (6.11) show cross plot of transit time against SNP for the entire Eocene/Paleocene carbonate section penetrated. The points fall into four approximate representative groups corresponding to the following lithologies.

1- Argillaceous Lime mudstone: 5750' - 5920' (1753m - 1804m)
2- Marl and argillaceous chalky Wackestone to Packstone: : 5920' - 6450' (1804m - 1966m)
3- Clean Lime stone with dolomitic intervals: 6450' - 7500' (1966m - 2286m)
4- Massive dolomite and dolomitic Limestone: 7500' - 8300' (2286m - 2530m)

Prediction of porosity from sonic log behaviour was fairly good in clean rocks. In the argillaceous lime mudstone or shaly environment BHCS are greatly influenced by the shale content and porosities derived from the charts without correction have a substantial high side error. As this type of tools do not detect the clay-bound water and shale porosity directly.

Plotting in shale lines (travel time shale 120 m.sec/ft) indicates a shale content of about 30% and gives porosities of 10 – 15%, compared to the 15 – 20% and 25 – 30% given by SNP and BHCS respectively.

In the tight massive dolomite section, the logs reflect the generally low (3 – 5%) porosities. This section also contains minor intervals where porosities reach 15 to 20%.

Samples from wells in eastern Sirt Basin show that calcite cementation, late dolomitization, - and compaction are the major factors controlling the reduction of the porosity in Upper Cretaceous carbonate formations whilst dissolution and fracturing have increased porosity and permeability (Hallett, 2002).

Well penetration does not significantly reach into the pre-rift section within the Ajdabiya Trough, stopping at the top Cambro-Ordovician at the trough margins. Here therefore I assumed that all pre-rift sediments (Triassic – Jurassic) were fully compacted (i.e. had zero porosity) prior to Early Cretaceous extension. This is not a viable assumption in the whole Sirt Basin, because oil is produced from primary porosity in Triassic sandstone reservoirs (e.g Gumati et al., 1996; Rusk, 2001; Hallat 2002; Burwood et al., 2003).

A correction for compaction was made using porosity-depth relationships based on the observed lithologies, standard mean exponential relationships, and material parameters (Sclater and Christie, 1980) (Table 6.5).

The sonic log is a porosity log that measures interval transit time (Δt) of a compressional sound wave travelling through the formation. Geologically this capacity varies with lithology, rock texture and, in particular, porosity.

Lithology	ϕ_0	c	Source
Conglomerate	0.45	3.3 x 10^{-4}	Stagpoole (2006)
Sandstone	0.45	3.3 x 10^{-4}	Funnel et. al. (1996)
Mudstone	0.5	4.4 x 10^{-4}	Armstrong et. al. (1998)
Siltstone	0.56	3.9 x 10^{-4}	Sclater and Christie (1980)
Limestone	0.7	7.1 x 10^{-4}	Stagpoole (2006)

Table 6.5: Porosity and compaction corrections used in this study

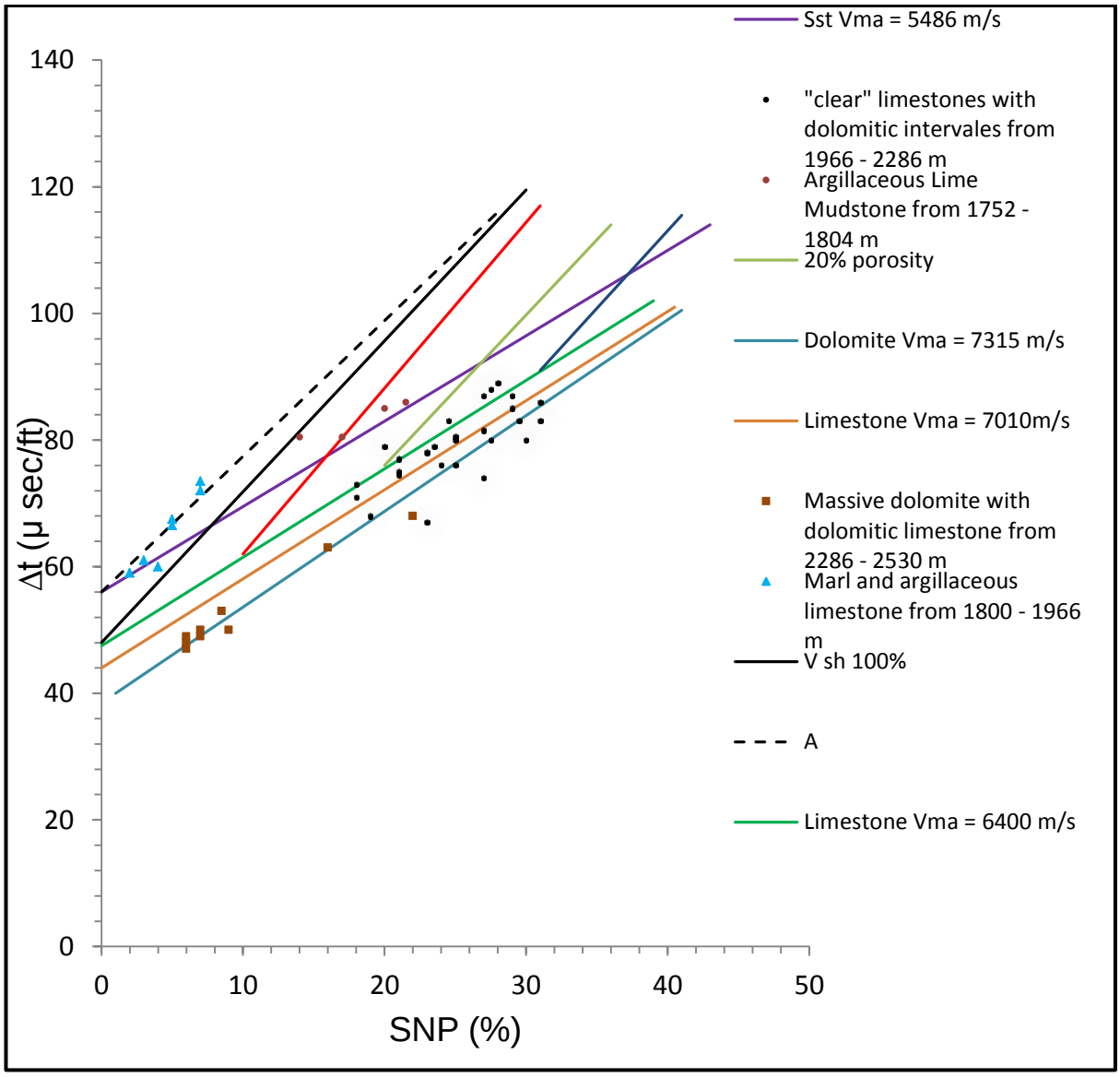

Figure 6.11: Show cross plot of transit time against SNP for the entire Eocene/Paleocene carbonate section penetrated in well A1-114 located at north-western Ajdabiya Trough.

In this study, porosity is also calculated from sonic logs for wells A1-114, U1-41, Q1-31, and A1-119, using Wyllie's time equation. Wyllie time average equation has been widely used for converting the recorded transit time to porosity, due to its simplicity.

$$\phi_{sonic} = \frac{\Delta t_{\log} - \Delta t_{ma}}{\Delta t_f - \Delta t_{ma}} \qquad \text{Equation (6.8)}$$

Where Δt_{log} is the travel time (μsec/feet) and Δt_{ma} is the matrix travel time and Δt_f is the fluids travel time.

Figure 6.12 show the relation between the sonic velocity Δt_{log} and a range of midpoint depths for the four wells. The velocities and corresponding travel times of the rock and matrix used are shown in (Table 6.6).

The lithology of the study area basically comprises argillaceous and carbonate rocks, and the formula between porosity and depth of each lithology is fitted based on the interpretation of sonic logging curves. Figure 6.13, shows four representative theoretical porosity depth curves from the four wells used in the backstripping analysis and an example of the conversion of sonic velocity to porosity.

Lithology	V_{ma} (ft/sec)	Δ_{ma} μsec/ft
Sandstone	18,000	55.5
Limestone	21,000	47.4
Dolomite	23,000	43.5
Anhydrite	20,000	50.0
Salt	15,000	66.7
Gypsum	19,000	53.0
Freshwater	5,300	189

Table 6.6: show ranges of velocity and equivalent matrix travel time for some lithology's (Rider 1986).

The predicted curves show an exponential reduction in porosity with increasing depth except for some high values attributed to either high porosity zones or possible overpressure zones formed by compaction. These could be also an indication post-compaction and apparent exhumation zones (e,g. Hillis, 1995). Disequilibrium compaction is typically the most important mechanism in the creation of overpressure (Swarbrick & Osborne, 1998). Hillis, (1995) suggested that in an area subject to exhumation, the wells with the highest Δ*t* (lowest velocity) for their given burial depth should be taken to be normally compacted, provided

their relatively high Δt is not due to phenomena that may inhibit normal compaction (such as overpressure or hydrocarbon-filled porosity).

Formations porosities have been checked for accuracy based on the SNP record of well A1-114.The interval (1966 m – 2286 m) in well A1-114 consists essentially of "clean" Limestone and there is generally good agreement between porosities derived from the SNP record and that calculated using Wyllie's equation (6.8). However it is necessary to correct for variations in matrix composition, e.g. presence of dolomite which usually indicated by low porosity values. In the massive Paleocene dolomite section from (2286 m to 2530 m), the porosity depth chart generally reflects low (3 – 5%) porosities.

The carbonate build up Paleocene section, was absent in well U1-41. It can be concluded that either Paleocene to early Eocene erosion, present elsewhere in western Cyrenaica, could have removed any Upper Paleocene sediments in this area, or due to environment (Bezan, (1996); Yanilmaz et al., (2008), it is possible that there was no generation of carbonate build-up at all on lower Paleocene dolomite section, but only intermittent corals were present, which were found reworked in the deeper marin Paleocene of A1-41 (Yanilmaz et al., (2008).

This latter interpretation is reinforced by the fact that during the Paleocene time an exhumation could be formed and indicated by a localized high within the Paleocene dolomite interval. The thick Cretaceous section of U1-41 in the northeastern part of the Ajdabiya Trough show that the configuration of the basement in this area seems to be more complex than the simple N-S alignment hitherto believed to exist at the western margin of the Cyrenaica Platform (e.g. Yanilmaz et al., (2008). The Eocene carbonate section (1628 m – 2193 m) consists essentially of marls and lime mudstone/wackstone, locally wackestone/packstone, argillaceous towards the top. Because of the shale content porosity values derived from the sonic log must be treated with caution. Apparent porosity values of 25 – 35% were derived from the interval (1878 m – 1923 m) which does not agree with the type of formation penetrated. This suggests a substantial high side error due to shaliness, compared with the cleanest packstone of the interval (1951 m – 2027 m) which has an apparent porosity of up to 20%. The Paleocene section (2493 m – 2993 m) consists of massive dolomite down to 2652 m (up to 5% porosity).

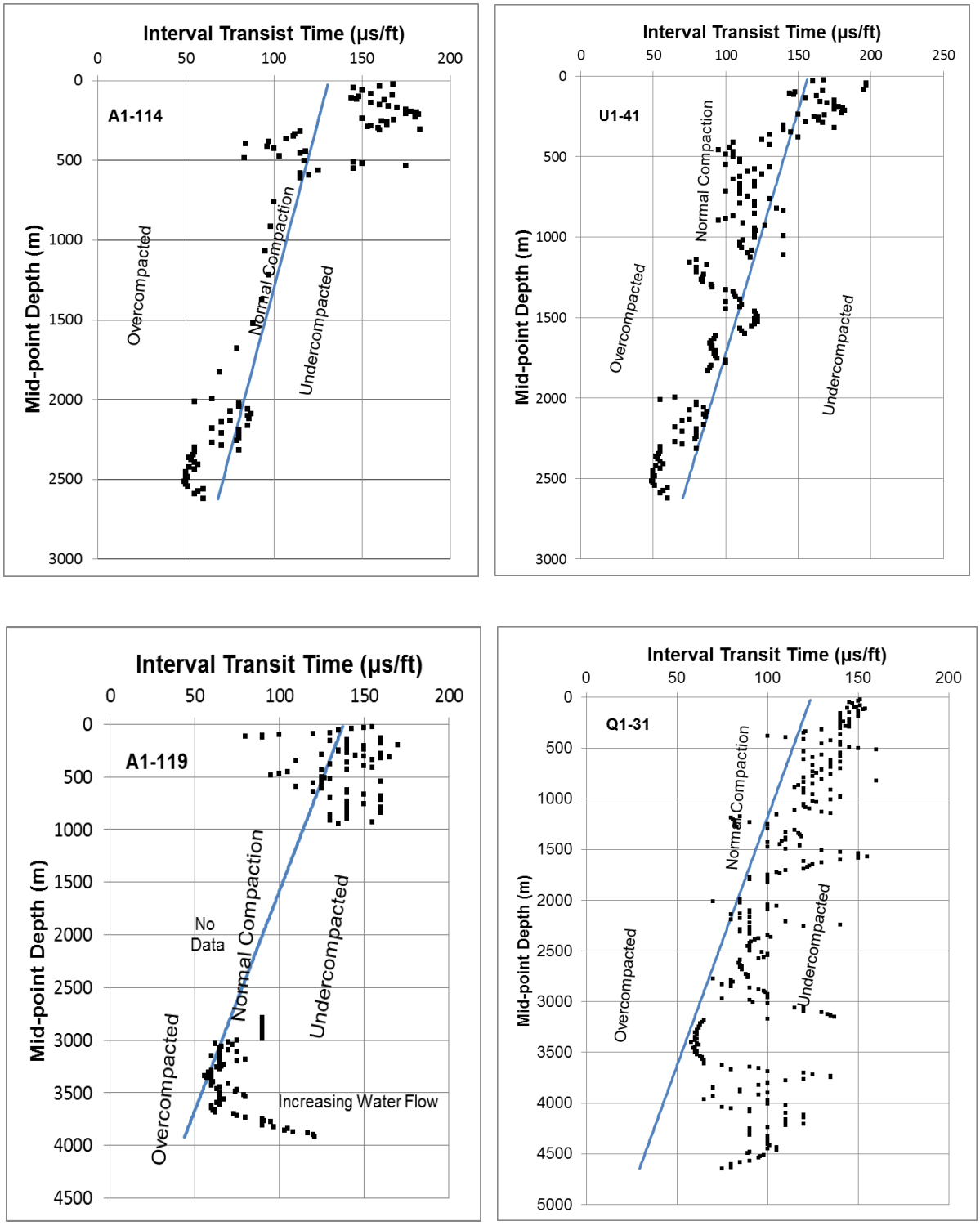

Figure 6.12: Mean adjusted sonic Δt /depth to unit midpoint plots for the sedimentary section in Ajdabiya Trough obtained from four wells with estimated normal compaction curve based on equations obtained from published works (e.g. Mavromatidis, 2006; Underdown et al., 2008)

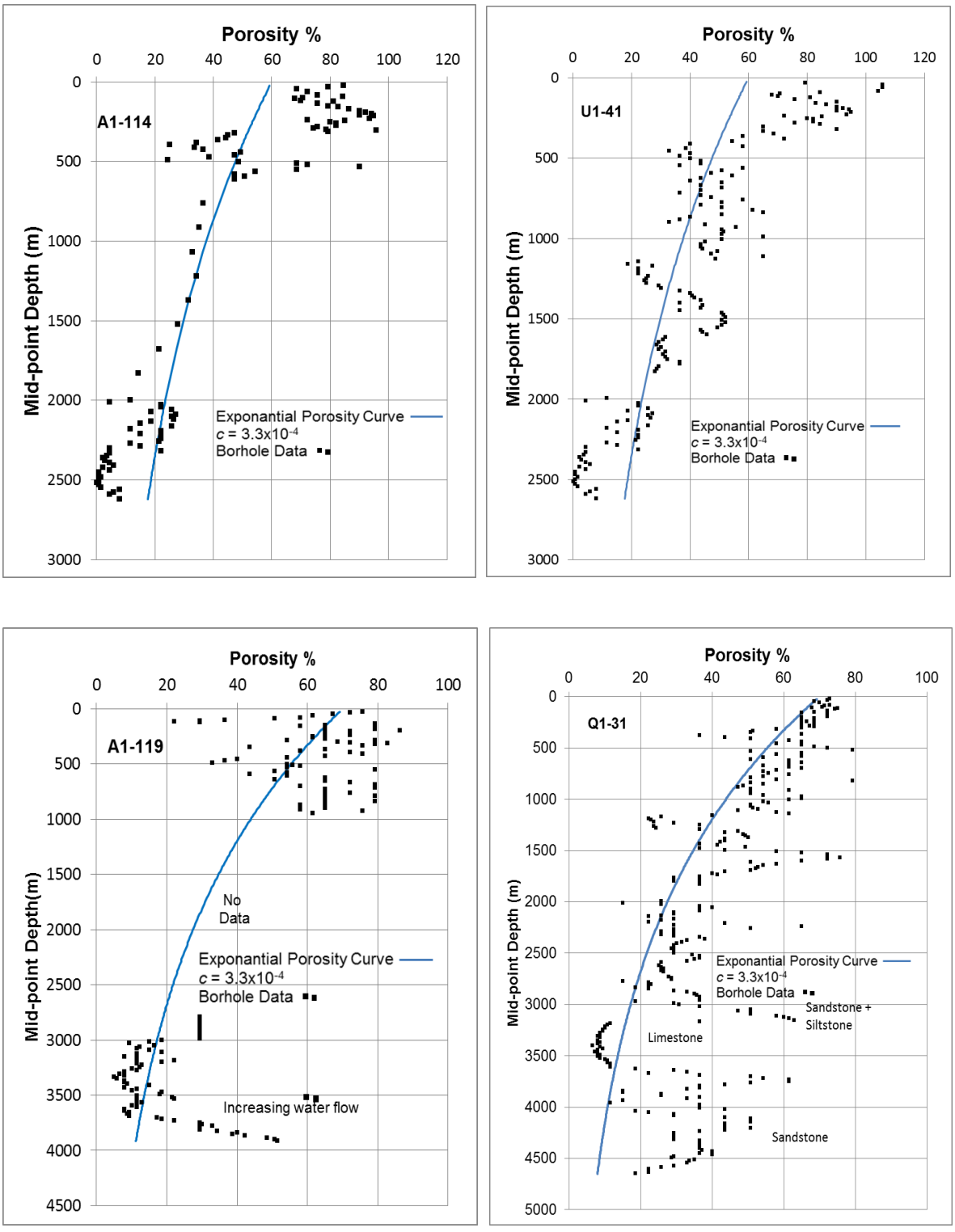

Figure 6.13: Porosity vs burial depth, determined from the sonic log for the backstripped wells with exponential-type curve derived in this study which gives the best-fit (blue line) to the data (black dots). It assumes a surface porosity of ~ 70% and a factor of exponential decrease, ***c*** of $3.3x10^{-4}$.

Thereafter porosity values are negligible. In the argillaceous lime wackestone/mudstone to wackestone of the Cretaceous section down to the top of the Rakb shale at 4179 m, porosity value of up to 15% was derived corresponding to the cleanest water bearing limestone at the top. The argillaceous limestone and clastic sediments in the section 4298 – 4712 are of low porosity (3 – 5%), with some minor intervals where porosities reach 7 – 10%. Down to the T.D the sonic log reflect the negligible porosity values in the limestone and in the clastic sediments.

The calculation of the porosity for the backstripped wells are in agreement with the relation between porosity and transit time given by the graph of Wyllie and Raymer (Figure 6.15). Moreover, the compaction correction is a multiplier only, which loses its utility at high transit times, where calculated porosity values are still more overestimated.

Higher value of transit time at about 70 % porosity is due to uncompaction effects as illustrated on Neutron Sonic transit time cross plot in Figure (6.12). Generally, consolidated and compact sandstones have porosities from 15 to 25%. However, in some higher porosity sandstones (30% or greater) that have very low water saturation. The increase of the sonic porosity is possibly due to increase of shale lamination.

Well Q1-31 located on the eastern flank of the Ajdabiya Trough (Amal Platform) show a superimposed general trend of decreasing porosities with increasing depth of burial, (Figure. 6.13). These variations in sediment porosity reflect changes in sediment composition as shown on Figure (6.14).

The drop in porosity values as show on the Q1-31 curve marks the beginning of an interval that shows only minor decreases in porosity with depth of burial at about 1500 m depth. The reason for this remains unexplained at present although it is worth noting that the top of this interval corresponds to a Mid to Upper Eocene unconformity (hiatus).

The compaction curve calculated for the sedimentary section show that Lower Paleocene (Lower Sabil Formation) composed of limestone, dolomite and trace anhydrite interval and was superimposed on the measured porosity-depth profile (Figure 6.13) despite that the compaction curve on the depth v.s sonic transit time show different trend due to uncertainty in the selection of the compaction parameters used in the calculations.

The Middle and lower Eocene beds in A1-119 consist of almost 100% limestone with associated shale and chert inclusions and minor shale interbeds. The limestones generally

reflect a quiet water depositional environment as interpreted from the associated microforaminifera and micritic matrix. The porosity of these lime times is generally a poorly developed non-crystalline type with associated fracturing.

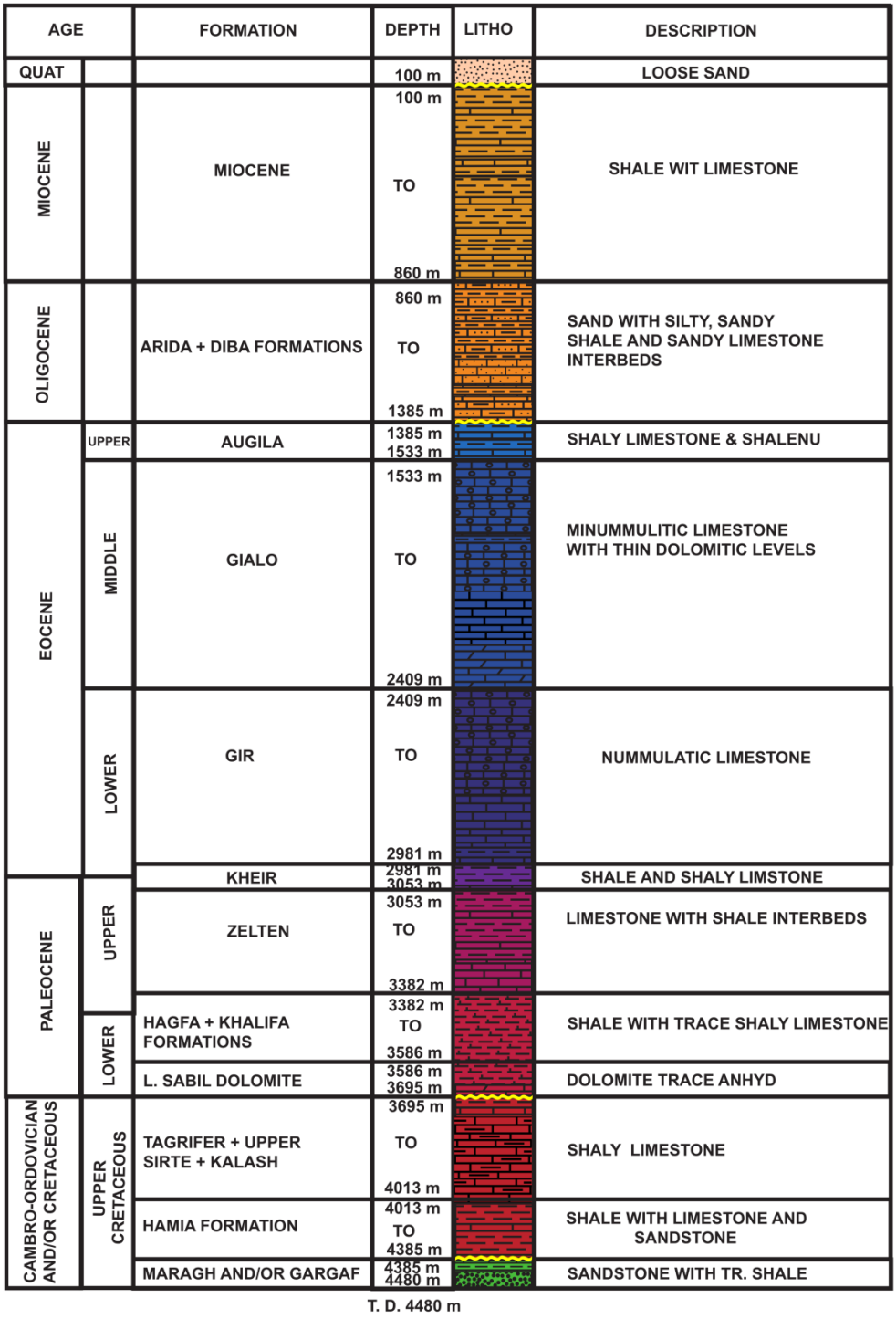

Figure 6.14: Stratigraphic chart of well Q1-31 showing thick section of remarkable post-rift sequence.

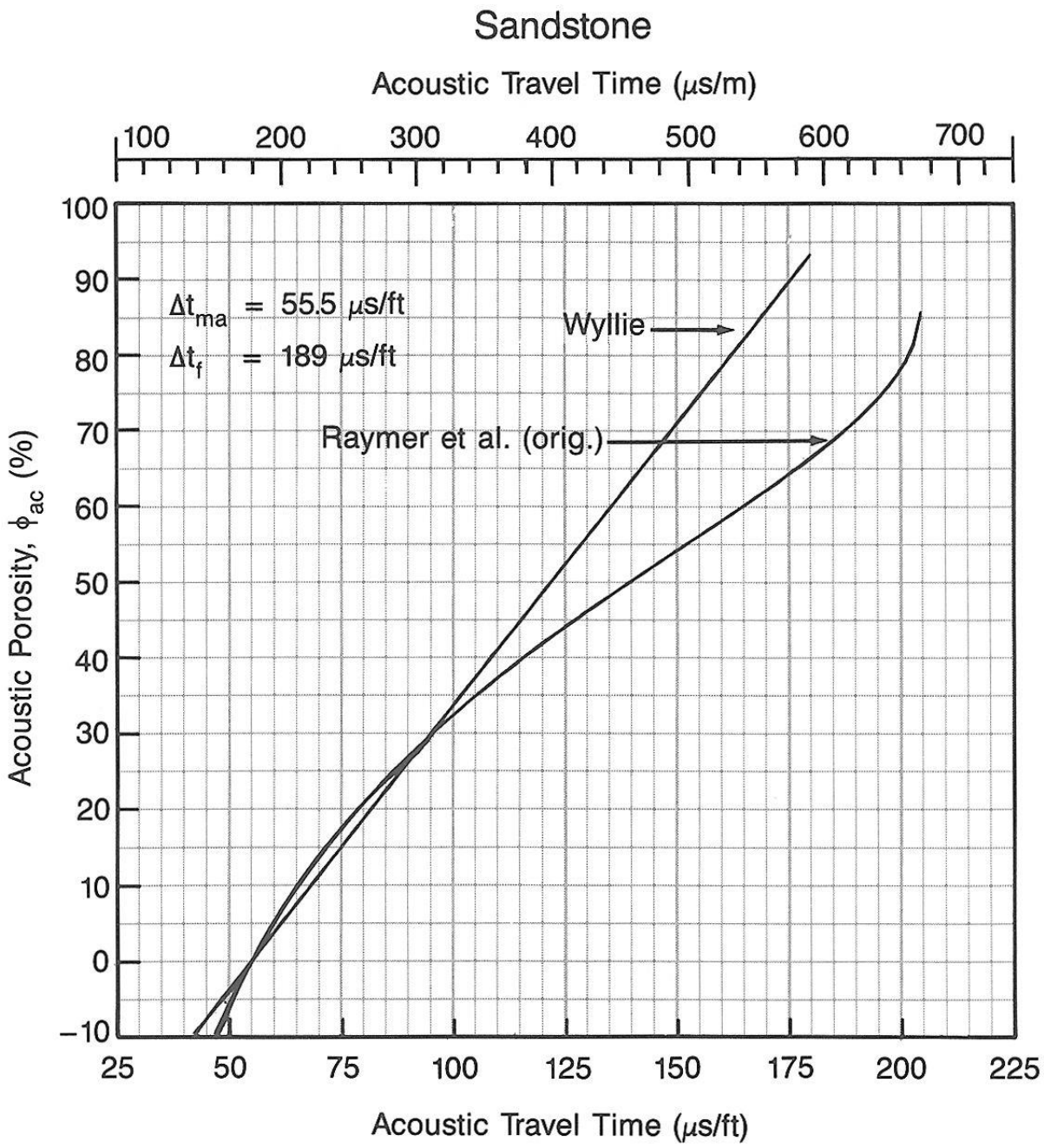

Figure 6.15: Graphical solutions of the Wyllie and Raymer velocity-porosity relationships (sandstone matrix)

From the well report of the well A1-119, it is noted that an increase in salinity was recorded toward the T.D accompanied by a noticeable water flow which took several days to control. This could be due to overpressure exist in the downhole which cause an increase of the porosity at this level.

6.4.3 Backstripping Results

The results of the subsidence calculations using the 1D Airy backstripping technique are presented on a series of contour maps obtained from a backstripping of number of wells in and around Ajdabiya Trough area, and subsidence obtained from curves for selected wells adjacent to Ajdabiya Trough borders (platform areas) and from one well obtained from the centre of the trough (A1-119 well) in addition to the pseudo well (PW 0360).

The tectonic subsidence contour maps were created through the interpolation of group of wells (Table. 6.1). The subsidence is calculated in each well individually using the same equations and parameters (Formation densities, porosity, and water depths) that used in constructing the subsidence curves from the selected wells. Then the final maps were compiled for distinct stratigraphic boundaries correlated with the tops of Paleocene, Eocene, Oligocene and Miocene time units. The obtained subsidence results from the wells were gridded using the Oasis Montaj gravity and magnetic mapping software. A 500 meter grid cell size was sufficient to overcome any possible gaps or spacing could exist on the maps. Due to the wide distribution of the wells, some isolated spots may occur, however the maps display a general spatial trends in the regional distribution of the subsidence within the study area. In addition, I present subsidence curves comprising two main curves in addition to the paleowater depth curve. The main curve describes the total subsidence the basement experienced as documented in the stratigraphy of the wells which comprises of two components, the effects of non-tectonic processes such as load induced subsidence driven by the presence of the sediments column and the water body, and the tectonically driven subsidence. The other curve is representing only the tectonic subsidence, i.e. that obtained after removing the effect of the loaded induced component from the total basement subsidence and it reflects solely the tectonic or driving mechanism of a basin (Bond and Kominz, 1984; Sclater and Christie, 1980).

Showing the subsidence variations on a map is the most desirable option. Tectonic subsidence maps have been used to study temporal and spatial variations in the Sirt Basin, Libya (Gumati and Nairn, 1991; Abadi et al., 2008).

Four maps were created for the four units of interest start from Paleocene to Miocene to create a map suite. These represent the Paleocene, Eocene, Oligocene, and Miocene time intervals. Tectonic subsidence maps show the progression of trends throughout the basin. The maps

provide an additional means of comparing the tectonic subsidence obtained from the subsidence curves.

6.4.3.1 Subsidence Curves

In this section subsidence analysis is performed to quantify vertical movements and associated subsidence rates, and to illustrate key features of the tectonic and thermal evolution across Ajdabiya Trough using selected wells. The wells used are, located in the trough margins LL1-6 (Zelten Platform to the west), A1-114 (Al Jahama Platform, to the northwest), Q1-31 (Amal Platform, to the east), U1-41(Northeast Ajdabiya Trough and close to the Soluqe flank or depression in Cyrenaica Platform), and A1-119 near to the centre of the trough (see Figures 6.3 & 6.4 for well locations).

At the central area, where no well data is available, a synthetic well (PW-360) is built by combining the lithology from the available wells (Figure 6.16), and the geological interpretation of the seismic line 05NC213-0360 located at the middle of the study area (Figure 6.17).

The reconstruction of the pseudo well is challenged and complicated by the fact that stratigraphic boundaries are often based on lithostratigraphic and chronostratigraphic boundaries approach using wells and seismic sections.

The syn-rift succession either eroded or has not been entirely drilled in most of the wells and the post-rift possibly has experienced sedimentary gaps within the sedimentary record due to erosion cycles during the Tertiary time and possibly in line with the western Sirt Basin major Late Miocene erosion reported by Gumati and Schamel, 1988. Therefore, the calculated subsidence possibly represents minimum values.

Due to well locations and nature of depth penetrations, subsidence curves are most accurate for the post-rift period along the platform areas.

Practically in all wells, the syn-rift package is unknown. In the subsidence curves, the initial point (depth = 0) is not considered with respect to the initiation of rifting due to this lack of control on the total syn-rift sedimentary thickness. The zero level depth has been associated with the time of the oldest drilled formation and differs from one well to another, and therefore, does not correspond to the beginning of the subsidence. This means that the sedimentation and the subsidence rates represent minimum values in most of the wells.

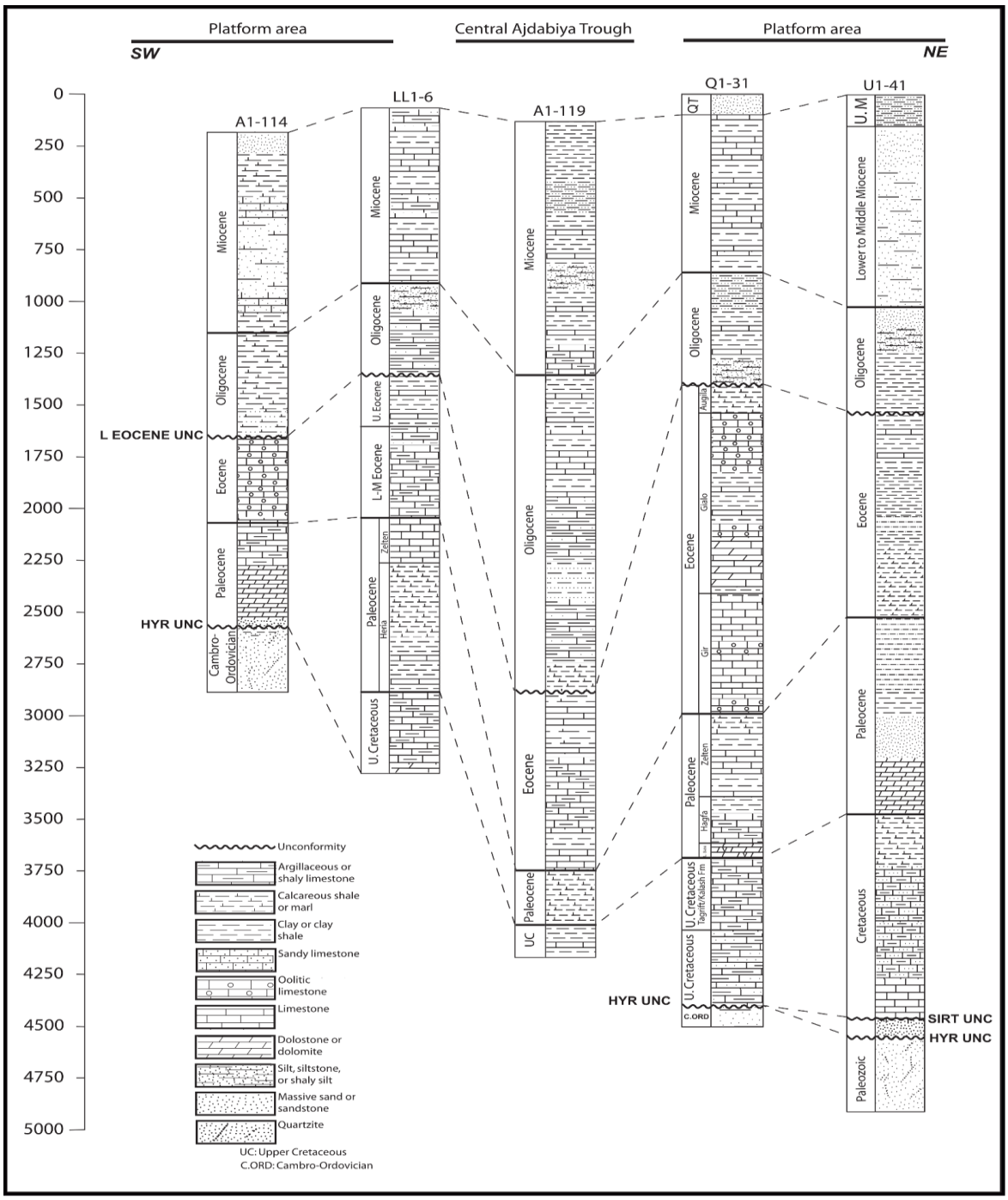

Figure 6.16: Lithostratigraphic correlation between the modelled wells U1-41, Q1-31, A1-114, LL1-6, and A1-119 located at the trough margins and the centre respectively.

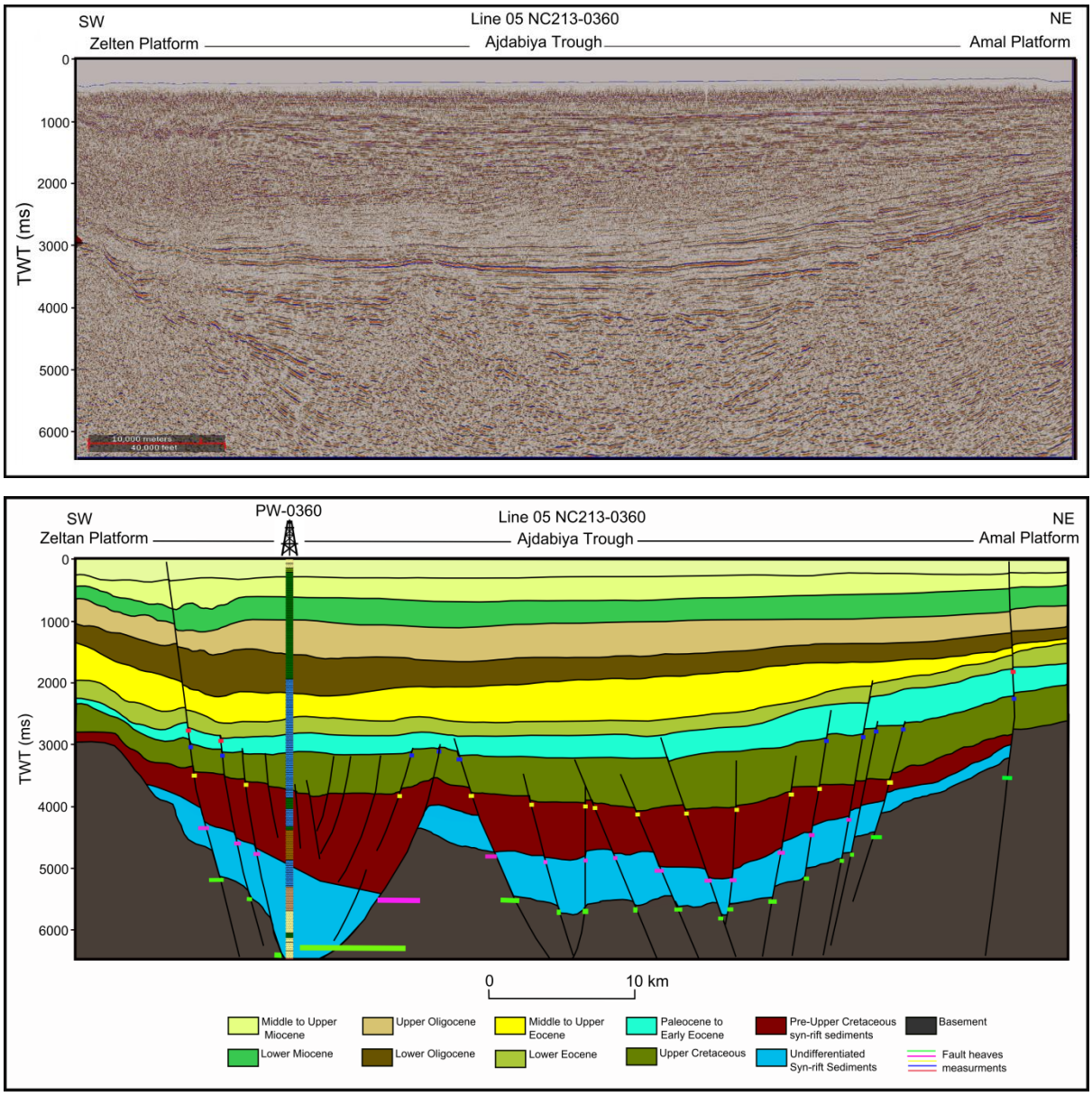

Figure 6.17: Seismic line 05NC213-0360 with geological interpretation (see location in figure 6.5). Green, purple, yellow, and blue lines are areas where fault heaves were measured for extension factor (β) prediction. Vertical column is the synthetic well (PW-0360) used in the subsidence calculation.

6.4.3.1.1 Observations from the Trough Margins

Accurate subsidence information obtained for the post-rift stage concern 5 locations, where wells transect the entire post-rift sequence reaching the base of the Upper Cretaceous section (Figure 6.17). The well coverage is rather broad, about 150 km along the coast and 100 km along a NE-SW axis from the platform areas towards the centre of the Ajdabiya Trough

(Figure 6.4). Therefore, observed similarities in subsidence histories reflect common geological history at a regional scale.

The subsidence observed can be resolved into two components: isostatic subsidence caused by the response to sediment-and water-loading; and tectonic subsidence, due to rifting of continental crust and subsequent thermal cooling. A maximum total subsidence of about 5.5 km is recorded in the NE part of the Ajdabiya Trough (U1-41 well), while in the NW the total subsidence does not exceed 3.0 km (A1-114 well), (Figure 6.18). The calculations are based on decompacted present-day thicknesses, and do not take into account the entire syn-rift period as any erosional periods. In the vicinity of the A1-114 well, a Cretaceous erosion or unconformity is recorded in the majority of the wells associated with larger gap time, especially in the north-western side. The Cretaceous formations are rarely found in the most proximal wells although in the eastern part of the platform, Cretaceous deposits can be largely observed. To the east of the trough the maximum total subsidence recorded is about 4.5 km (Q1-31well). In western Ajdabiya Trough the total subsidence observed is about 3.3 km (LL1-6 Well). Onlaping terminations are present, especially in the south-western part of the study area suggesting component of rifting and basin subsidence effecting this part during the Upper Cretaceous time.

The tectonic subsidence curves (Figures 6.18 & 6.19) show episodes of increased subsidence rates alternated with phases of slower subsidence, uplift and hiatuses indicated by curves flattening. Changes in subsidence rate can, in most cases, be correlated over the study area. The first phase is from the deposition of the Upper Cretaceous series ca. 100 Ma, and is characterized by declining rates of tectonic subsidence. The second phase is from 65 Ma to 54 Ma, and is characterized by much more rapid and accelerating rates of subsidence. Cretaceous sediments can thus be thought of as a result of incipient rifting post the nucleation of the Ajdabiya Trough bounding faults, when an increase in the subsidence rates, such as predicted in this study, would finally occur. During Early Cretaceous time, significant subsidence and sedimentation took place with the deposition, along almost the entire Ajdabiya Trough, of ~1.5 - 2 km on average of sediments (e.g. 2.0 km at pseudo well PW-360). This period of rapid subsidence lasted even longer than 10 Myr, and extending to 20 Myr on average (Figure 6.19B).

The increased subsidence interval would correspond to the Cretaceous to Middle Paleocene sediments, and the following slow decrease in the subsidence rates, with greater tectonic stability and progradation of the carbonate wedge basinwards, would be represented by the Late Paleocene – Early Eocene series. The depositional aggradation pattern at the lower part of the early Eocene (Gir sequence) (chapter 5) was accompanied by a maximum marine flooding in response to either maximum subsidence or sea-level rise during the Late Paleocene (e.g. Spring and Hansan, 1998).

The third phase is from 50 Ma to about 34 Ma with moderate to high subsidence rates observed on most of the wells. The fourth period is from about 34 Ma to recent and characterized by rapid subsidence at the western flank of Ajdabiya Trough (wells A1-114 and LL1-6) with moderate and gradual subsidence observed along the eastern flank (wells U1-41 and Q1-31). The backstripped subsidence history shows that 35% (~ 0.6 km) of the tectonic subsidence of the Ajdabiya Trough has been created since 65 Ma except for the pseudo well (PW-0360, figure 6.23B) which show a large difference in the tectonic subsidence by an amount of (~ 1.4 km) based on thick syn-rift stratigraphy.

The backstripping of A1-119 (Figure 6.23A) yields a very low syn-rift subsidence (~ 0.5 km) and total subsidence rate (15m/Myr), which are not representative of the thick syn-rift series preserved in the grabens and half grabens across the Ajdabiya Trough (Figure 6.20). Syn-rift subsidence illustrates the combined effect of two components, which are isostasy and normal faulting (e.g. Allen & Allen, 2005). In the hanging walls, subsidence is largely driven by normal faulting, as shown by the pseudo well PW-360 curve (Figure 6.23B), where the subsidence rate is 50 m/Myr, 3 times higher than that in A1-119. The Ajdabiya Trough was the site of continental-marine siliclastic deposition throughout the early and late-syn rift periods, and a more marine shales and shallow carbonates became established during the post-rift subsidence.

Numerous studies have shown that tectonic subsidence in the hanging-walls to normal faults is the primary control on the generation of accommodation space in extensional settings, e.g. Leeder and Gawthorpe (1987), Schlische and Olsen (1990), Prosser (1993), Gawthorpe et al. (1994). Sediment accumulations in the hanging-walls are affected by syn-depositional tectonic movements, e.g., differential subsidence. Distribution of sedimentary facies and the

morphology of onlapping strata during the syn-rift period are influenced by the subsidence within a hanging-wall of syn-depositional growth fault (Figure 5.45).

In the northeastern part of the Ajdabiya Trough, subsidence rates correspond to 85 m/Myr in well U1-41 mainly attributed to thermal component of lithosphere or due to movements along major bounding faults.

The minimum values observed in well A1-119 and the other wells drilled in the marginal areas (Platforms and structural highs) around the Ajdabiya Trough may account only for the upper part of the syn-rift, preserved in the footwalls of the main faults. This indicates a substantial increase of syn-rift subsidence rates towards the depocentre of the trough, in agreement with extension trend mentioned by previous investigators (e.g. Gumati, 1985; Gumatti and Naurm 1988 ; Abadi et al., 2008), and recently reported by Galushkin et al., (2014).

For the wells located on the platform areas, the strong basement subsidence is observed for the first 10 Myr of the early post-rift history (i.e. 65 to 54.8 Myr) with a value of 1.0 km on average as observed in well Q1-31.

The associated subsidence rates are also moderate to high, 30 m/Myr, 50 m/Myr, and 75 m/Myr respectively. This phase corresponds to the deposition of the Paleocene carbonate series. The early post-rift phase was tectonically quiescent, and was characterised by the progradation of marine sediments during stillstand or slower rise in sea level (dominated by a south-westwards-prograding clinoforms along the eastern margin. This phase was characterised by the establishment firstly of marginal-marine conditions and then of fully marine conditions during the the Late Paleocene (e.g. Bezan, 1996; Spring and Hansen, 1998)

Following the early post-rift phase, the Middle to Upper Eocene post-rift phase (50 – 33.7 Ma), is characterized, along an entire proximal domains, by an increase of subsidence rates (40 – 80 m/Myr).

For the period (33.7 – 0 Ma) post-rift accelerated subsidence occurred during the Early Oligocene at the western part of Ajdabiya Trough (80-100 m/Myr), as observed in wells A1-114 and LL1-6. Fault analysis during this period (chapter 7) show that there is a dramatically decrease in the numbers of active faults and fault growth rate which indicates that no active brittle crust extension occurred during post-rift period rather than fault re-activation. Regional

uplift in the Middle – Upper Eocene was followed by thermal sag, and deep to shallow marine deposition occurred through the remainder of the Cenozoic.

The Middle Eocene facies distribution in the Ajdabiya Trough is probably influenced by the structuration and subsidence of the region. The general configuration is characterised by a ramp model progressively deepening toward the northwest.

Regional slow subsidence due to thermal cooling began to occur during Late Oligocene. However, a significant rapid subsidence occurs in northern Ajdabiya Trough from late Miocene (about 10 Ma) to the present as observed from well U1-41 and A1-114. The post-rift sequence comprises marine shales and carbonates, deposited during the thermal subsidence stage. This indicates that possible extensional tectonics persisted during the Miocene, particularly in the northern parts of the study area. Subsidence during the Miocene continued to develop accommodation space subsequently the Miocene sediments thicken into the trough preserving more than 750 m in its axis. However in this case, corresponding high subsidence and equivalent sedimentation rates reach ~80 -100 m/Myr on average with sedimentation keep pace with the basin thermal subsidence. Following this rapid subsidence stage, a net decline of subsidence equivalent to a few hundred of metres and low associated sedimentation of less than 50 m/Myr are observed and concern a relatively short period. The duration of this second stage varies between 10 and 15 Myr depending on the location. The third post-rift phase that lasted since ~30 Ma corresponds to variable vertical movements of few hundred metres. Associated subsidence rates are medium to high, about 30 - 100 m/Myr. All over the platform areas, the amount of sediments deposited during the first 10 Myr of post-rift represents ~90% of the entire post-rift sequence thickness and corresponds to a high post-rift subsidence rate of ~80 m/Myr, equivalent to one third of the syn-rift rate.

The analysis shows that the syn-rift and post-rift sequences in the Ajdabiya Trough were affected significantly by basement structural relief. There is a ca. 1000 m syn-rift sequence correlated with the basement structural relief, and post rift sequences of more than 4000 m in sag or thermal subsidence stage.

It must be stated that the progression of depth level of the Pre-Cretaceous basement as was presented by Gumati (1985) indicates that the whole Sirt basin was progressively undergoing subsidence without interruption until the Late Eocene.

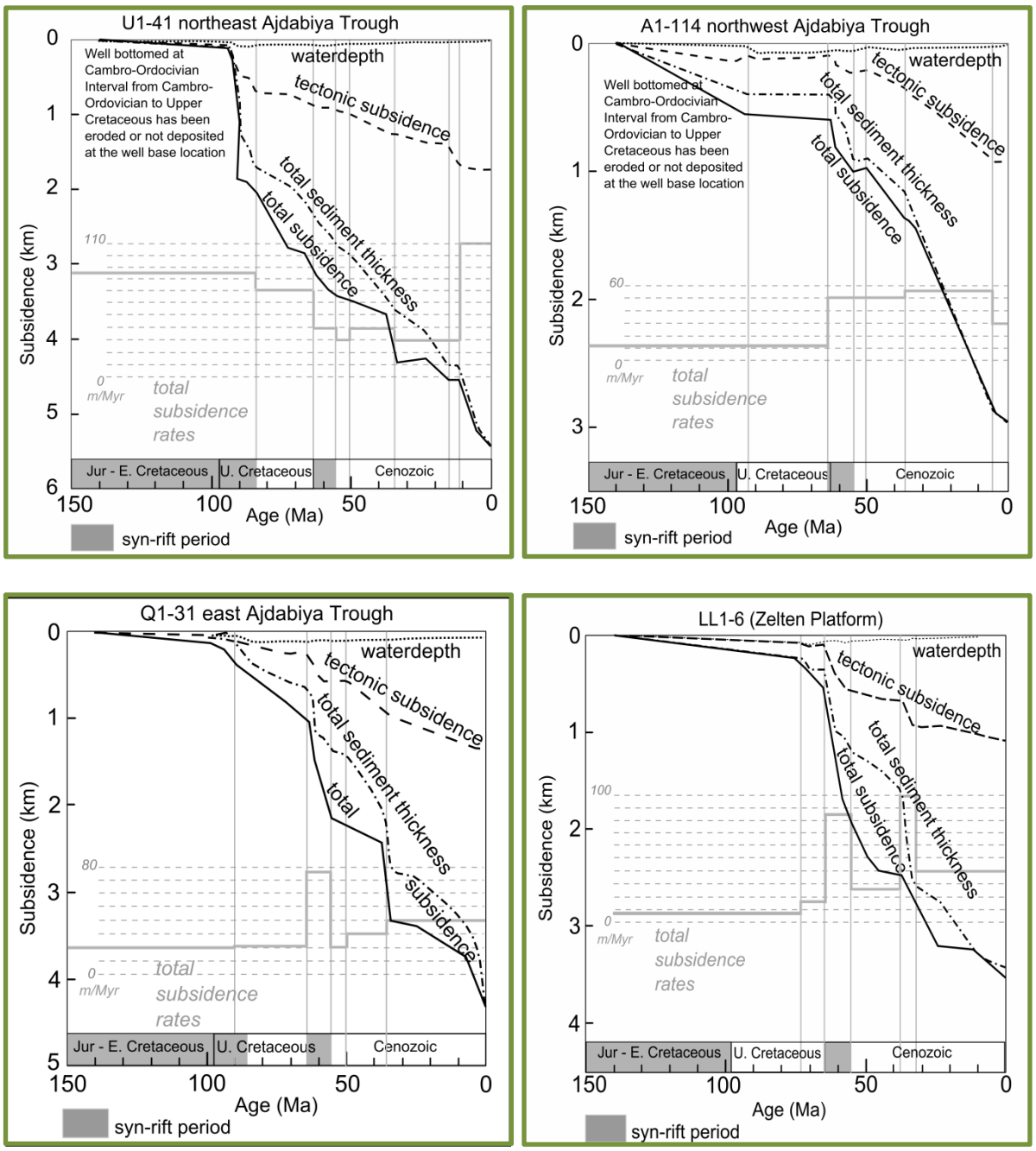

Figure 6.18: Subsidence curves inferred by backstripping for the wells U1-41 and Q1-31 located at the eastern side of the Ajdabiya Trough and the wells A1-114 and LL1-6 located to the west of the trough. For location of the wells see figure 6.5. The curves show the variations in the tectonic subsidence of the basement calculated with the assumption of isostatic response of the lithosphere to sediments and water load. The dashed line in the diagram denotes the tectonic subsidence of the basement calculated by the removal of the load of water and sediments from the surface of the basement within the basin (the backstripping technique); the thick line denotes the total subsidence of the basement obtained from the decompaction of the total sedimentary thicknesses: the dashed dotted line indicate the total sediment thickness encountered. The high subsidence rate is recorded at the well U1-41 located at the north-eastern part of the Ajdabiya Trough. The high subsidence is in agreement with observations obtained by previous investigators at this location (e.g. Abadi et al., 2008).

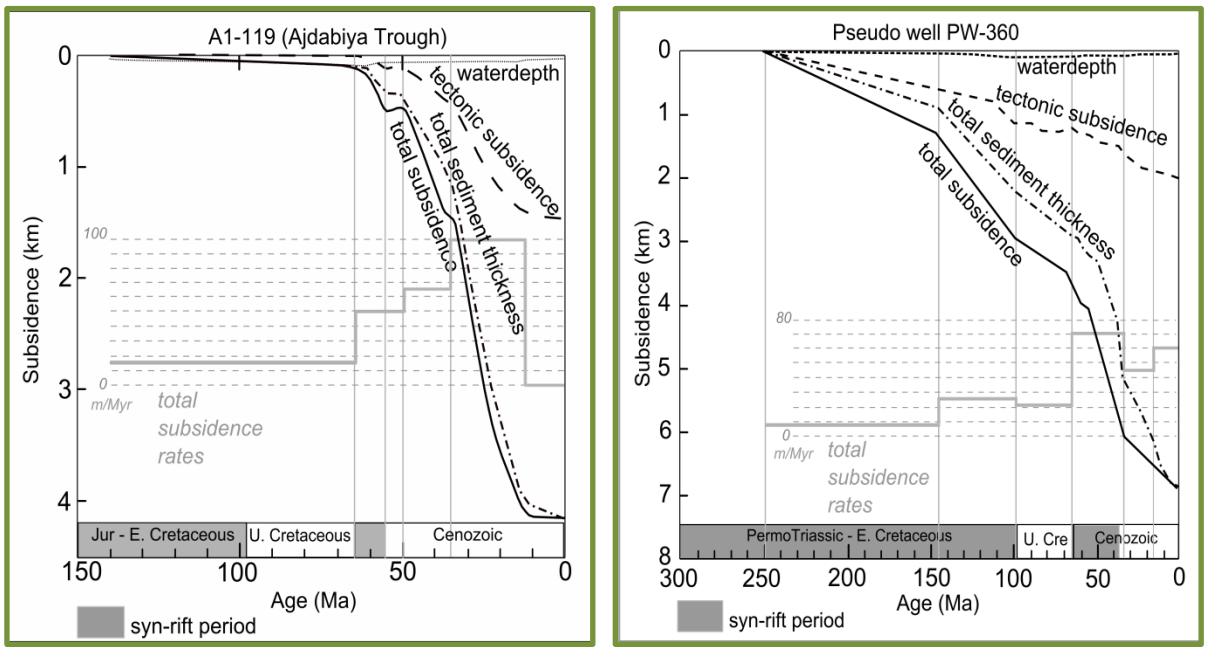

A **B**

Figure 6.19: Subsidence curves inferred by backstripping of the A1-119 well (A) and the pseudo well PW-360 (B). For location of the wells see figure 6.5.

6.4.3.2 Tectonic Subsidence Mapping

The tectonic subsidence contour maps were created through the interpolation of group of wells (Table 6.1). The subsidence is calculated in each well individually using the same equations and parameters (Formation densities, porosity, and water depths) that used in constructing the subsidence curves from 5 wells. Then the final maps were compiled for distinct stratigraphic boundaries correlated with the tops of Paleocene, Eocene, Oligocene and Miocene time units. The obtained subsidence results from the wells were gridded using the Oasis Montaj gravity and magnetic mapping software. A 500 meter grid cell size was sufficient to overcome any possible gaps or spacing could exist on the maps. Due to the wide distribution of the wells, some isolated spots may occur, however the maps display a general spatial trends in the regional distribution of the subsidence within the study area.

6.4.3.2.1 Subsidence Maps (map suites)

The tectonic subsidence maps are different from time and isopach maps, it provides knowledge about the subsidence pulses attributed to tectonic and thermal mechanisms rather than sediment accumulation centres. Before mapping any data, the tectonic subsidence and

the thickness can be cross plotted to look for trends and first-order relationships between the maps.

Subsidence maps presented here, outlining different estimates of thinning owing to variations in crustal stretching within the study area depending parameters derived from wells in the platforms, where tectonic subsidence is generally less than 1,000 meters, or from basins where the tectonic subsidence may exceed 1500 meters. The produced maps show that the subsidence in Ajdabiya Trough has occurred in pulses, based on temporal variations during the period of late Mesozoic (Upper Cretaceous) to Cenozoic (Paleocene – Miocene, 65 – 5.3 Ma).

The maps (Figure 6.20) show that a strongly spatially varying subsidence pattern is evident during the Paleocene and Eocene, with possibl minor uplift occurring during the Eocene to the southeast which would have stimulated tilting and erosion during this time (e.g. Gumati and Nairn, 1991; van der Meer and Cloetingh, 1993; Abadi et al., 2008). The mid Ajdabiya Trough shows a largely similar subsidence patterns during the same period. Subsidence is continued in the northern part of the trough during the Oligocene and Miocene time as shown on the maps.

The most noticeable features observed on the subsidence maps of the Ajdabiya Trough appears to be the increase of subsidence during the post-rift period (Eocene – Miocene) (Figure 6.20), which characterized by a gradual subsidence and occasionally high sedimentation rates, compared to the early syn-rift subsidence (e.g. Abadi et al., 2008; Baird et al., 1996; Bezan and Malek, 1996; Bezan, 1996; Gumati and Niurm, 1982). Although the 2D seismic data analysis restricts knowledge of the underlying structures essentially composed of pre-rift and syn-rift sequences, the preliminary results obtained here has a strong implication for the rifting history. As evidenced from the gravity and the magnetic data (chapter 4), the post-rift subsidence is presumably governed by thermal state of the lithosphere during early rifting stages (e.g. Gumati and Kanes, 1985; van der Meer and Cloetingh, 1993; Cloetingh et al., 2005; Abadi et al., 2008), and recently challenged by (Holt et al., 2010 and Galushkin et al., 2014).

The maps, shows that the Cenozoic subsidence in the Ajdabiya Trough can be divided into four major phases' post-rift subsidence and fault-reactivations.

The geometry of the Cenozoic post-rift sediments may give an impression that it possesses steerhead geometry (e.g. Graversen, 2002). However the thick interval above the central trough is due to a combination of post-rift compaction of the syn-rift sediments in the underlying graben fills.

Phase I: Paleocene - Early Eocene (65–56 Ma)

The most pronounced feature on the Paleocene map is the rapid subsidence rate recorded by wells situated on the south-western part of the Ajdabiya Trough (Figure 6.20). The maps show variations in subsidence in time and magnitude during the Paleocene with high subsidence rate at the southern part of the trough associated with possible re-new rifting or fault re-activation (Abadi et al., 2008) and the deposition of Paleocene carbonates (Bezan. 1996, Bezan and Malek, 1996). Sediment accumulation rates were even lower on the trough margins, which may be sites of Paleocene faulting and relative uplift, locally associated with compression (El Arnauti et al., 2008). Abrupt changes in sediment thickness towards the north are associated with numerous, small-offset faults on seismic data (Figure 6.21) and local thickenings into small graben-like depressions. Variation in subsidence rates across the trough strongly controlled the thickness and to a lesser extent, the facies distribution of the Paleocene units. This phase of high subsidence was followed by the deposition of lower Eocene carbonates and evaporites owing to continuous subsidence activity during this period (Abougares, 1996). To the north and north-east of the Ajdabiya Trough, low subsidence rates were succeeded by small uplift pulses marking the end of the Paleocene and the beginning of a period of almost zero subsidence. Uplift and erosion of Paleocene section has been documented from well (A1-114) near Al Jahamm Platform and well (A1-41) near Soluq Depression to the north-east (Yanilmaz et al., 2008). A sudden uplift pulse or very low subsidence rate is evident during the Eocene in this part as shown on the Eocene map (Figure 6.20) and is succeeded by a pronounced subsidence peak over the Soluq depression.

The Paleocene subsidence pattern shows the characteristic segmentation into narrow depocentres to the south of the study area (Figure 6.20) due to possible fault reactivations. Subsequent thermal cooling saw onset of a later Paleogene sag phase of subsidence, with the basin depocentre migrating into the north (Burwood et al., 2003), which probably caused by northward jumps of the Cretaceous and older faults. Conversely, the Paleocene–Eocene Sirt

basin tectonic regime is extensional, revealing a major stretching event under a NE–SW extensional regime (Schäfer et al., 1981; van der Meer and Cloetingh, 1993).

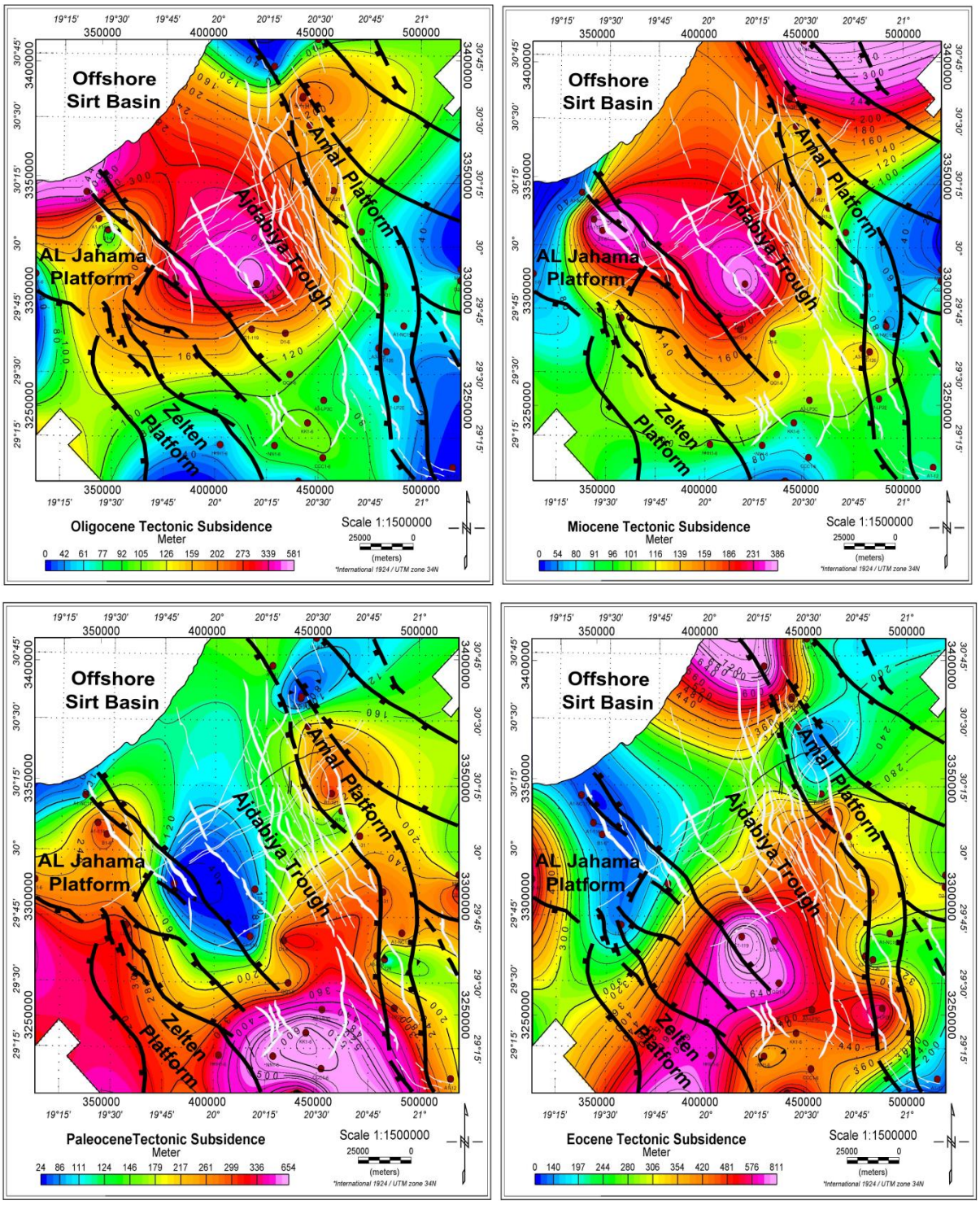

Figure 6.20: Tectonic subsidence maps of the Ajdabiya Trough obtained wells, displayed as a cumulative subsidence during the Paleocene, Eocene, Oligocene and Miocene times.

Seismic data and subsidence maps show that the oldest deposits are located at the southern part of the Ajdabiya Trough that accumulated within graben fill system of the main mapped faults. This mechanism is illustrated by the subsidence maps. The early narrow graben widened while moving to the north and mainly controlled by NW- and roughly N–S-trending faults. The Paleocene subsidence map show that the structural history of the trough is primary constrained to local fault-bounded depocentres.

During the Paleocene period, the tectonic subsidence increased in the southeastern part of the Ajdabiya Trough with the development of the narrow depocentres close to the eastern trough bounding fault zones. Seismic data (Figure 5.13) reveal that the main bounding fault zones were active in its southeastern part only, with vertical offsets ranging between 100 and 150 ms TWT.

Secondary fault activity along these fault zones antithetic faults has also controlled the development of the depocentres (Figure 6.20). Such an evolution demonstrates a concentration of the deformation with a significant fault activity bounding the Ajdabiya Trough.

Phase II: Eocene - Early Oligocene (56 – 33.9 Ma)

Eastward in the Sirt Basin, Paleocene and Early Eocene subsidence confirms that an extensional context prevailed in the Paleogene in the southern East Mediterranean domain (Anketell, 1996). The phase of rapid subsidence during both the Paleocene and the early Eocene times reflects either a re-new rifting phases (e.g. Gumati and Nairn, 1991; Abadi et al., 2008; Capitanio et al., 2009; Galushkin et al., 2014) or fault re-activation during which the lithosphere isostatically responds to crustal thinning; these are followed by a post-rift phase with decelerating tectonic subsidence rates driven by thermal re-equilibration modulated by plate interactions (Late Eocene - Miocene). The Sirt basin undergoes compression during Middle–Late Eocene tilting the basin northward, causing abrupt subsidence in the north and uplift on the basin southern shoulders, and possibly driving the latest stage of regional minor subsidence (van der Meer and Cloetingh, 1993).

The Eocene subsidence map (Figure 6.20) show that the Eocene subsidence within the Ajdabyia Trough resulted in a single elongated depression extended along NE-SW axial trend comparable to the trend strike slip faulting in Cyrenaica Platform at this time (e.g. Anketell,

1996; El-Arnauti et al., 2008). During the Eocene, deviations from this subsidence pattern can be observed affecting different parts in the Ajdabiya Trough concentrating in the south and gradually decreased to the north east suggesting component of uplifting and erosion (Baird et al., 1996). Early Eocene sediments depocentres (e.g. Gir Formation), were the result of strong tectonic movements and associated subsidence and rejuvenation of faulting during Early Eocene time (Gumati and Nairn, 1991; Abugares, 1996). During the Late Eocene a compression event caused regional tilting and subsidence in Ajdabiay Trough (e.g. Baaske et al., 2013), aside from that event, the Eocene was a period of minor tectonic activity.

Minor tectonism at the Oligocene-Miocene boundary as well as at the Eocene-Oligocene boundary is also reported in the western Sirt Basin by Anketell and Kumati, (1991).

Seismic data (Figure 6.21) show an evidence of low fault movement during the Late Eocene which indicates that sediment loading and thermal relaxation may play significant role in the subsidence mechanism during the Late Eocene. The faults are most active in the southern part of Ajdabiya Trough during the early Eocene and exhibit negligible throw across the Upper Eocene – Miocene strata. The absence of faulting during the late Eocene subsidence stage may also suggest a component of lithospheric folding (Cloetingh et al., 1999), and thermal activation reproduced by gradual uplifting of a top of a hot diapir with temperature 1100°C isotherm (Galushkin et al., 2014), which may be related to the mantle upwelling as evidenced from large areas in Europe (Cloetingh and Van Wees, 2005). Narrow to basin wide deposition caused by the post-rift thermal subsidence, mainly attributed to fluctuating of intraplate stress field and/or migration of rift activity caused by the strain burdening of the previously stretched lithosphere (Cloetingh et al., 2005; Abadi et al., 2008).

From the early Eocene to the Pliocene, interior sag dynamics persisted, with a gradual eastward shift of the sag axis (Rusk, 2002). I postulate that movement and new phase of rapid subsidence occurred close to NE-SW basement lithological trends and crustal fracture zone in the Ajdabiya Trough. Reactivated crustal scale fracture zone trending NE-SW is evidenced from the gravity and the magnetic data interpretation (Chapter 4). Crustal fracture zone correspond to major crustal scale zone of weakness (Anketell, 1996; Craig et al., 2008), and have been important reactivation zones through time.

The depositional environment within the Ajdabiya Trough was influenced by a combination of major subsidence interacting with minor local tectonics, climate and eustatic sea-level changes (Abugares, 1996; Wennekers et al., 1996; Spring and Hansen, 1998).

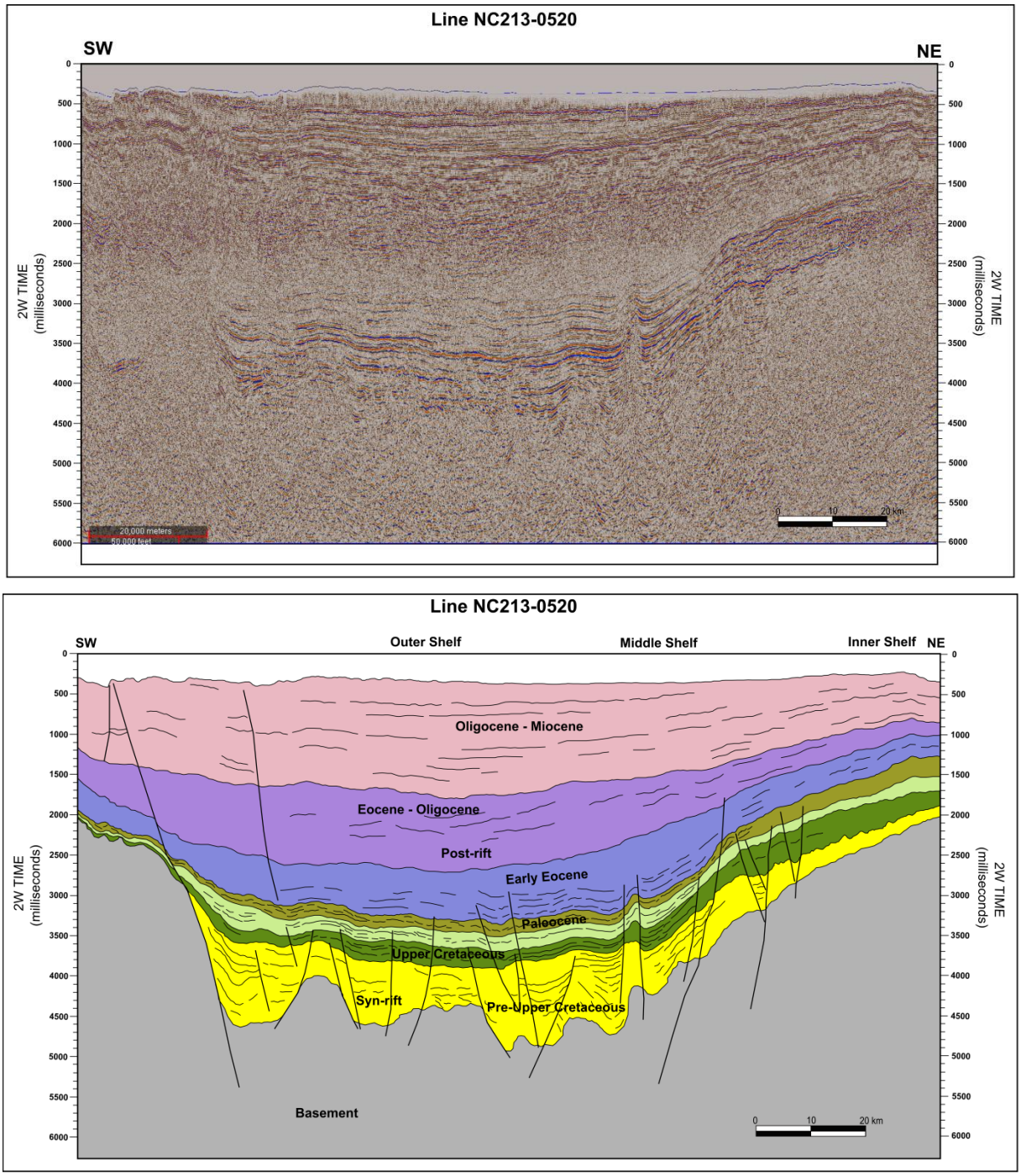

Figure 6.21: SW - NE transect line **05-NC213 0520**, across the Ajdabiya Trough (see location in figure 6.5), demonstrates the remarkably uniform subsidence that occurs throughout the Cretaceous and Tertiary. Also evident is an abrupt reorganisation of the margin at the end of the Cretaceous with a significant change to the location sediment accumulation in the Tertiary.

Phase III: Oligocene – Miocene (33.9 – 23.0 Ma)

An Oligocene rift phase is evident for many East African basins (e.g. Tenere, Sudan, and Anza basin; Genik, 1992). Although the geodynamic processes underlying this event are not clear, Guiraud et al., (1992) discussed the resumption of crustal stretching in terms of a renewed intraplate stress regime. In the sedimentary fill of the Sirt Basin this stretching event is evidenced by a widespread unconformity (Barr and Weegar, 1972; Benfield and Wright, 1983), marking the onset of a period of low and decelerating subsidence rates. According to the Oligocene map shown in Figure 6.20, the "tectonic" subsidence of the Ajdabiya Trough region since the late Oligocene has been approximately 580 m. This subsidence appears to have occurred at a fairly constant rate. The observed subsidence is characteristic of subsidence related to the evolution of passive continental margins (Steckler and Watts, 1978) and does not indicate active faulting. The main axis of the subsidence in the Ajdabiya Trough coincident well with thick section in excess of about 2500m of sediments, while in marked contrast, not far to the west at an Eocene exposure outlined by (Baird et al., 1996) (Figure 6.22), this sequence is entirely absent. This suggests that the central Ajdabiya Trough remained as actively subsiding during post-Eocene time. The sediments of this period also represent large scale regressive episode (Yanilmaz et al., 2008), the terminal phase of Sirt Basin development. During the Oligocene, subsidence in Sirt Basin decelerated and reefs developed along the platform areas (El Hawat et al, 2007; Yanilmaz et al., 2008) associated with flood basalt effusions in the west (Busrewil et al, 2008).

During the Late Oligocene the whole Sirt basin underwent exposure and, apart from a few troughs especially in their southern parts, remained uplifted during the Neogene. It has been suggested by Wilson and Guirand, (1998) that the NE transcurrent movement of Africa was slowed enough during the Oligocene for a mantle hotspot to accumulate magma for eruption.

After the regressive phase at the Oligocene–Miocene boundary and a short stop in the sedimentation influx, deformation was extended to the north-eastern part of the Ajdabiya Trough where a main depocentre developed (Figure 6.20). Seismic data show the development of onlap and downlap terminations, within parts of the Oligocene sequence which are interpreted in terms of sea-level variations and an increase of the subsidence during the Oligocene (Abadi et al., 2008). Contrary to the Late Eocene evolution, an oblique

orientation to the northeast during the Oligocene was possibly formed by reactivation along a crustal shear zone (Anketell, 1996; El-Arnauti et al., 2008).

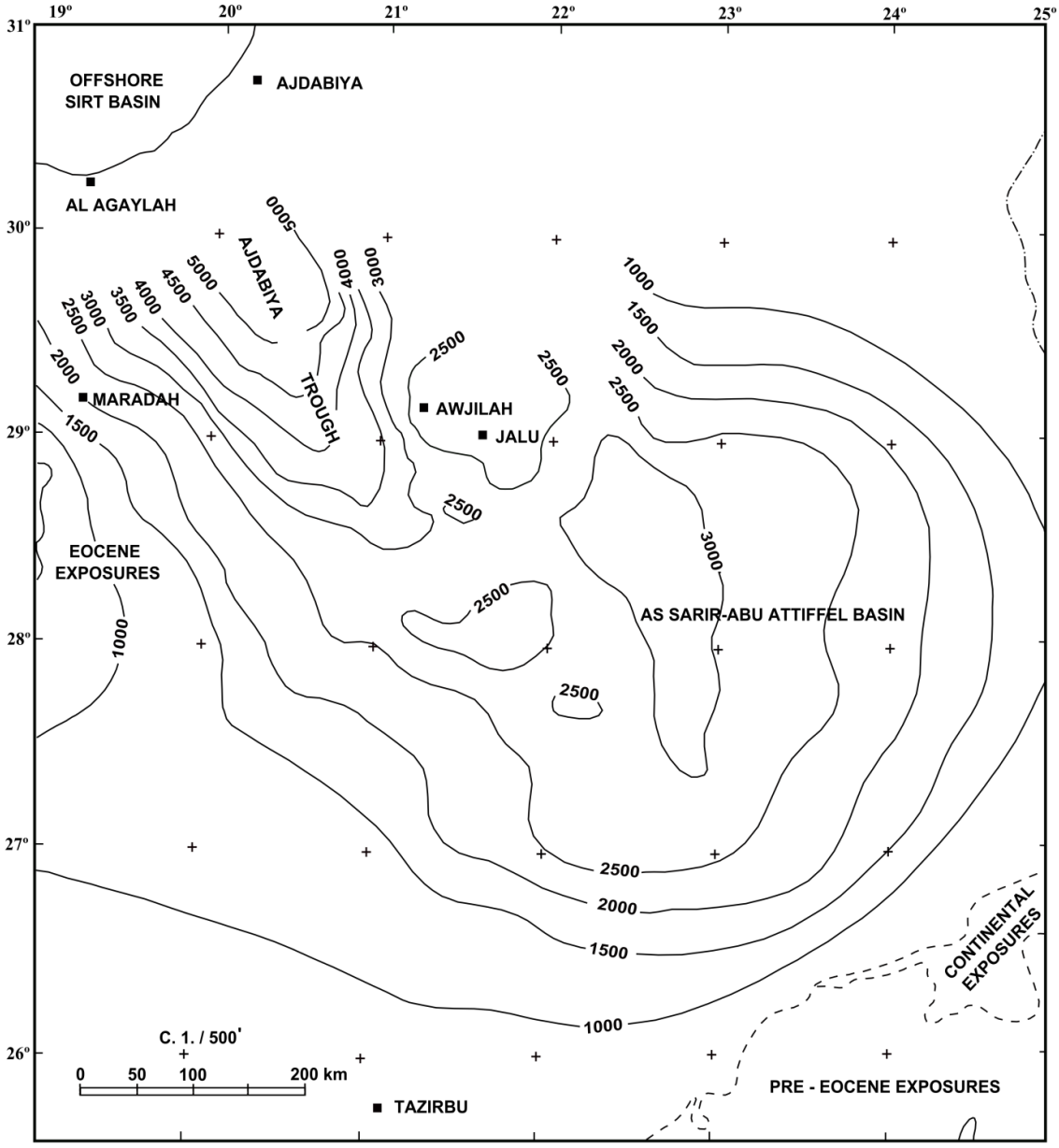

Figure 6.22: Isopach map of Oligocene to Miocene sediments section (post-Eocene) of the eastern Sirt Basin. Re-drawn from Baird et al., (1996)

The crustal shear zone must likely also has a strong influence on controlling the broad subsidence of the northern part of the Ajdabiya Trough during Oligocene to Miocene times at which the depocentre in the Ajdabiya Trough shifted from NNE-trending during the Paleocene-Eocene to nearly NW-trending latter during the Oligocene and at which rapid south

to north migration of the depocentre took place (Figure 6.20). During the Early Oligocene the axis of subsidence of the Ajdabiya Trough is migrated towards the north.

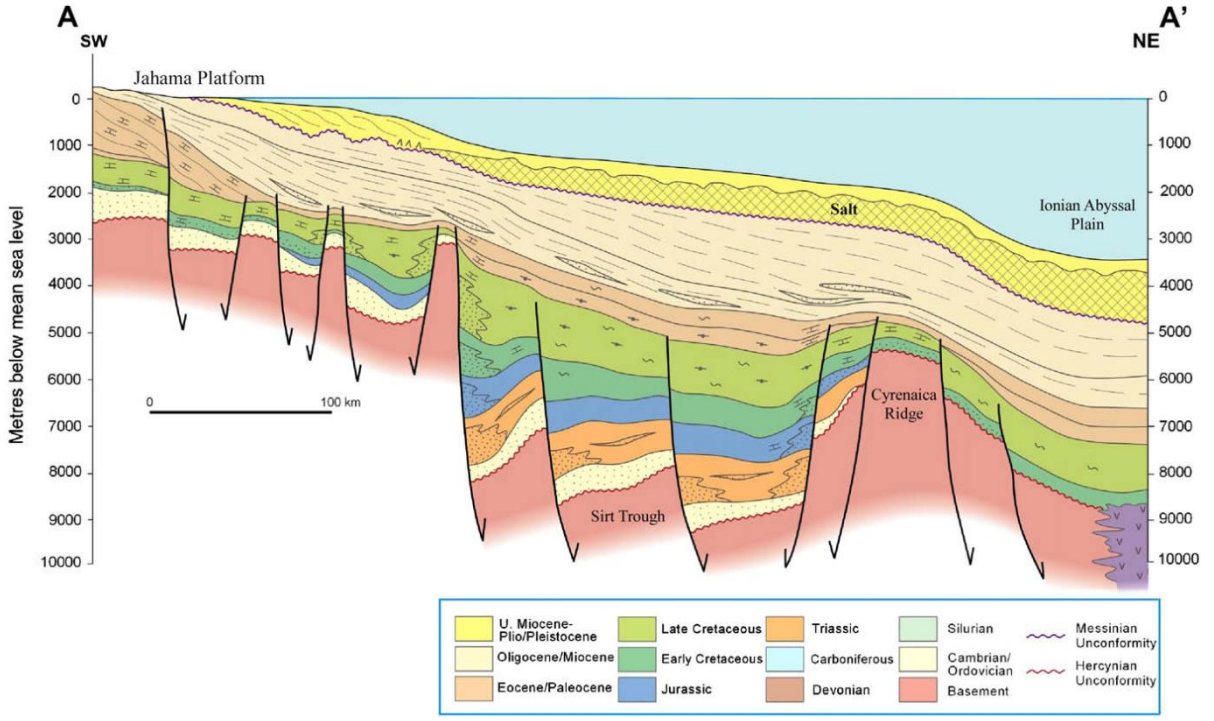

Figure 6.23: Cross-section **A–A'** is a south to north oriented schematic interpretation drawn across the Sirt Embayment see Figure (6.5) for location. It shows the progradational character of Cenozoic strata along the Sirt margin and a hypothetical wedge of halite associated with the Messinian section. The existence of the salt wedge was postulated to explain the loss of seismic reflections below the top Messinian unconformity. A wedge of salt, as shown, would be unstable and should show significant deformation. Cross-section obtained from Fiduk (2009).

The subsidence rates decelerate to very low levels during the Late Oligocene-Early Miocene at the southern part of the Ajdabiya Trough (Figure 6.20), However subsidence is continuing towards the offshore area to the north. Accordingly during the late Oligocene - early Miocene, the Ajdabiya Trough was still accommodating to the Eocene - early Oligocene subsidence, with low fault activity observed. The eastern side of the trough became the main source for siliciclastics starting in the latest Oligocene (El Hawat et al, 2007) with uplift followed by tilting through the early Miocene (Figure 6.20). The Oligocene – Miocene time is characterized by a northward tilting of the Ajdabiya Trough, (Baird et al, 1996) a sort of bending down of the north margin of the African continent to the west of the Cyrenican shelf (Fiduk, 2009), (Figure 6.23) with continued subsidence in the Ajdabiya Trough.

The overall tectonic framework of the Ajdabiya Trough during the Oligocene time varied considerably from that which had prevailed since the Upper Cretaceous. The tectonic activity gradually decreased during the Late Eocene (Bezan, 1996) and the subsequent filling of the trough helped to mask the older tectonics. Baird et al., 1996 suggested that the main phase of basin subsidence in Sirt Basin is coincident with thickening of Oligocene – Miocene sequence in the Ajdabiya Trough, while in marked contrast, not far to the west at an Eocene exposure, this sequence is absent. Mainly the eastern part of the Sirt Basin remained as actively subsiding during post-Eocene time. Regional uplift and possible exhumation of the northeast Ajdabiya Trough took place along the main trough bounding faults (e.g. van der Meer and Cloetingh, 1993; Yanilmaz et al., 2008) during the Late Eocene to Early Oligocene. Stratigraphic evidence and fossil assemblages (Yanilmaz et al., 2008) suggest that the Oligocene sediments were deposited in a near sea level basin, which has been uplifted in post-rift times.

Phase IV: Miocene - Recent (23 – 0 Ma)

The Miocene tectonic subsidence map (Figure 6.20) show a zone of rapid subsidence patterns towards the northern part of the Ajdabiya Trough near the offshore area.

Following a period of uplift and erosion associated with Late Oligocene uplift and erosion, a second relatively rapid subsidence observed during the Miocene which was succeeded by a generally exponentially decaying subsidence during the Late Miocene as observed from the subsidence curves (Figure 6.18). It is suggested also by Savostin et al., (1986), Livermore and Smith, (1985), that the phase of low subsidence rates during the Miocene coincides with the final change to north-eastward compressional motion of Africa relative to Europe that was accompanied by a rotation of the paleo-stress field to ENE-WSW compressional during Early-MiddIe Miocene and N-S during Late Miocene (Le Pichon et al., 1982).

The generally slow subsidence during the Miocene is followed by a relatively rapid concave-down subsidence since at least the early Pliocene. In particular, the Miocene rapid subsidence in the northeast part of the map nears to the Soluq Depression in Cyrenaica Platform and adjacent to area that formed the fault-bounded Ajdabiya Trough containing a block-faulted Miocene sequence attributed to strong strike slip component (e.g. El Arnauti et al., 2008). The cause of the subsidence increase in the centre of the trough is not well understood, but it may

reflect minor adjustments in the strain partitioning of the Sirt Basin extension also. It is therefore reasonable to suppose that the rapid subsidence at both the centre and the northeast part of the Ajdabiay Trough (Figure.6.20) may be due to some form of lithospheric extension. Post-rift subsidence rates for the Ajdabiya Trough during the Early - Mid Miocene are very high, slowing somewhat during the Late Miocene - Recent with up to 2 km of Miocene post-rift section having been deposited. Such thick accumulations of sediment have been cited as evidence for the formation of the Ajdabiya Trough as a downwarping basin (Baird et al., 1996). 2D seismic data show that few faults can experience low offset during the Miocene within the Ajdabiya Trough, suggesting that the subsidence during the Miocene mainly was not controlled by any large displacement faults, so no fault related cause as an extensional setting can be invoked.

6.5 Measurements of Brittle Extension and Stretching Factor

The northern part of the Ajdabiya Trough has subsided about 2 km with virtually no visible faulting, observed during the Oligocene and Miocene times, in contrast to the Cretaceous - Early Eocene time, which has recorded a large amount of subsidence possibly dissected by brittle extension. To gain insights about how the lithosphere deformed during extension, brittle extension measured from fault heaves is compared with extension estimated from crustal thinning measurements obtained from the gravity modelling (chapter 4).

The tectonic subsidence in any extensional settings such as rift basins is commonly described as the vertical movement of the basement due to isostatic compensation and thermal re-equilibrations of the continental lithosphere after stretching (Sleep, 1971; McKenzie 1978). Initially, there is an isostatic adjustment, or initial subsidence, due to the crustal thinning. This is followed by a thermal subsidence as heat is lost by conduction through the surface and the crust and lithosphere cools. This stage of subsidence consists of an exponential pattern associated with the thermal relaxation of the lithosphere. The amount of lithospheric extension is normally quantified by the so-called β factor which corresponds to the ratio of lithospheric thickness before and after stretching.

The lithosphere thermal anomaly correction using the lithosphere stretching and thinning model of McKenzie (1978) requires, the lithosphere stretching factor, β, to define the lithosphere thermal perturbation, and the lithosphere thermal re-equilibration.

The stretching model has been quantified by McKenzie (1978) (Figure 6.24), who gives the following expressions for the initial subsidence, S_i, and the thermal subsidence, S_t:

$$S_i = \frac{L\left\{(\rho_m - \rho_c)\frac{t_c}{L}\left(1 - \frac{\alpha T_m t_c}{2L}\right) - \frac{\rho_m \alpha T_m}{2}\right\}\left[1 - \frac{1}{\beta}\right]}{(\rho_m(1-\alpha T_m) - \rho_w)} \qquad (6.9)$$

$$S_t = \frac{4L\alpha\rho_m(T_m - T_o)}{\pi^2(\rho_m - \rho_w)}\left(\frac{\beta}{\pi}\right)Sin\left(\frac{\pi}{\beta}\right) \qquad (6.10)$$

L = Lithospheric thickness
ρ_m = density of Mantle lithosphere at 0 C°
ρ_c = density of crust at 0 C°
t_c = crustal thickness
α = coefficient of volume expansion
T_m = temperature of mantle
β = stretching factor
ρ_w = density of water
κ = thermal diffusivity
τ = thermal decay time constant of the lithosphere

$$\tau = \frac{L^2}{\kappa\pi^2}$$

The thermal subsidence in the McKenzie model is the subsidence of the basin in the absence of sediment loading. Hence, S_t is equivalent to the tectonic subsidence and uplift obtained by backstripping. Given the backstripping results, it is therefore possible to estimate β.

A simple expression can be derived from equation 6.10 (McKenzie, 1978), which relate the amount of tectonic subsidence (TS) to the amount of stretching (β) assuming an Airy isostatic model where the masses of the lithosphere are balanced everywhere (Watts, 1988; Stewart et al., 2000).

$$\beta^{-1} = 1 - \frac{TS(\rho_m - \rho_w)}{t_c(\rho_m - \rho_c)} \qquad (6.11)$$

Calculation of the lithospheric stretching factors and analysis of tectonic subsidence are essential for understanding the dynamic mechanism of the Ajdabiya Trough. In addition to the calculation of the stretching factor using equation (6.11), I adopted gravity and magnetic modelling (chapter 4) to quantify the stretching factor based on estimated approach to the crustal thickness before and after stretching. Modelling based on backstripping techniques provided stretching factors for the different rifting episodes of the Sirt Basin (Gumatti and Narin 1991; Abadi et al., 2008). These authors suggested mean Early Cretaceous to Paleocene stretching factors between 1.1 and 1.75 for different locations within the Ajdabiya Trough.

Based on the study of Galushkin et al., (2014) who adopted thermal modelling in their calculations, the maximum stretching factor obtained within Ajdabiya Trough is about 1.5 based on synthetic well analysis indicating high stretching within the trough depcentre, which can be attributed to Cretaceous rifting. The magnitude of the Late Cretaceous - Paleocene rifting is more difficult to determine using subsidence modelling owing to the lack of sufficient drilling penetration. These stretching factors are much higher than that obtained by the gravity and magnetic modelling and measurement of coeval normal fault heaves in this study. The whole crust stretching factor is preliminary derived from the Moho depth with incipient crust thickness varying from 26 to 35 km. The highest lithospheric stretching factor obtained based on the pseudo well PW-0360 is about 1.45 which nearly matches the results obtained by Galushkin et al., (2014). Extension estimate across rift margins at upper crustal level may have controlled the initiation of fault geometries (Davis and Kusznir, 2004). Extension measured from fault geometries is lower than that required to explain whole crustal and lithospheric thinning (Reston, 2009).

The geologic interpretation used in this study assumes that the early rift in Ajdabiya Trough composed of two possible phases of rifting during the period from Jurassic - Early Cretaceous. Though a simpler, single-phase interpretation of the rifting history of this part of the Sirt Basin is possible, a maximum estimate of brittle extension is desired.

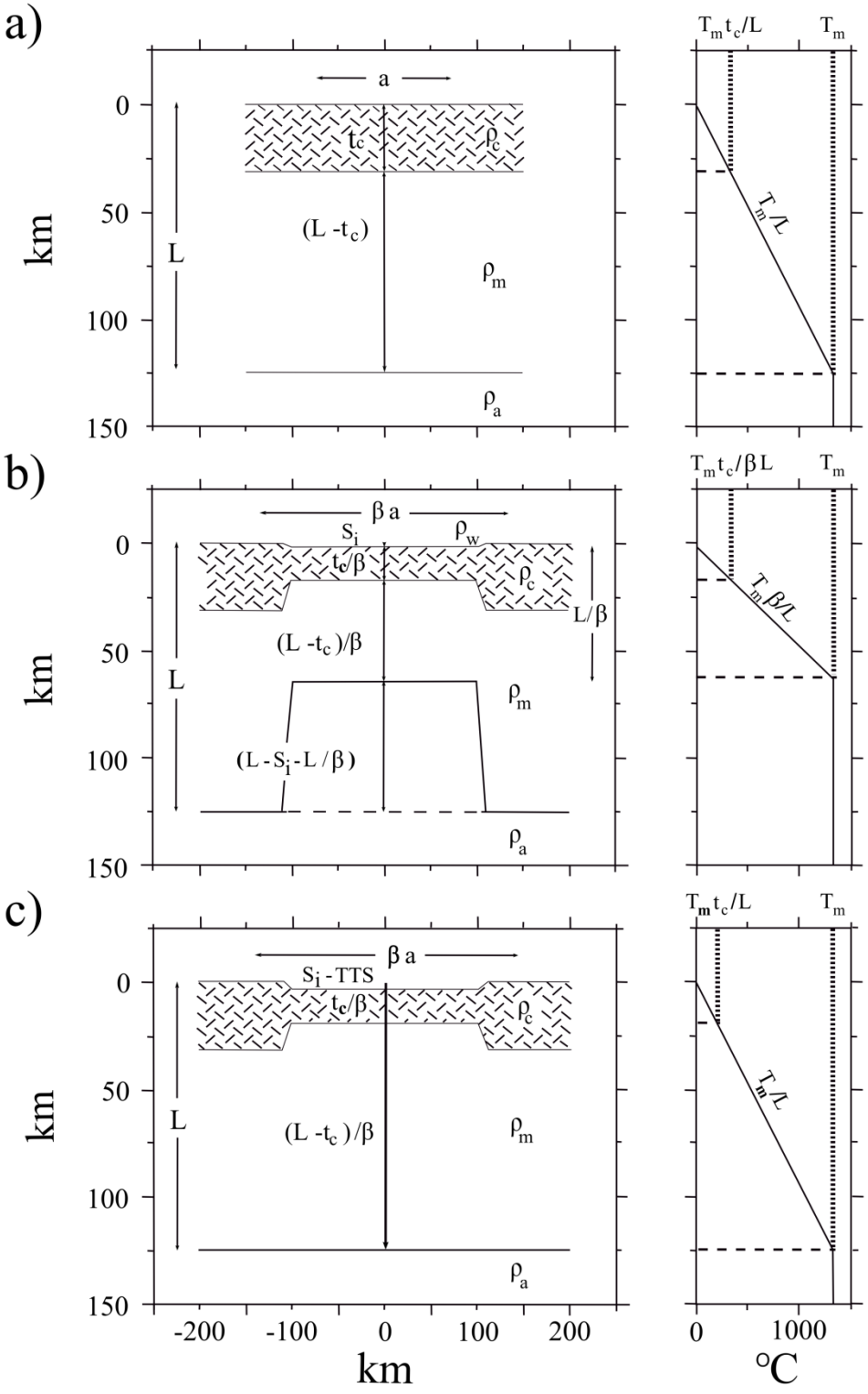

Figure 6.24: Stretching model proposed by McKenzie (1978), explaining the initial basin subsidence and the thermal structure of the lithosphere. a) Pre-stretched lithosphere. b) After instantaneous rifting event. c) After thermal relaxation of the lithosphere and recovery of the initial temperature gradient.

Seismic line 05NC213-0360, passing across the Ajdabiya Trough close to the active rifting zone, was chosen as the primary section along which to estimate brittle extension (Figure. 6.17). Extension factor is calculated using fault heaves obtained from system of extensional faults evolved during the rift periods. I also calculated the total extension length (Lt = 18.0 km), the stretch (E = L/Lt = 55.68%, where L is the present-day length), and the extension factor ($\beta = L/(L - Lt) = 1.3$) as shown in Table 6.7.

Due to complexity of the rift geometry within Ajdabiya Trough, the total extension is presumably underestimated. Complexity raising from possible contribution of mantle melting, effects of sub-seismic scale faulting (e.g. Scholz & Cowie 1990), and other factors.

As suggested by Marrett & Allmendinger (1992), 25 – 60% of extension a cross an extensional basin occurs by faulting on small faults below seismic resolution. In this case extension estimates within the Ajdabiya Trough could be minimum estimates due to the effect of sub-seismic faults that can not be observed on seismic profiles in addition to possible internal deformation. The low resolution of the used 2D seismic data in this study is most likely missing a large percent of sub seismic faults, and accordingly the data approximately underestimates extension in the Ajdabiya Trough area. Also the whole-crust extension determined using gravity data is possibly within error, and indicate low degree of whole-crust extension in the central Ajdabiya Trough; however a significant contribution of extension from unknown faults is expected.

Table 6.7: Extension factors caused by normal faulting in the southern Ajdabiya Trough, along seismic line 05 NC213-0360 with estimate of an average total crustal extension of 55.68% over the trough.

Region	Length (km)	Period	Deformed Length (km)	Stretch (%)	Total extension length (km)	Total extension (%)	Stretching factor (β^f) Crustal thickness & fault heaves	Stretching factor (β^f) Bckstripping	Stretching factor (β^f) Literature
South	85	Basement	18.0	21.17			~ 1.3		
Ajdabiya	85	und Pre-UC	11.0	12.94			~ 1.3	~ 1.35 - 1.5	1.263 -1.5
Trough	85	Pre-UC	5.5	6.47					
	85	UC	3.5	4.11	47.33	55.68		~ 1.145 - 1.45	
	85	Paleocene	1.5	1.76				~ 1.02 - 1.095	
	85	E. Eocene	0.75	0.88				~ 1.055 - 1.08	

The Ajdabiya Trough formed by lithospheric extension by a factor of about 1.45, lasting from Late Cretaceous – Miocene times. Streching factores calculated from subsidence curves agree

with those calculated from the geometry of the interpreted faults and from the crustal thining model obatained from the gravity and magnetic modelling.

6.5.1 Stretching Distribution

The stretching factor map (Figure 6.25) based on estimates of initial and final crustal thickness inferred from gravity and magnetic studies (chapter 4) show that extension occurred during early rifting stage (basin forming time), throughout the development of a local areas of thinning separated by areas of reduced stretching at the trough shoulders (platform areas). Data analysis in Ajdabiya Trough suggested that, initial, basin subsidence is shaped the study area during the 140 - 100Ma characterized with high stretching factor at the basin centre (β = 1.3), and followed by thermally-driven subsidence which interrupted by short period of fault activity along the Ajdabiya Trough shoulders (e.g., Baird et al., 1996).

Fault-dominated initial subsidence occurs only during rifting, and is limited to an active zone (McKenzie, 1978). Fault mapping using 2D seismic data, show that the trough bounding faults exhibit negligible throw across the Tertiary reflections, and do not cross cut the above reflections. The 2D seismic analysis show that fault-related differential subsidence abated during period from Late Eocene to Miocene.

This along strike variation in the timing of faulting is also reflected in sediment accumulation, with the thickest accumulations in the northern part of the trough occurring up to the Eocene reflector. The highest sediment accumulation rates occurred during times of greatest subsidence. The reason for this is possibly because the amount of preserved sediment was dependent directly on the amount of basement subsidence (depth dependant subsidence).

Modelling based on backstripping techniques, using number of stretching phases provided stretching factors for the different periods of extension and fault reactivation possibly linked to rifting episodes of the Sirt Basin (Anketell, 1996; Abadi et al., 2008; Baird eta l., 1996; El Arnauti et al., 2008; Gumatti, 1987; Gumatti and Nairn, 1991; Skuce 1996; van Wess and Clothings, 1996; Glukshtin et al., 2014).

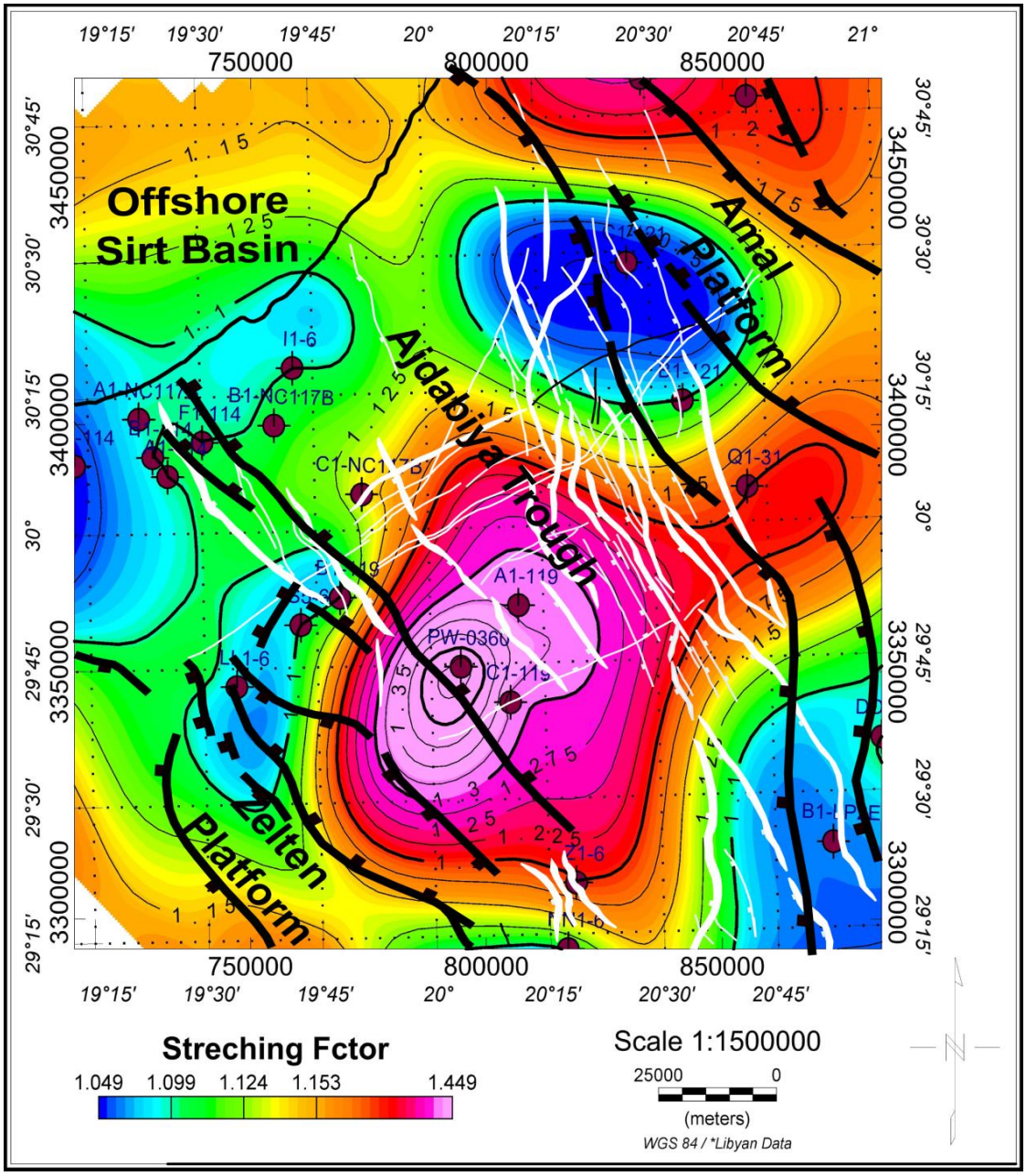

Figure 6.25: Stretching factor map for the Ajdabiya Trough calculated as the ratio of the initial crust thickness (~35 km) to the final crustal thickness, as inferred from gravity and magnetic modelling (chapter 4) and showed values ranging from 1 near basin shoulders to about 1.4 in the depocentre. Gumati and Nairn, 1991 suggested β values in the range of 1.1 – 1.75 for the Ajdabiya Trough, recently Abadi et al., 2008 derived an amount of 1.263 in the southern Ajdabiya Trough for 98.9 - 83.5 Ma stretching phase followed by thermal subsidence until 65 Ma.

These authors suggested different periods of basin evolution composed of rifting and subsidence. They determined mean Early Cretaceous stretching factors in the range of 1.06 and Late Cretaceous stretching factors between 1.2 and 1.263 for the southern part of Ajdabiya Trough. Abadi et al., (2008) have provided ß factors for different rifting events in

the Ajdabiya Trough using also backstripping analysis and considering different geometries for the Cenozoic infill. Their model with a thick Cenozoic geometry (similar to my interpretation) gives a mean post-early Cretaceous ß factor of around 1.266 as observed from the pseudo well PW-360 and the gravity and magnetic modelling.

The analysis by Abadi et al., 2008 show that the Ajdabiya Trough records a single stretching phase of about 1.108 during the Paleocene (65 - 49 Ma). Other short pulses with different time and magnitude are recorded during the Paleocene time at 65 - 61, 65 - 57.9, and 65 – 54 Ma obtained from different areas around the trough.

Using modelling worksheets (see Figures 6.26 and Appendix) which calculates decompacted burial histories and stratal thicknesses using the algorithms of Sclater and Christie (1980), the stretching factors were calculated using the derived McKenzie (1978) equation (6.11). By comparing the subsidence calculated from the sediment record (i.e. the backstripping) to the theoretical subsidence paths. An extension event (Rift Event) is defined and time at which extension started and the beta factor, and the output (green curve in the plot) (Figure 6.27) is added to the backstripping plot (red rectangles) for comparison with the data

Tectonic Subsidence/Time			
Time	Tectonic Subsidence(m)	Max Tectonic Subsidence(m)	Min Tectonic Subsidence(m)
0	1765	1732	1747
5	1554	1519	1537
11	1626	1594	1611
16	1438	1401	1423
23	1517	1487	1507
34	1453	1410	1440
37	1265	1203	1223
49	1237	1177	1197
55	1139	1081	1101
58	1208	1149	1179
62	1071	1000	1025
66	1115	1036	1070
72	1049	977	1005
84	979	910	952
86	904	858	888
90	822	794	814
90	732	693	713
92	531	508	523
94	181	167	167
95	0	-7	-7
140	0	0	0

Rift Event 1		Rift Event 2	
Beta Factor:	1.210	Beta Factor:	
Rift Start: (myrs)	93.5	Rift Start: (myrs)	
Calculate Rift Event 1		Calculate Rift Event 2	
Calculate Rift Events 1 & 2			

Figure 6.26: Example from the Excell dasta sheet used for calculating the stretching factors displayed in figure 6.29.

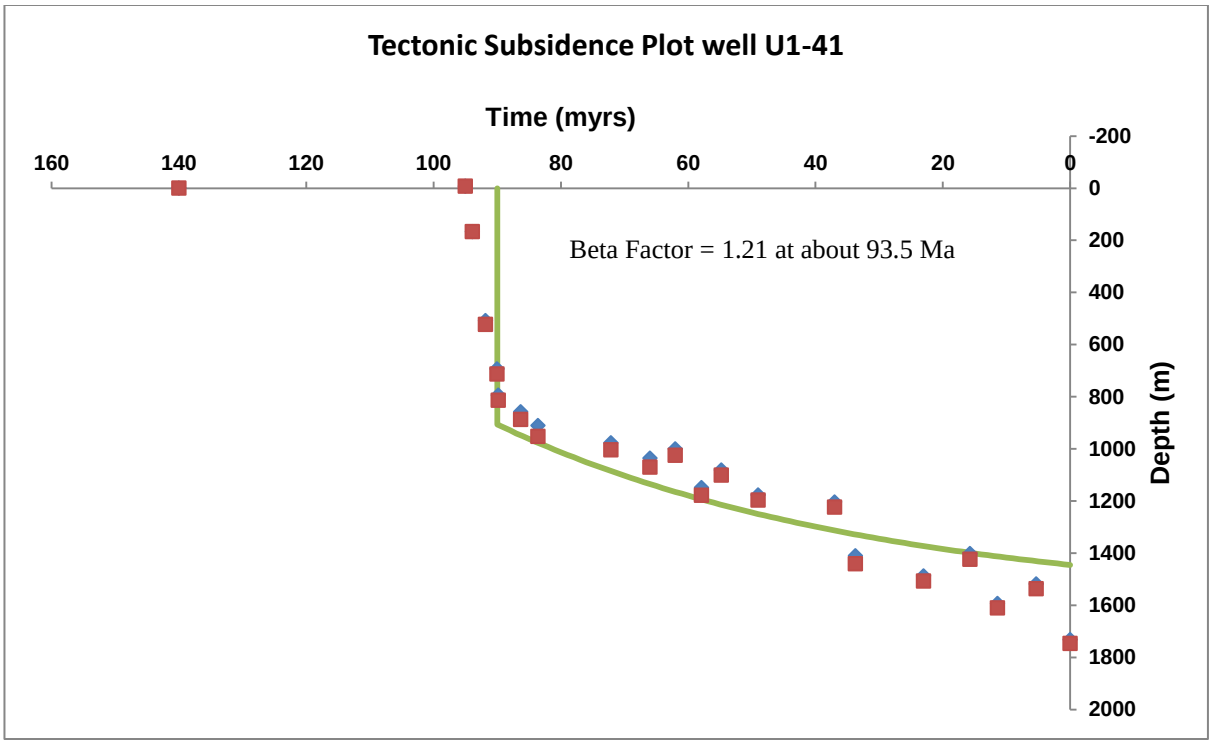

Figure 6.27: Results obtained from the stretching factor calculations.Theoretical subsidence is represented by green line with dots mark calculated tectonic subsidence including a Cretaceous rift at about 93.5 – 84 Ma given for well U1-41, as derived from 1D models.

Stretching factors obtained from the curves in figures 6.28 shows that the stretching is highly variable in amount and magnitude during the Late Cretaceous time, suggesting possible short lived rift phase with different stretching phases in agreement with subsidence rates obtained from the equivalent subsidence curves. Data coverage in most of the wells prevents further analysis of particular time intervals. Well Q1-31 from Amal Platform record short lived period of stretching during the Early Cretaceous time, attributed to thin Early Cretaceous section with a β of 1.046 followed by medium to short lived periods during the Upper Cretaceous and the Paleocene with a β values of 1.13 and 1.02 respectively

Well U1-41 located at the north-eastern side of the Ajdabiya Trough (Cyrenaica Platform/Sirt Basin boundary) record a longer stretching phase, with some recording continuous stretching from 93.5 to 84 Ma.

The backstripped curves of tectonic subsidence indicate that the post-rift subsidence displays a uniform, subsidence pattern in north-south direction (Figure 6.28). Significant differences in tectonic subsidence occur according to increasing stretching factors from the centre of the trough to the platform areas (Figure 6.28). This could be correlated with predicted subsidence

curves and range of beta factors as shown on figure 6.29. All curves show nearly a similar tectonic subsidence patterns, occasionally with differences in time and magnitude. Accordingly, the synthetic well show different sequence of events similar to those observed from well U1-41 for the Cenozoic sequence.

The curves show that the Ajdabiya Trough underwent a series of relative rapid post-rift subsidence until the Miocene after the cessation of the rift during the Early - Upper Cretaceous. The intensity of the post-rift subsidence is increasing towards the northern part of the trough. Wells A1-114 located at the north-west part of Ajdabiya Trough near Al Jahama platform records smooth tectonic subsidence of moderate gradient during the Upper Cretaceous indicate that a tectonic quiescence phase prevailed in this part from the basin. Short-lived uplift and erosion during the Late Cretaceous – Early Paleocene could be occurred and affected the north-western boundary of the Ajdabiya Trough followed by uniform and moderate subsidence during the Late Paleocene and continued until the end of the Oligocene 23.0 Ma.

The steeper overall gradient character of the subsidence curve during the Oligocene period indicates renewed subsidence acceleration followed by continuous thermal subsidence until recent. A main uplift event affected the Ajdabiya Trough during the Campanian time from 83.5 - 71.3 Ma, is observed on the subsidence curves predicted for the well A1-119 located at the centre of the Ajdabiya Tough. This uplift may be formed due to rising in thermal anomaly and mantle upwelling that represent component of lithospheric folding (e.g. Abadi et al., 2008).

The initial rift in the Ajdabiya Trough is affected by uniform stretching of the lithosphere, this result in increasing tectonic subsidence from the platform areas towards the centre of the trough. Tectonic subsidence increases to about 400 m of subsidence in the deeper parts as observed from well A1-119, with similar range of subsidence observed from well U1-41 to the north-east close to Solouq Flank or Depression. Slow subsidence rates observed from all subsidence curves are considered to be a periods of thermal uplift caused by possible underplating related to mantle upwelling (e.g. Abadi et al., 2008), this prevents the rift induced subsidence in areas with effective stretching factor in the range of 1.02 – 1.07 (Figure 6.28).

The stretching factors for the entire crust are appreciably higher because of the geometry of the thinned lower crust. As observed from the gravity and magnetic modelling (chapter 4) and also on figure 4.39, the crust within the Ajdabiya Trough experiences a thinning to less than 30 km. In the vicinity of the other wells on the platform areas, a thinning to 38 km is observed suggest that the crust under these areas is remained unstretched or slightly stretched after the cessation of the rift.

Within areas, where the β values reach their maximum, the crust was thinned to less than 26 km post-rift thickness. This observation is in agreement with crustal thickness estimation by (Doser et al., 1996; Marone et al., 2003). This conclusion aided with observations from the modelled subsidence curves indicates that post Upper Cretaceous tectonic phases did not lead to any further thinning of the crust. This could be related to sub-crustal thinning process and thermal cooling subsequent to rifting.

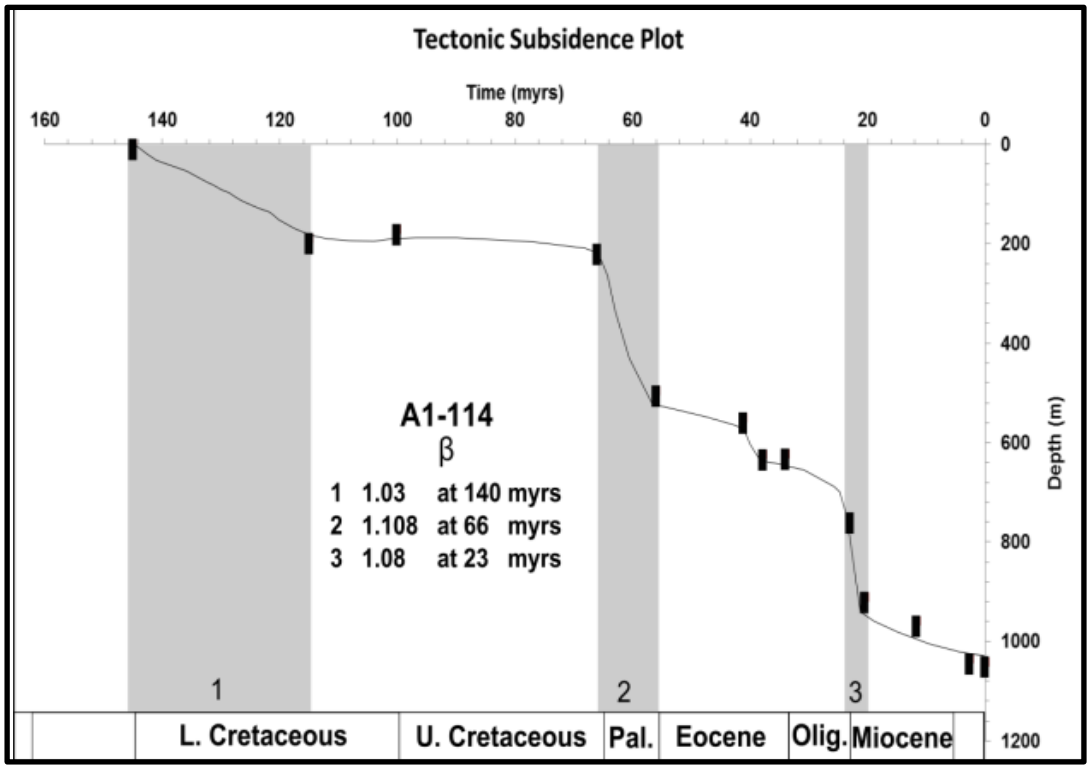

A

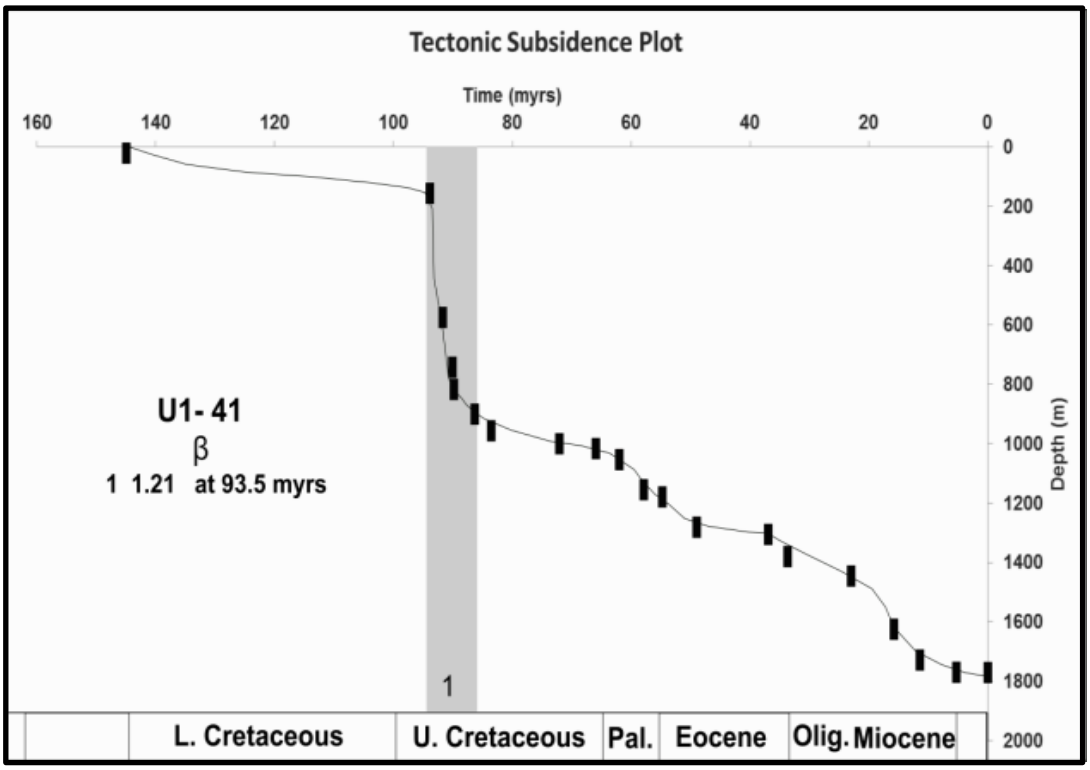
Tectonic Subsidence Plot
Time (myrs)
160
140
120
100
80
60
40
20
0
0
200
400
600
800
1000
1200
1400
1600
1800
2000
Depth (m)
U1- 41
β
1 1.21 at 93.5 myrs
1
L. Cretaceous
U. Cretaceous
Pal.
Eocene
Olig.
Miocene

B

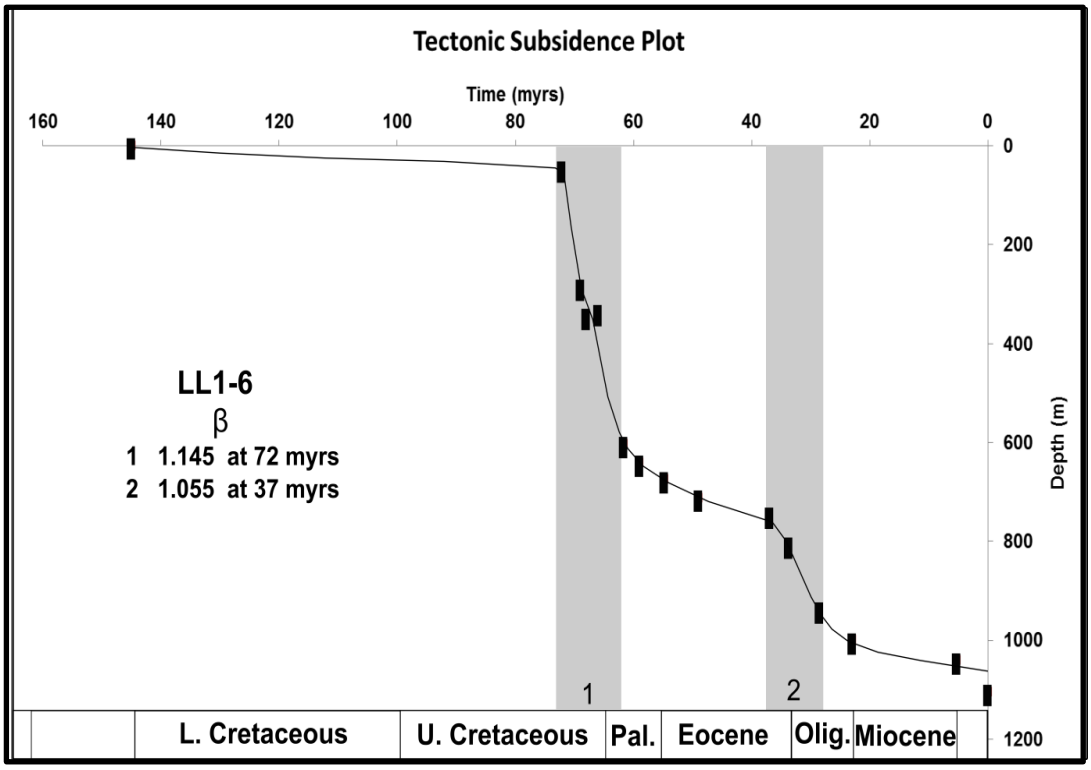
Tectonic Subsidence Plot
Time (myrs)
160
140
120
100
80
60
40
20
0
0
200
400
600
800
1000
1200
Depth (m)
LL1-6
β
1 1.145 at 72 myrs
2 1.055 at 37 myrs
1
2
L. Cretaceous
U. Cretaceous
Pal.
Eocene
Olig.
Miocene

C

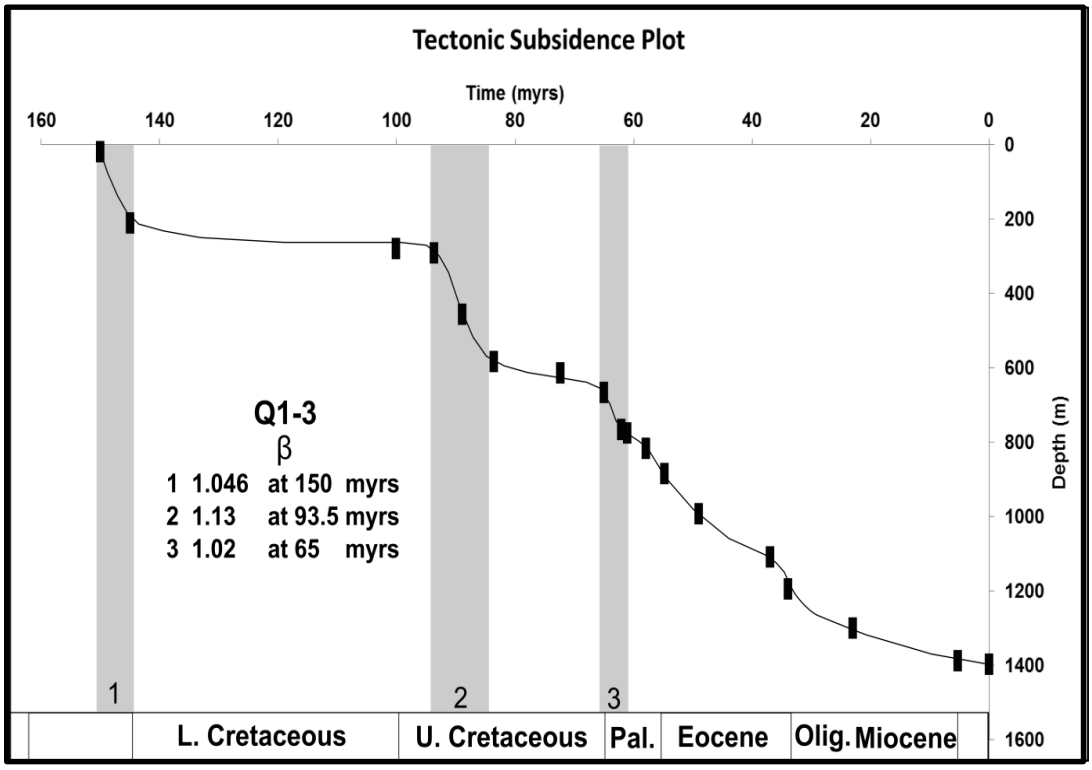
Tectonic Subsidence Plot
Time (myrs)
160
140
120
100
80
60
40
20
0
0
200
400
600
800
1000
1200
1400
1600
Depth (m)
Q1-3
β
1 1.046 at 150 myrs
2 1.13 at 93.5 myrs
3 1.02 at 65 myrs
1
2
3
L. Cretaceous
U. Cretaceous
Pal.
Eocene
Olig.
Miocene

D

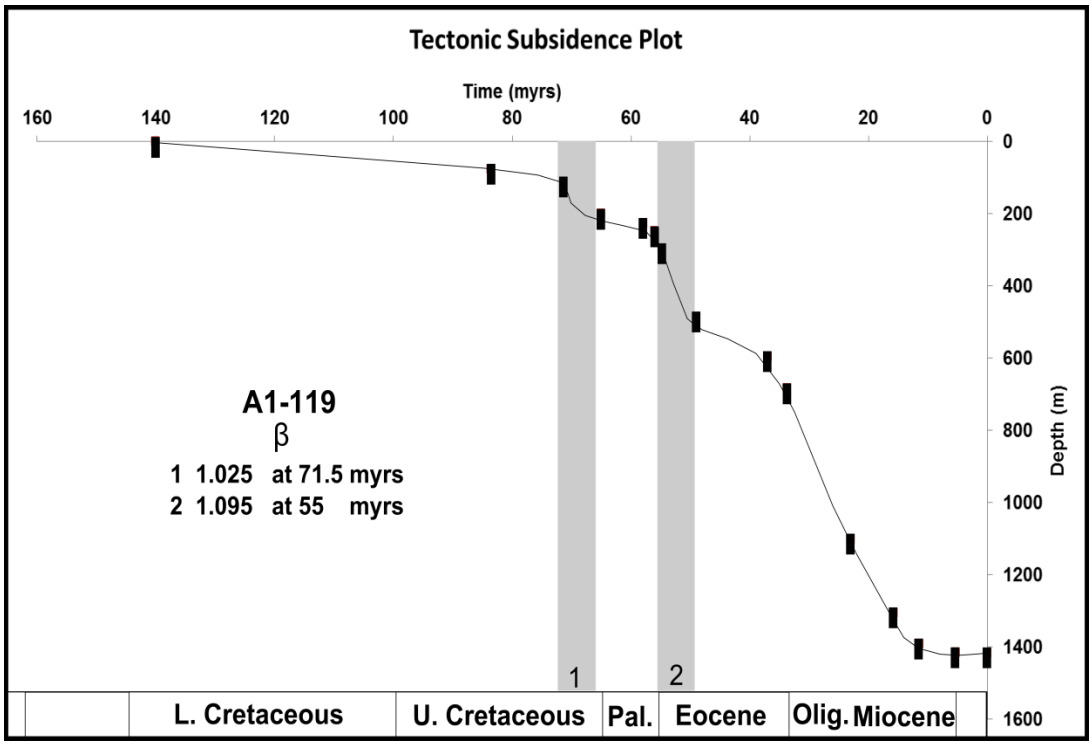
Tectonic Subsidence Plot
Time (myrs)
160
140
120
100
80
60
40
20
0
0
200
400
600
800
1000
1200
1400
1600
Depth (m)
A1-119
β
1 1.025 at 71.5 myrs
2 1.095 at 55 myrs
1
2
L. Cretaceous
U. Cretaceous
Pal.
Eocene
Olig.
Miocene

E

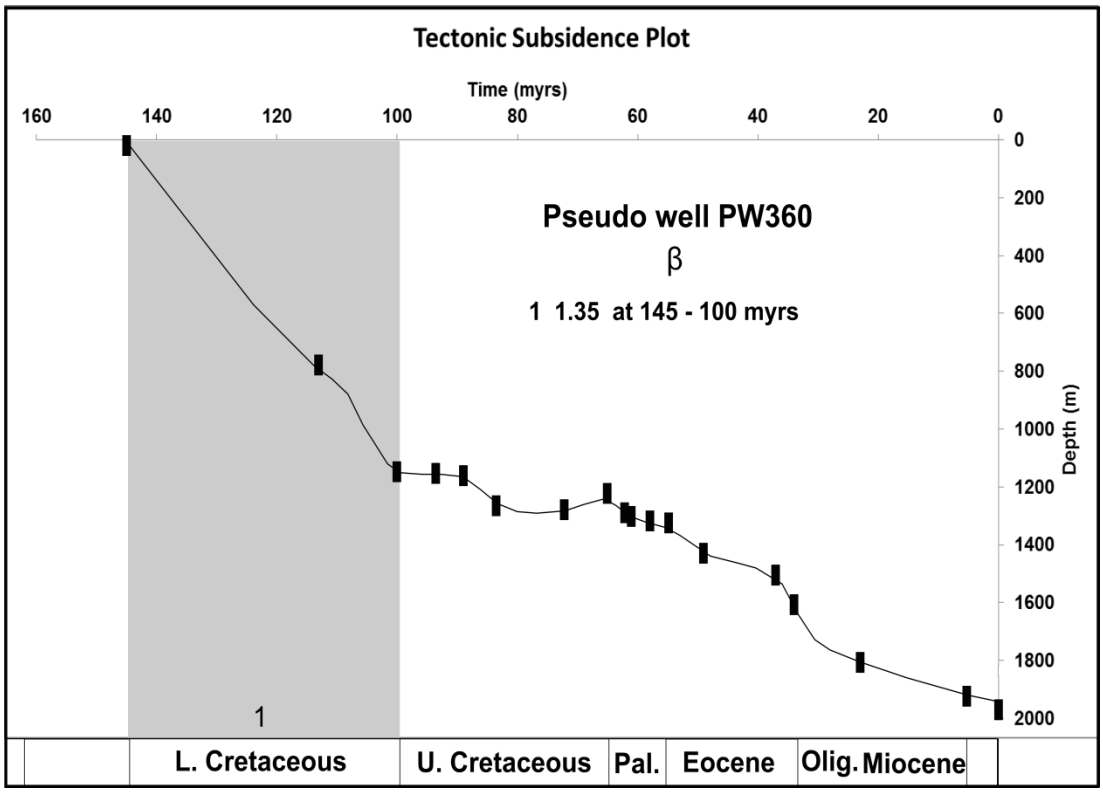

F

Figure 6.28: Modelled stretching factor for the subsidence curves for the backstripped wells. Vertical-shaded boxes correspond to possible stretching pulses and/or periods of fault re-activations. The β denotes values for the lithospheric stretching of each stretching phase.

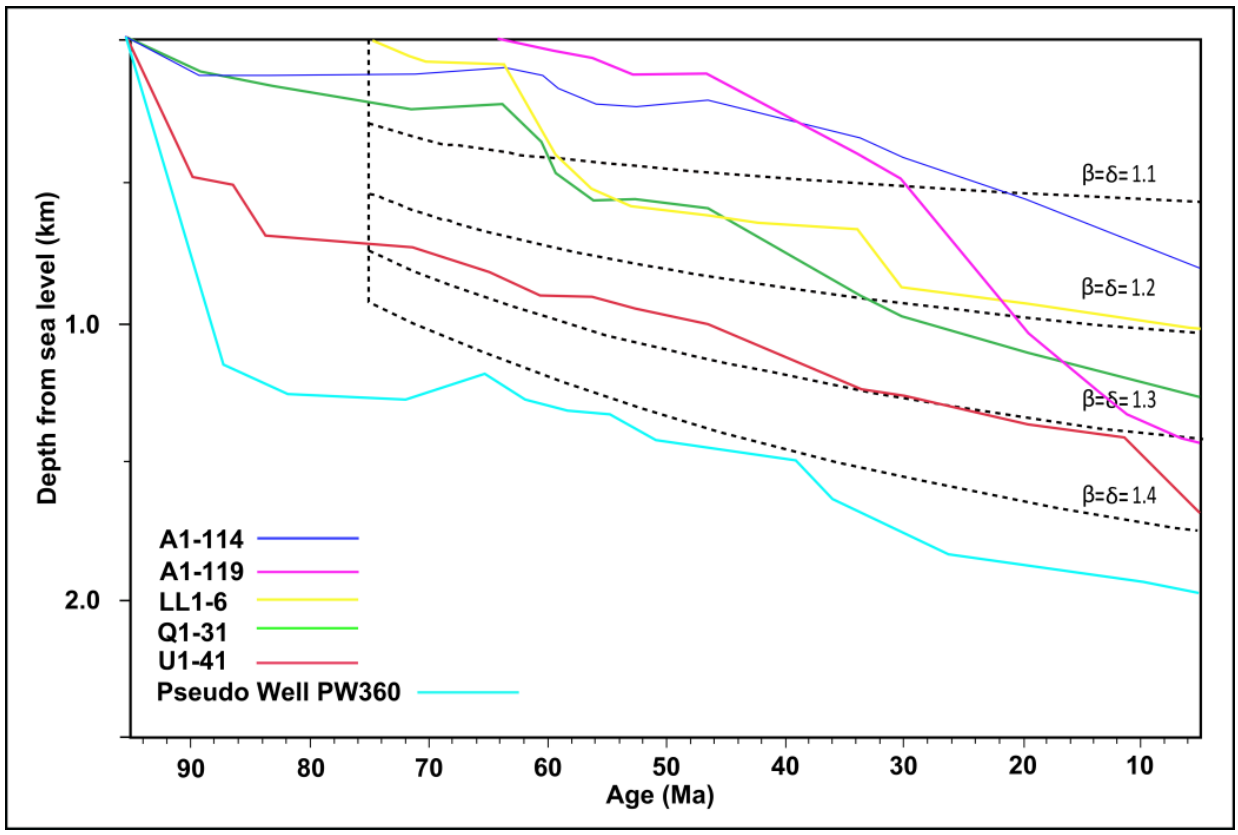

Figure 6.29: Comparison of observed tectonic subsidence (solid curves) and predicted synthetic subsidence (dashed curves) of the lithosphere using a two-layered stretching model (Royden and Keen, 1980) with an instantaneous rifting event at 75 Ma as adopted from van der Meer and Cloetingh, 1993. The instantaneous rifting model fails to account for the observed syn-rift subsidence during the Late Cretaceous-Paleocene. Our model show possible Mid Cretaceous rifting with short pulses during the Paleocene along the Ajdabiya Trough eastern and western shoulders as shown by the rapid subsidence rates observed from wells LL1-6 (Zelten Platform) and Q1-31 (Amal Platform), although the thermally driven post-rift subsidence is well approximated by the model for the wells except for the well A1-119 and the well A1-114.Well A1-119 show uplifting during the Paleocene – Eocene time, supported by it is location over a structural high as suggested by Hallett and El Ghoul, 1996. Over Al Jahama Platform, the Late Paleocene – Early Eocene was time of uplift and erosion (e.g. Bezan, 1993) as shown from the A1-114 curve.

6.6 Burial History

Burial history analysis of the study area, using well data, leads to the following conclusions:

The burial history curves for the backstripped wells in the Ajdabiya Trough are constructed using standard decompaction techniques, euastatic sea level data and estimated paleowater depths obtained fairly from sedimentological studies in the Sirt Basin. The curves indicate the main features of deposition occurred in and around the Ajdabiya Trough for the period from Cretaceous to recent.

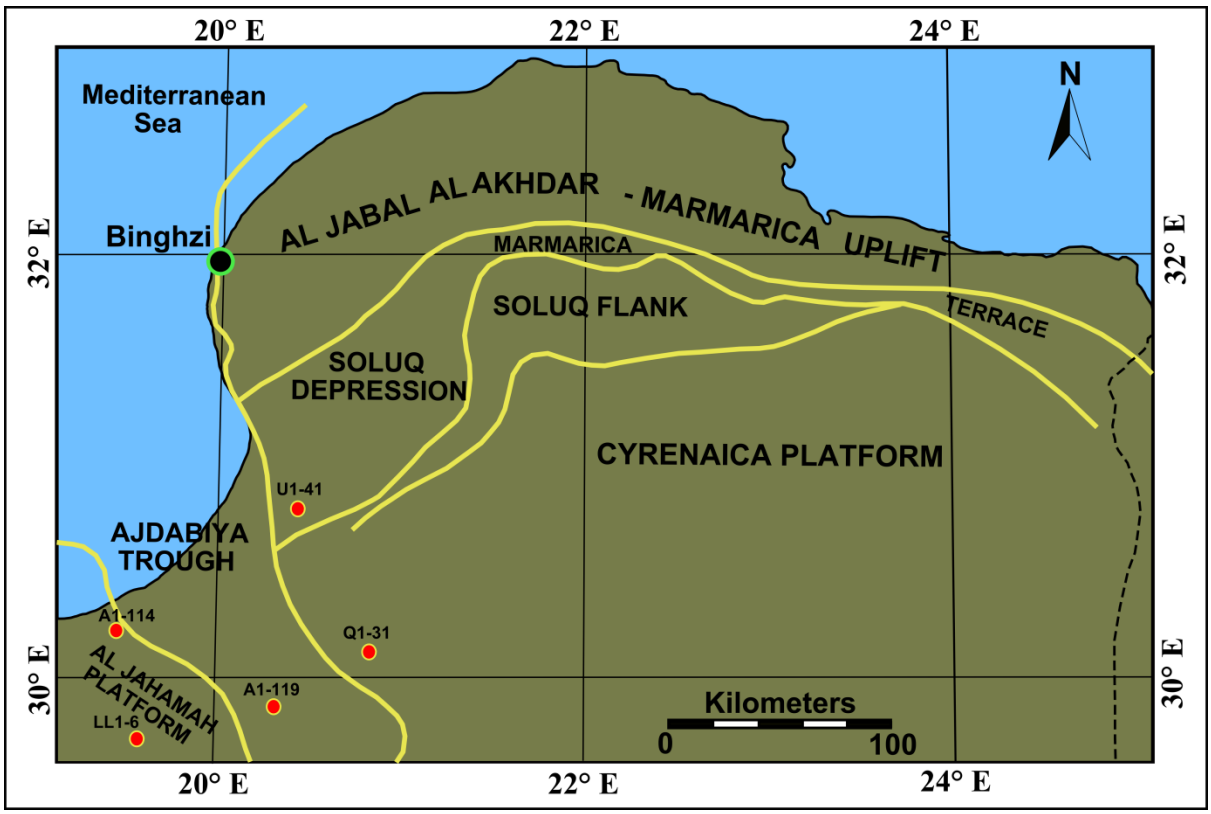

Figure 6.30: Map showing major tectonic elements in eastern Sirt Basin and Cyrenaica region. (Map redraws from El Arnauti et al., 2008)

The burial-history reconstruction for the well A1-114 (Figure 6.31 A), located at the north-western part of the Ajdabiya Trough (Figures 6.4 & 6.30) illustrates the burial depth reached in this part from the trough. From 113 Ma to about 65 Ma, subsidence and sedimentation rates appear to be fairly constant and relatively slow. Substantial increase in rate of deposition between 65 and about 56 Ma is observed when more than 1000 m of sediments were deposited. A major hiatus period seems to be occurred for about 15 million years between 56 - 41 Ma and ended with the resumed deposition of Upper Paleocene sediments.

At the near end of the Paleocene time, subsidence is decelerated in the north-west periphery of the Ajdabiya Trough and the south west part of the Cyrenaica Platform (Bezan, 1993). Upper Paleocene Harash and Kheir formations have been removed due to subsequent regional erosion which also reduced the underlying post-lower Sabil carbonates (Zelten Formation).

Sedimentation rates increased during the Middle to Upper Eocene (41 – 38 Ma). By the end of the Eocene, arelatively a brief period of uplifting and non-deposition occurred in this time

between 38 and 34 Ma. Maximum sediment burial is occurred around 12 Ma with total sediment thickness of about 2950 m.

The burial history curves for the well LL1-6 (Figure 6.31 B) is similar to that at A1-114, except that the rate of sediment accumulation was not as rapid during deposition of the Miocene sequence, resulting in about half the thickness of that unit here. A substantial increase in subsidence and sedimentation rate occurred during the Oligocene, yielding a unit that is about twice the thickness of this sequence at the well A1-114. These differences can be seen by the shift in the steepest part of the curves at each location.

The plot curves of the well U1-41 (Figure 6.31 C) indicate the main features of deposition in the north-eastern part of the Ajdabiya Trough close to the Soluq Depression in Cyrenaica Platform (Figure 6.30). The deep-basin burial-history setting is the Soluq Depression in the Cyrenaica area. Its history is most likely similar to that in Ajdabiya Trough in terms of the rapid rates of subsidence/sedimentation with approximately rate of 81m/Ma (Ghori and Mohamed, 2008), during Cretaceous - Paleocene deposition.

About 2500m of Upper Crertaceous marine sequence of limestone and shale is overlain disconformably by about 900 m of marine sediments of Paleocene age. El Arnauti et al., 2008 suggested that a phase of rejuvenated extension prevailed during Cenomanian - Santonian accompanied with block faulting associated with thickening of Cenomanian to Maastrichtian strata. During the early Eocene (about 49 Ma), a slow deposition rates prevailed indicating period of uplifting due to thermal activity (e.g. Galushkin et al., 2014). Rapid deposition of marine mudstone and siltstone took place in the Early Miocene and was followed by a thick sequence of about 1250 m of marine shale and carbonate sediments. The maximum burial in the area occurred around about 12 Ma.

Reconstruction of the burial history for the well Q1-31 (Figure 6.31 D), illustrates clearly rapid deposition in marine environments and high subsidence in the Late Cretaceous time.

During the Late Cretaceous, the subsidence rate in the Ajdabiya Trough was rapid but shorter than that at the well U1-41 in Soluq Depression. The subsidence rate during the Late Cretaceous was high due to rapid deposition of the marine sequence (Rakb Group) which mainly formed of carbonates and shales (Wennekers et al., 1993).

Based on data from oil and source maturity, Ceriani et al., 2002 and Burwood et al., 2003 concluded that generation of hydrocarbon in the eastern Sirt Basin including Ajdabiya Trough

commenced prior to maximum burial depth and that peak expulsion of oil occurred during the Late Cretaceous at depths ranging from 3750 m to 4875 m.

Two burial history locations within the Ajdabiya Trough are studied based on data obtained from the well A1-119 (Figure 6.31 E) which presumably located on a structural high within the trough (Hallett and El Ghoul, 1993) and other data obtained from the pseudo well PW-0360 (Figure 6.31 F). Their burial history curves are similar for the post-Cretaceous sequence, especially the steep decline of the curves between 98 and 60 Ma representing the rapid increase in subsidence and sedimentation rate during Cretaceous - Paleocene time. This time correlates with period of more acute fault movement in the area.

There are differences between the two occurs before and after this period. The thickness of the Oligocene sequence deposited at the A1-119 location is more than 2000m, nearly one half the thicknesses observed from the pseudo well (over 1500m).

The major Early Cretaceous subsidence (140 Ma) in the pseudo well location is evident from the thick and preserved section of the Early Cretaceous. This dramatic increase in subsidence marks the crustal thinning and the consequent rifting in the region. During the Early Cretaceous, the Ajdabiya Trough was subsiding at a faster rate. The process was reversed during the Late Cretaceous (99 Ma), where the subsidence rate slowed dramatically, then increased significantly during the period (94 Ma - 84 Ma) as shown from the subsidence curves (Figure6.28).

The well A1-119 has more complicated burial history due to it is location on a structural high. Although during the Cretaceous, the sediment accumulation rates appear to be fairly constant and relatively slow, a thicker section of sediments of this age was deposited in this area. The A1-119 and the pseudo well curves show that a number of episodes of uplift and erosion occurred and mainly concentrated around the Ajdabiya Trough boundaries compared with the trough depocentre. The first erosional event was relatively minor. The result of this event was the removal of part from the Cretaceous section (Galushkin et al., 2014). Later, from 94 to 65 Ma, the burial-history curve looks very similar to the others in the study area. The curve drops steeply, representing the rapid increase in sediment accumulation rate during the Paleocene time.

The Late Cretaceous interval is culminated with short – lived pulse of uplift possibly causing minor erosion during this time (e.g.Van der Meer and Cloetingh, 1993).

By the end of the Cretaceous, rapid sedimentation prevailed during the early Paleocene as a consequence of high subsidence rate due to extension rejuvenation (Ahlbrandt, 2001; El Arnauti et al., 2008; Bosworth, 2008; Abadi et al., 2008) and thermal cooling (Burwood et al., 2003; Cowie and Kusznir, 2012; Galushkin et al., 2014). The Late Cretaceous source rocks of the east Sirt Basin are likely to have reached initial stages of hydrocarbon generation in the Paleocene - Eocene, when the subsidence rate was relatively high, and became fully mature in the Oligocene. Cooling in the trough is consistent with a decelerating tectonic subsidence rate during the Late Eocene (Van der Meer and Cloetingh, 1993) and driven by thermal re-equilibration following the main rifting in the area.

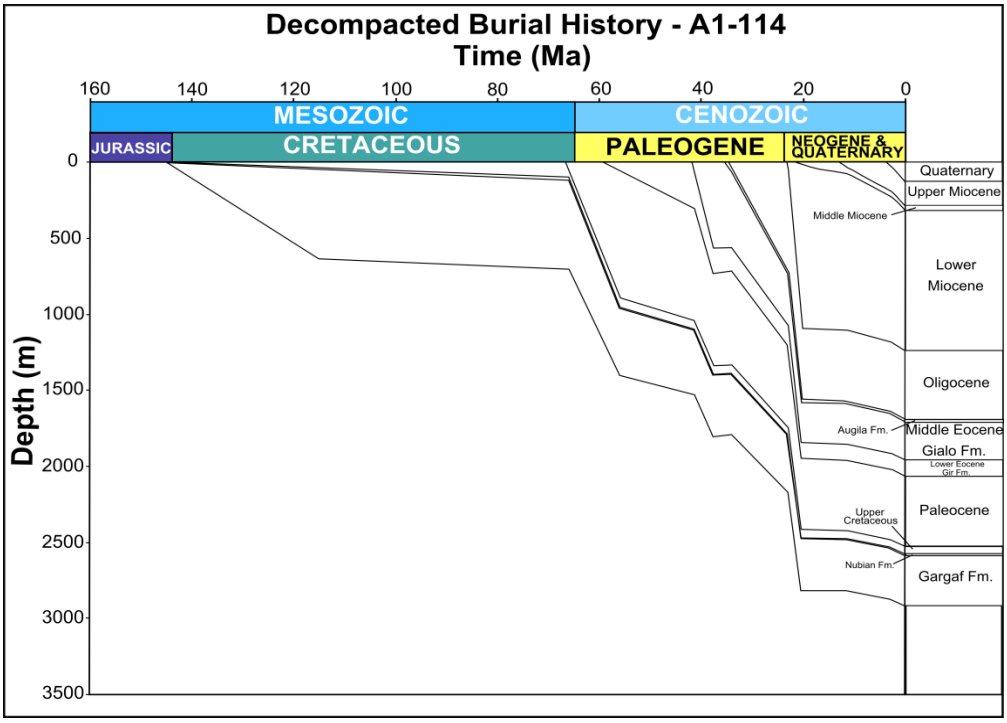

A

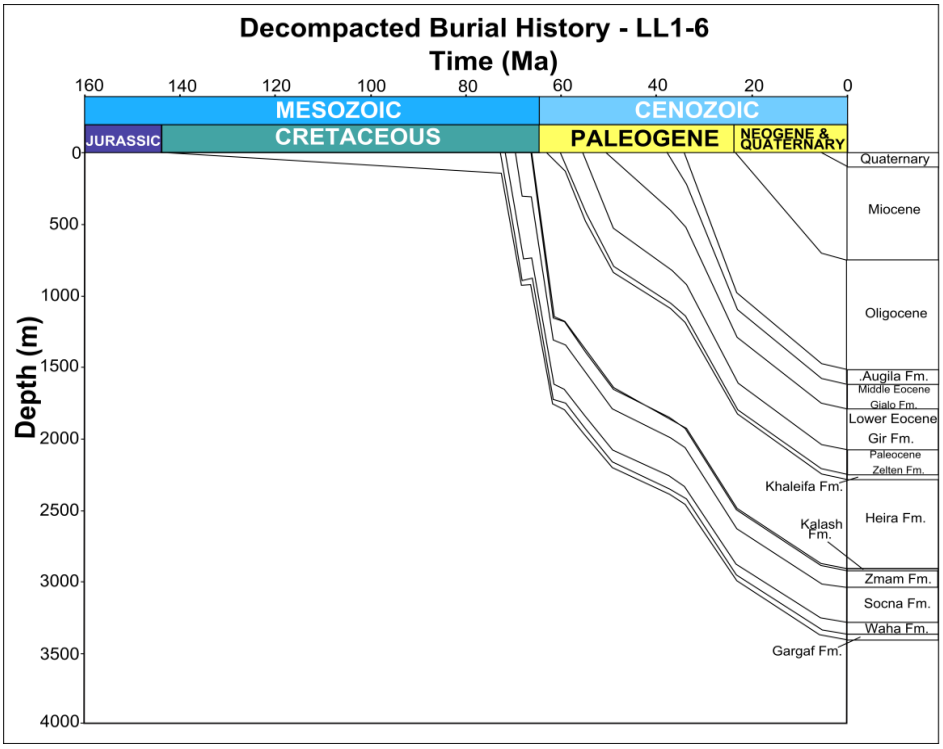
Decompacted Burial History - LL1-6
Time (Ma)
160
140
120
100
80
60
40
20
0
MESOZOIC
CENOZOIC
JURASSIC
CRETACEOUS
PALEOGENE
NEOGENE & QUATERNARY
Depth (m)
0
500
1000
1500
2000
2500
3000
3500
4000
Quaternary
Miocene
Oligocene
Augila Fm.
Middle Eocene
Gialo Fm.
Lower Eocene
Gir Fm.
Paleocene
Zelten Fm.
Khaleifa Fm.
Kalash Fm.
Heira Fm.
Zmam Fm.
Socna Fm.
Waha Fm.
Gargaf Fm.

B

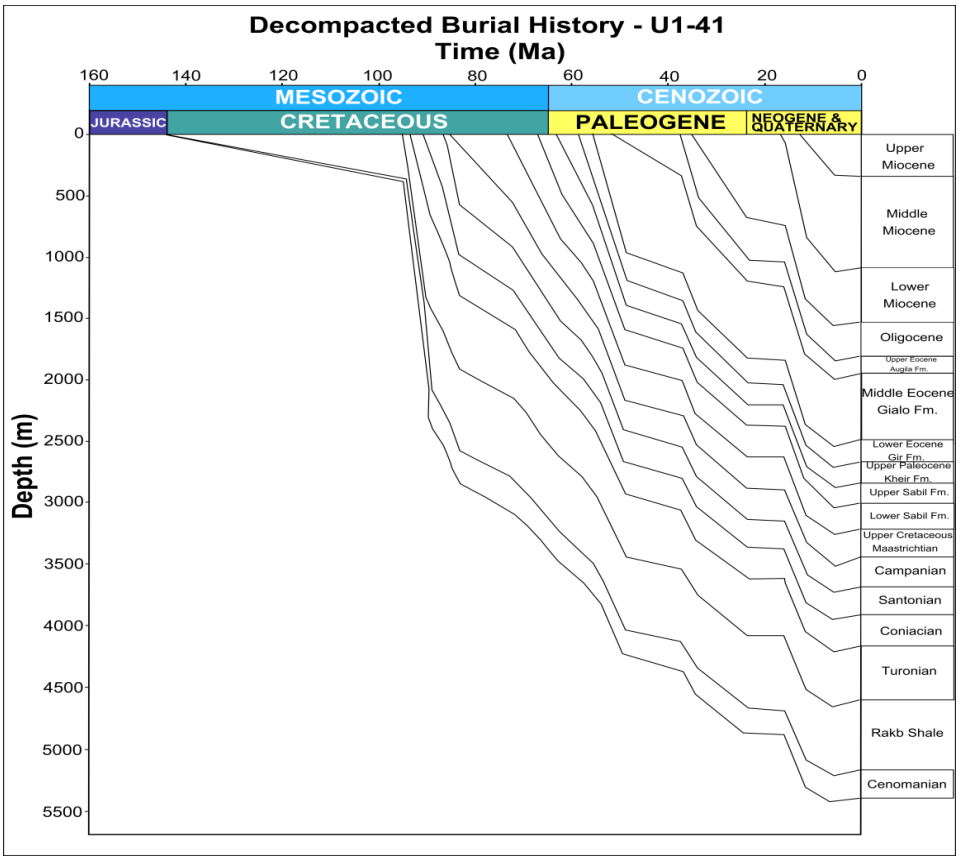
Decompacted Burial History - U1-41
Time (Ma)
160
140
120
100
80
60
40
20
0
MESOZOIC
CENOZOIC
JURASSIC
CRETACEOUS
PALEOGENE
NEOGENE & QUATERNARY
Depth (m)
0
500
1000
1500
2000
2500
3000
3500
4000
4500
5000
5500
Upper Miocene
Middle Miocene
Lower Miocene
Oligocene
Upper Eocene
Augila Fm.
Middle Eocene
Gialo Fm.
Lower Eocene
Gir Fm.
Upper Paleocene
Kheir Fm.
Upper Sabil Fm.
Lower Sabil Fm.
Upper Cretaceous
Maastrichtian
Campanian
Santonian
Coniacian
Turonian
Rakb Shale
Cenomanian

C

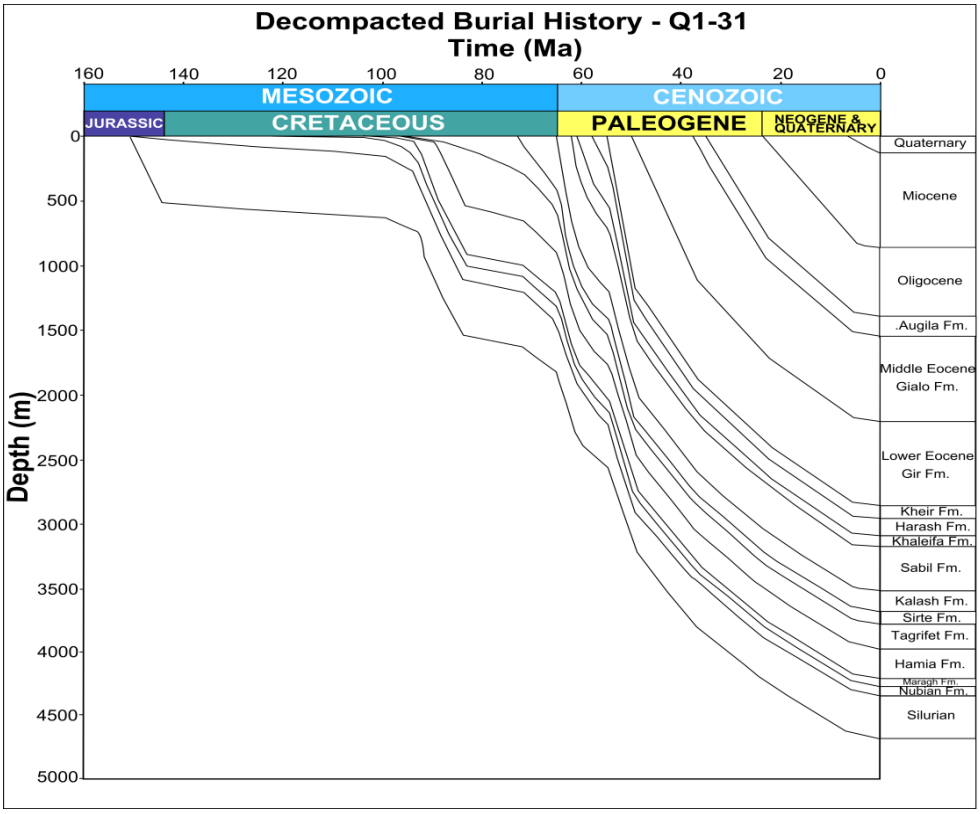
Decompacted Burial History - Q1-31
Time (Ma)
160
140
120
100
80
60
40
20
0
MESOZOIC
CENOZOIC
JURASSIC
CRETACEOUS
PALEOGENE
NEOGENE & QUATERNARY
Depth (m)
0
500
1000
1500
2000
2500
3000
3500
4000
4500
5000
Quaternary
Miocene
Oligocene
.Augila Fm.
Middle Eocene
Gialo Fm.
Lower Eocene
Gir Fm.
Kheir Fm.
Harash Fm.
Khaleifa Fm.
Sabil Fm.
Kalash Fm.
Sirte Fm.
Tagrifet Fm.
Hamia Fm.
Maragh Fm.
Nubian Fm.
Silurian

D

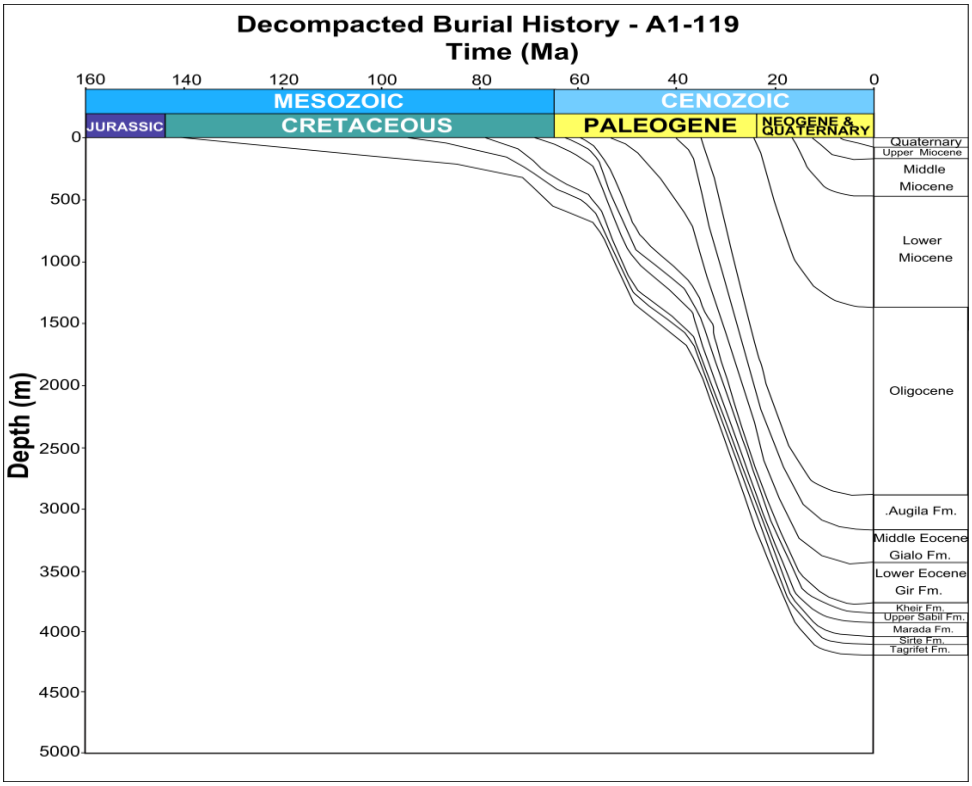
Decompacted Burial History - A1-119
Time (Ma)
160
140
120
100
80
60
40
20
0
MESOZOIC
CENOZOIC
JURASSIC
CRETACEOUS
PALEOGENE
NEOGENE & QUATERNARY
Depth (m)
0
500
1000
1500
2000
2500
3000
3500
4000
4500
5000
Quaternary
Upper Miocene
Middle Miocene
Lower Miocene
Oligocene
.Augila Fm.
Middle Eocene
Gialo Fm.
Lower Eocene
Gir Fm.
Kheir Fm.
Upper Sabil Fm.
Marada Fm.
Sirte Fm.
Tagrifet Fm.

E

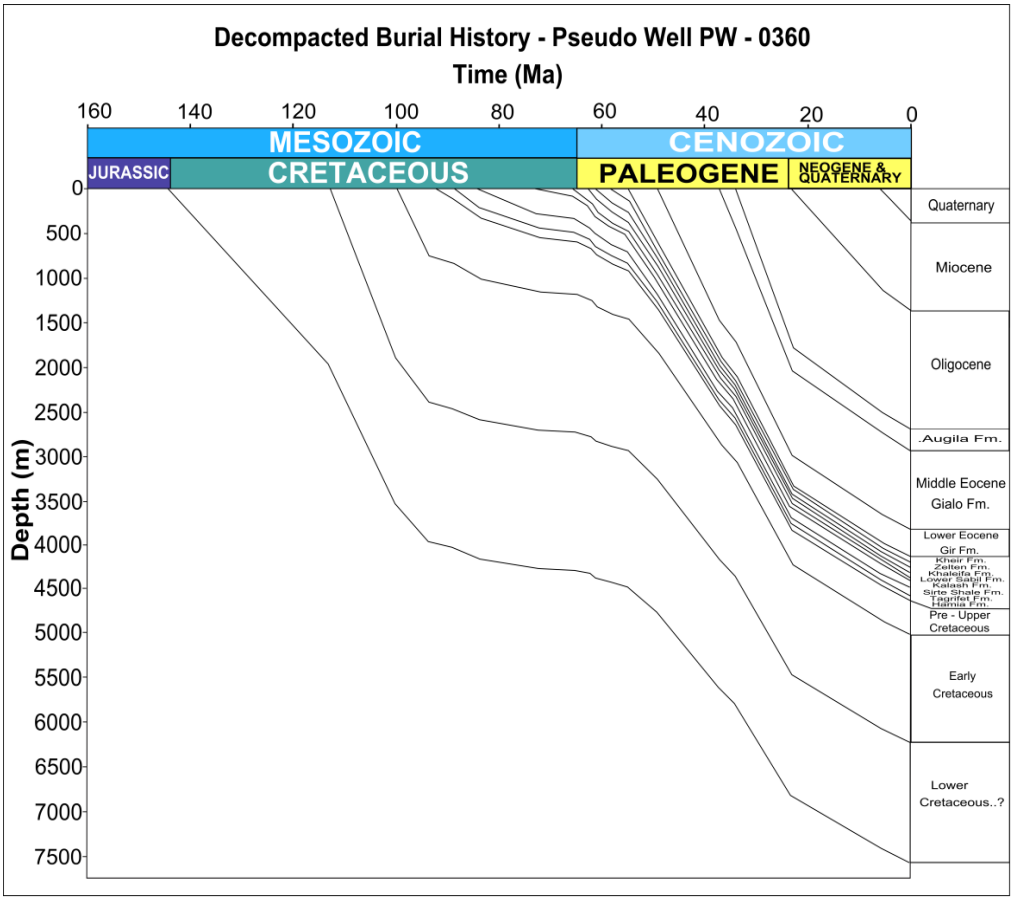

F

Figure 6.31: Burial history curves for the backstripped wells

6.7 Summary

In addition to initial subsidence (tectonic controlled), sag basins could be developed during post-rift thermal subsidence and thermal relaxation stages along the northern passive margin of the African Plate (e.g., Janssen et al. 1995). Backstripping analysis of well data aided with 2D seismic observations provides new constraints on the development of the tectonic subsidence and it is relation to structures of the Ajdabiya Trough during period from Late Cretaceous to Miocene. The greatest subsidence observed in the Ajdabiya Trough central area is about 2,000 meters based on pseudo well data. These show that at various times in the Late Cretaceous and Palaeocene - Eocene, renewed differential subsidence followed fault reactivation prevailed.

Tectonic subsidence maps show a systematic SE to NW shift in the loci of maximum and minimum subsidence, accompanied by seaward shift of the depocentre, which parallels the structural trend of the Ajdabiya Trough.

2D seismic profiles (chapter 5) show that seaward shift in depocentre is evidenced by the clear shift in Paleocene – Early Eocene progradding sequences at the shelf margin, indicating also change in sediment flux rate towards the basin, these all formed during major transgression followed by forced regressive sea level falling formed during slow subsidence rates.

The post-rift period in the Ajdabiya Trough can be divided into three main phases characterized by specific subsidence patterns and sedimentation rates. A first period of rapid subsidence (~ 65 – 54 Ma), of variable duration, is followed by a smoother and gentler transitional period (~ 50 – 34 Ma) associated with a decline of the subsidence and sedimentation rates, and eventually by a last stage (34 – 0) with quasi-null subsidence amplitude as observed from the subsidence curves in figures 6.18, 6.19.

Well A1-114 located in the vicinity of the seismic line 05NC213-0590 (Figures 5.14 & 6.4), record a rapid early post-rift subsidence period of about 10 Myr with sedimentation rates of 50 m/Myr. For the wells located on the platform areas, the strong basement subsidence is observed for the first 10 Myr of the early post-rift history (i.e. 65 to about 55 Myr) with a value of 1.0 km on average (e.g. Q1-31, Figure 6.18).

The analysis shows that the syn-rift and post-rift sequences in the Ajdabiya Trough were affected significantly by basement structural relief and increase gradually to the north. In conjunction with sedimentological and tectonic data, the subsidence patterns for the Ajdabiya Trough indicate deposition in a flexurally-loaded sag basin which migrated north-eastwards with time.

The subsidence induced a change in the basin configuration during the Cenozoic time as expressed on the subsidence curves by a different change in subsidence pattern: (1) a convex-upward profile denoting a short and rapid subsidence phase and a subsidence rate that increases through time at 100 m/Ma corresponding to deposition of the Late Palaeocene to Early Eocene sequences during the interval of 55 – 50 Ma; and (2) another convex-upward profile is noticed on the subsidence curve during the interval of 37 to 10 Ma expressing a long phase of rapid subsidence with a subsidence rate that increases through time at 40 –100 m/Ma

corresponding to deposition of the Upper Eocene to Middle Miocene sequences. There may be a period of stability or uplift between convex upward subsidence curves attributed to possible compression and inversion during the period of rapid subsidence.

The subsidence map of the Paleocene to Early Eocene period (65–49 Ma) shows that the southern part of the trough was affected by a high and rapid subsidence rates as result of possible renewed rifting.

During the Eocene, the subsidence map show that the subsidence is increasing towards the north in a NE-SW trend with high subsidence rate also observed to the northeast close to the Soluq Depression in Cyrenaica Platform. It is documented that the Sirt Basin undergoes compression during Middle - Late Eocene tilting the basin northward, causing abrupt subsidence in the north and uplift on the basin southern shoulders, possibly driving the latest stage of regional minor subsidence (van der Meer and Cloetingh, 1993; Anketell, 1996). Capitanio et al., (2009) suggested that an abrupt growth of tensile boundary force was recorded in the Sirt Basin, ~55–48 Ma, could have been induced by the avalanching of the Hellenic slab in the lower mantle after ~20 m.y. of stagnation on the 660-km discontinuity.

Gravity modeling provided evidence of mantle upwelling and crustal thinning which accelerating the subsidence rates and raising a low amplitude positive gravity anomaly at the centre of the Ajdabiya Trough.

The tectonic subsidence during this period is presumably attributed to thermal contraction following heating and thinning of the crust at the time of rifting (e.g. Galushkin et al., 2014).

The subsidence maps for the Ajdabiya Trough show an anomalous subsidence pattern both for the Oligocene and the Miocene times reflect a period of post-rift thermal subsidence. Gumati and Kanes, 1985; van der Meer and Cloetingh, 1993; Abadi et al., 2008, have also pointed to the anomalous subsidence pattern in the same period, with apparent subsidence acceleration. The Oligocene - Miocene subsidence increase, up to about 700 meter in magnitude, these anomalous, were not predicted by the previous works despite the existing models of lithospheric stretching (van der Meer and Cloetingh, 1993; Abadi et al., 2008). The subsidence maps and gravity modeling suggest that the excess subsidence is caused by surface and subsurface loading of a lithosphere with a large effective elastic thickness, and possibly a middle phase of Cenozoic stretching to have occurred.

In map view, the basin subsidence patterns reveal a tilting to the northeast toward the Mediterranean Sea. However, no fault activity in this interval is observed, which indicates that the basin subsided because of sediment loading and thermal relaxation.

6.7.1 General Overview

The Sirt Basin developed following a sequence of tectonic events that led to the break-up of the supercontinent Pangaea (Zigler, 2001). The timing of the structures varies significantly within the Sirt Basin, the rifting was active during at least the Late Cretaceous - Paleocene (Janssen et al., 1995; Baird et al., 1996; Rusk, 2001; Ceriani et al., 2002; Abadi et al., 2008), and it developed NW-SE faults in a wide area within the basin. The NW-SE faults are seems to be oblique to a system of E-W trending faults developed mainly during the opening of the Tethys Ocean (Coward and Ries, 2003; El-Arnauti et al., 2008). The collision between Gondwana and Laurasia during the mid Paleozoic to form the Pangaea supercontinent which inherited from the break-up of the Gondwana resulted in the formation of a number of fault bound grabens and half grabens with mainly NW-SE orientation filled with alternative siliciclastics and carbonate deposits, and the bounding faults played an important role in the initial subsidence of the Sirt Basin (Baird et al., 1996; Gumati and Kanes, 1985; van der Meer and Cloetingh, 1993; Cloetingh et al., 2005; Abadi et al., 2008).

The reviewed maps show that subsidence in the Ajdabiya Trough is associated with lithospheric extension and thermal components following the break-up of Pangaea during the Triassic – Cretaceous (Abadi et al., 2008; Cowi and Kusznir, 2012). Frizon de Lamotte et al., (2011) suggested that continuous subsidence in Sirt Basin during the period from Late Cretaceous – Neogene is related to an extensional deformations caused by two subduction zones located south of connection between Alpine Tethys and Neo-Tethys. A change in tectonic style is seen during near the Mesozoic - Tertiary boundary, (Upper Cretaceous - Paleocene) attributed to possible convergence on basement re-activated faults (e.g. El Arnauti et al., 2008). Tectonic subsidence also increases along the eastern Ajdabiya Trough and characterized by high fault activity due to strain partitioning along old faults and mainly modified by recent activity in Cyrenaica region (e.g. El Arnauti et al., 2008). The reactivation of these faults is interpreted as the direct consequence of the recent bending of the Cyrenaica region related to the flexural uplift in front of the propagating Mediterranean Ridge (El-

Arnauti et al., 2008). In the southern part of the Ajdabyia Trough, west-dipping growth faults with throws of up to 200 ms are evident (chapter 7), and their overall geometry show planar segments cut Mesozoic section with possibly listric geometry at higher depth (Baird et al., 1996). The interval subsidence maps from Eocene to Miocene show that in the following depocentres merged, and the subsidence increases to the northeast towards the offshore area, ideas supported by the tilting of the trough to the northeast and the steep of the Cenozoic strata towards the offshore area as indicated by Fiduk, (2009). Subsidence began initially during Early Cretaceous in the present day depocentre of the trough. As sediment accumulated and loaded the centre of the trough, flexure of the crust resulted in the growth of the depocentre. Sedimentation slowed during Paleocne from ~ 65 - 55 Ma, with increasing water depth. This may be due to either increased distance from the sediment source (carbonate factory), or a change in the uplift rates in the source area providing sediment as evidenced along the trough boundaries to the east and west respectively (Yanilmaz et al., 2008). In general the subsidence maps show substantial changes in form and magnitude during the development of the Cenozoic sequence. Due to uncertainties in gridding, contouring and interpolation processes it is difficult to differentiate between periods of rapid and decelerating subsidence based solely on the subsidence history of the four maps presented in this section. Nevertheless, what the subsidence data do show is a rift history that had finished by about 65 Ma, and then an ongoing long period of what is interpreted to be as fault re-activation and thermal subsidence.

CHAPTER 7: CENOZOIC STRUCTURAL EVOLUTION OF THE AJDABIYA TROUGH

7.1 Introduction

In this chapter structural analysis of subsurface data from the Ajdabiya Trough is aimed to analyse faults and construct a kinematic model for its Cenozoic structural evolution. The trough marks the boundary between the Early Cretaceous rift of the eastern Sirt Basin and the north Cyrenaica fold-thrust belt (e.g. El Arnauti et al., 2008), where subsidence and strike slip-related inversion (Bosworth et al., 2008), are compatible with lateral extensional regime that extended to the Cyrenaica, Western Desert of Egypt and the Syrian Arc (review in Bosworth et al., 2008; Capitanio et al., 2009) (Figure. 7.1).

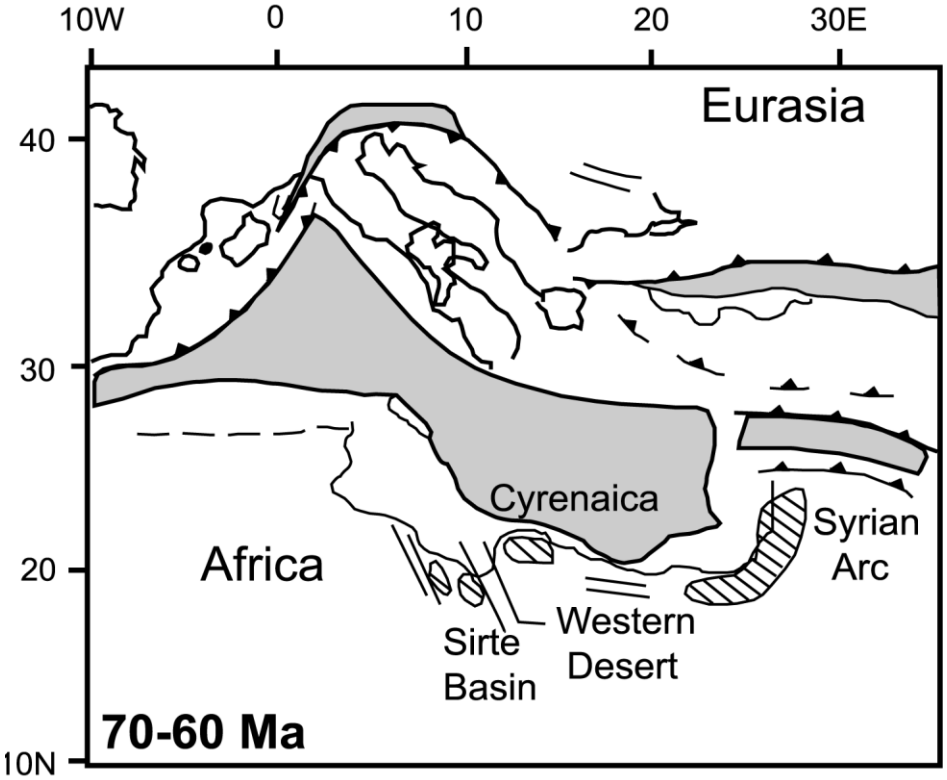

Figure7.1: Reconstruction of the Mediterranean area at early Tertiary, 70–60 Ma, in absolute reference frame. Oceanic domains are marked in grey. Extension in the Sirt Basin was concomitant with compression and uplift (shortening) in Northern Cyrenaica and the Western Desert. Area of tectonic inversion is hatched after (Bosworth et al., 2008); area in subsidence is marked by thin line, corresponding to faults, (from Capitanio et al., 2009).

The Ajdabiya Trough region which is 150 km wide and 200 km long is considered to be part of the rifted continental margin of the North Africa (Figures 7.2 & 7.3) that formed by rifting during the Cretaceous and developed thereafter due to post-rift subsidence related to basin downwarping and thermal relaxation (chapter 6). The tectonic evolution and corresponding geological units remained quite poorly known until hydrocarbon discoveries were made, thereby provoking a sharp rise in interest (Gumati & Nairn 1991; Baird et al., 1996; Ahlbrandt, 2001; Rusk, 2001; Craig et al., 2008). As part from Sirt Basin Libya, the Ajdabiya Trough belongs to a family of extensional provinces in North East Libya, but is quite different from other parts of the basin. The Cenozoic subsidence of the trough as addressed in chapter (6) is controlled by a combination of lithospheric thinning and different style polycyclic fault movements. The trough underwent a syn-rift and post-rift stages (e.g. Abadi et al., 2008; Gumati and Nairn, 1990, and references therein), but two episodic dextral movement events of strike-slip faults are believed to have modify the subsidence of the Ajdabiya Trough since the Oligocene (e.g. Anketell, 1996; Baird et al., 1996; El Arnauti et al., 2008).

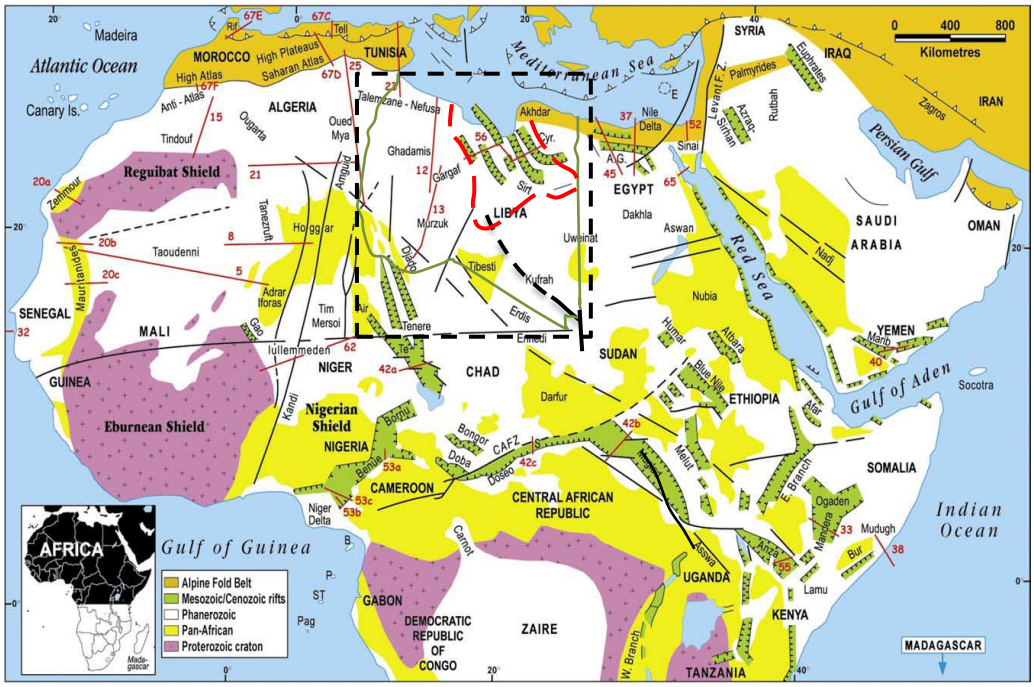

Figure 7.2: Schematic geological map of Northern Africa, Central Africa and Arabia, compiled from Wilson and Guiraud (1998), showing regional setting of Libya, almost surrounded by currently active plate boundaries. The major fault zones and Mesozoic-Cenozoic rifts are located. CAFZ, Central African Fault Zone; Cyr, Cyrenaica Platform. Rifting is moved northward from southern Atlantic during Late Jurassic-Early Cretaceous (e.g. El Arnauti et al., 2008), during this time the African plate moved to the ENE with respect to Europe and broke into sub-plates along major shear zones which were formed by the Central African Shear Zone (CASZ). Map obtained from Guiraud et al., 2005.

Existing stratigraphic data shows that the Sirt Basin is characterised by an early syn-rift sequence of mainly Triassic to Early Cretaceous age overlain by a post-rift sequence of Eocene to Miocene age (Gummati and Nairm, 1982; Baird et al., 1996; Wennekers et al., 1996). The Ajdabiya Trough Cenozoic structures developed upon pre-existing basins of Mesozoic (rift) age that modified above Late Palaeozoic basement grain.

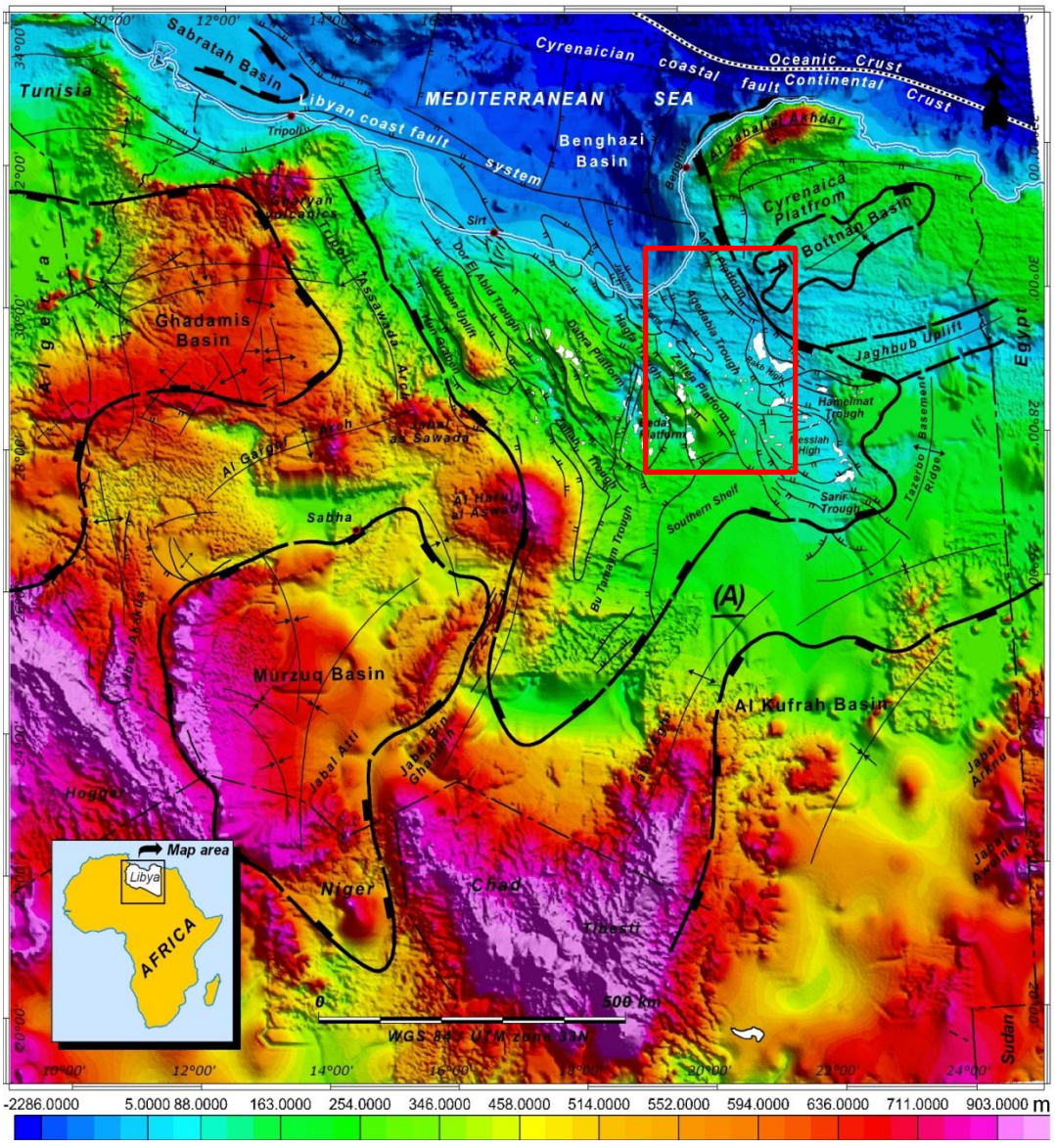

Figure 7.3: Regional tectonic setting of Libya with major structural features and interpreted bathymetry. Inset shows location of Libya along North Africa. The red box in panel outlines the location of the Ajdabiya Trough.

Palaeozoic (Cambro-Ordovician) basement rocks (Figure 7.4) within the Ajdabiya Trough area overlain by a moderate to thick sequence of undifferentiated permo-Triassic to

Cretaceous sediments separating the underlying basement from overlying thick sequences of Cenozoic clastic and carbonate cycles.

During rifting and basin initiation, the Ajdabiya Trough has been controlled by the multi-stage activity of several major fault zones (Anketell, 1996; Baird et al., 1996; Hallett, 2002; Guiraud et al., 2005). High sediment load in the Ajdabiya Trough also implies more compaction than in the structural highs (adjacent platform areas) (Skuze, 1994) which are mainly characterised by a thinner sedimentary infill. The resultant geometry after compaction consists of monocline and syncline like structures along the axis of the trough.

This chapter is based (1) on fault analysis inferred from 2D seismic data (Figures 7.4 & 7.5) and (2) on inspection of maps (Upper Cretaceous to Miocene sedimentation) resulting from mainly 2D seismic interpretation. The combination of these two approaches allows determination of fault activity during the different Mesozoic - Cenozoic time periods.

Preliminary fault analysis results in this study show the timing of variable structural events along mapped fault system correlated with periods of basin subsidence in the area. The hanging walls of the mapped faults display a broad syncline structures affecting Cretaceous and deeper strata with series of significant faulting dip in different directions. It is concluded that the most recent phase of deformation within the trough represents reactivation of the basement – Cretaceous faults with overall low levels of fault activity during the Cenozoic.

Structural and stratigraphic interpretations of the 2D seismic profiles highlight three stages of fault formation. The dominant fault direction is NW-SE with a conjugate set of ENE-WSW faults on the northern margin of the Ajdabiya Trough. Other faults trend NNW-SSE and E-W, and mainly cut Miocene and older strata. A concept of listric normal faulting in the northern Sirt Basin has the potential for more or less geometric variations (Baird et al., 1996). The Ajdabiya Trough area, which is characterised by dominantly NW-SE trending normal faults that display southwest dips and both planar and listric geometries, is strongly influenced by rift-related extension. These structures dissect Cretaceous and older rocks and are sealed by Paleocene - Eocene sediments.

The inferred faults within the Palaeozoic (Cambro-Ordovician) basement and the Cretaceous are probably reactivated Hercynian or older basement structures and others could have been initiated in the Early Cretaceous with activity ongoing until the Eocene in the Ajdabiya Trough.

The fault geometry has a large influence on the deformation of the hanging-wall within any formed half-graben (e.g. Schlische and Withjack, 1999; Jackson et al., 2002).

The chapter aimed to examine the nature of the geometrical relationships between the mapped faults by mapping fault surfaces and their relations to hanging-wall deformation within the underlying the syn-rift sequences. Undifferentiated Pre-Upper Cretaceous to Late Cretaceous successions on the seismic sections show intervals with uniform thickness as well as intervals that are wedge shaped bodies of syn-rift features bounded with unconformable onlap surfaces defined by strong reflectors.

At the base or within the wedge-shaped bodies, surfaces showing onlap towards fault block crests as well as fault scarps have been identified. Representative seismic cross sections, oriented perpendicular to the strike of the faults array, illustrate the key seismic reflectors mapped in the hanging-wall fault system. In the hanging-wall of each fault block, the top pre-rift is the deepest reflector then can be mapped. This is a marked onlap surface separating the well-defined, gently dipping reflectors of the pre-rift from the seismically transparent syn-rift strata.

Strike-slip faults within parts of the Ajdabiya Trough may have originated as reactivated basement structures (e.g. El Arnauti et al., 2008). In this case it is required to test the amount and sense of strike-slip displacement across these faults. The analysis in this chapter aimed also to quantify the amount of fault related extension as apparent low fault-related strains has been observed within the Tertiary section of the Ajdabiya Trough, despite the possibility of some fault reactivation.

I proposed an asymmetrical half graben geometry for the underlying Jurassic - Cretaceous structure of the Ajdabyia Trough (Baird et al., 1996). Most of the mapped faults within the trough have the component of normal faults that controlled thickness of the syn-rift sequence and, in general, the geometry of the structure. Despite the low resolution of the 2D seismic data at this level, the rift structures seem to be well preserved in the study area. However, most of the preserved faults were possibly inverted during the Tertiary time (e.g. El Aranauti et al., 2008). Inversion can be documented by structures such as thicker rift strata on the hanging wall and by variation of fault throw (Williams et al., 1989; Holdsworth et al., 1997). Inversion of rift faults in Ajdabiya Trough could be formed in line with the same movement that happened at Cyrenaica Platform to the east, during Cretaceous (Santonian) time and

lasted also through the Paleocene (Danian) (Röhlich 1980; Craig et al., 2008; El-Arnauti et al., 2008).

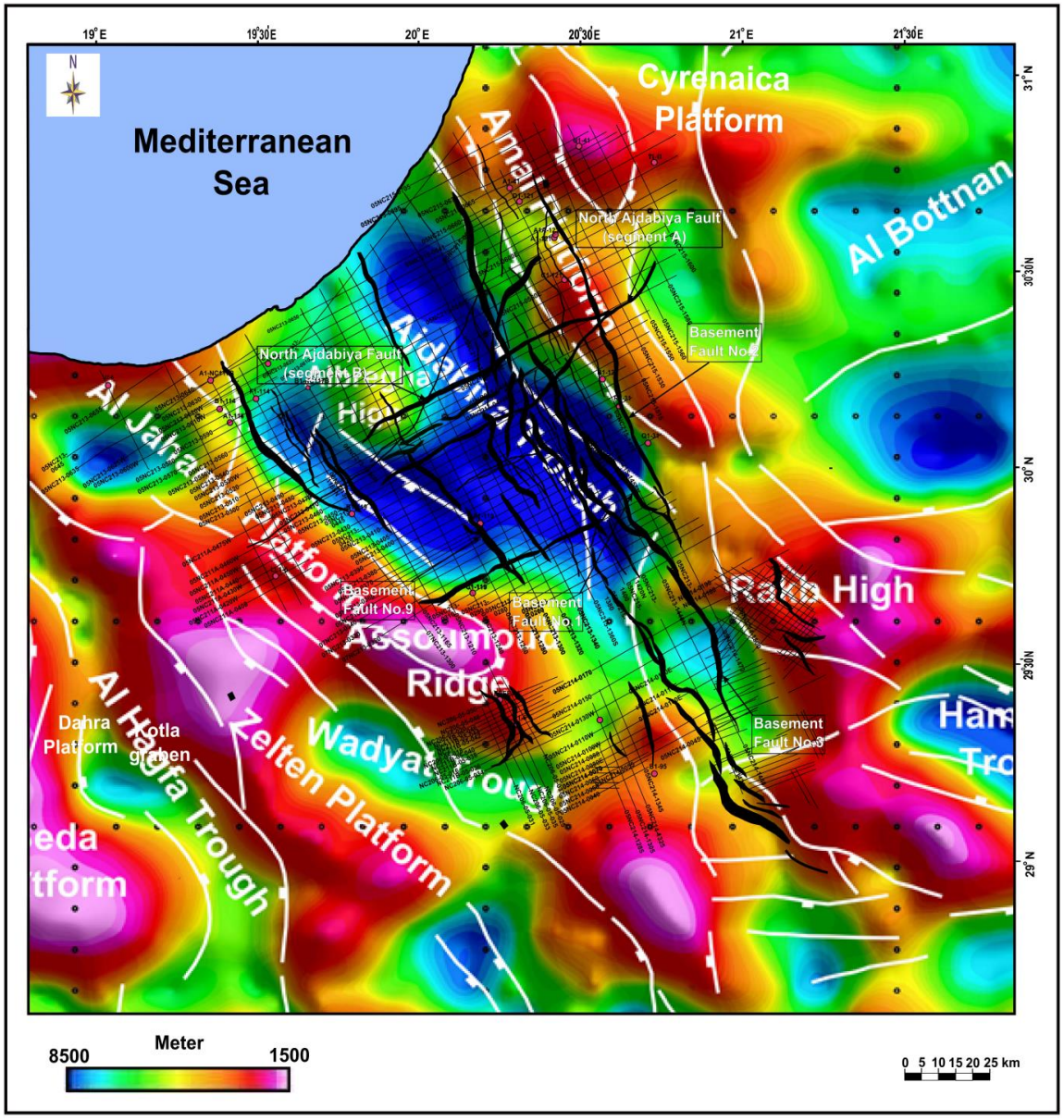

Figure 7.4: Map showing the 2D seismic survey acquired by Shell and Petro-Canada over the Ajdabiya Trough area. The burble circles are wells used for calibration with the seismic data for horizon interpretation and faults picking. The seismic and well data are superimposed on Structure contour map for the top of the basement in the region where the Sirt Basin Rift intersects. Data are from gravity profiles (chapter 4), and well data with prominent faults from literature. Locations of transects used to interpret faults and to derive their throws across the Ajdabiya Trough fault intersection are indicated and numbered. Warm and cold colours indicate high and low altitudes, respectively. The coastline is indicated.

Although analogous Cenozoic compressional folding has been reported along the Cyrenaica Platform, (El Arnauti et al., 2008), the formation of domes by compression in the Ajdabiya Trough is still controversial.

The fault analysis in this chapter is aided also by calculating fault displacements along strikes and fault throw profiles. For this purpose, I have picked fault sticks and horizon cut-offs against fault traces on seismic lines both perpendicular and parallel to the mapped faults strikes.

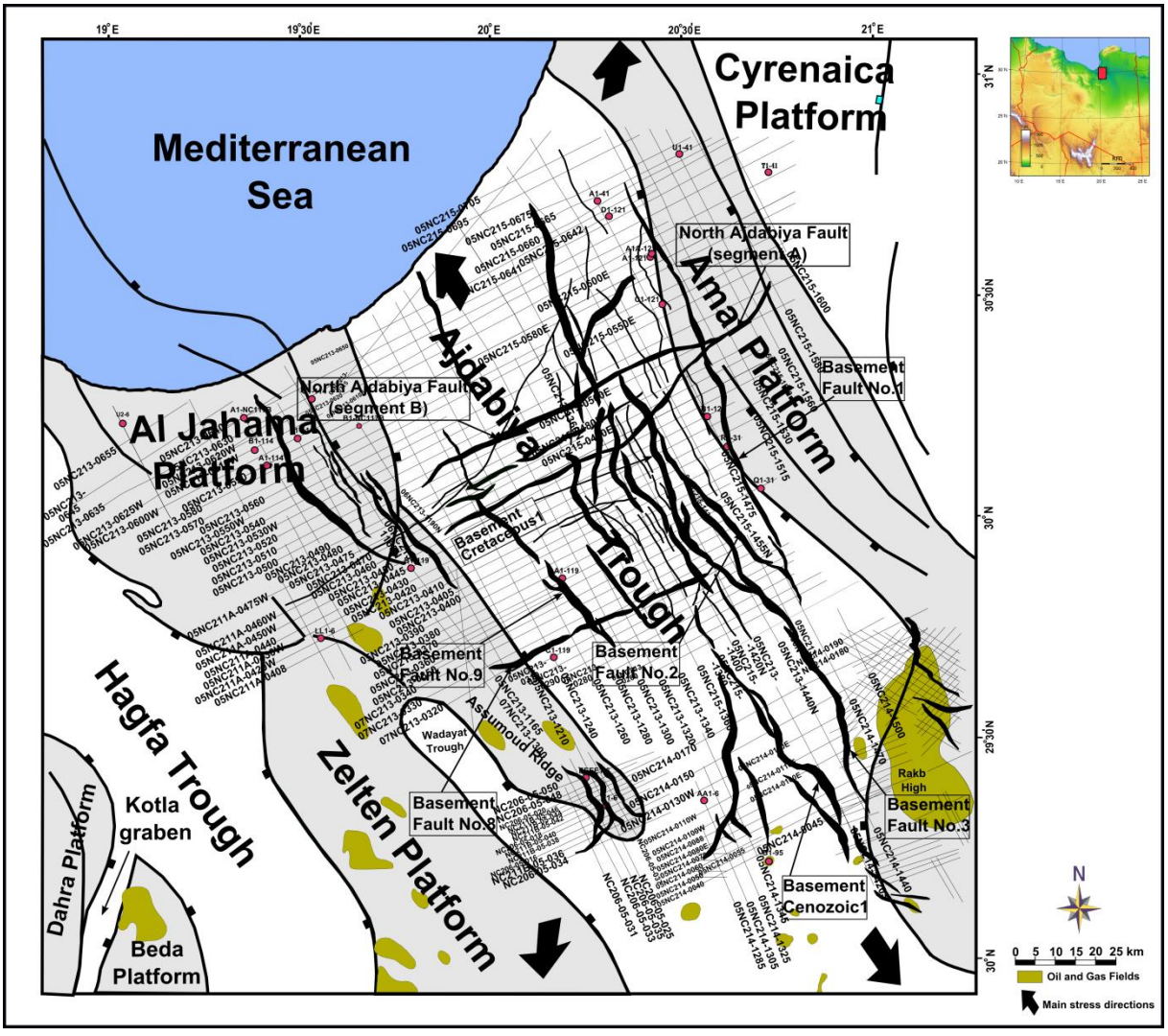

Figure 7.5: 2D seismic data coverage used in the fault interpretation with interpreted fault polygons related mainly to old basement faults subsequently reactivated during Cretaceous and latter stages. Black arrows are indicating stress field directions during permo-Triassic to Cretaceous times (e.g. Ouali, 1985; El Arnauti and Shelmani, 1985; Morgan et al., 1998; Hallett, 2002; Guiraud et al., 2005) which were predominant factors in the fault reactivation during the rifting cycles. An older generation of normal faults is interpreted in the landward-most part of the survey (grey).

For illustrating information on basin wide distribution of depocentres, a series of time thickness maps related to particular stratigraphic sequences have been produced based on the mapped reflectors. These will assist in defining the distribution of the sediments within areas of different tectonomorphic character of the Cenozoic record.

The maps were used to infer the sediment distribution during the Paleocene, Eocene, Oligocene and Miocene sequences and show details about the variability of thickness in the depositional dip and along strike directions within each sequence, and the migration of depocentres through time, from one sequence to the next.

In this study I integrate stratigraphic and tectonic evidence to reconstruct the three dimensional evolution of half-graben structures focusing, in particular, on the temporal and spatial characteristics of the faults and the distribution of the active fault populations. These are complemented by the analysis of the displacement-length scaling relationships of the structures, which includes examination of variations in syn-rift structures, fault displacements and stratigraphic evidence.

7.2 Methodology

7.2.1 Identifying Faults within Fault Blocks

Fault/horizon map has been constructed for the Ajdabiya Trough area using a combination of Landmark and Badley's Traptester™ software. Fault segments were picked on NE-SW oriented strike lines and other arbitrary lines (Table 7.1) in Landmark and then imported into Traptester™ to be modelled into gridded fault surfaces. In total 50 fault surfaces have been mapped and modelled using the Landmark and Traptester™ software. Fault polygons are interpreted using the Traptester™ software, where hangingwall and footwall cutoffs of a given stratigraphic horizons on a fault surface are picked using different criteria.

Two main parameters were used to control the generation of horizon cut-offs (Figure. 7.6).

Firstly, horizon picks within the trim distance of a fault are not used in cut-off generation, allowing the user to exclude horizon data points that fall into the area adjacent to the fault that is influenced by drag or fault-propagation folding. The second parameter used to create the cut-offs is the patch width which defines the size of the patch of the horizon data that fall outside the trim distance (Figure. 7.6).

Palaeozoic Fault Blocks	Start seismic line	End seismic line	Fault length in (km)	Fault trend
BF1	05NC213-0260	05NC213-0450	~70	NW-SE
BF2	05NC213-0280	05NC215-0665	~100	NW-SE
BF3	05NC214-0045	05NC213-0400	~120	NW-SE
BF4	05NC213-0380	05NC213-0470	~30	NW-SE
BF5	05NC213-0430	05NC213-0480	~25	NW-SE
BF6	05NC213-0400	05NC213-0480	~35	NW-SE
BF7	05NC213-0420	05NC213-0480	~23	N-S
BF8	05NC213-1165	05NC213-1420N	~55	NE-SW
BF9	05NC213-0290	05NC213-0540	~75	NW-SE
BF10	05NC213-0360	05NC213-0470	~18	N-S
BF11	05NC213-0445	05NC213-0530	~40	NW-SE
BF12	05NC213-0450	05NC213-0640	~55	NW-SE
BF13	05NC213-0410	05NC213-0530	~45	NW-SE
BC1	05NC213-0320	05NC213-0500	~77	NW-SE
BC2	05NC213-0290	05NC213-0445	~66	NW-SE
BCE1	05NC214-0045	05NC213-0240	~110	NW-SE

Table 7. l: Group of basement faults mapped in this study with their start and end seismic lines.

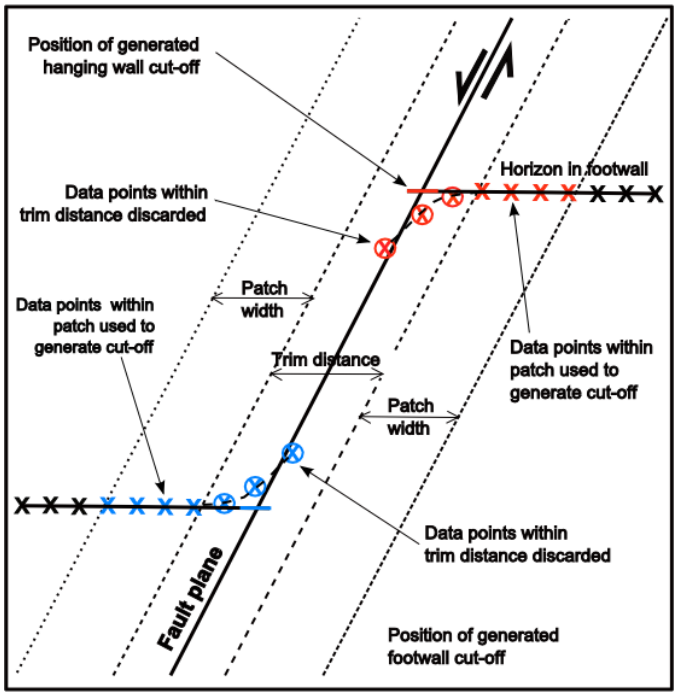

Figure 7.6: Diagram showing the significance of "trim distance" and "patch width" during the automatic creation of hanging-wall and footwall cut-offs (Re-draw from Wilson et al., 2013).

Finally a combination between a triangulated mesh and horizon patch is projected onto fault plane to produce the cut-offs. In this study, the trim distance is set to about 120 meter such that our estimates of throw include any possible deformation close to the seismically observable fault plane. The generated fault and horizon cut-offs are checked and edited manually for possible errors that could be formed due to uncertainties in fault and horizon picking. Maximum errors on throw measurements made in this study are obtained from polygon discontinuity between seismic lines and from deeper parts where seismic image quality becomes poor. Various fault attributes have been calculated using the Traptester™ for the mapped fault surfaces in the study area, including apparent throw (Figure 7.7) and apparent heave.

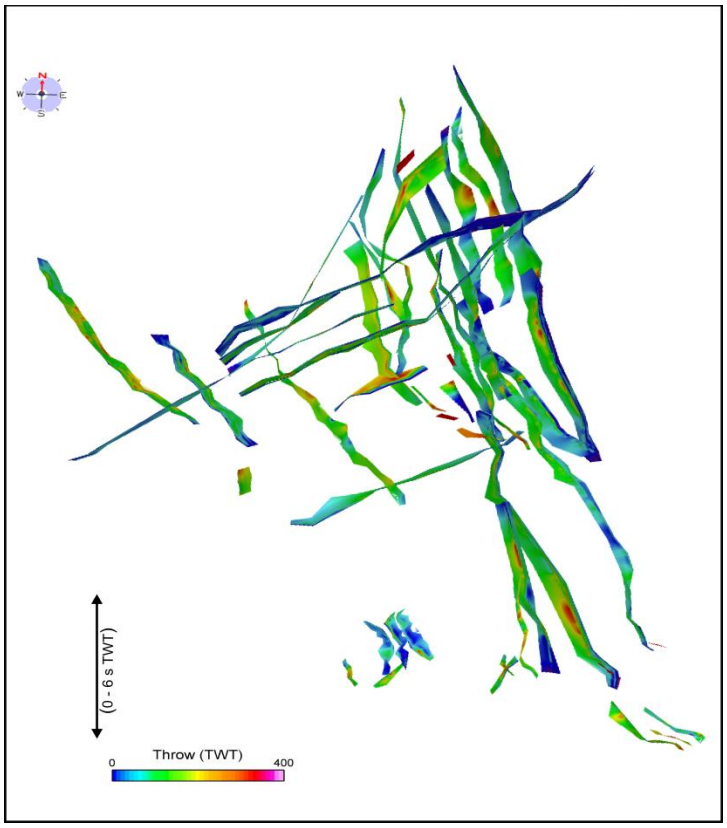

Figure 7.7: 3dimensional images of the modelled fault surfaces from Badley's Traptester software.

The software calculates and extracts fault attributes from the polygons utilizing two distinctive examining methods. The main technique utilizes a set of sample lines, each of which has an orientation orthogonal to the strike azimuth of the fault surface at each sample point. The second uses a matrix of sample lines with an azimuth that has been manually and physically set by the interpreter. The first step has been used to calculate azimuth and fault

offset, and depicts the geometrical character of the fault polygons without making any assumptions with respect to the direction of the fault slip, while, the second method measures the amount of offset in specific manner and has been utilized to estimate the time of fault movement. This can be achieved by measuring the last time substantial offset occurred across any mapped fault.

The Ajdabiya Trough comprises a north-westward narrowing fault complex of southwest dipping normal faults occasionally with characteristic of zigzag pattern (Figure 7.7).

Fault populations of this generation is concentrated at the eastern side of the trough owing to strain localization and tilting of the trough implying that the eastern faults are older than faults mapped at the western side of the trough. This observation could suggest a westward propagation of complexe basement topography and fault activity with time. Much of the Late Mesozoic – Early Cenozoic structures apparently results from compaction over the basement topography. Movements of basement blocks control the stratigraphy and localized most of the structures in the sedimentary section.

The most prominent fault system is found in the north-eastern flank of the trough consisting of a series of major NW – SE trending and moderate to widely spaced normal faults bounding thick Pre - Late Cretaceous graben structures.

Analysis of 3D geometry of the mapped faults from the Ajdabiya Trough area is based on the recognition of the geometry of each fault in plan-view and cross-section, variation in displacement and dip on the fault surface. The geometry of the faults is described using observations from fault surface topography or length of fault segments (e.g. Cowie et al. 1996). The maximum dimension of the fault surface constitute the fault length, while the fault displacement is refers to the total displacement accumulated through the life of the fault (Walsh & Watterson, 1988). Displacement gradients (Figure 7.8) are calculated using the ratio of maximum displacement (D) and the fault radius (R) or (D/R) (Barnet et al., 1987; Walsh and Waterson, 1988). Displacement gradients vary with fault size and with mechanical properties of the host rock (Barnett et al, 1987). The basement faults are thick-skinned faults that bound large rotated fault blocks and have sufficient displacement to offset the entire layers, thus coupling deformation of the basement and upper strata. The faults are generally planar in geometry and trending NW-SE with throw varying along strike between (100 ms) and (400 ms) TWTT. However the maximum displacement observed on the basement faults is

about 500 ms. Activity on the basement faults probably initiated synchronously in the Late Palaeozoic and Mesozoic times and they remained active into the Early Eocene, confirmed by majour offsets on stratigraphic horizons. The faults have a horizontal separation, measured in a direction approximately perpendicular to fault strike, of 5 km – 10km and a length in excess of 100km. Among a number of faults modelled using the Traptester™ software (Figure 7.7), eight pronounced fault blocks have been selected for detailed interpretation. The selection of these fault blocks is based on the clarity and the visibility of the fault trends, planes on seismic sections and the reflector terminations within formed grabens. The faults attached to these blocks are composed of normal fault segments with variable structural style and evolution. For descriptive purposes, the fault array is divided into a basement-restricted fault array (i.e. faults that tip-out upward into the Upper Cretaceous), and a basement-involved fault array (i.e. Faults offset both basement and Mesozoic - Cenozoic strata).

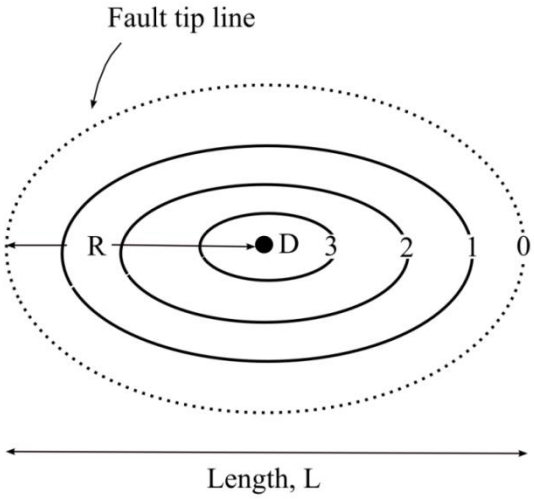

Figure 7.8: Schematic displacement contour diagram for a simple, isolated fault drawn normal to the fault surface (strike-view). Maximum displacement is in the fault centre (D_{max}) and with tip line loop corresponding to the zero displacement contours, R = radius and W = the width of the fault (from Barnet et al., 1987; Walsh and Waterson, 1988).

The faults that have been selected are named Basement Fault No.1 (BF1), Basement Fault No.2 (BF2), Basement Fault No.3 (BF3), Basement Fault No.9 (BF9), North Ajdabiya Fault (NAF), Basement Cretaceous1 (BC1), Basement Cretaceous2 (BC2), and Basement Cenozoic1 (BCE1) (Figure 7.10). The identified faults are considered to be reactivated pre-existing basement structures characterized by moderate to high segmented pattern and maximum throws.

Deviations from the extensional fault geometries can be generally related to the tensional reactivation of pre-existing crustal discontinuities (Bertotti et al., 2000). These geometric relationships provide important information about the spatial and temporal evolution of the fault systems, specifically that the larger faults, such as BF2 and BF3, were probably formed and grew first as a graben bounding faults during the early rifting stages.

7.2.1.1 Fault Correlation

Fault correlation using 2D seismic data in this study was a subjective task as a result of the large spacing (~2.5 – 3km) between the seismic lines. In this case the analyses focuse on the largest structures – ie 100km long faults. In addition to lateral association between lines, vertical association between horizons also was a main problem in fault correlation. This means that faults picked on vertical sections most correlate to the mapped horizons that offset by the mapped faults. Due to few mistakes in the vertical link between horizons as a result of vertical segmentation, fault pattern drawn for one horizon may not correspond to that produced for adjacent horizons. As a result of the manual interpretation, fault polygons often show heaves that are wider than the true heave on the fault they represent.

A fault correlation has been made in this study based on a series of fault sticks and traces lie along the same trend (Figures 7.9 & 7.10). Not all the interpreted fault traces could be used for construction of fault planes, as it was not always possible to find adequate traces in seismic lines nearby. Analysis of displacement patterns on single or multiple fault surfaces is a powerful way of testing lateral fault correlations in 2D and 3D datasets (e.g. Freeman et al., 1990; Waterson et al., 1997). Displacement patterns are used also to differentiate between isolated faults based on throw maxima (Figure 7.11) which strongly supports the idea that some correlated structures in fact consist of more than one fault segment. This led to the recognition of separate fault sets in the Ajdabiya Trough dataset and in general includes faults that show increase of displacement with depth possibly as a result of propagation of basement faults.

Faults can be analysied using 2D sampling methods as fault segments can be expressed in terms of changes in their maximum displacement and length (e.g. Walsh et al., 2002). In this case, car should be taken when calculating the length vs. displacement relationships. There is

a lote of scatter in displacement length correlation plots, which is caused by the process of segment linkage (e.g. Mansfield and Cartwright, 2001).

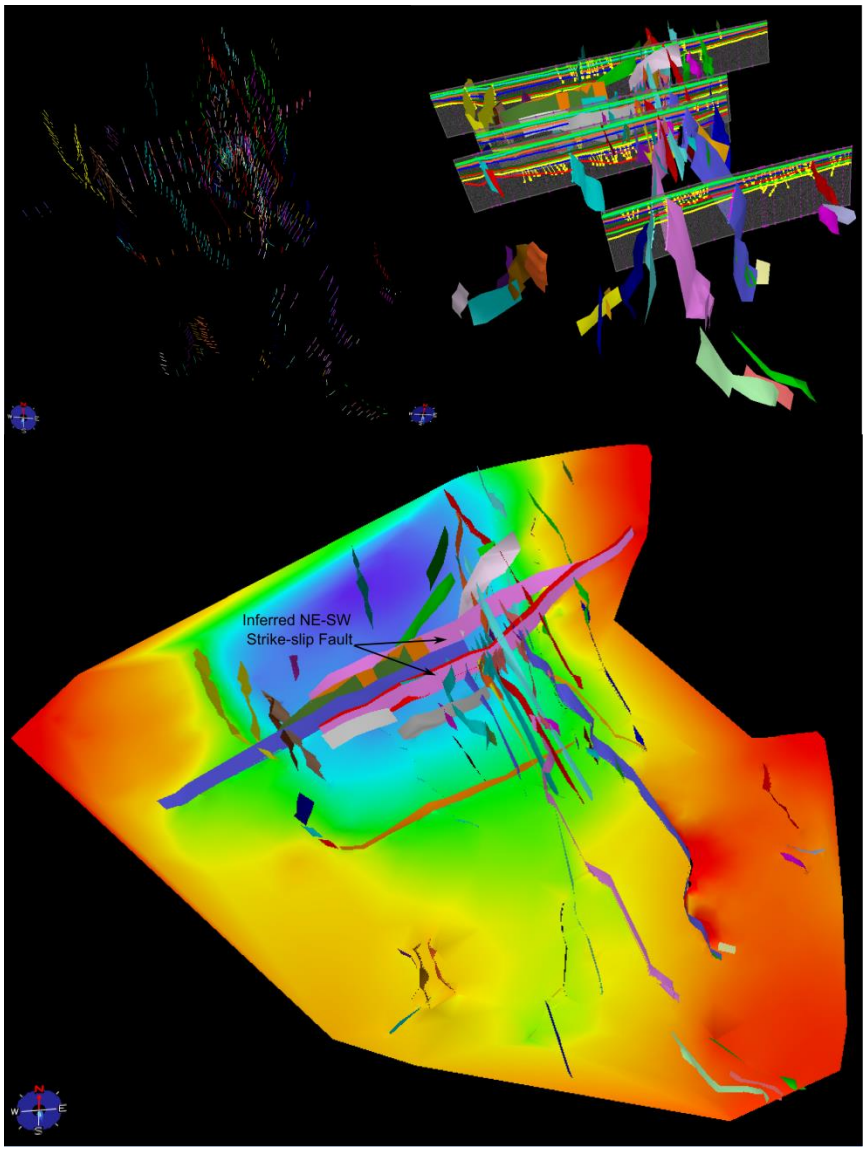

Figure 7.9: Distribution of variable fault sticks assigned to the picked faults within the Ajdabiya Trough with 3D structural model automatically built using faults, horizons and stratigraphic trends interpreted from 2D seismic data. Time structure map of Upper Cretaceous horizon with the mapped faults superimposed below. Note the major NE-trending strike-slip faults that are inferred to have been active during the Cenozoic period. According to Anketell (1996) and El Arnauti et al., (2008), the Cyrenaica Platform and the eastern Sirt Basin including the Ajdabiya Trough are characterized with strike-slip activities along major shear zones.

The concept of strike slip fault within the Ajdabiya Trough was also introduced and interpreted using careful correlation procedures, based on methods of strike slip recognition (e.g. Harding, 1990), because the fault traces do not provide direct evidence for the sense of movement.

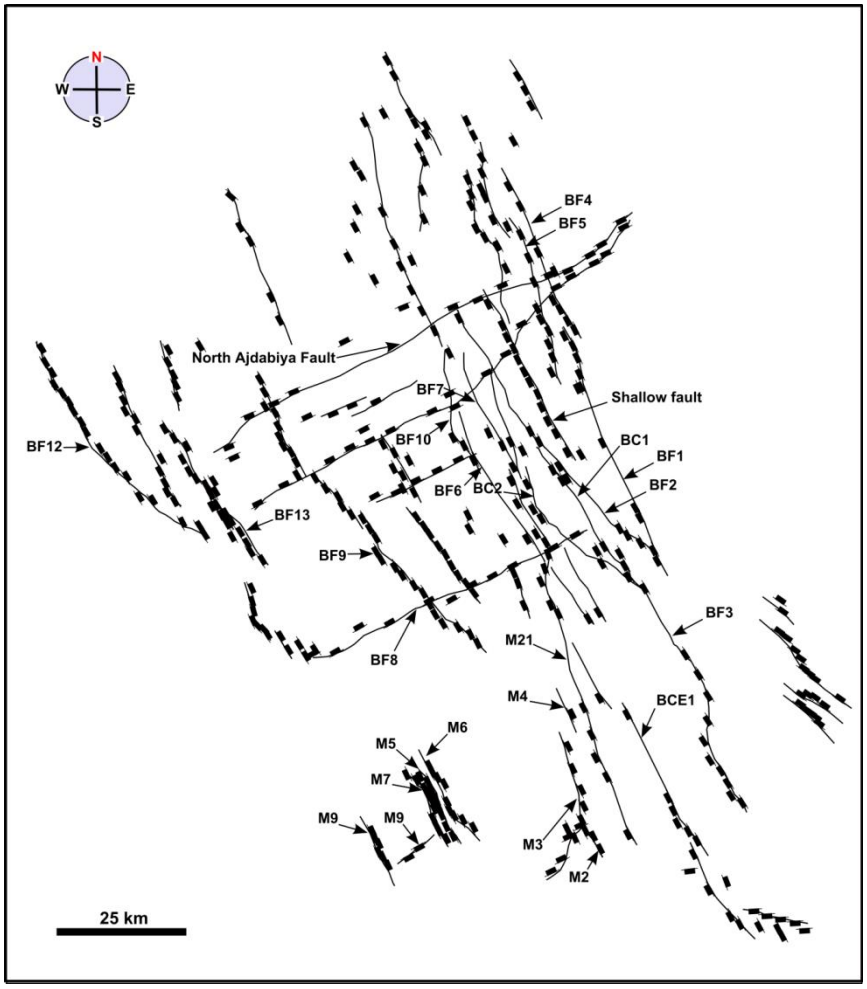

Figure 7.10: Small rectangles show the relative dip sense of the mapped faults. These were correlated as possible and assigned to particular faults within the Ajdabiya Trough fault system.

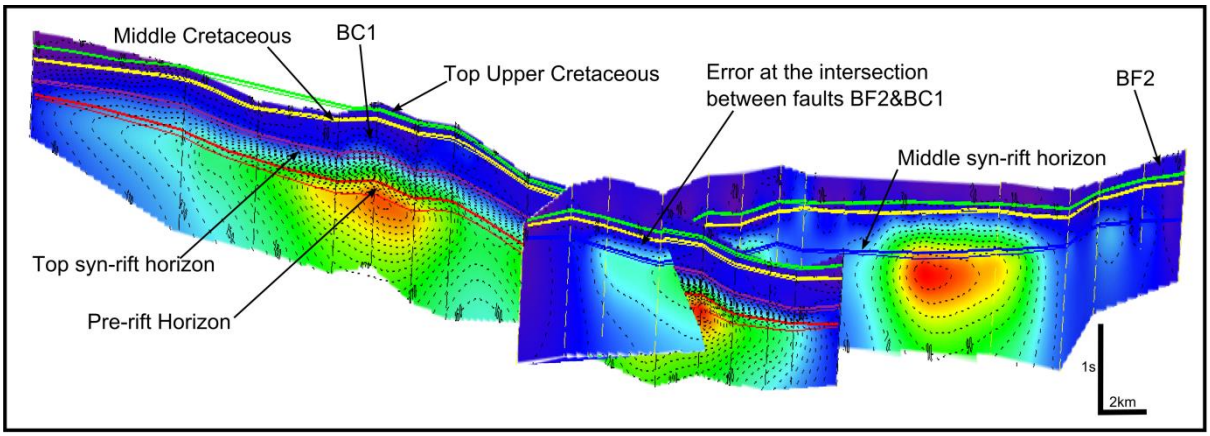

Figure 7.11: Displacement contour map of the BF2 and BC1 faults where black and yellow lines are fault sticks picked on 2D lines and coloured polygons are hanging wall/footwall horizon intersections. Coloured contours of throw show a complex growth history or, perhaps, unlikely correlation of faults. The centre of the fault is probably basement related, while at each end displacement is non-basement related.

A correlation procedure is applied in this study in order to quantify possible strike–slip movements. Additionally, other subordinate faults might be difficult to resolve on the seismic sections. Fault traces are grouped into different classes based on their characteristics on map and 2D seismic lines (stratigraphic separation, relative age, relative movement in 2-D) and are grouped in TrapTester environment. Fault surfaces were constructed and checked plausibility and at the end of the correlation process, a set of the most reasonable faults remained (Figure. 7.12).

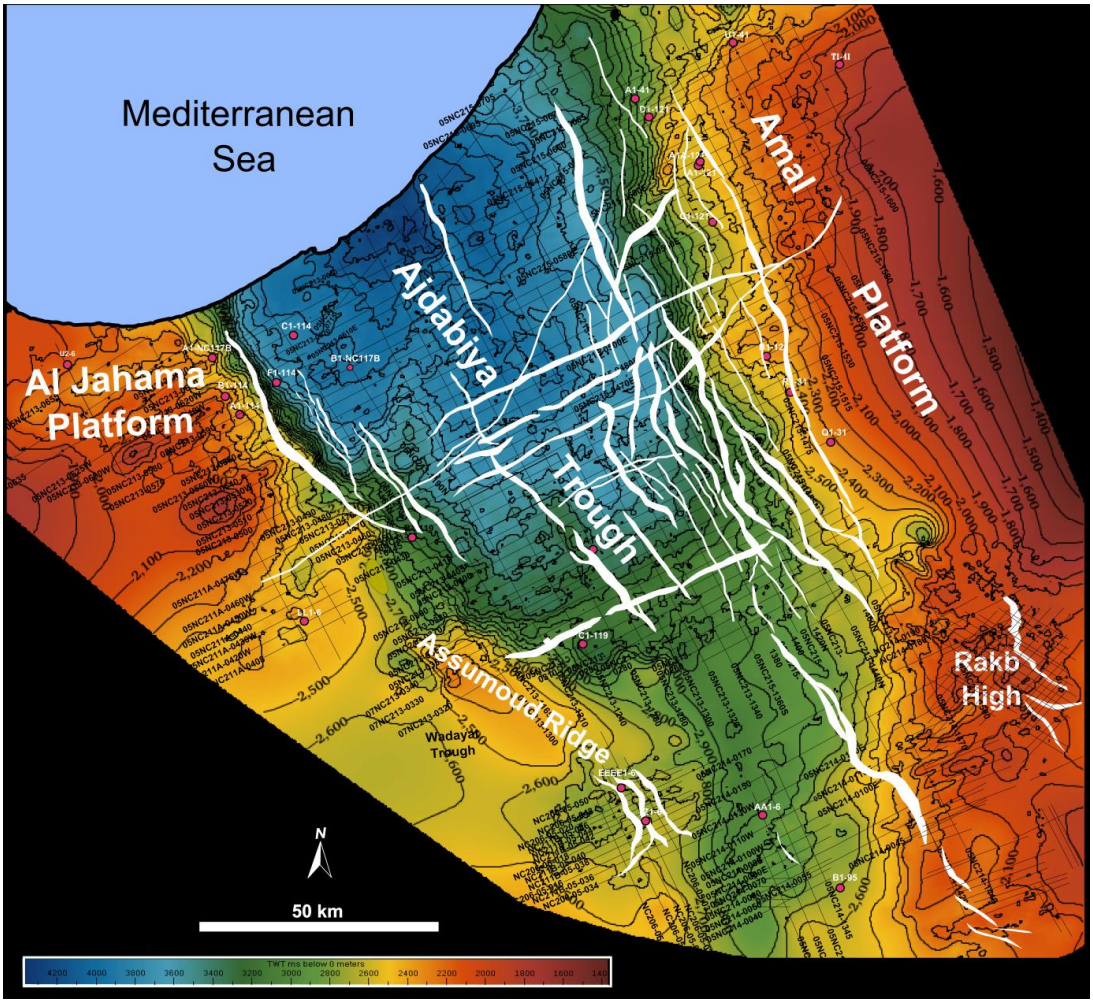

Figure 7.12: Time structure map of Upper Cretaceous horizon illustrating the general structural style of the Ajdabiya Trough with Pre – Upper Cretaceous rift related faults superimposed. Folds developed along the trough margins probably during the latest Cretaceous to the earliest Palaeocene that is during the final stage of intracontinental rifting prior to breakup of ca. 140 Ma but following the main phase of normal fault growth and linkage which was synchronous with the deposition of the Upper Cretaceous – Palaeocene sequence. These intrabasin structures (anticlines and synclines) are possibly the sites of fault linkage. Normal faulting and growth of strata during the Late Cretaceous, followed by intensive erosion that defined by an Upper Cretaceous Unconformity (e.g. Roohi, 1996b; Hallett, 2002). Any subsequent structures developed such as intrabasin highs are considered to be a non syndepositional transverse folds developed as a transpressional components.

7.2.1.2 The Fault Pattern

Faults mapped on 2D data in the Ajdabiya Trough, strike approximately parallel to basement structures identified using gravity and magnetic data (chapter 4). The faults have different orientations with a predominant NW-SE and NE-SW patterns (Figures 7.12, 7.13, and 7.14) and supposed to offset the basement to Eocene horizons. The majority of faults do not cut up through the Tertiary strata and may be related to short lived syn-rift faulting. Instead that there are a small number of faults seems to cut the Tertiary strata (Figures 7.13 & 7.14).

To the east of the trough the faults are dipping to the SW and formed along hinge zone separating Ajdabiya Trough from Cyrenaica Platform (e.g. Shary, 2008) while the NE-SW faults are mainly dipping to the NW and SE (Figure 7.15) some of which has component of strike-slip faulting (see below). The faults at the western side of the Ajdabiya Trough are dipping towards the NE along its length (Figure 7.15). The faults give off an impression of being widely dispersed, with occasionally very densely spaced with about 3 - 5 km between each other. These faults are probably reactivated Late Palaeozoic or older basement structures based on similarity in trends of the mapped faults and deepseated gravity and magnetic anomalies. Some faults show evidence of having slipped in various directions and appear to have both sinistral and dextral strike slip components and are possibly linked to seismic activity in Sirt Basin and the Cyrenaica Platform to the east (e.g. Anketell, 1996; El Arnauti et al., 2008, see below). Fault movement and fault splays can be observed within the Ajdabiya Trough suggest that faults may have been initiated around the trough first then latterly propagated towards the centre of the trough during periods of rifting and basin subsidence with development of local depocentres.

Vertical displacements on these faults are several hundred of milliseconds TWT and are defined by large throws on Cretaceous and underlying horizons. The modelled faults vary in size from 60 km to more than 100 km in length, with a mean length of about 65 km. The maximum offset during the Upper Cretaceous to Eocene on each modelled fault varies from 10 ms TWT to 85ms TWT.

Large fault offset in particular is comparable with strain localization in certain areas within the Ajdabiya Trough which characterized by large fault movement. In comparison with little movement on other faults which in this case can be considered as a blind faults.

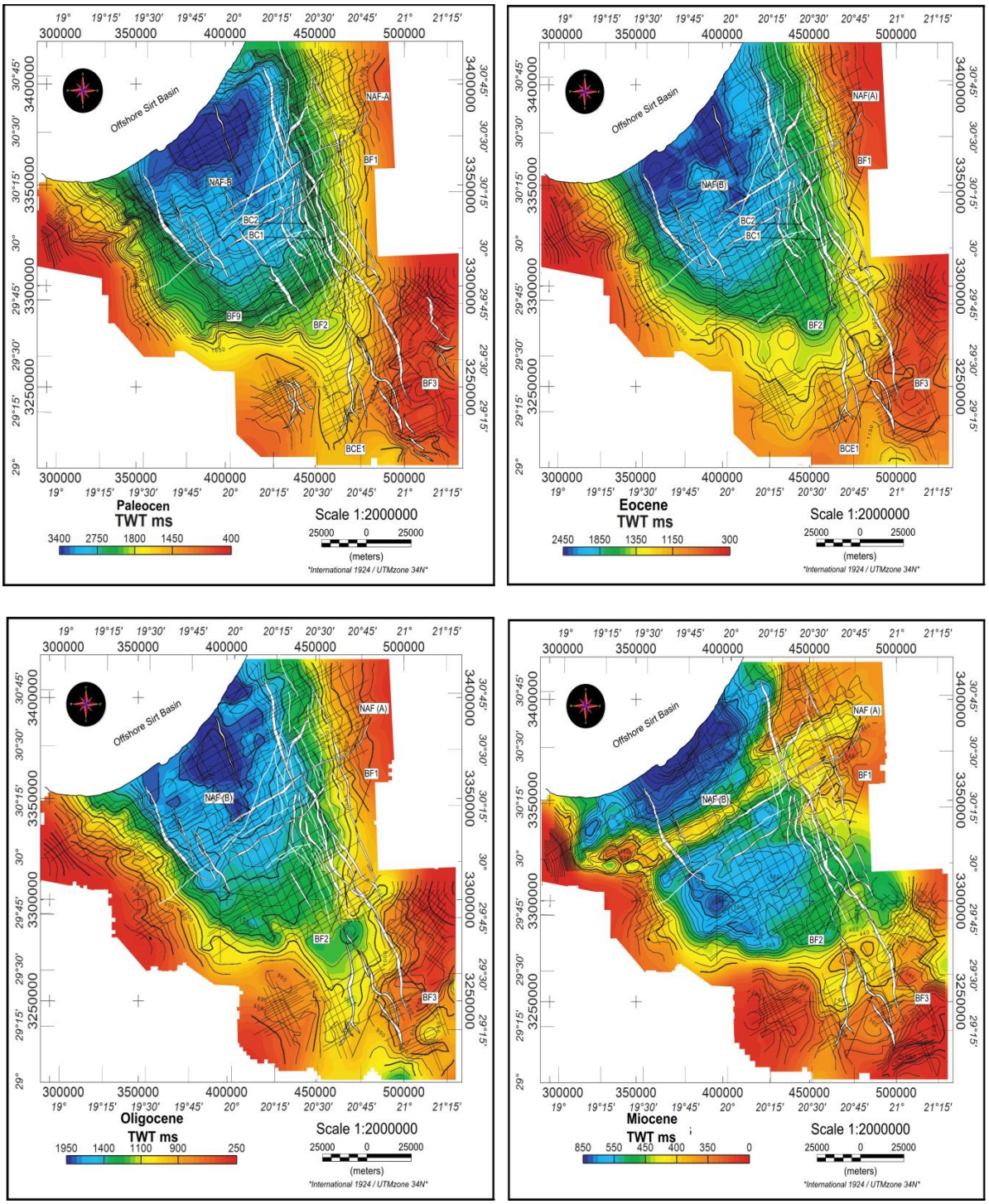

Figure 7.13: Time structure maps obtained from 2D seismic interpretations show the distribution of the top Paleocene, top Eocene, top Oligocene, and top Miocene sequences and their relations to the development of faults in the Ajdabiya Trough. Red and yellow are structurally high areas marking the Ajdabiya Trough margins. Within the centre of the trough, green and light blue colors are local structural highs and dark blue, purple, and pink colors are structural lows. Local depocentres are aligned in different directions in the centre and the northern area of the maps (dark blue).

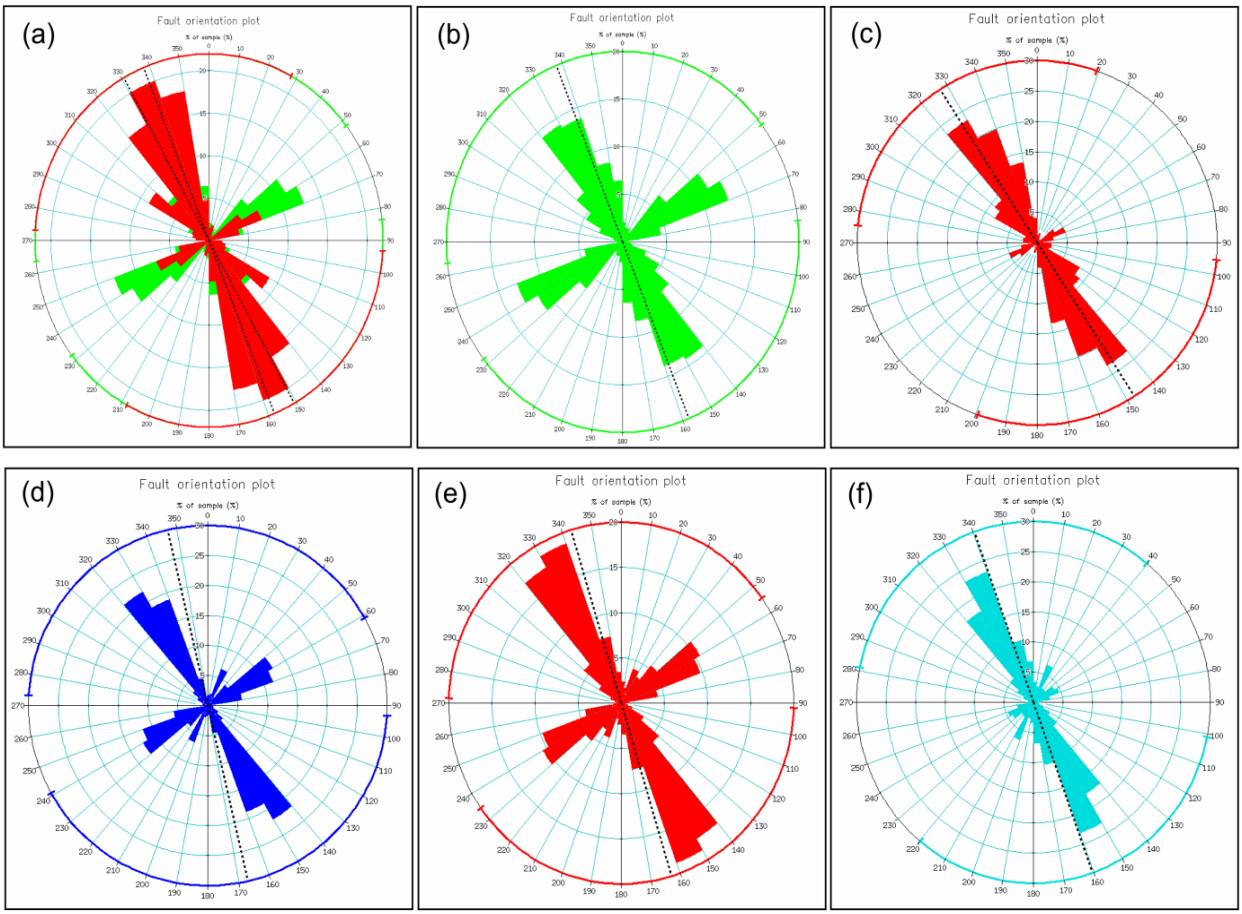

Figure 7.14: Fault orientation plots highlighting the mean vector (strike) azimuth and mean circular deviation of faults that intersect horizons moving progressively up sequence from (a) superimposed plot of Upper Cretaceous and Paleocene (b) Top Kalash (Upper Cretaceous) (c) Paleocene (d) Top Gialo (Middle Eocene) (e) Oligocene (f) Miocene. The plot shows variation of fault orientations through period from Cretaceous to recent. The dashed line indicates changes in the mean strike azimuth which increasing during the Cretaceous then progressively decreased during the Paleocene then become increasing again during the Eocene followed by slight decrease in azimuth during the Oligocene and Miocene.

In the Ajdabiya Trough area the Cabmro-Ordovician basement is cut and offset by set of normal faults. Reactivation of these faults may be influenced the development of the Cretaceous rift system in the study area. Rift related sedimentary wedges commonly thin onto the crests of fault blocks, where truncation and onlap are observed.

Reflectors diverge and thicken down dip from the footwall crest and towards the adjacent bounding fault. Some faults seems to be a blind fault in nature and mainly characterized by the development of fault propagation folds with anticline and syncline like structures formed above buried fault tips (e.g. Withjack and Callaway, 2000).

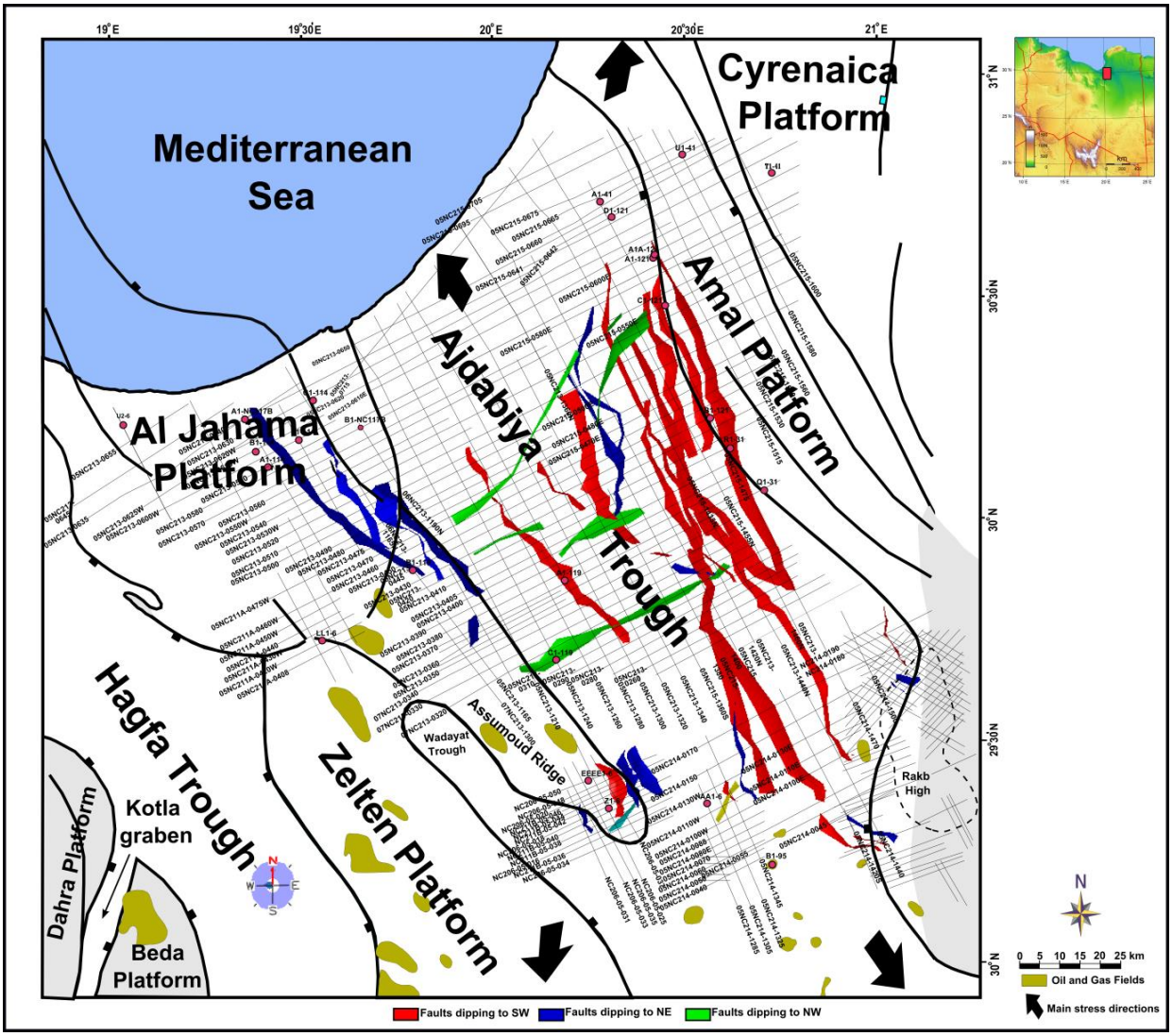

Figure 7.15: Faults in a 3D fault model show variations in fault dips along strike (different colour code) which mainly related to different types of fault populations within the Ajdabiya Trough structural domain.

7.2.1.3 Syn-sedimentary Faulting

Within the Sirt Basin area, Gras and Thusu (1998) recognised pre-rift (Palaeozoic) and syn-rift (Triassic to early Cretaceous) phases, and a post-rift phase characterised by graben fill, basin sag and subsidence (late Cretaceous to recent) (Figure 7.16). Subsidence history during Late Cretaceous is consistent with fault controlled sedimentation (Gumati and Nairn, 1991) followed by uniform stratigraphy implying little motion on bounding faults (Selley, 1997). A phase of extensional faulting in the Triassic to early Cretaceous of the Sirt Basin is also documented by Gras, 1996.

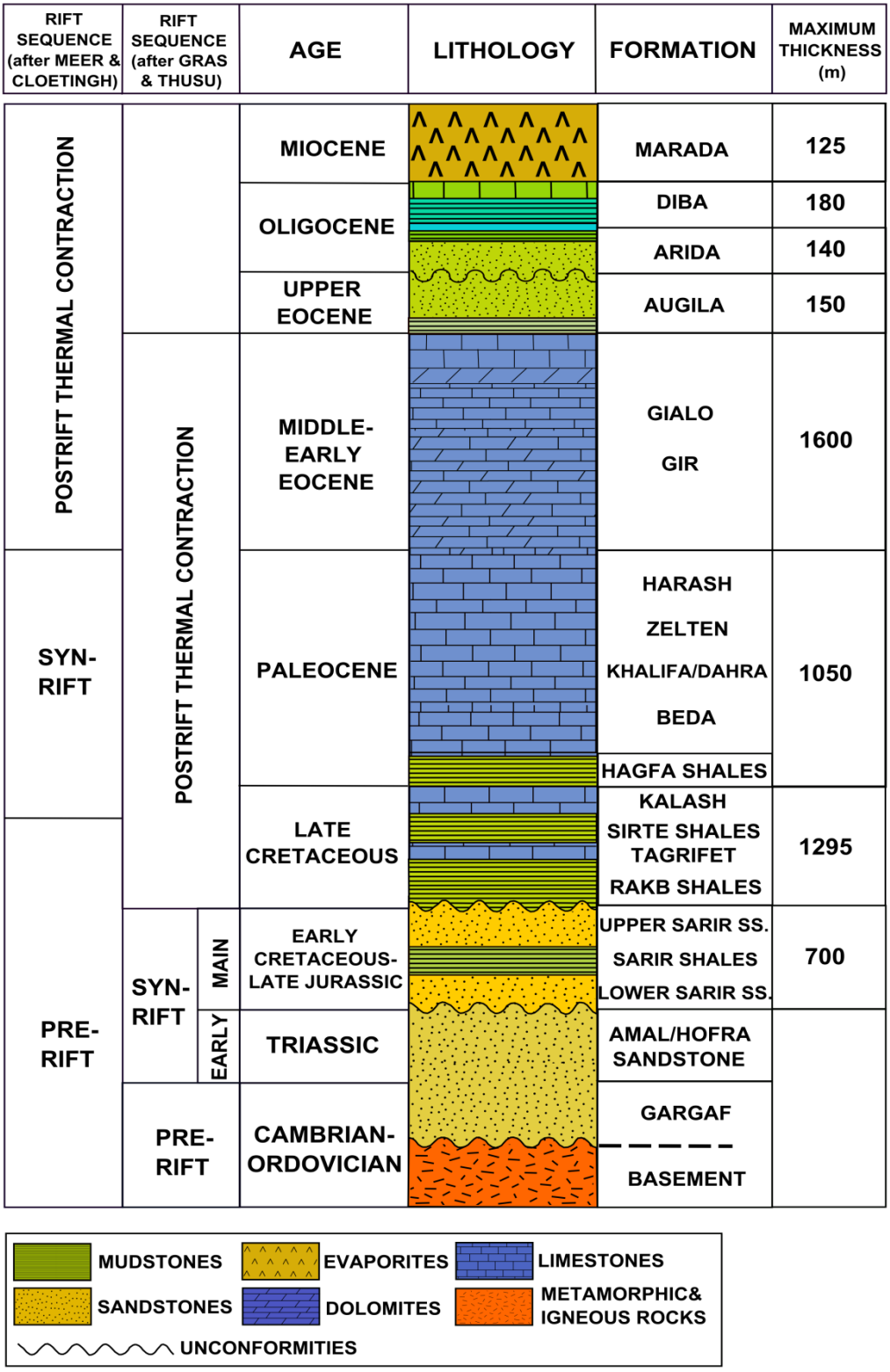

Figure 7.16: Stratigraphic framework showing the ages and representative lithologies of the formations present in the Ajdabiya Trough (redrawn from Ibrahim, 1991). Maximum thicknesses of different units are taken from Van der Meer and Cloetingh (1993). On the left, the related tectonic interpretations according to Van der Meer and Cloetingh (1993) and Gras and Thusu (1997).

Observations in this study show that the structure framework of the Ajdabiya Trough is dominated by normal faults and tilted blocks trending NW-SE, NE-SW, and NS with sedimentary fill locally up to 4 km thick. The uplifted edges of many fault blocks were eroded and subsequently overlain unconformably by Cenozoic structures.

Synsedimentary faulting can be recognised on seismic data based on stratal relationships and seismic character in addation to distribution of fault throw contours on strike projections (Figure 7.17) (Prosser, 1993; Child et al., 2003). The 2D seismic data in the Ajdabiya Trough show evidence of deep-seated faults terminating within possible Triassic or pre-Upper Cretaceous successions and sediment thickness variations suggesting syn-sedimentary growth faulting (Figures 7.21 & 7.22).

Several faults propagate upwards and terminate within the late Cretaceous sequences which occasionally display mildly chaotic and disrupted intervals. This type of internal seismic character may indicate syn-sedimentary disruption, as observed by wedging of reflectors.

Syn-sedimentary normal faulting continued during the Lower Cretaceous and produced a vertical displacement of 150 to 350 ms at top of pre-rift horizon. The amount of crustal extension calculated on basement horizon at 6000 ms TWT is about 21.17 %, and Pre Cretaceous horizons with TWT of 3500 ms is about 12.94 % (chapter 6).

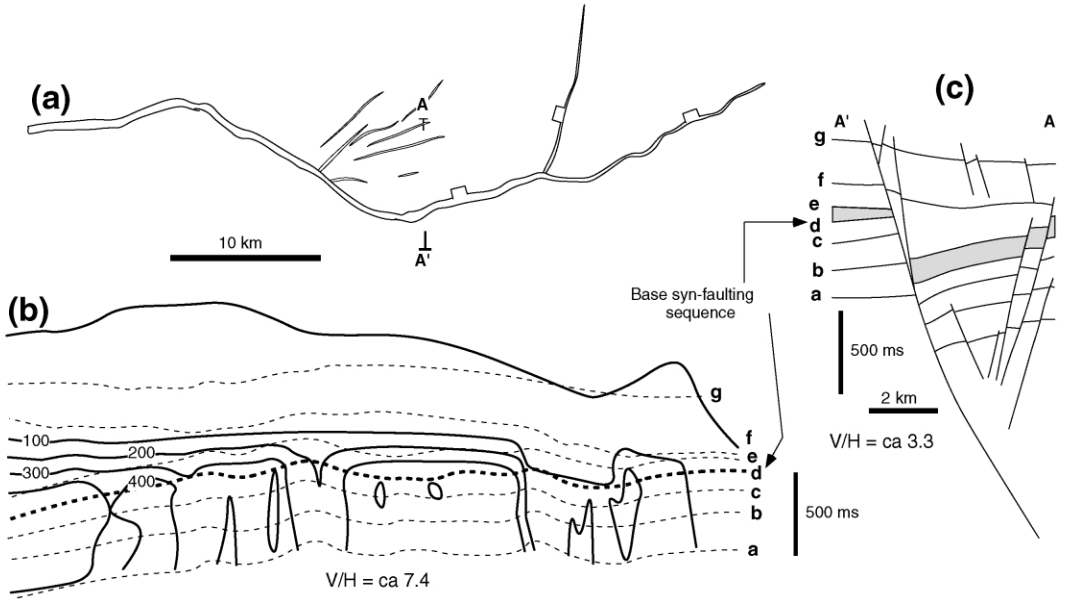

Figure 7.17: (a) Synsedimentary fault map from the North Sea (b) Throw contoured strike-projection of the fault (c) Cross-section along line A–A' on map (a). Figure obtained from Childs et al., (2003).

I postulate that the extension may have a regional character possibly driven by far-field stresses along the North African Margin (Hallett, 2002). The Ajdabiya Trough includes an Early Cretaceous succession bearing clear evidence for syn-sedimentary normal faulting, such as syn-sedimentary geometries related to well oriented NW-SE-striking faults, with lateral variations in the thickness and facies of formations. Three stages of syn-sedimentary fault activity can be proposed for the Ajdabiya Trough fault system. (1) Early Cretaceous rifting accompanied by localized normal faulting, creating growth-fault structures and differential subsidence. (2) Upper Cretaceous normal faulting, which contributed to the initiation of erosion on topographic highs and sedimentation in topographic lows. A transition from distributed to more localized faulting is observed in the eastern part of the Ajdabiya Trough, related to a final stage in the evolution of the Cretaceous extensional process and strain localization. (3) Paleocene and Eocene when a major reactivation of faults occurred.

True growth sequences have been constrained by the offsets on series of stratigraphic horizons which helped in breaking the age of fault movement.

The Cretaceous successions on the seismic sections show intervals with uniform thickness as well as intervals that are wedge shaped stratal geometry reflects differential accommodation development and associated differential sediment accumulation on the hanging-wall of the bounding faults, with the maximum of accommodation creation a geometrical depocentres located in the vicinity of major fault scarps and elongated with a lateral extension along the fault blocks truncated with a series of minor faults.

The structure of the trough is asymmetric with most large blocks tilted to the NE and their bounding faults dipping SW (Figures 5.21, 5.22 and 7.15). The footwalls of the mapped faults represent a series of structural highs extending NW-SE. The fault blocks occasionally characterized by basement section on its uplifted edge and tilted pre-rift sediments (Figures 5.21 & 5.22). Pre-Upper Cretaceous rocks overlie pre-rift rocks with possible angular unconformity showing that considerable tilting had occurred in this time. Uplift in the Ajdabiya Trough is likely to be part of a long wavelength uplift of the entire region, and may be related to the cause of rifting in the region. Short wavelength movements are also associated with normal faulting.

7.2.1.4 Identifying Strike-slip Faulting in 2D Seismic Reflection Datasets

The origin, evolution and recognition of strike–slip faults have been widely studied in experimental models and by using outcrops and subsurface structural data (e.g. Harding, 1990; McClay & Dooley, 1995 and references therein). There is sometimes a problem identifying listric faults on time migrated seismic due to the increase in velocity with depth. Therefore, it can be difficult to say with certainty that a fault is listric in nature.

The interpretation of strike-slip faults using seismic reflection profiles is based on their three-dimensional structural style (e.g. Harding, 1990). Based on this the characteristics observed on 2D seismic sections from different parts within the Ajdabiya Trough structural domain suggest possible existence of strike-slip faulting. The main criteria used in identifying strike-slip faults in the Ajdabiya Trough using the 2D seismic sections are (1) flower structures (positive or negative), (2) change in the amount and/or direction of dip of fault plane along strike, (3) reversal of or change in fault throw with depth, (4) basement involvement.

The seismic data show evidence of strike-slip faults within different parts from the Ajdabiya Trough structural domain based on the above assumptions. A major strike-slip component trending NE-SW from the western part of the Ajdabiya Trough towards the Cyrenaica Platform shown as a strike-slip segment with length in excess of 100 km and a width of up to about 3 km (Figure7.12). The fault zone comprises a group of sub-parallel faults rooted in the basement at depths of about 2.8 s TWT, whose geometry suggests the development of a possible negative flower structures (Figures 7.51 & 7.52 in section 7.3.4.8), markedly contrasting with the reverse fault geometry typically suggested for this strike-slip fault (e.g. Anketell, 1996; Baird et al., 1996; El Arnauti et al., 2008). Significantly, two main strike slip fault segments (North Ajdabiya Fault A&B) were interpreted (Figures 7.10).

The northern boundary fault NAF (A) dips to the northwest with an estimated maximum throw of ~100 ms TWT, on Upper Cretaceous horizons. Conversely, the southern segment NAF (B), dips to the southeast with a normal maximum throw of ~68 ms TWT on Upper Cretaceous horizons also (Figure 7.18).

I postulate that the fault zone may predominantly constitute of a dextral bend component (e.g. Anketell, 1996; El Arnauti et al., 2008) during the Mesozoic formed by kinematic movements of the fault zone during continental extension. There might be also several kinematic stages characterize this first order transfer fault and primarily related to sinistral strike-slip during

Hercynian continental collision, dextral transtension during continental extension, sinistral transpression during Early Eocene (Lutetian) and Late Miocene continental collision (e.g. El Arnauti et al., 2008).

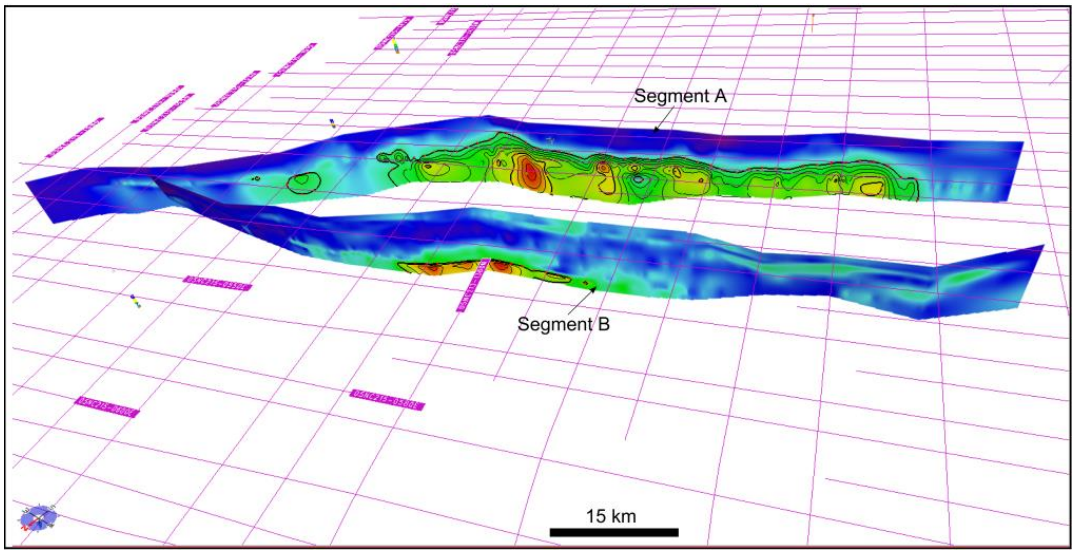

Figure 7.18: Fault surfaces as colour-coded attribute maps showing throw variations along strike of NAF fault segments (A), above and (B) below.

7.3 Geometry and Distribution of Faults in the Ajdabiya Trough

7.3.1 Interpretation and Correlation of Major Faults in the Ajdabiya Trough

The fault interpretation within the Ajdabiya Trough began with checking the consistency of picking the same fault from line to line to avoid as possible the miscorrelation of aliasing faults that may connect one two separate faults as one. The faults picked every line using lines orthogonal to the strike of the faults. Some faults have been interpreted as bifurcating faults with variable splays. However, a correlation between large- and small-scale faults is difficult because of their strong variations in orientations.

Fault throw measurements derived from regularly spaced lines across the fault plane are contoured and displayed in two-way travel time (TWT). Correlation of stratigraphy between hangingwall and footwall was good for shallow horizons but decreases for the deeper horizons, therefore errors in throw measurement are expected. Lithological variations and

compaction of sediments between hangingwall and footwall sequences within the Ajdabiya Trough has large impact on estimating accurate throw values (e.g. Cartwright et al., 1998).
Drag folds can introduce errors in throw calculations (e.g. Walsh and Watterson, 1988; Mansfield and Cartwright, 1996), but this is not considered in this study. Many of the faults are associated with growth strata and considered as synsedimentary faults evolved during the Cretaceous time.

7.3.2 Displacement-length Analysis

Displacement length profiles (Figure 7.19) have been constructed in this study for each mapped fault using data exported from the TrapTester software based on sampling grid spacing of (~2500 m) which set up orthogonal to each fault strike.
Throw data in milliseconds (TWT) were plotted against distance along the fault strike. The displacement profiles could have an uncertainty due to difficulties in constraining the dip of the faults as the data have not been depth-converted and secondly the profiles were recorded at mainly Upper Cretaceous level were possible footwall erosion can affect the displacement values due to low accuracy in the determination of the footwall and the hanging wall cut-offs in a good manner. Therefore the throw data measured along vertical planes is used as representative to the displacement. Variations in displacement of each mapped fault in addition to the assessment of fault segment interactions during fault growth process can be constrained from these profiles. The plots include throw data obtained from faults that tip-out within the limit of the 2D seismic dataset, by which the faults are well imaged with their end tips. In this case the maximum observed throw was assumed to be located in the centre of the faults, i.e. at a distance L/2 from the observed lateral tip. Thus, D_{max} is greater than or equal to the maximum observed throw. Tip lines and fault lengths are difficult to estimate based on the 2D seismic dataset used in this study, therefore the mapped faults are assumed to tip-out at the low displacements at both sides of the faults and not considering that the faults are extending further based on decrease of displacement gradient to zero.

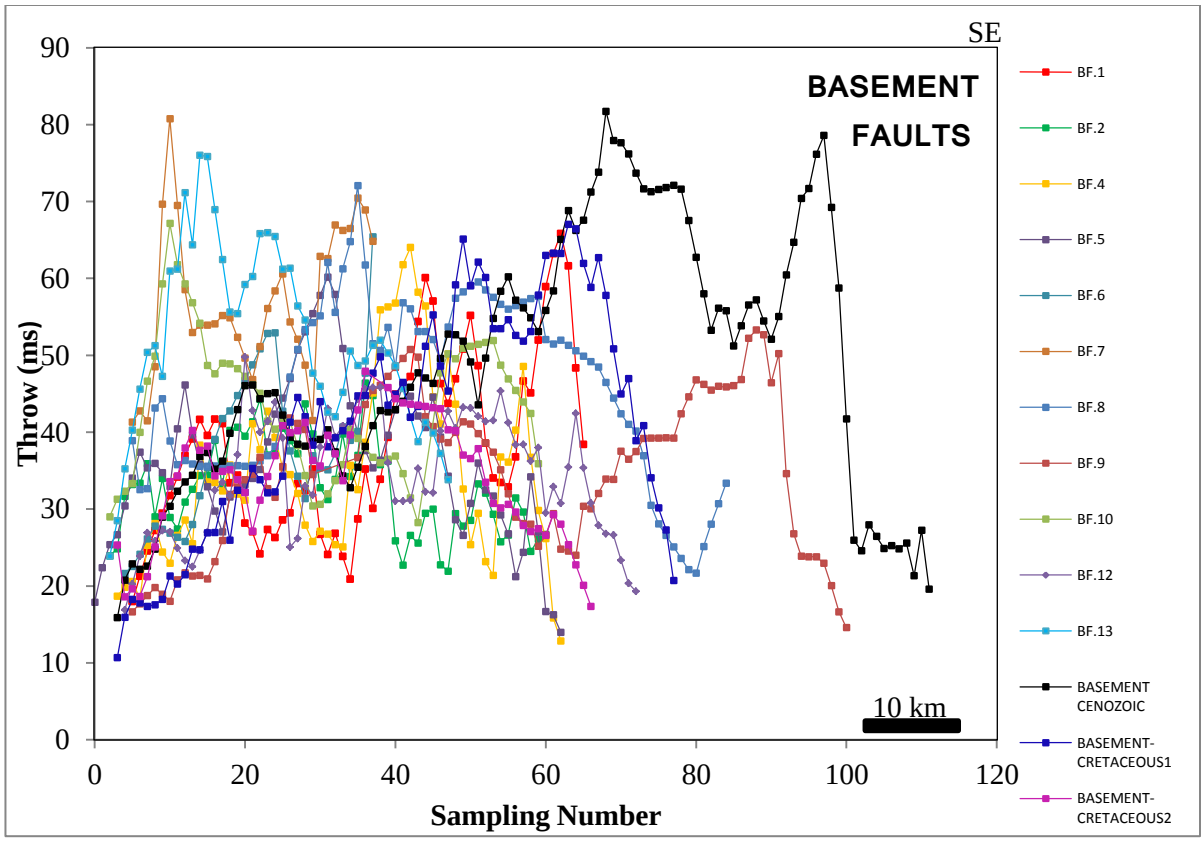

Figure 7.19: Displacement profiles for selected basement faults mapped in the study area. The basement fault sets may share a same single extension axis during Cretaceous time, then they are assumed to be kinematically compatible and may represent similar deformation event.

The Upper Cretaceous and the Pre-Upper Cretaceous syn-rift horizons can be mapped across major parts of the study area, but the deeper horizons such as those related to pre-rift and basement are hard to identify. However horizons have been extended as far as possible and appear to be representative of the structural system based on the 2D seismic interpretations. The fault interpretation has been built based mainly on identified horizons where it is possible to map cut-offs in the hanging walls and footwalls of most of the mapped faults. The fault system within the Ajdabiya Trough composed of variable fault populations trending northwest-southeast, north-south and northeast-southwest with approximately 5 – 10 km wide grabens and half graben features. The northwest-southeast trending grabens mainly filled with Pre-Upper Cretaceous sediments related to periods of rifting in the Ajdabiya Trough, which subsequently deformed by younger faults trending north-south and northeast-southwest (Figures 5.21, 5.22, 7.12, 7.13, and 7.14). However these faults are cross-cut and offset the Early Eocene strata (Figures 5.21, 5.22, and 7.45 – 7.48). The Palaeocene – Early Eocene

sequence thins and possibly onlaps onto a south west dipping relay ramp associated with fault (BF3) which presumably re-activated during the Early Cretaceous time (Figures 2 7.21 & 7.22). Faults are re-activated even post Upper Cretaceous unconformity and possibly the activity is ceased prior to Eocene unconformity. The 2D seismic data used in this study suffer from vertical resolution within the lower part of the Cretaceous sequence (e.g. Figures 7.21 & 7.22). In this case it was difficult to constrain the time of faulting but it is possible that the faults are developed during Pre - Cretaceous extension or subsequent re-activation. Some cross cut faults could be initiated as cut-off stretched faults orthogonal to the strike of the main faults. (Figures 7.7, 7.14, 7.15, 7.48, and 7.49).

Faults in the Ajdabiya Trough are possibly initiated sub-perpendicular or oblique to the main extension vector which leads to displacement partitioning between set of coeval dip slip faults.

7.3.3 Fault Description

The study of syn-depositional fault activity within the Ajdabiya Trough was based on significant differences in stratal thicknesses on both the footwall and hanging wall of each mapped fault and the thickening of sediments on the hanging wall of the active faults. In addition to the analysis of the vertical and lateral growth components of the faults.

The seven regional faults selected for detailed analysis are not isolated features but exhibit linear and curved fault traces and some of which may composed of variable fault segments that exhibits differential growth and displacement histories during fault development.

7.3.4.1 Basement Fault No.1 (BF1)

The **BF1** is characterized by a linear pattern with an estimated length of approximately 70 km (Figure 7.20) and linked segments on basement-Mesozoic horizons getting younger with increasing fault length, over several scales from 5 km to 10 km fault length. These are younger with increasing fault-length, because of possible progressive fault-growth by segment linkage. This supported by stratigraphic evidence along strike of the fault and shift in the depocentres (e.g. Dawers & Underhill, 2000).

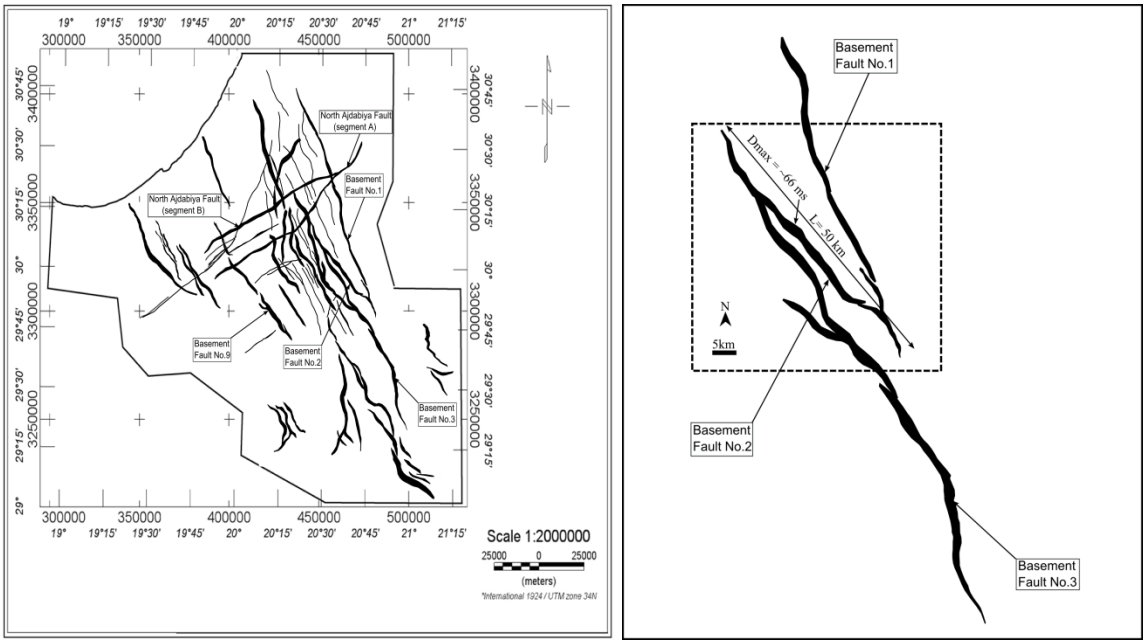

Figure 7.20: (a) Fault polygon map for the mapped faults in the Ajdabiya Trough. (b) Plan view of the basement fault BF1 with approximate length of about 70km measured from the seismic data and maximum displacement observed on pre-Cretaceous horizon of Dmax = 66 ms.

The fault has a planar geometry (Figures 7.21 & 7.22) and trends NW-SE dipping to the SW and exhibits along-strike variations due to changes in fault displacement. The fault possibly initiated in the south possibly as early as the Late Palaeozoic time and cut by Late Paleozoic (Hercynian) unconformity evidenced by moderate offsett on deeper horizons. The fault then to propagates to the north throughout Pre-Upper Cretaceous and terminated at middle Palaeocene strata.

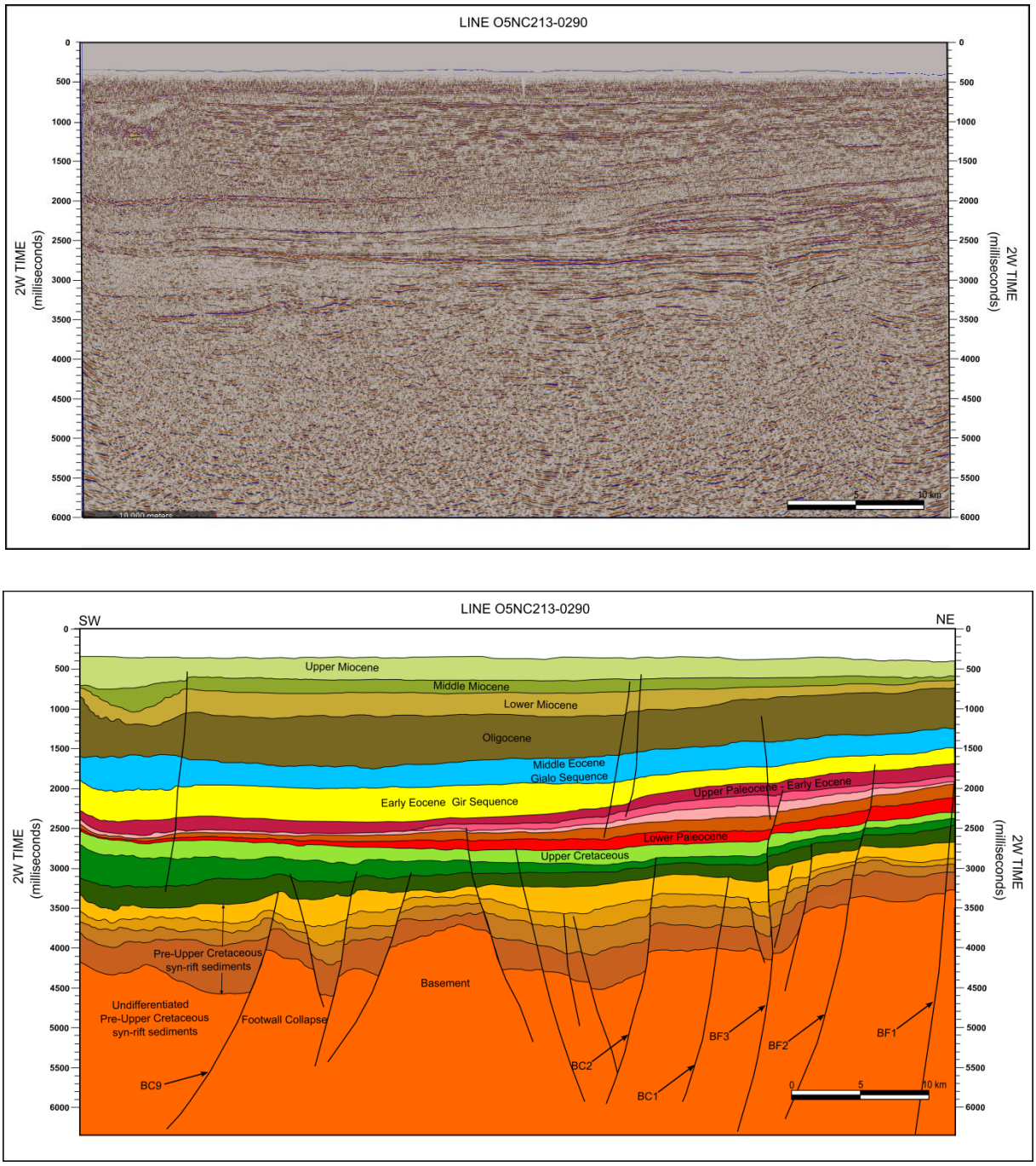

Figure 7.21: 2D seismic section 05NC213-0290 showing basement fault complex in the southern Ajdabiya Trough. The faults exhibit listric and planar normal fault geometry with components of synthetic splay faults dipping towards the southwest. Antithetic faults are also developed at the centre. Colour code for interpreted lithology is also shown. For line location see figures 7.4 & 7.5.

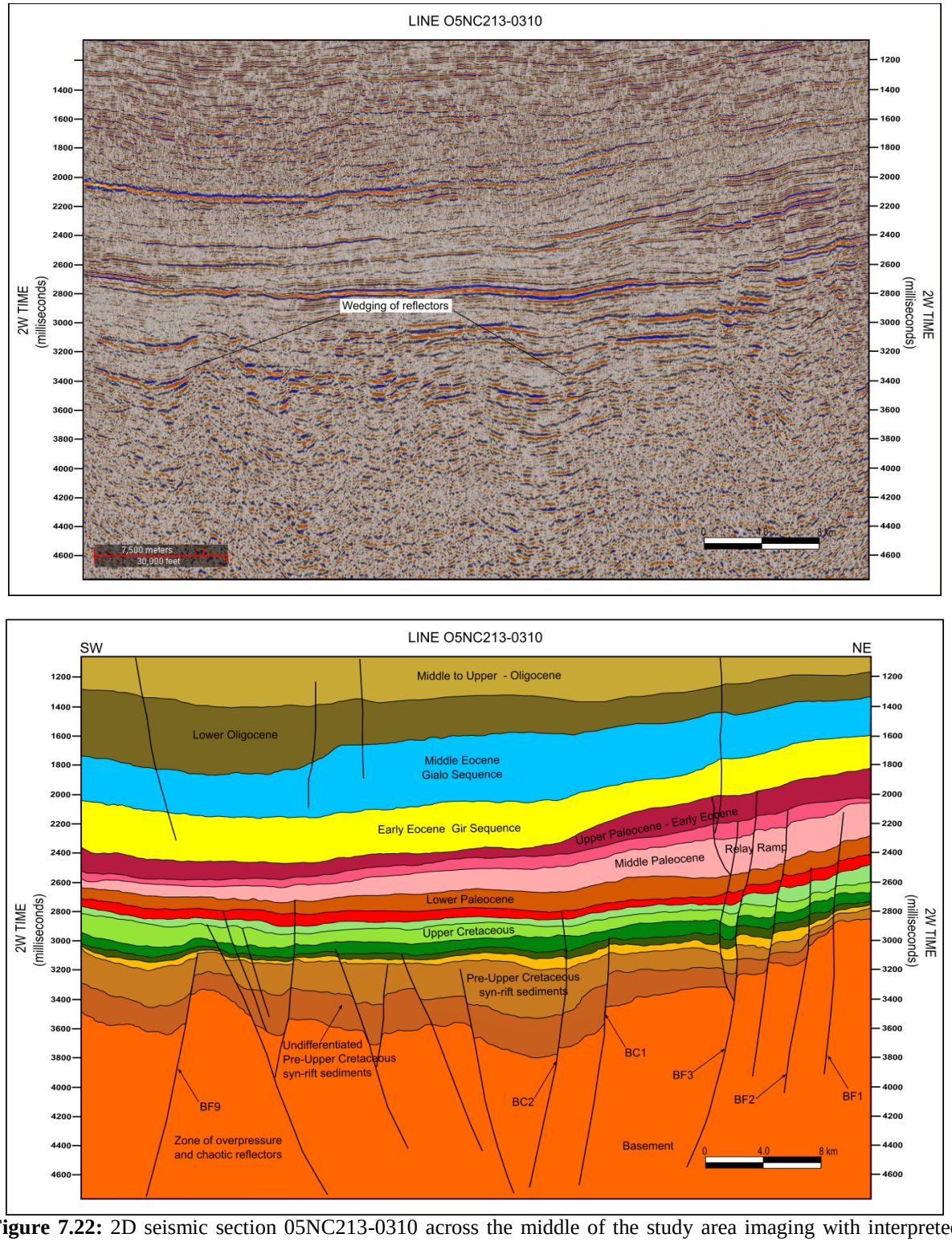

Figure 7.22: 2D seismic section 05NC213-0310 across the middle of the study area imaging with interpreted version below depicting the studied fault blocks on the hanging wall of a major planar and listric, growth-faults. The location of the cross section is shown on Figures 7.4&7.5. The footwall of the BF9 fault has been uplifted due either to tectonic movement or due to the presence of possible overpressure zone corresponds to a chaotic reflection pattern on seismic data. Paleozoic - Pre-Upper Cretaceous growth strata denote timing of main period of faulting which continued to propagate and offset the upper strata and show a complex fault array with multiple synthetic strands - potentially in overlap or relay ramp positions.

The patterns of the displacement (throw) contours shown on the fault surface image (Figure 7.23) are broadly elliptical with high displacement at the centre and outward decrease in value. The strike of the fault is parallel to the dominant NW-SE fault trend along the majority of its length, slightly changing to a NNW-SSE trend along the northernmost 10 km of the fault up to its tip-point (Figure 7.20). The fault, either initiated during the Pan African orogeny or during early rifting (140 – 115 Ma) and was compatible with a regional N-S direction of extension (e.g. Ahlbrandt, 2001). This event caused the reactivation of many of NS-oriented faults as normal faults as well as NW-striking faults as oblique slip faults (Benshati et al., 2006). The fault is propagating through the Early Tertiary strata, with maximum displacement (~180ms) at the centre of the fault, at zone of about 15 km from its northern and southern tip-points (Figure 7.23). The rate of change of displacement is higher on Cretaceous horizons compared with the overlying Tertiary horizons with nearly horizontal contour shape and displacement gradient of 0.013 implying possible syn-depositional fault style (e.g. Childs et al., 2003).

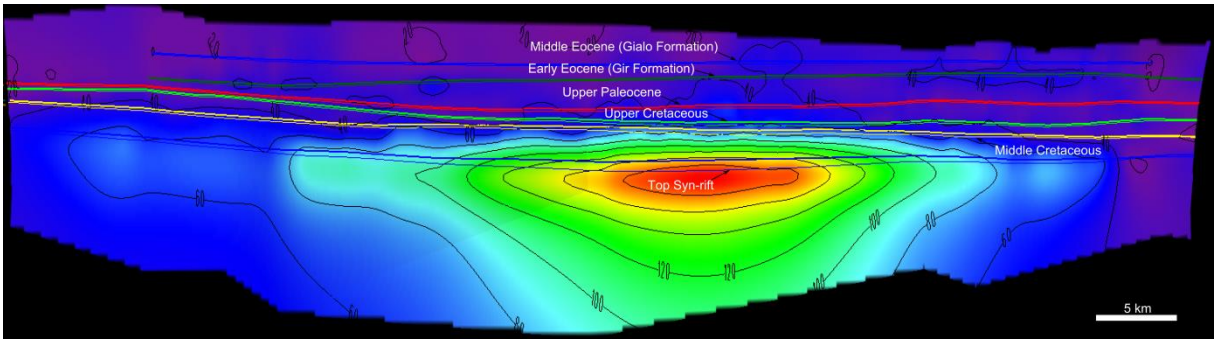

Figure 7.23: Throw contours for the BF1 measured in ms TWT. The throw contour plot exhibits throw values ranging from 0 to 180 ms TWT with contour spacing of 20 ms TWT, decreasing away from the centre towards the tips of the fault and from branch lines between fault segments.

At its maximum displacement the **BF1** fault offsets strata from the Early Paleozoic to the Early Eocene (Gir Formation), but as the fault losses displacement it is no longer offsets the upper strata. This could suggest that the **BF1** is presumably nucleate at basement level at the southern part of the Ajdabiya Trough and then progressively propagate up into the upper Tertiary strata during fault re-activation cycles.

Fault surface attribute (throw), (Figures 7.23) and displacement profile for the fault (Figure 7.24) show several sub-units with local minima and maxima, which point to different

segments, that merged during fault growth. Maximum displacement occurred close to the centre of the segments, whereas minima represent areas where fault segments are linked.

The use of only 2D seismic profiles, instead of a complete 3D interpretation, lowers the sampling rate significantly, and an incomplete identification of fault segments.

The fault loses displacement near fault tips and it is no longer able to impact on the deformation of the upper strata. Instead, displacement in the basement is transferred progressively onto BF3 located to the west of the BF1, which gains sufficient displacement to propagate the Cretaceous to Early Eocene strata (Figures 7.21 & 7.22).

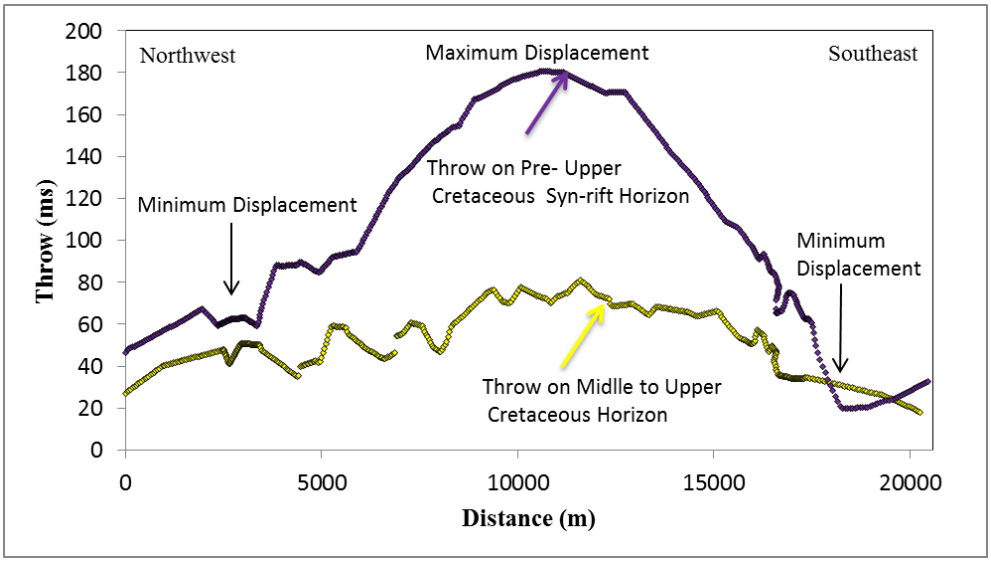

Figure 7.24: Displacement-length profile (throw) for the basement portion of basement fault No.1 (BF1) show the basement fault displacement is vary along the entire imaged and extrapolated length of the fault. The average displacement gradient in the basement is (0.013). The throw profile for the BF1 shows maximum throw at the centre during pre-rift period compared to little movement during the Upper Cretaceous time.

During the depositional interval between Upper Palaeocene to Miocene, fault BF1 becomes inactive as the depositional units above remain unaffected by the fault, but are offset by faults BF2 and BF3 that displace the footwall block of fault BC1 (Figure 7.22) instead the footwall of the BF1 fault not affected by these faults. The hanging wall of BF3 comprises in places a small rollover structure or reverse drag (Figures 7.33 & 7.36).

The eastern side of the trough exhibit more complex fault patterns. Along the eastern margin of the Ajdabiya Trough, the faults show possible transtensional style as both wrenching and extension are exist as the faults in the study area are mainly reactivated along pre-existing structures and the new fault trend is mainly oblique to the previous trend.

7.3.3.2 Basement Fault No.2 (BF2)

The basement fault **BF2** extend in a NNW-SSE direction along the eastern edge of the Ajdabiya Trough with a distance of about 100 km and dips in western direction displacing the footwall strata of fault BF3 (Figure 7.21 & 7.22). To the south, this fault is intersected by fault BF1, whereas its northern tip intersecting the BC1 fault segment. The maximum displacement of fault BF2 is ca. 135 ms (TWT) in the SE portion of the fault (Figures 7.25 & 7.26). The fault is segmented into more than two segments each with different dip and structural style. In cross-section the geometry of the fault cutting the upper strata changes along strike, from a shallow-dipping, listric fault in the south (Figure 7.21) to a progressively steeper-dipping more planar fault further north (Figures 7.22 & 7.27). The geometry of the fault surface is rotated towards the horizontal from north to south (Figures 7.21, 7.22, 7.45, and 7.47) indicating change in dip along strike. The change in geometry along strike of the BF2 fault is possibly related to transition between a planar component dominated by tectonic extension, to a listric component possibly formed due to gravity-driven deformation. The along strike dip variations of the fault indicate possible inversion (e.g. El Arnauti et al., 2008). This can be observed through the changes in dips along strike as shown on seismic cross-sections (Figure 7.48). A small rollover anticline develops in the hangingwall as the fault surface becomes increasingly listric unlikely no dip contours obtained for the fault surface to support these observations. The rollover anticlines are a common response to listric fault geometry during half-graben evolution (Xiao and Suppe, 1992). But the dip seems to be increasing from south to north provided that the basement portion shows more listric segment component at the southern part of the trough.

The Cretaceous isochron thickness map show thickening of Cretaceous strata to the northeast indicating syn-tectonic movement and owing also to high subsidence and growth during the Early Cretaceous time. In Cyrenaica region to the east, strike slip faulting is observed to be associated with thickening of Upper Cretaceous strata (e.g. El Arnauti et al., 2008).

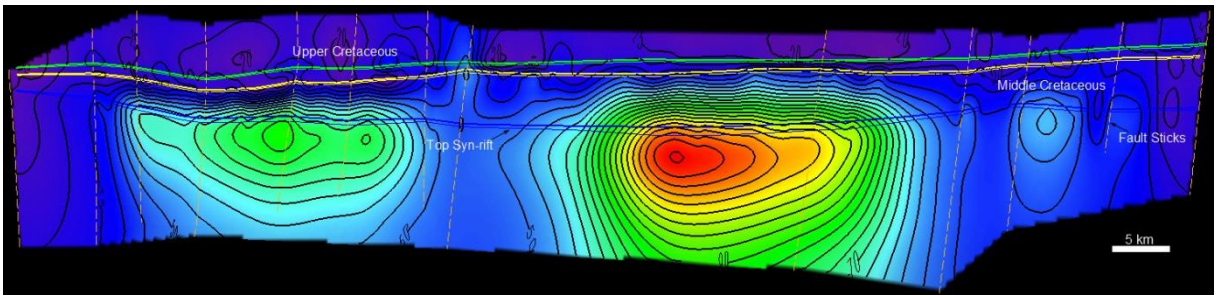

Figure 7.25: Throw contours for the BF2 measured in ms TWT. The throw contour plot exhibits throw values ranging from 0 to 135 ms TWT with contour spacing of 5 ms TWT, decreasing away from the centre towards the tips of the fault and from branch lines between fault segments.

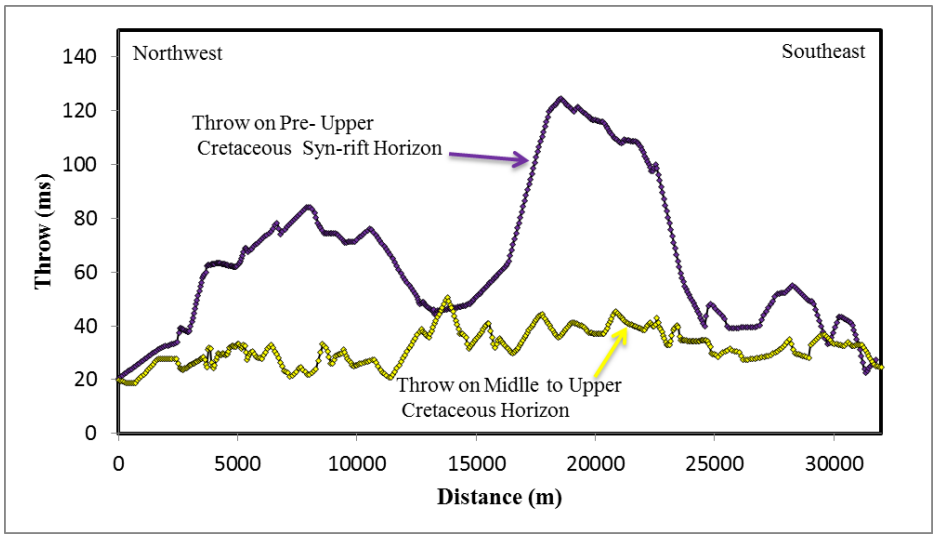

Figure 7.26: Displacement-length profile (throw) for the Pre-Upper Cretaceous syn-rift andUpper Cretaceous horizons of Basement fault No.2 (BF2) show that the fault displacement is vary along the entire imaged and extrapolated length of the fault. The throw profile for the BF2 shows maximum throws at two positions during syn-rift period compared to little movement during the Upper Cretaceous time suggesting segmentation during rifting stage.

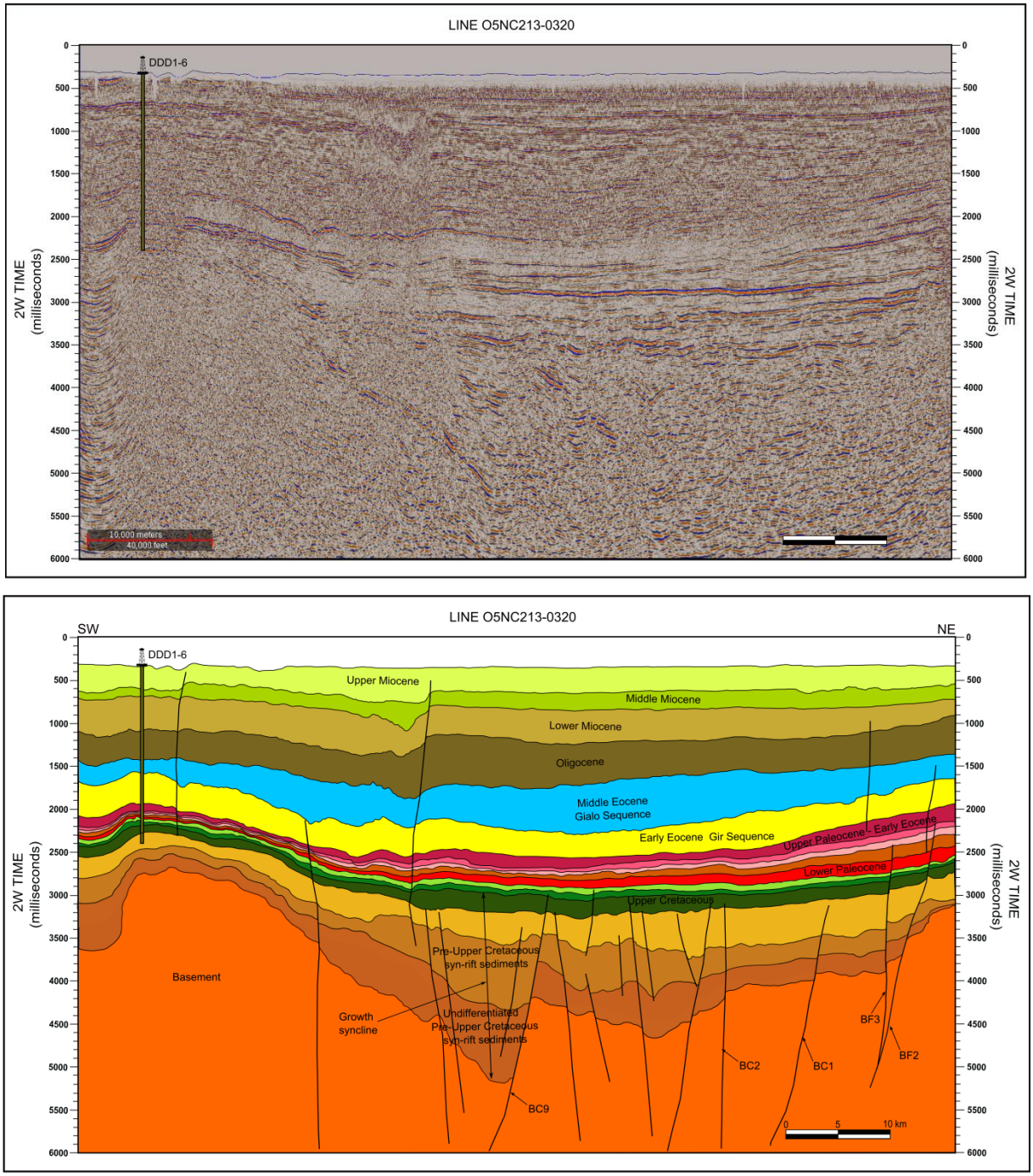

Figure 7.27: Uninterpreted 2D seismic section 05NC213-0320 above and, below interpretation of sedimentary horizons (Pre-Cretaceous–Upper Miocene) and basement reflector cut by normal faults. The rising of the basement to the west results in the progressive thinning of the sedimentary sequence west of the BF9 hangingwall depocentre. Intensive fault block rotation indicating fault growth and movement during rifting episodes. Tilting of strata in the hangingwall of the BF9 fault and growth strata date normal faulting to the Pre-Upper Cretaceous stage. The fault was re-activated during the Late Cretaceous.

Footwall uplift, and northward thickening of Late Cretaceous to Tertiary section as observed on the seismic section (Figure 7.45 & 7.48) and the isochron maps (Figures 7.58) suggest that

the BF2 is seems to be subjected to late phase of inversion during the Miocene (e.g. El Arnauti et al., 2008). The strike slip component of the BF2 is evident on the seismic line NC213-0590 (Figure 7.47) where a Pre-Paleocene - Early Eocene fold structures are active with possible development of flexural uplift.

The NW-SE prolongation of the BF2 is revealed as a NW striking reverse fault dipping to the SE that exerts significant control on sediment transfer towards the depocentre.

The change of orientation from NW-SE to N-S and then again to NW-SE indicate that the fault had normal slip during possible Mesozoic time and was reactivated by reverse slip during the Tertiary leading to positive structural inversion.

The fault propagates and dissects all the stratigraphic units up to Early Miocene section (Figure 7.47). The throw of this fault is about (135 ms TWT) measured on top of Upper Cretaceous horizons but decreased on shallower horizons. Thickening of Pre-Upper Cretaceous strata against the fault indicating that large displacement on this fault probably started in the Early Cretaceous or older.

7.3.3.3 Basement Fault No.3 (BF3)

The **BF3** fault zone is the longest mapped fault in the study area with an approximate length of about 120 km (Figures 7.4 & 7.5) and appears to extend NW-SE, but show a little change in orientation to mainly N-S near its southern tip before it is return to the main NW-SE trend. The fault is located in the footwall of BC1 fault trending over significant distances subparallel to fault BF2 (Figures 7.21 & 7.22).

The shape of the fault exhibits a series of connected arcs indicating that this fault formed from at least four linked fault segments (Figures 7.28 & 7.29) that grew through time into a single fault. The separation between these segments is correlated to an intersection with the BF2 and BC1 faults. On vertical seismic sections, this fault is slightly listric at depth.

Fault segments are linked along strike to a series of mainly basinward dipping fault segments (Figure 7.21). At least three different faults can be mapped on the upper tip of fault segment BF3 as shown on the 2D seismic section (Figures 7.21 & 7.22). In certain circumstances it is quite difficult to discriminate between linked fault segments at depth. For instance, the BF3 fault show a character of splay fault (Figures 7.4, 7.5, and 7.10) branching upward and linked to the BC1 and BC2 faults. The 2D seismic sections in figures 7.21 and 7.22 show that the

BC1 and BC2 faults are mainly formed as synthetic faults to the main fault BF3 and have changed their orientation along strike. Partial linkage of fault segments BC1 and BC2 with fault BF3 are developed through time each with different movement style and possibly sharing the same history with the BF3 which considered being a common root to the other faults. The spatial and temporal variation between the developments of fault segments in the Ajdabiya Trough is related to the differences between periods of fault activity during time of depositions.

In the immediate hanging-wall of the fault zone, the morphology of the strata seems to be dipping to the southwest, into the hanging-wall, with the thickest strata occurring in an asymmetric elongated syncline parallel to the strike of the fault zone. The attached graben is also influenced by a series of minor faults that splay off the fault plane and seems to extend hundreds of meters into the hanging-wall before they tip out.

There is a change in fault displacement along strike as shown in (Figure 7.29). The graph shows displacement increasing towards the centre of the fault. Maximum displacement extended along the fault block separated by a minimum displacement at distance of about 5 km from the south eastern edge of the fault block. The displacement has its maximum value of ca. 290 ms (TWT) at a distance of about 25 km from the SE edge of the fault and it decreases towards the NW part with a minimum displacement value of ca. 20 ms (TWT).

It is noticed that some subordinate faults are coupled with the BF3 at zones of high displacement (Figures 7.21 & 7.22). These faults are possibly initiated due to gravity-driven mechanical compaction (e.g. Skuce, 1994) or due to change in the extensional regime in the Ajdabiya Trough. The fault is cross-cut by an antithetic fault that cuts down in to the basement (Figure 7.21). The antithetic faulting that appears to cross the BF3 is providing an accommodation to the basement faults along the eastern side of the trough. Movement on these secondary faults is limited by their nature perhaps to the extensional movement dimension, complicated by the internal antithetic and synthetic faulting within the trough.

BF3 forms it is own Cretaceous depocentre to the south of the Ajdabiya Trough as observed from the Cretaceous isochron map (Figures 7.58) and the seismic cross-section (Figure 7.36). Seismic data indicate that displacement on the BF3 fault started in the Early Cretaceous and continued till the Early Eocene indicating that the fault is a long lived in nature and seems to control the trough major subsidence and representing part from its eastern bounding fault.

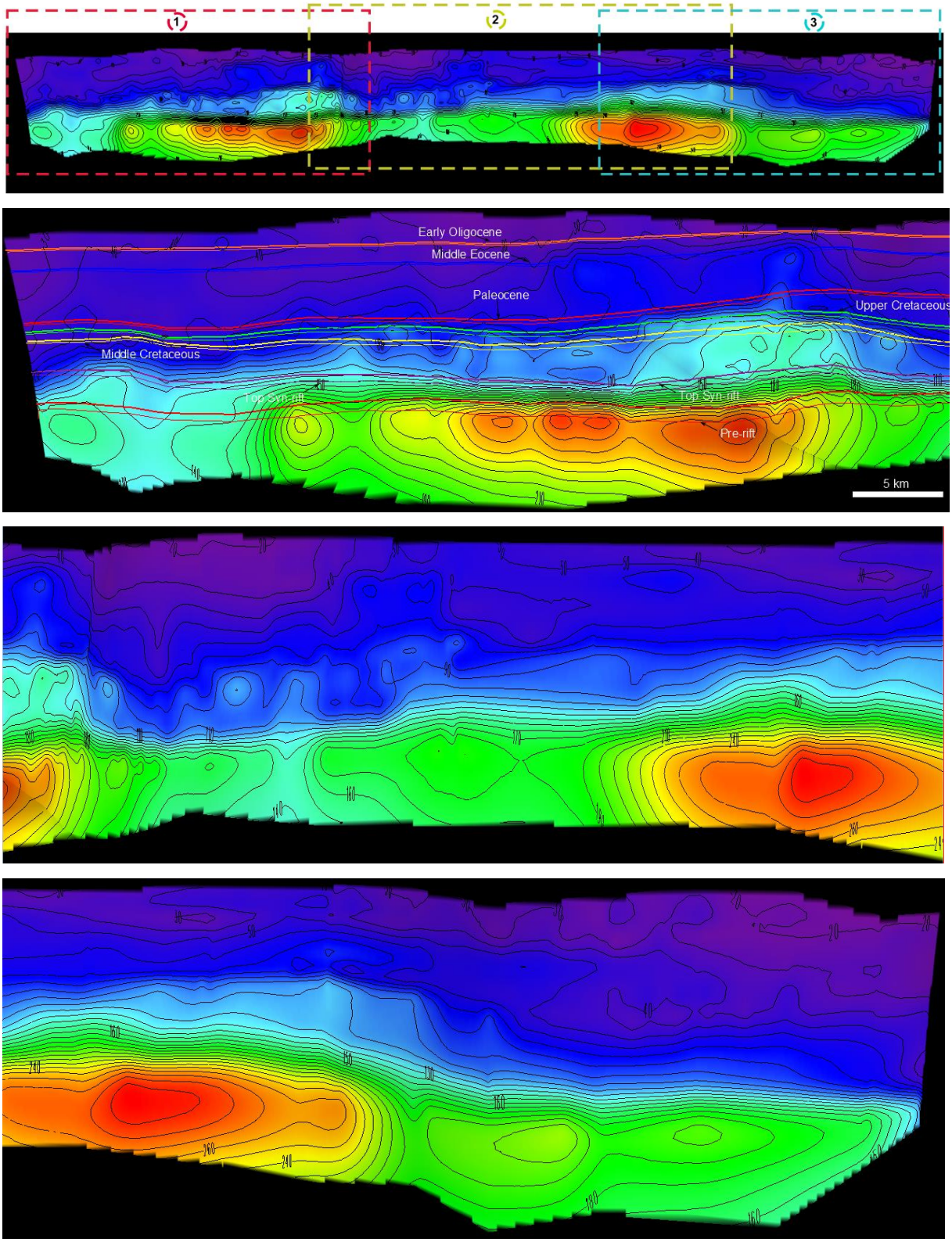

Figure 7.28: Throw contours for the BF3 measured in ms TWT. The throw contour plot exhibits throw values ranging from 0 to 290 ms TWT with contour spacing of 10 ms TWT, changing at about four locations along the fault strike suggesting fault segmentation.

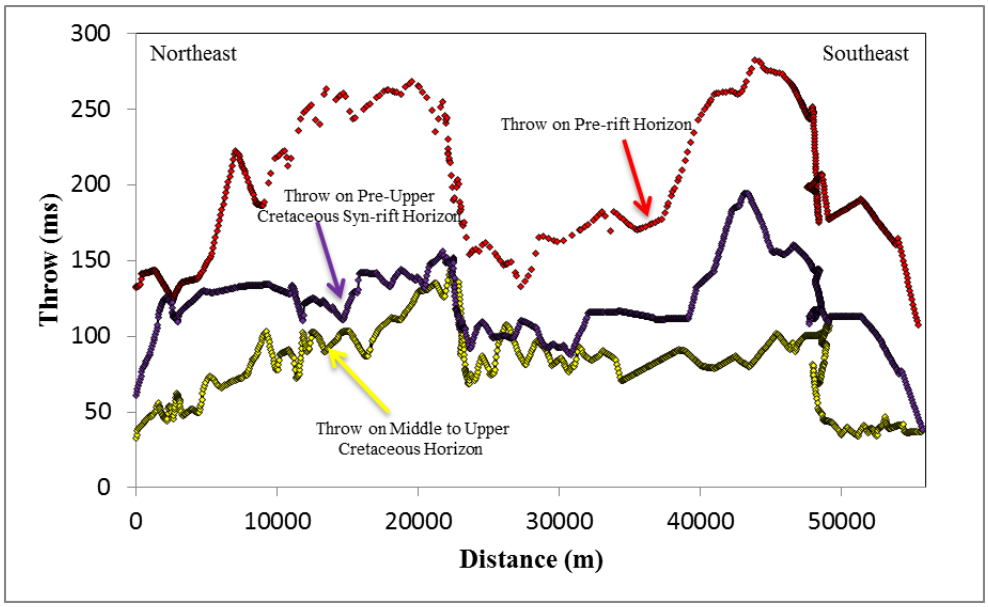

Figure 7.29: Throw distribution on the hangingwall of the BF3 fault shows throw values ranging from 0 to 290 ms TWT, contours spaced at 10 ms TWT decreasing away from branch lines. The throw is high on pre-rift horizons and progressively decrease until rift cessation during Upper Cretaceous.

Aggregate throws on BF1, BF2, and BF3 faults resulting in a more regular aggregate profile (Figure 7.30), resembling the throw profile for a single fault and these faults can be said to be geometrically coherent (Walsh & Watterson, 1991; Roberts & Yielding, 1994)

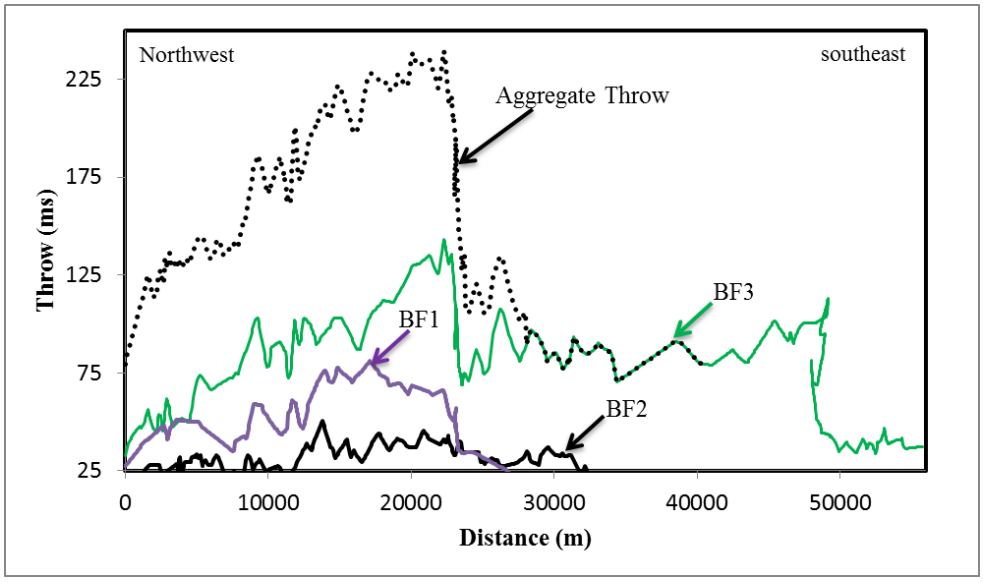

Figure 7.30: Throw profiles for faults BF1, BF2, and BF3 (solid lines) and aggregate throws (dotted line). The sum of fault throw produces a more regular profile suggesting that faults are a kinematically coherent structure. The steeper throw gradient is possibly related to the presence of an unconformity between the upper tip lines of the faults and the highest picked horizon (e.g. Freeman et al., 1990).

7.3.3.4 Basement Cretaceous 1(BC1)

The Basement Cretaceous fault **BC1** is located along the same fault zone as fault BF3, bounding a NW-SE extended graben with approximate length of about 77 km (Figures 7.4 & 7.5). In map-view, the fault is straight or slightly curved and has planar geometry, trending NW-SE and dips progressively towards the SW direction with change in the mean fault strike to N-S started at possible splay or relay ramp junction.

Displacement profile and fault surface mapping shows that displacement increases in two locations implying fault segmentation with throw values ranging from ca. 320 ms (TWT) in the northern portion to about 360 ms (TWT) near the junction with fault BF3. It decreases towards the northwest part with a minimum throw of ca. 10 ms (TWT) near the fault tip (throw gradient 0.025). The distance between successive displacement minima and maxima is about 10 - 20 km.

The fault generally tips out downward within the basement and tip out upward within Upper Cretaceous strata (Figures 7.33). Throw profile plot and fault surface mapping for the BC1 (Figure 7.31) are typically characterized by an asymmetric throw distribution. Throw decreases progressively toward the west where less throw occurs, the same gradual downward decrease in throw into the lower part of the Pre-Upper Cretaceous is observed.

The BC1 fault is appear to bifurcate along strike, into two, laterally separate segments. Seismic sections across the fault indicate that where throw on the structure is greatest (~360 ms), this coincides with asymmetrical throw distribution on the upper portion of the fault (Figures 7.31 & 7.32), whereas the lower portion of the fault has more symmetrically distributed. Throw strike-projections on the fault surface illustrating a concentric shape of throw distribution on the upper part of the fault and a symmetrical and elliptical shape on the lower part of the fault. Seismic cross sections and the Cretaceous isochron map (Figures 7.21, 7.22, and 7.58) indicate increased hanging wall thickness for the BC1 toward the southern tip. The isochron map of the Paleocene show increasing thickness above hanging wall depocentre that offset by the BC1 fault. At the same time footwall monocline could be developed as a result of compaction of Cretaceous – Paleocene strata.

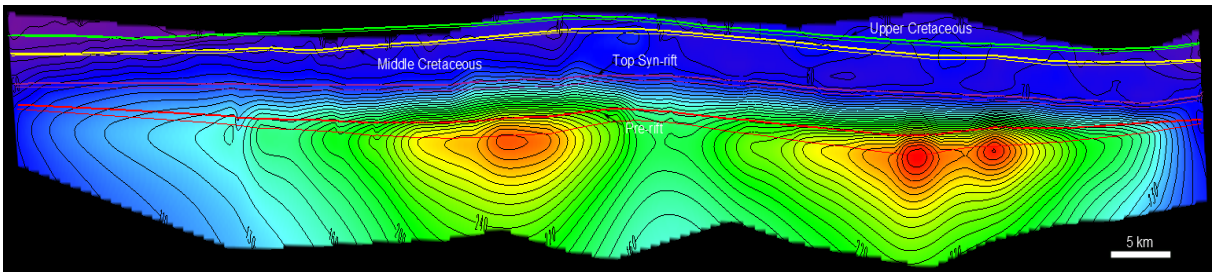

Figure 7.31: Throw strike-projections on the fault surface of fault BC1 illustrating a concentric shape of throw distribution at two main positions, with an elliptical and symmetrical shape. Horizontal lines are horizon polygons cut by the fault.

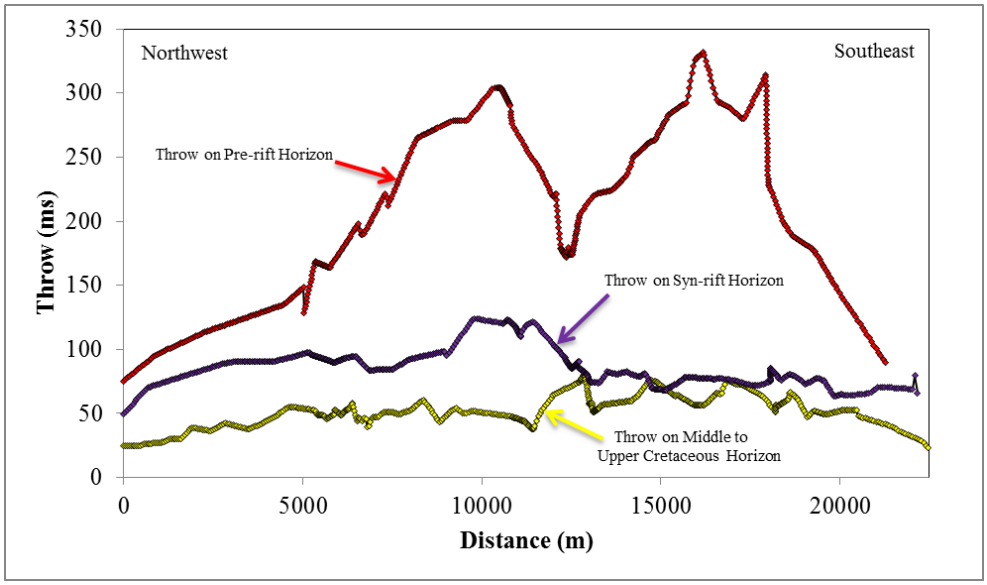

Figure 7.32: Fault throw profiles of BC1 fault on Middle - Upper Cretaceous horizons (yellow) and Pre-Upper Cretaceous syn-rift horizon (pink) with corresponding throw length profile along top pre-rift horizon of Pre-Upper Cretaceous age showing gradual increase in throw toward the centre of the fault and decrease towards the north-western fault tip.

7.3.3.5 Basement Cretaceous 2 (BC2)

The Basement Cretaceous **BC2** is located at the centre of the study area and trending NW-SE with maximum length of about 66km. There is a change in fault orientation to mainly N-S near an intersection with NE-SW trending faults (Figures 7.10 & 7.13). This fault parallels fault BC1 close to the edge of the study area and terminates in the north against NE-SW trending fault (NAF) and probably dies out towards the NW in a hanging wall of NE dipping fault. A maximum displacement of ca. 250 ms (TWT) is observed at the centre of the fault. The displacement on fault BC2 generally decreases towards the fault tips.

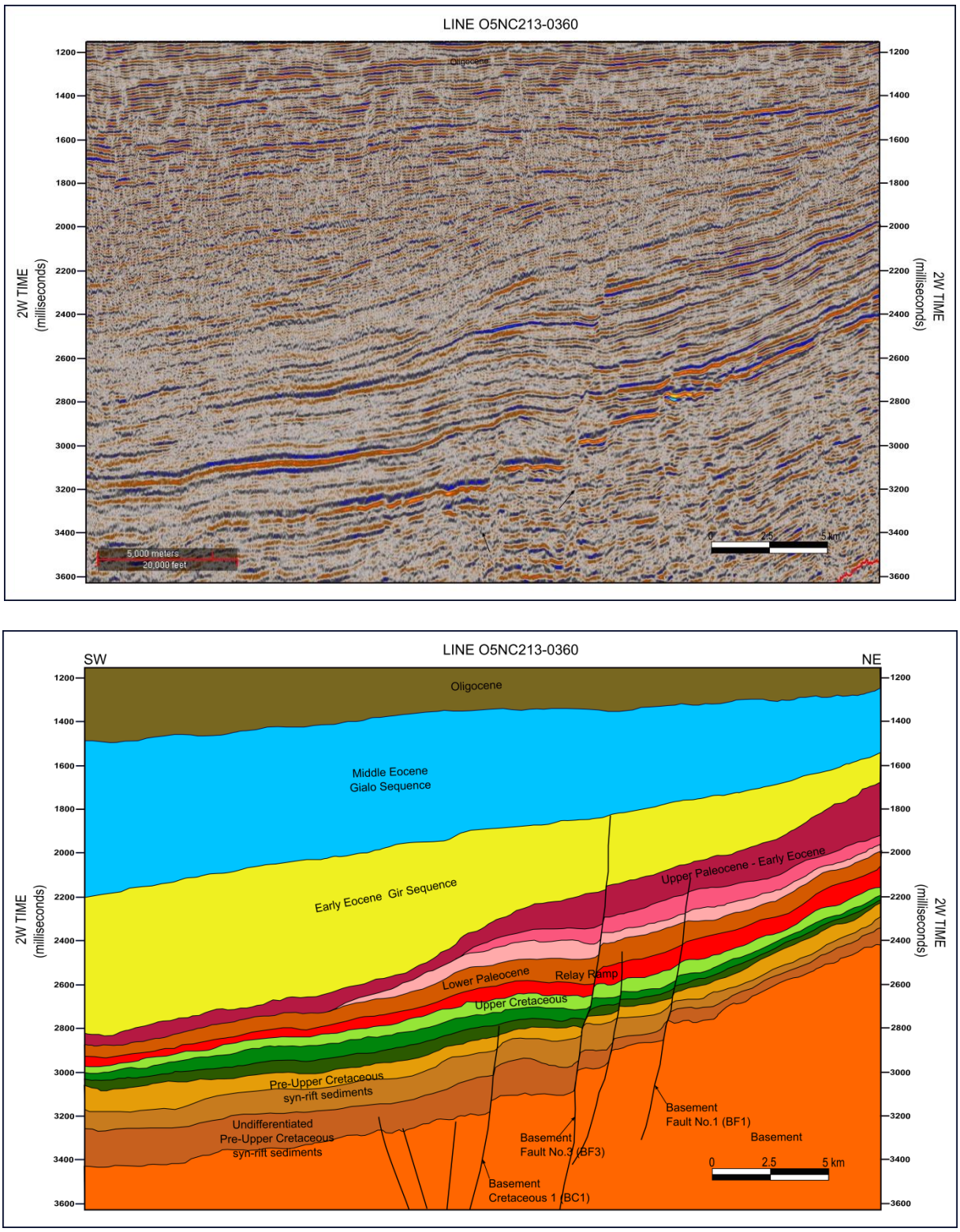

Figure 7.33: Part from seismic line 05NC213-0360 show the geometry of relay on synsedimentary normal fault. Possible relay ramp formed by fault bifurcation (splaying) of a small throw synsedimentary normal fault. The fault trace shown on the map (Figures 7.4&7.5) splays upwards from a single surface on basement horizons (orange) to a segmented fault (with a relay) on higher horizons.

Along strike the BC2 fault forms a through-going fault that can be divided into three segments, where a lower asymmetric portion has a throw maximum at top Cretaceous ca. 150 ms (TWT) (Figures 7.34 & 7.35) with a rapid upward decreasing throw gradient (0.0.06) up to the Early Paleocene level. Fault surface throw attribute display tightly spaced contours toward the upper fault tip (Figure 7.34), whereas the lowermost portion of the fault displays more elliptical contours that are centred on maximum throw at top of Cretaceous horizon. The isochron thickness map indicates increased hanging wall thickness for the Cretaceous and Paleocene strata (Figure 7.58). The Upper part of the Cretaceous strata is typically folded into very low relief syncline in the hangingwall of the fault to the south (Figures 7.21 & 7.22). The relief of the syncline increases with increasing fault throw.

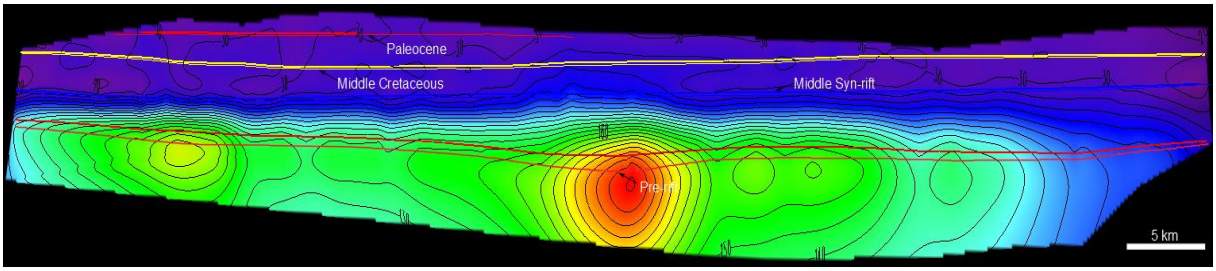

Figure 7.34: Throw strike-projections on the fault surface of BC2 fault illustrating a concentric shape of throw distribution on the central part of the fault segment, with an elliptical and symmetrical shape. Throw at the centre of the faults reaches about 250 ms (TWT) and is decreasing gradually to the northeast implying fault bifurcation into about three segments with variable range of throw.

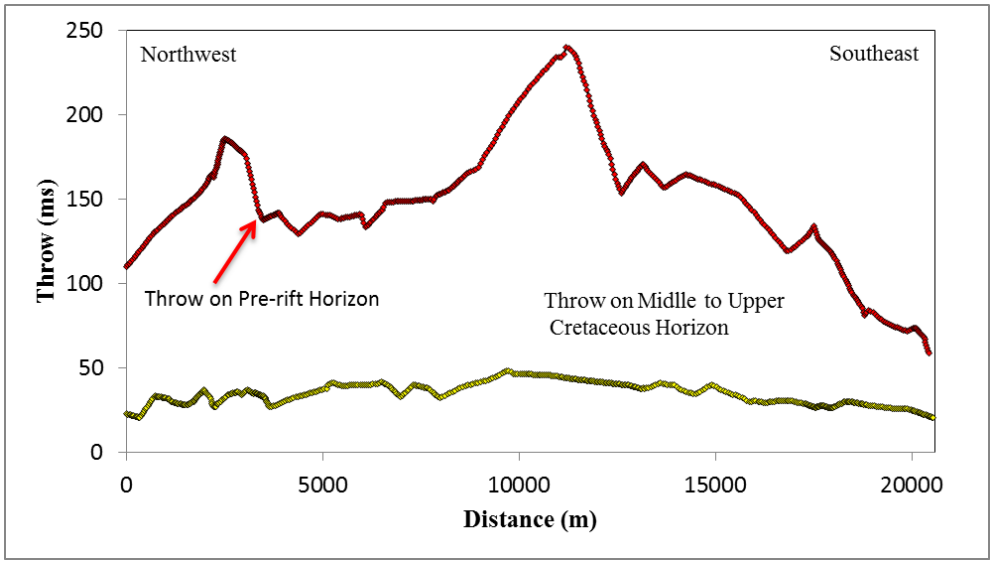

Figure 7.35: Fault orientation of BC2 fault on Upper Cretaceous horizons (green) and Pre-Upper Cretaceous horizon (yellow) with corresponding throw length profile along top of Pre-Cretaceous showing gradual decrease in throw toward the north-western fault tip.

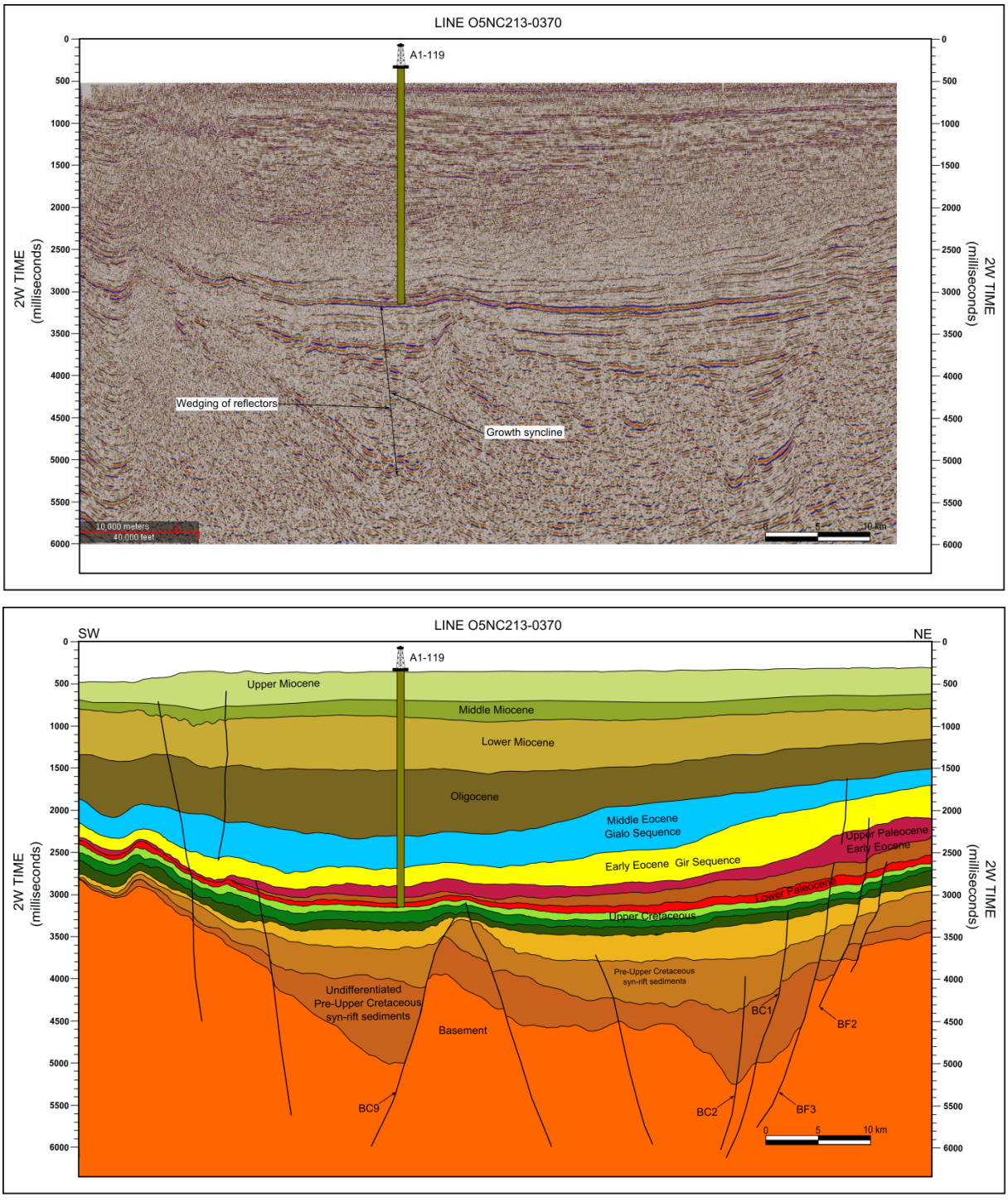

Figure 7.36: Uninterpreted 2D seismic section 05NC213-0370 above and, below interpretation of sedimentary horizons (Pre-Cretaceous–Upper Miocene) and basement reflector cut by normal faults. The rising of the basement to the west results in the progressive thinning of the sedimentary sequence west of the BF9 hangingwall depocentre. Footwall uplift and intensive fault block rotation indicating fault growth and movement during rifting episodes. Growth depocentre also observed to the east and controlled by movement along the BF3 fault and subsequently modified by movement along the synthetic BC1 and BC2 faults.

7.3.3.6 Basement Cenozoic No.1 (BCE1)

The **BCE1** fault extends along NW-SE trend with an undulated pattern (Figure 7.4 & 7.5). It has a curvilinear trace and trending NW-SE at the southern segment before changing the orientation into mainly NWW-SEE and then again to NW-SE. The changes in fault orientation coincide with the throw minima, representing segment linkage points. The length/throw profile (Figures 7.37 & 7.38) shows that the fault is segmented, with throw minima on most of the mapped horizons occurring approximately 8 km from the north-western end of the fault where fault displacement does not fall to minimum (zero) as a result of intersection with approximately northwest striking antithetic fault. The throw contours also illustrates the segmentation characteristics of the fault (Figure. 7.39). Two throw maxima are observed, on the fault surface with maximum throw values of about ca. 80 ms (TWT). The throw contours show an elliptical throw maximum along the more northwest-southeast striking segment of the fault, with throw decreasing rapidly upward. The displacement has its maximum value (80 ms) at a distance of 15 km from the SE edge of the fault and progressively decreases towards the NW with a minimum value of (20 ms). Movement on this fault can be substantial as the Cretaceous isochron map show thickening of strata within the hanging wall of the fault.

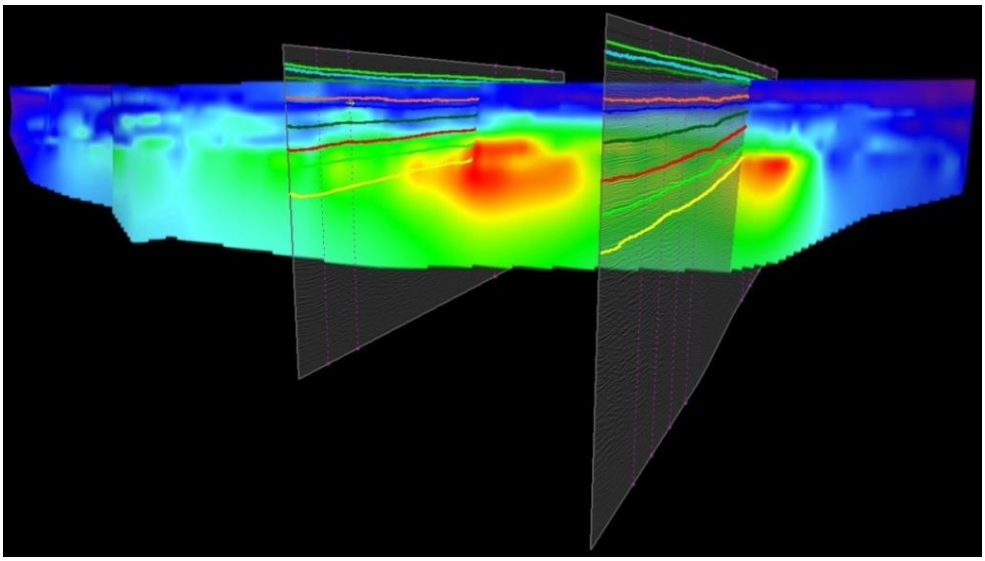

Figure 7.37: Throw strike-projections on the fault surface of fault BCE1 illustrating a concentric shape of throw distribution on the eastern part of the fault segment, with an elliptical and symmetrical shape. The figure also show fault orientation of BCE1 fault on Upper Cretaceous horizons (green) and Pre-Upper Cretaceous horizon (yellow) with corresponding throw length profile along top of Pre Upper-Cretaceous horizon showing fault segmentation and gradual decrease in throw toward the north-western fault tip.

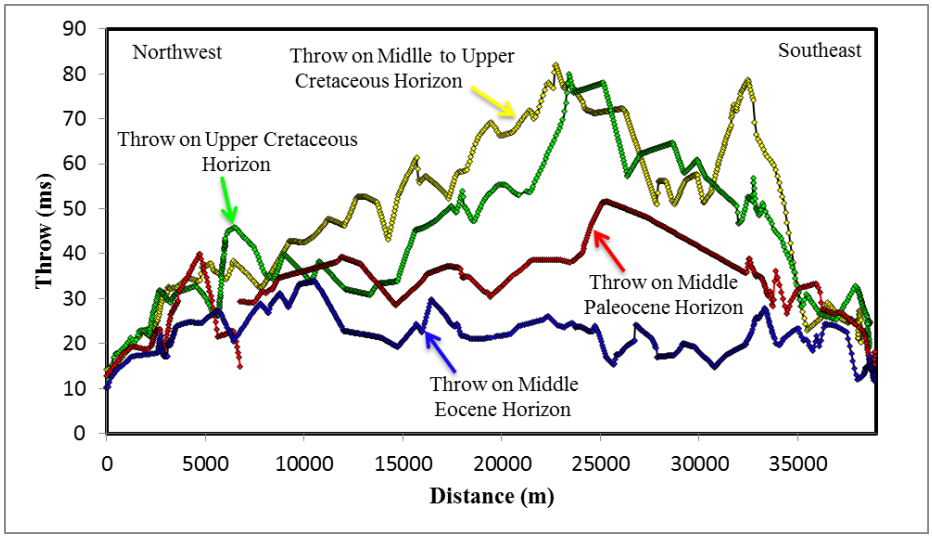

Figure 7.38: Fault orientation of BCE1 fault on Upper Cretaceous horizons (green) and Pre-Upper Cretaceous horizon (yellow) with corresponding throw length profile along top of Pre-Cretaceous showing gradual decrease in throw toward the north-western fault tip.

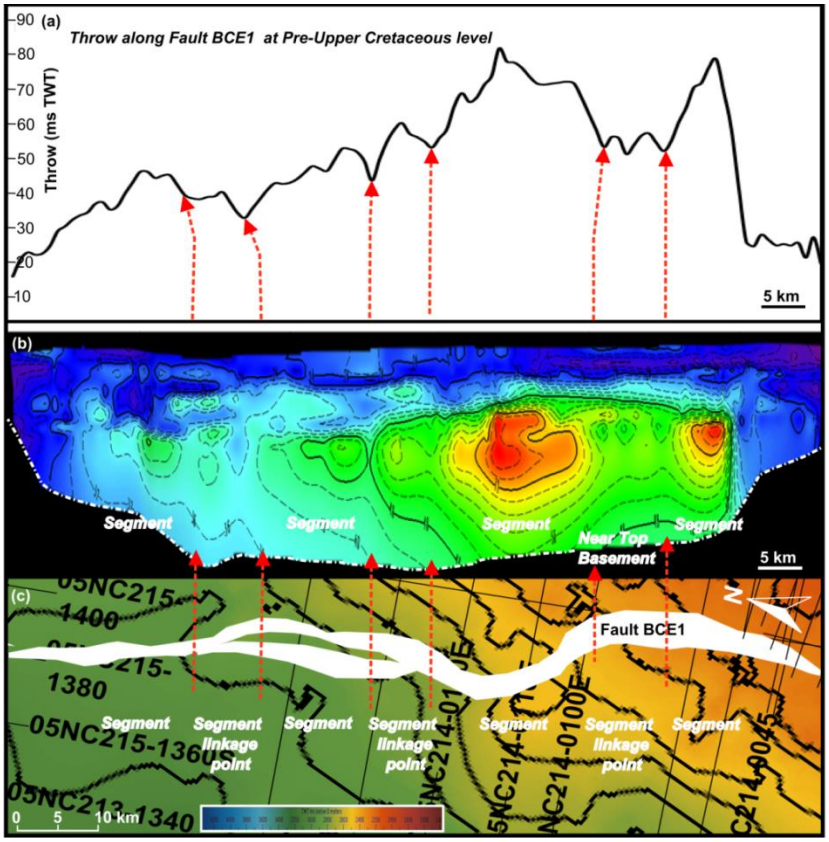

Figure 7.39: (a) Throw–Distance plot for fault BCE1 at Top Pre-Upper Cretaceouse level showing the segment linkage points at clear throw minima (arrowed). (b) Throw distribution map for Fault BCE1 showing the general increase in throw from the fault tips towards the fault centre, with localized throw minima representing segment boundaries.(c) Fault polygon showing the planform morphology of Fault BCE1 at Upper Cretaceous level, with two major changes in fault orientation coinciding with the throw minima, representing segment linkage points.

The displacement on fault BCE1 decreases towards the NW, contrasting the displacement pattern on the neighbouring fault BF3 to the east. At the same time the displacement is decreased upward implying that the southern part of the fault could be developed during post-rift period and not had any subsequent movement as the fault surface in this part has the concentric throw contour pattern typical of a post-fault sequence (e.g. Childs et al., 2003). This could be observed on the 2D seismic (Figure 7.40) section throughout the propagation upward with low stratal deformation away from the fault and possible reverse drag on both footwall and hanging wall of the fault.

7.3.3.7 Basement Fault (BF) No.9

The **BF9** is trending NW-SE along the western boundary of the Ajdabiya Trough and dipping toward the SW. The fault is continuous within the study area from the south east by about 75 km, tipping out in the northwest direction, (Figures 7.4 & 7.5). In strike oriented sections (Figures 7.21, 7.22, 7.27, and 7.36), the fault plane is planar at surface and become listric at depth and mainly located in chaotic seismic reflections that correspond to a zone of undercompaction and overpressure zone as evidenced from the well report of well A1-119 and the subsidence analysis (chapter 6) with throw varying along strike between ca. 20 ms and 400 ms (TWT). The fault zone is form with about three segments possibly linked via overlap zones.

The attached graben has broad wedge shaped geometry (Figures 7.36 & 7.47) with a width of about 30km showing overall expansion into the fault and thinning and onlap on to the hanging-wall dip towards the southwest. The BF9 intersects and terminates against NE-SW trending faults or transfer zones (Figures 7.4 & 7.5) and representing a syn-depositional fault style formed by set of linked fault segments. The fault dipping to the southwest and swings in strike from NW-SE at southern segments to NNW-SSE along its northern segment to become subparallel to the master fault. Thickening of Pre-Upper Cretaceous indicates that displacement on the BF9 continued till Paleocene time. The throw contours and profile (Figures 7.41 & 7.42) shows a gradual change in throw towards the fault tips. There are a variety of minimum and maximum displaced points with distances ranging from 15 to 20 km between them. Fault throw has maximum values ca. 400 ms (TWT) at the SE portion of the

fault and decreases to about ca. 210 ms (TWT) towards the northern segment of the fault. Throw values are decreasing upwards to about 20 ms (TWT).

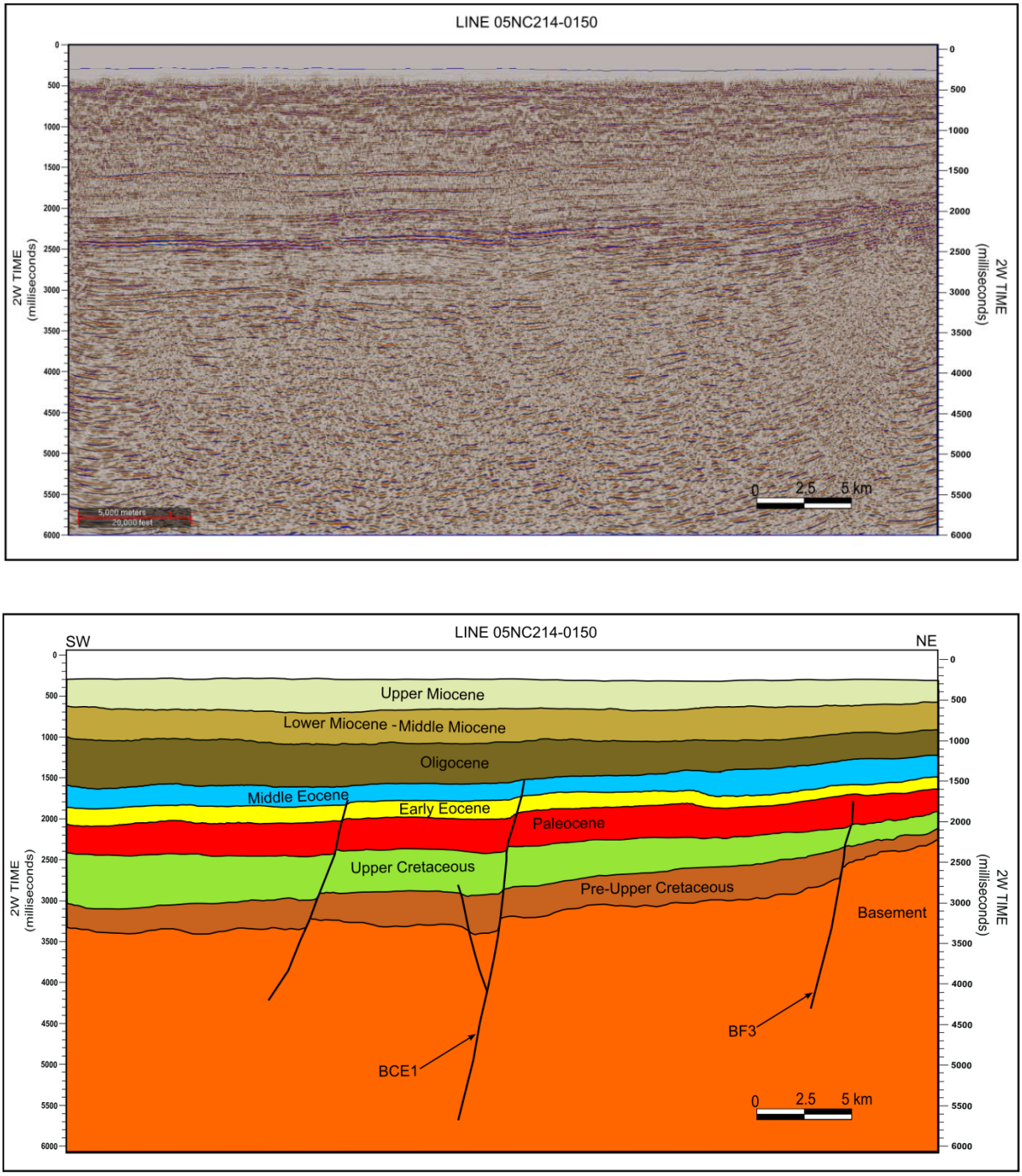

Figure 7.40: Seismic section 05NC214-0150 from the southern Ajdabiya Trough showing little fault activity compared with northern part of the trough. BCE1 fault dipping to the southwest and associated with small antithetic normal fault with larger movement observed on basement horizon.

These throw variations suggest that the fault zone may consist of variable segments linked via relay zones (Childs et al., 1995; Imber et al., 2004). The shape of the throw profiles for top Pre-Upper Cretaceous (syn-rift) – Paleocene horizons (Figure 7.42) is comparable on the fault surface attribute. By contrast, throws on the fault decrease towards the northwest. The majority of the decrease in throw occurs across intersections between the fault segments indicating possible segment overlaps. The decrease in throw on the fault, suggest that displacement has also been transferred by soft-linkage (Walsh and Watterson, 1991) or via transfer zones between overlapped segments (Morley et al., 1990). Instead throw increases at intersections with other faults trending NE-SW. In this case the dominant changes in vertical displacement of the BF9 are consistent with the opinion that displacement was transferred between the fault and the other faults.

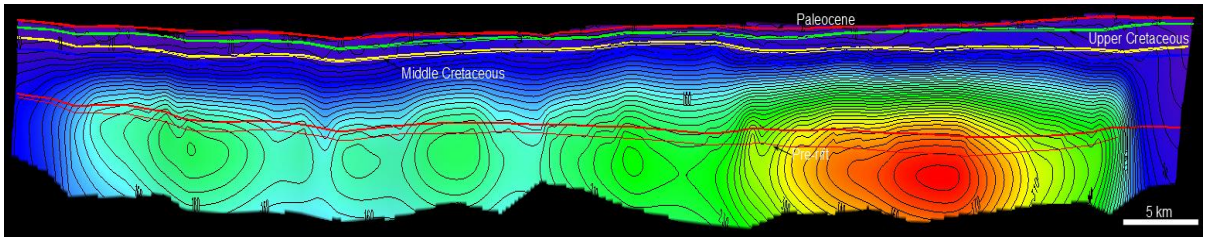

Figure 7.41: Throw strike projection on the fault surfaces of the BF9 fault illustrate variations along fault strike with characteristic of elliptical and concentric variations of throw indicating variable fault segments. Large throw observed at the southern portion of the fault and reaches about 400ms (TWT).

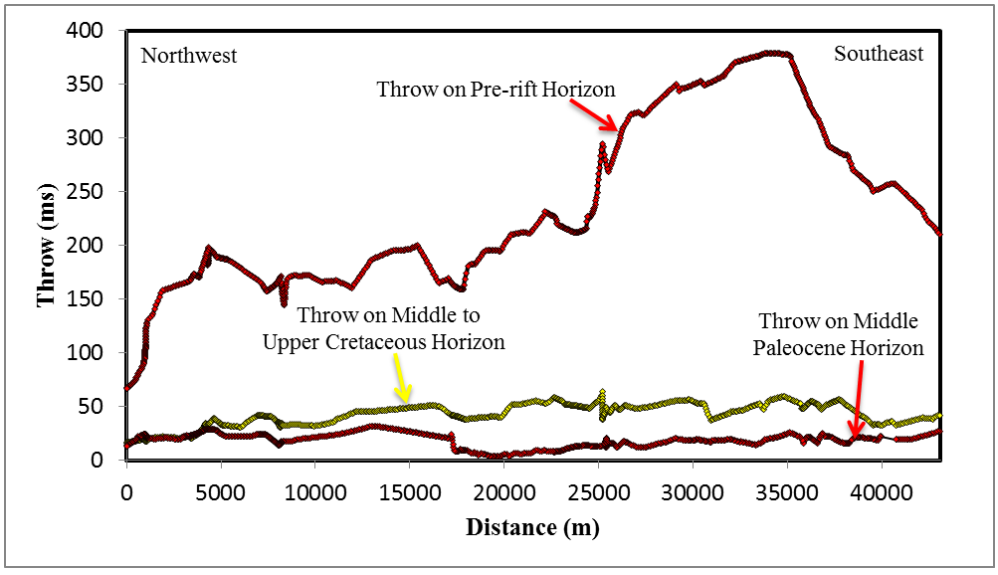

Figure 7.42: Displacement length profiles of BF9 with pre-Cretaceous, Upper Cretaceous, and Paleocene horizons.

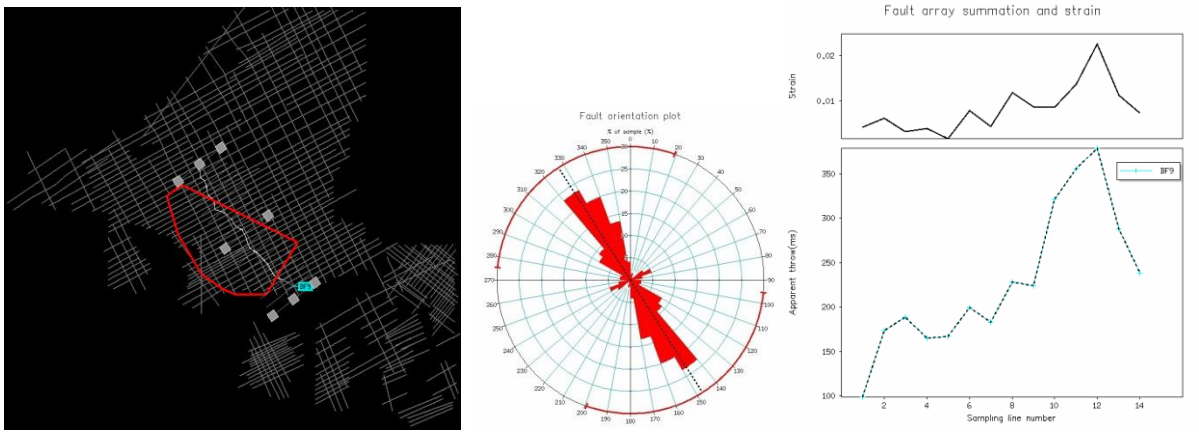

Figure 7.43: (a) fault trace of BF9 with zigzag pattern, (b) fault orientation diagram, (c) displacement length profile correlated with pre-rift horizon.

The fault surface attribute (Figure 7.41) show that the fault has an irregular surface shape in some places with a major smooth surface extended along the zones of high displacement. The irregular features along the surface of the fault may represent evidence of segment interactions or overlap zones formed during fault growth stages (Morley et al., 1990). In addition the throw pattern on the mapped fault surface is approximately horizontal, a characteristic of synsedimentary fault (e.g. Childs et al., 2003). Extensive syn-rift thickening of Lower Cretaceous sequences overlying pre-rift sequence is apparent along the BF9, indicating that tectonism was active until about Upper Cretaceous, ~100Ma. Upper Cretaceous hangingwall sequences (Figures 7.43 and 7.44) dip away from the BF9 fault and shallowing up towards a structural high or spur through a hangingwall syncline (Figures 7.45 -7.49). This geometry resembles a similar compaction-related geometry discussed by Skuce, (1994) for faulting in the Ajdabiya Trough which subsequently prevailed by the development of faulted monocline structures. These structures are interpreted to form in response to differential compaction as a consequence of varying hangingwall and footwall lithologies together in addition to effects from underlying structures. Decreasing throw along fault strike is indication of uplifting or/and erosion associated faults, it is also due to significantly less thermal subsidence and infilling as observed from subsidence data (chapter 6). On a smaller scale, onlap surfaces are well displayed on the dip slope of the formed graben and also in the immediate hanging-wall of the fault (Figure 7.22 & 7.45). During the end rifting stage, sedimentation is likely to be outpaced by subsidence and differential relief are created across fault scarp. Mapping the syn-rift surfaces using reflector terminations allows us to understand

the topographic variations through the interaction with the fault plane. Seismic data show that during the rift stage sediments are characterized by the thickening of strata against the fault (wedging of reflectors) related to continuous tilting of the hanging-wall during deposition. The infilling package represented by a wedge–shaped geometry of syn-rift topography and may also display divergent reflector configurations induced by compaction. Compaction during the Tertiary would cause movement most especially in the upper parts of the old Late Cretaceous faults and the compensatory thickening of the Tertiary deposits. This with compaction subsidence would cause a degree of disruption among younger rocks (Withjack et al., 1990).

Cross-sections through the Pre-Upper Cretaceous interval show uniform thickness distribution across the fault BF9. The divergent character of the seismic reflectors indicates that the fault was active during the deposition of this interval. The isochron map of the Cretaceous sequence (Figure 7.58) and the syn and pre-rift maps (Figures 7.44) provides evidence of thickness changes occur across the fault.

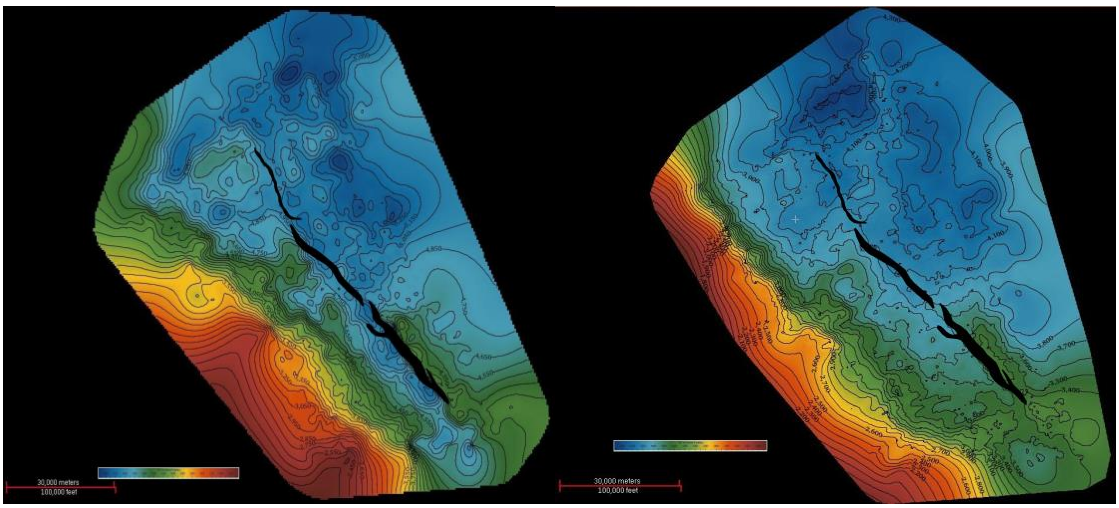

Figure 7.44: Time-structure map of the top syn-rift horizon to the left and pre-rift horizon to the right along the BF9 fault zone.

These variations in thickness implies that the fault represent a syn-sedimenatary fault growth. There are also variations in reflector thickness and dips across the hangingwall and footwall of the fault (Figures 7.45 - 7.47). The steep character of the Pre-Upper Cretaceous strata in the hangingwall compared to the more gentle strata in the footwall may suggest that the fault

could be initiated either before or at the same time of the deposition of the Pre-Upper Cretaceous sequence. The isochron thickness map of the Paleocene sequence (Figure 7.58) show no apparent thickness variations suggesting that this geometry is consistent with passive infilling of isolated half-graben depocentre (e.g. Paredes et al., 2013**).** The Paleocene interval in this part from the Ajdabiya Trough seems to be deposited in an environment of static sea level conditions with little fault activity (Spring and Hansan, 1998; section 5.4.1.2). Variations in throw are quantified using horizons assigned to the Pre - Upper Cretaceous level which was difficult to follow through many parts within the study area. Maximum throw observed along profile and from the fault surface attribute model (Figures 7.41 & 7.42) for Pre-Upper Cretaceous horizon shows that maximum values (210 and 400 ms TWT) are observed at the intersection with two major NE-SW trending faults known as the BF8 and the North Ajdabiya Fault (NAF) respectively. Throw decreases rapidly at an overlap zone between tow fault segments towards the north, until there is a sharp increase where the fault intersects the NAF fault. The BF9 fault is partly accommodating the difference in throw between the fault segments. Variations in throw corresponding to the positions of fault-perpendicular folds are seen along the identified fault segments (Figures 7.48 & 7.49), with throw minima associated with possible anticline like features formed perpendicular to the fault strike and occur at linkage or overlap zones between the segments (Figure 7.41, 7.42, and 7.44) There might be also possible displacement distribution onto normal faults formed antithetic to the BF9.

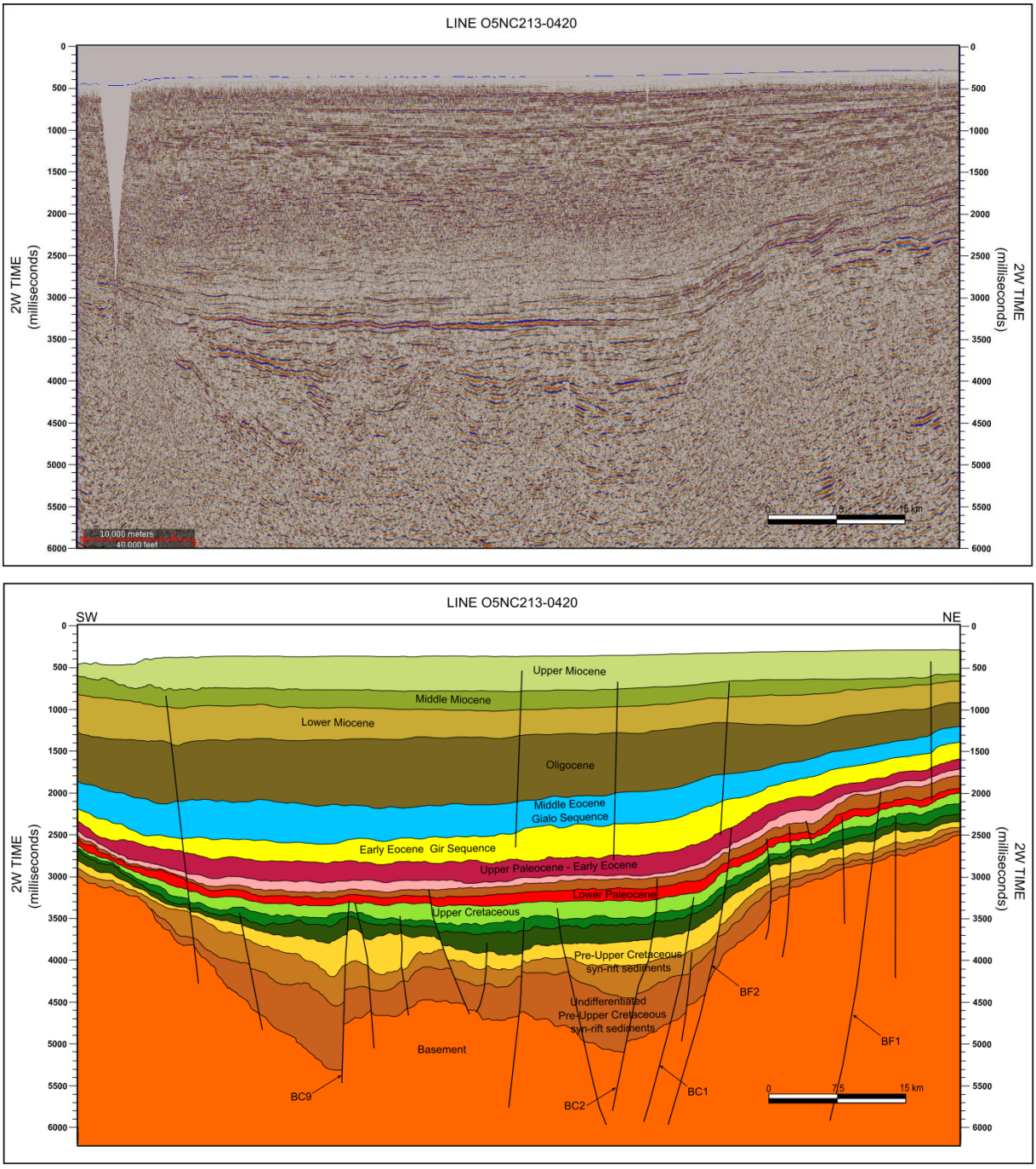

Figure 7.45: Uninterpreted SW-NE seismic line 05NC213-0420 illustrating large scale intrabasin fault blocks related to rifting in the Ajdabiya Trough (above), with an interpretation of the section with key seismic horizons identified (below).

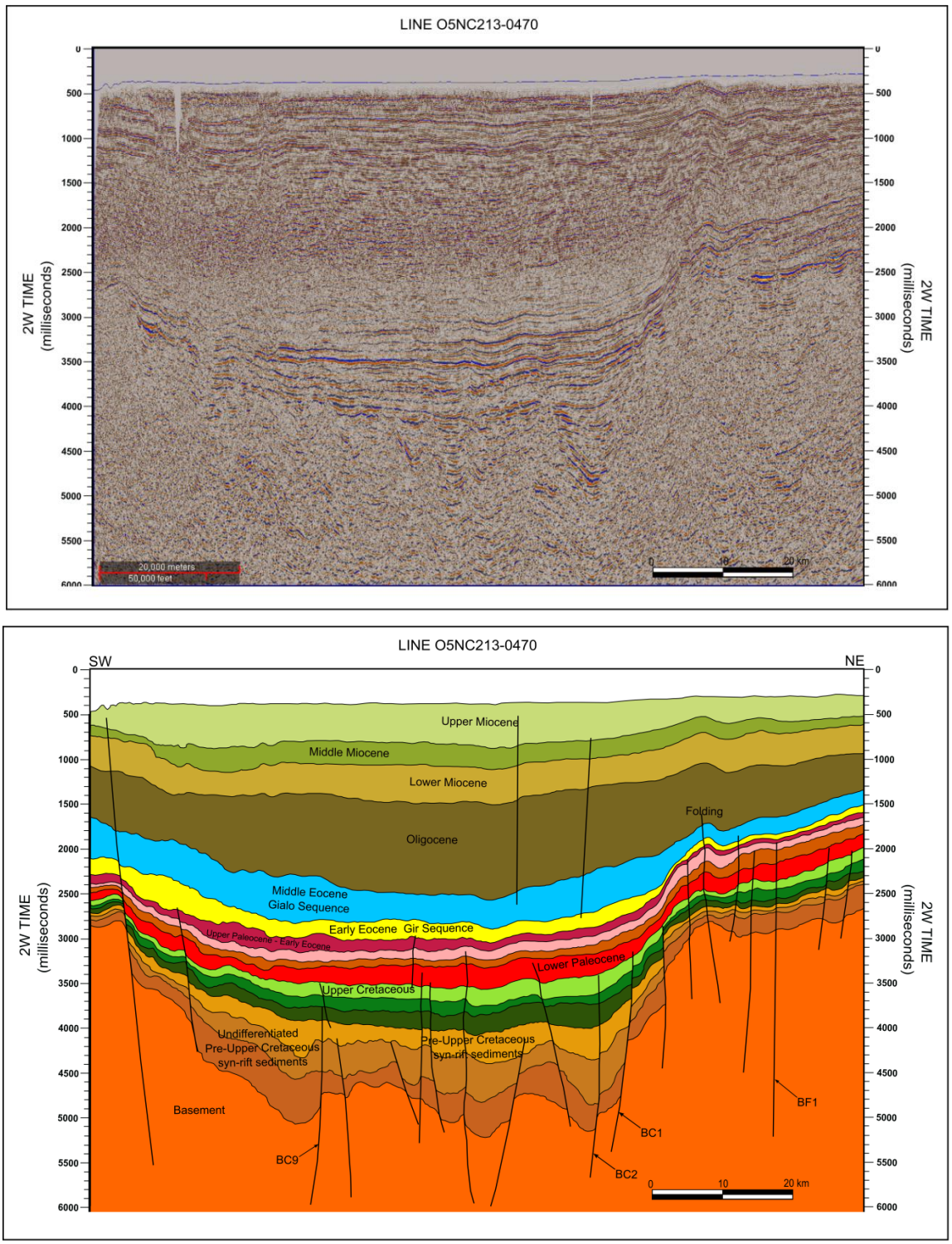

Figure 7.46: Uninterpreted version of seismic section 05NC213-0470 (above) with interpreted seismic copy (below). Note structural asymmetry and great thickness of sedimentary section contained in the central Ajdabiya Trough. Large normal faults which bound grabens and half-grabens show clear evidence of syn-rift growth across the Ajdabiya Trough faults. Large displacement faults are not as clear on NE margin, although some faults are observed in the basement. These faults are confined to the syn-rift sequence and do not offset overlying post-rift sequence. The deepest horizon mapped defines unconformable boundary between the base of syn-rift Pre-Upper Cretaceous sedimentary rocks and Cambro-Ordovician basement (orange section).

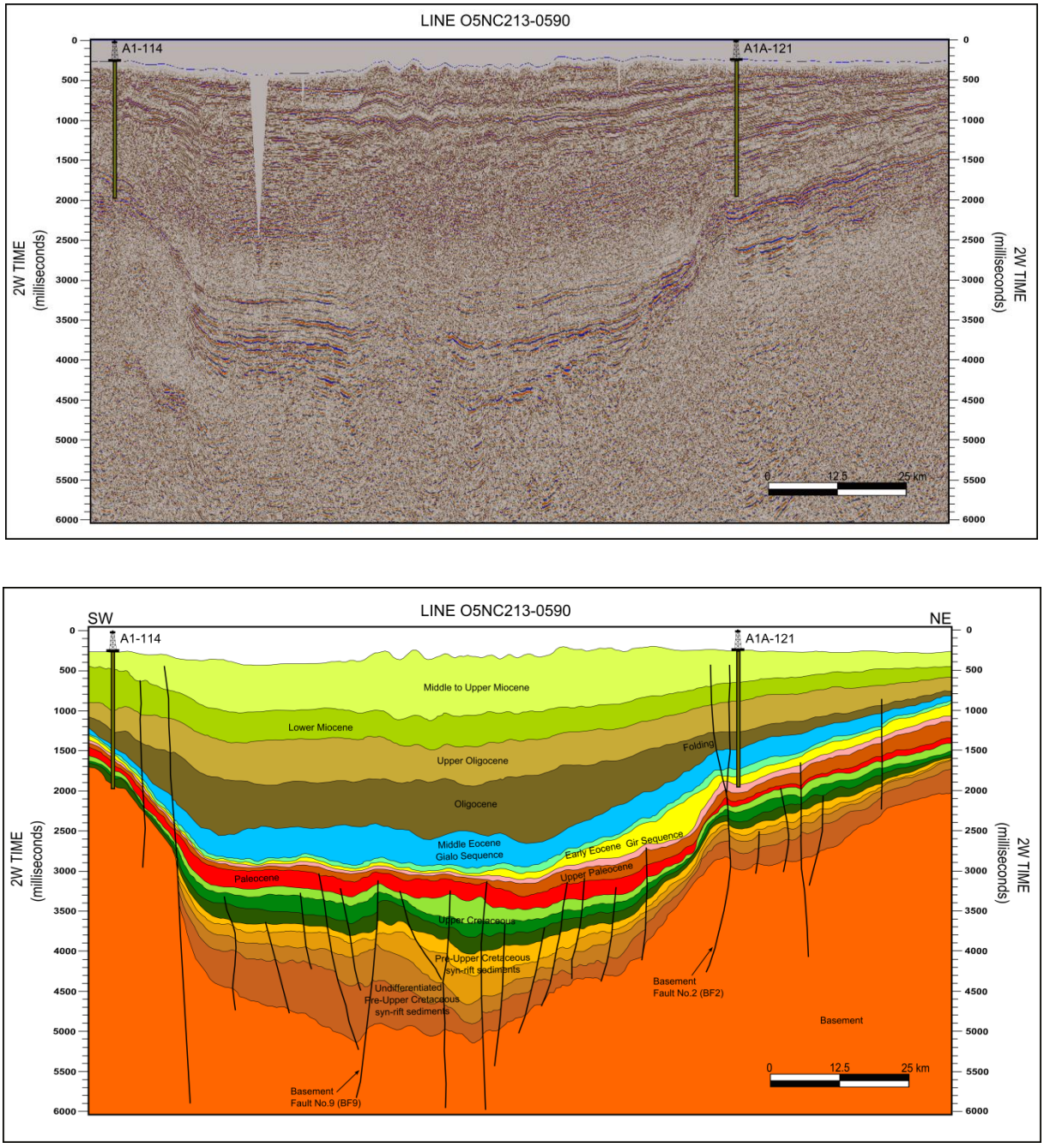

Figure 7.47: Seismic line 05NC-213-0590 above with interpreted copy below illustrating syn-rift seismic stratigraphic architecture in the northern part of the Ajdabiya Trough. The syn-rift package was probably generated by normal and strike-slip faulting. The seismic section shows that an intense tectonisation has occurred along the northern margin of the trough. The rift phase ended around Mid-Cretaceous or Cenomanian time. This time is characterized by a regional unconformity (Upper Cretaceous) that truncates rotated Early Cretaceous layers. Moderate to high relief faulted monocline is observed throughout much of the Cretaceous - Paleocene section and is interpreted to have formed because of differential compaction of the Cretaceous section over a buried fault block topography associated with the Pre-Upper Cretaceous fault zone. The section illustrating the development of wedge shaped sedimentary units that thicken towards the BF9 fault surface.

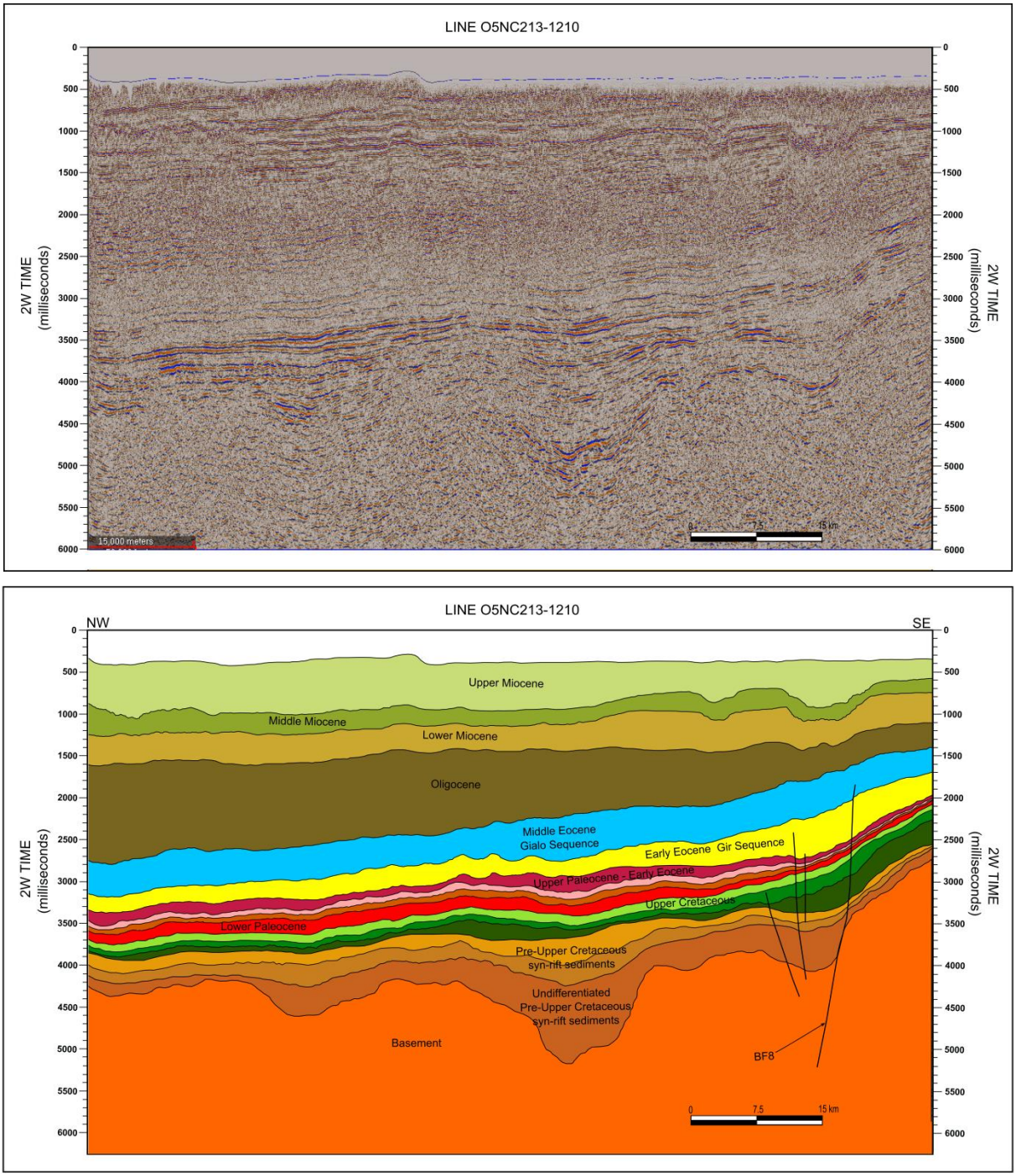

Figure 7.48: Seismic line 05NC213-1210 paralleling the strike of the BF9 showing drape sequences of Mesozoic – Cenozoic sediments over the basement and characterize the structural style of the hangingwall of the fault. The fault is segmented into variable segments with maximum throw at the centre suggesting possible fault nucleation zone. Axial surfaces of the drape sequence dip away from a basement highs. This helps to distinguish the succession from growth strata and indicates the fault formed prior to the Pre-Upper Cretaceous.

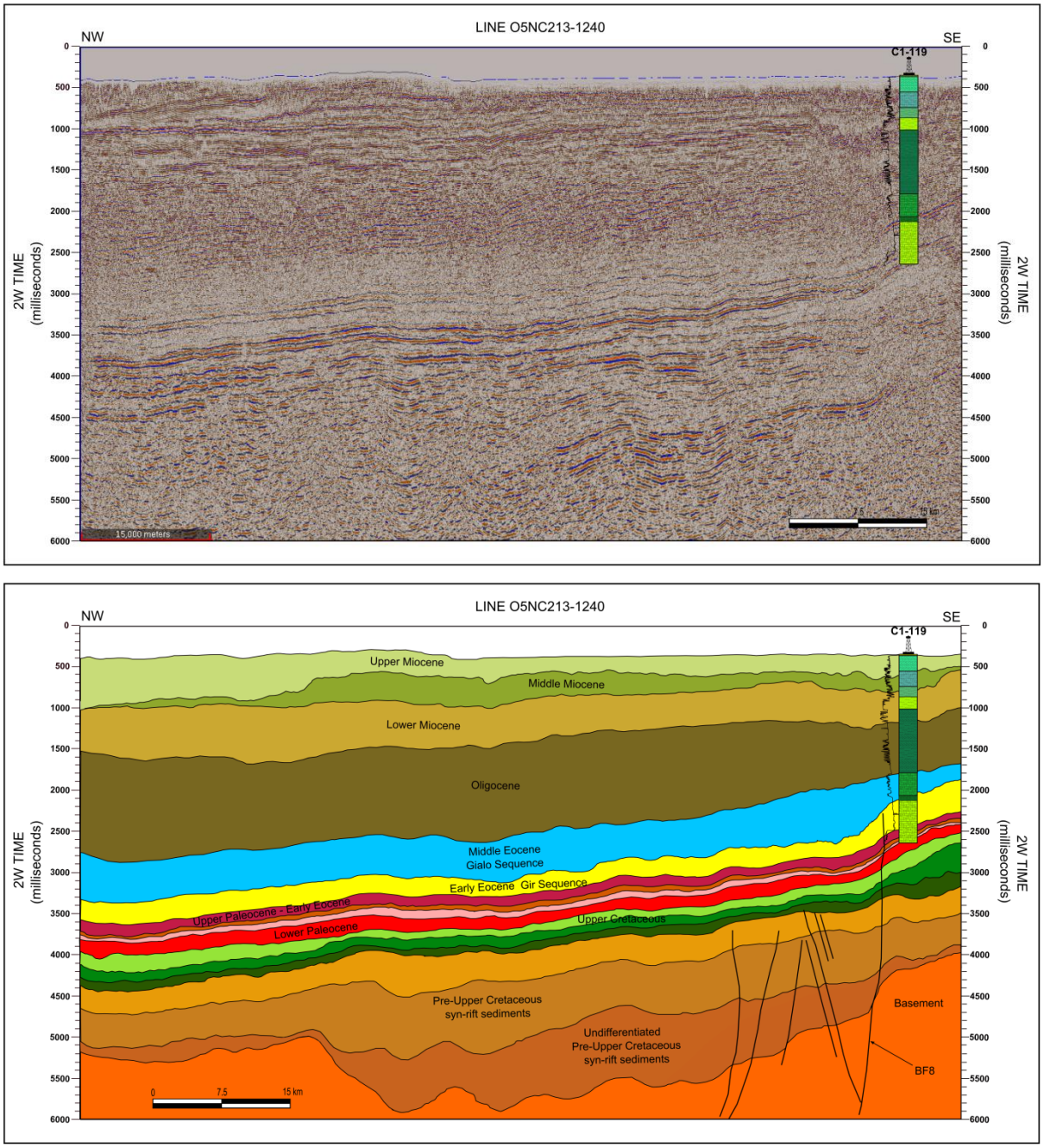

Figure 7.49: Uninterpreted copy of seismic line 05NC21301240 across the footwall of the fault BF9 in strike direction with interpreted copy below clearly show the different geometrical characteristics of the stratigraphic relationships along the footwall of the fault.

7.3.3.8 North Ajdabiya Strike Slip Fault (NAF)

7.3.3.8.1 Geometry and Structural Style

The recognition of strike slip deformation in the Ajdabiya Trough is based on the methodology advocated by Harding (1990). The criteria consistent with strike slip deformation include.

1- Steep fault segment at depth
2- Change in fault dip along strike
3- Basement involvement
4- Positive and negative flower structure
5- Coeval en-echelon faults (riedel shears) or folds

2D seismic data across the northern Ajdabiya Trough show a clear NE-SW trends of fault structures. These structures could be formed in response to inversion of previous rifts which led to the reactivation of pre-existing Paleozoic and Mesozoic faults into reverse faults, with an oblique-slip sense of movement (e.g. Brede et al., 1992; Craig et al., 2008). A hypothesis by El Arnauti et al., 2008 addressed the idea of possible phase of extension rejuvenation in Cyrenaica region which manifested as a planar block faulting and probably related to strike slip movement during the Upper Cretaceous time (Cenomanian – Santonian). This may be formed due to local inversion of the north Cyrenaica rift during this time as a result of relative subplate movement (El Arnauti et al., 2008; Fairhead et al., 2013) and could influenced the faults framework in north-eastern Ajdabiya Trough.

The North Ajdabiya Fault (NAF) (Figures 7.4 & 7.5) is an expression of a NE-SW trending strike-slip fault extending along the northern side of the Ajdabiya Trough for a distance of about 100 km. The trend of this fault and the geometry of the basement structure in the Ajdabiya Trough are not coincident to support an idea of possible reactivation. The variation is most likely attributed to local variations in stress field during stages of deformation, possibly reflecting strain partitioning during transtension regime which represent combination of dip-slip and strike-slip deformation (e.g. Dewey et al., 1998; Withjack and Jamison, 1986).

The structural style of the NAF is depicted from the 2D seismic profiles (Figures 7.51 & 7.52) shows clear planar geometry, dip-slip and normal separation criteria. The development of antithetic faults in the hanging wall at both deep and shallow levels gives the impression that flower structures (Harding, 1985, 1990) are developed. A remarkable feature of the fault in

this part of the area, and a criterion of strike slip movement, is a negative flower structure. A change in the fault throw direction from south to north (Figures 7.51 & 7.52) is also further evidence of strike-slip movement. Some of the structural features of the NAF could be observed on the Landsat images (Figures 7.55 & 7.56). It shows that the fault is segmented in two parts with development of en echelon folds on either side of the fault segments (Figure 7.50).

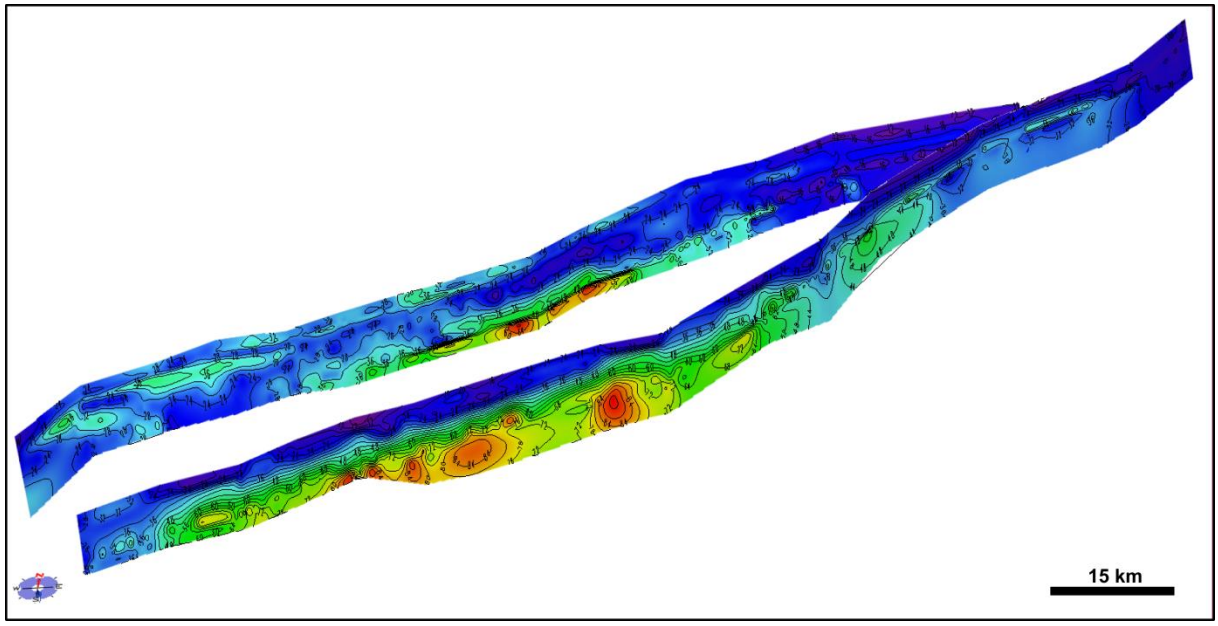

Figure 7.50: Fault surface as colour-coded attribute maps showing throw variations along two branches forming the NE-SW striking North Ajdabiya Strike Slip Fault (NAF). Throws are higher at the central area related to possible high strain partitioning zones.

The NE-SW trends are often consistent with NE-SW sinistral structures observed by El Arnauti et al., 2008 in Cyrenaica region (Figure 7.54). The strain field generated was of a sinistral rotational shear with variable extension limits; N-S extension, NE-SW shears and E-W oriented folds. Minor transpression could be partitioned between the NE-SW sinistral strike slip re-activation of the basement normal faults and the NW-SE faults in the Ajdabiya Trough. Strike-slip movement perpendicular to the NE-SW shearing is observed during the interpretation of the basement fault (BF2) (Figure 7.47) in addition of similar fault trends deduced from the gravity and magnetic interpretation near the Cyrenaica region (chapter 4). This could be induced by the rifting during the Triassic to Late Cretaceous times (Dercourt et al., 1986).

The NAF is possibly inherited also from Pan African orogeny event when acted as a sinistral strike-slip movement that was subsequently re-activated as a major transtensional fault during the Cretaceous time and associated with thickening of Upper Cretaceous strata (e.g. El Arnauti et al., 2008).

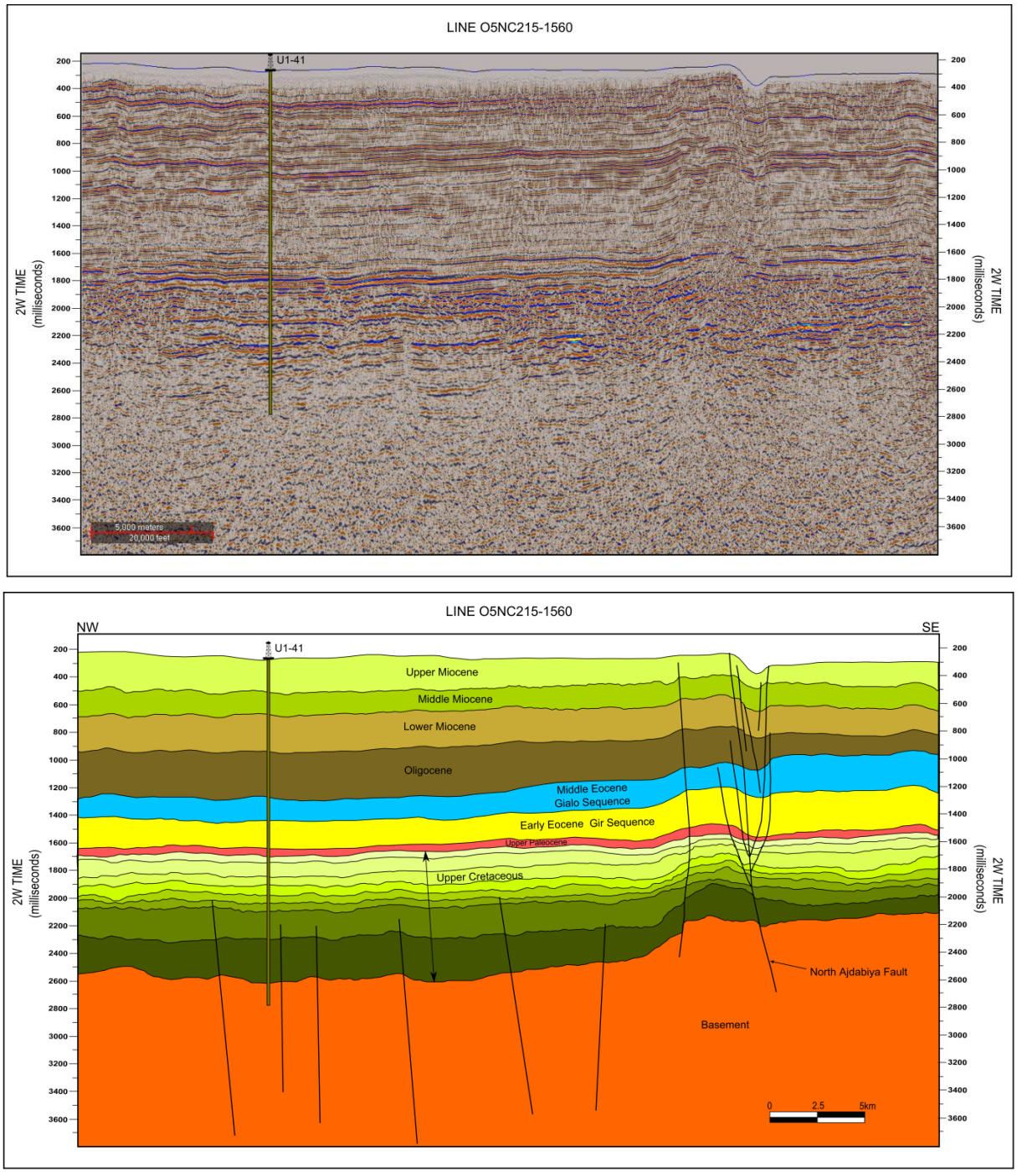

Figure 7.51: Seismic line 05NC215-1560 showing NE-striking negative flower structure

The regional strain field can be described in this phase as a sinistral rotational shear including two elements, the NE-SW shears and the N-S extension (Figure 7.54). However, the structural styles of basement relief indicate possible evidence of both sinistral and dextral deformation.

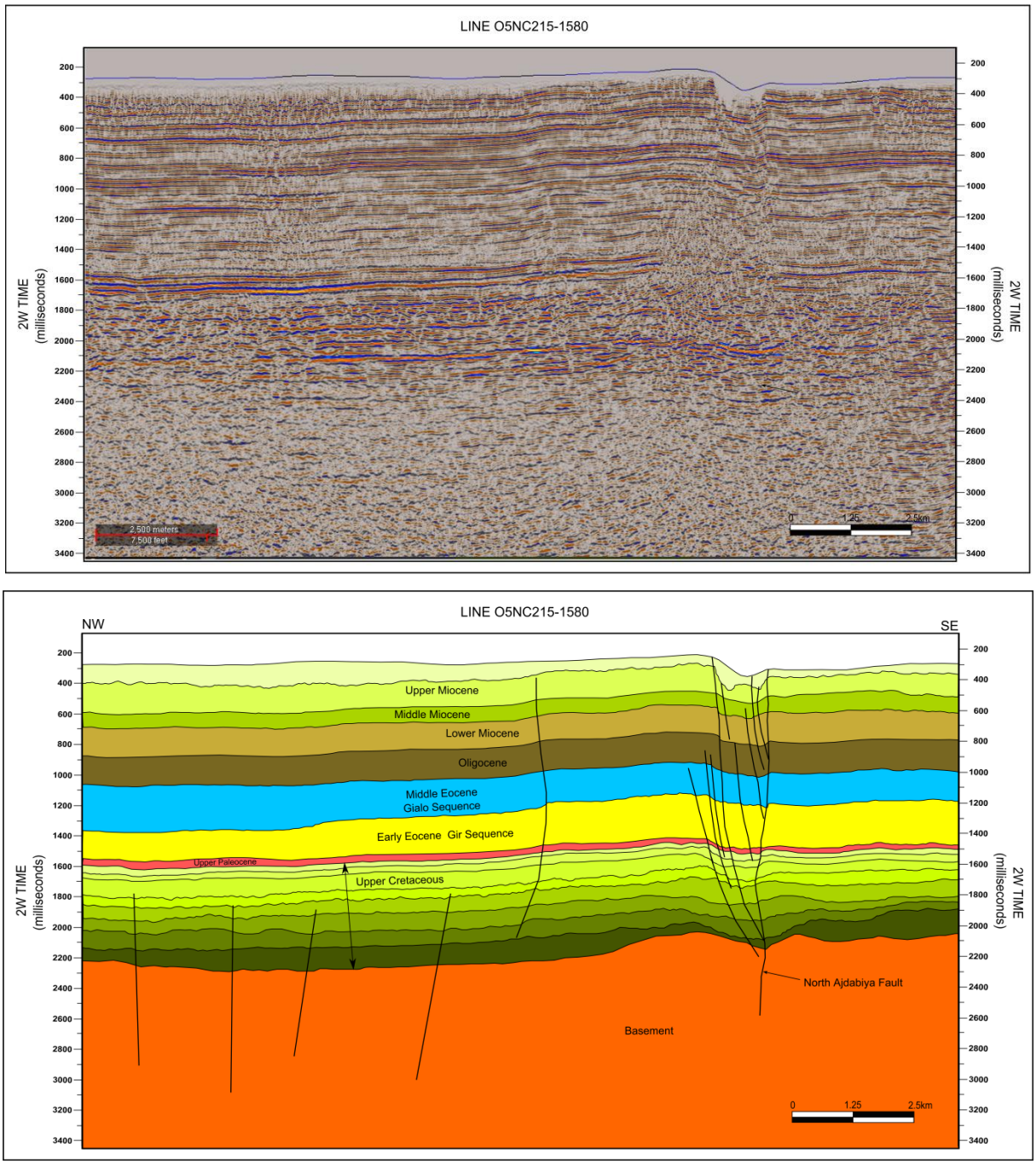

Figure 7.52: Seismic line 05NC215-1580 showing NE-striking negative flower structure

Fault activities in the Ajdabiya Trough are considered to be very rare during periods from Eocene to recent, even though during Upper Cretaceous to early Eocene faults show small offset possibly due to existence of low strain compatibility over large area owing to strain partitioning (De Paola et al., 2005b).

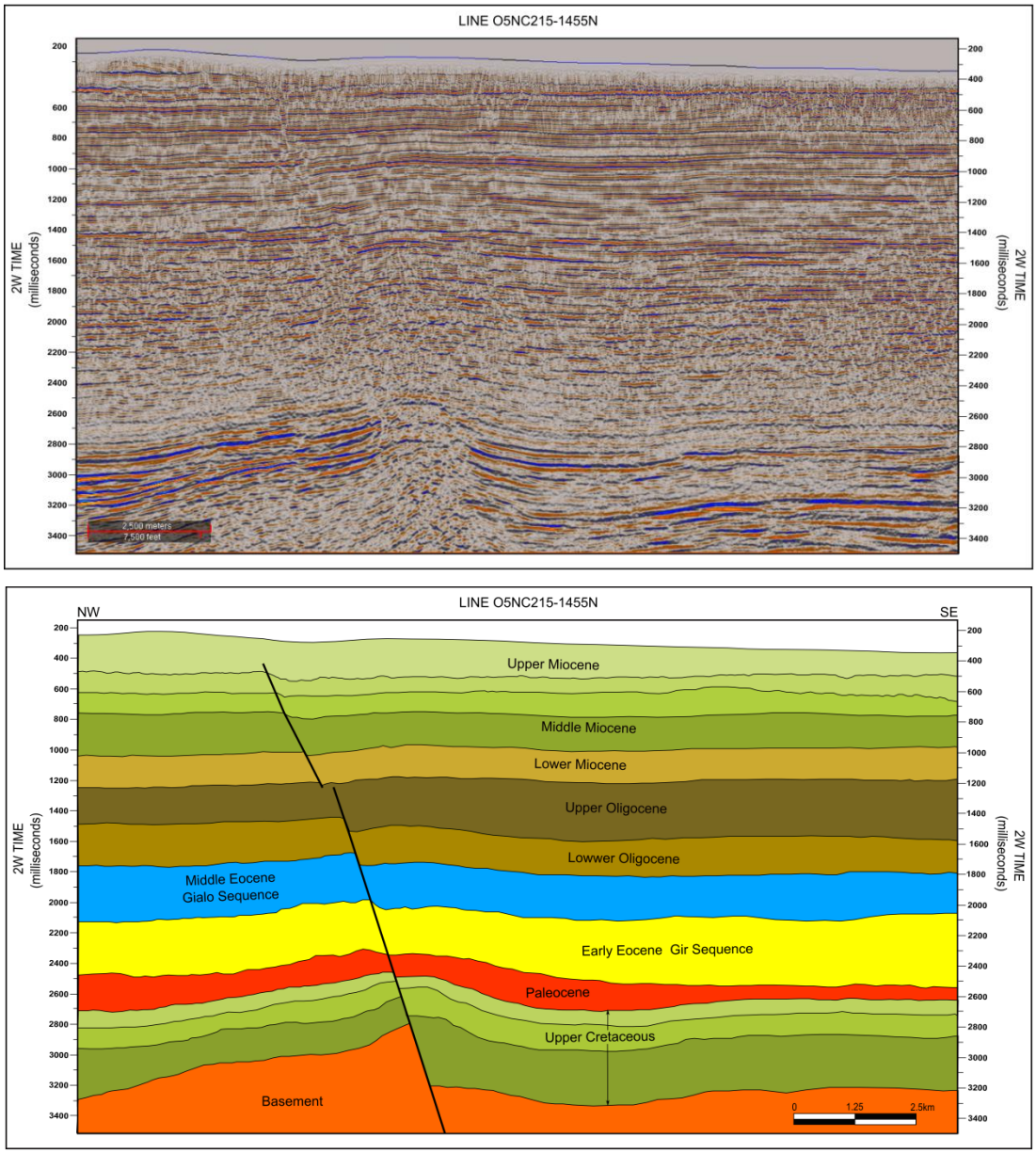

Figure 7.53: Above un-interpreted copy of line NC215-1455N crossing the Ajdabiya Trough in NW-SE direction (See figures 7.4 & 7.5 for location), with interpreted version below show part of a mapped fault trending NNE-SSW and dipping to the SE. the fault cross-cut NE-SW strike slip fault in the northern Ajdabiya Trough and show possible variable phases of re-activation. The line shows evidence for the timing of normal-fault activity in the Ajdabiya Trough characterized by period of differential growth across the fault during Cretaceous - Paleocene. Minor differential growth is also evident at higher stratigraphic levels (Late Eocene – Early Oligocene). This unit is usually regarded as marking the end of rifting in the Ajdabiya Trough.

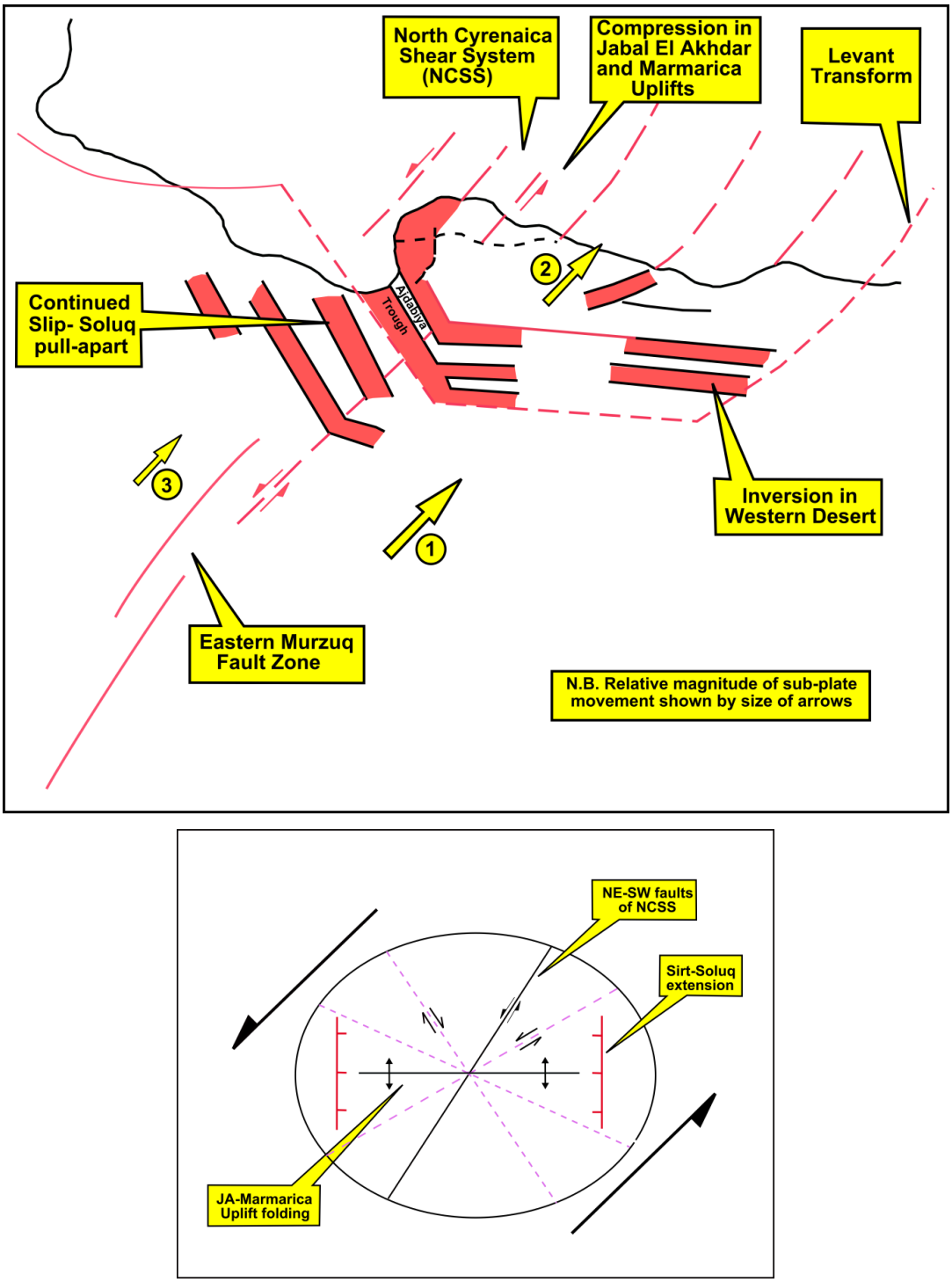

Figure 7.54: Structural analysis montage of Late Cretaceous (Santonian-Danian, above semi schematic of sub-plate separation and movements in NE Libya and parts of Egypt, below is regional strain field in NE Libya.
The regional strain field was a sinistral rotational shear with three elements; N-S extension, NE-SW shears and generally oriented E-W folding (El Arnauti et al., 2008). During Cenomanian-Santonian time a new NE-SW trending North Cyrenaica Shear System (NCSS) was established. NNE-SSW strike-slip movement affected the area and led to the development of depression in a sinistral pull-apart system with associated block faults along the eastern part of the Ajdabiya Trough including the Soluq Depression. E-W and WNW-ESE pull-apart basins formed and were subject to shortening resulting in compression and inversion (Guiraud and Bosworth, 1999).

Interpretation using Landsat images (Figures 7.55 & 7.56) has shown that right lateral movement may have occurred along the NAF zone. It is also observed that, splay faults or cross cut faults are oriented counter-clockwise of the main border fault, this resembles an en-echelon style fault geometry from which a component of sinistral shear could also be inferred along the North Ajdabiya Fault (NAF) segments in this area. The observed NE-SW strike-slip fault in the Ajdabiya Trough differs significantly from the normal faulting, which displays a NW-SE extension partitioned from the primary N-S extension in the Sirt Basin. Linear strike-slip fault segments belonging to the NAF can be traced as far northeast, but Cenozoic ages also provide clear evidence for active right-lateral movement along faults in the adjacent Cyrenaica region (El Arnauti et al., 2008; El Amawy et al., 2009).

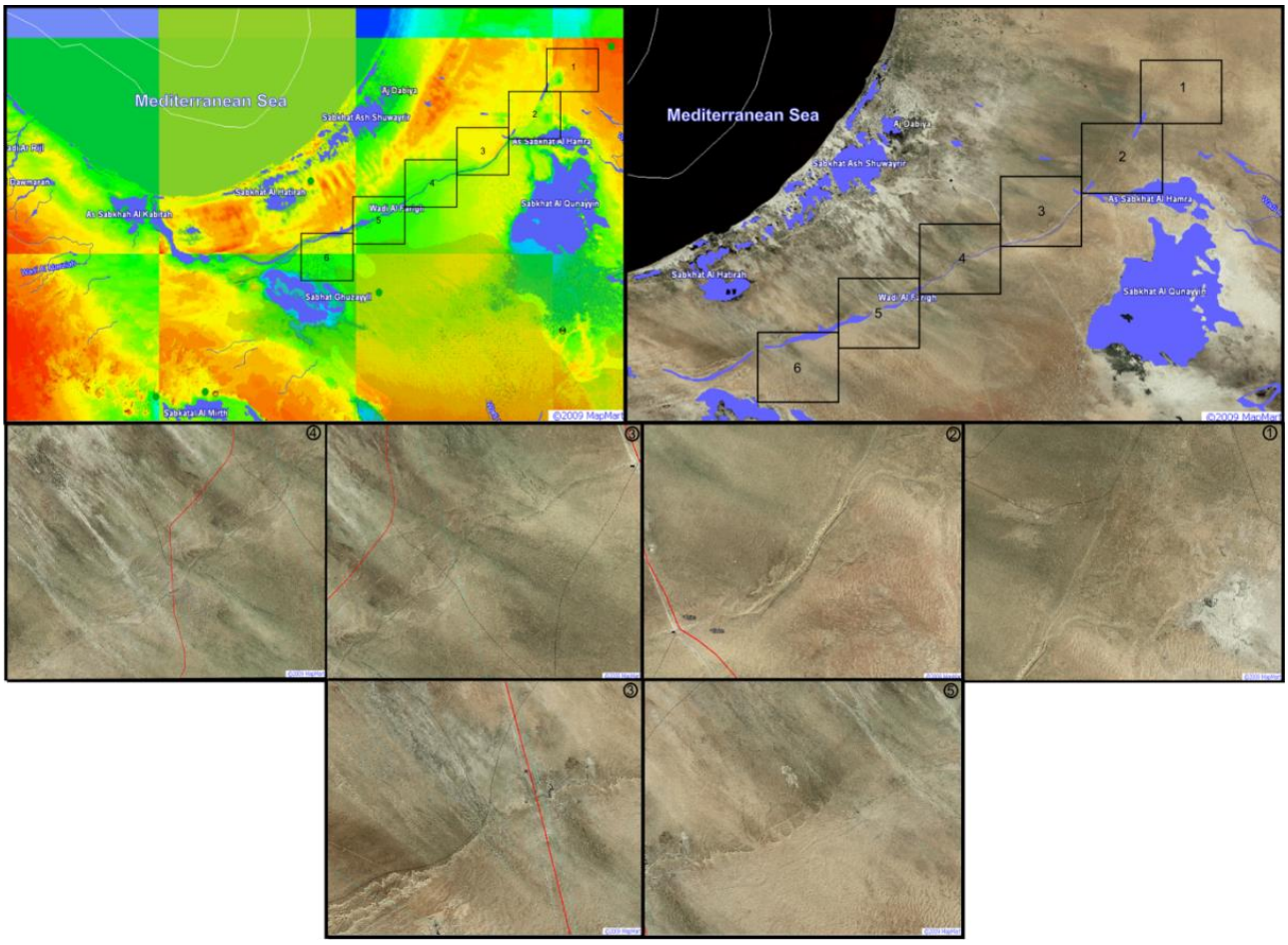

Figure 7.55: Digital elevation model (DEM) up to the left and Landsat image of the northern part of the Ajdabiya Trough, showing location and evidence of the North Ajdabiya Fault (NAF) zone with an amplified slices showing more detailed features along the fault zone.

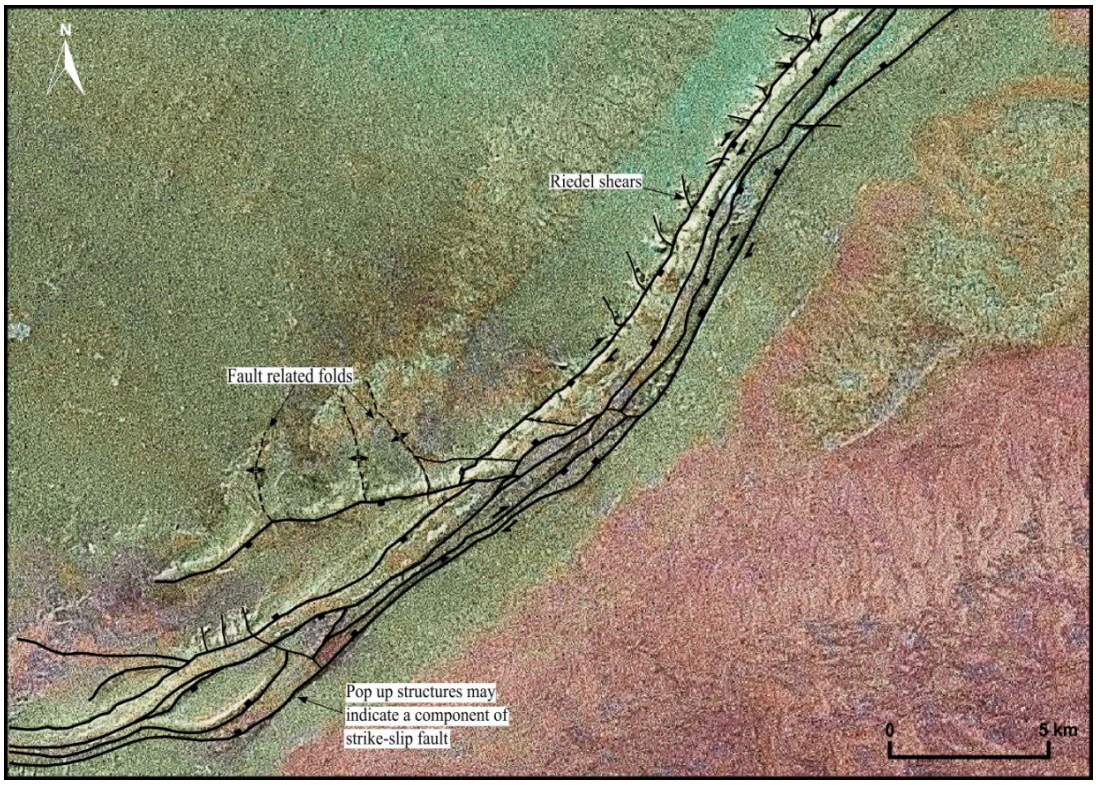
N
Riedel shears
Fault related folds
Pop up structures may indicate a component of strike-slip fault
0
5 km

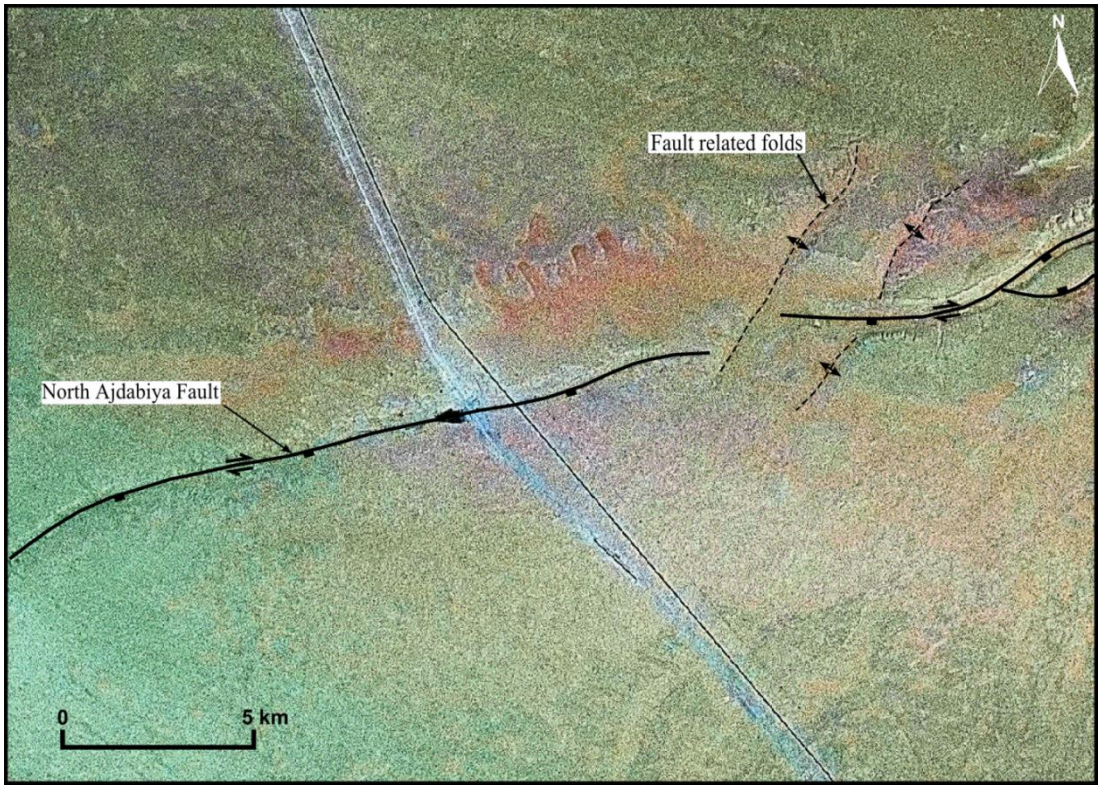
N
Fault related folds
North Ajdabiya Fault
0
5 km

Figure 7.56: Landsat images (from Google Earth) of North Ajdabiya fault system showing surface fault trace and fault strands drawn as black lines. Fault occasionally lacks surface expression. Semi-parallel right-lateral component can be traced. Trace of fault cutting drainage features and recent alluvial deposits. The central images show that the fault cuts along a NE-SW extending valley named Wadi Alfarigh which forms few meters south facing scarp.

7.3.3.8.2 The Timing of Movement on the NAF

The timing of movement on the NAF is difficult to establish precisely. The fault presumably initiated in Pre-Cretaceous time and was vertically propagated to the northeast with a maximum displacement of about (100 ms TWT). A displacement profile computed for the Upper Cretaceous horizon on the southern segment of the NAF is shown in figure 7.57.

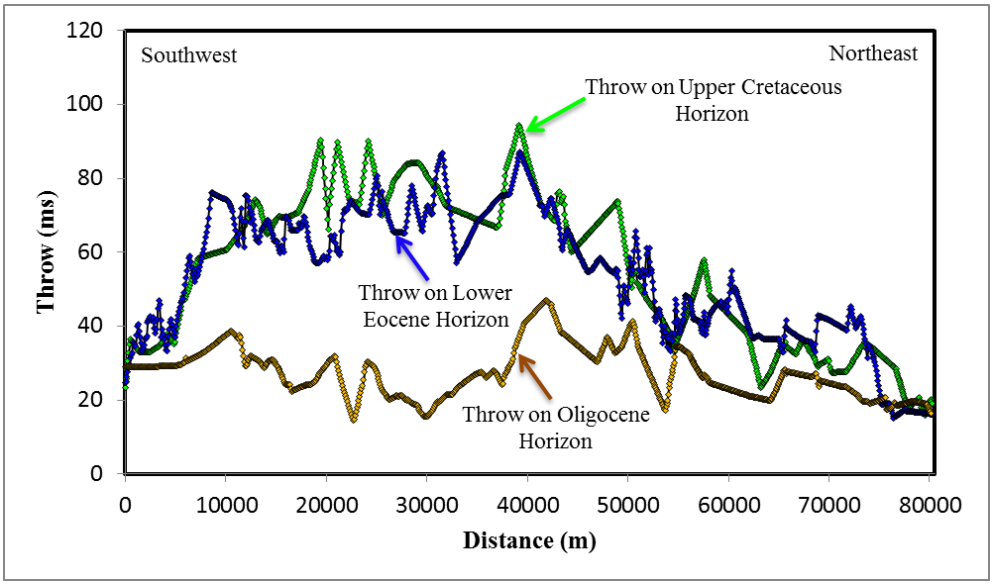

Figure 7.57: Throw profiles of NAF fault on Upper Cretaceous horizons (green), Lower Eocene horizon (blue), and Oligocene horizon (brown) showing gradual decrease in throw toward the north-eastern fault tip.

The patterns on the displacement profile are broadly identical, with displacement high at the centre and outward decrease in value (Figure). These results suggest that the fault correlation shown on seismic date is acceptable and the segmentation of the NAF is valid.

2D seismic profiles (Figures) show that the youngest rocks cut by post sedimentary fault activities are Oligocene to Miocene sedimentary rocks (Figures 7.51-7.53). On the Landsat images (Figures 7.55 and 7.56) there is also clear evidence for right lateral movement along a roughly ENE-WSW zone of asymmetric graben feature.

On the Landsat images and topographic maps, there is also a clear evidence of highly efficient systems of drainage features and linear valley (Wadi Al Farigh), formed along the NAF fault zone and cut an upper Pliocene strata.

The strike-slip fault cut across the Upper Cretaceous, Eocene, and Oligocene to lower Miocene rocks at minor scale, negative flower structures (Figures 7.51 and 7.52). This

younger episode of deformations which characterized by right-lateral strike slip faulting probably related to the evolution of the nearby Cyrenaica fault system and to the internal rift faults which were reversed later by two compressional events of contractional regime (e.g. El Arnauti et al., 2008) lasting from Late Cretaceous (Santonian) into the Palaeogene. It could be also due to recent seismic activity in the offshore and onshore Sirt Basin (Suleiman and Doser, 1994).

Left-stepping en-echelon faults were mapped along the North Ajdabiya Fault (NAF) (Figure 7.56). These faults formed as an oblique faults (Figures 7.51 & 7.52) to the NAF fault and propagated upward possibly till the Upper Pliocene. At the same time NW-SE striking faults were interpreted as dextral strike-slip faults associated with possible "pop-up" structures and seem to be active throughout the Late Miocene (Figure 7.47).

Thickening of strata during the Oligocene as observed on the the seismic cross-sections and isochron maps (Figures 7.51, 7.52, 7.53, and 7.58) is an indication of lateral displacement in the Ajdabiya Trough depocentre, possibly attributed to younger deformation. This lateral displacement is consistent with fold-axis data adjacent to the fault. However the en chelon arrangement of the fold structures with respect to the main fault is evidence of geometrical wrench deformation (Harding 1990). Oblique folds are everywhere oriented clockwise of the fault strike, an observation that is consistent with the regionally significant sinsitral re-activation of all NE-SW trending pre-existing rift related faults on the eastern Sirt Basin and Cyrenaica Platform (El Arnautii et al., 2008). Fold amplitudes are greatest adjacent to fault trace and decrease progressively within about 2km.

7.3.4 Syn-tectonic Stratigraphy and Fault Evolution

Isochron maps were generated from the 2D seismic data in order to identify major and subtle changes in thickness and to detect fault discontinuities from changes in dip and reflection character. The isochron maps show changes in time different between two successive horizons and therefore can be used to delineate changes in stratal distribution and their relation to active faulting as sedimentation rates are comparable to variation in displacements along strike of the faults. The anlysis in chapters 5 & 6 show that the internal stratigraphic architecture of the Ajdabiya Trough is complexe and mainly attributed to fault controlled sedimentation and subsequent pos-rift subsidence (e.g. Baird et al., 1996). Thickness

estimation is largely controlled by the nature of the stratal dips as high dips will lead to overestimated thickness. Variations in stratal dips are disregarded in this analysis and considered to be true variations in vertical thickness. The analysis of isochron maps for the syn-rift and post-rift sequences reveals preferential areas of deposition, which are accompanied by large areas of thinning and thickening of sediments. Sedimentation probably controlled by relay ramps and other growth faults (Figures 7.22 & 7.33). Folding in some areas probably formed due to compressive events (Figures 7.46 & 7.47).

The isochron map between the top of the Upper Cretaceous and undifferentiated Pre-Upper Cretaceous syn-rift strata (Figure 7.58) reflects variable thickness changes (wedge shaped sedimentary units) (Figures 7.33, 7.36, and 7.47) related to asymmetrical depressions and major elongate uplifts bound by syn-tectonic faults with variable trends and elongation. The observations suggest that the Ajdabiya Trough was deformed by Cretaceous faulting caused by diffuse crustal extension along the North African Margin (Guiraud, 1998; Coward and Ries, 2003). The isochron map between the Top Cretaceous and the Top Paleocene (Figure 7.58) shows abrupt changes in thickness of Palaeocene strata at the southern part of the trough. Based on the preliminary observations obtained from the Cretaceous and the Palaeocene isochron maps (Figure 7.58), I interpreted the BF3 and BC1 faults as a syn-sedimentary growth faults and have been active until the Palaeocene and possibly extended to the middle Eocene.

The southern Ajdabiya Trough was deformed by Palaeocene faulting associated with reactivation of early faults (Figures 7.21, 7.22, 7.33, and 7.59), possibly related to changes in spreading direction in the central Atlantic (Dewey et al., 1989). During this event, the boundary faults of the Ajdabiya Trough were relatively inactive (e.g. Hallett, 2002) however, the trough continued to subside as part of broader area, possibly representing a phase of thermal subsidence that followed the main rifting during Late Cretaceous.

A NW-SE compressive regional stress regime was established by Middle Cretaceous. Subsidence accelerated within the Ajdabiya Trough along reactivated NW-trending extensional faults (Figure 7.58). Dextral transpression is interpreted along the North Cyrenaica Fault system (Anketell & Ghellali, 1991; Giraud & Bosworth, 1997 ref in Ahlbrandt, 2001). The deformation was accompanied by localised uplift along Pan African fracture zones, concentrated in the northern part of the area.

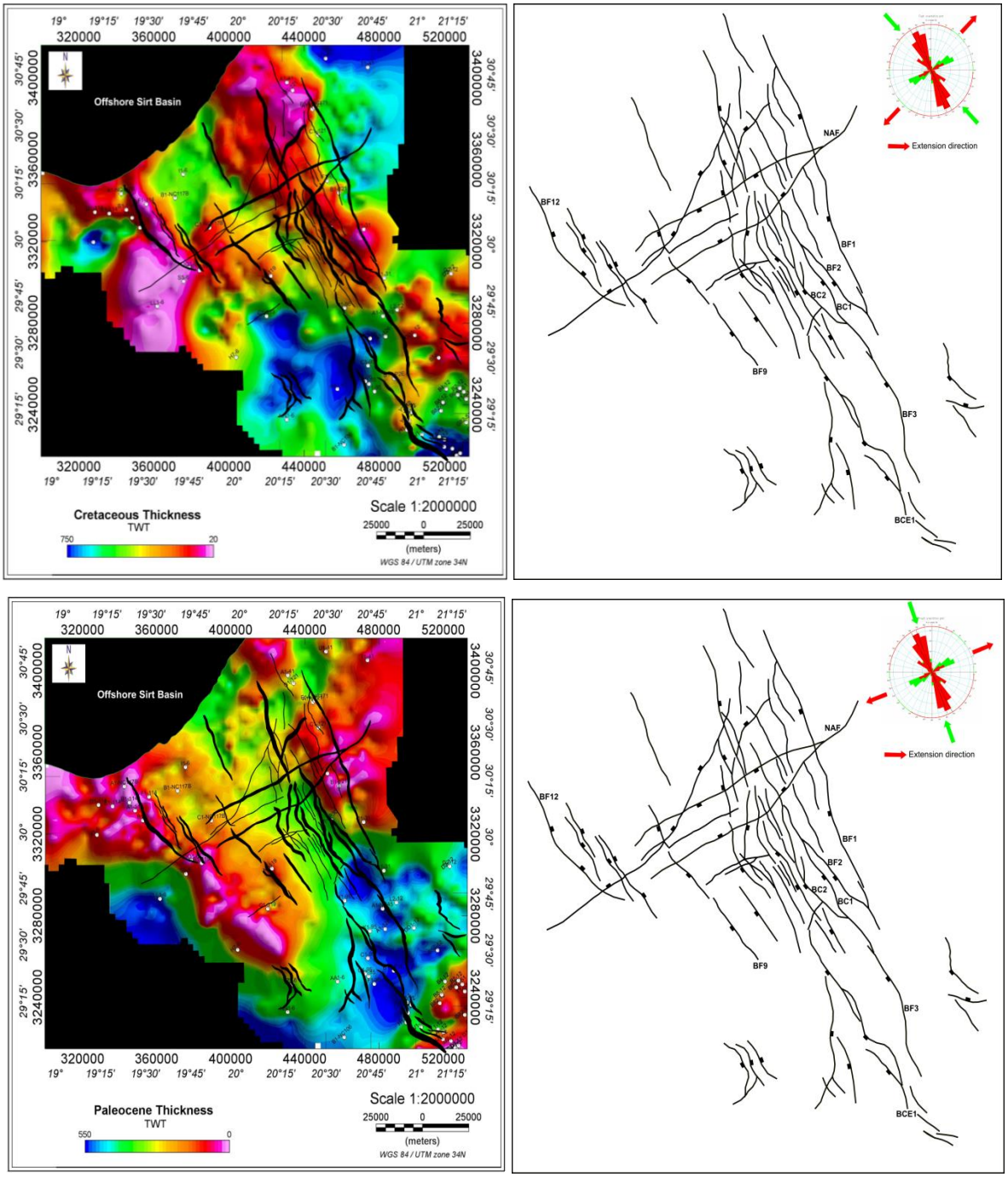

Figure 7.58: Isochron thickness maps illustrating sediment thicknesses and depocentre migration of the: (a) Pre – Upper Cretaceous with increased hanging wall thickness in the graben toward the southwest and northeast, indicative of syn-sedimentary faulting during this time. (b) Paleocene where the depocentre migrated southward. (c) Eocene where the main depocentre migrated north. (d) Oligocene where depocentre migrated further north with increasing sediment thickness (e) Miocene where the main depocentree slightly shifted to the north with increase in sediment thickness. Increase in thickness toward the NE indicating tilting of the Ajdabiya Trough towards the northeast and increase of fault activity along the main trough bounding faults. Internal unconformities are thought to have caused some of the thinning of the Cretaceous – Miocene sequences highlighted by areas of low thickness.

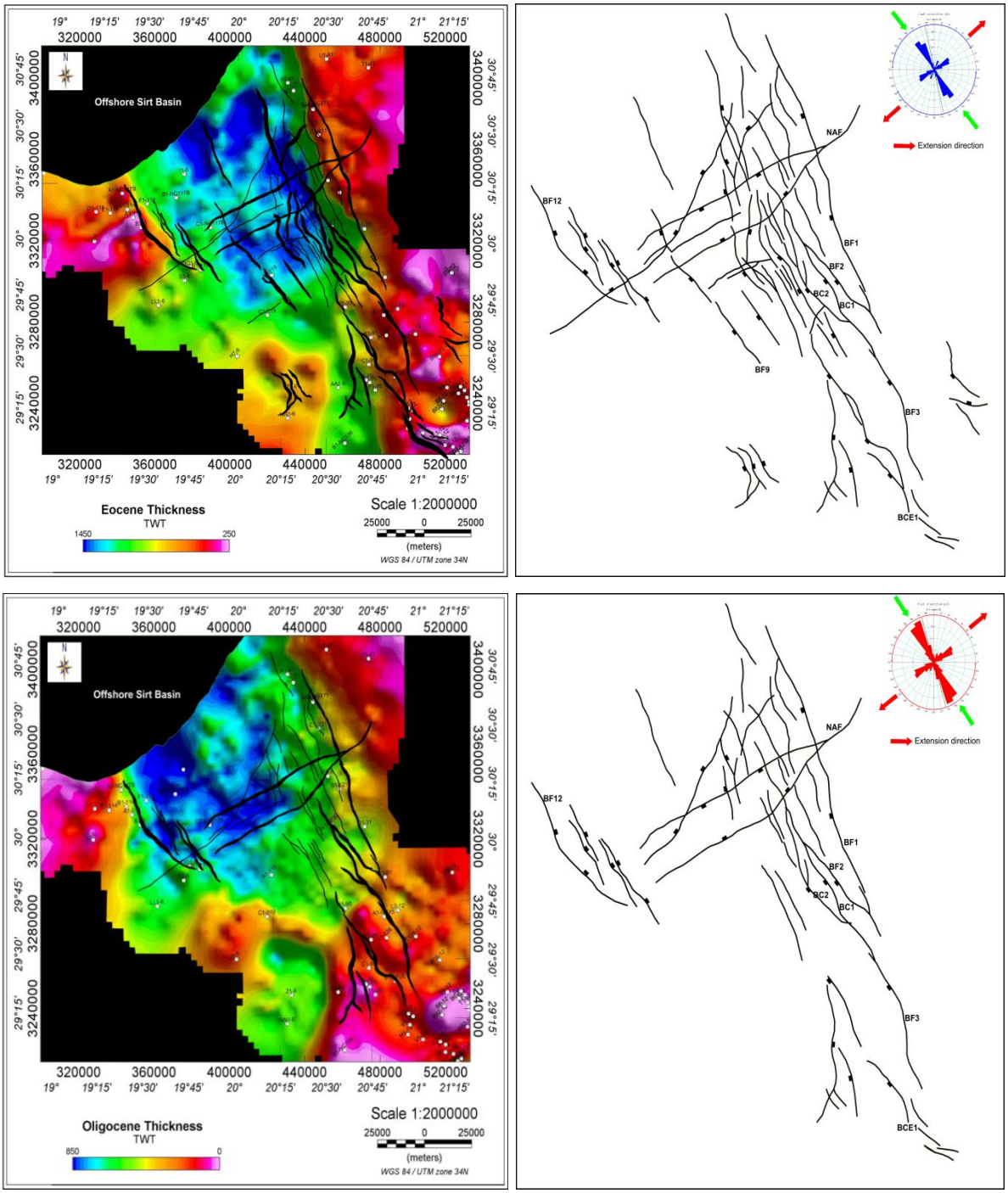

Figure 7.58 continued

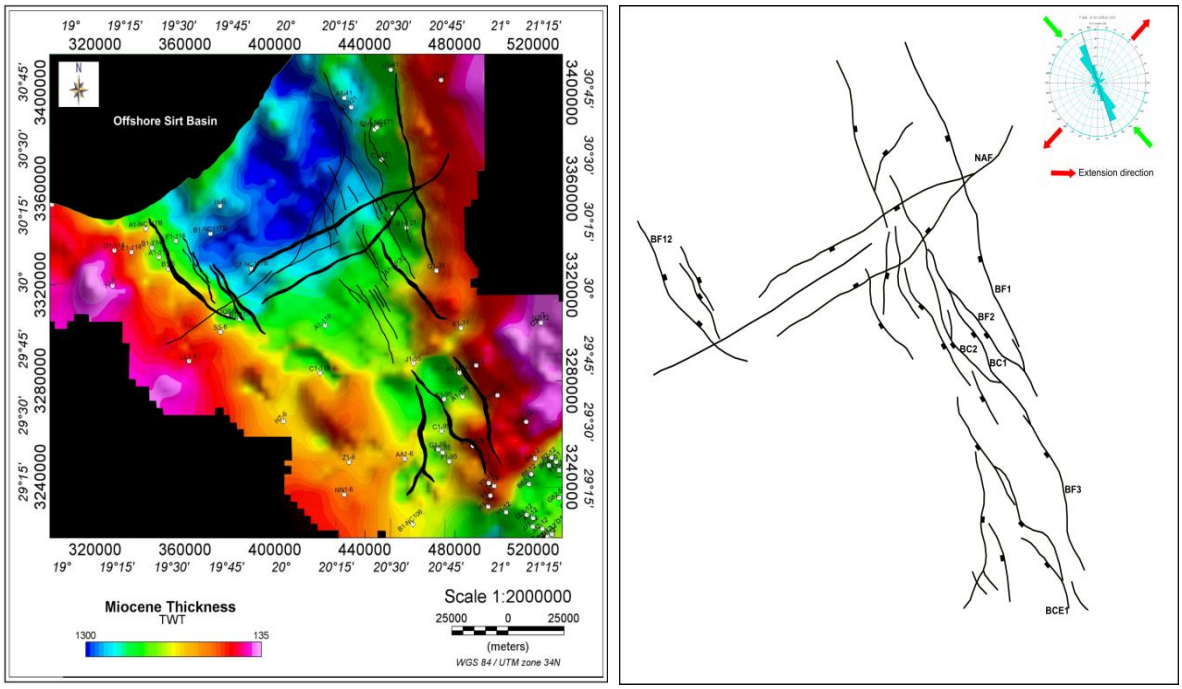

Figure 7.58 continued

An episode of transtension in the Sirt Basin corresponds to the second stage of the Syrian Arc inversion event affecting North Africa during the Paleocene – Eocene. Onset of the event coincides with slowing in rate of convergence between Africa and Europe (Klitgord & Schouten ref in Abadi, 2002) and change in spreading direction in central Atlantic (Dewey et al., 1989 ref in Abadi, 2002). Within the Ajdabiya Trough, a period of intense rifting resulted in abrupt deepening of the trough and finally deposition of thick Eocene sediments (Figure 7.58) (Abadi 2002). Along the North African Margin, NE-SW extension between Africa and Arabia continued into the Oligocene. Extension probably continued through to the early Mid Miocene during the Red Sea extension phase. Coupled NE extension and NW compression may have been the driver for renewed dextral strike-slip movement on E-W faults in eastern Ajdabiya Trough and Cyrenaica Platform with local development of normal fault arrays.

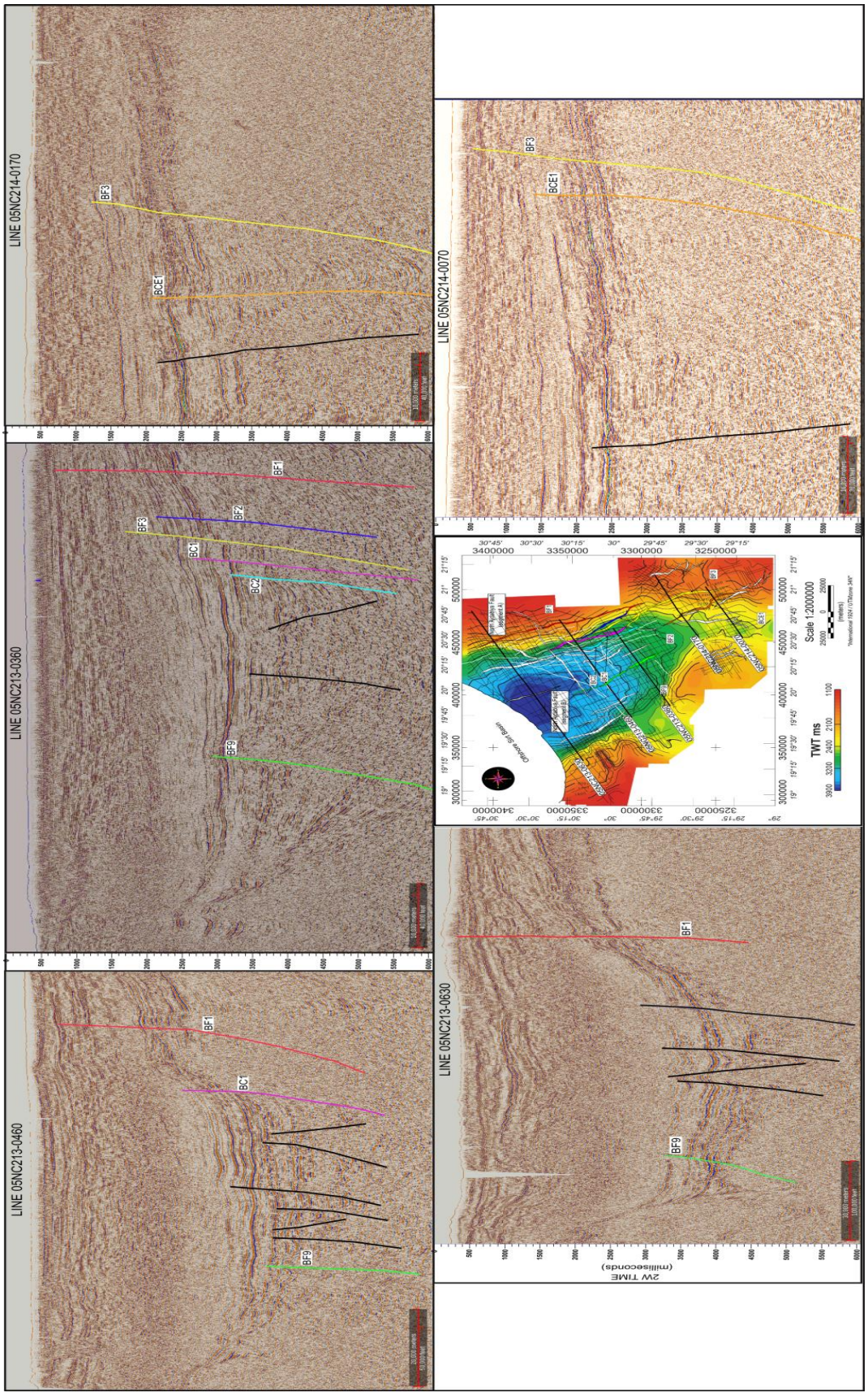

Figure 7.59: Series of NE - SW oriented reflectivity cross-sections across the study area illustrating the major regional variation in fault evolution along Strike and propagation caused by reactivation of the deep-seated fault segments.

7.3.5 Fault Array Summation and Strain

In order to estimate extension rates and strain accommodated by faulting. A group of fault displacement versus distance profiles were constructed for the selected faults in the Ajdabiya Trough. The profiles include plots of individual displacement, fault array displacement summation and strain. The TrapTester software extracts throw fault attributes from fault polygons along sample lines oriented perpendicular to the average strike of the faults. Sample line spacing (in the horizontal) was 5000 m and the initial and the last position of the sampling line are shown in the map views outlined by 8 small white rectangles.

7.3.5.1 Middle Cretaceous

Figure 7.60 show four different plots of fault array summation and calculated strain for faults cut middle Cretaceous surface with mainly NW-SE and slightly N-S strike. The first one is for the all mapped faults that cut the middle Cretaceous surface with NW-SE and NE-SW strikes (in the map view the area surrounded by the large sampling lines square and yellow outline). The second one is for the mapped faults with strike NW-SE along the eastern part of the Ajdabiya Trough (in the map view the area surrounded by the sampling lines square). The fault displacement versus distance profiles for these plots show the aggregate vertical offsets (throws > *ca*: 300ms TWT), the fault array summation, and the strain for variable fault numbers. The fault that shows a highest apparent throw in the two plots is fault BF3, which shows a throw of (> *ca*: 100ms TWT). It is observed from the seismic profiles that the BF3 has large fault movement on Pre-Upper Cretaceous horizons defined by growth of strata within the hangingwall of the fault. The first two plots show similar displacement and strain summation character and sharing the same effect of possible strain localization along the eastern part of the Ajdabiya Trough.

The faults along the western side of the trough also show an important aggregate vertical component of displacement (dashed line) ~*ca*: 160ms TWT and show also important strain range. In contrast, the last plot in the series is obtained for the faults mapped in the southern part of the Ajdabiya Trough with aggregate vertical displacement > *ca*: 250ms TWT, but the strain summation curve show that the strain is decreasing gradually towards the south.

For this analysis some faults did not have sufficient data which can result in underestimation of cumulative throw.

7.3.5.2 Upper Cretaceous

In the Upper Cretaceous data shown on figure 7.61, the BF3 is the dominant fault which has high displacement range (~ ca; 130ms TWT) compared with the other faults located in the footwall of the BF3 fault (BF1and BF2).

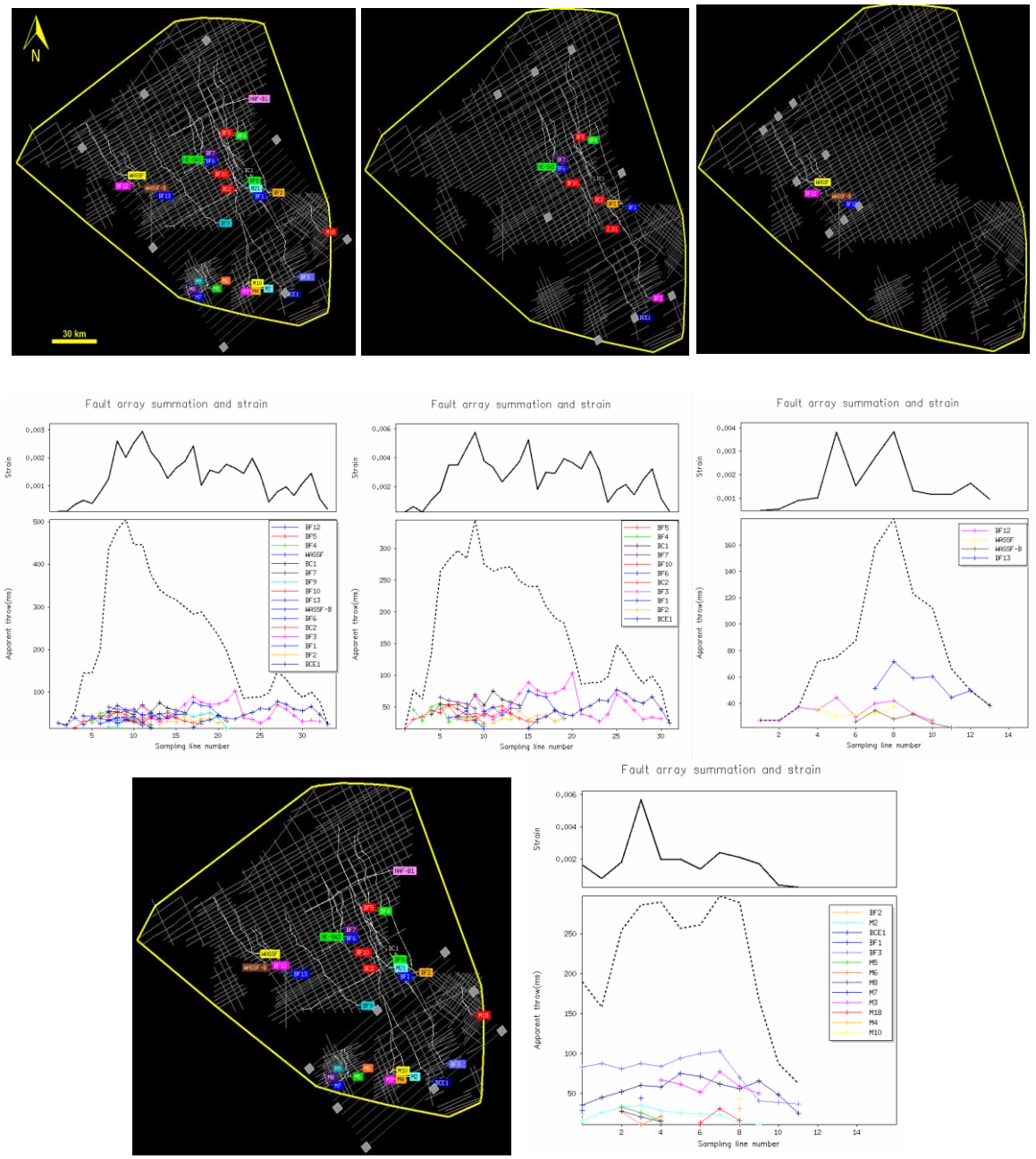

Figure 7.60: Plots of individual and aggregate fault throw, and fault related strain vs. distance with appropriate maps displaying the faults effecting Middle Cretaceous horizon outlined by yellow line. The maps show the sample lines with fault polygons corresponding to four different areas within the Ajdabiya Trough indicated by NW-SE and N-S striking faults.

At the same time the strain summation curve is characterized by three clear spikes with the highest range is observed at the southern part implying increase of strain as well as increase in the cumulative displacement as observed from the first plot in figure 7.61. At the region of high strain and high displacement, there is a good correlation between group of faults (BF2, BF3, BCE1, and M12).

The point of intersection between these faults suggests a zone of possible fault nucleation or re-activation during Upper Cretaceous time. In certain circumstances, the cumulative throw does not resemble a continuous curve due to the faults being widely spaced. In general, it is observed that the displacement in the northern part of the trough gradually increases up-section younger at region cut by the fault BF8 trending NE-SW which could represent a transfer zone where displacement is transferred between adjacent faults. In the third plot to the south, the cumulative displacement and strain curves show a gradual distribution with maximum values at the central area between the faults BCE1 and BF3 implying strain localization and wide range of fault activity in this region.

7.3.5.3 Paleocene

The strain value (Figure 7.62) ranging between 0.02 - 0.04 is lower than the observed strain for the Upper Cretaceous section. These values are seemingly generated by the Ajdabiya Trough bounding faults such as BF12 at the northwest and the BF3 to the east. Additionally to the high value of fault-related strain, fault BF3 has the second fault throw pattern and represent the dominant fault in the total cumulate throw curve supporting the idea that cumulative maximum displacements increase with the increases of fault length (e.g. Walsh & Watterson 1988, Cowie & Scholz 1992). Also Nicol et al., (1997) suggest that long term fault displacements rates are constant and strongly depend on the size of the moving faults. The fault plane with highest throw near the edges of the fault (Figures 7.28 and 7.29) is consistent with displacement pattern of segmented fault. The plots for faults with strike NW-SE show higher strain values than those for faults with strike NE-SW. The data show clear differences between individual segments of the faults concerning the total fault cumulative displacement. This suggests individual deformation histories of the studied fault segments, possibly depending on their orientations and the local stress conditions both influencing the time dependent strain accumulation pattern.

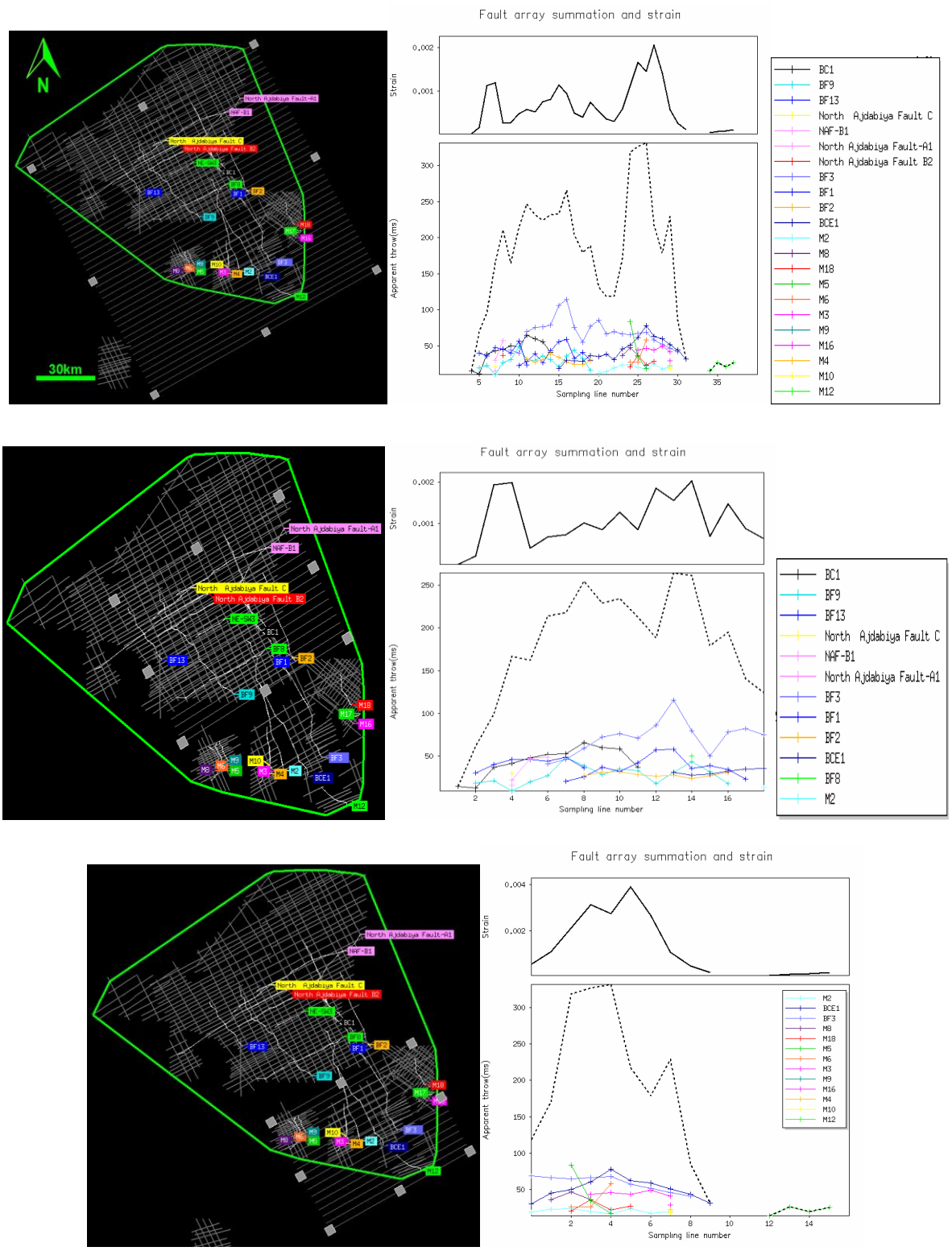

Figure 7.61: Plots of individual and aggregate fault throw, and fault related strain vs. distance with appropriate maps displaying the faults effecting Upper Cretaceous horizon outlined by green line. The maps show the sample lines with fault polygons corresponding to two different areas within the Ajdabiya Trough indicated by NW-SE and N-S striking faults.

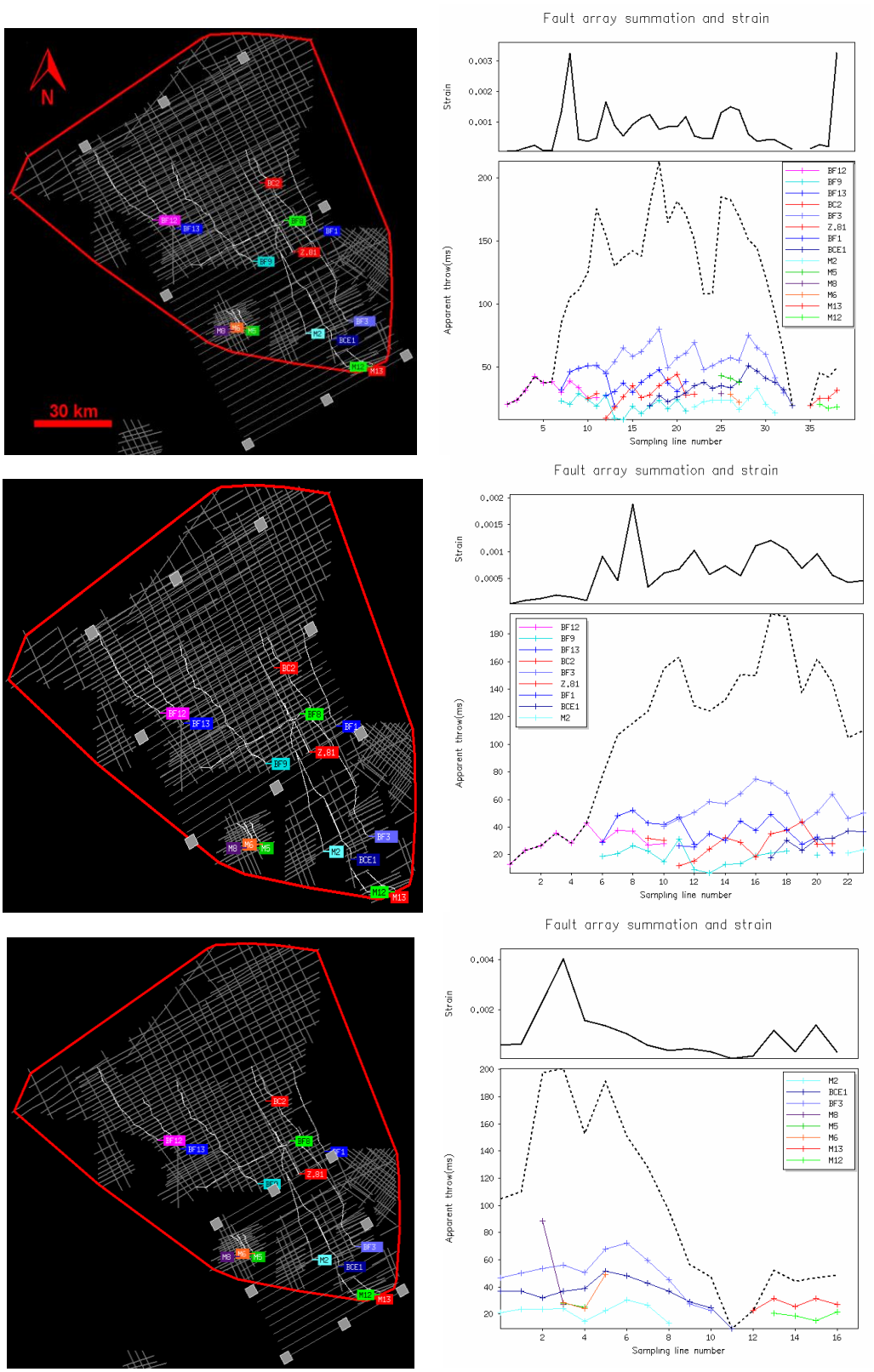

Figure 7.62: Plots of individual and aggregate fault throw, and fault related strain vs. distance with appropriate maps displaying the faults effecting Palaeocene horizon outlined by red line. The maps show the sample lines with fault polygons corresponding to two different areas within the Ajdabiya Trough indicated by NW-SE and N-S striking faults.

7.3.5.4 Eocene

During the Eocene displacement on faults is increased gradually towards the north (Figure 7.63) with increasing thickness of the Eocene sequence as observed on the Eocene thickness map (Figure 7.58) show possible fault growth activity in the north part of the Ajdabiya Trough. This can be correlated with the hypothesis that strain could be migrated to the north during possible period of Eocene extension following a distinctive period of uplifting (e.g. van der Meer and Cloetingh, 1996).

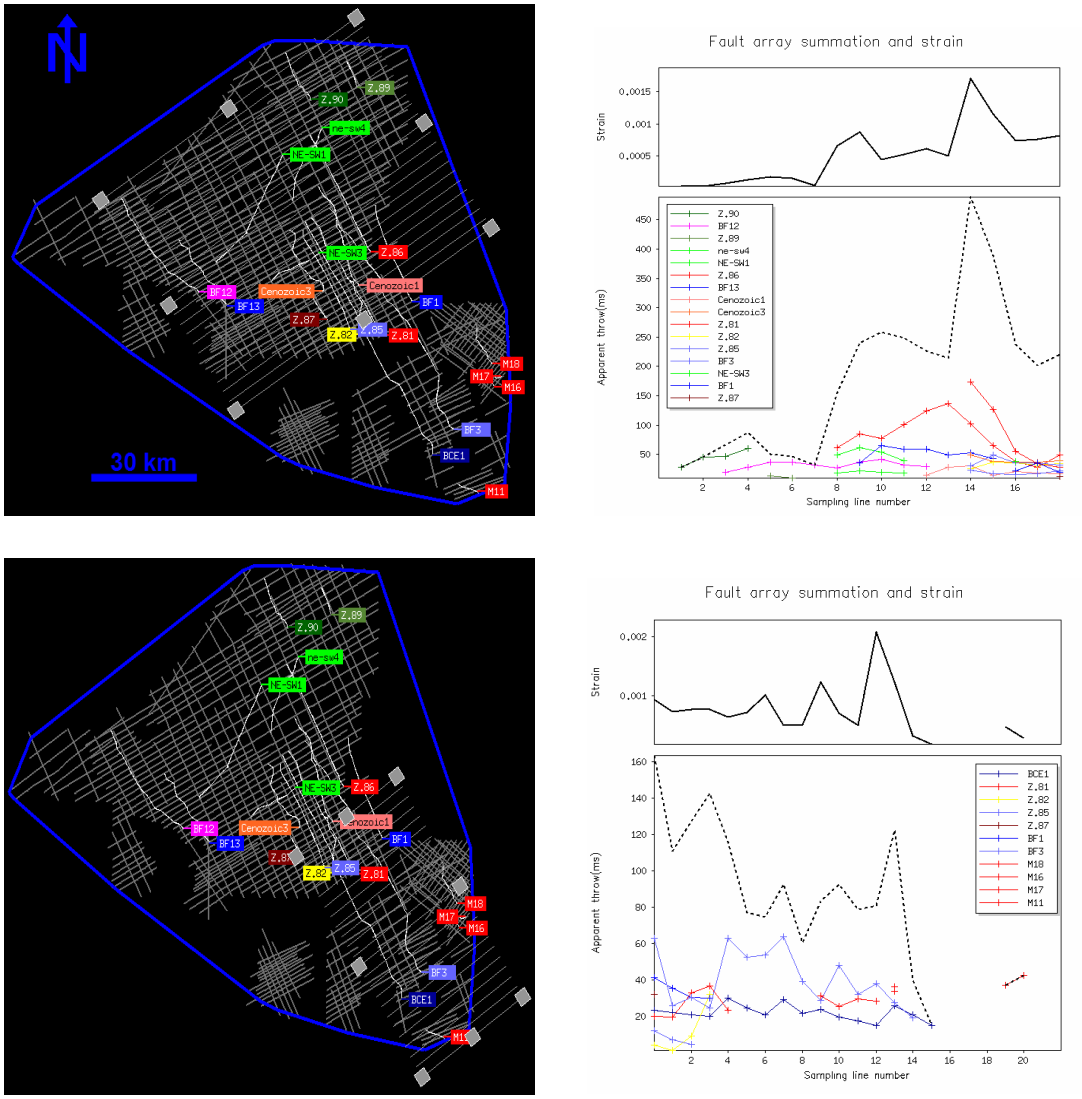

Figure 7.63: Plots of individual and aggregate fault throw, and fault related strain vs. distance with appropriate maps displaying the faults effecting Middle Eocene (Gialo) horizon outlined by blue line. The maps show the sample lines with fault polygons corresponding to two different areas within the Ajdabiya Trough indicated by NW-SE and N-S striking faults.

7.3.6 Spatial Distribution of Faults and Extension in the Ajdabiya Trough

In order to document faults activity and constrain their spatial development through time, a series of seismic horizons (Upper Cretaceous – Miocene) were mapped throughout the study area. The mapped horizons are used to produce thickness maps and to constrain the range of fault distributions and activities. Fault movements and syn-depositional fault activity can be expressed on isopach maps and seismic profiles through the variability in the thickness variations between hanging wall and footwall of the active faults, and throughout the development of possible rollover features (fold structures) and the thickening of sediments on the hangingwalls (wedging of reflectors) of the active faults.

The seismic data indicated that fault activity in the Ajdabiya Trough actually decreased through time and summarised that the number of active faults actually decreased through the Cenozoic period. Progressive extension could be continued during the Cenozoic owing to possible deformation that developed by a thermal regime as outlined from the subsidence analysis (chapter 6).

During the initial phase of extension, sediment supply presumably outpaced the rate of tectonic subsidence so that a true measure of fault activity can be inferred from the coeval syn-rift stratigraphy (e.g. McLeod et al., 2000). Unfortunately the lack of 3D seismic data and very detailed biostratigraphic information make it difficult to illustrate the depositional response to faulting, and make detailed interpretations of fault linkage, fault segmentation or changes in fault displacement rates.

Fault analysis using the 2D seismic data show that there is a dramatic decrease in the numbers of active faults and fault growth rate during the Cenozoic which suggest that no active brittle crust extension occurred during post-rift period.

The first extension period in Sirt Basin lasted ~119 – 130 Myr during the opening of the south Atlantic was associated with a large zone of diffuse deformation across the Ajdabiya Trough, which accompanied with deepening to the north of early formed Triassic basin associated with the opening of the eastern Mediterranean and characterized with continues regional extension along NW-SE trending faults with maximum fault throws of hundreds of milliseconds (TWT) observed from 2D seismic analysis in this study.

It has been suggested that Triassic faults initiated with diffuse crustal extension in North African basins including the Sirt Basin (Guiraud, 1998; Coward and Ries, 2003). Within the

Ajdabiya Trough, these faults trending NE-SW with several kilometres length and dipping SE and NW both towards and away from the eventual rift axis in the trough and could have been initiated during this Triassic incipient rift stage in the Sirt Basin.

However, some faults along the rift axis began to emerge as the dominant set controlling subsequent depocentre development within the trough with strain localised onto mainly basin ward dipping faults concentrated along the eastern boundary of the trough (e.g. Figures 7.12,7.13, 7.58, and 7.65). Strain localizations typically observed in basin scale faulting have been studied by incorporating movement along pre-existing structural elements, like earlier formed faults (e.g. McClay, 1989; Kusznir and Ziegler, 1992; Van Wees et al., 1996).

The seismic data (Figures 7.21, 7.22, 7.33, 7.40, and 7.47) show that during period from Paleocene to Eocene, deformation in the Ajdabiya Trough possibly reactivated earlier faults and produced an asymmetrical basin profile with increasing depth to north. Rapid subsidence during the Oligocene and Miocene observed from the subsidence analysis (chapter 6) was accompanied by additional deformation and faulting along the edges of the trough (Figures 7.22, 7.45, and 7.47).

Extension accommodated by variable structures including faults within the Ajdabiya Trough is quantified by summing fault heaves (cumulative heaves) along straight lines oriented at high angles to the main trend of the mapped faults. For each fault, I measured its distance from the start point of the line, and its heave. Uncertainty has not been considered in these measurements which could be related to errors due to early low accuracy heave estimation and variation of fault trends with respect to sampling lines. The obtained data from group of lines (Figure 7.64) can be examined by plotting the estimated heaves against the distance along the lines (Figures 7.65). The cumulative heave diagrams show the distribution of extension along each sample line.

Smaller and larger extensions are represented by low gradient and steep slopes respectively, while constant gradient indicate homogenous deformation. Localized deformation is indicated by rapid change in gradient.

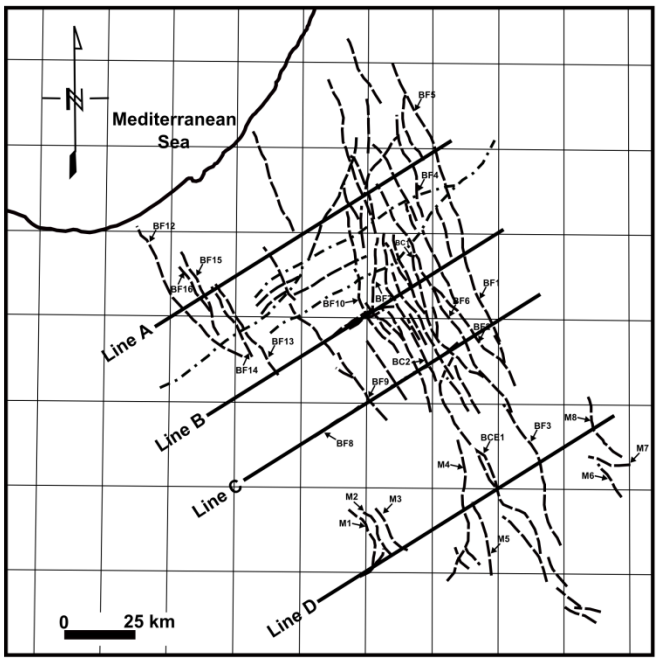

Figure 7.64: Map of the study area. Long dashed lines show fault traces mapped in this study. Locations of the modelled lines are shown by orthogonal thick lines.

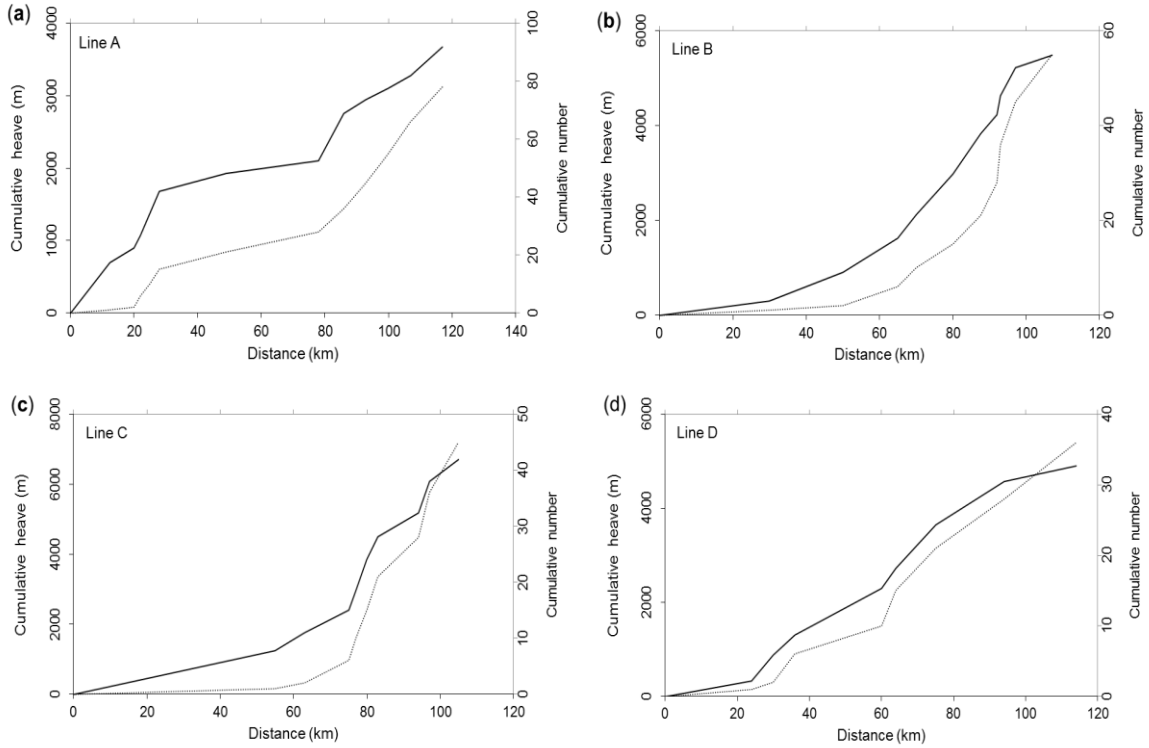

Figure 7.65: Cumulative heaves (solid lines) and numbers (dashed lines) plotted against corrected distance (traverse length) for selected NE-SW trending lines (A-C). Left vertical axes show the cumulative heave, right vertical axes show the cumulative number of modelled faults along each line.

Observations from the line (A) which has a length of about 120 km and intersects 12 mapped faults show abrupt increase in extension at the beginning of the line which indicate larger extensions followed by almost constant gradients indicate homogeneously distributed deformation extended for about 60 km along the centre of the trough and possibly suggesting a well-established fault segments whilst large steps and gradient changes indicate localized deformation. The faults along this line encountered heaves ranging from about 150 m to 700 m.

In line (B), the faults show lower total extension to the west compared with line (A), due to not crossing much faults. The largest accumulated heave encountered along this line is about 850 m and show a higher accumulated heave along the same fault zone compared to the line (A). However, the extensions recorded for the modelling lines does not compare well with variations of stretching factors obtained during subsidence analysis (chapter 6 and Figure 7.66) at certain areas due to not crossing any mapped faults.

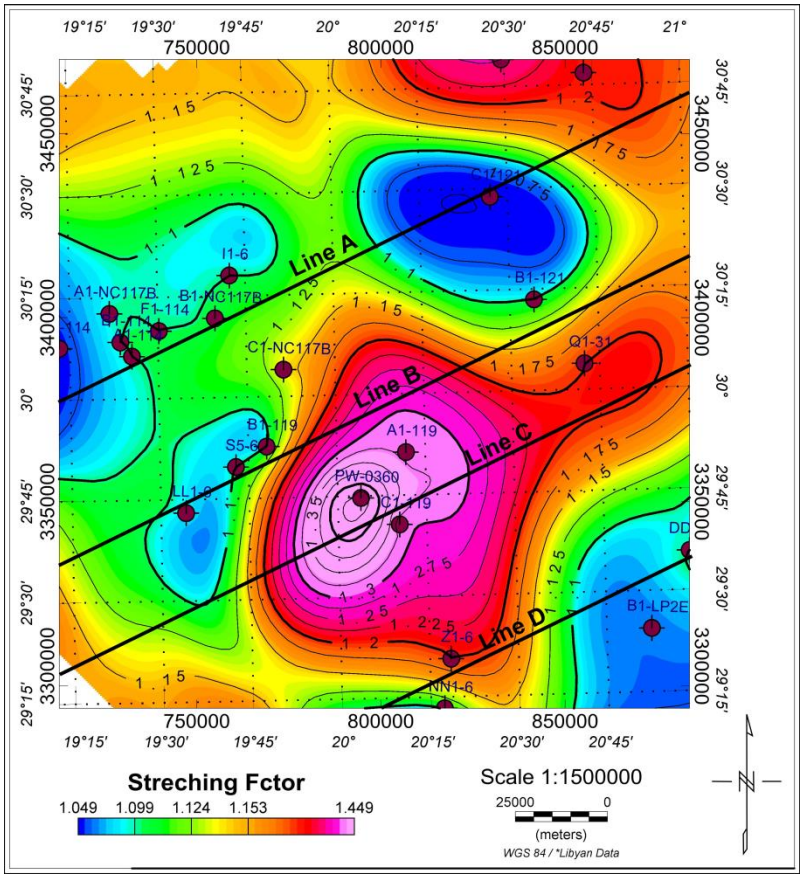

Figure 7.66: Map of Upper Cretaceous stretching factor distribution in the Ajdabiya Trough with location of modelling lines.

In correlation with the stretching factor data, the relatively low crustal stretching values are compared to moderate angle normal faults, in contrast in areas of high crustal stretching the faults become rotated to low dip with continues fault activity and possible generation of new set of faults (e.g. Reston, 2009).

The distinct distribution of the mapped faults within the Ajdabiya Trough provides information about their spatial and temporal evolution. The faults seem to be linked through time. The major faults in the study area most likely they nucleated at nearly the same time, with other subordinates probably continued to nucleate. Small faults mapped could be represent late stage features and may be accommodate low strain deformation. This can be supported by the idea that large faults are surrounded by low deformation zones with increase of fault length.

The cumulative heave plot (Figure 7.65) shows a gradual increase of the extension with low values at the about 60 km along line (C), due mainly the line not crossing any faults. The area of faulting along the line is represented by zones of increasing strain and can be seen as a change in slope of the heave-distance curve.

The line (D) has a length of about 120km and encounters 9 faults. Both cumulative heave and fault spacing appear homogenous. The mapped faults within the Ajdabiya Trough trend normally to the extension direction and some faults trend parallel to the early rift axis.

The line profiles show that faults at the eastern part of the trough have a wider range of extension than faults elsewhere and I conclude that these faults may form under distinct stress system oriented orthogonal to the man fault trend in the Ajdabiya Trough or possibly formed as a result of a secondary stress system localized along eastern boundary.

7.3.7 Fault Segmentation

Many of the mapped faults within the Ajdabiya Trough have longer fault lengths (up to 100km (Figure 7.4 & 7.5) and accumulate moderate throws on mainly Cretaceous horizons (Figure 7.65). The faults are possibly segmented by cross-cutting faults or have numerous faults that abut them. The displacements are consistent along strike of these faults and their cumulative throw profiles are symmetrical.

Fault throw attributes show that maximum throws are near the centre of the faults and minimum at the fault tips a characteristic of isolated fault. Along the fault surface, there are a

regions of alternating maximum and minimum throw indicating that the majority of the faults are composed of number of isolated segments as each segment has a throw range that is consistent with its adjacent segment, these can be considered as coherent structures and not isolated fault segments that have aligned and linked (Walsh et al., 2003).

7.4 Discussion

7.4.1 Timing of Fault Activity in the Ajdabiya Trough

Seismic data from the Ajdabiya Trough provides numerous examples of fault systems which must have an early origin. The timing of fault activity has been quantified for the mapped faults using 2D seismic profiles (divergent hangingwall reflectors), throw-depth plots and isochron/isopach maps. The 2D seismic part is based on an analysis of the amount of offset on each mapped horizon cut by the fault (e.g. Childs et al., 2003).

Vertical separations for the mapped horizons have been estimated by measuring the difference in elevation of these horizons in the footwall and hanging wall of the faults assuming that sedimentation keeps pace with subsidence produces a thicker sedimentary sequence in the hangingwalls (Childs et al., 2003). Because the sediments are being deposited whilst the faults are active, younger strata dip less steeply than older strata, which will have been subject to a longer history of fault movement and greater offset than the younger strata indicating syn-depositional rotation of the hanging wall blocks.

Studies on fault reactivations have reported that pre-existing faults serve as nucleation sites for new faults which mainly controlled by the fault fabric and the existence of possible zone of weaknesses in addition to the strain magnitude during variable phases of extensions (e.g. Henza et al., 2010). The 2D seismic data shows that Early Cretaceous fault initiation is the dominant fault population of the Ajdabiya Trough faults that dipping consistently to the SW and NE. It is represented by normal faults that bound NW-SE trending graben features. The timing of fault activity within the trough shows that the majority of the faults are initiated early during the basin forming time (Collapse of Sirt Arch during Early Cretaceous) and the number of faults are broadly increased and controlled by a continuing subsidence along the trough bounding faults, which accommodated the large amount of strains during extension

periods. This could be formed as oblique faults and controlled by underlying pre-existing Pan-African basement fabrics and ENE-WSW trending late Paleozoic structures

Some of the NW-SE trending faults are mostly formed during the initial rift stage, ie they are associated with the main trough bounding faults and formed by different extension stages during the Cretaceous time and probably reactivated during the Paleocene – Eocene times. In this case the early fault fabric has not adequately developed and the strain has been partitioned between faults. When the extension is rejuvenated within the trough (e.g. Guiraud and Bosworth, 1997), a system of oblique faults has been formed in the northern part of the trough as a consequence of well developed fault fabric. Along the north and eastern parts, these faults accommodated the whole strain.

A change in plate-motions occurred around 84Ma, and caused the African and Arabian Plates to strongly rotate in an anticlockwise direction and by doing so initiated the onset of collision with the Eurasian Plate (e.g. Guiraud and Bosworth, 1997; Guiraud et al., 2005). As a result the Late Cretaceous corresponded to a first episode of regional compression in North Africa, linked to the Alpine cycle. A regional NW-SE to NNE-SSW direction of shortening was established during this period, which caused major inversion of the Jurassic – Early Cretaceous rift basin in Cyrenaica Platform during the Santonian (e.g. El Arnauti et al., 2008). At the same time, major subsidence occurred in the Sirt Basin controlled by NW-trending structures. The range of fault orientations likely reflects the conflicting influences of the early NW-SE regional extension direction and the dominant ~N-S trending basement fabric within a regional context of a Gondwana wide extensional event or during second phase of Gondwana breakup (Late Permian – Jurassic). The Mid to Late Cambrian extension (510-490Ma) corresponds to a Gondwana wide event, with relatively minor effects in North Africa (e.g. Guiraud et al., 2005). Weak extensional deformation caused the systematic occurrence of hiatuses or unconformities in the continental and passive margin sequences that were deposited across Libya during the Cambrian and Ordovician. Evidence of major fault movement is scarce, and the inferred weak NW-SE tensional stresses likely only reactivated NE-SW faults striking almost perpendicularly to the direction of extension. Some NW-striking faults may also have been reactivated as transfer structures accommodating growth on the NE-oriented faults.

From about 195 Ma, the opening of the mid Atlantic was accompanied by separation of North Africa and Europe along a major sinistral transcurrent shear zone (e.g. Anketell, 1996). South of this zone throughout Libya and North Africa, NE-trending growth faults, some reactivated during the Late Permian-Triassic, developed along a marginal zone of extended crust, partitioned from unaffected areas to the south by major Pan African NW-trending crustal fracture zones (Najd faults). The magnitude of extension was controlled by the fabric of the basement terranes being extended. In the Ajdabiya Trough, the eastern boundary faults in this study are represented by series of linked faults among them the BF1 and BF3 fault zones (Figures 7.4 & 7.5). These faults die out northwards along strike, terminating in structural lows near the Amal Plarform to the northeast (Figures 7.4 & 7.5). Similarly, the BF9 and related fault blocks western Ajdabiya Trough die out northwards (Figures 7.4 & 7.5), producing the much wider hanging wall synclinal flexure to the southeast (Figures 7.36, 7.46, and 7.47). A comparable time-progressive but eastward evolution of the mapped faults is shown by the BF3 fault and the related, synthetic faults BC1 and BC2 (Figures 7.21, 7.22, 7.27, and 7.36). The critical observation regarding absolute timing of initiation of this oldest fault group is the possible occurrence of thickened pre-Cretaceous (Permo-Triassic and Jurassic?) strata adjacent to the faults in the lower parts of the Ajdabiya Trough. These basinal strata are in turn overlain by Upper Cretaceous deposits, indicating a prolonged fault activity. Deep-seated, local and regionally preserved Jurassic strata are also found in drilled wells eastern Ajdabiya Trough (e.g. El Arnauti, and Shelmani, 1985). BF3 and BF9 faults are characterised by a thick pre-Cretaceous strata at the base of their hangingwalls as shown on most of the seismic sections. Thus, the initiation of faults BF3, and BF9 may have covered a time span from the Permo-Triassic to Early Cretaceous. Another closely related fault set represents WNW-dipping planar normal faults that affected the strata up to the base-Cretaceous level and formed antithetically and exclusively in the hanging walls of BF3 and BF9. The faults define opposing fault systems that bounded initial pre-Cretaceous basins. These observations suggest that faults may have started as growth faults in an early-rift stage (likely Permo-Triassic and Jurassic), while the antithetic faults formed later in the time period Early Cretaceous and became further developed during a subsequent syn-rift stage during Early to Late Cretaceous time.

The BF3 fault plane has a complex throw contour geometry (Figure 7.29), and a complicated history. The horizontal zone of minimum throw occurs at the top of the growth sequence and, by definition, maximum displacements occur at the base of thickened hanging-wall sequences with minimum displacements at the top. There is a contrast between the timing of faulting from south to north. In the north there are two separate periods of growth; the main period occurred in the lower zones of the Upper Cretaceous level and the other period occurred during the Paleocene level. In the south, the growth faulting is less consistent. The decrease of the fault growth coincides with lower throws and the approximate N-S strike of the southern segment. In the Pre-Upper Cretaceous, the latest movements in the south post-date those of the north NE-SE striking segment in two episodes of rifting. In the south, growth occurred in the Pre-Upper Cretaceous interval, whilst an earlier Paleocene phase was significant in the north.

The 2D seismic data and the isochron maps indicates that most of the faults mapped in the southern Ajdabiya Trough had significant syn-sedimentary movements during deposition of the Pre-Upper Cretaceous sequence, while displacement across other faults was dominantly post-depositional. This is very consistent with the high subsidence rates obtained from the subsidence analysis (chapter 6) in this part from the trough. Lateral changes in the Late Cretaceous – Paleocene demonstrate active faulting coeval with rapid subsidence (Selley, 1997). The seismic interpretation indicates that most of the mapped faults displaces Eocene and older sedimentary rocks, but does occasionally not offsetting the Oligocene strata suggesting that fault movement in the Ajdabiya Trough was Eocene and older (Figure 7.38).

From the Eocene onwards, the Ajdabiya Trough is characterized by a uniform stratigraphy, implying little local movement on the faults and thin skinned deformations. The seismic data shows that the trough bounding faults exhibit negligible throw across the Tertiary reflections and do not cross cut the above reflections, which means that there is no clear and significant fault growth during the Cenozoic except for the Paleocene to early Eocene times. This along-strike variation in the timing of faulting is also reflected in the sediment accumulation, with the thickest accumulations observed in the hangingwalls of the faults indicating fault growth activity during Cretaceous – early Eocene.

The faults were not completely quiescent; however, there is evidence for an episode of inversion during the Miocene (Selley, 1971). This is recently challenged by El Arnauti et al., (2008) over the Cyrenaica region and the eastern Ajdabiya Trough.

The subsidence is punctuated by periods of decelerating subsidence rates from Early Cretaceous to Miocene time related to periods of tectonic quiescent or change in tectonic regimes. For instance, during the Maastrichtian movement on faults slowed, with progressive shallow upward of Upper Cretaceous to Lower Palaeocene carbonate facies (e.g. Kalash Formation). It is observed that the timing of movement on the BF2 fault (Figures 7.26, 7.27, 7.36, 7.45, and 7.47) is uncertain, although the fault appears to have been active during the formation of the Cretaceous – Early Eocene. The folding observed in the footwall of the fault is largely related to strike-slip movement on fault BF3.

The faults bounding graben features in the south-west are established along with a number of smaller faults. Thus during the early stages of faulting and graben formation, the main elements of the present-day structure were likely already established.

These faults appear to be focussed within the existing grabens, with very few forming in the centre of the area. The subsequent fault set, which formed prior to the deposition of Eocene show a similar fault pattern, particularly in the north-eastern part of the Ajdabiya Trough where several faults form within the hangingwalls of the bounding faults owing to strain migration and localization. However, this fault set includes some large faults in the centre of the area.

7.4.2 Fault kinematics

The analysis of the Ajdabiya Trough fault kinematics using the 2D seismic data can not be revealed properly and the subtle details of fault plane structure and localised deformation will generally be underestimated. The general structural framework of the Ajdabiya Trough fault system is built on a hypothesis of basement fabric reactivations and the fault arrays form complex dip slip fault pattern during rifting (e.g. Morley et al., 2004). Oblique slip faults are difficult to distinguish in the area owing to the lack of 3D data and outcrops. The mapped fault arrays in the Ajdabiya Trough can be subdivided into variable kinematically and geometrically distinct groups characterized by a thick skinned basement fault system and other cross cut faults formed during rifting and periods of fault reactivations and thin skinned

fault arrays that form due to gravity driven mechanism or mechanical compaction during basin subsidence. The cross-faults appear to reactivate older faults in the underlying basement.

The active fault system also includes a major NE-striking sinistral displacement zone located at the NE border of the Ajdabiya Trough near Cyrenaica Platform (e.g. Anketell et al., 1996; El Arnauti et al., 2008) and several NNE-striking normal faults branching off from the strike–slip system and formed as a riedel shears. Both Cyrenaica Platform and the Ajdabiya Trough are separated by a fault system, where NW-SE strike–slip faulting is combined with significant vertical movement. I presume that the majority of the active faults in the Ajdabiya Trough are reactivated basement structures with both dip slip and strike slip components. The strike slip is possibly due to strain partitioning formed during transtension regime which represents combination of dip-slip and strike-slip deformation. Subsidence during Cenozoic is higher and related to the reactivation of a Miocene extensional strike–slip duplex at a releasing bend along the NE-SW strike–slip fault in the north-eastern part of the Ajdabiya Trough.

7.4.3 Temporal and Spatial Fault Evolution

The NW-SE trends of the Sirt basin are related to the late Cretaceous extensional (Late Neocomian) phase and seem to truncate other tectonic trends. ENE trends are inherited Late Palaeozoic origin, and probably activated from earlier basement trends. This is especially characteristic of a major trend in central Libya extending from the Gargaf Arch in W Libya (Figures 7.2 & 7.3) to the eastern Libya. This trend was subsequently activated during the Triassic, Jurassic, early Cretaceous and even late Cretaceous and Paleogene. The eastern part of the Ajdabiya Trough is heavily faulted and is related to the underlying South Cyrenaica dextral wrench fault studied by Anketell, (1996). The largest displacement faults offset the Upper Cretaceous-Early Eocene strata and therefore decouple much of the deformation of the basement and the upper strata. Faults cut the Cretaceous interval display significant variations in thickness. The variations in thickness as shown on the isochron map of the Cretaceous sequence represent patterns of activity across some large faults interpreted on seismic sections occasionally show thick graben and wedge shaped half-graben geometry with divergent reflectors. The diverge character of the seismic reflectors correlate with an idea that

subsidence in certain areas are controlled by contribution of possible fault movement provided that the underlying basement faults are active during the Early Cretaceous. There are a clear growth of strata into the hanging-wall and thinning across the footwalls of the faults with development of southwest ward dipping ramp between overlap fault segments. Active faults were identified based on recognition of reflector geometries that define distinct syn-rift wedges (Prosser, 1993). Duration of growth through the recognition of thickness variations across two types of syn-sedimentary faults active and blind faults. The active faults are propagating upward and cut Cenozoic strata, the blind faults do not propagate beyond the Early Eocene. Growth across faults in the north east and south west was more pronounced owing to localized subsidence. Growth faults on the western margin of the Ajdabiya Trough indicate subsidence of over 700m during the late Eocene (Hallett, 2002). The eastern flank of the trough is more complex. It is abuts against the Cyrenaica Platform and the Amal Platform, with a series of terraces which may represent relay-ramp faulting. There has been shift in activity from south to north characterized by thick Cretaceous section observed. For instance fault BF9 display thick Cretaceous section correlated with it is southern segment with thinning across limbs of faulted monocline suggesting that activity across few basement faults continued during the Cretaceous-Early Tertiary. The Cretaceous section thicken to the northeast and southwest as observed from the interpreted seismic sections and the isochron map with noticeable thinning of Cretaceous section across a NW-SE trending boundary parallel to the BF9 fault.

Although many of the basement faults in the central part of the trough became inactive, the margin faults continued their activity. As a result, an imbalance in the rate of sedimentation occurs between the central and the marginal parts of the trough. This also caused the development of the inverted structures (e.g. El Arnauti et al., 2008).

The late Cretaceous was generally a period of extension, with some block faulting, except for a brief compressional phase during the Santonian (e.g. El Arnauti et al., 2008). Growth of compressional folds is observed to offset Paleocene – Eocene level where thinning and onlap over the crest of the folds and thickening around the folds is observed. The combination drag folds and wrench faults have produced spectacular flower structures possibly support the observations of possible pop-up structure from landsat imaging along the north-western part of the Ajdabiya Trough.

The Ajdabiya Trough has completed its first stage of development by the Oligocene (Baird et al., 1996). The wrench faults have been dated as post-Oligocene in age (Anketell, 1996; El Arnauti et al., 2008). Along the eastern side of the Ajdabiya Trough thickness variations of Cretaceous sediments across the mapped faults most likely represent fault activity in a low strain rate localized rift environment. However thickness is increasing across long lived faults of the same generation. There might be possible for new faults generated whilst activity continued on the basement faults. Fault orientation in this case presumably related to rotation of the horizontal extension to more NW-SE direction. Thickening of Cretaceous strata occasionally observed over footwalls and hangingwalls of few faults owing to movement along more steeply segments. There is a clear cessation of fault activity during the Cenozoic time across many parts of the study area with decrease of displacement on the main trough bounding faults. The Cenozoic is characterized by a structurally inactive period in the Palaeocene dominated by basin sag, and a reactivated period of faulting and graben-fill during the early Eocene (Hallett, 2002). The lack of faulting is attributed to the onset of thermal subsidence and relative tectonic quiescence.

7.5 Summary

The Sirt basin part of the Tethyan rift system, with significant rifting and syn-rift sediment deposition in the Permo-Triassic to Early Cretaceous and post-rift deposition in the Oligocene – Miocene. The basin geometry appears to be controlled by structural heterogeneities or weaknesses within the basement (e.g. Pan-African shear zones). The distance from the active plate boundary to the weak zone played a significant role in the structural development and reactivation of pre-existing faults.

In this study 2D seismic data has allowed the distribution of initial rift faults to be mapped across the Ajdabiya Trough, northeast Sirt Basin. It has been suggested that hot spots, active during the early stages of the Gondwana supercontinent break-up, may have weakened the lithosphere beneath the Sirt Basin area, playing a significant role in localization the basin deformation. Our mapping shows that on a smaller scale during rift initiation in the Permo-Triassic and Jurassic, faulting took place along numerous segmented basement faults, which eventually linked up, creating a set of basin master faults in the main rift phases (Triassic – Cretaceous), and probably after. Fault activity was much higher along the eastern boundary of

the Ajdabiya Trough due to strain localization above the pre-existing basement faults identified from the 2D seismic and potential field mapping. The initial rifting strongly influenced the depositional setting and lateral distribution of the post-rift Cenozoic sediments. The analysis revealed that the depositional history of the trough, show the typical subdivision for extensional fault blocks and sub-basins into syn-rift depositional sequences dominated by NW-SE, NE-SW, and E-W trending structures which form a complex, structurally coherent linked fault system and some of them show component of strike slip movement due to possible re-activation and variations in strain directions. Fault reactivation is observed throughout the up-dip clockwise rotation of some propagated basement fault surfaces between the Late Cretaceous and Eocene horizons. Displacement is transferred between different components of the fault system via possible transfer zones. Hard-linkage also occurs possibly across breached relay ramps formed at overlap zones and via NE-SW trending strike slip faults which comprise a minor component of the rift system (strain partitioning). However, seismic data indicate that fault block tilting occurred during the deposition of Pre-Upper Cretaceous strata. On a large scale, this package defines a profound eastward thickening sedimentary wedge, indicating fault block rotations followed by stratal thickening indicating the initiation of tectonic extension leading up to the early Mesozoic phases of rifting. Irregular discontinuous reflectors, rotated by normal faults and increasing thickness towards fault escarpments to the east, characterize the early rift phase and switch to Cretaceous rifting. In Early Tertiary, a post-rift phase controlled by thermal subsidence started. Subsidence data (chapter 6) shows that the transition from thermal cooling and subsidence following the early rift-phase to renewed rifting was gradual and complex. The Tertiary tectonic phases can be regarded as a time of crustal scale thermal cooling with uniform basin-wide subsidence, and with only minor tectonic movement along some of the larger basin faults. Progradding sequences of Upper Palaeocene to Early Eocene age (chapter 5) show a uniform east-west thickness distribution indicating no tectonic influence during deposition, as they were deposited within a relative short time-period.

The rift structures are well preserved in the study area. However, most of the preserved faults were possibly inverted during the Cenozoic time. Inversion can be documented by structures such as shortcuts, folding on footwalls, thicker rift strata on the hanging walls and by variation of fault throw along strike.

CHAPTER 8: DISCUSSIONS, CONCLUSIONS AND FUTURE WORK

8.1 Introduction

The discussion presented in this chapter will introduce the concepts and open questions highlighted in the thesis chapters. It will summarize the main evidence in the seismic data interpretation of the Ajdabiya Trough and demonstrates the distinct structures that correlate to the fault system and stratigraphy through the demonstration of both the existence of distinct phases of rifting, and the significance of individual regional geodynamic events that controlled the rift evolution and the Cenozoic stratigraphy of the Ajdabiya Trough.

Detailed interpretations of fault associated structures in the hanging walls of master faults are discussed in this chapter. The existence of contrasts in associated structures allow to divide up the hanging walls into several vertical stratigraphic segments; Pre-Cretaceous (~ Triassic – Jurassic), Early Cretaceous and Late Cretaceous-Early Cenozoic. The chapter also discusses the distinct subsidence patterns observed in different sectors within the trough.

The thesis outcomes demonstrate both the existence of different phases of rifting, and the significance of individual regional geodynamic events that controlled the rift evolution of the Sirt Basin and have implications for the Ajdabiya Trough rift infill. This introduce the Mesozoic rifting in the context of the break-up of Gondwana, the tectono-stratigraphic and kinematic model of the Ajdabiya Trough in the context of regional tectonics of the North African Platform. The results of each chapter are discussed in terms of their contribution to: the key issues of the thesis work. Finally, the main limitations to this work are discussed and accordingly an overview of the main open questions and suggestions for further work are presented.

The structural history of the Sirt Basin is characterized by a number of tectonic phases each of which played significant role in the structural development during the Mesozoic – Cenozoic period. Within the basin crustal stretching eventually lead to major rifting and crustal collapse and the formation of major grabens in which syn-rift sediments accumulated. The resultant subsidence and thickness of the syn-rift sediments are primarily controlled by local isostasy,

basement topography and fault controlled deformation. For instance structural styles, the intensity and timing of deformation vary spatially across the region. In the Ajdabiya Trough region the combined effect of tilting and late fault reactivation (Figure 8.1) would have occurred during the Cretaceous – Palaeogene (e.g. Baird et al., 1996).

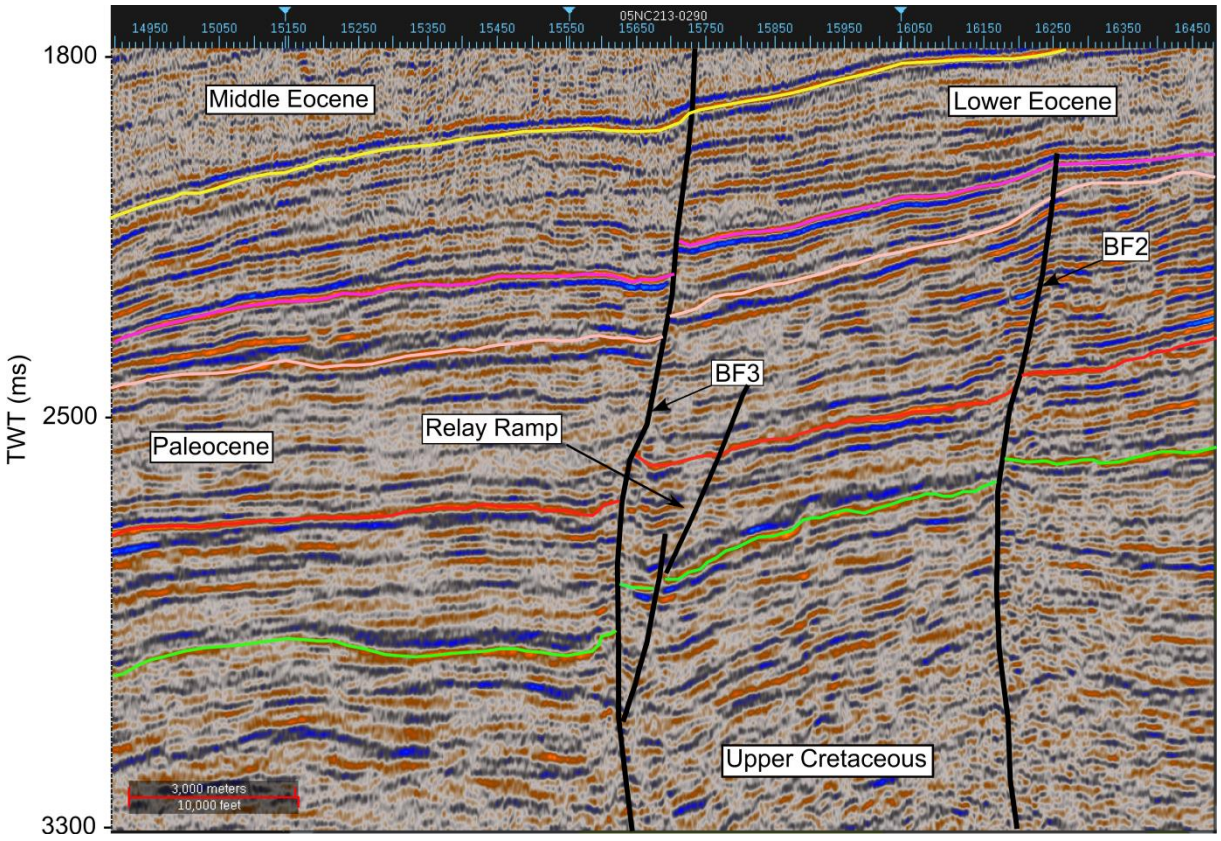

Figure 8.1: NE-SW oriented seismic section through the north-eastern part of the Ajdabiya Trough showing typical growth faulting in carbonates with relay ramp occur between normal fault segments.

Deferential isostatic loading and subsidence along the eastern margin of the trough possibly play significant role in the development of the high subsidence observed in the trough.

Evidence based on 2D seismic, potential field data analysis which was incorporated with results from commercial wells around the trough margins shows that the Ajdabiya Trough was created as a result of Cretaceous NE-SW extensive tectonic phase. Volcanic intrusions are interpreted as a rift associated structures (e.g. Busrewil et al., 2008). Isopach maps of Cretaceous – Palaeogene strata, illustrate well the generation of the Ajdabiya Trough and its structural evolution. This NW-SE trending rift system was created during the Early

Cretaceous time, reached its maximum during the Upper Cretaceous and was aborted in Late Eocene time.

The review and model of subsidence history of the trough helps to identify the influence of the trough main bounding faults on the distribution of the sedimentary sequences throughout the Mesozoic – Cenozoic period (e.g. Gumati, 1981; Gumati and Kanes, 1985; Baird et al., 1996; Abadi et al., 2008). Syn and post rift subsidence and displacement of normal and strike slip faults seem to be the most significant factors affecting the general depositional pattern in the Ajdabiya Trough. The transtensional opening of the NeoTethys during the early Mesozoic was associated with sinistral strike-slip movements which reversed during Late Cretaceus – Plaeocene time into dextral transpresional shear movements contemporaneous with the opening of the North Atlantic (Smith, 1971). The later changes were associated with loss of the Tethyan oceanic crust and inversion of the previously subsiding rift basins on the southern Tethyan margin (El Hawat and Abdulsamad, 2004).

Cenozoic post-rift sediments thins towards the trough margins especially in the early stages of post-rift subsidence, thicken considerably in the direction of increasing crustal thinning, producing the characteristic wedge shape of a passive-margin strata or "steer's head" geometry. Stratigraphic models suggest that basal onlap of the stratigraphic successions along the eastern margin of the trough is mainly due to increase in flexural rigidity with time. Throughout the Late Cretaceous – Cenozoic post-rift marine sedimentation influenced most of the study area and conditions were favourable for the depositions of sequences dominated by shallow water carbonates. Observed carbonate ramp on the eastern margin of the trough developed in the post-rift stage when subsidence became largely flexural. The eastern margin of the Ajdabiya Trough is characterized by substantial thickness of basinward dipping sediments. Increase in the basinward slop may occur due to differential subsidence between the trough margin and the trough depocentre. The large variations in the overall distribution of sediments along the eastern margin suggest that the main trough bounding faults may control the overall tectonic evolution of the trough.

8.2 The Influence of Basement in Structuring of the Ajdabiya Trough

The Sirt extensional system has been covered by numerous publications, all of which agree that it occurred during the break-up of Gondwana and the drifting of Africa from South America which coincided with the close of the Early Cretaceous (Albian - Cenomanian) (Guiraud and Bosworth, 1999). During the Hercynian orogeny (Late Carboniferous and Early Permian), uplifting in Sirt Basin was manifested in a very broad NNW-SSE to NW-SE anticlinorium, the centre of which underwent erosion (Guiraud et al., 2005). Quantifying basement terrains within the Ajdabiya Trough is important for acquiring an understanding about the underlying tectonic trends which were seemingly re-activated throughout the Mesozoic – Cenozoic. The Precambrian basement depth within the Ajdabiya Trough approaches over 7000m within the central of the trough which reflects, the subsidence figures discussed in chapter 6. The basement within the trough forms a local NW–SE-trending horst that is characterized by a low amplitude positive gravity anomaly in the centre of the trough as seen on Bouguer gravity map (chapter 4). Gravity and magnetic modeling show that the internal geometry of the trough is characterized by a system of asymmetric graben vary greatly in the orthogonal direction to the main basin axis, possibly due to the presence of intra-basement heterogeneities. The NW-SE trend also related to the late Cretaceous extensional phase and seems to truncate other ENE tectonic trends in the region. From the analysis of the sedimentary sequences of the trough, it is evident that the ENE trends are of Late Palaeozoic origin, activated from earlier basement trends (e.g. Tawadros, 2002; Hallett, 2002; Guiraud et al., 2005). This trend was subsequently activated during the Triassic, Jurassic, early Cretaceous and even late Cretaceous and Paleogene.
The tectonic interpretation of the basement structures in seismic reflection profiles of the Ajdabiya Trough is particularly difficult due to its complex nature and due to low seismic resolution at depth. The complexity of the basement further increases due to presence of volcanics required to break the crust. The presence of a basement compositional change in the area resulting from higher density material (possibly intrusives or metamorphics) in the basement causing a relatively high gravity anomaly. This could be related to a deep ridge identified by Hallett and El Ghoul (1996) in the central trough area.

The most impressive African Rift system which started in the early to late Cretaceous has its roots deep in the Pan African N-S and E-W trends (Ziegler et al., 1999; Maurin and Guirand, 1993). Gumati (1985) indicated that during the Cretaceous-Tertiary boundary times the Pre-Upper Cretaceous basement reached a maximum subsidence of 1200m in the Ajdabiya Trough area. The northern part of the Ajdabiya Trough showed much lower subsidence which might suggest a present day thinning of the Upper Cretaceous sequence towards the north. It must be stated that the progression of depth level of the Pre-Cretaceous basement as was presented by Gumati (1985) indicates that the whole Ajdabiya Trough was progressively undergoing subsidence without interruption until the Late Eocene.

The gravity and magnetic interpretations shows significant variations in the orientation, geometry and deep crustal structure. The forward gravity modeling provided a better control in the Ajdabiya Trough to determine crustal type distribution and crustal boundary identification. It has been described that entire rifting history from rift initiation to continental breakup went through several phases, including stretching and thinning. The main features of the Ajdabiya Trough include a multi-phase rifting history, distinct structural and stratigraphic architecture, a mantle upwelling as a result of extreme extension, a set of kinematically related faults developed during different phases of deformation. A high-angle NW-SE trending faults are mainly crustal-scale and represent the stretching phase of deformation. These faults cut through the entire syn-rift stratigraphic section and are passively onlapped and buried by a large amount of post-rift sedimentation.

As observed in chapter 7, the faults in the Ajdabiya Trough probably generated during the Late Paleozoic (Hercynian orogeny) which may had major episodic movement again in the Permo-Triassic to Early Cretaceous time, in Late Cretaceous to early Tertiary time, and perhaps in mid-Tertiary time. The offset detectable on the basement faults on the seismic sections in this study represents the sum of all previous movements which mainly governed by the stress field orientation for each mapped fault. The basement influence on faults is reflected by depositional patterns throughout the Mesozoic section as observed on the seismic sections. However, assessing the direct relationship between the fault architecture and the pre-existing structures is often difficult because the basement is overlain by thick syn - to post-rift strata.

8.3 Seismic Mapping and Observations

Interpretation of the seismic reflection data involves identifying major acoustical boundaries between formations that exhibit different seismic acoustic impedance; for example, a carbonate/shale interface or unconformities. Interpretation of the data has focused on features that would be critical to the study objectives, namely identifying potential faults as they may affect the continuity and integrity of the host strata.

The resolution of the 2D seismic data used in this study is not sufficient to suggest with high confidence that the mapped faults are all accurately identified as faults or possibly artefacts, which remain following data processing. However, some conditions provide higher confidence with interpretation of seismic anomalies, for example, where shallow seismic reflection events appear to be continuous and flat, confidence is gained in the quality of the data at such locations.

For illustrating information on basin wide distribution of depocentres, a series of time structure and time thickness maps related to particular stratigraphic sequences have been produced using the 2D seismic data. Isopach maps were made for each of the mapped horizons in order to understand the dynamic stratigraphy of the area. These assist in defining the distribution of the sediments within the Mesozoic - Cenozoic record. The maps were used to infer the sediment distribution during the Upper Cretaceous, Paleocene, Eocene, Oligocene and Miocene sequences (chapters 6 and 7) and show details about the variability of thickness in the depositional dip and strike directions within each sequence, and the migration of depocentres through time. Isopach maps indicate that the Upper Cretaceous unit is variable in thickness due to infilling of paleo-depressions in the underlying strata formed during rifting in Sirt Basin.

The Cretaceous sediments in the Ajdabiya Trough show different tectonic and stratigraphic history. It is thickest in the southern part and along the north-eastern part of the Ajdabiya Trough and becomes thinner northward towards a structural high (Albregha High, figure 4.41) (Hallett and El Ghoul, 1996), possibly formed by uplifting due to heating and stretching that caused by rifting. Accordingly, the thicknesses of the Upper Cenozoic units are approximately inversely proportional to the Cretaceous thickness in southern and north-eastern portions of the Ajdabiya Trough. The Eocene, the Oligocene and the Miocene units tended to preferentially fill similar depocentres in the north part of the trough.

The Cenozoic sediments were deposited over most of the study area and are mostly limestone and shale with a deep basinal shale facies becoming predominant in the depocentres. This depocentres developed during the Middle Eocene deposition and well log facies indicate that it correlates to the carbonate platform/ramp facies identified in the Gialo Formation (e.g. Spring and Hansan, 1998; Yanilmaz et al., 2008). The Eocene thins to the northwest away from this depocentres due to intensive erosion in shallow water (e.g. Gumati and Schamel, 1988) result during sea level lowstands and characterized by channel incision. This is subsequently consistent with sea level rise and deposition of thick section during the Oligocene where accommodation space is increased (e.g. Spring and Hansan, 1998). Westward thickening of the Oligocene strata is interpreted to be controlled by rapid basin subsidence.

8.3.1 Tectono-stratigraphic Observations

The seismic interpretation was a combination of traditional mapping of distinct reflectors or unconformities and determination of stratigraphic sequences through the identification of seismic reflection geometries (e.g. downlap, onlap, erosional truncation; after Mitchum et al., 1977). Stratigraphic sequences were attributed to the broad classification of pre-rift, syn-rift or post-rift, defined by the nature of the internal geometries (after Prosser, 1993). The geometry of sedimentary loads is constrained by wells (isochron maps) with low resolution lateral extent due to wide spacing between wells, or by seismic data (limited regional extend) due also to large spacing between the 2D seismic lines.

The stratigraphy of the Ajdabiya Trough can be divided using sequence stratigraphy principles. This approach works well in the study area where the lack of deep drill holes restricts lateral correlation. Six Cenozoic mega-sequences have been identified within the Ajdabiya Trough (Chapter 5). The movement along major faults influences the geometry of these packages. The overall uniform thickness of Cenozoic sediments indicates subsidence and depositional rates remained comparable throughout basin evolution. Wedge shape geometries with package thickening towards bounding faults are observed along the eastern part of the trough.

Sequence boundaries mark changing depositional environments, depositional hiatuses and periods of tectonic instability. Sequence boundaries in the Ajdabiya Trough are largely

identified on the basis of onlap, and erosional truncation. Gamma-ray (GR) logs also defined sequence boundaries on the basis of the abrupt GR log response.

Initial deposition in the trough has been dated as Early Cretaceous (Gras and Thusu, 1998, Hallett, 2002). This was restricted to the northern part of the Ajdabiya Trough, as indicated by the seismic and by the limited number of data holes.

I proposed asymmetrical half graben geometry for the underlying Early - Late Cretaceous structure of the Ajdabiya Trough (see also Baird et al., 1996). The bounding faults of the eastern side of the trough have the component of normal faults that controlled thickness of the syn-rift sequence and, in general, the geometry of the structure. Subsidence and displacement of the normal faults seem to be the most significant factors affecting the general depositional pattern in the Ajdabiya Trough. Despite the low resolution of the 2D seismic data at this level, the rift structures are seen to be well preserved in the study area. However, some of the preserved faults were possibly inverted during the Cenozoic time.

Inversion can be documented by structures such as thicker rift strata on the hangingwall and by variation of fault throw (Williams et al., 1989; Holdsworth et al., 1997). Inversion of rift faults in the Ajdabiya Trough (Figures 7.46 & 7.47) could be formed in line with the same movement that happened at Cyrenaica Platform to the east, during Cretaceous (Santonian) time and lasted also through the Paleocene (Danian) (Röhlich, 1980; Craig et al., 2008; El-Arnauti et al., 2008). Sediments are considerably thick towards the subsiding edges and missed on a high folded structure. Extension is more pronounced with an increase in subsidence and vertical throw of major graben-bounding faults proceeding southeast ward. Inversion of the subsidence probably related to rejuvenation of the NE-SW and NW-SE faults.

The mapped Lower – Middle Eocene (Gir and Gialo) sequences (chapter 5), shows high thickness changes along seismic profiles; however seismic profiles and isochon maps clearly exhibits sigmoidal prograding shape and wedge-like geometry along the eastern and south-eastern parts of the Ajdabiya Trough.

Major sequence boundaries (Unconformity surfaces) are identified throughout the seismic dataset. They are tentatively correlated with Late Mesozoic transgression and Paleocene lowstand progradding sequences. I suggest that during the Cenozoic, most of the stratigraphic record is formed by falling stage systems tracts with forced-regressive deposits, which confers

a general progradational vertical stacking pattern as observed on some 2D seismic profiles. Transgressive systems tracts are represented by continuous units over previously eroded (incised) surfaces developed during highstand system tract. Retrograding facies observed during late Paleocene and at the end of Early Eocene are considered to be part from transgressive system tracts (TST).

Highstand system tracts (HST) are generally recognized on the outer shelf and slope and are marked by shelf margin aggradaing and progradaing parasequences during the Middle Eocene (Gialo Sequence). Parasequences are indicated by short-lived sea level rises and falls developed within the Eocene sequences.

Still stand deposits are difficult to recognize in the available dataset, which need to be confirmed with relevant wells also.

8.3.2 Various Stages of Rift Evolution

The results presented in this work demonstrate that in common with other areas in the Sirt Basin, the Ajdabiya Trough has undertaken noteworthy crustal thinning resulting from repeated cycles of rifting. The lower part of the trough shows typical geometries of syn-rift strata associated with the extension of a deformed Palaeozoic metamorphic basement, above which, at least two rift-related Megasequences were accumulated possibly from Triassic to Upper Cretaceous time. Above these units, the post-rift Megasequences record the progressive thermal subsidence of the trough, followed by discrete uplift and compression periods that resulted in rift-dependent inversion and shortening architectures. Syn and post rift architecture reveals that the Ajdabiya Trough record the progressive migration of the dominant locus of subsidence during the different phases of the evolution of the Sirt Basin. Each sector within the trough shows distinct patterns of subsidence/uplift, as expressed from seismic and well data. In chapter 6, the trough depocentre was modelled using synthetic well PW0360 that confirmed both the multiphased nature of extension of the trough and the significance of the subsidence pulses during the Mesozoic – Cenozoic.

In the Sirt Basin, rifting and orogenic events have likely controlled faulting and subsidence within the northwest-southeast trending grabens while faulting has mainly associated with basement reactivation of high-angle normal fault system (e.g. Burke and Dewey, 1974; Van Houten, 1980; Van Houten, 1983).

Reactivation of the South Cyrenaica Shear Zone (SCFZ) (Figure 8.2) and other basement structures during the earlier stages of rifting was accompanied by the partitioning of extensional strain and formation of NE-SW and NW-SE trending normal faults in the Ajdabiya Trough (e.g. El Arnauti et al., 2008).

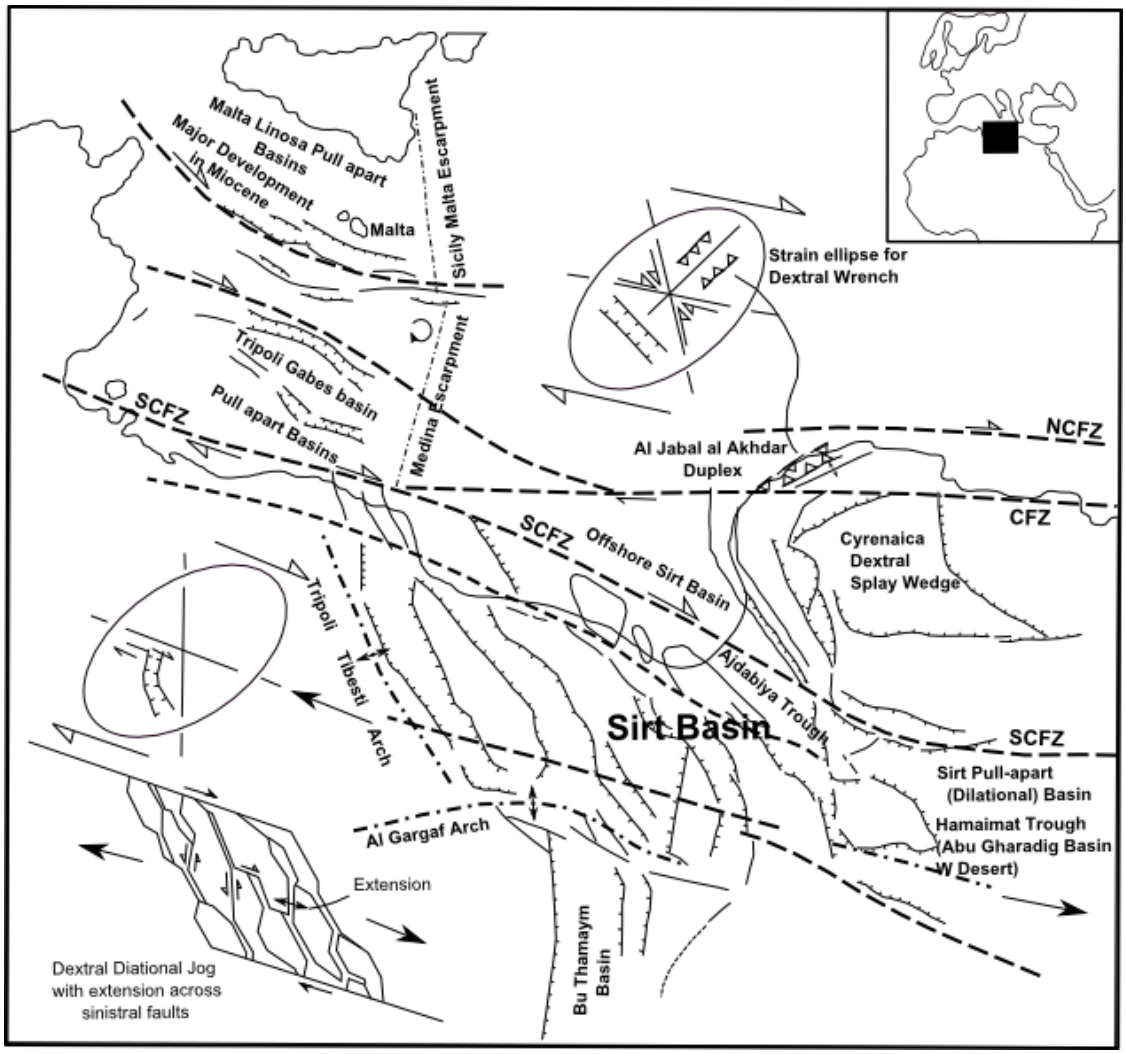

Figure 8.2: Tectonic and morphologic elements map showing the relationship between Sabratah- South Cyrenaica Fault Zone (SCFZ), the Jifarah fault, Sirt basin and Pelagian shelf (redrawn from Anketell, 1996).

During Mid – Late Cretaceous NE-SW crustal extension associated with the formation of NNW-SSE and NW-SE trending normal fault systems some of which has component of strike-slip faulting (e.g. Anketell and Ghellali, 1991; Anketell, 1996; Guiraud and Bosworth, 1997; Ahlbrandt, 2001). Seismic data show that the faults cross-cutting earlier Palaeozoic

structures which mainly folds formed at high angle and possibly parallel to some basement shear zones (e.g. Anketell, 1996).

The onset of major rifting during mid - Late Cretaceous resulted in block faulting and rapid subsidence (Selley, 1997; Ahlbrandt, 2002; Hallet, 2002; Coward and Ries, 2003). Seismic data reveal that the Cretaceous successions commonly thicken dramatically towards syn-depositional faults (e.g. Figures 7.33, 7.45 – 7.47).

The main syn-rift deposition occurred in the early Cretaceous when the pre-Upper Cretaceous, Nubian (Sarir) Sandstone (Figure 5.4) accumulated in rift troughs and topographic lows on the irregular pre-Cretaceous surface and passing into a quartzitic facies in the northern Ajdabiya Trough (e.g. Hallett, 2002).

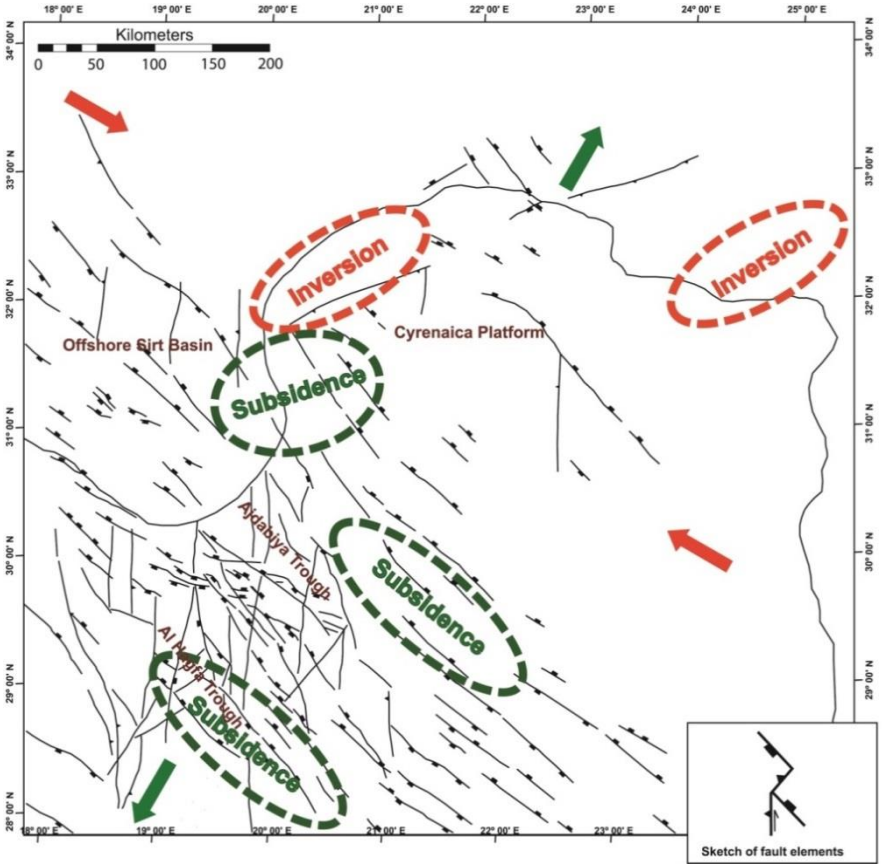

Figure 8.3: Shortening in North Africa during the Alpine event (49-34 Ma), resulted from change in the rate and direction of opening of central, south and north Atlantic Oceans (Guiraud et al., 2005). The Eocene time corresponds to phase of major subsidence in some parts from Sirt Basin and Cyrenaica Platform.

Following extension, thermally-driven subsidence in response to Cretaceous rifting dominated much of the Cenozoic (Figure 8.3) with relatively minor pulses of fault movements and

inversion in Cyrenaica Platform (e.g. Gumati and Nairn, 1991; Gumati et al., 1996; El Arnauti et al., 2008). The Ajdabiya Trough experienced the greatest subsidence and attendant sedimentation patterns that dramatically attenuated between marine and clastic sediments with influx of debris flows and turbidites.

8.3.3 Mesozoic Rifting and Continental Break-up

8.3.3.1 Permo Triassic - Early Cretaceous

The North African Margin was subjected to the Caledonian and the Hercynian main orogenies during the Palaeozoic. The Silurian Devonian Caledonian orogeny had a NW-SE tectonic stress template and developed NW-SE oriented gentle arches and faults in NE Sirt Basin. The Triassic and Jurassic are marked by rifting developed in response to the break up of Pangea (e.g. Dewey and Bird, 1970; Bond and Kominz, 1984). This rifting and crustal stretching formed a large E-W trending sub basin that covers most of the eastern part of the Sirt Basin. In a classic rift development, basins are formed as rift grabens on stretched and thinned crust over a thermal feature (e.g. Reston, 2009) .

The extensional phase of rifting in the Sirt basin probably started during the Permo Triassic - early Cretaceous with E-W trending graben development, which became especially more active during the Aptian-Albian (e.g. Hallett, 2002). This was followed by a NW-SE trending extension system (started during the Cenomanian) which influenced the flanks of the Sirt basin at first, then migrated towards the middle during the Maastrichtian. The most recent phase of extension was the NNE trending graben development in the SW which extended into the Tibesti region in central Libya (Guiraud et al., 2005). This latter trend was probably initiated during the latest Cretaecous and earliest Paleocene.

Based upon the apparent juxtaposition of Pre-Upper Cretaceous strata on the 2D seismic data (chapters 5 and 7), one may suggest a Pre - Upper Cretaceous age for the rift phases in the Ajdabiya Triugh. Overlying the pre-rift sediments, a set of superimposed reflectors exists in the Cretaceous interval rotating towards the west showing a wedge shaped geometry (Figure 5.45). A wedge shape geometry is one common criteria to identify rifting (Cartwright, 1987; Prosser, 1993) and characterize syn-rift sediments. The wedge shape of syn-rift reflector sequences may indicate that sedimentation kept pace with subsidence (Prosser, 1993).

The seismic data indicate, however, that fault block tilting occurred during the deposition of presumably Triassic - Jurassic strata. On a regional scale, the Triassic - Jurassic package

defines a profound eastward thickening sedimentary wedge, indicating fault block rotations followed by stratal thickening indicating the initiation of tectonic extension leading up to the early Mesozoic phases of rifting. Irregular discontinuous reflectors, rotated by normal faults and increasing thickness towards fault escarpments to the east, characterize the early rift phase and switch to Cretaceous rifting.

This type of sediment accumulation provides an indication for growth faults. Growth faults are produced during simultaneous faulting and sedimentation. Differences in thickness occur due to rapid accumulation of sediments (Thusu 1996; Wilson and Guiraud, 1998; Gudarzi, 1981; Busrewil et al., 2008).

8.3.3.2 Early Cretaceous – Late Cretaceous

The Sirt extensional system has been covered by numerous publications, all of which agree that it occurred during the break-up of Gondwana and the drifting of Africa from South America which coincided with the close of the Early Cretaceous (Albian-Cenomanian). Moreover, it has been suggested (Vail, 1991; Wilson and Guirand, 1991; Ziegler et al., 1999 etc.) that the African rift system responsible for the development of the Sirt basin has inherited its trend from the Pan African Precambrian orogenesis.

The 2D seismic data fairly images the deeper structure of the Ajdabiya Trough area, the interpretation of which reveals a previously un-proven but inferred Early - Late Cretaceous rift underlying the Cenozoic strata (e.g. Ahlbrandt, 2001; Burwood et al., 2003).

The age of rifting is inferred as no wells have penetrated such a deep succession in this area of the basin. The inference is based upon recognised rift events which have affected the Sirt Basin area and the trend behaviour of the major fault systems (e.g. Goudarzi, 1981; Anketell, 1996; Gras and Thusu, 1998; Guiraud et al., 2001; Capitanio et al., 2009 and references therein). Evidence for rifting is through the wedging of stratigraphically seismic reflectors towards normal faults at depth, which provide evidence of deposition during active extension and initial rapid subsidence. This is visible in different parts within the Ajdabiya Trough (Figures 7.27, 7.33, 7.36, and 7.45). The top of the syn-rift sequence is difficult to identify as much depends upon whether the Cretaceous sequence infills a sediment starved Late Jurassic – Early Cretaceous rift (e.g. Gras and Thusu, 1998) or whether rifting continued until the Paleocene time (e.g. Abadi et al., 2008; Capitanio et al., 2009). The interpretations presented

implies the presence of a Cretaceous syn-rift sequence which links chronologically with other Early Cretaceous rift systems in North Africa in line with north of Tunisia and was responsible for the separation of the Apulian Platform from Africa, Algeria and the West African Craton (e.g. Coward and Ries, 2003) in which rifting had concluded by the Early Cretaceous. Yet both interpretations of the deeper rift structure indicates the Lower Cretaceous sequence to thicken into the Ajdabiya Trough fault system which may be evidence of Neocomian aged NW-SE extension as proposed by Lundin & Doré (1997).

8.3.3.3 Syn-rift Depositional Models

In the Ajdabiya Trough, crustal stretching eventually led to major rifting and crustal collapse and the formation of major grabens and half-grabens in which syn-rift sediments accumulated in. These sediments are primarily controlled by local isostasy and deposited to infill rift topography. The Ajdabiya Trough contains more than 7000 m of Mesozoic – Cenozoic sedimentary fills (e.g. Hallett, 2002). However, the sediment-basement interfaces mainly hard to observe on seismic data, so total sediment thicknesses are difficult to determine. The identification of syn-rift depositional sequences within the Ajdabiya Trough is based on the stratal geometries observed on the seismic data, in the absence of any other source of data. These observations shows that the identified syn-rift sequences are varied along different fault blocks, showing different depositional packages formed during rifting and subsidence stages. Although there is a limitation, concerning the subsidence mechanism and sedimentation within the study area, it may be possible to establish some idea about these mechanisms during rifting evolution.

The syn-rift sediments were uplifted and eroded particularly from the highs prior to faulting in Cretaceous time. These faults are generally NNW-SSE trending and arcuate around basement uplifts. The Cretaceous faulting represents the start of the Late Cretaceous basin development. Major basin boundary faults as rotated on seismic, were generally active until lower Eocene and died out in Middle to Late Eocene. Important ones, however continued into Oligocene and Miocene.

Many of the mapped NW-SE trending faults within the Ajdabiya Trough cut some of the syn-rift seismic surfaces, indicating that the syn-rift structures were active until the end of rifting and may be accommodated by minor extension during immediate post-rift periods. The syn-

rift package show different depositional features attributed to more than one rifting event. It could be that there is evidence of more than one rift phase in the mapped fault blocks as suggested, which can be defined by an onlap surfaces within the syn-rift packages. Distinctive seismic facies can be recognized within the syn-rift sequences on the basis of reflection character, intensity of acoustic contrast at bounding surfaces, and external shape of the unit. The southeastern part of the study area shows thin syn-rift wedges (Figure 7.40), within which only one phase rifting can be resolved.

8.4 Stratigraphy Synthesis

Sequence stratigraphic analysis of well logs, and 2-D seismic data provided a stratigraphic framework of the study area, through which six sequence boundaries were identified. Most sequence boundaries are interpreted as partially or fully eroded surfaces caused by subaerial erosion and submarine channels or bypass sediments (debris flows). Seismic reflection characteristics including amplitude, and reflection configuration were examined and each sequence was subdivided into separate seismic facies.

Depositional sequences (Mitchum et al., 1977) are formed in response to the interaction of eustatic change, tectonic activities (subsidence or uplift), sediment supply, accommodation space and paleogeography (Posamentier and Allen, 1999). A combination of tectonic, structural movement and sea-level changes probably had controlled the variations in cycle characteristic in the study area. The lithology of the Ajdabiya Trough is variable in response to sediment input and depositional environments that result in different relative sea level variations. The eastern margin of the trough is represented by a prograding complex; sigmoidal clinoforms indicate a mixture of high and low energy pulses, depositing sediments on the slope and margin of the rifted parts of the trough. In general this sequence pinches out towards the trough margin. In the shallower part of the Ajdabiya Trough the Paleocene – Mid Eocene sequences are made up of carbonates and some shale of restricted shallow platform to deeper platform environment. In the deeper parts of the trough, the shale is probably dominated as indicated by the seismic signature of the sequences.

In this study, the importance of tectonic control was highlighted and stated as a major parameter of submarine canyon and channel-levee formation in Middle Eocene time. In the following time interval of the Late Eocene (corresponding to the deposition of the Oligocene

and Miocene sequences), a more stable tectonic regime was dominant and tectonically induced subsidence rate diminished.

During the Cenozoic period, most of the basement involved normal faults have lost their activities and sedimentation prevailed by the development of sedimentary sequences. Particularly during the Late Paleocene – Early Eocene, shoreline transgression was characterized by a clastic-carbonate mixed system. The carbonate production started depending on the configuration of the topography throughout the basin. During the highstand position of the sea-level, the carbonate production increased and a large platform was developed in Middle to Late Eocene. Gradual shoreline transgression also caused the partial drowning of the carbonate platform and the backstepping of facies.

Under a transpressional tectonic regime in latest Eocene and Upper Oligocene, the eastern and central Ajdabiya Trough were gradually elevated above the sea (e.g. Yanilmaz et al., 2008).

A right lateral strike-slip fault system has begun to develop in the Oligocene (El Arnauti et al., 2008; Yanilmaz et al., 1997). This time interval was recognized as the transition from deeper to shallower depositional environments throughout the Sirt Basin.

A relatively wider shelf and gentle angle slope gradient dominated the multi-channel system within the Ajdabiya Trough. These channels fed fine to medium-grained sandstone rich turbidites, slide and slump deposits in the north-eastern part of the study area.

The amount of sediment arriving in the deep basin depends on the nature of the clastic material transported (sand or mud-dominated). Differences in slope morphology, such as between a margin with a well-defined shelf break or a ramp-type margin (Van Wagoner et al. 1988), may influence the morphology of the turbidite systems within the Ajdabiya Trough.

An unconformity was formed on the shelf as a consequence of uplifting during the Middle Eocene (e.g. Hallett, 2002), and most of the clastic material bypassed the shelf through incised valleys (Figures 5.26, 5.30, 5.36, and 5.38). Major submarine canyons were also incised in the slope, and supplied coarse-grained clastic sediments to the turbidite systems (e.g. Baaske et al., 2014).

My interpretations suggest that the end of the Early Eocene is characterized by shoreline transgression. In this time interval, the facies exhibits retrogradational stacking patterns. Northeast to southwest oriented seismic lines demonstrate relative sea-level rise and landward

shift in facies in the Late Eocene (Figure 5.27). Shallow marine clastics are possibly the first products of transgression of high energy shoreface.

This suggested that facies distribution in the early part of the Middle Eocene in the Ajdabiya Trough was mostly controlled by the sea floor subsidence. The uppermost Eocene mostly exhibited retrogradational stacking patterns. The evolution of the carbonate platform was characterized by shoreline transgression and landward shift of the facies in Early Eocene.

8.5 Review on Subsidence Analysis

The analysis of subsidence and burial history within the Ajdabiya Trough was accomplished by modelling key wells located along the margins of the Ajdabiya Trough, and by the tentative modelling of a single pseudo-well close to the depocentre. The analysis aimed to estimate the magnitude of subsidence variation across the trough and to estimate the importance of uplift events on the overall rift-related tectonic subsidence, as well as the relation between the principal events controlling the evolution of the trough. When possible, depths of stratigraphic markers and main unconformities were obtained from well reports provided by the National Oil Company of Libya (NOC). Ages of marker horizons assigned to sequence boundaries were obtained also from the well reports and occasionally interpreted in accordance with the regional lithostratigraphic framework presented in introductory chapters.

Subsidence curves in the study area show some variations in the subsidence patterns for each well typical of a sag basin. Additionally, they all record short and long period rapid pulses of subsidence during deposition of the Upper Cretaceous - Lower Eocene shown by the steeply sloping section of the subsidence curves (Figures 6.18 & 6.19) punctuated by periods of tectonic quiescent during the Cenozoic, indicated by the gentle slope of the curves. This could be in accordance with periods of hiatuses (erosion or non-deposition) and their quantification in time, were estimated mainly on the basis of the architecture of the sequences and their stratigraphic relationships as observed on the seismic data.

The rapid subsidence quantified is interrupted by a pre Cretaceous unconformity event along the NW part of the Ajdabiya Trough. This unconformity was possibly responsible for removing Permo-Triassic and Jurassic strata along the eastern portions of the trough.

Subsidence in the Ajdabiya Trough was the main control on deposition and sedimentation patterns during the Late Cretaceous time. During the Palaeocene, subsidence continued in the Ajdabiya Trough in response to fault reactivations and possible strike slip movement. Accordingly folding and uplift events appeared to have taken place along the same axial trends in the Late Eocene and Oligocene (Martin et al., 2008). Burk (1996) postulated that the African Plate became stationary relative to the mantle at this time, resulting in plate wide uplift as mantle plume buoyed up the lithosphere. Late Eocene and mid Oligocene unconformities have traditionally been attributed to fall in sea level, while Oligocene - Miocene period was marked by rapid subsidence along the NW to NNW-trending Ajdabiya Trough.

8.5.1 How does Subsidence Vary within the Ajdabiya Trough?

The tectonic subsidence history in the Ajdabiya Trough is formed by pulses of stretching periods punctuated by periods of tectonic quiescence and thermal subsidence amplified by sediment load. Cretaceous times are marked by the evolution of basement highs and graben features and occasionally hiatuses in the sedimentary record. I postulate that thermal cooling commences subsequent to the Cretaceous - Palaeocene rifting phase and uniform continuous subsidence creates a depocentre consistent with present-day basement depth which exceed 7000 meter within the entire Ajdabiya Trough. Post-rift thermal cooling becomes more effective during the Cenozoic time. These could be attributed to possible variations in mantle lithosphere density during possible mantle upwelling and crustal thinning stages as evidenced from the gravity and the magnetic interpretations.

Repeated cycles of subsidence recorded in the Mesozoic - Cenozoic sequences of the Ajdabiya Trough, as observed from the subsidence analysis (chapter 6) are basically attributed to one or more rifting phase (e.g. Gumati and Kanes, 1985; van der Meer and Cloetingh, 1993; Baird et al., 1996; Schroeter, 1996; Abadi et al., 2008, and others). Its postulated that subsidence during the Cenozoic time (Paleocene - Eocene) might be explained by downwarping of the Sirt Basin when the rifting is cessed and the extension gives way to the collision and formation of sag basin that overlies the graben system in place of rift. The transtensional opening of the NeoTethys during the early Mesozoic was associated with sinistral strike slip movements which were reversed during Late Cretaceous - Paleocene time

into dextral transpressional shear movements contemporaneous with the opening of the north Atlantic (Smith 1971). The latter changes were associated with the onset of the formation of the Tethyan oceanic crust and inversion of the previously subsiding rift basins on the southern Tethyan margin (El Hawat and Abdulsamad, 2004). These were associated with increased magmatism that peaked during the Late Cretaceous (Turonian) time in Sirt Basin (Meneisy, 1990; El Hawat and Argnami, 2001). There might be periods of multiple spatially irregular extensions without clear inversion within the Ajdabiya Trough. The study suggests that the Ajdabiya Trough was developed during the Mesozoic - Cenozoic time as a structure of intense downwarping of the Earth's crust with maximum subsidence exceeding 2000m.

Within the Ajdabiya Trough sequences can be identified in filling grabens and onlapping the basement highs (Figure 8.4).

In the western portion of the study area, well A1-114 show hiatuses in the upper Cretaceous sequence attributed to lowering in the tectonic subsidence as observed from the subsidence curve of the well and lists till about Late Upper Cretaceous (~ 66 Ma).

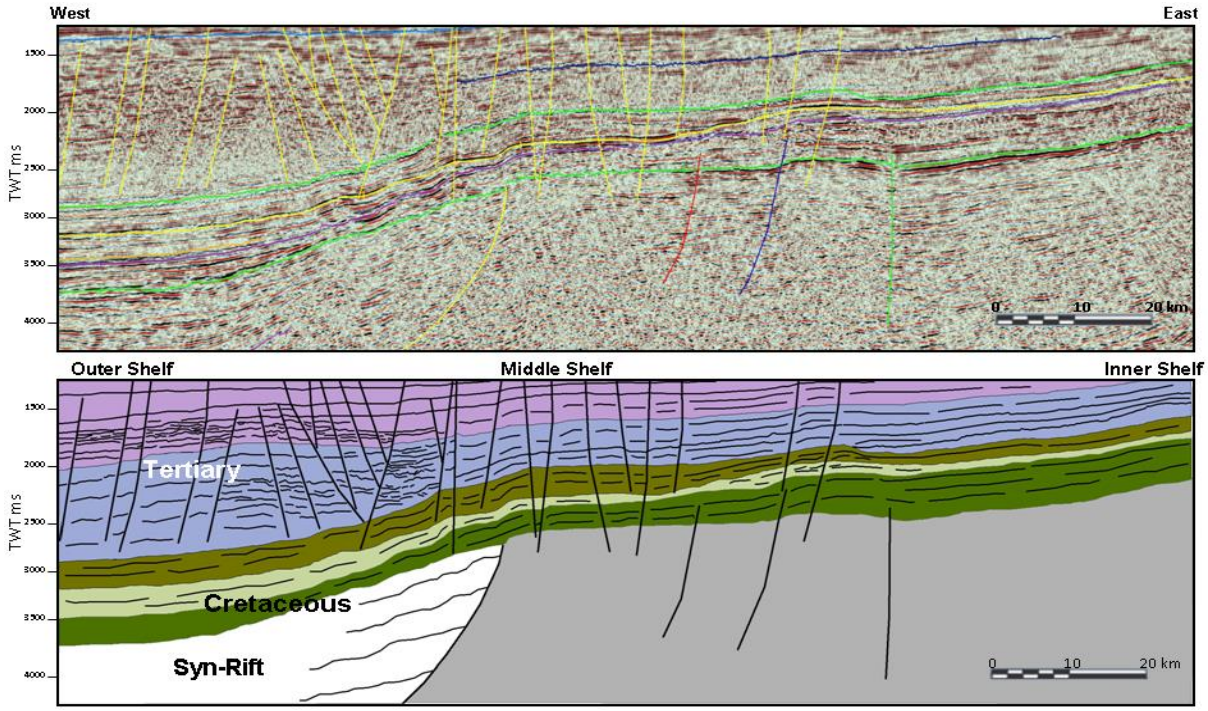

Figure 8.4: SW - NE transect line **05-NC213 0460**, across the Ajdabiya Trough, demonstrates the remarkably uniform subsidence that occurs throughout the Cretaceous and Tertiary. Also evident is an abrupt reorganisation of the margin at the end of the Cretaceous with a significant change to the location sediment accumulation in the Tertiary.

The spatial variations in subsidence in the western part of the trough indicate the occurrence of a relatively narrow NW-SE-trending sub-basin in the west along the Al Jahama Platform as observed from the Cretaceous isochron map, most likely controlled by NW-SE-trending boundary faults.

During the Cenozoic time an accelerated subsidence resulting in a thickness of post-rift sediments of over 4000 m. The early post-rift subsidence patterns are interpreted to be linked to thermal anomaly formed during the early rifting stage (e.g. Galushkin et al., 2014). The majority of the post-rift period is characterized by high sediment rate compared to the syn-rift subsidence as observed from the steep slope gradient of the burial history curves (Figure 6.31).

8.5.2 Correlation of Subsidence Results with Plate Motion Changes

In numerous publications, the Sirt extensional system has been considered as the result of the break-up of Gondwana and the drifting of Africa from South America which this coincided with the close of the Early Cretaceous (Albian - Cenomanian). Moreover, it has been suggested that the development of Sirt Basin during this time is linked to the main African rift system which has been inherited from Pan African Precambrian orogeny (Vail, 1991; Wilson and Guiraud, 1998; Ziegler et al., 1999). As the Gondwana moved northward from southern high latitude, it began to colliding with Laurasia during the mid-Palaeozoic to form the Pangaea supercontinent. The Palaeozoic tectonic history in North Africa shows an alternation of long periods of predominantly gentle basin subsidence and short periods of gentle folding and occasionally basin inversion (Guiraud et al., 2005). This compressional event marks an important change in the relative movement of Africa and Eurasia. Plate motions evolve with various time-scales; some are clearly related to mantle convection. Changes in basin subsidence rates are mainly attributed to changes in far-field stresses related to changes in plate boundaries (e.g. Xie and Heller, 2009).

The African plate is considered traditionally as a rigid plate (Fairhead et al., 2013), provided that intra-plate deformation of Africa is primarily attributed to far field interactions between the African Plate itself and the other plates such as the Eurasia and Arabia. Fairhead et al., 2013 also suggested that internal sub-plates within the African continent may played

significant role in developing different structural styles and deformations including different cycles of extension rejuvenations formed as a result of local stress fields.

The tectonic development of North Africa was dominated by multiple phases of rifting phase's in it is complex history along the established Tethys margin, and a post-rift phase in which the Tethys Ocean closed with dominated compressive tectonism prevailed (Hallett, 2002). The Sirt Basin is formed during Late Cretaceous break-up of Gondwana, however, data analysis suggest an extended period of subsidence in the basin. Holt et al., 2012 among others suggested that subsidence in Sirt Basin is formed due to cooling and thickening of the lithosphere and mainly coincides with supercontinent breakup and a broad extensional regime. Paleogeographic re-construction (Jansen et al., 1995) shows that a major change in the African Plate motion with respect to the Eurasia is occurred during the Upper Cretaceous (Santonian) 86 – 83 Ma (Westphal et al., 1986). Sinistral and extensional movement had to be reversed resulting in collision between Africa and Eurasia (Dercourt et al., 1986; Ziegler, 1988). This compressional event caused a period of strong tectonic activity in the North Africa with deceleration in the tectonic subsidence in most of the African basins including Sirt Basin.

The tectonic and basement subsidence curves for the Ajdabiya Trough obtained in this study correlate well with subsidence curves obtained from studies in Sirt Basin (Gumati, 1981; Gumati and Kanes, 1985; van der Meer and Cloetingh; 1992; Ceriani et al., 2002; Abadi et al., 2008). The subsidence curves show linear profile character during the interval of 90 – 0 Ma. The linear subsidence curve shape is characteristic of tectonic and thermal stages of lithospheric extension (McKenzie 1978), and in the Ajdabiya Trough depocentre it resembles that of a passive continental margin characterised by medium to high subsidence rate at about 20 - 100 m/Ma i.e. The curves show striking differences both in the timing of acceleration and deceleration of subsidence and in the magnitude of subsidence attributed to changes in stress fields related to major changes in plate motions (e.g. Cloetingh et al., 1985; Cloetingh, 1988). The subsidence is punctuated by period of decelerating subsidence rates from Early Cretaceous to Miocene time related to periods of tectonic quiescent or change in tectonic regime.

8.5.2.1 Upper Cretaceous

Tectonic subsidence analysis has been performed for period from the Upper Cretaceous until present which cover the main phases of rifting related to the opening of the south and Equatorial Atlantic Ocean. The backstripped tectonic subsidence curves shows generally subsidence patterns related to uplift and subsidence phases formed during basin evolution stages related to plate tectonic changes. Janssen et al., (1995) presented results of backstripped wells from numerous African rifted basins, including the Sirt Basin (Figures 8.5 & 8.6). He established a close correlation between subsidence patterns in these basins and the changes of plate motions.

An increase in subsidence and sedimentation rate is observed from the subsidence and the burial history curves after the Santonian time (~ 86 – 83 Ma), consistent with the Janssen et al., (1995) model of plate motions that recorded renewed subsidence for the Campanian and Maastrichtian following an inversion and associated erosion similar to tectonic inversion in Cyrenaica Platform that formed by block rotations associated with the change in extension direction from NW-SE to NE-SW (Guiraud, 1993). Subsidence curves show a major break during the Late Cretaceous associated with plate rotation (e.g. Janssen et al., 1995), and modified by reactivation of the pre-existing fault systems and the development of new faults. The Early Cretaceous event is most likely linked to the increase of slab forces following the subduction of the Neo-Tethys along the north-eastern African margin (Janssen et al., 1995; Capitanio et al., 2009). The tectonic subsidence curves show a gradual to stepwise character, with short lived rapid subsidence interrupted by periods of uplift or erosion subsequently followed by periods of lower subsidence, indicating periods of possible fault re-activation alternating with periods of tectonic quiescence. Evidence of fault reactivation is observed on the 2D seismic data, where the mapped faults are observed to dirupt the Cenozoic sediments. The presence of inversion structures (Figures 7.46 & 7.47) indicates that another reactivation mechanism possibly formed as a result of far field force acting on early extensional structures. It has been suggested that shift in plate motion during the Early Cretaceous, produced change in the state of the stress field within the African Plate and the development of intracratonic rifting within the Sirt Basin (Janssen et al., 1995). Fairhead et al., 2013 noticed that plate motion changes are well correlated with timing of the stratigraphic unconformities associated with the continental margin of the Atlantic and correlate also with stratigraphic data from

African basins formed within different sub-plates. Their observations show that the effect at the sub-plates boundaries is manifested and influenced by tectonism as it is located within the heart of the sub-plates where the underlying crust has been weakened due to vertical load caused by the sedimentary column at each basin.

This presumably the case in the Ajdabiya Trough subsidence during the Late Cretaceous which virtually oscillates between periods of moderate to rapid subsidence (Figures 6.18 & 6.19) possibly related to variations in the local stress field produced by interactions of sub-plate boundaries.

The crust is prone to flexural response as a result of change in stress field which latter form changes in elastic strength of the crust resulting in change in the isostatic response.

Rotation of the African stress field caused by changes in relative plate motion which form changes in deformation regime, such as compression (e.g. Santonian inversion (see review in El-Arnauti et al., 2008) or extension that split into different directions with possible strike slip movement prevailed along the axis of the rifts (e.g. Anketell, 1996).

Tension or compression has been generated as a result of plate motion during this time giving rise to vertical movements during Late Cenomanian to Early Turonian, as a result of global sea level rise with up of 300 m along old rifts (e.g. Mitchum, 1977).

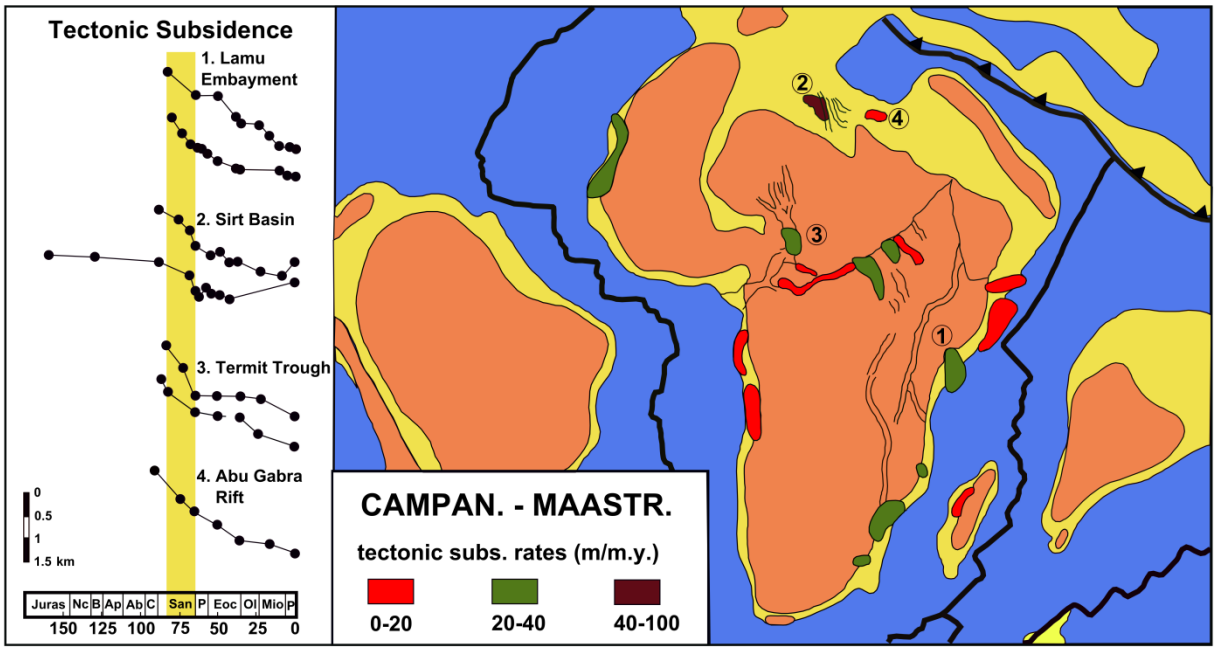

Figure 8.5: Tectonic subsidence curves of selected wells from selected sedimentary basins in Africa including Sirt Basin, and paleogeographic reconstruction, showing the mean tectonic subsidence rates, for the Campanian and Maastrichtian. Note the increase in subsidence rate in the Sirt Basin after the Santonian compressional event. The map is redrawn from Janssen et al., (1995).

8.5.2.2 Tertiary (the post-rift subsidence phase)

Convergence between Africa and Europe slowed down about the Cretaceous - Tertiary time (Dewey et al., 1989). Large parts from the African continent has been uplifted during the Late Tertiary (Bond, 1978), and accompanied by tilting and rapid subsidence.

The Sirt Basin has experienced an abrupt increase in depth at the Cretaceous - Paleocene boundary (Gumati and Kanes, 1985). During periods of major crustal extension and fault re-activations, the subsidence in Sirt Basin reached a climax during the Paleocene - Eocene, (e.g. Gumati and Kanes, 1985; Gumati and Nairn, 1991; Abadi et al., 2008; van der Meer and Cloetingh, 1993), while post-rift phase with decelerating subsidence driven by thermal re-equilibration modified by plate interactions during Eocene - Early Miocene (Galushkin et al., 2014). Within the Ajdabiya Trough coupled processes of sediment loading, compaction and flexure induced subsidence could be correlated to plate tectonic process including the changes in thermo-tectonic subsidence rates (e.g. van der Meer and Cloetingh, 1993; Galushkin et al., 2014).

The burial history curves (chapter 6) show that the Ajdabiya Trough is characterised by a continuous sedimentation rate and an abrupt deepening around the Cretaceous – Paleocene boundary. Subsequently during lower to middle Paleocene depocentre was formed (Al Hagfa Formation) (Bezan, 1996) and controlled by both NNW-SSE directed shortening during a late Paleocene as a result of convergence between Africa and Europe (Dewey et al., 1989) and northwest-southeast to north-south–oriented stress field during the early Eocene (Cloetingh et al., 2005). It is possibly that an asymmetric Palaeocene carbonate ramp or wedge was controlled by strike –slip displacement along a right-lateral movement.

During the Mid – late Eocene, basin tilting and subsidence is caused by compressional event (Figure 8.2). However the Late Eocene period was a period of minor tectonic activity. The increase in subsidence rate in the Ajdabiya Trough during the Cenozoic time as observed from the subsidence curves are probably correlated with short duration of extensional rejuvenation phases (Figures 8.5 & 8.6) (e.g. Janssen et al., 1995; Galushkin et al., 2014), related to changes in the orientation of the main stress fields during Paleocene – Eocene time (Capitanio et al., 2009), this could cause reactivation of previous northwest-southeast trending basins. Deviations from the subsidence rates observed during the Eocene time could be

related to short period changes in tectonic stress rather than thermal influence (e.g. van der Meer and Cloetingh, 1993).

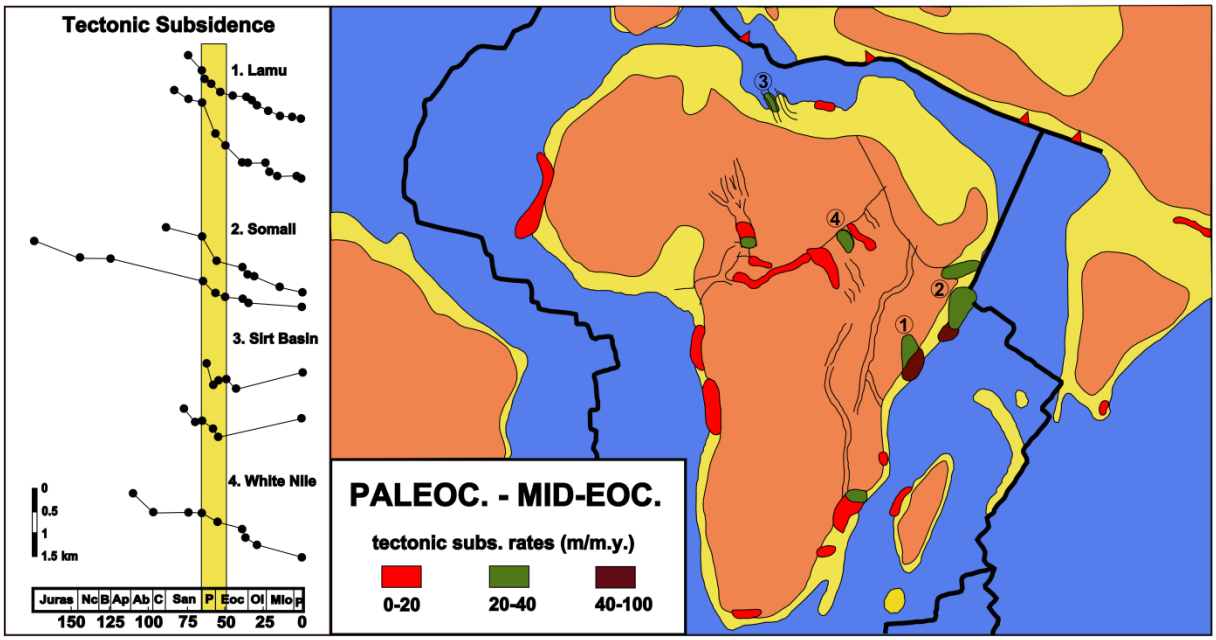

Figure 8.6: Tectonic subsidence curves of selected wells from selected sedimentary basins in Africa including Sirt Basin, and paleogeographic reconstruction, showing the mean tectonic subsidence rates, for the Paleocene through mid-Eocene. Note the moderate subsidence rate in Sirt Basin coeval with extensional rejuvenation and fault re-activation in Sirt Basin correlated well with plate motion. The map is redrawn from Janssen et al. (1995).

Uplift and subsidence cycles terminated by the end of the Late Eocene related to changes in the motion vector of the African Plate (Janssen et al., 1995; van der Meer and Cloetingh, 1993). Throughout the North African Margin, it has been documented that post - Eocene phase of compression is dominated (Gealey, 1988). Guiraud et al. (1992) attributed these compressional events to a major stage in the collision between the African and European plates. An increase in basin subsidence during the Neogene can be related to compressional due to collision between the Africa and Europe (van der Meer and Cloetingh, 1993). Fairhead and Binks, 1991 attributed this event to change in directions during the opening of the Atlantic and the change in drift pattern of the African Plate.

Based on paleo stress analysis in Sirt Basin by Schafer et al. 1981, the stress regime changed from NE-SW extensional to NW-SE compressional during the Neogene time. Collision between the African-Arabian and Eurasian plates has also intensified from the earliest

Miocene times (Guiraud et al., 2005). The rapid subsidence observed during the Miocene coincides well with this regional compression regime (e.g. Schafer et al., 1981).

8.5.3 Integration of Subsidence and Sequence Stratigraphic Analysis

Back-stripping analysis, incorporating over 5 wells in conjunction with seismic and potential field data indicates a temporal and spatial correlation between a multiphase of uplift and rapid subsidence. This shows that the transition from thermal cooling and subsidence following the early rift-phase to renewed rifting was gradual and complex. Progradding sequences of Upper Paleocene to Early Eocene age show a uniform east-west thickness distribution indicating no tectonic influence during deposition, as they were deposited within a relative short time-period. The Cenozoic tectonic phases can be regarded as a time of crustal scale thermal cooling with uniform basin-wide subsidence, and with only minor tectonic movement along some of the larger bounding faults.

Retrogradational stacking pattern recognized within Paleocene and Eocene regressive parasequences provides evidence of a longer-term increase of accommodation space, probably reflecting the regional subsidence regime that shaped the study area which most likely consistent with the general increase in thickness of depocentres from Paleocene to Eocene. However the Paleocene thickness has a reduced thickness at the depocentre compared to the Eocence sequence due to possible erosion following the deposition. Possible causes would be a decreasing rate of regional subsidence, or drop in sea level. A static conditions of the sea level could be also influenced the deposition of the Paleocene sediments in different parts within the trough.

Within the Ajdabiya Trough, factors such as compaction, palaeobathymetry, faulting, erosion and global sea level changes are the primary factores affecting the sedimentation and the tectonic subsidence. Decompaction and backstripping are used to quantify the tectonic subsidence of the Ajdabiya Trough area. Uncertainties in the input parameters are related mainly to constraints on stratigraphic resolution, and water depths. The key issue is that the subsidence data must be used in conjunction with other lines of evidence in order to determine basin controlling mechanisms. The tectonic and basement subsidence curves for the Ajdabiya Trough obtained in this study correlate well with subsidence curves obtained from studies in Sirt Basin (Gumati, 1985; Gumati and Kanes, 1985; van der Meer and Cloetingh;

1992; Ceriani et al., 2002; Abadi et al., 2008). The subsidence curves (chapter 6) show linear and exponential profiles during the interval of 90 – 0 Ma, probably related to syn-rift and thermal subsidence (McKenzie 1978). The subsidence of the Ajdabiya Trough depocentre resembles that of a passive continental margin characterised by medium to high subsidence rate at 20 - 100 m/Ma (e.g. Allen and Allen, 2005). From the middle Eocene onward fault-related differential subsidence abated. Fault mapping using 2D seismic data shows that the trough bounding faults exhibit negligible throw across the Cenozoic reflections, and do not cross cut the above reflections which mean that there is no clear and significant growth in the Cenozoic strata. This along strike variation in the timing of faulting is also reflected in sediment accumulation, with the thickest accumulations in the northern part of the trough occurring up to the Eocene reflector.

The subsidence is punctuated by periods of decelerating subsidence rates from Early Cretaceous to Miocene time related to periods of tectonic quiescent or change in tectonic regime. It is documented that the Sirt basin undergoes compression during Middle - Late Eocene tilting the basin northward, causing abrupt subsidence in the north and uplift on the basin southern shoulders, possibly driving the latest stage of regional minor subsidence (van der Meer and Cloetingh, 1993; Anketel, 1996). Capitanio et al., (2009) suggested that an abrupt growth of tensile boundary force was recorded in the Sirt Basin, ~55 - 48 Ma, could have been induced by the avalanching of the Hellenic slab in the lower mantle after ~20 Myr of stagnation on the 660 km discontinuity.

Although this study concentrates on the Mesozoic - Cenozoic history of the Ajdabiya Trough, it is necessary to go back to the Early Cretaceous to understand the events and episodes that took place in this time better. During the late Cretaceous - Paleocene, all the Ajdabiya Trough marginal areas considered herein was part of a wide and generally shallow carbonate platform (e.g. Yanilmaz et al., 2008). The subsidence in the Ajdabiya Trough area was rather homogeneous and moderate, becoming greater during the Paleocene, probably announcing the tectonism that would occur, during the Cretaceous time and letter during the Late Paleocene and the earliest Eocene. In fact the consistent pattern of overall subsidence of the Upper Cretaceous ceased, when a tectonic event took place in the Sirt Basin (e.g. Abadi et al., 2008). That fault system was to play an essential role in the later evolution of the trough, with final inversion during the Cenozoic compressional episodes.

The rift faults in the study area, caused differential subsidence by rotation of blocks, and determined that sedimentation was mainly restricted to graben and half-graben basins. These patterns can be recognised in figure. 6.16, where the tectonic subsidence curves of the Ajdabiya Trough show comparable shapes for this period but very different rates. The sedimentary record of the Paleocene and Early Eocene interval includes two successive sequence sets each of which, in the studied area, consists of shallow and deep marine sediments (carbonates, evaporits, and marine shales). Both sequence sets are separated by a regional unconformity that could be induced by minor regional tectonic pulses. Sedimentation was strongly controlled by the formation and movement of normal faults, which generated considerable differences of facies and thickness within the trough. This interval, between Paleocene and Early Eocene, is characterised by an increase of the accommodation throughout the region. This was determined mainly by the continuation of the extensional tectonics and also by a global long-term sea-level rise (e.g. Haq et al., 1987). An important fact is that the extensional tectonics spread into the Ajdabiya Trough which had been stable during the later Cenozoic times, became moderately affected by fault movements, which were particularly active during the latest Paleocene – Early Eocene interval.

The Early Eocene to Miocene sedimentary record of the trough includes four sequence sets bounded by regional unconformities that were possibly induced by successive tectonic events. The early Eocene sequence is unequally represented in the region. Within the Ajdabiya Trough domain it consists of limestones, and evaporites. Eastwards of the Ajdabiya Trough, the unit is also dominated by mixed facies but of coastal origin. In this zone, the maximum extension of the sequence set occurred at its end, when a wide shallow marine carbonate platform developed. Middle Eocene facies were deposited on a vast and shallow marine carbonate platform which covered the subsiding domain of the Ajdabiya Trough. The Middle Eocene sequence can be divided into three depositional sequences which show variable thickness as a consequence of possible fault movements. The Oligocene sequence consists of a mixed facies ranging from shallow to open marine ranging from carbonate, shale and marls. Sedimentation of this sequence set took place over the whole region in a stable tectonic regime. From a geodynamic perspective, this generalised but decreasing tectonism could be related to the end of the rifling in the Sirt Basin and the onset of basin dawn-warping (Baird et al., 1996).

A new interval of overall post-rift subsidence was probably controlled by the cooling of the lithosphere and also by eustatic changes. From a sequence stratigraphic perspective, the interval corresponds to the Oligocene and Miocene sequences. The whole interval lasted nearly ~20 m.y., which was recorded in very homogeneous successions of shallow marine carbonates, siliciclastic sands, detrital clays, and sandy limestones.

8.6 Thermal Evolution

The thermal evolution induced by lithospheric stretching in rift basins is mainly calculated, during finite syn-rift phases and thereafter, using a 1D forward modelling technique of lithospheric stretching (Van Wees and Stephenson, 1995). Heat conduction rising away from the thermal anomaly in rift basins is responsible for the thermal equilibrium state since the lithosphere is defined by an isothermal boundary (Stephenson et al., 1989). Thermal subsidence is mainly produced by cooling and increases in density of the hotter asthenosphere due to decrease in temperature perturbation (McKenzie, 1978; White, 1989).

During extension isotherms within the lithosphere are raised, and the stretched portion of the lithosphere cools and subsides after extension cessation (McKenzie, 1978). Magmatic activity associated with rifts in oceanic and continental domains can be accounted for by lithospheric extension – driven uplift of mantle isotherms and the generation of melting of mantle material (McKenzie, 1984).

Extension implies that material move apart laterally and offset from, each other. Isotherms at the base of the lithosphere move up during upward movement of material within the lithosphere and advection of heat. This implied by vertical motion of material in response to lateral extension which required mass conservation (Buck et al., 1988).

Recent modelling of the thermal evolution of the Sirt Basin by Galushkin et al., (2014) demonstrated that the temperature at the base of the sedimentary section changed from 1150°C to 1160ºC. In forward modelling by Abadi et al., 2008, the temperature 1333°C is kept at a depth of about 100 km which assumed to be high in modelling by Galushkin et al, 2014.

Forward modelling of subsidence data for the AA1-6 well in the southern part of the Ajdabiya Trough, including potentially important effects of heat production predicts a gradual

shallowing of 1100°C isotherm by 42 km during 20 Ma and which would cause isostatic uplift and erosion, accompanied by heating and thinning of the lithosphere in the Sirt Basin in the Albian - Cenomanian (Galushkin et al., 2014). Based on tectonic analysis, the similar rise of the isotherm by 24 km during 12 Ma also occurred in the mid - Eocene.

The thermal rising of the lithosphere, which had different amplitudes and variations, is responsible for the sediment erosion in Sirt basin at the Upper and Lower Cretaceous, the Upper and Lower Eocene, and the Upper Miocene – Pleistocene boundaries (e.g., Gumati and Schamel, 1988; Galushkin et al., 2014).

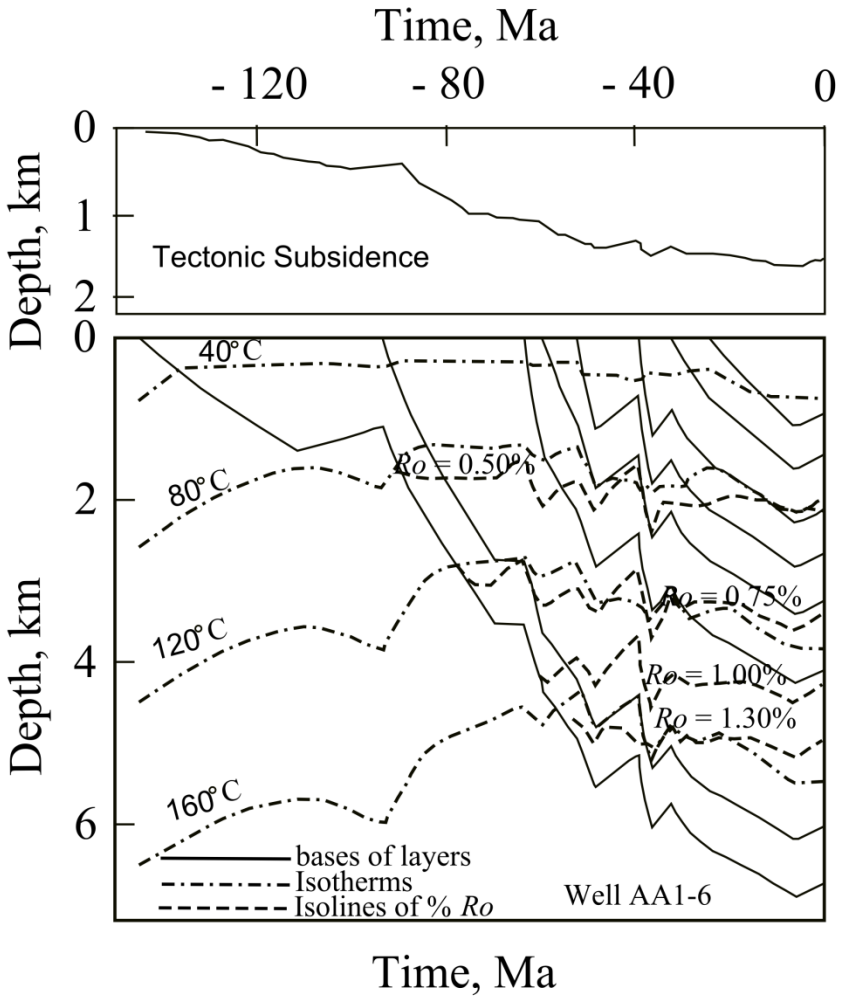

Figure 8.7: The solid line (1) in the upper diagram denotes the tectonic subsidence of the basement calculated by the removal of the load of water and sediments from the surface of the basement using data from well AA1-6 from southern Ajdabiya Trough (Figure 6.5), the lower part of the diagram show the changes in the temperature and catagenesis of the rocks during the subsidence history of the Ajdabiya Trough (curves re-drawn from Galushkin et al., 2014).

Erosin could occured after cooling and strengthen of the lithososphere. For example, the variations in the tectonic subsidence according to the AA1-6 well data (Figure 8.7) suggest different intervals of thermal activities of the lithosphere within the basin with alternating intervals of lithospheric extension (Galushkin et al., 2014). Thermal effects account for a relatively slow subsidence of the basin in the Early Cretaceous are possibly play significant role in increasing the maturation of the Cretaceous source rocks in the basin as modelled by Galushkin et al., 2014, (Figure 8.7).

Pre-Upper Cretaceous - Upper Cretaceous boundary reflects the top of Early Cretaceous sub-basins which developed during early extension phases at the Ajdabiya Trough depocentre and transected by a NW-SE trending basin faults, bounding thick sedimentary strata and re-activated during subsequent periods from Cretaceous to Eocene and possibly after (e.g. Abadi et al., 2008; El Arnauti et al., 2008). Each interval of intense sediment accumulation corresponds to a separate stage of lithospheric extension and fault re-activation in the basin.

The interval of rapid subsidence observed from the subsidence curves are due to fault re-activation periods or possibly attributed to intervals of extension that shaped large parts from Sirt Basin, as outlined in Abadi et al., 2008. The events of thermal activation or lithospheric extension change the distribution of density across the basement column (Dewey, 1998; Galushkin et al., 2014). Stretching factors obtained from subsidence curves (chapter 6) agree with those determined from the geometry of normal faulting and from crustal thinning suggesting uniform stretching model which could account for the nature of the stretching mechanism in Ajdabiya Trough (e.g. Abadi et al., 2008; Galushkin et al., 2014).

From the subsidence curves of the well A1-119 and the pseudo-well PW-0360, I noticed that subsidence rate is slower during the late Upper Cretaceous - Paleocene time owing for possible post-rift thermal subsidence, during short time duration. Possible uplift shaped the Sirt Basin during the Upper Cretaceous related to major plate movements (e.g. van der Meer and Cloetingh, 1993; Janssen et al. 1995), and hypothesised intraplate interactions (e.g. Fairhead et al., 2013), this followed by abrupt and rapid subsidence during Paleocene (66 Ma – 56 Ma) and Middle – Late Eocene (49 – 33.7 Ma).

At the A1-119 well, the subsidence rate during these periods is lower than the subsidence observed from the pseudo well (PW 0360), because the well A1-119 is possibly located on structural high or ridge as suggested by Hallett and El Ghoul 1996. The area under the pseudo

well PW360 is possibly uplifted during the period from Upper Cretaceous - Paleocene then subsequently modified by more basin subsidence during the Mid – Late Eocene as observed by the development of the depocentre and the tilting of the old strata. Stretching normally produces domino style fault array within the brittle crust (Glennie, 1986) and tilted fault blocks have been imaged on some seismic sections within Ajdabiya Trough (this study). The relative movement between such blocks requires a combination of simple shear and rotation (Jackson, 1987). If the faults are assumed to be planar, it is very straightforward to estimate the amount of horizontal extension (Jackson and McKenzie, 1984a, b)

8.7 Fault Systems Evolution

8.7.1 Preface

Study of fault system evolution such as fault growths and timing requires detailed analysis of the syn-rift sequences within each defined fault block. Depositional patterns such as thickness and onlap patterns within syn-rift tectonic stratal units provide details on the spatial characteristics of fault zone at particular stages of evolution (Jackson et al., 2002). Within the core of the thesis (chapter 7), I have introduced the results of research on the normal fault displacements and geometry, fault segmentation, and fault growth associated with basin evolution within the Ajdabiya Trough. The discussion presented in chapter (7) is based purely on the interpretation of the geometric evolution of the faults and the associated grabens or half-grabens. Despite the obvious limitations in the range of data, it is my hope that the analysis provided sufficient framework for interpreting the faulting and the stratigraphic record of the area. Seismic lines have been used to highlight the Mesozoic - Cenozoic structure and evolution of the Ajdabiya Trough. Northern terminations of the Ajdabiya Trough fault system comprise NW-SE trending normal faults that form grabens and/or half graben morphologies (Figures 5.21 & 5.22). In seismic cross sections (e.g. Figure 5.21) some faults show decrease in dip with increasing depth indicating listric fault geometry (e.g. Baird et al., 1996). Some faults are characterized by different segments based on strike directions. The segments suggest a linked fault system indicating an important mechanism for fault growth (Cartwright, Trudgill, & Mansfield, 1995; Peacock, 1991).

Drag folds form within hanging-walls as a result of fault propagation into monocline structures developed by differential compaction of strata. This geometry resembles a similar compaction-related geometry discussed by Skuce, (1994) for faulting in the Ajdabiya Trough which subsequently prevailed by the development of faulted monocline structures.

Relay ramp occur between normal fault segments, which eventually becoming breached by hard linkage of the fault segments. Both the seismic cross sections and thickness maps show that BF2 and BF3 developments with depth (Figure 5.7 and Figure 5.8A) are almost identical with the description of an interpreted breached relay ramp structure.

8.7.2 Faults Geometry and Graben Evolution

The cross sectional faults geometries in the Ajdabiya Trough are dominated by planar fault segments trending mainly in NW-SE direction with other fault orientations towards the NE-SW and N-S. Curvature observed in some areas, suggests that some structures are listric in form at depth. The fault segments separating Pre-Cretaceous pre-rift lithologies in the footwalls from Upper Cretaceous syn-rift sequences in the hanging walls of the mapped fault blocks. The change in fault orientations along strike gives some mapped fault zones a curvilinear pattern in plan view.

Fault segments are tipping out along strike with evidence of linkage along the immediate hanging-wall of some mapped fault blocks. A series of fold structures are observed that have axes oriented in a NW-SE direction, mainly parallel to the direction of the mapped faults. The mapped faults along the eastern portion of the Ajdabiya Trough are associated with displacement maxima and extensional hanging-wall basins. Displacement maxima and transverse hanging-wall synclines indicate the location and length scales over which paleosegments were active (e.g. Young et al., 2001). The faults are strongly segmented with evidence of segment linkage and segment overlapping forming possible intra basin highs at segment interaction zones. Minor folding observed in the area is also likely to be due to ductile deformation in a relay ramp formed between two overlapping faults along the eastern margin of the trough.

There are a number of NW-SE trending faults separated into sub-populations of synthetic and antithetic faults of variable arrays that can be observed on the 2D seismic data. Some faults

terminate against these faults at possible overlap zones, and crossing both the foot-walls and the hanging-walls in some places.

Within extensional environments the fault depth and dip may be determined from the associated roll-over anticline, as long as the hanging-wall stratigraphy is accurately determined (Kerr and White, 1994). It can be proposed from the fault analysis that probably during extension there is a net rotation of each fault block accommodating regional extension, with changes in the dip of the faults along strike. Syn-rift sequences related to the Cretaceous rift episodes can be identified on seismic sections within the Ajdabiya Trough area (e.g. Baird et al., 1996). Fault blocks are assumed to rotate rigidly with a different accommodation zone at their base (Cartwright et al., 1995). The syn-rift sediment package along the western side of the Ajdabiya Trough becomes more symmetric as rotation continues and onlaping on the foot-wall blocks. Onlap of Cretaceous strata against faults, later deformed by compaction (e.g. Skuze, 1994), demonstrates the progressive post-rift sedimentary infill in deep-water environment (e.g. Baaske et al., 2014).

8.7.3 Growth and Segmentation

Characterization of normal fault architectures in the Ajdabiya Trough has been achieved through the interpretation of the 2D seismic data. This has enabled the recognition of a significant amount of segmentation of the fault systems in the area. The identified faults have been initially segmented. Linkages between segments occurred through the development of NW-SE oriented connecting faults. Tip line shapes of the mapped faults located along the same fault zone in the eastern part of the study area indicate that segmentation has an impact on the growth tendencies of the faults and can be used to recognize locations of fault segment boundaries. From the displacement-distance profiles, a series of fault segments of 5-10 km length have been recognized. The analysis illustrates that the growth of these faults was characterized by, initially isolated segments that linked to form a single, through going faults. The isolated segments grow by both linkage and radial tip propagation, with maximum rates of displacement at the centre of the segments (evidenced by along-strike throw profiles and models). Consequently, the positions of maximum displacement on some faults are tilted from the centre of some faults towards the adjacent structures. Relay ramp structures may be developed as stated above and probably breached during segment linkage stages. With

linkage the lengths of the faults increases whilst the maximum displacement is hardly changed hence, the ratio of maximum displacement to length decreases significantly. The effects of the faults interactions are considered to be the primary control on the rate of displacement along the identified faults arrays.

8.7.4 Comparison of the Structural Trends Inferred from Gravity/Magnetic Data with the Fault Interpretation from 2D seismic Data

Interpretation of the 2D seismic data provided key geometric and geologic constrains for a 2D structural model along seismic profiles. Gravity and magnetic depth estimates provided constraints for basement depth and geometry. Density, magnetization and geometry were tested to improve the data fit for gravity and magnetic modelling purposes.

Gravity-derived anomalies were used as guides for the fault orientations and indicative of the tectonic control influencing the Mesozoic and Cenozoic strata. These anomalies possibly related to narrow structural highs and lows bound by system of extensional faults and underlain by pre and syn-rift rocks. An example of this is the thickness of the Lower Cretaceous units where strong NW-SE trending gravity highs and lows exist and where the few wells located on these highs and lows show substantial thinning and thickening of strata. The thickness of the pre and syn-rift section is interpreted by using the 2D seismic and well-log information, supplemented by indirect inferences that can be made from gravity data analysis. For instance the syn-rift section is considered as one package, because gravity and magnetic data cannot distinguish individual units.

Mainly high angle fault and a homogeneous basement terrene were interpreted for comparison. The seismic images show that the Ajdabiya Trough fault zone is characterized by west-tilted and chaotic fault blocks across a 3–5 km wide zone, as shown in the 2D seismic profiles. Faults interpreted from the gravity and magnetic data provide additional evidence for the Ajdabiya Trough fault system, especially in the southern part, where its magnetic expression is unclear. Part of the expression of the Ajdabiya Trough fault system in the gravity and magnetic data coincides with several north-south trending, elongated gravity and magnetic anomalies within the trough.

8.7.5 Comparison of the Timing and Magnitude of Faulting with the Timing and Magnitude of Tectonic Subsidence

Within the Ajdabiya Trough, the subsidence data show that thermal cooling at the post-rifting stage leads to thermal subsidence and basin formation. Broad-scale downwarping patterns, in the absence of faulting, may also suggest a component of lithospheric folding in the late stage post rift evolution (e.g. Cloetingh et al., 1999). Fault activity within the Ajdabiya Trough is relatively small during the Cenozoic compared with the observed high rate of tectonic subsidence which mainly controlled by low fault movement and component of thermal relaxation and sediment loading. The rifting which formed the Sirt Basin started in the Permo-Triassic (at ca; 298 - 200 Ma) and resulted in large scale crustal faulting and tectonic subsidence (e.g. Gumati and Kanes, 1985; van der Meer and Cloetingh, 1993; Anketell, 1996; Baird et al., 1996; Schroeter, 1996; Hallett, 2002; Guiraud et al., 2005; Abadi et al., 2008, and references therein). During early stages of basin subsidence, the fault system has experienced large fault movement characterized by stratigraphic growth signatures which are recognised on seismic profiles throughout the study area. Maximum fault throws and fault heaves are obtained from faults trending approximately NW-SE and following the main trend of the Ajdabiya Trough and mainly superimposed along the basement fabric. There is a good correlation between the timing of normal faulting identified in seismic data and the identified periods of accelerated subsidence determined by theoretical analyses, which suggests that the cause of subsidence in the Ajdabiya Trough is primarily lithospheric extension. The oldest sediments are present mainly in the eastern part of the trough. They consist of locally deposited coarse conglomerate of the Bahi Formation (e.g. Hallett, 2002) suggesting that faulting was coavel with the initiation of basin subsidence. However the trend of faults associated with these strata is unknown. There is a clear evidence that northeast-southwest trending faults with a strike slip component, may have played a significant role in the formation of small, north-south extending, pull-apart basin formed during the Neocomian, prior to the dextral wrenching in the western Sirt Basin (Anketell, 1996). Younger sediments of Oligocene – Miocene age vary in thickness as the locus of subsidence shifted during deposition. The greatest thickness of Oligocene – Miocene strata are >2500m and occur in the north-central part of the trough. The fine grained character of the sediments (e.g. Hallett, 2002) and the fact that local remnants of similar strata are found south of the basin, indicate

that faulting along the present margins of the basin was not intense during the Oligocene and Miocene. Strata in the eastern part of the Ajdabiya Trough extended eastward into the Cyrenaica region over the Amal Platform and the Rakb High, where it can be shown that graben formation is began contemporaneous to the establishment of the Ajdabiya Trough due to rapid and continuous subsidence during the Turonian time equivalent to same subsidence in the Hameimat Trough to the southeast (e.g. Abadi et al., 2008) and the Solouq Depression in the northeast (El Arnauti et al., 2008). Triassic – Early Cretaceous sediments were deposited over a broader region and their present distribution is partly a result of Permo-Triassic – Early Cretaceous faulting. However the strata that were deposited along the margins of the Ajdabiya Trough are much thinner than those in the east, indicating that faulting and tectonic subsidence were greatest in the trough during this time period.

8.8 Tectonic Model for Cenozoic Evolution of Ajdabiya Trough

The tectonic evolution model for the Ajdabiya Trough (Figure 8.8) is set in a framework of plate tectonic events. This model is based on the Cretaceous tectono-stratigraphic evolution of the Sirt Basin. The first rift episode contains an initiation phase (Figure 8.8), followed by a linkage phase during which individual basement and Cretaceous faults begin to link up and form through-going fault systems. As displacement is facilitated by fewer faults, the depocentres that border these faults are subject to higher subsidence rates and may become under filed. During the second rift episode, strain is accommodated by reactivation of pre-existing faults resulting in rift climax without preceding rift initiation or linkage stages.

Pronounced subsidence and fault block rotation and subsequent post-rift thermal subsidence produces deep basin and reversals of sedimentary system.

The model shows rotated block structures and half-grabens at the top of the crystalline basement that confirms the traditional structural style of rifting in the Sirt Basin (Rossi et al., 1991; Guiraud and Bosworth, 1997). These structures could reflect Early Mesozoic syn-rift sedimentary rocks deposited in grabens and/or half-grabens that developed during brittle extensional reactivation of pre-existing shear zones (Anketell, 1996).

The internal crustal structures beneath the Ajdabiya Trough would then be expressions of Mesozoic - Cenozoic compressional and extensional tectonics.

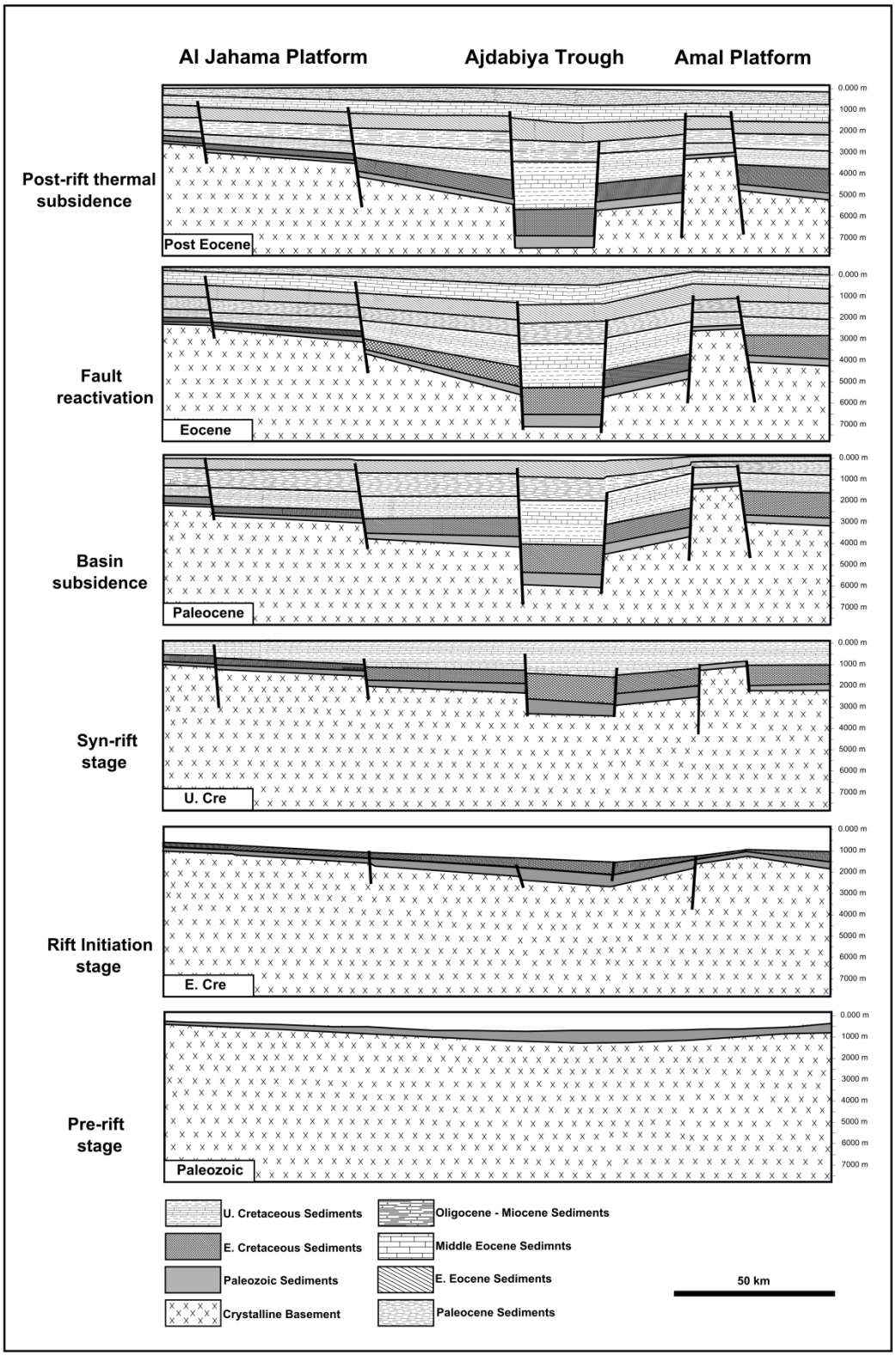

Figure 8.6: Hypothesised tectonic model for the Ajdabiya Trough shows the structural development and basin evolution of the area.

The regional Lower Cretaceous tectonic models published by Guiraud and Maurin (1991, 1992) indicate a second phase of Lower Cretaceous rifting with a NW-SE trend.

This was supported by a set of NW-SE trending gravity and magnetic anomalies obtained from the gravity and magnetic study (chapter 4). The tectonic model reflects a simple asymmetric rift basin with steeply dipping basin-bounding faults in the upper crust. It is most likely that Permo Triassic – Jurassic extension reactivated pre-existing basement faults of Palaeozoic age (Thusu 1996) and thereby created a series of sub-basins and half-grabens typically lead to complex stratigraphic relationships produced by a combination of sea level changes and progressive burial. The subsidence data in the Ajdabiya Trough suggest that this part of the basin formed through stretching factors (β) of about 1.5, which are more typical of intra-continental rifting.

8.9 Future Work

Although the Ajdabiya Trough has been fairly investigated during the last decade, there are still a number of issues which remain unresolved, such as: (1) The syn-rift stratigraphy (2) the structure of the deep crust (3) The uplift and erosion of the internal structures during the Cenozoic (3) Acurate fault analysis (4) The differences in the amount of basement subsidence between different areas within the trough.

In order to improve our current understanding of the Ajdabiya Trough rift, as well as provide further constraints for future works, it is crucial that additional geological and geophysical datasets are evaluated. 3-D seismic data, for example, would be essential to determine, in detail, the architecture" of the main rift basin and fault systems. This will further improve the understanding of the interplay between ongoing rift evolution and sedimentation. It would also be useful to investigate in a systematic way the influence of the fault farmwork and the Cenozoic sequence stratigraphy on the evolution of the observed relay ramp structure along the eastern margin of the trough. Mapping for example the displacement variations on the faults in relation to nearby faults or in relation to intersection with other faults, or comparing fault orientations in modelled accommodation zones with natural ones can provide further insight in the intriguing complexity of fault interactions.

More wells (cores and wireline logs) from Ajdabiya Trough should be used for further detailed sedimentological and sequence stratigraphic interpretations. It is strongly

recommended to drill the sediments within the main depocentres, in order to quantify the pre-, syn- and post-rift sequences, and establish good correlations with the well-known stratigraphy of the near areas. In this case selection of surface sections (outcrop) in the Cyrenaica Platform for detailed study, including structural, stratigraphic and sedimentological aspects, would be useful. This would be particularly important for documenting various factors influencing structural styles and facies distribution, and explain issues of facies cyclicity, and sequence stratigraphy. The 3D seismic and well data could be used to gain insights into the complex deformation history of the Ajdabiya Trough, and to understand more about the tectonic subsidence and uplift history of the trough. This requires re-evaluation of any previous and available 3D and well data. However, since the seismic coverage is sparse and widely spaced within particular areas, it may be advisable to shoot an additional set of 2D seismic lines to improve resolution of the structure.

More work is required in order to validate the subsidence analysis. A key subject that can bring clarification to the understanding of the tectonic subsidence of the Ajdabiya Trough relates with a more detailed lithostratigraphic, chronostratigraphic and paleontological controls that allow dating the main subsidence events resulting from crustal extension and subsequent thermal relaxation. This must be validated by using bottom-hole temperature and heat flow data also.

Results from such task would have major impact on dating the exact age of the main regional depositional units and their related widespread unconformities, thus allowing to better constrain subsidence periods within the trough, as well as their variable magnitude, in addition to precise kinematic controls of strike-slip Mesozoic deformation along the eastern margin of the Ajdabiya Trough.

8.10 Conclusions

- The Mesozoic - Cenozoic of the Ajdabiya Trough consists of thick successions of shallow marine carbonates, evaporites and deep marine shales which have been divided into six mega-sequence sets or stratigraphic units bounded by tectonically induced unconformities.

- The recognized stratigraphic architecture of the Ajdabiya Trough is influenced by sea-level changes and minimal tectonic effects during the Cenozoic, while observed progradation along the trough margin is attributed to increasing sedimentation rates presumably under control of main basin bounding faults and deep rift related sequences observed within Cretaceous and older strata.
- The development of carbonate platform along the eastern margin of the Ajdabiya Trough during Paleocene – Middle Eocene suggest that the history of this part is dominated by interaction between regional effects, and governed by thermal subsidence consequent upon extension.
- During the Early to Middle Eocene, the stratigraphic sequences are characterized by erosional unconformities and channel incision during lowstand system tracts (LST).
- Conversely highstand system tract carbonates are associated with sheet-like debris flows, mass transport deposits and turbidites supply sediment into deep water settings.
- Tectonic subsidence maps show a systematic SE to NW shift in the loci of maximum and minimum subsidence, accompanied by seaward shift of the depocentre, which parallels the structural trend of the Ajdabiya Trough.
- The post-rift period in the Ajdabiya Trough can be divided into three main phases characterized by specific subsidence patterns and sedimentation rates.
- The analysis revealed that the depositional history of the trough, show the typical subdivision for extensional fault blocks and sub-basins into syn-rift depositional sequences dominated by NW-SE, NE-SW, and E-W trending structures which form a complex, structurally coherent linked fault system and some of them show component of strike slip movement possibly associated with re-activation of faults and strain partitioning.
- Hard-linkage across breached relay ramps formed at overlap zones and via NE-SW trending strike slip faults which comprise a minor component of the rift system.
- The timing of fault activity within the Ajdabiya Trough shows that the majority of the faults are initiated early during the basin forming time (collapse of Sirt Arch during Early Cretaceous) and the number of faults are broadly increased and controlled by a continuing subsidence along the trough bounding faults.

APPENDIXE

Analysis of Fault Zone Characteristics Using Potential Field and Seismic Data, Al Hagfa Trough, Sirt Basin - Libya

H.B. Ghanoush (Department of Earth Sciences)

Department of Earth Sciences, Conference 3-6- 2013, Durham University

Abstract: In this study, gravity data has been used in conjunction with seismic data to map and model the structural and stratigraphic elements in and around the Al Hagfa Trough, central Sirt Basin, Libya. 2D seismic data reveal erosion and truncation of pre-rift strata and the thinning and onlapping of syn-depositional sequences onto normal fault scarps, suggesting that the basin experienced rifting and erosion. The rift-related fault zone is about 150 km long and is composed of three 45-50 km long planar, normal fault segments. These segments are bounded on the east by NW-SE trending gravity high which results from the density contrast between the Palaeozoic basement and Mesozoic-Cenozoic rocks and defines the Zaltan Platform structural trend. The western boundaries are marked by both gravity highs and lows which includes Al Bayda Platform and Al Hagfa Trough. The gravity minima are associated with longitudinal synclines developed during fault growth and characterized by thick wedges, of syn and post- rift sediments. The structural framework has important consequences for the Cretaceous hydrocarbon plays associated with the rifted province of Al Hagfa Trough. A possible breached relay ramp as evidenced from seismic and gravity data probably has a great influence on the hydrocarbon migration and entrapment in the study area.

Cenozoic Subsidence and Lithospheric Stretching Deformation of the Ajdabiya Trough Area, Northeast Sirt Basin, Libya*

H.B. Ghanoush[1], J. Imber[1], and K. McCaffrey[1]

Search and Discovery Article #10695 (2014) Posted December 29, 2014
*Adapted from extended abstract prepared in conjunction with poster presentation at AAPG 2014 Annual Convention and Exhibition, Houston, Texas, April 6-9, 2014,

1.Structural Geology Group, Department of Earth Sciences, University of Durham, Science Site, South Road, Durham DH1 3LE, UK (ganoush@hotmail.com)

Abstract

The Ajdabiya Trough is a failed rift that represents the deepest part of the Sirt Basin, Libya It is postulated that more than 7000 m of Mesozoic-Cenozoic sediments accumulated in this depocentre (Rusk, 2001; Hallett, 2002). The Ajdabiya Trough has significant petroleum potential. However, most exploration activity has focused on the relatively shallow basin flanks and adjacent platforms. As a result, the structural and stratigraphic development of the central Adjabiya Trough is poorly known. The aim of this study is to use 2D seismic reflection profiles, potential field data and information from exploration wells to illustrate key features of the tectonic evolution across the Ajdabiya Trough. In particular, these data are used to determine the tectonic subsidence during the latest syn-rift (Cretaceous to Palaeocene) to post-rift periods, and to estimate syn-rift crustal stretching. Our study builds on previous research by Gumati (1981), Gumati and Kanes (1985), van der Meer and Cloetingh (1993) and Abadi et al. (2008).

Subsidence is calculated by assuming 1D Airy isostatic equilibrium, which allows backstripping based on sedimentary thicknesses, horizon ages, lithologies, and paleo-water depths obtained from well information and crosschecked against sediment isopach and structural maps. The combination of these two approaches allows quantification of tectonic and total subsidence and their relationship to fault activity during the syn- to post-rift stages. The syn-rift sedimentary package has not been encountered or entirely drilled in most of the wells. For this reason, a pseudo (synthetic) well derived from 2D seismic interpretation has also been modeled. In addition to the syn-rift package, the location of the pseudo-well was chosen in order to evaluate the history of the deepest parts of the basin, which are not yet drilled.

Potential Field Data

Gravity Data

1- The process of preparing a gravity compilation of Libya was started in 2002 with data gathering and preprocessing to be carried out mainly in Libya. (the final project in this compilation was formerly agreed in a contract signed 20 July 2000 which called addition of available data).

2- The project comprised: Addition of new data, Correction, compilation and integration of data, map production for the whole country and subareas, data interpretation, report preparation for whole Libya and subareas.

The objectives of the project are.

1- The project was envisioned to provide a reference text and maps for ongoing research in the Libyan Petroleum Institute (LPI) and to highlight areas for priority of new data.

2- It was also direct use in areas where seismic is of poor quality such as over the Sirt volcanics, the Jabal Al Kdhar cavity limestones and areas of large sand dunes in south of country.

These objectives have been addressed as providing a wide selection of enhanced displays.

By direct modeling for such parameters as densities and gravity regional fields plus area depth solutions from Euler deconvoltion.

Additions of a magnetic data grid provided by Getech, Leeds which produced a further set of displays.

Data additions

1- The dataset output from work in 1998 formed the input to further work in 2000/2001, and was incremented by archived data originally collected by the operators Braspetro and the Waha Oil company.

2- Geological information were loaded to a spreadsheet, with assistance of LPI staff, for reference in interpretation. (Geological map of Libya were loaded from LPI image and provided a useful alternative base for the display of gravity data).

3- Oil/ Gas fields and pipelines were also added to the basemap.

4- The area of compilation extended to latitude 34N to 35N, the area was eventually extended to 35N in order to provide an adequate background for offshore concessions.

5- The Getech magnetic data grid was used during interpretation stage.

Editing and compilation

1-After suspension of the work 1998, some irregularities, apparent spikes or misties were highlighted, and were queries regarding the large shift applied to some of surveys in order to obtain a levelled dataset.

2- The merging of onshore and offshore gravity had also produced noise in the coastal zone.

3- Large shifts had been applied in 1998 to surveys in the Sirt basin.

4-Offshore data was added from the global open-satellite altimetry gravity compiled by Sandwell and others at San Diego, available from various sources including the Internet. These are not direct gravity measurements but measurements of ocean high from satellites in items of deviation from a lower order harmonic goid.

DATA PROCESSING:

Gravity processing

1- Bouguer Gravity The full dataset after compilation is of Bouguer gravity onshore and free air gravity offshore. This tends to be standard display for combined land-marine displays.

2- A correction density of 2.67cgs was used .

3- 1980 formal was used in the whole country.

1- Magnetic Data

2- The data provided by GETECH were already in residual form ,after subtraction of the appropriate reference field

2D Seismic Data

2D Acquired as coarse grid (2 to 5 km) of some 10,000km – Designed for deep targets but well suited to image shallow structures – Symmetrical 480 channel split spread, 25m receiver-group spacing, 6km maximum offset, and a vibroseis shot interval of 25m. Nominal fold is 240. – Coarse grid allows only interpretation of major features.

The 2D Seismic line spacing is quite large (2 to 5km) resulting in some uncertainty with the tie from line to line.

Well Data

B-NC213_NC215_Wells_Checkshots(1)

							Depth						TWT						Vel	seismi	Gialo Factor	intvl to Gialo	gialo - Gir Factor	gialo - hagfa	gir-UC	gialo - td
con	dee	well	X	Y	KB	Source	Gialo	Gir	Hagfa	UC	Gargaf	TD	Gialo	Gir	Hagfa	UC	Gargaf	TD	*(check); s(sonic)							
1	1	A1-114	348285	3331477	54	F	1803	2041		2469	2606	2953	1483	1611		1805	1863	1993	*	1	1.17996615	2358.732299	1.859375	3718.75			2.206186	4412.371	2.254902	4509.804
1	1	A1-41	430814	3397736	39	F	2658	3387		3993		4180	2184	2608		2896		2990	*	1	1.199175824	2398.351648	1.71934	3438.679			2.104167	4208.333	1.868337	3776.675
1	1	A1A-121	444286	3384636	72	F	2056	2534		3065	3263	3500	1500	1736		1936	2004	2088	*	1	1.322666667	2645.333333	2.025424	4050.847			2.655	5310	2.455782	4911.565
1	1	A1-NC117B	342489	3343332	69	F	2178			2784	2823	1696				1944		1954	*	1	1.243514151	2487.028302							2.5	5000
1	1	A1-NC45	482018	3283389	21	F	1256	2192	3154		3531	1010	1430	1960			2168	s		1	1.222772277	2445.544554	2.228571	4457.143	1.997895	3995.789			1.964594	3929.188
1	1	AA1-6	457695	3247720	69	F	1508	2551		3989		4406	1156	1644		2328		2544	av area6	1	1.244809689	2489.619377	2.137295	4274.59			2.102339	4204.678	2.087896	4175.793
1	1	B1-114	345223	3335437	40	F	2185	2500			2692	2804	1706	1854			1914	1950	A1-NC117B	1	1.257327081	2514.654162	2.128378	4256.757					2.536885	5073.77
1	1	B1-119	384272	3305770	27	F	2530	2763			3050	3308	2150	2284			2444	2584	i'd b	1	1.164186047	2328.372093	1.738806	3477.612					1.792627	3585.253
1	1	B1-121	458485	3343707	39	F	1827	2384		3063	3265	3408	1370	1628		1854	1920	1980	*	1	1.305109489	2610.218978	2.158915	4317.829			3.004425	6008.85	2.591803	5183.607
1	1	B1-6	352511	3326654	36	F	1845	2043		2534	2667	2710	1486	1628		1864	1904	1916	A1-NC117B	1	1.217362046	2434.724092	1.394366	2788.732			2.080508	4161.017	2.011628	4023.256
1	1	B1-LP2E	488007	3253094	59	F	1128	1838	2955			3088	888	1318	1830			1896	av area6	1	1.203828829	2407.657658	1.651163	3302.326	1.93949	3878.981			1.944444	3888.889
1	1	B1-NC117B	371253	3341215	-4	F	3414	3890				4004	2718	2956				3014	*	1	1.257542311	2515.084621	2	4000					1.993243	3986.486
1	1	C1-119	419982	3283394	32	F	2064					3460	1804					2662	B1-119	1	1.126385809	2252.771619							1.62704	3254.079
1	1	C1-121	447341	3372060	43	F	2140	2367		2989	3716	3780	1588	1712		1992	2274	2316	*	1	1.320528967	2641.057935	1.830645	3661.29			2.221429	4442.857	2.252747	4505.495
1	1	C1-95	474061	3259151	46	F	1442	2381	3338			3688	1160	1620	1960			2084	s	1	1.203448276	2406.896552	2.041304	4082.609	2.37	4740			2.430736	4861.472
1	1	C1-NC117B	389529	3326636	14	F	3420					3504	2632					2658	*	1	1.294072948	2588.145897							3.230769	6461.538
1	1	D1-114	328516	3334249	35	F	1161	1637		2417	2672	2740	1044	1320		1692	1788	1816	*	1	1.078544061	2157.088123	1.724638	3449.275			2.096774	4193.548	2.045337	4090.674
1	1	E1-114	336117	3333594	48	F	1310	1698		2538	2721	2780	1144	1366		1730	1794	1818	*	1	1.103146853	2206.293706	1.747748	3495.495			2.307692	4615.385	2.181009	4362.018
1	1	E1-95	474526	3250225	49	F	1387	2280	3495			3657	1110	1530	2000			2064	s	1	1.205405405	2410.810811	2.12619	4252.381	2.368539	4737.079			2.379455	4758.91
1	1	E1A-NC171	445367	3385450	basin was F+PT		2038	2393	2839	3002	3464	3514	1494	1660	1868	1908		2088	A1A-121	1	#VALUE!	#VALUE!	2.017045	4034.091	2.085938	4171.875	2.455645	4911.29	2.443709	4887.417
1	1	F1-114	355842	3338216	mixed cari F		2762	2911		3082	3266	3302	2268	2380		2492	2624	2648	B1-NC117B	1	#VALUE!	#VALUE!	1.330357	2660.714			1.526786	3053.571	1.421053	2842.105
1	1	F1-6	452229	3349689	followed t F		2019	2603		3208	3512	3522	1466	1720		1906	2012	2020	B1-121	1	#VALUE!	#VALUE!	2.299213	4598.425			3.252688	6505.376	2.712996	5425.993
1	1	F1-95	477511	3246525	the basin F		1315	2213	3475			3572	1020	1500	2110			2156	s	1	#VALUE!	#VALUE!	1.870833	3741.667	1.981651	3963.303			1.986796	3973.592
1	1	G1-95	472574	3251537	successi F		1417	2355	3216			3353	1120	1570	1920			1975	s	1	#VALUE!	#VALUE!	2.084444	4168.889	2.24875	4497.5			2.264327	4528.655
1	1	I1-6	375521	3352787	transgres F		3650	4100	4502			4604	2822	3052	3252			3304	B1-NC117B	1	#VALUE!	#VALUE!	1.956522	3913.043	1.981395	3962.791			1.979253	3958.506
1	1	J1-95	461551	3287350	an admix F		1748	2612	3752			4109	1280	1660	2140			2290	s	1	#VALUE!	#VALUE!	2.273684	4547.368	2.330233	4660.465			2.337624	4675.248
1	1	K1-31	482720	3302072	deposits. F		1353	2062	3191	3533		4115	1144	1544	1928	2224		2760	s	0	#VALUE!	#VALUE!	1.7725	3545	2.344388	4688.776	2.163235	4326.471	1.709158	3418.317
1	1	K1-95	475195	3272476	to shallow F		1432	2222	3173			3326	1120	1472	1900			1968	s	1	#VALUE!	#VALUE!	2.244318	4488.636	2.232051	4464.103			2.233491	4466.981
1	1	L2-12	489467	3286458	time dural F		1224	1981		3204		3802	1000	1396		1968		2256	av area6	1	#VALUE!	#VALUE!	1.911616	3823.232			2.138112	4276.224	2.052948	4105.096
1	1	L-L1-6	361730	3288262	setting in F		1595	1771	2257			3383	1412	1570	1952			2624	B1-119	1	#VALUE!	#VALUE!	1.113924	2227.848	1.225926	2451.852			1.475248	2950.495
1	1	M1-11	231760	3352908	152	F+Mas	406	874		2073	2635	2700	220	524		1196	1528	1544	av D1-11 & F	1	1.154545455	2309.090909	1.539474	3078.947			1.784226	3568.452	1.732628	3465.257
1	1	NW1-6	430747	3232771	95	F+Mas	1447				N.R.	4048	1124					2352	av area6	1	1.202846975	2405.69395							2.118078	4236.156
1	1	OO1-6	378678	3307061	12	F	2408	2530	2696		2920	2934	2072	2161	2254		2377	2387	B1-119	1	1.156370656	2312.741313	1.370787	2741.573	1.582418	3164.835			1.669841	3339.683
1	1	Q1-31	471758	3325863	57	F	1552	2199	3039	3471	4195	4648	1280	1610	1980	2150	2530	2744	s	0	1.16796875	2335.9375	1.960606	3921.212	2.124286	4248.571	2.355556	4711.111	2.114754	4229.508
1	1	S5-6	375733	3300444	31	F	2183	2263	2664		2738	2868	1890	1952	2226		2266	2346	B1-119	1	1.138624339	2277.248677	1.290323	2580.645	1.431548	2863.095			1.502193	3004.386
1	1	T1-41	473845	3405149	66	F	1118	1408	2112	2371	3676	3711	750	918	1248	1376	1916	1928	*	1	1.402666667	2805.333333	1.72619	3452.381	1.995984	3991.968	2.10262	4205.24	2.201188	4402.377
1	1	T1A-11	235644	3361966	89	F+Mas	460	1356	1781	2230	3091	3101	332	840	1080	1316	1792	1796	av b1-11 & F	1	1.11746988	2234.939759	1.76378	3527.559	1.766043	3532.086	1.836134	3672.269	1.803962	3607.923
1	1	U1-41	451440	3409442	87	F	1791	2193		2493		5422	1280	1480		1636		2792	*	1	1.33125	2662.5	2.01	4020			1.923077	3846.154	2.401455	4802.91
1	1	Z1-6	422933	3246270	77	F+Mas	1568	2043	2965	3809	N.R.	4478	1180	1400	1832	2272		2572	av area6	1	1.263559322	2527.118644	2.159091	4318.182	2.148368	4285.276	2.116972	4233.945	2.090517	4181.034
																					#VALUE!	#VALUE!	1.863063	3726.107	2.008287	4016.575	2.221679	4443.357	2.113335	4226.669

Stratigraphic data used in the subsidence calculation

Stratigraphic Data

	Unit Name	Lithology	Depth to Top (metres)	Depth to Base (metres)	Age Top (myrs)	Age Base (myrs)	ax Bathymetr (metres)	in Bathymetr (metres)	Eustasy (metres)
WELL A1-114	Quternary	1	0	118	0	2.6	15	5	25
	Top Miocene	2	118	274	2.6	11.6	30	10	30
	Middle Miocene	2	274	304	11.6	20.4	35	35	35
	Lower Miocene	4	304	1219	20.4	23	40	25	40
	Oligocene	2	1219	1668	23	33.9	50	35	67
	Augila	2	1668	1684	33.9	37.8	35	35	70
	Gialo	4	1684	1943	37.8	41.2	60	40	75
	Gir	3	1943	2049	41.2	56	65	35	73
	Paleocene	4	2049	2511	56	66	55	35	77
	U Cretaceous	2	2511	2552.4	66	100	40	10	78
	Nubian	1	2552.4	2563.4	100	140	20	5	80
	Gargaf Group	1	2563.4	2899.9	140	140	20	0	78
WELL U1-41	Quaternary	1	0	0	0	5.3	25	10	30
	Upper M	2	0	304	5.3	11.4	28	10	32
	Middle Miocene	3	304	1036	11.4	15.7	32	15	33
	Lower Miocene	2	1036	1097	15.7	23	34	12	34
	Oligocene	3	1097	1524	23	33.7	40	20	35
	Augila	3	1524	1791	33.7	37	45	15	40
	Gialo Formation	4	1791	1944	37	49	55	35	67
	Gir Formation	4	1944	2493	49	54.8	60	40	70
	Paleocene	4	2493	2660	54.8	57.9	70	50	75
	Upper Sabil Formati	3	2660	2826	57.9	62	75	45	73
	Lower Sabil Formati	4	2826	2993	62	66	65	40	77
	Maastrich	3	2993	3230	66	72.1	67	33	78
	Campanian	3	3230	3467	72.1	83.6	70	42	80
	Santonian	3	3467	3704	83.6	86.3	85	43	78
	Coniacian	3	3704	3941	86.3	89.8	80	50	67
	Turonian	3	3941	4179	89.8	90	85	65	65
	Rakb Shale	3	4179	4634	90	91.8	60	40	55
	Cenomanian2	3	4634	5213	91.8	93.9	35	20	30
	Cenomanian1	3	5213	5421	93.9	95	0	0	10
	T.D	1	5421	5421	95	140	0	0	5
WELL LL1-6									
	Quaternary	1	0	500	0	5.3	25	10	30
	Miocene	2	500	750	5.3	23	30	10	35
	Oligocene	3	750	1595	23	33.7	35	15	40
	Augila	3	1595	1771	33.7	37	45	15	67
	Gialo	4	1771	1956	37	49	50	20	68
	Gir	4	1956	2054	49	54.8	50	20	70
	Zelten	4	2054	2225	54.8	59	60	25	75
	Cra	3	2225	2258	59	61.6	65	27	73
	Heira	3	2258	2896	61.6	66	55	21	77
	Kalash	3	2896	2900	66	68	60	27	80
	Zmam	4	2900	3020	68	69	75	30	78
	Socna	3	3020	3265	69	71.3	70	28	67
	Waha	4	3265	3383	71.3	72.1	75	31	65
	TD	1	3383	3383	72.1	140	60	25	45
WELL Q1-31									
	Quaternary	1	0	100	0	5.3	25	10	30
	Miocene	2	100	840	5.3	23	30	10	35
	Oligocene	3	840	1385	23	33.9	35	15	40
	Augila	3	1385	1533	33.9	37	45	15	67
	Gialo	4	1533	2199	37	49	50	20	70
	Gir	4	2199	2860	49	54.8	60	20	75
	Kheir	3	2860	2961	54.8	57.9	65	25	73
	Harash	4	2961	3095	57.9	61	55	27	77
	Khalifa	4	3095	3183	61	62	57	21	78
	Sabil	3	3183	3527	62	65	60	27	80
	Kalash	3	3527	3686	65	72.1	75	30	78
	Sirte	3	3686	3770	72.1	83.5	70	28	67
	Tagrifet	4	3770	3962	83.5	89	75	31	65
	Hamia	3	3962	4186	89	93.5	20	25	45
	Maragh	3	4186	4250	93.5	100	10	5	25
	Nubian	1	4250	4328	100	145	0	0	0
	Silurian	3	4328	4648	145	160	0	0	15

WELL A1-119									
	Quaternary	1	0	0	0	5.3	35	10	30
	Upper Miocene	1	0	126	5.3	11.4	40	10	35
	Middle Miocene	1	126	431	11.4	15.7	45	15	40
	Lower Miocene	1	431	1330	15.7	23	55	15	67
	Oligocene	1	1330	2859	23	33.7	55	20	70
	Augila Formatior	4	2859	3137	33.7	37	60	20	75
	Gialo Formation	4	3137	3413	37	49	60	25	73
	Gir Formation	4	3413	3749	49	54.8	65	27	77
	Kheir	4	3749	3807	54.8	56	65	21	78
	Upper Sabil Format	4	3807	3828	56	57.9	70	27	80
	Marada Fm	3	3828	3885	57.9	65	85	30	78
	Marad Shale	3	3885	4030	65	71.3	80	28	67
	Sirt Shale	4	4030	4066	71.3	83.5	75	27	65
	Tagrift	3	4066	4145	75	140	70	26	45
WELL Pseudo Well PW0360									
	Quaternary	1	0	92	0	5.3	35	20	10
	Upper Miocene	1	92	398	5.3	11.4	40	20	25
	Middle Miocene	1	398	763	11.4	15.7	45	25	26
	Lower Miocene	1	763	1250	15.7	23.8	55	25	27
	Oligocene	1	1250	2640	23.8	33.7	55	25	30
	Augila Formation	4	2640	2940	33.7	37	60	30	40
	Gialo Formation	4	2940	3900	37	49	60	30	67
	Gir Formation	4	3900	4500	49	54.8	65	32	68
	Paleocene	4	4500	4620	54.8	57.9	65	34	70
	Upper Sabil	4	4620	4700	57.9	61	70	35	75
	Lower Sabil	3	4700	4950	61	65	85	37	73
	U. Cretaceous	3	4950	5650	65	98.9	80	40	79
	Lower Cretaceous	1	5650	6230	98.9	145	75	36	70
	Triassic - Jurassic	1	6230	6700	145	250	10	10	37
	Basement	1	6700	6850	250	260	5	0	30

Stratigraphic Data

Unit Name	Lithology	Depth to Top (metres)	Depth to Base (metres)	Age Top (myrs)	Age Base (myrs)	lax Bathymetr (metres)	lin Bathymetr (metres)	Eustasy (metres)
Quternary	1	0	118	0	2.6	15	5	25
Top Miocene	1	118	274	2.6	11.6	30	10	30
M.Miocene	2	274	304	11.6	20.4	35	35	35
L.Miocene	4	304	1219	20.4	23	40	25	40
Oligocene	2	1219	1668	23	33.9	50	35	67
Augila	2	1668	1684	33.9	37.8	35	35	70
Gialo	4	1684	1943	37.8	41.2	60	40	75
Gir	4	1943	2049	41.2	56	65	35	73
Paleocene	4	2049	2511	56	66	55	35	77
U Cre.	1	2511	2552.4	66	100	40	10	78
Nubian	1	2552.4	2563.4	100	115	20	5	80
Gargaf G	2	2563.4	2899.9	115	145	20	0	78

Stratigraphic Data

Unit Name	Lithology	Depth to Top (metres)	Depth to Base (metres)	Age Top (myrs)	Age Base (myrs)	lax Bathymetr (metres)	lin Bathymetr (metres)	Eustasy (metres)
Quaternary	1	0	0	0	5.3	25	10	30
Upper M	1	0	304	5.3	11.4	28	10	32
M. Miocene	1	304	1036	11.4	15.7	32	15	33
L. Miocene	1	1036	1097	15.7	23	34	12	34
Oligocene	2	1097	1524	23	33.7	40	20	35
Augila	2	1524	1791	33.7	37	45	15	40
Gialo. F.	2	1791	1944	37	49	55	35	67
Gir. F.	2	1944	2493	49	54.8	60	40	70
Paleocene	2	2493	2660	54.8	57.9	70	50	75
U. Sabil. F.	2	2660	2826	57.9	62	75	45	73
L. Sabil. F.	4	2826	2993	62	66	65	40	77
Maastrich	4	2993	3230	66	72.1	67	33	78
Campanian	2	3230	3467	72.1	83.6	70	42	80
Santonian	2	3467	3704	83.6	86.3	85	43	78
Coniacian	2	3704	3941	86.3	89.8	80	50	67
Turonian	4	3941	4179	89.8	90	85	65	65
Rakb Shale	2	4179	4634	90	91.8	60	40	55
Cenomanian	4	4634	5213	91.8	93.9	35	20	30
TD	1	5213	5421	93.9	145	0	0	10

Stratigraphic Data

Unit Name	Lithology	Depth to Top (metres)	Depth to Base (metres)	Age Top (myrs)	Age Base (myrs)	lax Bathymetr (metres)	Min Bathymetr (metres)	Eustasy (metres)
Quaternary	2	0	80	0	5.3	25	10	30
Miocene	2	80	750	5.3	23	30	10	35
Oligocene	2	750	1495	23	33.7	35	15	40
Augila	2	1495	1595	33.7	37	45	15	67
Gialo	4	1595	1771	37	49	50	20	68
Gir	2	1771	2054	49	54.8	50	20	70
Zelten	4	2054	2225	54.8	59	60	25	75
Khaleifa	2	2225	2258	59	61.6	65	27	73
Heira	4	2258	2896	61.6	66	55	21	77
Kalash	4	2896	2900	66	68	60	27	80
Zmam	2	2900	3020	68	69	75	30	78
Socna	2	3020	3265	69	71.3	70	28	67
Waha	4	3265	3350	71.3	72.1	75	31	65
TD	4	3350	3383	72.1	145	60	25	45

Stratigraphic Data

Unit Name	Lithology	Depth to Top (metres)	Depth to Base (metres)	Age Top (myrs)	Age Base (myrs)	lax Bathymetr (metres)	Min Bathymetr (metres)	Eustasy (metres)
Quaternary	2	0	100	0	5.3	25	10	30
Miocene	2	100	840	5.3	23	30	10	35
Oligocene	2	840	1385	23	33.9	35	15	40
Augila	2	1385	1533	33.9	37	45	15	67
Gialo	4	1533	2199	37	49	50	20	70
Gir	4	2199	2860	49	54.8	60	20	75
Kheir	2	2860	2961	54.8	57.9	65	25	73
Harash	4	2961	3095	57.9	61	55	27	77
Khalifa	4	3095	3183	61	62	57	21	78
Sabil	2	3183	3527	62	65	60	27	80
Kalash	2	3527	3686	65	72.1	75	30	78
Sirte	2	3686	3770	72.1	83.5	70	28	67
Tagrifet	4	3770	3962	83.5	89	75	31	65
Hamia	2	3962	4186	89	93.5	25	25	45
Maragh	1	4186	4250	93.5	100	10	5	25
Nubian	1	4250	4328	100	145	0	0	0
Silurian	1	4328	4648	145	160	0	0	15

Stratigraphic Data

Unit Name	Lithology	Depth to Top (metres)	Depth to Base (metres)	Age Top (myrs)	Age Base (myrs)	lax Bathymetr (metres)	Min Bathymetr (metres)	Eustasy (metres)
Quaternary	1	0	0	0	5.3	35	10	30
Upper Miocen	1	0	126	5.3	11.4	40	10	35
Middle Miocen	1	126	431	11.4	15.7	45	15	40
Lower Miocen	1	431	1330	15.7	23	55	15	67
Oligocene	1	1330	2859	23	33.7	55	20	70
Augila Formatic	4	2859	3137	33.7	37	60	20	75
Gialo Formatio	4	3137	3413	37	49	60	25	73
Gir Formation	4	3413	3749	49	54.8	65	27	77
Kheir	4	3749	3807	54.8	56	65	21	78
er Sabil Forma	4	3807	3828	56	57.9	70	27	80
Marada Fm	3	3828	3885	57.9	65	85	30	78
Marad Shale	3	3885	4030	65	71.3	80	28	67
Sirt Shale	4	4030	4066	71.3	83.5	75	27	65
Tagrift	3	4066	4145	83.5	140	70	26	45

Stratigraphic Data

Unit Name	Lithology	Depth to Top (metres)	Depth to Base (metres)	Age Top (myrs)	Age Base (myrs)	lax Bathymetr (metres)	lin Bathymetr (metres)	Eustasy (metres)
Quaternary	2	0	339	0	5.3	35	10	10
Miocene	2	339	1329	5.3	23	40	10	25
Oligocene	2	1329	2064	23	33.9	45	15	26
Augila	2	2064	2100	33.9	37	55	15	27
Gialo	4	2100	3017	37	49	55	20	30
Gir	2	3017	3356	49	54.8	60	20	40
Kheir	2	3356	3410	54.8	57.9	60	25	67
Zelten	2	3410	3472	57.9	61	65	27	68
Khaleifa	2	3472	3523	61	62	65	21	70
Lower Sabil	2	3523	3583	62	65	70	27	75
Kalash	4	3583	3600	65	72.1	85	30	73
Sirt Shale	2	3600	3710	72.1	83.5	80	28	79
Tagrift	2	3710	3790	83.5	89	75	31	70
Hamia	4	3790	3843	89	93.5	10	5	37
Pre-U. Cre.	4	3843	4223	93.5	100	5	3	30
E. Cret	2	4223	5435	100	113	5	3	10
E. Cret	1	5435	6795	113	145	5	3	7

Unit Name	Lithology	Depth to Top (metres)	Depth to Base (metres)	Age Top (myrs)	Age Base (myrs)	lax Bathymetr (metres)	lin Bathymetr (metres)	Eustasy (metres)
Quaternary	2	0	261	0	5.3	35	10	10
Miocene	2	261	1066	5.3	23	40	10	25
Oligocene	2	1066	1765	23	33.9	45	15	26
Augila	2	1765	2306	33.9	37	55	15	27
Gialo	4	2306	2893	37	49	55	20	30
Gir	4	2893	3142	49	54.8	60	20	40
Kheir	2	3142	3235	54.8	57.9	60	25	67
Zelten	4	3235	3297	57.9	61	65	27	68
Khaleifa	4	3297	3340	61	62	65	21	70
Lower Sabil	2	3340	3402	62	65	70	27	75
Kalash	2	3402	3452	65	72.1	85	30	73
Sirt Shale	2	3452	3545	72.1	83.5	80	28	79
Tagrift	4	3545	3651	83.5	89	75	31	70
Hamia	2	3651	3728	89	93.5	10	5	37
Pre-U. Cre.	1	3728	4056	93.5	100	5	3	30
E. Cret	1	4056	5247	100	145	5	3	10
Tri - Jur	1	5247	6009	145	200	5	3	7
Basement	1	6009	7440	200	250	0	0	5

Stratigraphic Data

Unit Name	Lithology	Depth to Top (metres)	Depth to Base (metres)	Age Top (myrs)	Age Base (myrs)	lax Bathymetr (metres)	lin Bathymetr (metres)	Eustasy (metres)
Quaternary	2	0	339	0	5.3	35	10	10
Miocene	2	339	1329	5.3	23	40	10	25
Oligocene	2	1329	2689	23	33.9	45	15	26
Augila	2	2689	2922	33.9	37	55	15	27
Gialo	4	2922	3817	37	49	55	20	30
Gir	2	3817	4127	49	54.8	60	20	40
Kheir	2	4127	4181	54.8	57.9	60	25	67
Zelten	2	4181	4243	57.9	61	65	27	68
Khaleifa	2	4243	4294	61	62	65	21	70
Lower Sabil	2	4294	4354	62	65	70	27	75
Kalash	4	4354	4371	65	72.1	85	30	73
Sirt Shale	2	4371	4481	72.1	83.5	80	28	79
Tagrift	2	4481	4561	83.5	89	75	31	70
Hamia	4	4561	4614	89	93.5	10	5	37
Pre-U. Cre.	4	4614	4994	93.5	100	5	3	30
E. Cret	2	4994	6206	100	113	5	3	10
E. Cret	1	6206	7566	113	145	5	3	7

			A1-12	Quaternary	2	0	410	0	5.3	25	10	30
				Miocene	2	410	798	5.3	23	30	10	35
				Oligocene	2	798	834	23	33.7	35	15	40
				Augila	2	834	1072	33.7	37	45	15	67
				Gialo	4	1072	1140	37	49	50	20	68
				Gir	2	1140	1405	49	54.8	50	20	70
				Zelten	4	1405	1961	54.8	59	60	25	75
				Khaleifa	2	1961	2069	59	61.6	65	27	73
				Heira	4	2069	2171	61.6	66	55	21	77
				Lower Sabil	4	2171	2300	66	68	60	27	80
				Kalash	2	2300	2698	68	90	75	30	78
				Rakb a	2	2698	2874	90	91.8	70	28	67
				Nubian	4	2874	3009	100	145	75	31	65
				TD	4	3009	3033	145	150	60	25	45
				Quaternary	2	0	80	0	5.3	25	10	30
HHH1-6	Etel Eocene	3336.00		Miocene	2	80	750	5.3	23	30	10	35
HHH1-6	Sheghega	3655.00		Oligocene	2	750	1495	23	33.7	35	15	40
HHH1-6	Gialo	3655.00		Augila	2	1017	1114	33.7	37	45	15	67
HHH1-6	Domran	5831.00		Gialo	4	1114	1777	37	49	50	20	68
HHH1-6	Ruaga	7212.00		Gir	2	1777	2054	49	54.8	50	20	70
HHH1-6	Hagfa	8017.00		Zelten	4	2054	2225	54.8	59	60	25	75
HHH1-6	Heira	8017.00		Khaleifa	2	2225	2443	59	61.6	65	27	73
HHH1-6	Zmam	9968.00		Heira	4	2443	3038	61.6	66	55	21	77
HHH1-6	Kalash	9968.00		Kalash	4	3038	2900	66	68	60	27	80
HHH1-6	Socna	10328.00		Zmam	2	2900	3148	68	69	75	30	78
HHH1-6	Waha	10843.00		Socna	2	3148	3305	69	71.3	70	28	67
HHH1-6	Nubian	10903.00		Waha	4	3305	3350	71.3	72.1	75	31	65
				Nubian	1	3350	3383	72.1	145	60	25	45
				Quaternary	2	0	80	0	5.3	25	10	30
C1-119	Oligocene	4360.00		Miocene	2	80	1329	5.3	23	30	10	35
C1-119	Middle Eocene	6772.00		Oligocene	2	1329	2000	23	33.7	35	15	40
C1-119	Gialo	6772.00		Augila	2	2000	2064	33.7	37	45	15	67
C1-119	Tamet	6772.00		Gialo	4	2064	3017	37	49	50	20	68
C1-119	Lower Eocene	9900.00		Gir	2	3017	3664	49	54.8	50	20	70
C1-119	Paleocene	12022.00		Paleocene	4	3664	3670	54.8	59	60	25	75
B1-119	Miocene	295.00		Quaternary	2	0	90	0	5.3	25	10	30
B1-119	Oligocene	3900.00		Miocene	2	90	1188	5.3	23	30	10	35
B1-119	Upper Eocene	7960.00		Oligocene	2	1188	2426	23	33.7	35	15	40
B1-119	Tamet	8298.00		Augila	2	2426	2529	33.7	37	45	15	67
B1-119	Gialo	8298.00		Gialo	4	2529	2810	37	49	50	20	68
B1-119	Middle Eocene	8298.00		Gir	2	2810	2840	49	54.8	50	20	70
B1-119	Gattar	9065.00		Paleocene	4	2840	2873	54.8	65	60	25	75
B1-119	Lower Eocene	9220.00		Cretaceous	2	2873	3050	65	100	65	27	73
B1-119	Nabiha	9244.00		Cam-Ord	1	3050	3038	100	115	55	21	77
B1-119	Paleocene	9320.00		Gargaf	1	3038	3308	115	145	60	27	80
B1-119	Kotla	9426.00										
B1-119	Marada	9426.00										
B1-119	Cambro Ordovic	10006.00										
B1-119	Gargaf	10006.00										
B1-6		16.00	Pliocene	Quaternary	2	0	161	0	5.3	25	10	30
B1-6		16.00	Fortino	Miocene	2	161	1400	5.3	23	30	10	35
B1-6		530.00	Zaggut	Oligocene	2	1400	1700	23	33.7	35	15	40
B1-6		530.00	Miocene	Augila	2	1700	1766	33.7	37	45	15	67
B1-6		530.00	Tamet	Gialo	4	1766	2600	37	49	50	20	68
B1-6		5795.00	Sheghega	Gir	2	2600	2659	49	54.8	50	20	70
B1-6		5795.00	Gialo	Zelten	4	2659	2663	54.8	65	60	25	75
B1-6		5795.00	Zmam	Kalash	2	2663	2667	65	100	75	30	78
B1-6		8750.00	Kalash	Nubian	1	2667	2670	100	145	75	31	65
B1-6		8750.00	Nubian	TD	1	2670	2674	145	150	60	25	45
B1-6		8772.00	TD									
U2-6		16.00	Pliocene	Quaternary	2	0	30	0	5.3	25	10	30
U2-6		16.00	Muailah	Miocene	2	30	527	5.3	23	30	10	35
U2-6		1672.00	Etel Eocene	Oligocene	2	527	1005	23	33.7	35	15	40
U2-6		2400.00	Tamet	Augila	2	1005	1463	33.7	37	45	15	67
U2-6		3198.00	Sheghega	Gialo	4	1463	2072	37	49	50	20	68
U2-6		3198.00	Gialo	Gir	2	2072	2588	49	54.8	50	20	70
U2-6		3198.00	Zmam	Zelten	4	2588	2590	54.8	65	60	25	75
U2-6		8490.00	Kalash	Kalash	2	2590	2744	65	71.3	75	30	78
U2-6		8490.00	Socna	Socna	1	2744	2865	71.3	100	75	31	65
U2-6		9002.00	Waha	Gargaf	1	2865	2926	100	150	60	25	45
U2-6		9326.00	Gargaf									
				Quaternary	2	0	30	0	5.3	25	10	30
				Miocene	2	30	527	5.3	23	30	10	35
				Oligocene	2	527	3368	23	33.7	35	15	40
	I1-6			Augila	2	3368	3566	33.7	37	45	15	67
				Gialo	4	3566	3985	37	49	50	20	68
				Gir	4	3985	4383	49	54.8	50	20	70
				Ruaga	2	4383	4501	54.8	61.6	60	25	75
				Heira	2	4501	4604	61.6	66	75	30	78
F1-41	Miocene	900.00	Quaternary	2	0	274	0	5.3	25	10	30	
F1-41	Oligocene	3050.00	Miocene	2	274	930	5.3	23	30	10	35	
F1-41	Upper Eocene	3900.00	Oligocene	2	930	1189	23	33.7	35	15	40	
F1-41	Middle Eocene	4350.00	Augila	2	1189	1326	33.7	37	45	15	67	
F1-41	Lower Eocene	6150.00	Gialo	4	1326	1875	37	49	50	20	68	
F1-41	Paleocene	6509.00	Gir	4	1875	1984	49	54.8	50	20	70	
			Paleocene	2	1984	2000	54.8	61.6	60	25	75	
	Quaternary	0										
	Miocene	120										
	Oligocene	1370		Quaternary	1	0	40	0	5.3	25	10	30
	Augila	2523		Miocene	1	40	418	5.3	23	28	10	32
A1-126	Gialo	2723.00		Oligocene	2	418	769	23	33.7	40	20	35
A1-126	Etla	3352.00		Augila	2	769	829	33.7	37	45	15	40
A1-126	Gir	4064.00		Gialo. F.	2	829	1239	37	49	55	35	67
A1-126	Upper Pale	6171.00		Gir. F.	2	1239	1881	49	54.8	60	40	70
A1-126	Upper Sabil	6288.00		Kheir	2	1881	1917	54.8	57.9	70	50	75
A1-126	Hagfa	7052.00		U. Sabil. F.	2	1917	2149	57.9	62	75	45	73
A1-126	Lower Sabil	7097.00		Hagfa	4	2149	2163	62	66	65	40	77
A1-126	Kalash	8334.00		Lower Sabil	4	2163	2540	66	72.1	67	33	78
A1-126	Rakb A	8507.00		Kalash	2	2540	2593	72.1	83.6	70	42	80
A1-126	Rakb B	8906.00		Rakb A	2	2593	2715	83.6	86.3	85	43	78
A1-126	Rakb C	9317.00		Rakb B	2	2715	2840	86.3	89.8	80	50	67
A1-126	Rakb D	9930.00		Rakb C	4	2840	3027	89.8	90	85	65	65
A1-126	Bahi	9969.00		Rakb D	2	3027	3039	90	100	60	40	55
A1-126	Granite Wash	11075.00		Bahi	4	3039	3376	100	120	35	20	30
A1-126	Basement	11149.00		Granite Wash	1	3376	3398	120	140	0	0	10
				Basement	1	3398	3420	140	150	0	0	5

				Quaternary	2	0	50	0	5.3	35	10	10
				Miocene	2	50	500	5.3	23	40	10	25
				Oligocene	2	500	1026	23	33.9	45	15	26
				Augila	2	1026	1186	33.9	37	55	15	27
				Gialo	4	1186	1920	37	49	55	20	30
	A1-NC154			Gir	2	1920	2415	49	54.8	60	20	40
				U.Sabil	2	2415	2844	54.8	57.9	60	25	67
				Shetrat	2	2844	2893	57.9	61	65	27	68
				Lower Sabil	2	2893	3260	61	62	65	21	70
				Kalash	2	3260	3332	62	65	70	27	75
				Sirt Shale	2	3332	3436	65	72.1	85	30	73
				Tagrift	4	3436	3546	72.1	83.5	80	28	79
				Rachmate	2	3546	3798	83.5	89	75	31	70
				Etel	4	3798	4279	89	93.5	10	5	37
				Maragh	1	4279	4348	93.5	100	5	3	30
A3-126	Augila	2259.00		Quaternary	1	0	40	0	5.3	25	10	30
A3-126	Rashda Horizon	2704.00		Miocene	1	40	398	5.3	23	28	10	32
A3-126	Smara	2913.00		Oligocene	2	398	689	23	33.7	40	20	35
A3-126	Gialo	2913.00		Augila	2	689	888	33.7	37	45	15	40
A3-126	Budaffar	3248.00		Gialo. F.	2	888	1299	37	49	55	35	67
A3-126	Etla	3522.00		Gir. F.	2	1299	1933	49	54.8	60	40	70
A3-126	Mesdar	4262.00		Kheir	2	1933	1985	54.8	57.9	70	50	75
A3-126		5643.00		U. Sabil. F.	2	1985	2197	57.9	60	75	45	73
A3-126	Abu Fas	6343.00		Hagfa	4	2197	2210	60	61	65	40	77
A3-126	Upper Sabil	6512.00		Lower Sabil	4	2210	2592	61	65	67	33	78
A3-126	Sheterat	7208.00		Kalash	2	2592	2683	65	71.3	70	42	80
A3-126	Lower Sabil	7253.00		Rakb A	2	2683	2783	71.3	86.3	85	43	78
A3-126	Kalash	8505.00		Rakb B	2	2783	2919	86.3	89.8	80	50	67
A3-126	Rakb A	8803.00		Rakb C	4	2919	3183	89.8	94	85	65	65
A3-126	Rakb B	9130.00		Rakb D	2	3183	3213	94	100	60	40	55
A3-126	Rakb C	9578.00		Bahi	1	3213	3218	100	120	35	20	30
A3-126	Rakb D	10442.00		Nubian	1	3218	3225	120	140	0	0	10
A3-126	Bahi	10541.00										
A3-126	Nubian	10559.00										
B1-LP2E	Miocene	54.00		Quaternary	2	0	16.5	0	5.3	25	10	30
B1-LP2E	Arida	2273.00		Miocene	2	16.5	693	5.3	23	30	10	35
B1-LP2E	Muailah	2680.00		Oligocene	2	693	1028	23	33.7	35	15	40
B1-LP2E	Augila	3372.00		Augila	2	1028	1129	33.7	37	45	15	67
B1-LP2E	Etel Eocene	3464.00		Gialo	4	1129	1875	37	49	50	20	68
B1-LP2E	Gialo	3703.00		Gir	4	1875	2647	49	54.8	50	20	70
B1-LP2E	Smara	4468.00		Paleocene	2	2647	2954	54.8	57.9	60	25	75
B1-LP2E	Budaffar	4504.00		SABIL	4	2954	3000	57.9	62	60	20	65
B1-LP2E	Etla	4685.00										
B1-LP2E	Mesdar	6030.00										
B1-LP2E	Zelten	8686.00										
B1-LP2E	Sheterat	9622.00										
B1-LP2E	Sabil	9693.00										
EEE1-6	Muailah	1257.00		Quaternary	2	0	16.5	0	5.3	25	10	30
EEE1-6	Etel Eocene	2192.00		Miocene	2	16.5	383	5.3	23	30	10	35
EEE1-6	Sheghega	2390.00		Oligocene	2	383	668	23	33.7	35	15	40
EEE1-6	Gialo	2390.00		Augila	2	668	728	33.7	37	45	15	67
EEE1-6	Domran	3990.00		Gialo	4	728	1216	37	49	50	20	68
EEE1-6	Uaddan	3990.00		Gir	4	1216	2359	49	54.8	50	20	70
EEE1-6	Hagfa	7738.00		Paleocene	2	2359	2484	54.8	57.9	60	25	75
EEE1-6	Heira	7738.00		Upper Cre.	4	2484	2639	57.9	65	60	20	65
EEE1-6	Zmam	8149.00										
EEE1-6	Kalash	8149.00										
EEE1-6	Gargaf	8658.00										
A1-NC117B	Ajdabiya	57.00		Quaternary	2	0	16.5	0	5.3	25	10	30
A1-NC117B	Najah	1010.00		Miocene	2	16.5	308	5.3	23	30	10	35
A1-NC117B	Augila	6740.00		Oligocene	2	308	2043	23	33.7	35	15	40
A1-NC117B	Gialo	7145.00		Augila	2	2043	2178	33.7	37	45	15	67
A1-NC117B	Zelten	7583.00		Gialo	4	2178	2287	37	49	50	20	68
A1-NC117B	Megraf	7997.00		Gir	2	2287	2311	49	54.8	50	20	70
A1-NC117B	Gargaf	9134.00		Paleocene	4	2311	2438	54.8	65	60	25	75
				Upper Cre.	2	2438	2784	65	100	60	20	65
				Gergaf	1	2784	2823	100	140	40	20	60
D1-114	Lower Miocene	1596.00		Quaternary	2	0	40	0	5.3	25	10	30
D1-114	Oligocene	3475.00		Miocene	2	40	1059	5.3	23	30	10	35
D1-114	Upper Eocene	3712.00		Oligocene	2	1059	1131	23	33.7	35	15	40
D1-114	Middle Eocene	3810.00		Augila	2	1131	1161	33.7	37	45	15	67
D1-114	Gialo	3824.00		Gialo	4	1161	1636	37	49	50	20	68
D1-114	Lower Eocene	5370.00		Gir	2	1636	1932	49	54.8	50	20	70
D1-114	Paleocene	6340.00		Paleocene	4	1932	2417	54.8	65	60	25	75
D1-114	Gheriat	7930.00		Upper Cre.	2	2417	2661	65	100	60	20	65
D1-114	Upper Cretaceo	7930.00		Gergaf	1	2661	2740	100	140	40	20	60
D1-114	Gargaf	8730.00										
A1-NC103	Oligocene	1015.00		Quaternary	2	0	40	0	5.3	25	10	30
A1-NC103	Etel Eocene	5340.00		Miocene	2	40	309	5.3	23	30	10	35
A1-NC103	Sheghega	5910.00		Oligocene	2	309	1628	23	33.7	35	15	40
A1-NC103	Gialo	5910.00		Augila	2	1628	1801	33.7	37	45	15	67
A1-NC103	Zelten	10250.00		Gialo	4	1801	2601	37	49	50	20	68
A1-NC103	Hagfa	10973.00		Gir	2	2601	3124	49	54.8	50	20	70
				Paleocene	4	3124	3345	54.8	62	60	25	75
				Hagfa	2	3345	3400	62	63	60	20	65
A3-LP3C	Miocene	505.00		Quaternary	2	0	154	0	5.3	25	10	30
A3-LP3C	Arida	2665.00		Miocene	2	154	812	5.3	23	30	10	35
A3-LP3C	Muailah	3505.00		Oligocene	2	812	1280	23	33.7	35	15	40
A3-LP3C	Augila	4200.00		Augila	2	1280	1477	33.7	37	45	15	67
A3-LP3C	Etel Eocene	4480.00		Gialo	4	1477	2336	37	49	50	20	68
A3-LP3C	Gialo	4845.00		Gir	2	2336	2920	49	54.8	50	20	70
A3-LP3C	Budaffar	5667.00		Kheir	4	2920	3185	54.8	57.9	60	25	75
A3-LP3C	Etla	5985.00		Intisar	4	3185	3326	57.9	60	60	20	65
A3-LP3C	Mesdar	7665.00		Heira	2	3326	3415	60	61	50	20	45
A3-LP3C	Kheir	9580.00		Lower Sabil	2	3415	3450	61	66	50	20	35
A3-LP3C	Intisar	10452.00										
A3-LP3C	Heira	10911.00										
A3-LP3C	Lower Sabil	11205.00										
CCC1-6	Zaggut	16.00		Quaternary	2	0	80	0	5.3	25	10	30
CCC1-6	Tertiary	16.00		Miocene	2	80	750	5.3	23	30	10	35
CCC1-6	Etel Eocene	4642.00		Oligocene	2	750	1415	23	33.7	35	15	40
CCC1-6	Tamet	4956.00		Augila	2	1415	1510	33.7	37	45	15	67
CCC1-6	Sheghega	4956.00		Gialo	4	1510	2534	37	49	50	20	68
CCC1-6	Gialo	4956.00		Gir	2	2534	3199	49	54.8	50	20	70
CCC1-6	Domran	8313.00	Gir	Ruaga	4	3199	3499	54.8	56	60	25	75
CCC1-6	Uaddan	8313.00	Gir	Heira	4	3499	3857	56	57.9	55	21	77
CCC1-6	Ruaga	10494.00		Sabil	4	3857	4327	57.9	60	50	3	73
CCC1-6	Fogaha	10494.00		Dahra	4	4327	4450	60	65	50	20	70
CCC1-6	Heira	11480.00		Kalash	2	4450	4517	65	71.3	45	20	69
CCC1-6	Sabil	12654.00		Socna	2	4517	4600	71.3	83.5	45	15	67
CCC1-6	Dahra	14195.00										
CCC1-6	Zmam	14600.00										
CCC1-6	Kalash	14600.00										
CCC1-6	Socna	14820.00										
				Quaternary	2	0	15	0	5.3	25	10	30
				Miocene	2	15	838	5.3	23	30	10	35
				Oligocene	2	838	1696	23	33.7	35	15	40
D1-6				Augila	2	1696	1844	33.7	37	45	15	67
				Gialo	4	1844	2904	37	49	50	20	68
				Gir	2	2904	3416	49	56	50	20	70
				Heira	4	3416	3749	56	57.9	60	25	75

HHH1-59	Augila	2082.00		Quaternary	2	0	40	0	5.3	25	10	30	
HHH1-59	Gialo	2394.00		Miocene	2	40	300	5.3	23	30	10	35	
HHH1-59	TEM	2394.00		Oligocene	2	300	635	23	33.7	35	15	40	
HHH1-59	Gialo B	2630.00		Augila	2	635	730	33.7	37	45	15	67	
HHH1-59	Al Gata	3038.00		Gialo	4	730	1113	37	49	50	20	68	
HHH1-59	Gir	3650.00		Gir	4	1113	1670	49	54.8	50	20	70	
HHH1-59	TEL	3650.00		Kheir	4	1670	1728	54.8	57.9	60	25	75	
HHH1-59	Kheir	5478.00		Harash	4	1728	1780	57.9	59	75	45	73	
HHH1-59	Harash	5669.00		Zelten	4	1780	1978	59	59.5	65	40	77	
HHH1-59	Zelten	5904.00		Khaleifa	4	1978	2034	59.5	60	67	33	78	
HHH1-59	Marginulina	6490.00		Pale	2	2034	2035	60	60.5	55	21	77	
HHH1-59	Hagfa	6672.00		Upper Beda	2	2035	2153	60.5	61	60	27	80	
HHH1-59	Khalifa	6672.00		Hagfa	2	2153	2469	61	65	75	30	78	
HHH1-59	Upper Beda	6975.00		Cretaceous	2	2469	2509	65	71.5	70	28	67	
HHH1-59	Hagfa	7065.00		Sirte Shale	2	2509	2630	71.5	83	75	31	65	
HHH1-59	Cretaceous	7905.00		Tagrift	4	2630	2941	83	100	60	25	45	
HHH1-59	Sirte	8232.00		Pre-U.C.	1	2941	3000	100	113	60	25	75	
HHH1-59	Waha Pay	8630.00											
HHH1-59	Pre Cretaceous	9650.00											
HHH1-59	Volcanics	9650.00											
KK1-6	Fortino	16.00		Quaternary	2	0	80	0	5.3	25	10	30	
KK1-6	Zaggut	16.00		Miocene	2	80	750	5.3	23	30	10	35	
KK1-6	Tertiary	16.00		Oligocene	2	750	1439	23	33.7	35	15	40	
KK1-6	Etel Eocene	4721.00		Augila	2	1439	1565	33.7	37	45	15	67	
KK1-6	Sheghega	5133.00		Gialo	4	1565	2612	37	49	50	20	68	
KK1-6	Tamet	5133.00		Gir	2	2612	3112	49	54.8	50	20	70	
KK1-6	Gialo	5133.00		Ruaga	4	3112	3335	54.8	56	60	25	75	
KK1-6	Domran	8570.00		Zelten	4	3335	3349	56	57.9	55	21	77	
KK1-6	Uaddan	8570.00		Heira	4	3349	4163	57.9	60	50	3	73	
KK1-6	Ruaga	10210.00		Sabil	4	4163	4255	60	65	50	20	70	
KK1-6	Fogaha	10210.00		Kalash	2	4255	4300	65	71.3	45	20	69	
KK1-6	Zelten	10942.00											
KK1-6	Heira	10988.00											
KK1-6	Sabil	13660.00											
KK1-6	Zmam	13960.00											
KK1-6	Kalash	13960.00											
NN1-6	Zaggut	16.00		Quaternary	2	0	80	0	5.3	25	10	30	
NN1-6	Tertiary	16.00		Miocene	2	80	750	5.3	23	30	10	35	
NN1-6	Etel Eocene	4334.00		Oligocene	2	750	1321	23	33.7	35	15	40	
NN1-6	Tamet	4747.00		Augila	2	1321	1447	33.7	37	45	15	67	
NN1-6	Sheghega	4747.00		Gialo	4	1447	2452	37	49	50	20	68	
NN1-6	Gialo	4747.00		Gir	2	2452	2782	49	54.8	50	20	70	
NN1-6	Domran	8046.00		Ruaga	4	2782	3048	54.8	57.9	60	25	75	
NN1-6	Uaddan	8046.00		Zelten	4	3048	3103	57.9	60	50	3	73	
NN1-6	Ruaga	9127.00		Heira	4	3103	3923	60	65	50	20	70	
NN1-6	Fogaha	9127.00		Socna	2	3923	4048	65	71.3	45	20	69	
NN1-6	Cra	10000.00											
NN1-6	Heira	10180.00											
NN1-6	Socna	12870.00											
QQ1-6	Fortino	16.00		Quaternary	2	0	5	0	5.3	25	10	30	
QQ1-6	Zaggut	16.00		Miocene	2	5	935	5.3	23	30	10	35	
QQ1-6	Tertiary	16.00		Oligocene	2	935	1465	23	33.7	35	15	40	
QQ1-6	Muailah	3067.00		Augila	2	1465	1650	33.7	37	45	15	67	
QQ1-6	Gehenna	3067.00		Gialo	4	1650	2628	37	49	50	20	68	
QQ1-6	Etel Eocene	4807.00		Gir	2	2628	3183	49	54.8	50	20	70	
QQ1-6	Sheghega	5412.00		Ruaga	4	3183	3345	54.8	57.9	60	25	75	
QQ1-6	Tamet	5412.00		Heira	4	3345	3400	57.9	60	60	20	65	
QQ1-6	Gialo	5412.00											
QQ1-6	Domran	8621.00											
QQ1-6	Uaddan	8621.00											
QQ1-6	Ruaga	10442.00											
QQ1-6	Fogaha	10442.00											
QQ1-6	Cra	10937.00											
QQ1-6	Heira	10973.00											
				Quaternary	2	0	100	0	5.3	25	10	30	
A1-121	Miocene	O	LIGOCENE	Miocene	2	100	1105	5.3	23	30	10	35	
A1-121	Middle Eocene	6840.00		Oligocene	2	1105	2085	23	33.7	35	15	40	
A1-121	Gialo	7688.00		Augila	2	2085	2343	33.7	37	45	15	67	
A1-121	Lower Eocene	8260.00		Gialo	2	2343	2518	37	49	50	20	68	
				Gir	2	2518	2590	49	54.8	50	20	70	
				Quaternary	2	0	100	0	5.3	25	10	30	
A1-41	Diba	4480.00		Miocene	2	100	1365	5.3	23	30	10	35	
A1-41	Gialo	8720.00		Oligocene	2	1365	1465	23	33.7	35	15	40	
A1-41	Kheir	12445.00		Augila	2	1465	2658	33.7	37	45	15	67	
				Gialo	4	2658	3387	37	49	50	20	68	
				Gir	2	3387	3793	49	54.8	50	20	70	
				Kheir	2	3793	3993	54.8	65	50	20	70	
				U.C	2	3993	4180	65	71.3	60	25	75	
A1A-121	Oligocene	4490.00		Quaternary	2	0	120	0	5.3	25	10	30	
A1A-121	Upper Eocene	6620.00		Miocene	2	120	1369	5.3	23	30	10	35	
A1A-121	Tamet	6743.00		Oligocene	2	1369	2018	23	33.7	35	15	40	
A1A-121	Gialo	6743.00		Augila	2	2018	2055	33.7	37	45	15	67	
A1A-121	Middle Eocene	6940.00		Gialo	4	2055	2527	37	49	50	20	68	
A1A-121	Lower Eocene	8290.00		Gir	2	2527	3048	49	54.8	50	20	70	
A1A-121	Maastrichtian	10000.00		Maastricht	2	3048	3179	54.8	71.3	50	20	70	
A1A-121	Upper Cretacec	10000.00		Turonian	4	3179	3234	71.3	93.5	50	20	70	
A1A-121	Turonian	10430.00		Gargaf	1	3234	3500	93.5	140	60	25	75	
A1A-121	Gargaf	10610.00											

			Quaternary	2	0	40	0	5.3	25	10	30	
B1-121	Gialo	6090.00	Miocene	2	40	1000	5.3	23	30	10	35	
B1-121	Operculina	7890.00	Oligocene	2	1000	1820	23	33.7	35	15	40	
B1-121	KUM	9950.00	Augila	2	1820	1844	33.7	37	45	15	67	
B1-121	Kalash	9950.00	Gialo	4	1844	2384	37	49	50	20	68	
B1-121	Cambro Ordovic	10695.00	Gir	2	2384	2405	49	54.8	50	20	70	
			Paleocene	4	2405	3057	54.8	65	60	25	75	
			U. Cretaceous	2	3057	3261	65	140	60	20	65	
			Gargaf	1	3261	3408	140	150	60	15	55	
			Quaternary	2	0	40	0	5.3	25	10	30	
			Miocene	2	40	1000	5.3	23	30	10	35	
			Oligocene	2	1000	1820	23	33.7	35	15	40	
			Augila	2	1820	2140	33.7	37	45	15	67	
C1-121			Gialo	4	2140	2367	37	49	50	20	68	
			Gir	2	2367	2405	49	54.8	50	20	70	
			Paleocene	4	2405	2989	54.8	65	60	25	75	
			U. Cretaceous	2	2989	3716	65	140	60	20	65	
			Gargaf	1	3716	3780	140	150	60	15	55	
D2-12	Arida	1334.00	Quaternary	1	0	40	0	5.3	25	10	30	
D2-12	Gabal Al Akhdar	1334.00	Miocene	1	40	195	5.3	23	28	10	32	
D2-12	Augila	2503.00	Oligocene	2	195	763	23	33.7	40	20	35	
D2-12	Augila Ss	2566.00	Augila	2	763	843	33.7	37	45	15	40	
D2-12	Rashda	2601.00	Gialo. F.	2	843	1125	37	49	55	35	67	
D2-12	Rashda Horizon	2620.00	Gir. F.	2	1125	2026	49	54.8	60	40	70	
D2-12	Gialo	2766.00	Kheir	2	2026	2045	54.8	57.9	70	50	75	
D2-12	Smara	2766.00	U. Sabil. F.	2	2045	2240	57.9	60	75	45	73	
D2-12	Smara F	3296.00	Hagfa	4	2240	2270	60	61	65	40	77	
D2-12	Budaffar	3344.00	Lower Sabil	4	2270	2671	61	65	67	33	78	
D2-12	Etla	3497.00	Kalash	2	2671	2780	65	71.3	70	42	80	
D2-12	Salih	3692.00	Rakb A	2	2780	2845	71.3	86.3	85	43	78	
D2-12	Mesdar	4573.00	Rakb B	2	2845	2952	86.3	89.8	80	50	67	
D2-12	Abu Fas	6647.00	Rakb C	4	2952	3004	89.8	140	85	65	65	
D2-12	Upper Sabil	6709.00										
D2-12	Sheterat	7350.00										
D2-12	Lower Sabil	7448.00										
D2-12	Kalash	8763.00										
D2-12	Kalash B	9120.00										
D2-12	Rakb A	9335.00										
D2-12	Rakb B	9685.00										
D2-12	Basement	9855.00										
D2-12	Granite	9855.00										
K1-31	Augila	4103.00	Quaternary	2	0	50	0	5.3	25	10	30	
K1-31	TEM	4530.00	Miocene	2	50	700	5.3	23	30	10	35	
K1-31	Gialo	4530.00	Oligocene	2	700	1250	23	33.7	35	15	40	
K1-31	Al Gata	5590.00	Augila	2	1250	1381	33.7	37	45	15	67	
K1-31	TEL	7034.00	Gialo	4	1381	2144	37	49	50	20	68	
K1-31	Gir	7034.00	Gir	4	2144	2839	49	54.8	50	20	70	
K1-31	Kheir	9313.00	Kheir	2	2839	2924	54.8	57.9	60	25	75	
K1-31	Zelten	9594.00	Harash	4	2924	3195	57.9	59	75	45	73	
K1-31	Hagfa	10481.00	Zelten	4	3195	3429	59	60	65	40	77	
K1-31	Lower Paleocer	11250.00	Hagfa	2	3429	3514	60	65	75	30	78	
K1-31	Cretaceous	11530.00	Cretaceous	2	3514	3777	65	71.5	70	28	67	
K1-31	Sirte	12390.00	Sirte Shale	2	3777	4090	71.5	83	75	31	65	
K1-31	Hamia	13420.00	Tagrift	4	4090	4115	83	100	60	25	45	
N1-31	Augila	558.00	Quaternary	2	0	10	0	5.3	25	10	30	
N1-31	TEM	1390.00	Miocene	2	10	80	5.3	23	30	10	35	
N1-31	Gialo	1390.00	Oligocene	2	80	170	23	33.7	35	15	40	
N1-31	Kheir	5309.00	Augila	2	170	424	33.7	37	45	15	67	
N1-31	Zelten	5327.00	Gialo	4	424	1174	37	49	50	20	68	
N1-31	KUM	6925.00	Gir	4	1174	1618	49	54.8	50	20	70	
N1-31	Maastrichtian	6925.00	Kheir	2	1618	1624	54.8	57.9	60	25	75	
N1-31	Kalash	6925.00	Zelten	4	1624	2111	57.9	65	75	45	73	
N1-31	Cretaceous	6995.00	Kalash	2	2111	2132	65	71.3	65	40	77	
N1-31	Hamia	7865.00	Cretaceous	2	2132	2397	71.3	89	75	30	78	
N1-31	Nubian	8483.00	Hamia	4	2397	2586	89	100	70	28	67	
N1-31	Tanezzuft	9136.00	Nubian	1	2586	2784	100	140	75	31	65	
N1-31	Lower Silurian	9448.00	Tanezzuft	2	2784	2880	140	420	60	25	45	
N1-31	Gargaf	10222.00	Lower Silurian	2	2880	3116	420	440	60	20	40	
Q1-31	Oligocene	2755.00	Quaternary	2	0	40	0	5.3	25	10	30	
Q1-31	Augila	4801.00	Miocene	2	40	840	5.3	23	30	10	35	
Q1-31	Gialo	5275.00	Oligocene	2	840	1463	23	33.7	35	15	40	
Q1-31	Gir	7399.00	Augila	2	1463	1608	33.7	37	45	15	67	
Q1-31	Kheir	9383.00	Gialo	4	1608	2255	37	49	50	20	68	
Q1-31	Harash	9715.00	Gir	4	2255	2860	49	54.8	50	20	70	
Q1-31	Khalifa	10155.00	Kheir	2	2860	2961	54.8	57.9	60	25	75	
Q1-31	Sabil	10443.00	Harash	4	2961	3000	57.9	59	75	45	73	
Q1-31	Kalash	11571.00	Zelten	4	3000	3095	59	59.5	65	40	77	
Q1-31	Sirte	12092.00	Khaleifa	4	3095	3183	59.5	60	67	33	78	
Q1-31	Tagrifet	12368.00	Sabil	2	3183	3527	60	65	55	21	77	
Q1-31	Hamia	13000.00	Kalash	2	3527	3686	65	71.3	60	27	80	
Q1-31	Maragh	13735.00	Sirte Shale	2	3686	3770	71.3	83	75	30	78	
Q1-31	Nubian	13945.00	Tagrift	4	3770	3962	83	89	70	28	67	
Q1-31	Silurian	14199.00	Hamia	4	3962	4186	89	100	75	31	65	
			Maragh	1	4186	4250	100	120	60	25	45	
			Nubian	1	4250	4328	120	140	60	25	75	
			Silurian	2	4328	4648	140	420	60	20	60	
R1-31	Diba	2972.00	Quaternary	2	0	40	0	5.3	25	10	30	
R1-31	Augila	5250.00	Miocene	2	40	906	5.3	23	30	10	35	
R1-31	Gialo	6045.00	Oligocene	2	906	1600	23	33.7	35	15	40	
R1-31	Jakhira	6858.00	Augila	2	1600	1843	33.7	37	45	15	67	
R1-31	Al Gata	6968.00	Gialo	4	1843	2627	37	49	50	20	68	
R1-31	Gir	8617.00	Gir	4	2627	3188	49	54.8	50	20	70	
R1-31	Kheir	10460.00	Kheir	2	3188	3282	54.8	57.9	60	25	75	
R1-31	Harash	10768.00	Harash	4	3282	3300	57.9	59	75	45	73	
R1-31	Zelten	10828.00	Zelten	4	3300	3411	59	59.5	65	40	77	
R1-31	Khalifa	11190.00	Khaleifa	4	3411	3463	59.5	60	67	33	78	
R1-31	Lower Sabil	11365.00	Sabil	2	3463	3478	60	65	55	21	77	
R1-31	Kalash	11412.00	Kalash	2	3478	3580	65	71.3	60	27	80	
R1-31	Sirte	11745.00	Sirte Shale	2	3580	3692	71.3	83	75	30	78	
R1-31	Tagrifet	12112.00	Tagrift	4	3692	3812	83	89	70	28	67	
R1-31	Lower Sirte	12507.00	Hamia	4	3812	3991	89	100	75	31	65	
R1-31	Maragh	13095.00	Maragh	1	3991	3994	100	120	60	25	45	
R1-31	Gargaf	13105.00										

Subsidence calculation

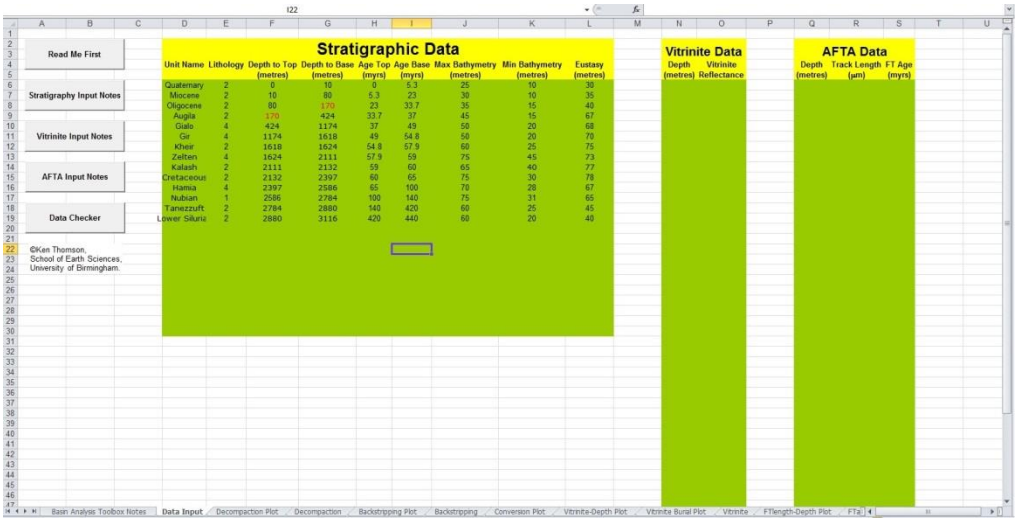

Burial history calculation

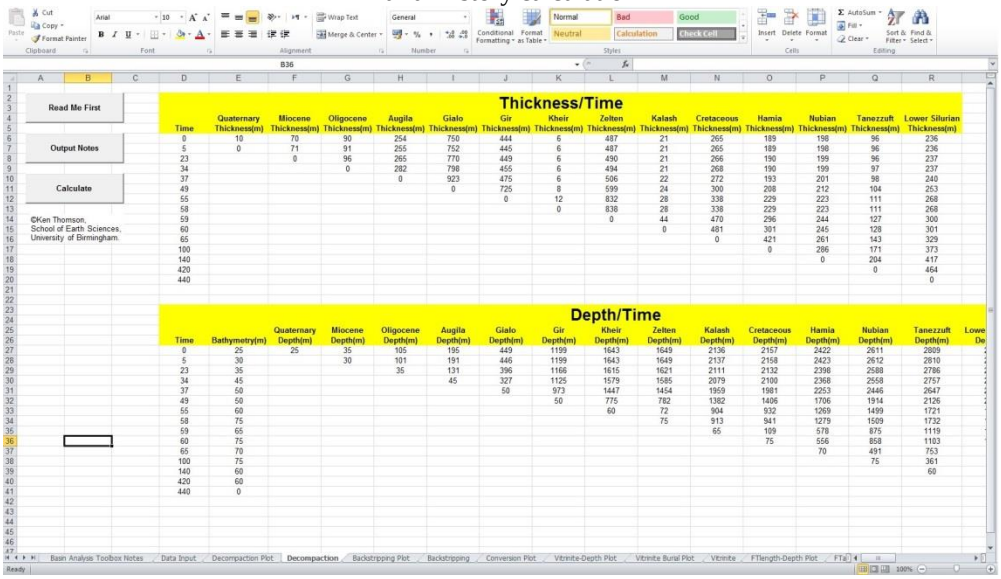

Stretching factor calculation

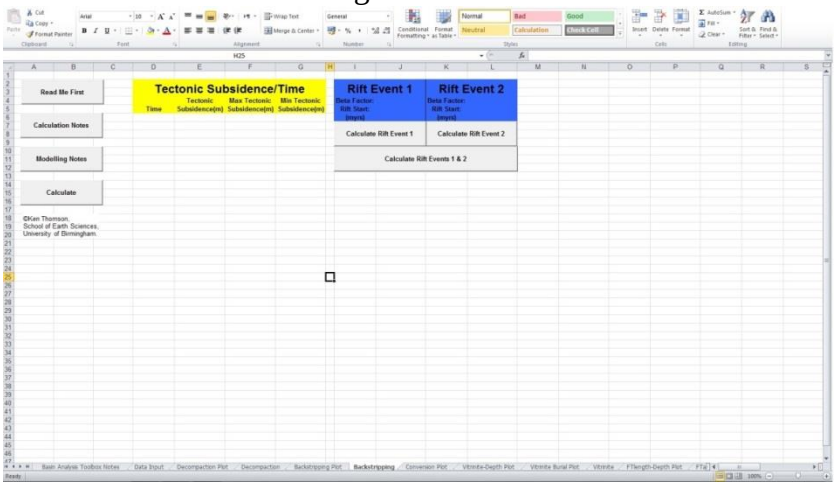

REFERENCES

Abadi, A.M., van Wees, J.D., van Dijk, P.M., Cloetingh, S.A.P.L., 2008. Tectonics and subsidence evolution of the Sirt Basin, Libya. Am. Ass. Petrol. Geol. Bulletin 92,993–1027.

Abouessa, A., Pelletier, J., Philippe, D., Mathieu, S., Schaeffer, P., and Métais, E., 2012. New insight into the sedimentology and stratigraphy of the Dur At Talahtidal-fluvial transition sequence (Eocene–Oligocene, Sirt Basin, Libya): Journal of African Earth Sciences, v. 65, p. 72-90.

Abugares, I. Y., 1996. Sedimentology and hydrocarbon potential of the Gir Formation, Sirt Basin, Libya, *in* M. J. Salem, M. T. Busrewil, A. A. Misallati, and M. A. Sola, eds., The geology of the Sirt Basin: Amsterdam, Elsevier, v. 2, p. 31–64.

Abuhajar, M.I., and Roohi, M., 2003. Giant Fields in the Sirt Basin, Libya: 1st EAGE North African/Mediterranean Petroleum & Geosciences Conference & Exhibition, October 6, 2003.

Ade-Hall, J. M., Reynolds, P. H., Dagley, P., Mussett, A. E., Hubbard, T. P., & Klitzsch, E. H., 1974. Geophysical studies of North African Cenozoic volcanic areas: I. Haruj Assuad, Libya. Canadian Journal of Earth Sciences, 11, 998–1006.

Ahlbrandt, T., 2001. Sirte Basin Province: Sirte-Zelten Total Petroleum System, U.S. Geol. Surv. Bull., 2202–F, 29 pp.

Airy, G. B., 1855, On the computations of the effect of the attraction of the mountain masses as disturbing the apparent astronomical latitude of stations in geodetic surveys, Trans. Roy. Soc. (London), ser. B, vol. 145.

Allen, P.A., and Allen, J.R., 2005, Basin analysis: principles and applications: Oxford, Blackwell Scientific Publications, 549 p.

Almond, D.C., 1986. Geological evolution of the Arabo-Nubian dome. Tectonophysics 131, 301–332.

Ambrose, G., 2000. The geology and hydrocarbon habitat of the Sarir Sandstone, SE Sirt Basin, Libya: Journal of Petroleum Geology, v. 23, p.165–192.

Anketell, J.M., and Kumati, S.M., 1991. Structure of Al Hufrah Region – Western Sirt Basin, G.S.P.L.A.J. In The Geology of Libya Volume V, Salem, M.J. and M.N. Belaid (eds), 2353-2370.

Anketell, J. M., and Ghellali, S. M., 1991. **A** palaeogeological map of the pre-Tertiary surface in the Jifarah plain and its implication to the structural history of northern Libya, *in:* Salem, M. J., Sbeta, **A.** M. and Bakbak, M. R. (eds.), The Geology of Libya, v. VI, p. 2381-2406.

Anketell, J.M., 1996. Structural history of the Sirte Basin and its relationship to the Sabratah Basin and Cyrenaican Platform, northern Libya. *In*: *The Geology of the Sirte Basin*, 3 (*eds* M.J. Salem, M.T. Busrewil, A.A. Misallati, and M.A. Sola).

Ashour, M.M., 1996. Microbiostratigraphical analysis of the Campanian–Maastrichtian strata in some wells in Sirt Basin: in M.J. Salem, A.J.

Baaske, U.P., Tricker, P., Itterbeeck, J.V., Griffiths, H., and Pickens, J., 2013. Gravity-induced deep-water carbonate deposits: Potential new plays in the Eocene of the Sirte Basin, Libya. Shell Exploration and Production Libya GmbH, Abunawas 2, Gagaresh Road, Tripoli, Libya.

Baird, D. W., Aburawi, R. M., Bailey, N. J. L., 1996. Geohistory and Petroleum in the Central Sirt Basin, The geology of Sirt Basin. v.3, p. 3 – 56.

Baldwin, B., and C. O. Butler, C.O., 1985. Compaction curves, Am. Assoc'. Pet. Geol. Bull., 69, 622-626.

Barbieri, R., 1996. Micropaleontology of the Rakb Group (Cenomanian to early Maastrichtian) in the Hameimat Basin, northern Libya: in M.J.

Barnett, J. A. M., J. Mortimer, J. H. Rippon, J. J. Walsh, and J., 1987. Watterson, Displacement geometry in the volume containing a single normal fault, AAPG Bulletin., 71, 925– 937, 1987.

Barr, F.T., and A.A. Weegar, 1972. Stratigraphic nomenclature of the Sirt Basin, Libya: Petroleum Exploration Society of Libya, 179 p.

Bayoumi, A.I. and Lofty, H.I., 1989. Modes of structural evolution of Abu Gharadig Basin, Western Desert of Egypt as deduced from seismic data. : Journal of African Earth Sciences, v. 9, p. 273-287.

Bebout, D., and Pendexter, **C**., 1975, Secondary carbonate porosity as related to Early Tertiary depositional facies, Zelten Field, Libya: AAPG Bulletin, v.59, no.4, p. 665-693.

Bellini, E. and Massa, D., 1980. A stratigraphic contribution to the Palaeozoic of the southern basins of Libya. *In: The Geology of Libya. Volume I.* (eds M.J. Salem, and M.T. Busrewil). Academic Press, London, 3-56.

Beloussov, V.V., 1969. Interrelations between the earth's crust and mantle. - In: The earth's crust and upper mantle, P.J. Hart, Ed., Am. Geophys. Union Geophys. monograph, 18, 698--712.

Benfield, A.C., and Wright, E.P., 1980. Post-Eocene sedimentation in the eastern Sirt Basin, Libya. In: Salem, M. J. and Busrewil, M. T. (eds.), The Geology of Libya. Academic Press, London, II, 463-499.

Berggren, W., 1969. Cenozoic chronostratigraphy, planktonic forminiferal zonation and the radiometric time scale, ***Nature,*** 224, 1072.

Bertotti, G., Podlachikov. Y., Daehler, A., 2000. Dynamic link between the level of ductile crustal flow and style of normal faulting of brittle crust. Tectonophysics 320:195–218.

Bernasconi, A., Poliani, G., and Dakshe, A., 1991. Sedimentology, petrography and diagenesis of Metlaoui Group in the offshore northwest of Tripoli, *in* M.J. Salem and M.N. Belaid, eds., The Geology of Libya: Third Symposium on the Geology of Libya, held at Tripoli, September 27–30, 1987: Amsterdam, Elsevier, v. 5, p. 1907–1928.

Bezan, M. A., 1996. The Paleocene sequence in Sirt Basin, in M. J. Salem, M. T. Busrewil, A. A. Misallati, and M. A. Sola, eds., The geology of the Sirt Basin: Amsterdam, Elsevier, v. 1, p. 97–118.

Bezan, A. M, and Malak, E. K, 1996. Oligocene sediments of Sirt Basin, Libya. 179p. PESL, Tripoli.

Biju-duval, B., Dercourt, J., Le Pichon, X., 1977. From the Tethys ocean to the Mediterranean seas: a plate tectonic model of the evolution of the western Alpine system. International symposium on the structural history of the Mediterranean basins, Split 1976, p. 143—164, Paris (Editions Technip).

Bijwaard, H., Spakman, W., Engdahl, E.R., 1998. Closing the gap between regional and 465 global travel time tomography. J. Geophys. Res. 103, 30055–30078.

Blakely, R.J., Simpson, R.W., 1986. Approximating edges of source bodies from magnetic and gravity anomalies. Geophysics 51, 1494–1498.

Blakely R.J., 1995. Potential theory in gravity and magnetic applications. Cambridge University Press, 441p. Blakely R.J. & Simpson R.W., 1986, Approximating edges of source bodies from magnetic or gravity anomalies. Geophysics 51, 1494-1498.

Blakely, R. J., 1996. Potential theory in gravity and magnetic applications: Cambridge University Press.

Blakely, R.J., Jachens, R.C., Calzia, J.P., Langenheim, V.E., 1999. Cenozoic Basins of the Death Valley Extended Terrane as Reflected in Regional-scale Gravity Anomalies. Geological Society of America,333, 16

Boote, D.R.D., D.D., Clark-Lowes, D.D., Traut, M.W., 1998. Palaeozoic petroleum systems of North Africa. In D.S. Macgregor, R.T.J. Moody and D.D. Clark-Lowes (eds), Petroleum Geology of North Africa, Geological Society Special Publication No132, p. 7-69.

Boote, D.R.D., 2009. Stratigraphic Controls of Petroleum Systems in the Sirt Basin, Libya, AAPG Annual Convention and Exhibition, 7-10th June 2009, Denver, USA (oral presentation)

Bond, G., and Kominz, M. A., 1984. Construction of tectonic subsidence curves for the early Paleozoic miogeocline, south Canadian Rocky Mountains: Implication for subsidence mechanisms, age of break up, and crustal thinning: Geological Society of America Bulletin, v. 95, p. 155–173.

Bosworth, W., 1985**.** Discussion on the structural evolution of extensional basin margins. Geological Society of London Journal 142, 939–942.

Bosworth, W., 1992. Mesozoic and early Tertiary rift tectonics in east Africa. Tectonophysics, **209**, pp. 115-137.

Bosworth W., El-Hawat A.S., Helgeson D.E., Burke K., 2008. Cyrenaica "shock absorber" and associated inversion strain shadow in the collision zone of northeast Africa, Geology, 36(9), 695–698

Bott, M. H. P., 1992. The stress regime associated with continental break-up. - In: Storey, B. C., Alabaster, T. & Pankhurst, R. J. (eds) (1992) *Magmatism and theCauses of Continental Break-up*, Geological Society Special Publication No. 68, pp. 125-136.

Boullier, A. M, Bertrand, J. M., 1981. Tectonique tangentielle profonde et couloirs mylonitiques dans le Hoggar central polycyclique (Algérie). *Bulletin de la Société géologique de France,* XXIII, 17-22.

Boullier, A. M., 1991. The Pan-African Trans-Saharan belt in the Hoggar shield (Algeria, Mali, Niger); a review. In: R.D. Dallmeyer and J.P. Lecorche, Editors, *The West African Orogens and Circum-Atlantic Correlatives*, Springer-Verlag, Berlin (1991), pp. 85–105.

Buck, W.R., 1991. Mode of continental lithospheric extension. *Journal of Geophysical Research* **96**, 20161-20178.

Buck, W.R., Martinez, F., Steckler, M.S., & Cochran, J.R., 1988. Thermal consequences of lithospheric extension: Pure and simple. *Tectonics* **7**, 213-234.

Bumby, A. J. and Guiraud, R., 2005. The geodynamic setting of the Phanerozoic basins of Africa, J. African Earth Sci., 43, 1–12.

Burbank, D.W. and Anderson, R.S., 2001. Tectonic Geomorphology. Sheridan Books, Malden, Massachusetts, 274 pp.

Burke, K., and Wilson, J. T., 1972. Is the African Plate stationary? Nature, 239, 387-390.

Burke, K., & Whiteman, A.J., 1973. Uplift, rifting and break-up of Africa. In: "Implications of Continental Drift to the Earth Sciences", D. H. Tarlino & S. K. Rvncorn, Eds., London (Academic Press), Vol. 2, 735--755.

Burke, K.C.A., Dewey, J.F., 1974. Two plates in Africa during the Cretaceous? Nature 249, 313–316.

Burke, K. C., 1977. Aulacogens and continental breakup, *in* F. A. Donath, ed., Annual Review of Earth and Planetary Sciences, v. 5, p. 371-396.

Burwood, R., Redfern, J., Cope, M. J., 2003. Geochemical evaluation of East Sirte Basin (Libya) petroleum systems and oil provenance. *In:* ARTHUR, T. J., MACGREGOR, D. S. & CAMERON, N. R. (eds) *Petroleum Geology of Africa: New Themes and Developing Technologies.* Geological Society of London, Special Papers, 207, 203-240.

Busrewil, M.T., and Esson, J., 1991. Chronology and Composition of the Igneous Rocks of Jabal As Sawda. In: Salem, M.J., Busrewil, M.T., Ben Ashour, A.M. (eds.): The Geology of Libya, VII: 2599-2604. Elsevier, Amsterdam.

Busrewil, M.T., Oun, K.M., 1991. Geochemistry of the Tertiary Alkaline Rocks of Jabal Al Hasawinah, West Central Libya. In: Salem, M.J., Busrewil, M.T., Ben Ashour, A.M. (eds.): The Geology of Libya, VII: 2587-2598. Elsevier, Amsterdam.

Busrewil, M.T.,Wadsworth,W.J., 1980a. The Basanitic Volcanoes of Gharyan Area, NW Libya. In: Salem,M.J., Busrewil,M.T. (eds.). The Geology of Libya, III: 1095-1105. Academic Press, London.

Busrewil, M. T., Oun, K. M., and Haman, M., 2008. Neoproterozoic – Lower Cretaceous Tectono – Sedimentary evolution of the Sirt Basin, Geology of east Libya, v. 4. Pp. 251 – 268.

Brede, R., Hauptmann, M., and Herbig, H., 1992. Plate Tectonics and Intracratonic Mountain Ranges in Morocco—The Mesozoic-Cenozoic Development of the Central High Atlas and the Middle Atlas," *Geologische Rundschau*, Vol. 81, No. 1, pp. 127-141. doi:10.1007/BF01764544

Briggs, I.C., 1974. Machine contouring using minimum curvature. Geophysics 39, 39-48.

Brown, L. F., Jr., and Fisher, W. L., 1977. Seismic stratigraphic interpretation of depositional systems: examples from Brazilian rift and pull apart basins. In: Payton, C. E. (ed.), Seismic Stratigraphy – Applications to Hydrocarbon Exploration. American Association of Petroleum Geologists Memoir **26**, 213–248.

Browne, S.E., Fairhead, J.D., Mohamed, I.I., 1985. Gravity study of the White Nile Rift, Sudan and its regional tectonic setting. Tectonophysics 113, 123–137.

Brun, J.P., 1999. Narrow rifts versus wide rifts: inferences for the mechanics of rifting from laboratory experiments. Philosophical Transactions of the Royal Society of London 357, 695–712.

Cacace, M., Bayer, U. and Marotta, A.M., 2008. Strain localization due to structural inhomogeneities in the Central European Basin System. International Journal of Earth Sciences, 97: 899-913.

Cahen L., Snelling N.J., Delhal J., 1984. The geochronology and evolution of Africa. Clarendon Press, Oxford.

Capitanio F.A., C. Faccenna, C., Funiciello, R., 2009. The opening of Sirte basin: Result of slab avalanching. Earth and Planetary Science Letters, 285, 210–216.

Capitanio, F. A., Faccenna, C., Funiciello, R., and Salvini, F., 2011. Recent tectonics of Tripolitania, Libya: an intraplate record of Mediterranean subduction, Geological Society, London, Special Publications, 357, 319–328.

Carr, I.D., 2003**.** A Sequence stratigraphic synthesis of the North Africa Mesozoic. Journal of Petroleum Geology, 26, 133-152.

Cartwright, J.A., Bouroullec, R., James, D., Johnson, H.D., 1998. Polycyclic motion history of some Gulf Coast growth faults from high-resolution displacement analysis. Geology 26 (9), 819–822.

Cartwright, J.A., Trudgill, B.D., Mansfield, C.S., 1995. Fault growth by segment linkage - an explanation for scatter in maximum displacement and trace length data from the Canyonlands grabens of SE Utah. Journal of Structural Geology 17, 1319±1326.

Casten, U. and Snopek, K., 2006. Gravity modelling of the Hellenic subduction zone—a regional study, Tectonophysics 417, 183–200.

Casero, P., and F. Roure, F., 1994. Neogene deformation at the Sicilian-North African plate boundary, in Peri-Tethyan Platforms, edited by F. Roure, pp. 27–45, Ed. Technip, Paris.

Catuneanu, O., V. Abreu, J.P. Bhattacharya, M.D. Blum, R.W. Dalrymple, P.G. Eriksson, C.R. Fielding, W.L. Fisher, W.E. Galloway, M.R. Gibling, K.A. Giles, J.M. Holbrook, R. Jordan, C.G.St.C. Kendall, B. Macurda, O.J. Martinsen, A.D. Miall, J.E. Neal, D. Nummedal, L. Pomar, H.W. Posamentier, B.R. Pratt, J.F. Sarg, K.W. Shanley, R.J. Steel, A. Strasser, M.E. Tucker, and C. Winker., 2009. Towards the standardization of sequence stratigraphy: Earth-Science Reviews, v. 92, p. 1-33.

Catuneanu, O., Galloway, W.E., Kendall, G.St.C., Miall, A.D., Posamentier, H.W., Strasser, A., and Tucker, M. 2011. Sequence stratigraphy: Methodology and nomenclature: Newsletters on Stratigraphy, v. 44, p. 173–245.

Cavazza W., Roure, F., Ziegler, P., 2004. The Mediterranean Area and the Surrounding Regions: Active Processes, Remnants of Former Tethyan Oceans and Related Thrust Belts. In: W. Cavazza, F. Roure, W. Spakman, G.M. Stampfli and P Ziegler (Eds), The TRANSMED Atlas. p. 1-29.

Ceriani A., Di Giulio A., Goldstein R.H., Rossi C., 2002. Diagenesis associated with cooling during burial: and example for Lower Cretaceous reservoir sandstones (Sirt basin, Libya), AAPG Bulletin, 86(9), 1573–1591.

Childs, C., Watterson, J., and Walsh, J. J., 1995. Fault overlap zones within developing normal fault systems: Journal of the Geological Society (London), v. 152, p. 535–550.

Childs, C., Nicol, A., Walsh, J.J., Watterson, J., 2003. The growth and propagation of synsedimentary faults. Journal of Structural Geology 25, 633–648.

Church, K.D. and Coe, A. L., 2003. Processes controlling relative sea level change and sediment supply. In: Coe, A.L. (ed.) *The sedimentary Record of Sea-Level Change*. Cambridge University Press, Cambridge, 99-117.

Cloetingh, S., Van der Beek, P.A., Van Rees, D., Roep, T. B., Biermann, C., and Stephenson, R. A., 1992. Flexural interaction and the dynamics of Neogene extensional basin formation in the Alboran-Betic region, Geo. Mar. Lett., 12, 66 – 75, 1992.

Cloetingh, S., van Wees, J.D., van der Beek. RA. and Spadini, G., 1995. Role of pre-rift rheology in kinematics of basin formation: constraints from thermomechanical models of Mediterranean and intracratonic basins. Mar. Pet. Geol., 12: 793-807.

Cloetingh, S., Burov, E., Poliakov, A., 1999. Lithosphere folding: primary response to compression? (from central Asia to Paris basin). Tectonics 18, 1064–1083.

Cloetingh, S. and Van Wees, J.D., 2005. Strength reversal in Europe's intraplate lithosphere: Transition from basin invers on to lithosphere folding: Geology, v. 33, pp. 285–288.

Cloetingh, S., Ziegler, P.A., Beckman, F., Andrieesen, P.A.M., Matencol, L., Bada, G., Garcia-Castellanos, D., Hardebol, N., Dezes, P., Sokoutis, D., 2005. Lithospheric memory, state of stress and rheology: neotectonic controls on Europe's intraplate continental topography. Quat. Sci. Rev. 24, 241–304.

Cloetingh, S., Burov, E., Matenco, L., Beekman, F., Roure, F., Ziegler, P.A., 2013. The Moho in extensional tectonic settings: Insights from thermo-mechanical models. Tectonophysics 609, 558-604.

Coe, Angela, Dan Bosence, Kevin Church, Steve Flint, John Howell and Chris Wilson, 2002, *The Sedimentary Record of Sea Level Change* , Cambridge University Press, 288 pp.

Coffeen, J., 1984. Interpreting seismic data. PennWell Books, United States.

Colley, B. B.. 1964**.** Libya: petroleum geology and development**.** ***Proceedings of the 6th World Petroleum Congress,*** Section I, p. I-io. Hamburg (Verein zur Fordernng des. 6. Welt-Erad-Kongresse**s).**

Conant, L.C., and Goudarzi, G.H., 1967. Stratigraphic and tectonic framework of Libya. Bull. Am. Assoc. Pet. Geol. 51, 719–730.

Corti, G., Bonini, M., Conticelli, S., Innocenti, F., Manetti, P. and Sokoutis, D., 2003. Analogue modelling of continental extension: A review focused on the relations between the patterns of deformation and the presence of magma. *Earth-Science Reviews*, 63 (3-4), 169-247.

Cordell, L., 1979. Gravimetric expression of graben faulting in Santa Fe Country and the Espanola Basin, New Mexico, in Guidebook to Santa Fe Country, 30th Field Conference, edited by R. V. Ingersoll, New Mexico Geological Survey, pp. 59–64.

Cordell, L., and Grauch, V.J.S., 1985. Mapping basement magnetization zones from aeromagnetic data in the San Juan basin, New Mexico. In: Hinze, W.J., (Ed.), The utility of regional gravity and magnetic anomaly Maps: Society of Exploration Geophysicists, 181–197.

Coward, M.P., 1986. Heterogeneous stretching, simple shear and basin development. *Earth and Planetary Science Letters* **80**, 325-336.

Coward, M.P., and Ries, A.C., 2003. Tectonic development of North African basins. In: Arthur, T.J., MacGregor, D.S., Cameron, M.R. (Eds.), Petroleum Geology of Africa: New Themes and Developing Technologies. The Geological Society, London. Special Publication No. 207. pp. 61–83.

Cowie, P. A., Knipe, R. J., Main, I. J., 1996. Special issue: Scaling laws for fault and fracture populations - Analyses and applications - Introduction. *J. Struct. Geol.*, 18(2-3), R5-R11.

Cowie, L and Kusznir, N.J., 2012. Mapping crustal thickness and oceanic lithosphere distribution in the Eastern Mediterranean using gravity inversion. Petroleum Geoscience, 18. pp. 373-380.

Craig, J., Thusu, B., Lüning, S., Meciani, L., Trombetti, A., Erchi, G., 2008. Structural Styles and Prospectivity in the Precambrian and Palaeozoic Hydrocarbon Systems of North Africa Snowball Earth and Global Neoproterozoic Petroleum Systems. Geology of East Libya, vol. 4. pp. 51 – 122.

Daly, M.C., Chorowicz, J., Fairhead, J.D., 1989. Rift basin evolution in Africa: the influence of reactivated step basement shear zones. *In*: cooper, M.A. & williAms, C.D. (eds) *Inversion tectonics*. *Geological Society, London, Special Publications*, **44**, 309–334.

Dautria, J.M. and Lesquer, A., 1989. An example of the relationship between rift and dome: recent geodynamic evolution of the Hoggar swell and of its nearby regions (Central Sahara, Southern Algeria and Eastern Niger). *Tectonophysics,* **163**, 45-61.

Davis, M., and Kusznir, N.J., 2004. Depth-Dependent Lithospheric Stretching at Rifted Continental Margins. In: Karner, G.D., ed Proceedings of NSF Rifted Margins Theoretical Institute, p 92-136. Columbia University Press, New York, pp. 92-136. ISBN 0-231-12738-3.

Davison, I., 1997. Wide and narrow margins of the Brazilian South Atlantic. Journal of the Geological Society of London, **154**, 471-476.

Dawers, N. H., and Anders, M. H., 1994. Displacement-length scaling and fault linkage: Journal of Structural Geology, v. 16 (in press).

Dawers, N.H., and Underhill, J.R., 2000. The role of fault interaction and linkage in controlling synrift stratigraphic sequences: Stratfjord East area, Northern North Sea. AAPG Bulletin, 84;1, 45-64.

De Paola, N., Holdsworth, R.E., Mccaffrey, K.J.W., 2005a. The influence of lithology and pre-existing structures on reservoir-scale faulting patterns in transtensional rift zones: Journal of the Geological Society, v. 162, p. 471-480.

De Paola, N., Holdsworth, R.E., McCaffrey, K.J.W., Barchi, M.R., 2005b. Partitioned transtension: an alternative to basin inversion models: Journal of Structural Geology, v. 27, p. 607-625.

Dercourt, J., Zonenshain, L.P., Ricou, L.E., Kazmin, V.G., Le Pichon, X., Knipper, A.L., Grandjacquet, C., Sbortshikov, I.M., Geyssant, J., Lepvrier, C., Pechersky, D.H., Boulin, J., Sibuet, J.-C., Savostin, L.A., Sorokhtin, O., Westphal, M., Bazhenov, M.L., Lauer, J.P., Biju-Duval, B., 1986. Geological evolution of the Tethys belt from the Atlantic to the Pamirs since the Lias. Tectonophysics, 123: 241-315.

Dercourt, J., Ricou, L. E., Vrienlinck, B., 1993. Atlas Tethys Palaeoenvironmental Maps. Gauthier-Villars, Paris.

Dewey, J.F. and Bird, J.M., 1970. Mountain belts and the new global tectonics. J. Geophys. Res., 75, 2625–2647.

Dewey, J. F., Pitman, W. C., Ryan, W. B. F., Bonnin, J., 1973. Plate tectonics and volution of Alpine system. Geol. Soc. Am. Bull. 84:3137-3180.

Dewey, J. F., Cande, S., and Pitman, W. C., 1989. Tectonic evolution of the India/Eurasia collision zone: Eclogae Geologicae Helvetiae, v. 82, p. 717–734.

Dewey, J.F., Holdsworth, R.E., and Strachan, R.A., 1998. Transpression and transtension zones: Geological Society, London, Special Publications, v. 135, p. 1-14.

Dickinson, W.R., 1974. Plate tectonics and sedimentation. In: Tectonics and Sedimentation (Ed. by W.R. Dickinson), Spec. Publ. 22,1^27.Society of Economic Paleontologists and Mineralogists, Los Angeles.

Dobrin, M.B., and Savit, C. H., 1988. *Introduction to Geophysical Prospecting* (4th ed.), New York, McGraw-Hill, 867 pp.

Doser, D.I., Keller, G.R., Harder, S., Miller, K. C., Dial, P. J., 1996. Development of a lithospheric model and geophysical data base for North Africa. University of Texas/El Paso, Department of Geophysical Sciences final report, TX 79968 – 0555.

Duval, B. C., C. and Vail, P. R., 1992. Types and hierarchy of stratigraphy cycles. Abstract for conference on sequence stratigraphy of European Basin. CNRS-IFP, Dijon, France (18 **th** - 20th May 1992), P. 44-45.

Echikh, K., 1998. Geology and hydrocarbon occurrences in the Ghadamis Basin, Algeria, Tunisia, Libya. In: Petroleum Geology of North Africa (eds D.S. Macgregor, R.T.J. Moody, D.D. Clark-Lowes). *Geol. Soc. London,* Sp. Publ., 132, 109-129.

El Arnauti, A., and Shelmani, M., 1985. stratigraphy and structural setting. In: B. Thusu and B. Owens (Eds.), Palynostratigraphy of Northeast Libya. Jour. Brit. Micropal. Sco. London.

El-Arnauti, A., and Shelmani, M., 1988. A contribution to the northeast Libyan subsurface stratigraphy with emphasis on Pre-Mesozoic. *In : Subsurface playnostratigraphy of Northeast Libya* (eds A. El-Arnauti, B. Owens, and B. Thusu). Benghazi, Garyounis University Publications, 1-16.

El-Arnauti, A., and Shelmani, M, A., Lawrence, S.R., Mansouri, A., Sengör, A.M.C., Soulsby, A. and Hassan, M., 2008. Structural styles in .N.E. Libya. *Sedimendary Basins of Libya, Third Symposium, Geology of East Libya vol. 4*.pp. 153-178.

El Amawy, M.A., Muftah, A.M., Abd El-Wahed, M., and Nassar, A., 2009. Wrench structural deformation in Ras Al Hilal-Al Athrun area, NE Libya: a new contribution in Northern Al Jabal Al Akhdar Belt: Arab J Geosci (2011) 4:1067–1085 DOI 10.1007/s12517-009-0114-5.

El-Badrawy, H.T and Soliman, M.R., 2000. Continuation of geophysical data in delineating the subsurface tectonic structures of Sirt Basin, Libya. 5th International Conference on the Geology of the Arab World, Cairo University, p. 683-698.

El-Batroukh, S. I., and Zentani, A. S., 1980. Gravity interpretation of Raguba field, Sirte basin, Libya. *Geophysics, 45,* 1153-1163.

El-Hawat A.S., and Abdulsamad E.O., 2004. The Geology of Cyrenaica: A Field Seminar. Special publication, 130pp., Earth Sciences Society of Libya (ESSL), Tripli.

E-Hawat, A.S., and Argnani, A., 2001. Libya and the Pelagian shelf. In: Stampfli, G., Borel, G., Cavazza, W., Mosar, J., Ziegler, P., (eds.).The palaeotectonic atlas of the Peri-Tethyan Domain. The European Geophysical Society. IGCP 369 project CD-ROM.

El-Hawat, A. S., 1992. The Nubian Sandstone sequence in Sirt Basin, Libya: sedimentary facies and events. In: Sadek. A. (ed.), *Geology of the Arab World*.Cairo Univ. **1**, 317-327.

El-Hawat, A.S., 1997. Sedimentary basins of Egypt: an overview of dynamic stratigra-phy. In: Selley, R.C. (ed.). Sedimentary basins of the world, vol. 3, African Basins: p. 39-85. Elsevier, Amsterdam.

El-Hawat, A.S. and Shelmani, M.A., 1993. Short notes and guidebook on the geology of Al Jabal la Akhdar, Cyrenaica NE Libya. Interprint, Malta, 70 pp.

Eliagoubi, B.A., and Powell, J.D., 1980. Biostratigraphy and paleoenvironment of Upper Cretaceous (Maastrichtian) foraminifera of northcentral and northwestern Libya: in M.J. Salem and M.T. Busrewil (eds), The geology of Libya: London, Academic Press, v. 1, p. 137-153.

El-Makhrouf, A.A., 1988. Tectonic interpretation of Jabal Eghei area and its regional application to Tibesti orogenic belt, south central Libya (S.P.L.A.J.). *Journal of African Earth Sciences*, 7, 7-8, 945-967.

El-Makhrouf, A. A., 1996. The Tibisti-Sirt orogenic belt, Libya, G.S.P.L.A.J. In: *The Geology of Sirt Basin* (eds M.J. Salem, A.A. Busrewil, A.A. Misallati, M.A. Sola). Amsterdam, Elsevier, 3, 107-121.

El-Makhrouf, A. A., 2004. field excursion report on the Geology of Eastern Jabal Nafusa and the NE of Al-Hamada Al Hamra area- Ghadamis Basin: From Tethys Ocean to the Mediterranean sea, The first conference on the microfossiles around the Tethys Margins, Tripoli – Libya.

El Sogher, A., 1996. Late Cretaceous and Paleocene ostracodes from the Waha Limestone and Hagfa Shale formations of the Sirt Basin: in M.J. Salem, M.T. Busrewil, A.A. Misallati, and M.A. Sola (eds), The geology of the Sirt Basin: Amsterdam, Elsevier, v. 1, p. 287–382.

Embry, A.F. and Johannessen, E.P. 1992. T–R sequence stratigraphy, facies analysis and reservoir distribution in the uppermost Triassic- Lower Jurassic succession, western Sverdrup Basin, Arctic Canada, *in* T.O. Vorren, E. Bergsager, O.A. Dahl-Stamnes, E. Holter, B. Johansen, E. Lie, and T.B. Lund, eds., Arctic Geology and Petroleum Potential: Norwegian Petroleum Society (NPF), Special Publication, v. 2, p. 121-146.

Emery, D. & Myers, K.J., (eds.) 1996. Sequence Stratigraphy. Blackwell Science, Oxford.

Essed, A. S., 1978. A reconnaissance Bouguer gravity map of Libya, M.Sc. thesis, Purdue University.

Etheridge, M.A., Symonds, P.A., and Lister, G.S., 1989. Application of the detachment model to reconstruction of conjugate passive margins, *in* Tankard, A.J., and Balkwill, H.R., eds., Extensional Tectonics and Stratigraphy of the North Atlantic Margins: American Association of Petroleum Geologists Memoir 45, p. 23–40.

Fairhead, J. D., 1988. Mesozoic plate tectonic reconstruction of the central south Atlantic Ocean: The role of the west and central African rift system. Tectonophysics, **155**, pp. 181-195.

Fairhead, J. D. and Binks, R. M., 1991. Differential opening of the Central and South Atlantic Oceans and the opening of the West African rift system, Tectonophysics, 187, 191–203, 1991.

Fairhead, J.D., Green, C.M., Masterton, S.M., and Guiraud, R., 2013. The role that plate tectonics, inferred stress changes and stratigraphic unconformities have on the evolution of the West and Central African Rift System and the Atlantic continental margins. Tectonophysics 594 (2013) 118–127.

Fekirine, B., and Abdallah, H., 1998. Palaeozoic lithofacies correlatives and sequencestratigraphy of theSaharan Platform, Algeria. *In: Macgregor, D.S., Moody, R.T.J. & Clark-Lowes, D.D. (eds.),Petroleum geology of North Africa. Geological Society, London, Special Publications*, **132**, 97-108.

Fiduk, J.C., 2009. Evaporites, petroleum exploration, and the Cenozoic evolution of the Libyan shelf margin, central North Africa. Marine and Petroleum Geology 26, 1513–1527.

Finetti, I. 1982. Structure, stratigraphy and evolution of central Mediterranean. Bollettino di Gefisica Teorica and Applicata, v. 24, p. 247-312.

Freeman, B., Yielding, G. and Badley, M., 1990. Fault correlation during seismic interpretation, First Break, 8, no. 3, 87-95.

Frizon de Lamotte., Shirazi, S. T., Leturmy, P., Averbuch, O., Mouchot, N., Raulin, C., Leparmentier, F., Blanpied, C., and Ringenbach, Jean-Claude., 2013, Evidence for Late Devonian vertical movements and extensional deformation in northern Africa and Arabia: Integration in the geodynamics of the Devonian world. Tectonics, Vol. 32, 1-16.

Funnel, R., Chapman, D., Allis, R., and Armstrong, P., 1996. Thermal state of the Taranaki Basin, New Zealand. *Journal of Geophysical Research* **101**(B11):25,197-25,215.

Gaina, C., T. H. Torsvik, D. J. J. van Hinsbergen, S. Medvedev, S. C. Werner, and C. Labails., 2013, The African Plate: A history of oceanic crust accretion and subduction since the Jurassic, Tectonophysics, 604, 4–25.

Galloway, W.E., 1989. Genetic stratigraphic sequences in basin analysis, I. Architecture and genesis of flooding-surface bounded depositional units: American Association of Petroleum Geologists Bulletin, v. 73, p. 125-142.

Galushkin, Yu. I., El Maghbi, A., El Gtlawi, M., and Sitar, K. A., 2015. Variations in the Degree of Catagenesis and Hydrocarbon Generation in the Source Rocks of the Sirt Basin, Libya. ISSN 0016_7029, Geochemistry International, 2015, Vol. 53, No. 2, pp. 150–161. © Pleiades Publishing, Ltd., 2015. Original Russian Text © Yu.I. Galushkin, A. El Maghbi, M. El Gtlawi, K.A. Sitar, 2015, published in Geokhimiya, 2015, No. 2, pp. 162–173.

Gawthorpe, R. L., Fraser, A. J. and Collier, R. E. L., 1994. Sequence stratigraphy in active extensional basins: implications for the interpretation of ancient basin-fills. *Marine and Petroleum Geology*, 11 (6), 642-658.

Gawthorpe, R.L., Sharp, I., Underhill, J.R., and Gupta, S., 1997. Linked sequence tratigraphic and structural evolution of propagating normal faults: Geology, v. 25, p. 795-798.

Gawthorpe, R.L., 1997. Implications of fault scarp degradation for Brent Group prospectivity, Ninian feld, Northern North Sea. American Association of Petroleum Geologists Bulletin 81, 999 - 1022.

Gawthorpe, R. L., and Leeder, M. R., 2000. Tectono–sedimentary evolution of active extensional basins. Basin Research, 12, 195–218.

Gealey, W. K., 1988. Plate tectonic evolution of the Mediterranean–Middle East region: Tectonophysics, v. 155, p. 285–306.

Genik, G.J., 1992. Regional framework and structural aspects of rift basins in Niger, Chad and the Central African Republic (CA.R.). In: P.A. Ziegler (Editor), Geodynamics of Rifting, Volume II. Case History Studies on Rifts: North and South America and Africa. Tectonophysics, 2\3: 169-185.

Ghori, K.A.R., and Mohammed, R.A., 1996. The application of petroleum generation modelling to the eastern Sirt Basin, Libya, *in* M.J. Salem, A.S. El-Hawat, and A.M. Sbeta, eds., Geology of the Sirt Basin: Amsterdam, Elsevier, v. 2, p. 529–540.

Glennie, K. W., (Ed.), 1986. Introductiont o the Petroleum Geology of the North Sea, 2nd ed., 278 pp., Blackwell Scientific, Boston, Mass.

Goudarzi, G.H., 1981. Structure - Libya. In: Salem, N.J., Busrewil, M.T. (Eds.), Geology of Libya. Al-Fateh Univ., Tripoli, pp. 879–892.

Gras, R., 1996. Structural style of the southern margin of the Messlah High, *in* Salem, M.J., El-Hawat, A.S., and Sbeta, A.M., eds., The geology of Sirt Basin: Amsterdam, Elsevier, v. III, p. 201–210.

Gras, R., and Thusu, B., 1998. Trap architecture of the Early Cretaceous Sarir Sandstone in the eastern Sirt Basin, Libya, *in* MacGregor, D.S., Moody, R.T.J., and Clark-Lowes, D.D., eds., Petroleum geology of North Africa: Geological Society, Special Publication 132, p. 317–334.

Graversen, O., 2002. A structural transect between the central North Sea Dome and the South Swedish Dome: Middle Jurassic-Quaternary uplift-subsidence reversal and exhumation across the eastern North Sea Basin, Geological Society, London, Special Publications, v.196.

Gupta, S., Cowie, P. A., Dawers, N. H., and Underhill, J. R., 1998. A mechanism to explain rift-basin subsidence and stratigraphic patterns through fault-array evolution: Geology, v. 26, p. 595-598.

Guiraud, R., Bellion, Y., Benkhelil, J., Moreau, C., 1987. Post-Hercynian tectonics in Northern and Western Africa. *Geological Journal*, 22, 433-466.

Guiraud, R., and Maurin, J.C., 1992. Early Cretaceous rifts of Western and Central Africa: an overview. Tectonophysics, 213, pp 153-168.

Guiraud, R., and Bellion, Y., 1995. Late Carboniferous to Recent geodynamic evolution ofthe West Gondwanian cratonic Tethyan margins. In: A. Nairn, L. E. Ricou, B. Vrielnck and J. Dercourt, The ocean basins and margins, 8, pp 101-124.

Guiraud, R., Binks, R.M., Fairhead, J.D., Wilson, M., 1992. Chronology and geodynamic setting of Cretaceous Cenozoic rifting in West and Central Africa. Tectonophysics 213, 227–234.

Guiraud, R., and Bosworth, W., 1997. Senonian basin inversion and rejuvenation of rifting in Africa and Arabia: synthesis and implications to plate-scale tectonics. Tectonophysics 282, 39–82.

Guiraud, R., 1998. Mesozoic rifting and basin inversion along the northern African Tethyan margin: an overview. In: MacGregor, D.S., Moody, R.T.J., Clark-Lowes, D.D. (Eds.), Petroleum Geology of North Africa. Geological Society, London, Special Publication 133, pp. 217–229.

Guiraud R., and Bosworth W., 1999. Phanerozoic geodynamic evolution of northeastern Africa and the northwestern Arabian platform, Tectonophysics, 315, 73

Guiraud, R., 2001. Northern Africa. In: Stampfli, G., Borel, G., Cavazza, W., Mosar, J., Ziegler, P.A. (Eds.), The Paleotectonic Atlas of the PeriTethyan Domain. European Geophysical Society.

Guiraud, R., B. Issawi, and W. Bosworth, 2001. Phanerozoic history of Egypt and surrounding areas, in P. A. Ziegler, W. Cavazza, A. H. F. Robertson, and S. Crasquin-Soleau,

eds., Peri-Tethys memoir 6: Peri-Tethyan rift/wrench basins and passive margins: Me´moires Museum National d'Histoire Naturalle, Paris 186, p. 469–509.

Guiraud R., Bosworth W., Thierry J., Delplanque A., 2005. Phanerozoic geological evolution of Northern and Central Africa: an overview, J. Afric. Earth. Sci., 43, 83–143.

Gumati, Y.D., Kanes, W.H. and Schamel, S., 1996. An evaluation of the hydrocarbon potential of the sedimentary basins of Libya. *Journ. Pet. Geol.* vol. 19, p. 39-52.

Gumati, Y.D., and Nairn, A.E.M., 1991. Tectonic subsidence of the Sirt Basin, Libya. J. Pet. Geol. 14, 93 –102.

Gumati, Y.D., and S. Schamel., 1988**.** Thermal maturation history of the Sirte Basin, Libya: *Jour. Petrol.Geol.,* 11, 205-218.

Gumati, Y.D, and Kanes, W.H., 1985. Early Tettiary Subsurface and Sedimentary Facies, Northern Sirt Basin, Libya. Bull. A.A.P.G. 69(1): 39-52.

Gumati, Y.D., 1985. Crustal extension, subsidence, and thermal history of the Sirt basin, Libya. Occasional publication No.3. Earth Sciences and Resources Institute, University of South Carolina, 207p.

Hallett, D., 2002. *Petroleum Geology of Libya*, ELSEVIER Amsterdam Boston.

Hallett, D., and El Ghoul, A., 1996. Oil and gas potential of the deep trough areas in the Sirt Basin, Libya, *in* Salem, M.J., El-Hawat, A.S., and Sbeta, A.M., eds., The geology of Sirt Basin: Amsterdam, Elsevier, v. II, p. 455–484.

Haq, B.U., Hardenbol, J., and Vail, P.R., 1987. Chronology of fluctuating sea levels since the Triassic (250 million years ago to present): Science, v. 235, p. 1156-1166.

Harding, T.P., 1984. Graben hydrocarbon occurrences and structural styles: AmericanAssociation of Petroleum Geologists Bulletin, v. 68, p. 333–362.

Harding, T., 1990. Identification of wrench faults using subsurface structural data: Criteria and pitfalls. AAPG Bulletin, 74, 1590–1609.

Hatton, L., Worthington, M. H., Makin, J., 1986. Seismic data processing: theory and practice. Oxford, Blackwell Scientific Publications.

Hay, W. W., Behensky Jr. J. F., Barron, E. J., and Sloan II, J. L., 1982. Late Triassic Liassic paleoclimatology of the proto-central North Atlantic rift system. Palaeogeogr.Palaeoclimatol., Palaeoecol., 40: 13--30.

Heller, P.L., and Paola, C., 1992. The large- scale dynamics of grain- size variation in alluvial basins, 2: application to syntectonic conglomerate. Basin Res., 4, 91-102.

Henza, A.A., Withjack, M.O., Schlische, R.W., 2010. Normal-fault development during two phases of non-coaxial extension: an experimental study. Journal of Structural Geology 32, 1656e1667.

Hillis, R. R., 1995. Quantification of Tertiary exhumation in the United Kingdom southern North Sea using sonic velocity data. AAPG Bulletin, 79, 130–152.

Hladil, J., Krejci, Z., Kalvoda, J., Ginter, M., Galle, A., Berousek, P., 1991. Carbonate ramp environment of Kellwasser time-interval (Lesni lom, Moravia, Czechoslovakia). Bull. Soc. Géol. Belg. 100, 57–119.

Holdsworth, R., Butler, C., and Roberts, A., 1997. The recognition of reactivation during continental: Journal of the Geological Society of London, V.154, p. 73-78.

Holford, S.P., Schofield, N., Jackson, C. A.-L., Magee, C., Green, P.F., Duddy, I.R., 2013. Impacts of Igneous Intrusions on Source and Reservoir Potential in Prospective Sedimentary Basins Along the Western Australian Continental Margin, West Australian Basins Symposium 2013.

Holt, P.J., 2012. Subsidence Mechanisms of Sedimentary Basins Developed over Accretionary Crust. PhD Thesis, Durham University.

Hunt, D., and Tucker, M.E., 1992. Stranded parasequences and the forced regressive wedge systems tract: deposition during base-level fall: Sedimentary Geology, v. 81, p. 1-9.

Ibrahim, M.W., 1991. Petroleum geology of the Sirte Group Sandstone, eastern Sirt Basin. In: Salem, M.J. and Busrewil, M.T., (eds), The Geology of Libya, Al-Fateh University, Tripoli, VII, 2757-2779.

Imber, J., Tuckwell, G.W., Childs, C., Walsh, J.J., Manzocchi, T., Heath, A.E., Bonson, C.G., Strand, J., 2004. Three-dimensional distinct element modelling of relay growth and breaching along normal faults. Journal of Structural Geology 26, 1897–1911.

Jackson, J. A., 1987**.** Active normal faulting and crustal extension, in ContinentaEl xtensionalT ectonicse, dited by M.P. Coward, J. F. Dewey, and P. L. Hancock, Geol. Soc. Spec. Publ., 28, 3-17.

Jackson, J. A. and McKenzie, D. P., 1984a. Active Tectonics of the Alpine Himalayan Belt Between Western Turkey and Pakistan, Geophys. J. R. Astron. Soc., 77, 185-246.

Jackson, J. A. and McKenzie, D. P., 1984b. Rotational Mechanism of Active Deformation in Greece and Iran, The Geological Evolution of the Eastern Mediterranean (Eds: J. E. Dixon, A. H. F. Robertson), 743-754.125

Jackson, J.A., and White, N. J., 1989. Normal faulting in the upper continental crust: Observations from regions of active extension, J. Struct. Geol., 11, 15-36.

Jackson, C. A., Gawthorpe, R.B., and Sharp, I.R., 2002. Growth and linkage of the East Tanka fault zone, Suez Rift: structural style and synrift stratigraphic response, J. Geol. Soc., 159, 175 – 187.

Jacobsen, B.H., 1987. A case for upward continuation as a standard separation filter for potential field maps. Geophysics 52, 1138–1148.

Janssen, M. E., Stephenson, R.A., Cloetingh, S., 1993, Changes in plate motions and their control on the subsidence of rifted basin in the African plate, in M. Thorweihe, Schandelmeier, H., ed., Geoscientific research in Northeast Africa, Rotterdam, Balkema, p. 185-188.

Janssen, M. E., Stephenson, R. A., and Cloetingh, S., 1995, Temporal and spatial correlations between changes in plate motions and the evolution of rifted basins in Africa: Geological Society of America Bulletin, v. 107, p. 1317–1332.

Jarvis, L., 1992. Sedimentology, geochemistry and origin of phosphatic chalk: the Upper Cretaceous deposits of NW Europe. *Sedimentology*, v. 39, p. 55-97.

Jervey, M. T., 1988. Quantitative geological modelling of siliciclastic rock sequences and their seismic expression. In: WILGUS C. K. (ed.) Sea Level Change." An Integrated Approach. Society of Economic Paleontologists and Mineralogists, Special Publication, 42, 47-69.

Johnson, J.G., and Murphy, M.A., 1984. Time-rock model for Siluro-Devonian continental shelf, western United States: Geological Society of America Bulletin, v. 95, p. 1349-1359.

Johnson, J.G., Klapper, G., and Sandberg, C.A., 1985. Devonian eustatic fluctuations in Euramerica: Geological Society of America Bulletin, v. 96, p. 567-587.

Jurdy, D.M., Stephanik, M., Scotese, C.R., 1995. Paleozoic plate dynamics, Journal of Geophysical Research 100 (1995), pp. 17965–17975.

Kearey, P., Brooks, M., and Hill, I., 2002. An Introduction to Geophysical Exploration: Blackwell Publishing.

Keen, C.E., C. Peddy, B. de Voogd, and D. Matthews, 1989. Conjugate margins of Canada and Europe: Results from deep reflection profiling, Geology1, 7, 173-176,1.

Kerr, H., and White, N., 1994. Application of an automated method for determining normal fault geometries, J. Struct. Geol., 16, 1691–1709.

Kaminski, M.A., Gradstein, F.M., Berggren, W.A., Geroch, S. & Beckmann, J.P., 1988. Flysch-type agglutinated foraminiferal assemblages from Trinidad: taxonomy, stratigraphy and paleobathymetry. Abhandlungen der Geologischen Bundesanstalt ,41, 155227.

Kleyn, A., 1983. Seismic reflection interpretation: Applied Science Publishers, New York.

Klitzsch, E., 1966. Comments on the Geology of the Central Parts of Southern Libya and Northern Chad. In: Williams, J.J. & Klitzsch, E. (eds): South-Central Libya and Northern Chad: 1-17. PESL 8th Annual Field Conference.

Klitzsch, E. and Ziegert, H., 2000. Short Notes and Guidebook on the Geology of the Dor el Gussa – Jabal Bin Ghanimah Area. Sedimentary Basins of Libya, 2nd Symp., Geology of Northwest Libya. 52 p. ESSL, Tripoli.

Kominz, M. A., 1984. Oceanic ridge volumes and sea-level change and error analysis. Mem Am. Assoc. Petrol. Geol., 36, 109-127.

Kominz, M.A., Miller, K.G., and Browning, J.V., 1998. Long-term and short-term global Cenozoic sea-level estimates. Geology, 26, 311–314.

kusznir, N.J. and Ziegler, P.A., 1992. The mechanics of continental extension and sedimentary basin formation: a simple-shear/pure-shear flexural cantilever model. *Tectonophysics* 215, 117-131.

Lambiase, J.J., 1989. The framework of African rifting during the Phanerozoic. Jour. African Earth Sciences, 8, 183-190.

Lambiase, J. J., and Bosworth, W., 1995, Structural controls on sedimentation in continental rifts, *in* Lambiase, J. J., ed., Hydrocarbon habitat in rift basins: Geological Society [London] Special Publication 80, p. 117–144.

Larsen, P.-H., 1988, Relay structures in a Lower Permian basement-involved extension system, East Greenland: Journal of Structural Geology, v.10, p. 3-8.

Laubscher, H. and Bernoulli, D., 1977. Mediterranean and Tethys, in Nairn, E.M., Kanes, W.H., and Stehli, F.G. (eds). *The Ocean Basins and Margins*. Plenum Publishing Corporation (New York) 4A 1–28.

Le Pichon, X., Angelier, J., & Sibuet, J.C., 1982. Plate boundaries and extensional tectonics. *Tectonophysics* **81**, 239-256.

Leeder, M. R., and R. L., Gawthorpe, R. L., 1987. Sedimentary models for extensional tilt-block/half-graben basins, *in* M. P. Coward, J. F. Dewey, and P. L. Hancock, eds., Continental extensional tectonics: London, Geological Society Special Publication 28, p. 139–152.

Leeder, M. R., 1995. Continental rifts and proto-oceanic troughs. In: *Tectonics of Sedimentary Basins* (Ed. by C. J. Busby and R. V. Ingersol).

Lister, G.S., Etheridge, M.A., and Symonds, P.A., 1986. Detachment faulting and the evolution of passivlistere continental margins. *Geology* **14**, 246-250.

Lister, G. S., Etheridge, M.A., and Symonds, P.A., 1991. Detachment models for the formation of passive continental margins. *Tectonics* 10:1038–1064.

Libyan Gravity Compilation Project, Libyan Petroleum Institute LPI (2001)

Lonergan, L., and White, N., 1999. Three-dimensional seismic imaging of a dynamic Earth. Phil. Trans. R. Soc. Lond. A357, 3359{3375.

MacGregor, D. S., and Moody, R.T.J., 1998. Mesozoic and Cenozoic petroleum systems of North Africa, in D. S. MacGregor, Moody, R.T.J., Clark-Lowes, D.D., ed., Petroleum Geology of North Africa, London, Geological Society Special Publication, v. 132: p. 201-216

Makris, J., and Yegorova, T., 2006. A 3-D density–velocity model of the East Mediterranean Ridge between Crete and Libya. Tectonophysics 417, 201–220.

Marone, F., Van der Lee, S., and Giardini, D., 2003. Three-dimensional upper-mantle S-velocity model for the Eurasia-Africa plate boundary region: Geophysical Journal International, v. 158/1, p. 109-130.

Marsh, N. A., 2008**.** The in_uences of crustal extension, salt tectonics and gravity-driven deformation on the structural evolution of the Halten Terrace, o_shore mid-Norway: new sights from 3D seismic data and fault analysis, PhD Thesis.

Martin, M., Starkie, S., Yanilmaz, E., Hufman, D. P., Gutteridge, P., Coles, G., El-Arnauti, A., and Keegan, J. B., 2008. Sequence Stratigraphy of the Precambrian to Middle Miocene of NE Libya. The Geology of East Libya 2008, vol. 1, pp. 263-294.

Massa, D., and Delort, T., 1984. Evolution du Bassin de Syrte (Libya) du Cambrien au Cretace Basal: Bulletin Société Géologique de France, Series 7, v. 26, no. 6, p. 1087–1096.

Maurin, J-C., and Guiraud, R., 1993. Basement control on the development of the interior Sudan rifts, Central Africa. Tectonophysics 228, 81-95.

Mavromatidis, A., 2006. Burial/exhumation histories for the Cooper – Eromanga basins and implications for hydrocarbon exploration, Eastern Australia. Basin Research, 18 (3): 351-373.

McClay, K. R., 1989, Analogue models of inversion tectonics, *in* Cooper,M. A., and Williams, G. D., eds., Inversion tectonics: Geological Society [London] Special Publication 44, p. 41–59.

McClay, K., Dooley, T., 1995. Analogue models of pull-apart basins. Geology 23, 711– 714.

McClay, K. R., Dooley, T., Gloaguen, R., Whitehouse, P., & Khalil, S., 2001. Analogue modeling of extensional fault architectures: comparisons with natural rift fault systems. In: Hill, K. C. & Bernecker, T. (eds) Eastern Australian Basins Symposium (2001). A refocused

energy perspective for the future, Petroleum Exploration SocieO' of Australia Special Publications, 573-584.

McKenzie, D. P., 1970. The plate tectonics of the Mediterranean region, Nature, 226, 239-243.

Mckenzie, D.P., 1978. Some remarks on the development of sedimentary basins. *Earth and Planetary Science Letters* **40**, 25-32.

Megerisi, M., and Mamgain, V.D., 1980. The Upper Cretaceous–Tertiary formations of northern Libya: in M.J. Salem and M.T. Busrewil (eds), The Geology of Libya: London, Academic Press, v. 1, p. 67-72.

Merle, O., 2011. A simple continental rift classification. *Tectonophysics,* 513 (1-4), 88-95.

Miall. A. D., 1985. Architectural-element analysis: a new method of facies analysis applied to fluvial deposits. Earth-Sci Rev 22: 261-308.

Meneisy, M., 1990. Volcanicity. In Said, R (ed). The Geology of Egypt, Balkema, Rotterdam, pp 157-172.

Mitchum R.M. Jr., 1977. Seismic stratigraphy and global changes of sea level. Part 11: glossary of terms used in seismic stratigraphy, Am. Assoc. Petrol. Geol. Mem., 26, 205–212.

Mitchum, R.M., Jr., Vail, P.R., **and Thompson, S**.,1977. Seismic stratigraphy and global changes of sea-level, part 2: the depositional sequence as a basic unit for stratigraphic analysis, *in* C.E. Payton, ed., Seismic Stratigraphy - Applications to Hydrocarbon Exploration: American Association of Petroleum Geologists Memoir, v. 26, p. 53-62.

Montgomery, S., 1994, Sirte Basin, North-Central Libya, prospects for the future: Petroleum Frontiers, Petroleum Information Corporation, v. 11, no. 1, 94 p.

Morgan, W.J., 1983. Hotspot tracks and the early rifting of the Atlantic. Tectonophysics 94, 123–139.

Morgan, M.A., Grocott, J., and Moofy, R.T., 1998. The structural evolution of the ZaghouanRessa Structural belt, northern Tunisia. In: MacGregor, D.S., Moody, R.T.J. and Clark-Lowes, D.D. (Eds.), Petroleum Geology of North Africa. Geol. Soc. Spec. Publ., 132, 405-422.

Morley, C. K., Gabdi, S., and Seusutthiya, K., 2007. Fault superimposition and linkage resulting from stress changes during rifting: Examples from 3D seismic data, Phitsanulok Basin, Thailand. Journal of Structural Geology, 29, 646–663.

Morley, C.K., Harayana, C., Phoosongsee, W., Pongwapee, S., Kornsawan, A., Wonganan, N., 2004. Activation of rift oblique and rift parallel pre-existing fabrics during

extension and their effect on deformation style: examples from the rifts of Thailand. Journal of Structural Geology 26, 1803e1829.

Morley, C.K., 1999. How successful are analogue models in addressing the influence of pre-existing fabrics on rift structures? Journal of Structural Geology 21, 1267-1274.

Morley, C. K., Nelson, R. A., Patton, T. L., and Munn, S. G., 1990. Transfer zones in the East African rift system and their relevance to hydrocarbon exploration in rifts: American Association of Petroleum Geologists Bulletin, v. 74, p. 1234-1253.

Morley,C .K., 1988. Variable extension in LakeTanganyika, Tectonics, 7, 785-801.

Moulin, M., Aslanian, D., and Unternehr, P., 2010. A new starting point for the South and Equatorial Atlantic Ocean: Earth-Science Reviews, v. 98, p. 1–37, doi:10.1016/j.earscirev.2009.08.001.

Mouzughi, A. J., and Taleb, T. M., 1981. Tectonic elements of Libya: Libya, National Oil Corporation, scale 1:2,000,000, 1 sheet.

Muftah, M.A., 1996. Agglutinated foraminifera from Danian sediment of northeastern Sirt Basin: in M.J. Salem, M.T. Busrewil, A.A.

Nicol, J.L., Forster, K.I., & Veres, C., 1997. Subject-verb agreement processes in comprehension. *Journal of Memory and Language*, *36*(4), 569–587.

Olsen, K. H., 1995. Continentarl ifts: Evolution, structure, tectonics, Developmenitns Geotectonis, Elsevier Amsterdam 4, 26 pp., 1995.

Paredes, J.M., S. Plazibat, C. Crovetto, J. Stein, E. Cayo, and A. Schiuma, 2013. Fault kinematics and depocentre evolution of oil-bearing, continental successions of the Mina del Carmen Formation (Albian) in the Golfo San Jorge basin, Argentina: Journal of South American Earth Sciences, v. 46, p. 63-79.

Parsons, M.G., Zagaar, A.M., and Curry., J.J., 1980. Hydrocarbon occurrence in the Sirte Basin, Libya, *in* A. D. Maill, ed., Facts and principles of world petroleum occurrence: Canadian Society of Petroleum Geology Memoir 6, p. 723–732.

Paul, M.K., Datta, S., Banerjee, B., 1966. Direct interpretation of two-dimensional structural faults from gravity data. Geophysics 31, 940–948.

Pawellek. T. 2007. A field guidebook to the geology of Sirt Basin, Libya.

Peacock, D. C. P., and Sanderson, D. J., 1991. Displacements, segment linkage and relay ramps in normal fault zones: Journal of Structural Geology, v. 13, p. 721-733.

Peregi, Z.S., Less, G.Y., Konrad, G.Y., Fodor, L., Gulacsi, Z., Gyalog, L., Turki, S.M., Suwesi, S.K., Sherif, K., Dalub, H., 2003. Geological map of Libya, 1:250.000, Al Haruj Al Abyad sheet NG 33-8 with explanatory booklet. 250 p. IRC, Tripoli.

Pereira, R. and Alves, T.M., 2012. Tectono-stratigraphic signature of multiphased rifting on divergent margins (deep-offshore southwest Iberia, North Atlantic). *Tectonics 31: doi: 10.1029/2011TC003001. issn: 0278-7407.*

Pique., A, and Laville., E, 1996. The Central Atlantic Rifting: Reactivation of Palaeozoic Structures, Journal of Geodynamics, 21(3):235-255.

Posamentier H.W., Jervey M.T., Vail P.R., 1988. Eustatic controls on clastic deposition: I. Conceptual framework, in: Sea Level Changes-An Integrated Approach, SEPM Special Pub. Vol. 42, pp. 110–124, eds Wilgus C.K., Hastings B.S., Kendall C.G.St.C., Posamentier H.W., Ross C.A., Van Wagoner J.C., Society of Economic Paleontologists and Mineralogists, Tulsa, OK.

Posamentier H.W., and Allen G.P., 1999. Siliciclastic sequence stratigraphy: concepts and applications, in SEPM Concepts in Sedimentology and Paleontology, 7, Society of Economic Paleontologists and Mineralogists, Tulsa, OK, 204pp., doi:10.1017/S0016756801216082.

Prosser, S., 1993. Rift-related linked depositional systems and their seismic expression. in *Tectonics and Seismic Sequence Stratigraphy*. G. D. Williams and A. Dobb, Geological Society of London. 71, 35-66.

Ralph, B., Cope, M., Redfern, J., (in prep) Petroleum Systems of the Eastern Sirt Basin (Libya).

Ravnås, R., and Steel, R. J., 1998. Architecture of marine rift-basin successions. AAPG Bulletin, 82 (1), 110-146.

Reading, H. G., 1980, Characteristics and recognition of strike-slip fault systems: International Association of Sedimentologists, Special Publication, v. 4, p. 7–26.

Regan, R.D., and Hinze, W.J., 1976. The effect of finite data length in the spectral of ideal gravity anomalies. Geophysics 41, 44–55.

Reid, A. B., Allsop, J. M., Granser, H., Millett, A. J., and Somerton, I. W., 1990. Magnetic interpretation in three dimensions using Euler deconvolution: Geo-physics, 55, 80{91.

Reston, T.J., 1990. Mantle shear zones and the evolution of the northern North Sea Basin. *Geology* **18**, 272-275.

Reynolds, D. J., Steckler, M.S., and Coakley, B.J., 1991, The Role of the Sediment Load in Sequence Stratigraphy: The Influence of Flexural Isostasy and Compaction: J. Geophys. Res., v. 96.

Reynolds, J.M., 1997. *An Introduction to Applied and Environmental Geophysics*, John Wiley and Sons Ltd, Chichester, 796 pp, first edition.

Reynolds, J.M. 2011. *An Introduction to Applied and Environmental Geophysics*. John Wiley & Sons Ltd, Chichester, 2nd ed.,712 pp.

Rider, M. H., 1986. The geological interpretation of well logs: Blackie Halsted Press, New York, 192 p.

Rider, M.H., 1991. *The Geologic Interpretation of Well Logs* (2nd ed.): Caithness (Whittles Publishing).

Robertson, A.H.F., and Dixon, J.E., 1984. *Aspects of the geological evolution of the Eastern Mediterranean.* In J.E. Dixon and A.H.F. Robertson (Eds.), The Geologic Evolution of the Eastern Mediterranean, Geological Society of London, Special Publication, 17, 1-74.

Robertson, A. H. F., Dixon, J. E., Brown, S., Collins, A., Morris, A., Pickett, E. A., Sharp, I., and Ustaomer, T., 1996, Alternative tectonic models for the Late Paleozoic-Early Tertiary development of Tethys in the Eastern Mediterranean region, in: Morris, A. and Tarling, O. H. (Eds): Paleomagnetism and tectonics of the Mediterranean region, Geol. Soc. London, Special Publications, 105, 239–263.

Roberts, A. M., and Yielding., G., 1991. Deformation around basin-margin faults in the North Sea/mid Norway rift. In; Roberts, A. M., Yielding, G. & Freeman, B. (eds) The Geometry of Normal Faults. Geophysical Society, London, Special Publications, 56, 61-78.

Roberts, A.M., Kusznir, N.J., Yielding, G., Styles, P., 1998. 2D flexural backstripping of extensional basins: the need for a sideways glance. Pet Geosci 4:327–338

Roohi, M., 1996a. A geological view of source-reservoir relationships in the western Sirt Basin, in M.J. Salem, A.S. El-Hawat, and A.M. Sbeta, eds., Geology of the Sirt Basin: Amsterdam, Elsevier, v. 2, p. 323–336.

Roohi, M., 1996b. Geological history and hydrocarbon migration pattern of the Az Zaahra-Al Hufrah Platform. In: Salem, M. J., Busrewil, M. T., Misallati, A.A. and Sola, M. A. (eds.). The Geology of the Sirt Basin. Elsevier, Amsterdam, **I**, 195- 232.

Röhlich P., 1980. Tectonic development of Jabal al Akhdar, in: The Geology of Libya, Vol. 3, pp 923–931, eds Salem M.J., Buserwil M.T., Academic Press, London.

Rosenbaum, G., Lister, G., Duboz, C., 2002. Relative motions of Africa, Iberia and Europe 553 during Alpine orogeny. Tectonophysics 359.

Rosenbaum, G., Weinberg, R. F., and Regenauer-Lieb, K., 2008. The geodynamics of lithospheric extension. *Tectonophysics*, 458, 1-8. DOI: 10.1016/j.tecto.2008.07.016.

Rosendahl, B.L., 1987**.** Architecture of continental rifts with special reference to east Africa. Annual Reviews of Earth and Planetary Sciences, 15, 445–503.

Rosendahl, B. R., Kilembe, K., and Kaczmarick, K., 1992. Comparison of the Tanganyika, Malawi, Rukwa, and Turkana rift zones from analyses of seismic reflection data, *Tectonophysics*, *213*, 235-256.

Rossi, M.E., Tonna, M., Larbash, M., 1991. Latest Jurassic – Early Cretaceous deposits in the subsurface of the Eastern Sirt Basin (Libya): facies and relationships with tectonics and sea-level changes. In: Salem, M.J., Sbeta, A.M., Bakbak, M.R. (Eds.), The Geology of Libya, vol. 6. Elsevier, Amsterdam, pp. 2211–2225.

Royden, L. H., and Keen, C. E., 1980. Rifting process and thermal evolution of the continental margin of eastern Canada determined from subsidence curves. *Earth planet.Sci. Lett.* **51,** 343-361.

Rusk, D. C., 2001, Libya: Petroleum potential of the underexplored basin centres - A twenty-first-century challenge, *in* M.W. Downey, J. C. Threet, and W. A. Morgan, eds., Petroleum provinces of the twenty-first century: AAPG Memoir, 74, p. 429–452.

Sandiford, M., Frederiksen, S., & Braun, J., 2003. The long-term thermal consequences of rifting: implications for basin reactivation. Basin Research, 15, 23–24.

Savostin, L.A., Sibuet, J.C., Zonenshain, L.p. Lepichon, X. & Roulet, M.J., 1986. Kinematic evolution of the Tethys belt from the Atlantic to the Pamirs since the Triassic. *Tectonophysics*, 123, (1-4), 1-35.

Sawyer, D. S., 1985. Total Tectonic Subsidence: A Parameter for Distinguishing Crust Type at the U.S. Atlantic Continental Margin. *J. Geophys. Res.*, 90(B9): 7751â€“7769

Schroeter, T., 1996. Tectonic and sedimentary development of the central Zallah trough (west Sirt Basin, Libya), in M. J. Salem, M. T. Busrewil, A. A. Misallati, and M. A. Sola, eds., The geology of the Sirt Basin: Amsterdam, Elsevier, v. 3, p. 123–135.

Schäfer, K., Kraft, K.H., Hausler, H., Erdman, J., 1980. In situ stresses and paleostresses in 561 Libya. In: Salem, N.J., Busrewil, M.T. (Eds.), Geology of Libya. InAl-Fateh Univ, Tripoli, 562 pp. 907 - 922.

Schlische, R. W., and Olsen, P. E., 1990. Quantitative filling model for continental extensional basins with applications to early Mesozoic rifts of eastern North America: Journal of Geology, v. 98, p. 135-155.

Schlische, R. W., 1993. Anatomy and evolution of the Triassic–Jurassic continental rift system, eastern North America: Tectonics, v. 12, p. 1026–1042.

Schlische, R. W., and Anders, M. H., 1996. Stratigraphic effects and tectonic implications of the growth of normal faults and extensional basins, in Beratan, K. K., ed., Reconstructing the Structural History of Basin and Range Extension Using Sedimentology and Stratigraphy: GSA Special Paper 303, p. 183-203.

Schlische, R.W., and Withjack, M.O., 1999. Rift basin architecture and evolution, *in* Olsen, P.E. and Kent, D.V., ed., Climatic, biotic, and tectonic pole-to-pole coring transect of Triassic-Jurassic Pangaea: International Continental Drilling Program

Schmoker, J. W., and Halley, R.B., 1982. Carbonate porosity versus depth: A predictable relation for south Florida, Am. Assoc. Pet. Geol. Bull., 66, 2561-2570.

Schultz, R.A., Hauber, E., Kattenhorn, S., Okubo, C.H., Watters, T.R., 2010. Interpretation and analysis of planetary structures, Journal of Structural Geology, 32, 855-875, doi:10.1016/j.jsg.2009.09.005.

Sclater, J., and Christie, P., 1980, Continental Stretching: An explanation of the post-mid-Cretaceous subsidence of the central North Sea Basin: Journal of Geophysical Research, v. 85, no. B7, p. 3711-3739.

Selley, R. C., 1971. Structural control of the Miocene sedimentation in the Sirt Basin, in C. Gray, ed., Symposium on the geology of Libya: Tripoli, Libya, University of Libya Science Faculty, p. 99–106.

Selley, R.C., 1997. The Sirte Basin of Libya in African Basins, *in* Selley, R.C., ed., Sedimentary basins of the world: Amsterdam, Elsevier, v. 3, p. 27–37.

Şengör, A. M. C., and Kidd, W. S. F., 1979. The post-collisional tectonics of the Turkish-Iranian Plateau and a comparison with Tibet: *Tectonophysics*, 55, 361-376.

Sengör, A.M.C., 1987. Cross-faults and differential stretching of hanging walls in regions of low-angle normal faulting: examples from Western Turkey.Geological Society, London, Special Publications**,** v. 28, **p. 575-589**

Shaw, J. H., Hook, S. C., Sitohang, E. P., 1997. Extensional Fault-Bend Folding and Synrift Deposition: An Example from the Central Sumatra Basin, Indonesia, Search and Discovery Article #40004.

Shelley, D., and Bossière, G., 2000, A new model for the Hercynian Orogen of Gondwana France and Iberia. *Journal of Structural Geology* 22, pp. 757–776.

Sheriff R.E., and Geldart L.P., 1995. Exploration Seismology. Cambridge University Press, 592 p.

Shepherd, M., 2009. Structural geology: Faults, *in* M. Shepherd, Oil field production geology: AAPG Memoir 91, p. 107-122.

Skuce, A.G., 1994. A structural model of a graben boundary fault system, Sirte Basin, Libya: Compaction structures and transfer zones: Canadian Journal Exploration Geophysics, v. 30/2, p. 84-92.

Skuce., A. G., 1996. Forward modelling of compaction above normal faults: an example from the Sirt Basin, Libya. Geological Society Special Publication No. 99, pp. 135-146.

Sleep, N.H., 1971. Thermal effects of the formation of Atlantic continental margins by continental break up, Geophysical Journal of Royal Astronomic Society, 24, 325–350.

Smith, A. G., 1971. Alpine deformation and the oceanic areas of Tethys, Mediterranean and Atlantic. Bulletin Geological Society of America, 82, 2039-70.

Smith, R.P., Grauch, V.J.S., and Blackwell, D.D., 2002. "Preliminary Results of a High-Resolution Aeromagnetic Survey to Identify Buried Faults at Dixie Valley, Nevada", Geothermal Resources Council Transactions, 26, 543-546.

Spector, A., and Grant, F.S., 1970. Statistical models for interpreting aeromagnetic data. Geophysics 35, 293–302.

Spring, D., and Hansen, O.P., 1998. The influence of platform morphology and sea level on the development of a carbonate sequence: The Harash Formation, eastern Sirt Basin, Libya, *in* D.S. MacGregor, R.J.T. Moody, and D.D.. Clark-Lowes, eds., Petroleum geology of North Africa: Geological Society of London, p. 335–354.

Stampfli G.M., and Borel G., 2000. Mesozoic Plate Tectonic of the Western Tethyan Domain, 6th Int. Cretaceous Symp, Vienna.

Stampfli, G.M. and Borel, G.D., 2002. A plate tectonic model for the Paleozoic and Mesozoic constrained by dynamic plate boundaries and restored synthetic oceanic isochrons. Earth and Planetary Science Letters, 196: 17-33.

Stampfli, G.M., Mosar, J., Favre, P., Pillevuit, A., Vannay, J.C., 2001. Permo-Mesozoic evolution of the western Tethys realm: the Neo-Tethys East Mediterranean Basin connection. In: P.A. Ziegler, W. Cavazza, A.H.F. Robertson, and S. Crasquin-Soleau (Eds.), Peri-Tethys Memoir 6: Peri-Tethyan Rift/Wrench Basins and Passive Margins, Me´moires du Muse´um national d_Histoire naturelle de Paris 186, pp. 51–108.

Starkie, S., Keegan, J.B., Mansouri, A. L., Yanilmaz, E., Hufman, D., and Martin, M., 2008. Development of an integrated Stratigraphical Nomenclature for the Precambrian to Middle Miocene of NE Libya. The Geology of East Libya, vol.1, pp. 239-262.

Steckler, M. S., and Watts, A.B., 1978. Subsidence of the Atlantic-type continental margin off New York: Earth and Planetary Science Letters, v. 41, p. 1–3.

Stewart, J., Watts, A.B., and Bagguley, J.G., 2000. Three-dimensional subsidence analysis and gravity modelling of the continental margin onshore Namibia, Geophys. J. Int., 141, 724–746.

Stephenson, R.A., Zelt, C.A., Ellis, R.M., Hajnal, Z., Morel-a-l'Hussier, P., Mereu, R.F., Northey, D.J., West, G.F., and Kanasewich, E.R., 1989. Crust and upper mantle structure and origin of the Peace River Arch. Bulletin of Canadian Petroleum Geology, v. 37, p. 224-235.

Suleiman,I .S., 1985**.** Gravity and heat flow studies in the Sirte Basin, Libya, Ph.D. thesis, 187 pp., Univ. of Tex. at E1 Paso.

Suleiman, I.S., Keller, O. R., and Suleiman, A. S., 1991. Gravity study of the Sift Basin, Libya, in The Geology of Libya, vol. 6, Edited by M.J. Salem, AIv[Sbeta, and 1V[R. Bakbak, Elsevier, Amsterdam, pp. 2462-2469.

Suleiman, A., and Doser, D., 1994. The seismicity, seismotectonics and earthquake hazards of Libya, with detailed analysis of the 1935 April 19, M=7.1 earthquake sequence, Geophys. J. Int., vol.120, pp: 312-322.

Swarbrick, R.E., and Osborne, M.J., 1998. Mechanisms that generate abnormal pressures: an overview. In: Abnormal Pressures in Hydrocarbon Environments, AAPG Memoir 70 (eds Law BE, Ulmishek GF, Slavin VI), pp. 13–34. American Association of Petroleum Geologists, Tulsa, OK.

Swezey, C. S., 2009. Cenozoic stratigraphy of the Sahara, Northern Africa: Journal of Africa Earth Sciences, v.53, no.3, p. 89-121.

Swire, P. H., and Gashgesh, T. M., 2003. Sedimentology of Jefarah Basin, NW Libya. Eds.: Salem, M., J. and Khaled M. Oun" The Geology of NW Libya l. Sedimentary Basin of Libya. Second Symposium, pp 173-215.

Talwani M, Worel,J.L., Landisman M., 1959. Rapid gravity computations for twodimensionalbodies with application to the Mendocino submarine fracture zone. Journal of Geophysical Research, 64, 49-59.

Tawadros E.E.M., 2001. Geology of Egypt and Libya. Taylor & Francis., London, 468pp.

Telford, W. M., L. P. Geldart, and R. E. Sheriff., 1990. Applied Geophysics. *Cambridge University Press.*

Tmalla, A.F.A., 1996. Late Maastrichtian and Paleocene planktonic foraminiferal biostratigraphy of well A1a-NC29A, northern Sirt Basin, Libya: in M.J. Salem, M.T.

Busrewil, A.A. Misallati, and M.A. Sola, (eds), The Geology of the Sirt Basin: Amsterdam, Elsevier, v. 1, p. 195–232.

Thompson, D.T., 1982. A new technique for making computer assisted depth estimates from magnetic data. Geophysics 47, pp 31-37.

Thomas, D., 1995. Exploration limited since 70s in Libya's Sirte basin. Oil and Gas Journal. 93(11): 99-104.

Thusu, B., and Mansouri, A., 1995. Reassignment of the Upper Amal Formation to Triassic and its implications for exploration in southeast Sirte, Libya. In: First Symposium on Hydrocarbon Geology of North Africa, London, 2&30 November 1995,
Abstracts, p. 48.

Thusu, B., 1996. Implication of the discovery of reworked and *in situ* Late Palaeozoic and Triassic palynomorphs on the evolution of the Sirt Basin, Libya. In: Salem, M.J., Mouzughi, A.J. and Hammuda O.S., (Eds), *The Geology of Sirt Basin*, **I**, Elsevier, Amsterdam, Netherlands, pp. 455-474.

Trudgill, B., and Cartwright, J., 1994. Relay-ramp forms and normal fault linkages, Canyonlands National Park, Utah: Geological Society of America Bulletin, v. 106, p. 1143-1157.

Turcotte. D.L., and Schubert, G., 1982. Geodynamics applications of continuum physics to geological problems. Wiley, New York, 450 pp.

Tucker, M. E., 1991. Sedimentary petrology: an introduction to the origin of sedimentary rocks. Blackwell Science Publications, Oxford, 260p.

Underdown, R., Redfern, J., Lisker, F., 2008**.** Constraining the burial history of the Ghadames Basin, North Africa. An integrated analysis using sonic velocity, vitrinite reflectance and apatite fission track ages. Basin Research, 19, 557-578.

Vail, P.R., Mitchum, R.M., Thompson, S. III, Sangree, J.R., Dubb, J.N., HaSlid, W.G., 1977. Sequence stratigraphy and global changes of sea level. In: Seismic Stratigraphy . Applications toHydrocarbon Exploration (Ed. byC.E. Payton),Mem.Am. Assoc. Petrol.Geol., 26, 49^205.

Vail, P.R., and Todd. G.R., 1981. Northern North Sea Jurassic Unconformities, Chronostratigraphy and Sea-level changes from seismic stratigraphy, eds Illing L. V., Hobson G. D. (Institute of Petroleum, Heyden, London), pp 216–235.

Vail P.R., 1987. Seismic stratigraphy interpretation using sequence stratigraphy. Part I: seismic stratigraphy interpretation procedure. in: Atlas of Seismic Stratigraphy, AAPG Studies in Geology No. 27, pp. 1–10, ed. Bally A.W., American Association of Petroleum Geologists, Tulsa, OK.

Vail, P.R., Audemard, F., Bowman, S.A., Eisner, P.N., and Perez-Cruz, **C.,** 1991, The stratigraphic signatures of tectonics, eustasy and sedimentology - an overview, *in* G. Einsele, W. Ricken, and A. Seilacher, eds., Cycles and Events in Stratigraphy: Springer-Verlag, p. 617-659.

Van der Meer, F.D., and Cloetingh, S.A.P.L., 1993. Intraplate stresses and the subsidence history of the Sirt basin, Libya. In: Tectonophysics : international journal of geotectonics and the geology and physics of the interior of the earth, 226 (1993)1-4, pp. 37-58.

Van Houten, F.B., 1980. Latest Jurassic–Early Cretaceous regressive facies, northeast Africa Craton: American Association of Petroleum Geologists Bulletin, v. 64, p. 857–867.

Van Houten, F.B., 1983. Sirt Basin, north-central Libya-Cretaceous rifting above a fixed mantle hot-spot. Geology 11, 115–118.

Van Wagoner J.C., Posamentier H.W., Mitchum R.M., Vail P.R., Sarg J.F., Loutit T.S., Hardenbol J. , 1988. An overview of sequence stratigraphy and key definitions. in: Sea Level Changes-An Integrated Approach, SEPM Special Pub. Vol. 42, pp. 39–45, eds Wilgus C.K., Hastings B.S., Kendall C.G.St.C., Posamentier H.W., Ross C.A., Van Wagoner J.C. Society of Economic Paleontologists and Mineralogists, Tulsa, OK.

Van Wagoner, J.C., Mitchum, R.M., Campion, C.M., and Rahmanian, V.D., 1990. Siliciclastic sequence stratigraphy in well logs, core, and outcrops: concepts for high-resolution correlation of time and facies, *American Association of Petroleum Geologists Methods in Exploration Series* **vol. 7** (1990) 55 pp.

Van Wees, J.D., and Stephenson, R.A., 1995.Quantitative modeling of basin and rheological evolution of the Iberian Basin. (Central Spain): implications for lithospheric dynamics of intraplate extension and inversion. Tectonophysics 163–178.

Van Wees, J.D., and Cloetingh, S., 1996. 3D flexure and intraplate compression in the North Sea Basin. Tectonophysics 266, 343–359.

Van Wees, J.D.,Cloetingh, S. and de Vicente, G., 1996. The role of pre-existing faults in basin evolution: constraints from 2D finite element and 3D flexure models, in Modern Developments in Structural Interpretation, Validation and Modelling, eds Buchanan, P.G. & Nieuwland, D.A., Geol. Soc. Spec. Publ., 99, 283–296.

Walsh, J.J., and Watterson, J., 1988. Analysis of the relationship between the displacements and dimensions of faults. Journal of Structural Geology 10, 239– 247.

Walsh, J.J., and Watterson, J., 1991. Geometric and kinematic coherence and scale effects in normal fault systems. In: Roberts, A.M., Yielding, G., Freeman, B. (Eds.), The Geometry of Normal Faults Geological Society of London Special Publication 56, pp. 193–203.

Walsh, J.J., Nicol, A., Childs, C., 2002. An alternative model for the growth of faults. Journal of Structural Geology 24, 1669-1675.

Walsh, J., C. Childs, J. Imber et al., 2003. Strain localisation and population changes during fault system growth within the Inner Moray Firth, northern North Sea. J. Struct. Geol. 25:307–315.

Walsh, J.J., Bailey, W.R., Childs, C., Nicol, A., Bonson, C.G., 2003. Formation of segmented normal faults: a 3D perspective. J. Struct. Geol. 25, 1251e1262.

Watts, A. B., Cochran, J.R., and Selzer, G., 1975. Gravity anomalies and flexure of the lithosphere: A three-dimensional study of the Great Meteor Seamount, J. Geophys Res., 80, 1391-1398.

Watts, A. B., and. Ryan, W. B. F., 1976. Flexure of the lithosphere and continental margin basins, *Tectonophysics*, 36, 25-44, doi:10.1016/0040-1951(76)90004-4.

Watts, A.B. and Steck[er, M.S., 1979. Subsidence and eustasy at the continental margin of eastern North America Maurice Ewing Syrup. Series 3, AGU Washington, D.C., 218-234

Watts, A.B., Karner, G.1., and Steckler, M.S., 1982. Lithosphcric flexure and the evolution of sedimentary basins, in: The evolution of sedimentary, basins (Eds. Kent, P.S. Bott, M.H.P.. McKenzic, D. P., and Williams, C.A., Phil, Trans. Roy. Soc. London 305A, 249-281.

Watts, A. B., and Torné, M., 1992. Subsidence history, crustal structure and thermal evolution of the Valencia through: A young extensional basin in the western Mediterranean, J. Geophys. Res., 97, 20,021–20,041.

Watts, A. B., and Marr, C., 1995. Gravity anomalies and the thermal and mechanical structure of rifted continental margins. *In:* Banda E., Torne M. & Talwani M. eds. *Rifted Ocean–Continent Boundaries*, pp. 65–94. Kluwer Academic Publishers, Dordrecht.

Watts, A.B., 2001. Isostasy and Flexure of the Lithosphere. Cambridge University Press. Cambridge, United Kingdom.

Watterson, J., 1986. Fault dimensions, displacement and growth, Pure Appl. Geophys., 124, 365-373.

Waterson, P.E., Clegg, C.W. and Axtell, C.M., 1997. The dynamics of work organization, knowledge, and technology during software development, *Journal of Human-Computer Studies*, Vol. 46 No. 1, pp. 79-101.

Wennekers, J.H.N., Wallace, F.K. and Abugares., 1996. The Geology and Hydrocarbons of the Sirt Basin: A Synopsis.–In: The Geology of Sirt Basin (Salem, M.J. et al., eds.), Elsevier, Amsterdam, 1, 3–58.

Wernicke, B., 1981. Low-angle normal faults in the Basin and Range province: nappe tectonics in an extending orogen. Nature, London, 291, 645-648.

Wernicke, B., and Burchfiel, B.C., 1982. Modes of extensional tectonics. *Journal of Structural Geology* **4**, 105-115.

Westphal, M., Bazhenov, M.L., Laurer, J.P., Bijou-Duval, B., 1984. Presentation of 9 paleogeographic maps at 20.000.000 scale from the Atlantic to the Pamir between Lias and Present. Bulletin de la Societe Geologique de France 8, 637– 652.

White, N., 1989. Nature of lithospheric extension in he North Sea. *Geology* **17**, 111-114.

Widiyantoro, S., van der Hilst, R.D.,Wenzel, F., 2004. Deformation of the Aegean slab in 590 Q4 the mantle transition zone. Int. J. Tom. Stat. D04, 1–14

Wilkerson, M.S., Apotria, T., Farid, T., 2002. Interpreting the geologic map expression of contractional fault-related fold terminations: lateral/oblique ramps versus displacement gradients. Journal of Structural Geology 24, 647–662.

Willemse, E. J., Pollard, D.D., and Aydin, A., 1996. Three-dimensional analyses of slip distributions on normal fault arrays with consequences for fault scaling, J. Struct. Geol., 18, 295– 309.

Williams, GD., Powell, CM., Cooper, MA., 1989. Geometry and kinematics of inversion tectonics. In: Cooper MA, Williams GD (eds) Inversion tectonics. Geol Soc Spec Publ 44 : 3 - 15.

Wilson, J.T., 1963. Evidence from Islands on the Spreading of the Ocean Floor. *Nature*, 197: 536-538.

Wilson, M., and Guiraud, R., 1992. Magmatism and rifting in western and central Africa, from Late Jurassic to Recent times. In: Ziegler, P.A. (Ed.), Geodynamics of rifting, volume II. Case history studies on rifts: North and South America and Africa. Tectonophysics, 213, pp. 203–225.

Wilson, BM., and Guiraud, R., 1998. Late Permian to Recent magmatic activity on the Africa-Arabian margin of Tethys, In: MacGregor, D.S., Moody, R.T.J. and Clark-Lowes, D.D. (Ed) *Petroleum Geology of North Africa*, Geological Society of London Special Publication, 132, Geological Society of London, pp231-263.

Wilson, T., Wells, A., and Koperna, G., 2009. Seismic evaluation of the Fruitland Formation with implications on leakage potential of injected CO2: on the proceedings CD for the 2009 International Pittsburg Coal Conference, 11p.

Wilson, P., Elliott, G.M., Gawthorpe, R.L., Jackson, C.A.L., Michelsen, L. & Sharp, I.R., 2013. Geometry and segmentation of an evaporite-detached normal fault array: the southern Bremstein Fault Complex, offshore mid-Norway. J. Struct. Geol., 51, 74‑91.

Withjack, M.O., and Jamison, W.R., 1986. Deformation Produced by Oblique Rifting: Tectonophysics, v. 126, p. 99-124

Withjack, M.O., Olson, J., and Peterson, E., 1990. Experimental models of extensional forced folds: AAPG Bulletin, v. 74, p. 1038-1054.

Withjack, M.O., Olsen, P.E., and Schlische, R.W., 1995. Tectonic evolution of the Fundy rift basin, Canada: Evidence of extension and shortening during passive margin development: Tectonics, v. 14, p. 390-405.

Withjack, M.O., Schlische, R.W., and Olsen, P.E., 1998. Diachronous rifting, drifting, and inversion on the passive margin of central eastern North America: An analog for other passive margins: AAPG Bulletin, v. 82, p. 817-835.

Withjack, M.O., and Callaway, S., 2000. Active normal faulting beneath a saltlayer: physical study of deformation patterns in the cover sequence. American Association of Petroleum Geologists Bulletin 84, 627–651.

Withjack, M. O., Schlische, R.W, and Olsen, P.E., 2002. Rift-basin structure and its influence on sedimentary systems, in Sedimentation in Continental Rifts, edited by R. Renaut, and G. M. Ashley, Spec. Publ. SEPM Soc. Sediment. Geol., **73**, 57–81.

Witte, S., 2008. Basin Evolution from integrated Seismic, Gravity and Magnetic Data Interpretation in North Africa, North African Conference and Exhibition, Marrakech, Moroco.

Woller, F., and Fediuk, F., 1980. Volcanic Rocks of Jabal As Sawda. In: Salem, M.J., BusrewilL, M.T. (eds.). The Geology of Libya, III: 1081-1093. Academic Press, London.

Woollam, R. and Pearce, T., 2006. A New Approach to Stratigraphic Analysis in the Pre-Upper Cretaceous of the Sirt Basin, Libya, (on line source).

Wyllie, M . R. J., Gregory, A. R., and Gardener, L. W., 1956. Elastic wave velocities in heterogeneous and porous media. Geophysics, 21, 41 - 70.

Xiao, H.-B., and Suppe, J., 1992. Orgin of rollover, AAPG Bulletin, 76 (4), 509-529.

Xie, X., and Heller, P.L.L., 2009. Plate tectonics and basin subsidence history: Geological Society of America Bulletin, v. 121, no. 1-2, p. 55, doi: 10.1130/B26398.1.

Yilmaz, Ö., 1987. Seismic Data Processing, S.*e.g*

Yanilmaz, E., Huffman, D.P., Martin, M., and Gutteridge, P., 2008. Facies Analysis and Depositional Systems of Defined Sedimentary Sequences from Precamberian to Late Miocene in NE Libya. The Geology of East Libya, vol. 1, pp.3-84.

Yielding, G., Freeman, B., and Needham, D. T., 1997. Quantitative fault seal prediction: AAPG Bulletin, v. 81, p. 897–917.

Zarudski E.F.K., 1972. The Strait of Sicily - a geophysical study, Revue de Géographie physique et de Géologie dynamique, Vol.14, p.11-28.

Zeigler, P.A., 1988. Evolution of the Artic-North Atlantic and the Western Tethys, Am. Assoc. Petrol. Geol. Mem., 43, 198.

Ziegler, P. A., 1989. Evolution of Laurussia. A study in Late Palaeozoic plate tectonics, Kluwer Acad. Publ., Dordrecht, 102 p.

Ziegler, P.A., 1990. Geological Atlas of Western and Central Europe, 2nd edn. Shell Internationale Petroleum Maatschappij, The Hague, 239 pp.

Ziegler, P.A., Cloetingh, S., Van Wees, J.D., 1995. Dynamics of intra-plate compressional deformation: the Alpine foreland and other examples. Tectonophysics 252, 7–59.

Ziegler, P. A., 1996. Geodynamic processes governing development of rifted basins. *In* Roure, F., Ellouz, N., Shain, V. S. & Skvortsov, I. (eds.): *Geodynamic evolution of sedimentary basins*, 19-67. Paris, Ed. Technip.

Ziegler, P.A., 1999. "Petroleum systems of Alpine-Mediterranean foldbelts and basins". In B. Durand, L. Jolivet, F. Horvath and M. Séranne. The Mediterranean Basins - Tertiary extension within the Alpine Orogen. Geol. Soc., London, Spec. Publ. **156**. pp. 517–540.

Ziegler, P.A., Cloetingh, S, Guiraud, R, and Stampfli, G.M., 1999. PeriTethys Platfroms: Constraints on dynamics of rifting and basin inversion. Peri-Tethys Memoir No.6, IGCP. 369,pp 1-41.

Ziegler, **M**., 2001. Late Permian to Holocene paleofacies evolution of the Arabian Plate and its hydrocarbon occurrences. GeoArabia, 6, 445–504.

Ziegler, P.A., and Cloetingh, S.A.P.L., 2004. Dynamic processes controlling evolution of rifted basins. Earth Sci. Rev. 64, 1– 50.

Zouaghi, T., B´edir, M. and Inoubli, M. H., 2005. 2D seismic interpretation of strike-slip faulting, salt tectonics, and Cretaceous unconformities, Atlas Mountains, central Tunisia, *J. Africa Earth Sci.*, **43,** 464–486.